UNIVERSIDADE DE LISBOA

INSTITUTO SUPERIOR TÉCNICO

Durability of pultruded GFRP profiles and adhesively bonded connections between GFRP adherends

João Pedro Girão Meireles de Sousa

Supervisor:	**Doctor João Pedro Ramôa Ribeiro Correia**
Co-Supervisors:	**Doctor Susana Bravo Cabral da Fonseca**
	Doctor Fernando António Baptista Branco

Thesis approved in public session to obtain the PhD Degree in

Civil Engineering

Jury final classification: Pass with Distinction and Honour

2018

UNIVERSIDADE DE LISBOA

INSTITUTO SUPERIOR TÉCNICO

Durability of pultruded GFRP profiles and adhesively bonded connections between GFRP adherends

João Pedro Girão Meireles de Sousa

Supervisor: **Doctor João Pedro Ramôa Ribeiro Correia**

Co-Supervisors: **Doctor Susana Bravo Cabral da Fonseca**

Doctor Fernando António Baptista Branco

Thesis approved in public session to obtain the PhD Degree in

Civil Engineering

Jury final classification: Pass with Distinction and Honour

Jury

Chairperson: Doctor Eduardo Nuno Brito Santos Júlio, Instituto Superior Técnico da Universidade de Lisboa

Members of the Committee:

Doctor Jorge Manuel Caliço Lopes de Brito, Instituto Superior Técnico da Universidade de Lisboa

Doctor João Pedro Ramôa Ribeiro Correia, Instituto Superior Técnico da Universidade de Lisboa

Doctor José Manuel de Sena Cruz, Escola de Engenharia da Universidade do Minho

Doctor Augusto Martins Gomes, Instituto Superior Técnico da Universidade de Lisboa

Doctor Maria Paula Marques da Costa Rodrigues, Laboratório Nacional de Engenharia Civil

Funding Institutions

Fundação para a Ciência e Tecnologia

2018

Abstract

The durability problems experienced by traditional materials (such as steel or reinforced concrete) and the need for increased construction speed in civil engineering applications, have been fostering the development of new structural solutions, using alternative construction materials, more durable and with lower maintenance requirements.

In this context, fibre reinforced polymer (FRP) materials are playing an increasingly important role; their demand for both new construction and rehabilitation of existing structures has been steadily increasing in the construction sector. In particular, pultruded glass fibre reinforced polymer (GFRP) profiles are now being used in a growing number of applications, including structural parts or components of bridges and buildings. Compared to conventional solutions, these profiles offer low self-weight, high specific strength, ease of handling, electromagnetic transparency, non-corrodibility and low maintenance operations. The main disadvantages are their brittle behaviour, the low elasticity and shear moduli, the relatively high initial costs, the low development of connection technology and the generalised lack of specific design codes.

In spite of practical evidence of improved performance under harsh conditions, namely when compared with more traditional materials, comprehensive and validated data on the durability of pultruded GFRP profiles is still scarce. The quantification of the durability and of the damage tolerance of GFRP constructions is becoming critical to their structural design. In addition, the connection technology for pultruded GFRP profiles also presents challenges, and despite the potential benefits of adhesively bonding these materials, there are also concerns about their durability, namely with respect to the influence of the exposure conditions on both the adhesives and the GFRP adherends.

The main objective of the present thesis was to study the durability of pultruded GFRP profiles and their adhesively bonded connections. The thesis thus focused on the following four research topics: (i) the durability of pultruded GFRP profiles for civil engineering applications; (ii) the long-term behaviour of structural adhesives typically used to bond GFRP elements; (iii) the durability of GFRP bonded connections in civil engineering applications; and (iv) the performance of a GFRP structure after more than 10 years in service conditions.

The research on the durability of pultruded GFRP profiles comprised an extensive experimental campaign, in which the physical, viscoelastic, mechanical and aesthetical properties of profiles made of vinylester or unsaturated polyester resins were monitored. The profiles were subjected to hygrothermal ageing, natural weathering, thermal cycles, and synergistic effects of different

ageing conditions and sustained loading for periods up to two years. Results obtained showed that hygrothermal degradation was the most severe conditioning, when compared to thermal cycling or natural weathering, which produced relatively small changes over the exposure period. Post-curing phenomena were observed for all ageing environments. For immersion in water and salt water, the long-term material properties were predicted using Arrhenius models and none of the estimated properties fell below 50% after 100 years. Sustained loading produced small effects when acting synergistically with the different ageing environments.

Two different structural adhesives (epoxy and polyurethane) were experimentally studied regarding their durability. Although post-curing effects were observed, hygrothermal ageing had negative effects on both adhesives, causing irreversible degradation mechanisms. In a similar way as for the GFRP profiles, the effects of natural weathering were much less severe.

Single lap bonded joints were produced with the above-mentioned adhesives and GFRP adherends, and exposed to similar ageing conditions, *i.e.* hygrothermal ageing, natural weathering and thermal cycles. The degradation of the mechanical performance of such joints, in terms of ultimate load and stiffness and failure modes, was monitored during the exposure period. Alongside the experiments, numerical models were developed in order to simulate the tests and to obtain a better understanding of the mechanical behaviour of the bonded joints, including the effects of ageing. Both hygrothermal and thermal cycles caused detrimental effects on the joints' response and influenced their failure modes, while natural weathering produced smaller changes. Effects from post curing were also visible on the performance of such joints.

Regarding the case study of a GFRP construction, the visual inspection and the laboratory tests performed on the GFRP material and profiles extracted from the construction showed that its structural safety is presently largely fulfilled and that its structural reliability should not be compromised, at least in the near future.

The results obtained in this thesis showed that the degradation levels exhibited by pultruded GFRP profiles and their bonded connections, although relevant and needed to be duly accounted for at design, seem to be compatible with their structural use in civil engineering applications.

Key-words: Glass fibre reinforced polymers (GFRP), pultrusion, structural adhesives, adhesively bonded joints, durability.

Sumário

Os problemas de durabilidade dos materiais de construção tradicionais (aço e betão armado) e a exigência de maiores velocidades de construção têm contribuído para o estudo e desenvolvimento de soluções estruturais inovadoras, utilizando materiais de construção alternativos, mais duráveis e com menores exigências de manutenção.

Neste contexto, os polímeros reforçados com fibras (PRF) estão a desempenhar um papel cada vez mais relevante. Em particular, os polímeros reforçados com fibras de vidro (PRFV) têm vindo a aumentar as suas aplicações em componentes estruturais de pontes e edifícios. Estes materiais oferecem várias vantagens quando comparados com as soluções tradicionais, como o reduzido peso próprio, os elevados valores de resistência mecânica, a facilidade de transporte e montagem, a transparência electromagnética, a não corrosibilidade e as reduzidas operações de manutenção. As suas principais desvantagens consistem no comportamento frágil, os reduzidos valores de rigidez, os custos iniciais relativamente elevados, o reduzido desenvolvimento da tecnologia das ligações e a falta de regulamentação específica consensual.

Não obstante a boa durabilidade observada em diversas construções, ainda existem poucos resultados válidos e abrangentes sobre a durabilidade de perfis pultrudidos de PRFV para aplicações da engenharia civil. A quantificação da durabilidade e da tolerância ao dano são cada vez mais relevantes para o dimensionamento destes componentes estruturais. Em paralelo, existem também dúvidas e preocupações sobre a durabilidade de ligações coladas entre perfis de PRFV, nomeadamente no que se refere à influência das condições de exposição ambiental que afectam tanto os adesivos de colagem, como os perfis a ligar.

O principal objectivo desta tese consistiu em estudar a durabilidade de perfis pultrudidos de PRFV e das suas ligações coladas. Para tal, a tese aborda os seguintes quatro tópicos de investigação: (i) a durabilidade de perfis pultrudidos de PRFV para aplicações em engenharia civil; (ii) o comportamento a longo prazo de adesivos estruturais utilizados na colagem de materiais PRFV; (iii) a durabilidade de ligações coladas entre perfis de PRFV para aplicações estruturais; e (iv) a avaliação do desempenho de uma estrutura PRFV após mais de 10 anos de utilização.

A investigação acerca da durabilidade de perfis de PRFV incluiu um extenso programa experimental, em que foram monitorizadas as propriedades físicas, químicas, viscoelásticas, mecânicas e estéticas de perfis com matrizes de poliéster e viniléster. Os perfis foram submetidos a envelhecimentos acelerados artificialmente, como exposições higrotérmicas e ciclos térmicos, a envelhecimento natural e também a efeitos sinergéticos entre vários tipos de envelhecimento e diferentes condições de carregamento em

flexão. Os resultados obtidos mostraram que os envelhecimentos higrotérmicos afectaram de modo mais pronunciado as propriedades de ambos os tipos de perfis de PRFV por comparação com os ciclos térmicos ou o envelhecimento natural, cujos efeitos globais foram reduzidos durante os períodos de exposição. Foram observados efeitos de pós-cura em todos os envelhecimentos considerados. Várias propriedades mecânicas foram estimadas por recurso a modelos de previsão de longo prazo baseados na equação de Arrhenius e, após 100 anos, nenhuma apresentou reduções superiores a 50%. Acrescenta-se ainda que os efeitos sinergéticos dos ambientes de envelhecimento e de carregamento em flexão foram reduzidos.

Dois adesivos estruturais de epóxi e poliuretano foram sujeitos a ambientes de envelhecimento semelhantes aos utilizados no estudo dos perfis de PRFV. De uma forma geral, os ambientes higrotérmicos afectaram de forma negativa ambos os adesivos, tendo-se verificado mecanismos de degradação irreversíveis, mesmo quando ocorreram fenómenos de pós-cura. De uma forma análoga aos perfis de PRFV, os efeitos do envelhecimento natural também foram menos severos nos adesivos.

Foi também estudada a durabilidade de perfis colados por sobreposição simples utilizando os perfis e adesivos acima mencionados. Estas ligações foram sujeitas a diferentes tipos de envelhecimentos, nomeadamente envelhecimentos higrotérmicos, envelhecimento natural e ciclos térmicos, tendo-se quantificado o seu efeito na degradação das propriedades mecânicas das ligações. Os envelhecimentos higrotérmicos e os ciclos térmicos reduziram o desempenho das ligações, tendo também influenciado os modos de rotura; o envelhecimento natural provocou efeitos mais reduzidos. Ao nível das ligações, também foram visíveis os efeitos de pós-cura já mencionados. Paralelamente, foram também desenvolvidos estudos numéricos que permitiram aprofundar o efeito da degradação ambiental dos diferentes materiais no comportamento das ligações.

Por último, em relação ao caso de estudo da estrutura em PRFV, a inspecção visual e os ensaios de laboratório efectuados no material retirado da obra mostraram que a segurança da estrutura está assegurada e que não deverá ser comprometida ou chegar a um nível crítico num futuro próximo.

Os resultados obtidos nesta tese mostram que os níveis de degradação apresentados pelos perfis de PRFV e pelas suas ligações coladas, não obstante serem relevantes e terem que ser devidamente considerados na fase de projecto, parecem ser compatíveis com a sua utilização em aplicações estruturais de engenharia civil.

Palavras chave: Polímeros reforçados com fibras de vidro (PRFV), pultrusão, adesivos estruturais, ligações coladas, durabilidade.

Acknowledgements

The work presented in this thesis marks the end of almost five years of research, and although it is mostly regarded as an individual work, there were periods I often had to rely on my colleagues and friends, and their contribution was essential in many ways. The next section is dedicated to them.

To begin with, I would like to express my deepest gratitude to my thesis scientific supervisors. Professor João Ramôa Correia and Doctor Susana Cabral-Fonseca were instrumental in the success of this thesis, both in their own way, and their combined efforts made this project possible. Their support, availability, confidence, encouragement, and ever constant optimism allowed me to overcome all difficulties that appeared during this period (even when I thought it was not possible!). Their contribution, guidance and experience allowed me to accomplish the difficult task of successfully combining very diverse research subjects into a coherent outcome. I consider myself privileged to have experienced and shared the dedication, exigence and rigour they put into their daily work, and I am also thankful for the friendship that we developed during these years. Collaborating with Professor João Correia changed my way of seeing research in civil engineering, and helped me to improve myself day after day, while Doctor Susana Fonseca made me realise the importance of the microscopic scale of materials and their chemistry.

I am also grateful to Professor Fernando Branco, my scientific co-supervisor, for sharing his immeasurable experience and ever valuable advice, in particular his ability to see practical applications and research guidance. During this period, I also had the opportunity to work during six months at the *École Polytechnique Fédérale de Lausanne* (EPFL), under the supervision of Professor Thomas Keller, to whom I want to extend my gratitude for welcoming me in his lab. His vast experience in composites for construction applications, and personal contributions allowed me to further enrich my research path, namely in what concerns adhesively bonded joints between composites materials.

This thesis was conducted in collaboration with *Laboratório Nacional de Engenharia Civil* (LNEC), where most of this thesis experimental work was conducted. I am deeply thankful for the opportunity to work at the *Núcleo de Materiais Orgânicos* (NMO). I thus want to thank Doctor Maria Paula Rodrigues and Doctor Susana Fonseca for making me feel always welcome, and for providing me with a unique learning experience in a different work environment.

I would also like to thank my friends, colleagues and fellow researchers at *Instituto Superior Técnico* (IST), particularly Adriana Azevedo, André Castelo, Cristina Sánchez, David Martins, Francisco Nunes, Inês Rosa, Inês Teotónio, João Firmo, João Pacheco, José Gonilha, Lourenço Fernandes, Luís Valarinho, Mário Arruda, Mário Sá, Mário Garrido, Mateus Hofmann, Miguel Proença, Tiago Morgado and Wallace Maia. Their friendship, support, and availability to help in both experimental and numerical work is greatly appreciated.

My period at the Composite Construction Laboratory (CCLab) in EPFL was short. However, I had the opportunity to meet and discuss with colleagues to whom I am also very grateful, namely Aida Molares, Alireza Moshtaghin, Anastasios Vasilopoulos, Haifeng Fan, Júlia de Castro, Kyriaki Goulouti, Maria Savvilotidou, Myrsini Angelidi, Saira Banu, Sonia Armas, Vahid Movahedirad, Victor Oladipo and Xing Zhao. Their contribution is also not forgotten.

Also from IST, I would also like to thank the interest and support from Professor António Correia Diogo in the execution of scanning electron microscopy tests. The extensive amount of experimental work would also not be possible without the help from the lab personnel, namely Mr. Fernando Alves, Mr. Fernando Costa, Mr. Leonel Silva and Mr. João Lopes. In addition, I would also like to thank Mrs. Maria Helena Salvado and Ms. Elaine Gregório for all their administrative work and kindness towards our group of PhD colleagues.

The valued help from Ana Marinho, João Carvalho, Pedro Rodrigues, and Rodrigo Borges in the context of their MSc dissertations is greatly appreciated. Throughout our work together we had the opportunity to overcome many difficulties and shared good moments in the lab.

All NMO personnel made me feel at ease and they were always available and helpful, assisting me in different experimental tests. In particular, I would like to thank Filomena Castro, Filomena Nobre, Helena Silva, Joana Pereira, Nuno Silvestre, Otília Lourenço, and Rúben Rocha.

I am also thankful for the support from the Portuguese Foundation for Science and Technology (FCT, through the individual doctoral scholarship SFRH/BD/88467/2012), which allowed me to have financial conditions to carry out this research, and also to the Civil Engineering Research and Innovation for Sustainability (CERIS) research unit from IST, which provided me with the work conditions needed to develop this work.

Moreover, I would also like to thank the industry partners which provided the materials for this work, namely *ALTO Perfis Pultrudidos, Sociedade Técnica de Estruturas Pultrudidas*

(STEP) for providing the pultruded materials, and to SIKA for providing the structural adhesives.

To all my personal friends, it would be an extremely difficult task to name all of them, but they surely know who they are. Their friendship, support, and encouragement through the hardships that I encountered during these years, are deeply appreciated.

To Ana's family, especially her parents and brother, I would like to thank their motivation and support towards me. Their confidence in me was unwavering during these years.

To my family I extend my deepest gratitude. They are a part of me every day, and surely without their unconditional love, encouragement, belief and support in times when I had near no belief in myself, this thesis would not be finished today. To my mother, father, sister and brother and grandmother, thank you for shaping me to be the person I am today. To all my grandparents who are not with me anymore, thank you for helping me distinguish right from wrong, and remaining in my heart every single day. To my brother and sister in law, you really give another definition to words like love and friendship. To my little Sofia, Diana and José, who are our future, I thank you for being the joy of our days, you never fail to cheer me!

I believe that we are in control of our destinies and dreams. However, if not for this period of my life, I would not have met my soulmate. My gratefulness and love to my fiancée, Ana, cannot be measured. The love, belief, endurance and patience that she has makes me feel like there is nothing that cannot be accomplished, no obstacle that cannot be overcome. You continue to amaze me every single day.

To my dear grandmother Madalena,

To F & Z,

To Ana, may we build our dreams together.

Contents

List of figures

List of tables

Notation

Roman Lower Case

a*	colour variation in the green-red axis
b*	colour variation in the blue-yellow axis
d	displacement
d_{max}	maximum vertical displacement
d_{yy}	single lap joint deformation in the longitudinal direction
h	thickness (w.r.t. diffusion)
k	relaxation constant
l	length (w.r.t. diffusion)
t	time
s	deflection
tan δ	loss factor
w	width (w.r.t. diffusion)
x	distance in the thickness direction (w.r.t. diffusion)
x_l	longitudinal deformation

Roman Capital

A	approximate fickian diffusion
B	two-stage fickian diffusion
C	concentration of sorbate per unit of sorbent
Cf	anomalous ascending fickian deviation
C_0	initial uniform distribution of sorbent
C_1	constant surface concentration
D	diffusion coefficient
D_d	diffusion coefficient of the denser phase
D_1	diffusion coefficient of the less denser phase
Df	anomalous descending fickian deviation
E	elasticity modulus
E_a	activation energy
E_{app}	apparent modulus of elasticity

$E_{c,0^\circ}$	elasticity compressive modulus in the longitudinal direction
$E_{c,90^\circ}$	elasticity compressive modulus in the transverse direction
E_d	activation energy for diffusion
E_{eff}	effective modulus of elasticity
E_f	elasticity flexural modulus
$E_{f,0^\circ}$	elasticity flexural modulus in the longitudinal direction
$E_{f,90^\circ}$	elasticity flexural modulus in the transverse direction
E_m	dielectric strength
E_t	elasticity tensile modulus
$E_{t,0^\circ}$	elasticity tensile modulus in the longitudinal direction
$E_{t,90^\circ}$	elasticity tensile modulus in the transverse direction
E'	storage modulus
E''	loss modulus
F	load
F_u	failure load
G	shear modulus
G_{eff}	effective distortion modulus
H	barcol hardness
J	energy
K	overall bond stiffness
K_{local}	local bond stiffness
L	span in structural beam tests
Lf	fickian diffusion
$L*$	colour variation in the black-white axis
M_{max}	maximum water absorption
M_t	total weight change of substance over time
M_∞	maximum equilibrium moisture absorption
$M_{\infty,F}$	fickian asymptote
$M_{\infty,R}$	absorbed water content due to relaxation
$M_{0\infty}$	pseudo-equilibrium moisture content
P	concentrated load
P_{max}	maximum load
R	universal gas constant
S	moving diffusion front
$S13$	longitudinal out-of-plane stress
$S33$	peeling stress

T	temperature
T_g	glass transition temperature
$T_{g,\ E'onset}$	glass transition temperature from the storage modulus curve
$T_{g,\ tan\,\delta}$	glass transition temperature from the loss factor peak
V_d	volume fraction of the denser phase

Greek symbols

α	thermal expansion coefficient
α_{long}	longitudinal thermal expansion coefficient
α_{trans}	transverse thermal expansion coefficient
$\alpha_{,\ 0°}$	thermal expansion coefficient in the longitudinal direction
δ	displacement in the structural beam tests
δE_c	elastic strain energy due to applied stress
$\delta\sigma$	energy required to create a crack surface
δW	energy expended in plastic deformation
Δ	coefficient of variation
ΔE^*	colour variation
ε_c	dielectric constant
ε_t	tensile strain
ε_{tu}	strain at tensile failure
ε_f	flexural strain
ε_{fu}	strain at flexural failure
γ	distortion
γ_u	distortion at failure
ν	poisson ratio
$\nu_{,\ 0°}$	poisson ratio in the longitudinal direction
$\nu_{,\ 90°}$	poisson ratio in the transverse direction
λ	thermal conductivity
ρ	density
σ_c	compressive strength
$\sigma_{c,\ 0°}$	compressive strength in the longitudinal direction
$\sigma_{c,\ 90°}$	compressive strength in the transverse direction
σ_{cB}	bearing strength

$\sigma_{cB,\ 0^\circ}$	bearing strength in the longitudinal direction
$\sigma_{cB,\ 90^\circ}$	bearing strength in the transverse direction
σ_{f}	flexural strength
σ_{fu}	ultimate flexural strength
$\sigma_{f,\ 0^\circ}$	flexural strength in the longitudinal direction
$\sigma_{f,\ 90^\circ}$	flexural strength in the transverse direction
σ_{sbs}	interlaminar shear strength
$\sigma_{sbs,\ 0^\circ}$	interlaminar shear strength in the longitudinal direction
σ_{t}	tensile strength
σ_{tu}	ultimate tensile strength
$\sigma_{t,\ 0^\circ}$	tensile strength in the longitudinal direction
$\sigma_{t,\ 90^\circ}$	tensile strength in the transverse direction
τ	in-plane shear strength
τ_{max}	maximum in-plane shear strength
$\tau_{,\ 0^\circ}$	in-plane shear strength in the longitudinal direction

Acronyms

AA	Aliphatic Amines
AH	Aromatic hydrocarbon
AFM	Atomic Force Microscopy
A-glass	Window glass
ALTO	Alto Perfis Pultrudidos, Lda.
AR-glass	Alkaline Resistant glass
ASCE	America's Infrastructure Report Card
ASTM	American Society of Testing and Materials
BED	1,3-bis(2,3-epoxypropoxy)-2,2-dimethylpropane
BPA	Bisphenol-A
BJ	Butt joint
BS	British Standard
CCLab	Composite Construction Laboratory
CE	Controlled Environment
Cov	Coefficient of variation
C40	Continuous Condensation
CERIS	Civil Engineering Research and Innovation for Sustainability

CFRP	Carbon Fibre Reinforced Polymer
CSM	Continuous Strand Mat
CTE	Coefficient of thermal expansion
DDA	Dicyandiamide
DDS	4,4'-diaminodiphenyl sulfone
DGEBA	Diglycidyl ether of bisphenol-A
DMA	Dynamic Mechanical Analysis
EDS	Energy Dispersive Spectrometer
E-glass	Electrical glass
EN	European Norm
EP	Epoxy
EPFL	École Polytechnique Fédérale de Lausanne
FE	Finite Element
FRP	Fibre Reinforced Polymer
FTIR	Fourier Transform Infrared Spectroscopy
F+R	Fickian and Relaxation model
GFRP	Glass Fibre Reinforced Polymer
IF	Inorganic Filler
IPDA	3-aminomethyl-3,5,5-trimethyl cyclohexylamine
IR	Infrared
ISO	International Standards Organization
IST	Instituto Superior Técnico
LNEC	Laboratório Nacional de Engenharia Civil
MAPE	Mean Absolute Percentage Error
MDI	Methylene Diphenyl Isocyanate
mDPA	Metaphenylene diamine
MXD	M-xylenediamine
NE	Natural weathering Exposure
NMO	Núcleo de Materiais Orgânicos
NOL	Naval Ordinance Laboratory
NPE	Nonylphenol
NA	Not Available
PEI	Polyethylenimine
PUR	Polyurethane
QUV	Q-Lab UV Accelerated Weathering Tester
RH	Relative Humidity

SATU	Urban Transport Automated System
SBS	Short Beam Shear
SEM	Scanning Electron Microscopy
S-glass	Structural glass
SLJ	Single Lap Joint
SM	Structural Modification
SMC	Sheet Moulding Compound
STEP	Sociedade Técnica de Estruturas Pultrudidas
S20	Salt water immersion at 20 °C
S40	Salt water immersion at 40 °C
S60	Salt water immersion at 60 °C
TC	Thermal Cycles
TDI	Toluene diisocyanate
TGA	Thermogravimetric Analysis
TGDDM	Tetraglycidyl-4,4'-diaminodiphenyl
TGMDA	Tetraglycidlymethylene dianiline
UP	Unsaturated Polyester
US	United States
UTM	Universal Testing Machine
UV	Ultraviolet
VARTM	Vacuum Assisted Resin Transfer Moulding
VE	Vinylester
W20	Water immersion at 20 °C
W40	Water immersion at 40 °C
W60	Water immersion at 60 °C
3D	Three-dimensional

Part I

Introduction

Preamble

Pultruded glass fibre reinforced polymers (GFRP) result from the combination of glass fibres and different polymeric matrices, being manufactured through the pultrusion method. Over the last 30 years, the use of these materials in the construction sector has significantly increased: in 2017, 34% of the GFRP production in Europe was applied in this industry. Despite these significant growing trends, there is still potential to further increase the production and use of pultruded elements in construction. One of the factors that is hampering the further use of pultruded GFRP in construction is the unquantified and/or unknown susceptibility of these materials when subjected to different ageing conditions.

Part I of this thesis presents an overview of pultruded GFRP profiles, their constitution, manufacturing method, typical properties, shapes, connection technology and current civil engineering applications. In addition, the GFRP European market and the current positioning of pultruded elements is also discussed.

Chapter 1.
Introduction

1.1. Context and motivation

In the past few decades, the durability problems of civil engineering structures built with conventional materials (namely steel, concrete, and timber) have increased significantly and so have the costs involved in the corresponding repair, retrofit and maintenance operations. As an example, the ASCE 2017 infrastructure report card [1.1] refers that almost four out of ten bridges in the United States (US) are at least 50 years old and in need of rehabilitation. In addition, in 2016 9.1% of the 614 387 bridges in the US were classified as structurally deficient; this number reflects a growing trend, with the most recent estimates regarding bridge repair needs amounting to a 123 billion dollar investment [1.1].

The limited durability of civil infrastructure has been fostering the search for alternative construction materials and structural systems. Over the past few decades this pursuit for lighter and more durable materials, with lower maintenance requirements, has raised the interest in innovative materials and connection systems [1.2–1.4].

Among those materials, pultruded glass fibre reinforced polymer (GFRP) profiles are being used in a growing number of applications, because they offer the above-mentioned advantages at a relatively competitive life cycle cost. There are already several examples of bridges and buildings comprising GFRP structural elements, in both new construction and rehabilitation of degraded infrastructure [1.2-1.4]. The field of application of GFRP profiles includes the replacement of deteriorated bridges decks made of reinforced concrete or steel, especially those located in cold environments (where de-icing salts are used), or new structural (*e.g.* pultruded frames and trusses) and non-structural components (*e.g.* hand-rails) exposed to relatively harsh environmental or chemical conditions, such as water treatment plants [1.5].

The main disadvantages of GFRP profiles are their brittle behaviour and low elasticity and shear *moduli*, with their design being often governed by deformability or instability phenomena and seldom allowing the full exploitation of the material's resistance [1.6, 1.7]. In spite of practical evidence of improved durability, another factor that is delaying the widespread acceptance of GFRP profiles for civil engineering structural applications is the lack of comprehensive and validated data about their durability. In fact, although there is a wealth of information available concerning their short-term behaviour, the durability of GFRP profiles has not yet been

investigated to an extent that provides enough confidence to construction agents, namely when compared with traditional materials. The need to document, evaluate and quantify the durability performance of GFRP profiles is particularly relevant for civil engineering structural applications, as the majority of the projects are developed considering relatively long service lives, often higher than 50 years [1.1, 1.8].

The connection technology for pultruded GFRP profiles also presents challenges due to the brittle and anisotropic nature of the material. GFRP profiles are usually connected via bolting and/or adhesive bonding. While mechanical bolting typically needs drilling operations and often leads to overdesigned GFRP components [1.5, 1.6], adhesively bonding offers more uniform load transfer, being also more material-adapted, as both the substrate and the adhesive are of a polymeric nature [1.7, 1.8]. Moreover, adhesives can potentially confer some ductility to joints, compensating the brittle nature of GFRP components, thus providing some energy dissipation capacity under cyclic/seismic actions and/or load redistribution in redundant structures [1.9]. Sections assembled by means of adhesive bonding may also benefit the construction process, by reducing installation times and production costs [1.10, 1.11].

As such, the use of adhesives to join GFRP components has been increasing in the construction industry, in parallel with other industries. However, among other concerns (*e.g.* the behaviour at elevated temperature), a broader use of bonded joints is pending on obtaining a better understanding of their long-term behaviour [1.12]. Nowadays, a wide range of adhesives is available to bond structural components made of different materials. Some industries, such as aerospace, naval and automotive, provide anecdotal evidence of good durability properties of bonded joints. However, limited comprehensive data is usually available regarding their long-term performance [1.13]. Moreover, structural adhesive bonding in civil engineering applications has very diverse requirements compared to those industries, namely different (longer) design service lives and exposure environments. In order to properly design such structural adhesive joints, such information is needed, namely about the environmental degradation underwent by the adhesives (and the adherends) throughout the service life of the construction [1.14].

The work presented in this PhD thesis follows the previous work conducted within the author's MSc dissertation [1.15], where preliminary and exploratory studies were conducted about the durability of pultruded GFRP profiles. The results obtained then established the backbone that supported the present research.

1.2. Objectives and methodology

The main objectives of the present thesis were to overcome some of the aforementioned limitations, namely: (i) to obtain in-depth understanding about the durability of pultruded GFRP profiles for civil engineering applications; (ii) to study the long-term behaviour of structural adhesives typically used to bond GFRP structural elements; (iii) to investigate the durability of GFRP bonded connections in civil engineering applications; and (iv) to evaluate the performance of a GFRP structure after more than 10 years in service conditions.

Regarding the first objective, the **assessment of the long-term behaviour of pultruded GFRP profiles**, it was addressed through the following tasks: (i) study of the main degradation mechanisms caused by different critical factors that affect the durability of pultruded GFRP profiles; (ii) characterisation of long-term material properties (mechanical, physical, and aesthetical) when GFRP profiles are subjected to different ageing environments; (iii) prediction of the long-term behaviour at the material level, attempting to correlate and compare the effects of the different ageing conditions on the durability of pultruded GFRP profiles.

The first task was supported by a literature review, which allowed (i) identifying the most pertinent issues that affect the GFRP material durability, and (ii) supporting the definition of the materials to be used in the experimental campaign, in terms of nature of the polymeric matrix and fibre architecture. Based on such study, two types of commercial "*off-the-shelf*" GFRP profiles made of either unsaturated polyester or vinylester resins were produced by the pultrusion method at company *Alto Perfis Pultrudidos, Lda.*, and their mechanical, physical, viscoelastic, chemical and aesthetical properties were initially characterised through several experimental tests.

This task motivated the second one, in which the long-term durability behaviour of pultruded GFRP profiles applied in mild Mediterranean climates was assessed through four different and comprehensive experimental programmes (each one involving up to two years of ageing or 600 thermal cycles): (i) hygrothermal ageing comprising a desorption period, (ii) outdoor (natural) and QUV (artificial) accelerated ageing, (iii) thermal cycling ageing, and (iv) synergistic effects of different ageing conditions and sustained loading (bending). For all these experimental programmes, different physical, chemical, viscoelastic and mechanical properties were monitored and their changes were thoroughly analysed and discussed.

Finally, the third task involved applying long-term prediction models to different mechanical properties in order to estimate their long-term behaviour. As such, analytical Arrhenius type models were successfully implemented, whenever applicable. In addition, an attempt was also made to correlate natural and QUV artificial ageing.

Regarding the second main objective of this thesis, the **durability of commonly used structural adhesives**, analogous tasks were performed towards the experimental characterisation of their long-term behaviour. As such, two structural adhesives, an epoxy and a polyurethane, were subjected to two environmental conditions - (i) hygrothermal ageing, and (ii) natural ageing. The results obtained provided relevant information about the deterioration of those adhesives when subjected to similar conditions to those used to assess the performance of pultruded GFRP profiles.

Based on the information obtained about both the adherend (GFRP profiles) and adhesive (epoxy and polyurethane) materials, further investigations were performed about the **durability of GFRP adhesively bonded connections**, the third objective of this thesis. Single lap bonded joints were produced and subjected to different ageing conditions, namely (i) hygrothermal ageing, (ii) natural ageing, and (iii) thermal cycles. Single lap shear tests were then performed in order to quantify the degradation of the mechanical performance of such joints, in terms of ultimate load and stiffness and failure modes. The changes in the performance of the bonded joints due to the different ageing conditions was analysed in light of the changes underwent by both the GFRP adherends and the adhesives. Alongside the experimental tests, numerical models were developed in order to simulate the tests and to obtain a better understanding of the mechanical behaviour of the bonded joints, including the effects of ageing. The numerical models were also used to assess the magnitude of the stresses developed in the materials due (i) to the hygrothermal ageing of the materials, and (ii) the mismatch between the coefficients of thermal expansion of the GFRP and the adhesives, due to thermal cycles.

Finally, the fourth main objective consisted of the **characterisation of the durability of a GFRP structure under actual service conditions**: the *Urban Transport Automated System in Oeiras* (SATU-Oeiras), which was exposed to a maritime influence during 11 years of service. To fulfil such objective, a detailed visual inspection was conducted and an experimental campaign was performed on GFRP components, which included: (i) assessment of physical, mechanical and aesthetical properties of the GFRP material; and (ii) assessment of the flexural behaviour of full-scale GFRP beams. It is worth noting that despite the importance of results obtained from accelerated and controlled laboratory artificial ageing, the

correlation between such results and those obtained from natural weathering is not an easy task. In fact, the environmental aggressiveness is not always easy to quantify and there are numerous parameters that may influence the material and structural behaviour, and their complex interactions (*e.g.* changing temperatures, humidity levels, direct contact with water, creep, fatigue, ultraviolet (UV) radiation, among others). Natural weathering studies provide more reliable results regarding the long-term behaviour, however very few works were published until now [1.7].

1.3. Main scientific contributions

The research presented in this thesis about the durability of pultruded GFRP profiles and their adhesively bonded connections provided relevant scientific contributions, for both the construction industry and the scientific community. The main contributions are highlighted in this section.

The research about the durability of pultruded GFRP profiles deepened the understanding about the long-term behaviour of these materials when subjected to different ageing conditionings. The amount of experimental data obtained was paramount - over 3000 tests were performed, some corresponding to significantly long periods of hygrothermal ageing – such information was very scarce in the current technical literature. Comprehensive information was obtained about the physical, viscoelastic and many mechanical properties of pultruded GFRP material made of either unsaturated polyester of vinylester, comprising a robust database on the effects of hygrothermal ageing (up to 2 years) after a desorption period. These data allowed quantifying the changes suffered by those properties, analysing the degradation mechanisms that affect GFRP profiles and applying long-term prediction models, whenever possible. In addition, it was also possible to correlate results obtained from 3000 hours of QUV artificial ageing with natural ageing up to 8.5 years, deepening the long-term information about these materials. For this type of ageing, even for low to moderate degradation of mechanical properties, the importance of fibre blooming (observed for relatively short exposure periods) was highlighted. This thesis also provided useful and new information about the effects of thermal cycles (up to 600 cycles) typical of mild Mediterranean climates on the physical and mechanical properties of GFRP profiles.

The research about the durability of structural epoxy and polyurethane adhesives also contributed to increase the knowledge about their long-term performance when subjected to several ageing conditions representative of different civil engineering applications, namely (i) hygrothermal ageing and (ii) natural ageing. The effects of these environments on several

physical, viscoelastic and mechanical properties of two common structural adhesives was assessed. The results obtained provided a better understanding of the degradation mechanisms that affect these adhesives and the impact of those mechanisms on the adhesive properties. The thesis provided also a wealth of experimental data (over 800 tests were performed in adhesive specimens), which, for some properties (*e.g.* in plane shear properties), was not available in the literature. The results obtained also allowed comparing the hygrothermal and weathering resistance of the two structural adhesives - epoxy (with higher stiffness) and polyurethane (with higher deformation capacity).

The research on adhesively bonded joints between GFRP adherends allowed assessing the effects of hygrothermal, outdoor ageing and thermal cycles on the performance of such joints. To the author's best knowledge, no test results were available in the literature about the influence of those environments on bonded joints between all-GFRP adherends. The information obtained in this thesis allowed filling a specific gap, improving the current knowledge about the susceptibility of such bonded joints to different types of ageing and providing relevant and extensive data (over 260 tests were performed on bonded joints) to both researchers and practitioners. The numerical models developed provided also interesting insights about the stress distributions in all-GFRP bonded joints, including (i) the effects of hygrothermal ageing on the stress peaks at the overlap ends and (ii) the magnitude of thermal stresses caused by thermal cycles.

In the final part of this work, a real GFRP structure - the SATU Oeiras - was thoroughly assessed, allowing quantifying and evaluating its mechanical and structural performances after 11 years in service conditions, under maritime influence. After a detailed visual inspection, it was possible to identify the occurrence and severity of the most significant anomalies, and the overall state of conservation of the construction. Mechanical tests on small-scale coupons and flexural tests on beams allowed quantifying the degradation underwent at the material and structural levels, by comparing the performance of similar unaged pultruded material and beams. In summary, the main contributions of this part of the work comprised the assessment of the structural safety and long-term performance of a full-scale GFRP structure in real service conditions.

The following ISI-indexed journal publications resulted from the contributions described above:

- Sousa JM, Correia JR, Cabral-Fonseca S, Diogo AC. Effects of thermal cycles on the mechanical response of pultruded GFRP profiles used in civil engineering applications. *Composite Structures*. 2014; 116:720–31;

- Sousa JM, Correia JR, Cabral-Fonseca S. Durability of glass fibre reinforced polymer pultruded profiles: Comparison between QUV accelerated exposure and natural weathering in a mediterranean climate. *Experimental Techniques*. 2016; 40:207–19;
- Sousa JM, Correia JR, Cabral-Fonseca S. Durability of an epoxy adhesive used in civil structural applications. *Construction and Building Mater*ials. 2018; 161:618–33;
- Sousa JM, Correia JR, Cabral-Fonseca S. Some permanent effects of hygrothermal and outdoor ageing on a structural polyurethane adhesive used in civil engineering applications. *International Journal of Adhesion and Adhesives*. (doi:10.1016/j.ijadhadh.2018.04.010) 2018;
- Cabral-Fonseca S, Correia JR, Custódio J, Silva HM, Machado AM, Sousa JM. Durability of FRP - concrete bonded joints in structural rehabilitation: a review. *International Journal of Adhesion and Adhesives* (in press) 2018;
- Sousa JM, Correia JR, Firmo JP, Cabral-Fonseca S, Gonilha, J. Effects of thermal cycles on adhesively bonded joints between pultruded GFRP adherends. *Composite Structures* (in press). 2018;
- Sousa JM, Correia JR, Gonilha, J, Cabral-Fonseca S, Firmo JP, Keller, T. Durability of adhesively bonded joints between pultruded GFRP adherends under hygrothermal and natural ageing. *Composites Part B: Engineering* (under review) 2018.

In addition to the above-mentioned publications in ISI journal papers, the research developed in this thesis was published in the proceedings of the following International and Portuguese conferences:

- Sousa JM, Correia JR, Cabral-Fonseca S. Durabilidade de ligações coladas entre perfis pultrudidos de GFRP com adesivos estruturais, *Proceedings of the 5as Jornadas Portuguesas de Engenharia de Estruturas (JPEE 2014)*, LNEC, Lisbon, Portugal. November 2014;
- Sousa JM, Correia JR, Cabral-Fonseca S. Durabilidade de ligações coladas entre perfis pultrudidos de GFRP com adesivos estruturais, *Proceedings of the XIII Congresso Latino-Americano de Patologia da Construção (CONPAT 2015)*, IST, Lisbon, Portugal. October 2015;
- Sousa JM, Correia JR, Cabral-Fonseca S. Durabilidade de perfis pultrudidos de GFRP em aplicações estruturais – Caso de estudo SATU-Oeiras, 2º Encontro Nacional sobre Qualidade e Inovação na Construção (QIC 2016), LNEC, Lisbon, Portugal. November 2016;
- Cabral-Fonseca S, Correia JR, Custódio J, Silva HM, Machado AM, Sousa JM. Durability of FRP - concrete bonded joints in structural rehabilitation: a review, 4th International Conference on Structural Adhesive Bonding (AB 2017), FEUP, Porto, Portugal. July 2017;

- Sousa JM, Correia JR, Cabral-Fonseca S. Durability of adhesively bonded joints between pultruded GFRP adherends under hygrothermal ageing, 20th International Conference on Composite Structures (ICCS 20), Paris, France. September 2017;
- Sousa JM, Correia JR, Cabral-Fonseca S. Effects of thermal cycles on the mechanical behaviour of adhesively bonded joints between pultruded GFRP profiles, 20th International Conference on Composite Structures (ICCS 20), Paris, France. September 2018.

1.4. Document outline

This thesis is organised in thirteen individual chapters, which were grouped into the following six parts:

- Part I - Introduction (chapters 1 and 2);
- Part II - Durability of pultruded GFRP profiles (chapters 3 to 7);
- Part III - Durability of structural adhesives for civil engineering applications (chapters 8 and 9);
- Part IV - Durability of adhesively bonded joints between pultruded GFRP profiles (chapters 10 and 11);
- Part V - Natural weathering performance of a GFRP structure (chapter 12);
- Part VI - Conclusions and future developments (chapter 13).

The present chapter introduces the thesis subject, describing the motivation and context that encompassed this thesis, as well as the main objectives and methodologies that were implemented. The main scientific contributions are also highlighted and the structure of the different parts and chapters is outlined.

The second chapter presents a brief overview of the use of pultruded GFRP profiles in civil engineering applications. The general constitution of these materials is introduced, as well as their typical properties and shapes, and the pultrusion manufacturing process is abridged. An insight is provided on the connection technology and current GFRP applications in the construction industry, and the current advantages and disadvantages of pultruded GFRP profiles are addressed. In addition, the current trends of GFRP materials in the European composites market are discussed, specifically in what concerns pultruded elements.

The third chapter presents a literature review on the durability of pultruded GFRP profiles. After an introduction to this topic, the review addresses first the effects on the durability of those materials of moisture and water, temperature, ultraviolet radiation, and creep. Next,

insights on the effects of alkaline environments and fatigue load are briefly presented. Then, diffusion modelling of pultruded GFRP profiles is discussed w.r.t. the analytical models used in the current thesis. Finally, a discussion about predictive degradation models for GFRP materials is also presented.

The fourth chapter addresses the hygrothermal ageing of pultruded GFRP profiles made of unsaturated polyester and vinylester resin systems. The experimental programme carried out to investigate the effects of such ageing on different GFRP material properties is first outlined, and then a detailed description is presented about the exposure conditions, ageing environments and durations, and characterisation methods. Next, the performance for each selected property is presented and discussed, and the results of different diffusion models applied for each tested environment and profile are presented. The results obtained are used to make comparisons between the susceptibility to hygrothermal ageing of two alternative polymeric resin systems. In addition, long-term prediction models are implemented at a material level, and the results obtained are presented and discussed.

The fifth chapter concerns the effects of natural weathering (monitored conditions) on the durability of pultruded GFRP material and its correlation to QUV artificial accelerated ageing. In the first of the chapter, the experimental programme is described and the characterisation techniques are outlined; next, the results obtained regarding several aesthetical, chemical and mechanical properties are presented and discussed. As in the preceding chapter, two types of GFRP profiles are compared (made of two resin systems), allowing to draw conclusions about their susceptibility to both types of ageing, their correlation, and the comparison with other ageing conditions.

The sixth chapter outlines the effects of thermal cycles, typical of mild Mediterranean climates, on the two same types of pultruded GFRP profiles. Similarly to the preceding chapter, the susceptibility to thermal cycles is assessed in terms of the changes presented by several properties; the results of those tests are complemented with detailed scanning electron microscopy analysis. As in previous chapters, the results obtained allow comparing both types of profiles, as well as the influence of this type of ageing in comparison to others.

The seventh chapter refers to a smaller experimental investigation on the synergistic effects between different ageing environments under sustained loading on the flexural properties of the two same types of GFRP profiles. The first part of the chapter outlines the experimental programme, and the second presents and discusses the results obtained about the combined effects of such ageing conditions.

The eighth chapter introduces the second part of this thesis, describing the experimental investigations on the hygrothermal and natural weathering of cold curing epoxy adhesive. The chapter first details the selected ageing conditions and the duration of the experimental programme, as well as the characterisation techniques. Then, the results obtained are presented and discussed, regarding the effects of the several degradation mechanisms that affect such adhesives. In addition, the implementation of diffusion modelling with non-Fickian analytical approaches is also presented and the results obtained are discussed.

The ninth chapter presents a parallel study to that described in the eighth chapter, now regarding the long-term behaviour of a structural polyurethane adhesive when subjected to the same conditions.

The tenth chapter introduces the third part of this thesis, addressing the hygrothermal and natural ageing of adhesively bonded joints between pultruded GFRP adherends and epoxy or polyurethane adhesives. The first part of the chapter describes the experimental programme, which was defined taking into account the changes experienced by the constituent materials, presenting the joint geometry, the preparation and manufacturing of the specimens, the selected ageing environments and the characterisation techniques. Next, the results obtained from the tests are presented and discussed, and the performance of the two types of bonded joints (w.r.t. the nature of the adhesives) is compared. The second part of the chapter describes the numerical investigations developed in order to simulate the behaviour of the adhesively bonded joints, namely in what concerns the effects of ageing on the mechanical properties of the constituent materials and, as a consequence, on the stress distributions in different parts of the joints.

The eleventh chapter describes the effects of thermal cycles on adhesively bonded joints between pultruded GFRP components. Bonded joints similar to those investigated in the preceding chapter were produced and subjected to mild thermal cycles. The first part of the chapter outlines the experimental programme. Next, the results obtained from the tests are presented and discussed, including the comparison of both joint systems (w.r.t. the nature of the adhesive). The second part of the chapter presents the numerical investigations that were performed to quantify the magnitude of the different stress fields during the heating and cooling stages of the thermal cycles, caused by the dissimilar coefficients of thermal expansion between the adherends and the adhesives.

The twelfth chapter (the single chapter of the fourth part of the thesis) presents the detailed visual inspection and experimental tests performed on a real GFRP structure subjected to

natural weathering during 11 years in service conditions – the SATU Oeiras. The tests performed at both material and structural levels are accompanied with a detailed visual inspection of the construction and a description of the severity of the main anomalies.

Finally, the last chapter (and part) summarizes the main conclusions that can be drawn from the research performed in this thesis and indicates future directions of research in this field.

1.5. References

[1.1] ASCE. ASCE 2017 Infrastructure Report Card - Bridges. 2018.

[1.2] Bakis C, Bank L, Brown V, Cosenza E, Davalos J, Lesko J, et al. Fiber-reinforced polymer composites for construction - State-of-the-art review. J Compos Constr 2002;6:73–87.

[1.3] Karbhari VM. Durability of Composites for Civil Structural Applications. Boca Raton, Florida: Woodhead Publishing; 2007.

[1.4] Cabral-Fonseca S, Correia JR, Rodrigues MP, Branco FA. Artificial accelerated ageing of GFRP pultruded profiles made of polyester and vinylester resins: Characterisation of physical-chemical and mechanical damage. Strain 2012;48:162–73.

[1.5] Keller T, De Castro J. System ductility and redundancy of FRP beam structures with ductile adhesive joints. Compos Part B Eng 2005;36:586–96.

[1.6] Keller T, Vallée T. Adhesively bonded lap joints from pultruded GFRP profiles. Part I: Stress-strain analysis and failure modes. Compos Part B Eng 2005;36:331–40.

[1.7] Keller T, Theodorou NA, Vassilopoulos AP, Castro J De. Effect of natural weathering on durability of pultruded glass fiber–reinforced bridge and building structures. J Compos Constr 2015;20:1–9.

[1.8] Gonilha JA, Barros J, Correia JR, Sena-Cruz J, Branco FA, Ramos LF, et al. Static, dynamic and creep behaviour of a full-scale GFRP-SFRSCC hybrid footbridge. Compos Struct 2014;118:496–509.

[1.9] Castro J de, Keller T. Design of robust and ductile FRP structures incorporating ductile adhesive joints. Compos Part B Eng 2010;41:148–56.

[1.10] Heshmati M, Haghani R, Al-Emrani M. Durability of bonded FRP-to-steel joints: Effects of moisture, de-icing salt solution, temperature and FRP type. Compos Part B Eng 2017;119:153–67.

[1.11] Lee SW, Hong KJ, Park S. Current and future applications of glass-fibre reinforced polymer decks in Korea. Struct Eng Int 2010;20:405–8.

[1.12] Custódio J. Structural Adhesives. In: Gonçalves MC, Margarido F, editors. Mater. Constr. Civ. Eng. Sci. Process. Des., Springer International Publishing; 2015, p. 717–71.

[1.13] Pethrick RA. Design and ageing of adhesives for structural adhesive bonding - A review. J Mater Des Appl 2015;229:349–79.

[1.14] Hutchinson AR, Hollaway LC. 6 – Environmental durability. Strength. Reinf. Concr. Struct., 1999, p. 156–82.

[1.15] Sousa JM. Durability of pultruded GFRP profiles made with vinylester resin. o Superior Técnico, University of Lisbon (in portuguese), 2011.

Chapter 2.
Pultruded GFRP profiles for civil engineering applications

2.1. Introduction

Fibre reinforced polymer (FRP) composites result from the combination of at least two distinct constituent materials (differing in terms of their properties), where the combined properties are usually superior to those of the constituent materials. In addition, the constituent materials of FRPs remain distinct and separate within the composite, with the reinforcement phase (usually, fibrous materials) remaining distinct from the matrix phase (typically, polymeric resins) [2.1].

Throughout history, the use of combined materials has been attempted, in order to increase their individual performance and to enhance their use, such as the application of straw reinforcement in mud, by the ancient Israelites (which can be traced back to 5000 BC), or the combination of different veneer orientations forming plywood [2.2].

Although the concept of composite materials dates back to ancient times, the manufacturing of FRP composites is much more recent. The first exploratory experiments started around 1930 and begun to widespread in the 1940's, in the naval and aerospace industries associated to defence applications [2.3]. A generalized spread to other industries occurred from the 1950's with the continuous development of new manufacturing techniques and FRP systems [2.1].

Although some early interest in civil engineering applications can be traced back to the 1950's, these materials only started to be competitive in the 1990's, due to the development and improvement of automated FRP production methods, such as pultrusion [2.4]. An increasing interest and growth of FRP materials in the construction industry has been occurring in the last 30 years, in particular in what concerns pultruded elements [2.5]. Currently, about 34% of GFRP production in Europe is applied in the construction and infrastructure sector (the second most relevant in 2017). More specifically, the estimate for the production of pultruded elements in Europe was about 53 kton in 2017 [2.5], with this manufacturing technique being the one that grew the most compared to previous years and other processes.

This chapter presents an overview of the general constituent elements of pultruded GFRP profiles. Next, a description of the pultrusion manufacturing technique is provided, followed by the typical characteristics of pultruded GFRP elements and their structural shapes. A brief overview of the current connection technology is also presented, as well as typical applications of pultruded GFRP profiles in the construction industry.

2.2. Constitution of pultruded GFRP elements

As mentioned, pultruded GFRP composite materials are the result of a combination of two primary raw materials - a polymeric resin matrix and the glass fibre reinforcement - that are combined through the pultrusion process. Besides these two elements, additional constituents are usually incorporated with the purpose of improving and optimizing the final properties or the processing characteristics (*e.g.* polymerization agents, fillers or additives) [2.6].

2.2.1 Polymeric matrix

Strictly speaking, the word matrix refers to the continuous phase of a composite material that contains another dispersed phase [2.6]. The main purposes of the polymeric matrix are to ensure the position and orientation of the fibre layup in the profile (*e.g.* preventing buckling effects due to fibre compression), to distribute the internal stresses through the glass fibres, and to absorb energy from impact loads, while protecting the fibres from environmental degradation agents [2.4, 2.6, 2.7].

Organic polymers have different characteristics depending upon the number and type of functional groups existing in a polymeric chain, as well as the extent of interaction between them [2.8]. These polymers are typically divided into two separate groups: thermosetting and thermoplastic. The main difference between these two groups is the polymeric chain structure. Thermosetting resins are crosslinked, forming continuous three-dimensional networks connected through strong covalent bonds. This is not the case of thermoplastic resins, whose molecular chains are comprised by weaker wan der Waals or hydrogen bonds [2.9]. The described molecular differences translate in significantly different material properties. Thermoplastic resins, despite being often reprocessable and recyclable, have higher viscosity values (which significantly increase the difficulty in impregnation and adhesion). On the contrary, thermoset resins do not allow welding after curing; however their lower viscosity provide them with better impregnation and adhesive properties [2.4].

The majority of pultruded GFRP profiles are manufactured with thermosetting polymers. The most commonly used thermosetting polymers are unsaturated polyester, vinylester, or phenolic

resins. Epoxy resins are widely used as structural adhesives, and also incorporated in many FRP products. However, they are typically applied in carbon fibre reinforced polymer (CFRPs), and not commonly used in pultrusion of large scale FRP components, due to their higher costs and processing difficulties [2.9].

Unsaturated polyester is widely used in structural pultruded GFRP profiles. According to Correia [2.3], this resin represents about 75% of the FRP market, due to the good balance between its properties, ease of handling and cost efficiency. Three types of unsaturated polyester (orthophthalic, isophthalic, and terephthalic) are typically produced, based on the type of acid monomer chosen. Ortophthalic polyester exhibits the lowest physical and mechanical properties, while terephtalic is the best performing one. These low viscosity resins are easily filled and pigmented, and can be formulated in different ways, which makes them quite versatile [2.9].

Vinylester was developed in the last 30 years and tried to combine the properties of both epoxy and unsaturated polyesters. It became increasingly attractive for pultruded components, due to its higher environmental degradation resistance when compared to unsaturated polyesters. More specifically, the superior resistance to alkaline corrosion makes it more suitable for rebar applications in concrete elements [2.9].

Phenolic resins can also be used in the pultrusion of GFRP components, when there are requirements for superior fire resistance properties, since they char and release water when burned. However, they are difficult to pigment and usually their mechanical properties compare to those of low performance polyesters [2.4].

Other polymeric systems, such as polyurethane, which has a wide array of formulations and extensive use as structural adhesives and foams, have recently started being incorporated in the pultrusion process (mostly in research activities). High-density polyurethane formulations used in pultrusion are able to produce GFRPs with high transverse tensile and impact strengths [2.9].

Nowadays, most manufacturers usually present both unsaturated polyester and vinylester alternatives in their production catalogues – this was the main reason for selecting these two resin systems for the experimental programme of the thesis on the durability of pultruded GFRP profiles. Table 2.1 presents typical ranges of variation for the tensile properties, density and glass transition temperature (T_g) of both resins systems.

Table 2.1. Properties of unsaturated polyester and vinylester resins for pultruded GFRP components, adapted from [2.4, 2.7, 2.9].

Resin system	Tensile Strength [MPa]	Tensile Modulus [GPa]	Maximum Tensile Strain [%]	Density [g/cm^3]	T_g [°C]
Unsaturated polyester	20-70	2.0-3.5	1.0-5.0	1.20-1.30	70-120
Vinylester	68-82	3.5-4.0	3.0-6.0	1.12-1.16	102-150

2.2.2 Glass fibre reinforcement

The glass fibre reinforcement of pultruded GFRP profiles consists of several thousands of individual filaments. These continuous fibres are used at a relatively high volume percentage in pultrusion (30-70%), and their typical mechanical properties are significantly higher than those of the polymeric matrix [2.10]. The diameter of the individual filaments ranges from 3 to 24 μm, although 17 μm is usually the most common for GFRP structural applications. Glass fibres have a distinctive white and bright colour, and are usually considered as an isotropic material.

The main purpose of glass fibres is to provide mechanical properties to the GFRP profile, such as strength and stiffness. However, other characteristics (*e.g.* electrical properties), also depend on the grade of the glass fibres [2.6].

Glass fibres combine good mechanical properties at a relatively low cost (especially in comparison to carbon fibres), which makes them the most common type of reinforcing fibres in the construction industry [2.3]. However, they are particularly sensitive to moisture, especially in the presence of salts and alkaline environments. In addition, they are also susceptible to lose strength under sustained stress, being prone to creep rupture for relatively low stress levels [2.9].

There are several grades of glass fibres used in the production of GFRP components. Borosilicate glass presents high electrical resistivity and is typically known as electrical glass (E-glass). This fibre grade is the most widely used in FRP components for the construction industry (80-90%) [2.4, 2.9]. Presently, two types of E-glass fibres are typically considered in the market: regular or boron free. The difference stems from the boron oxide percentage (usually 5-6% in weight), or the absence of it in order to have a lower environmental impact [2.11]. Alkaline resistant glass (AR-glass), and window glass (A-glass) fibres are typically used in specialized products that need specific fibre performance. Structural glass (S-glass) fibres are usually employed in high-performance applications and are significantly more expensive [2.9]. Table 2.2 presents typical properties of common grade glass fibres.

Table 2.2. Properties of common grades of glass fibres, adapted from [2.9, 2.11].

Grade	Tensile Strength [MPa]	Tensile Modulus [GPa]	Max. Tensile Strain [%]	Density [g/cm^3]	Softening temperature [°C]
E	3100-3800	73-78	2.5-4.9	2.57	830-860
A	2410-2760	73-75	2.5-4.5	2.46	770
C	2350-3100	74-80	2.5-4.9	2.46	880
S	4380-4590	88-91	3.0-5.8	2.47	1056

Glass fibres are incorporated in pultruded GFRP elements after being subjected to several secondary operations to produce different types of fibre systems and architectures [2.9]. These are usually supplied in the form of continuous and unidirectional rovings (untwisted) and yarns (twisted). These types of fibres are mainly used for the longitudinal direction of reinforcement [2.12]. In addition, these fibres and also short fibres can be further processed in order to produce mats, sheets and fabrics, with random or oriented reinforcement in several directions, such as chopped (short fibres) or continuous (long fibres) strand mats and fabrics (woven, stitched, braided and knitted). In addition, a thin outer layer mat can be applied at the surface of the pultruded component (surface veil) to confer additional protection, and strengthen the resin rich surface of composite parts [2.3, 2.12]. Synthetic surface veils made of polyester are also used in order to diminish the susceptibility to fibre blooming effects [2.13]. Figure 2.1 displays typical examples of different fibre systems for pultruded GFRP components.

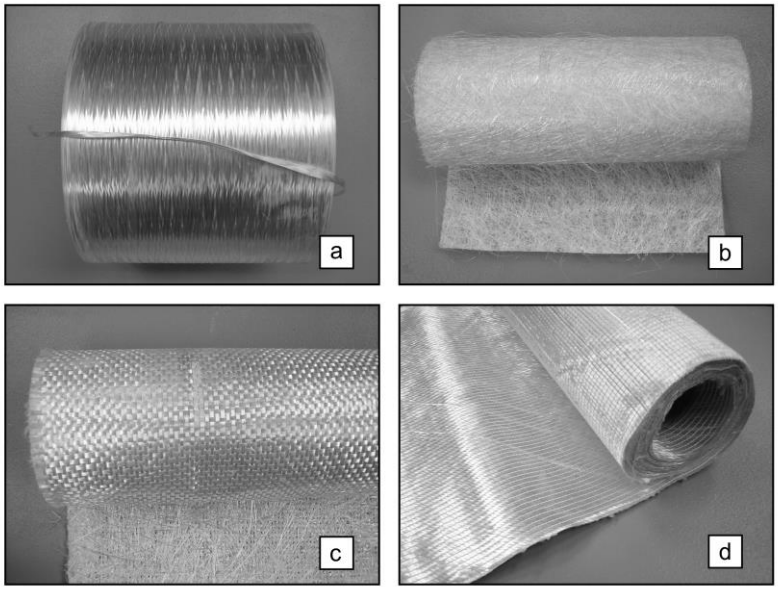

Figure 2.1. Typical glass fibre reinforcement for GFRP components: (a) unidirectional glass roving, (b) glass continuous filament mat, (c) woven glass roving fabric, and (d) stitched glass fibre fabric, adapted from [2.9].

2.2.3 Additional constituents

According to Bank [2.9], the following three types of additional constituents can be added to promote the polymerization reaction, modify processing variables, or even to tailor the properties of the GFRP final product: polymerization agents, fillers, and additives.

Polymerization agents are usually catalysts, curing agents or hardeners, that depend on the type of polymeric matrix that will be used in the GFRP element. These have the function of inducing the curing reaction and preventing curing in the resin bath, before proper impregnation. Thus, these catalysts only cause the polymerization process to occur at a controlled time and position in the pultrusion line. In unsaturated polyester and vinylester resins, organic peroxides are typically used, in quantities that can vary in the 0.25-1,50% range of the resin weight; however, higher quantities can be used (up to 15%) to aid in processing, since peroxides usually reduce the resin viscosity and reduce costs [2.4, 2.9].

Fillers are inorganic chemical inert products, whose main goal is three-fold: (i) to reduce production costs, (ii) to improve processing dynamics, and (iii) to improve some characteristics of the final cured product [2.14]. The particle geometry is usually spherical or plate-like and dimensions range between 0.5-8 μm. In pultrusion, calcium carbonate, aluminium silicate, alumina trihydrate, and calcium sulphate are typically used [2.3]. The last two additives are also used as fire-retardant additives [2.3, 2.9]. In terms of quantities, the amount of incorporated filler content can range between 10-30% for the usual pultruded GFRP profiles made of unsaturated polyester and vinylester; however, small pultruded parts can present much lower content (0-5%). In addition, the recent incorporation of nanosized particle fillers can increase corrosion resistance [2.9].

Finally, additives can be used to modify the properties of the final components, and also to improve processing during manufacturing. Chemical release agents can be used to prevent curing of the final GFRP component inside the mould, and foaming agents are employed to remove entrapped air from the resin bath [2.4]. Pigments can be used to confer different colours, and ultraviolet (UV) stabilizers can also be added in specific elements, where high sunlight due to outdoor exposure is expected. In addition, flame retardant additives, such as antimony trioxide, may also be added. Moreover, toughening, thickening and viscosity control agents are also available for pultruded GFRP profiles. All the aforementioned additives correspond to usually less than 1% in weight of the resin. The only exception is additives that prevent shrinkage (low profile additives) [2.9].

2.3. Pultrusion manufacturing process

The term pultrusion arises from the combination of the words "*pull*" and "extrusion". Extrusion, very succinctly, consists of the forced passage of material through spindles of specific geometry, to obtain the desired shapes [2.15].

Pultrusion is a fully automated closed mould and continuous method used for manufacturing of GFRP profiles. In the 1950's, Brant Goldsworthy developed a process based on a manufacturing line in which continuous fibres, rovings and mats (*cf.* Section 2.2.2), pass through a resin bath, and are subsequently drawn through a preforming die that shape the profile configuration, and lastly cured in a heated die [2.1, 2.10]. The preforming and heating die can also be joined in a single die. The several stages of the pultrusion process are illustrated in Figure 2.2.

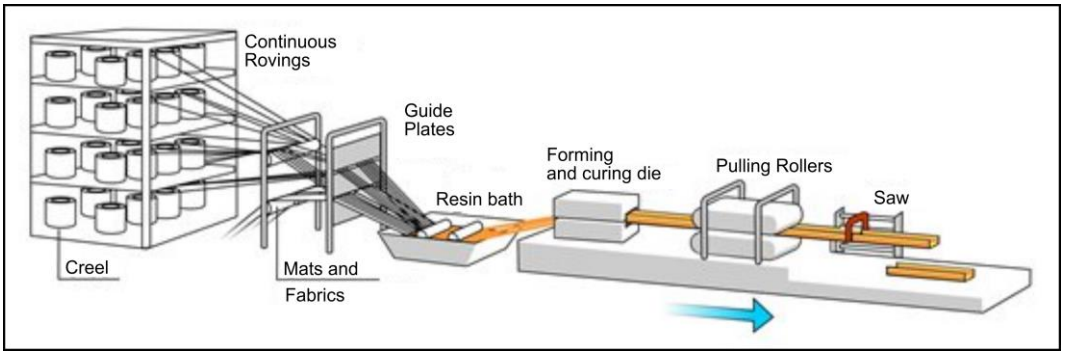

Figure 2.2 Pultrusion line: components and stages of manufacturing, adapted from [2.16]

The automated process is designed to evenly distribute fibre rovings, mats and other fabrics or veils, in the cross section to be produced, conferring the selected fibre architecture [2.10]. The fibres are completely impregnated in the resin bath (in newer pultrusion equipment the resin bath can be closed, and the resin is injected under pressure inside an injection chamber, which is commonly part of the die [2.4]). The composite is then compacted in the die, eliminating most voids and possible defects, and also heated and cured. The curing temperature depends on the resin system used. Afterwards, the profile detaches from the die due to curing shrinkage, being pulled by pulling rollers and cut to the desired length with an automated saw [2.3]. Production rates strongly depend on the pultrusion equipment, with average values around 2 m/min and 20 m^2/min for profiles and panels, respectively [2.3].

The continuity and automation make the pultrusion process a high-production manufacturing process with no limitations in terms of profile length [2.7]; it results in high quality GFRP materials, while reducing the waste of raw materials. This process also allows for higher fibre

contents (especially when compared to traditional processes, such as hand layup) and reduces the probability of defects and voids [2.1]. In addition, typically 80-90% of the production cost is the unit cost of the raw materials themselves [2.4]. The main disadvantages stem from the fact that it only enables the production of constant cross-section elements, and also the predominant unidirectional fibre architecture [2.10].

The most common pultruded GFRP profiles have a general fibre architecture that is illustrated in Figure 2.3. While the fibre architecture of most GFRP profiles has the same backbone, there may be differences regarding the inclusion of different types of mats and fabrics or the use of surface veils, and the resulting fibre architecture may considerably affect the final properties and performance of pultruded GFRP profiles.

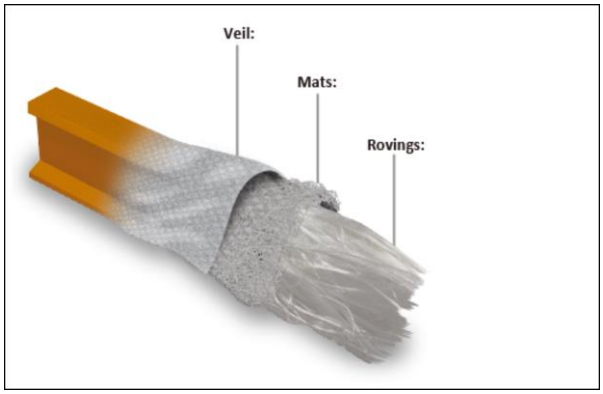

Figure 2.3. Typical fibre architecture of pultruded GFRP elements [2.17].

Quality control is a crucial factor in the processing of FRP products, and GFRP pultrusion is no exception. The performance, overall integrity and durability of the resulting components is strongly affected by a sound and effective quality control system. In the global scope of engineering structures, these facts gain relevance as the components are likely to be exposed to aggressive and constantly changing environmental exposure conditions for extended periods of time, and in several cases, without regular inspection and maintenance procedures [2.18]. Even considering fully automated methods, such as pultrusion, achieving a reliable product relies on the use of good quality procedures, high quality labour training, and appropriate levels of process monitoring and control of the manufacturing environment. Aspects such as storage and handling of raw materials, mixing of resin components, and correct fibre orientation through the guiding plates must be taken into account to avoid possible defects or problems (usually related to incorrect curing and shrinkage) [2.2]. Defects attributed to material reception, or related to processing, can have a substantial effect on the durability and reliability of the final installed products [2.18].

Figure 2.4 presents a general view of *ALTO* pultrusion line, where the pultruded profiles used in this present thesis were manufactured.

Figure 2.4. *ALTO* pultrusion line.

Several types of pultruded structural shapes can be manufactured. The first and most frequent shapes reproduced those from metal construction, namely open or closed thin-walled sections, as illustrated in Figure 2.5. Recent research has shown that these shapes are not fully material adapted, being quite prone to instability phenomena.

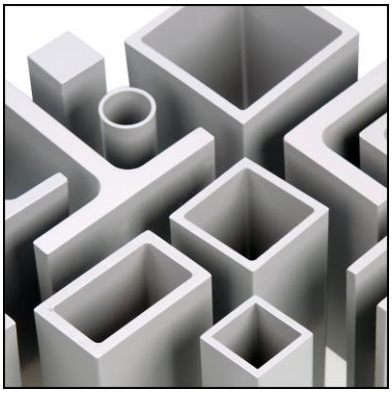

Figure 2.5. Typical pultruded structural profile shapes, open or closed sections, adapted from [2.19].

New structural shapes have emerged, more material-adapted, aiming to improve the performance of GFRP profiles and widen their application fields in the construction industry. Nowadays, besides the standard shapes mentioned above, several producers provide multicellular panels, forming plate elements (*e.g.* bridge deck panels or load bearing flooring systems) that are usually joined through interlocking mechanisms or bonding operations. Figure 2.6 highlights recent pultruded shapes.

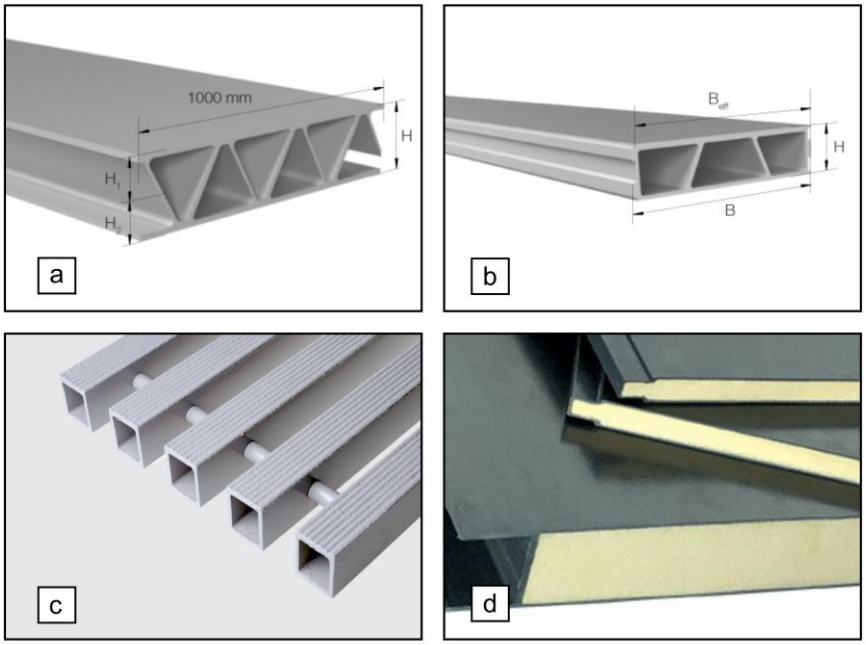

Figure 2.6. Pultruded GFRP profile structural systems: (a) Fiberline FBD600 bridge deck for heavy vehicles, (b) Fiberline FBD300 bridge deck for access road bridges, (c) Fiberline pultruded gratings, and (d) Strongwell DURASHIELD fibreglass foam and hollow core structural building panels, adapted from [2.19, 2.20].

In addition, other systems are available, such as pultruded gratings (Figure 2.6 (c)), entire staircases made only with pultruded elements (and bolted connections) and handrails systems. Pultruded sandwich panels are also emerging (*e.g.* Figure 2.6 (d)), combining the lightness and insulation properties of a multitude of different core materials with the high mechanical properties of pultruded GFRP laminates.

According to Keller [2.12], there are two main reasons for an historical regularity in the shapes of new building materials and the evolution of their structural forms. The first one is related to the lack of knowledge of the most adaptable forms when a new material is introduced – thus, there is a "scientific or technical" reason for a substitution phase. On the other hand, the reproduction of structural forms of materials that are already widely known guarantees a better acceptance of the newer material – there is also a "commercial" reason for this replacement stage [2.21].

2.4. Typical properties of pultruded GFRP profiles

The properties of pultruded GFRP profiles depend on the type and relative proportion of polymeric matrix and glass fibre reinforcement; as aforementioned, the typical combinations comprise E-glass fibres with unsaturated polyester or vinylester resins. The fibre architecture and the fibre-matrix interaction also influence the properties of GFRP profiles [2.3]. Comparing

with steel profiles, which exhibit isotropic material properties, pultruded GFRP profiles have strongly anisotropic behaviour [2.12].

The various possibilities of combining these elements make the characterisation of typical material properties harder, since they can significantly change among manufacturers. Table 2.3 provides a summary of the physical, electrical and mechanical properties of GFRP profiles produced by six different pultrusion companies. The table lists also the requirements set in EN 13706-3 [2.22] for some of those properties, namely the minimum values that structural pultruded profiles should present.

From the analysis of Table 2.3, one can see that a significantly wide range of properties can be found considering different manufacturers. In addition, although many standards are available for pultruded GFRP materials at the laminate level [2.9], there is no consensus between material suppliers, manufacturers and structural engineers on precisely which test methods to use, with different test methods being usually reported by different manufacturers[1] (*e.g. Creative Pultrusion* uses ASTM standards and *Roechling* uses ISO standards). The inexistence of standardised formats for providing mechanical and physical properties, which often can be incomplete, results in a high variability of test methods and results (especially in heterogeneous materials) [2.9].

Full-scale standardised tests, such as the ones described in EN 13706-2 standard [2.23] (which defines specifications for pultruded elements) are still scarce [2.7, 2.9], and some manufacturers still rely on unspecialized standardisation, such as the Appendix B of ASTM D 198 standard [2.24] (applicable to structural wood) for determining the full-scale properties of pultruded beams [2.25].

In spite of the abovementioned difficulties, it is possible to set a typical range of variation for the mechanical and physical properties (*cf.* Table 2.3) of pultruded GFRP properties, which is in general agreement with data reported elsewhere [2.3, 2.4, 2.7].

Figure 2.7 presents the constitutive relation and physical properties of one typical commercial GFRP profile (produced by *ALTO*) comparing them with other materials [2.3, 2.26].

[1] Take as an example the numerous standards for FRP materials of the American Society for Testing and Materials (ASTM) and the International Organisation for Standardisation (ISO).

Table 2.3. Typical mechanical, physical and electrical properties of pultruded GFRP profiles (standard shapes) from different pultrusion manufacturers.

Property(1)	**Abv.**	***C. Pultrusions***	***Fiberline***	***Top Glass***	***Alto***(3)	***Strongwell***	***Roechling***	**Summary**	**EN 13706-3**(4)
Material properties(2)									
Tensile strength 0° [MPa]	$\sigma_{t,\,0°}$	208-317	240	300-400	450	138-207	300-600	207-450	170-240
Tensile strength 90° [MPa]	$\sigma_{t,\,90°}$	52-82	50	20-30		48-69		20-82	30-50
Tensile modulus 0° [GPa]	$E_{t,\,0°}$	17-29		22-26		12-18		12-29	17-23
Tensile modulus 90° [GPa]	$E_{t,\,90°}$	6-10		7-8		5-7		6-10	5-7
Compressive strength 0° [MPa]	$\sigma_{c,\,0°}$	227-258	240	160-220	350	165-207	150-250	150-258	
Compressive strength 90° [MPa]	$\sigma_{c,\,90°}$	113-138	70	55-70		103-121		55-138	
Compressive modulus 0° [GPa]	$E_{c,\,0°}$	21		15-18	23	12-18		12-21	
Compressive modulus 90° [GPa]	$E_{c,\,90°}$	7-8		6-7		5-7		5-8	
Flexural strength 0° [MPa]	$\sigma_{f,\,0°}$	227-258	240	300-400	450	207-241	300-600	207-600	170-240
Flexural strength 90° [MPa]	$\sigma_{f,\,90°}$	76-86	100	60-70		69-124	100-250	60-300	70-100
Flexural modulus 0° [GPa]	$E_{f,\,0°}$	11-14			20	8-11	10-20	8-20	
Flexural modulus 90° [GPa]	$E_{f,\,90°}$	6-7		6-7		6-9		6-9	
Interlaminar shear strength 0° [MPa]	$\sigma_{sbs,\,0°}$	31	25			31		25-31	15-25
In-plane shear strength 0° [MPa]	$\tau_{,\,0°}$	48		20-30				20-48	
Bearing strength, 0° [MPa]	$\sigma_{cB,\,0°}$	206-261		130-170		207-221		130-261	90-150
Bearing strength, 90° [MPa]	$\sigma_{cB,\,90°}$	124-182		60-70				60-182	50-70
Poisson ratio 0°	$\nu_{,\,0°}$	0.35	0.23	0.28		0.31-0.33		0.23-0.35	
Poisson ratio 90°	$\nu_{,\,90°}$	0.15	0.09	0.12				0.09-0.15	
Full section properties									
Elasticity modulus [GPa]	E	19-22	23-28	25	28	17-19		17-25	17-23
Shear modulus [GPa]	G	2.9	3.0	2.4-3.0		2.9		2.4-3.0	
Physical properties									
Barcol hardness [°B]	H	45		45-50	50	40-45		40-50	
Water absorption [% max]	M_{max}	0.6		0.4	0.15	0.6		0.2-0.6	
Density [g/cm^3]	ρ	1.66-1.93		1.80-2.00	1.8	1.66-1.94	1.65-2.10	1.65-2.10	
Thermal exp. coeff. 0° [10^{-6}/K]	$\alpha_{,\,0°}$	8		9-11	11	7-8	5-15	5-15	
Thermal conductivity [W/m.K]	λ	0.58		0.3-0.35		0.58		0.3-0.58	
Electrical properties									
Dielectric Str. 0° [kV/mm]	E_m	1.58		5-10		1.38		1.4-10	
Dielectric constant [50-60 Hz]]	ε_c	5.2		5				5	

(1) Properties are available in the manufacturers technical data sheets; (2) 0° and 90° refers to the longitudinal and transverse directions, respectively;
(3) *ALTO* supplied the profiles for the present thesis; (4) EN-13706 range values correspond to E17 (lower grade) and E23 (upper grade) of minimum material requirements.

In comparison to steel (the main competitor), pultruded GFRP presents linear elastic behaviour up to failure, without ductility. In addition, GFRP profiles present lower stiffness (10-20%), which is one of the main limitations in design, due to high deformability and susceptibility to instability; however, pultruded GFRP profiles exhibit lower density, usually 20-25% less compared to steel, and also much lower thermal conductivity. In terms of thermal expansion, typically the coefficients of these two materials are similar, being slightly lower for pultruded GFRP profiles [2.3].

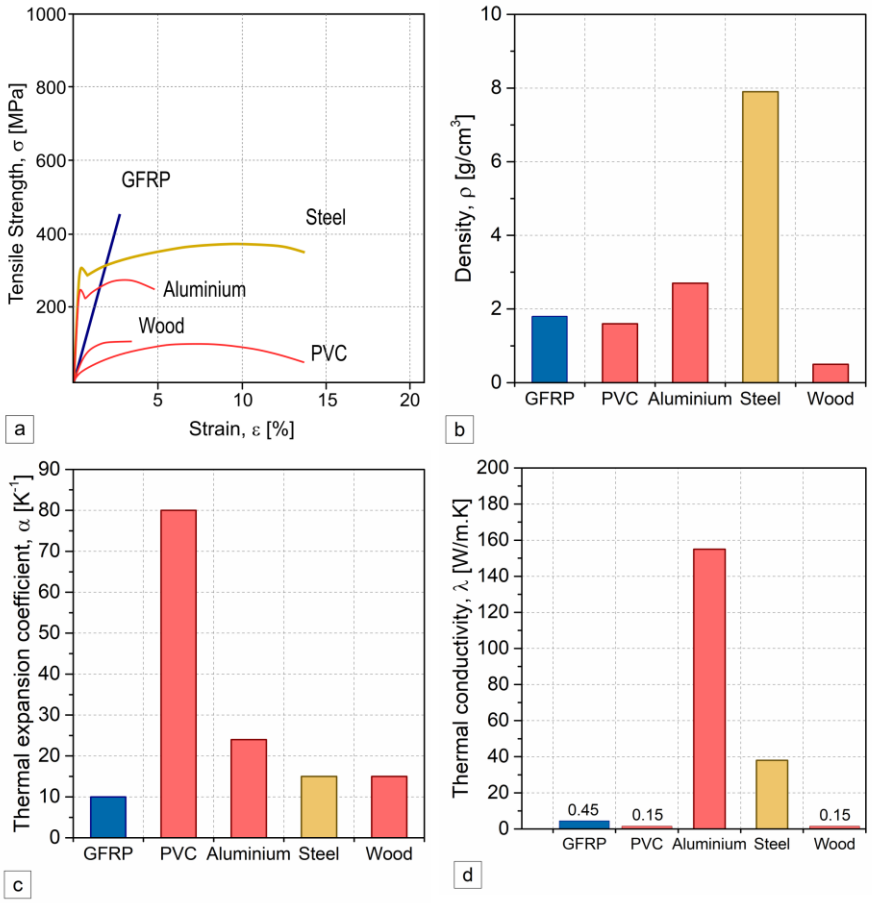

Figure 2.7. Properties of pultruded GFRP profiles in comparison with other materials, adapted from [2.3, 2.26].

2.5. Connection technology of pultruded GFRP profiles

Connections between pultruded GFRP profiles are typically divided into four categories, regarding the type of connection: (i) bolted, (ii) bonded, (iii) mixed, and also (iv) interlocking connections. The first three are the most usual connections types; the latter, despite being adequate from a conceptual point of view, presents significant technical limitations, such as high geometrical tolerance requirements [2.3].

In terms of structural role, the Eurocomp Design Code and Handbook [2.27] classifies three types of connections: (i) primary joints, which provide major strength and stiffness throughout the structural components service life; (ii) secondary structural joints, comprising only local failure without compromising the remaining structure; and (iii) non-structural connections, with main roles of protection against environmental agents [2.28].

Typical joint design comprises the following procedures: (i) identifying the joint requirements; (ii) selecting the adequate joint category and type; (iii) selecting the joint configuration, *cf.* Figure 2.8 (all types can be fastened bonded or combined with the exception of scarf and butt joints, which can only be bonded); (iv) detailing joint design; and (v) performing design and analysis verifications [2.1].

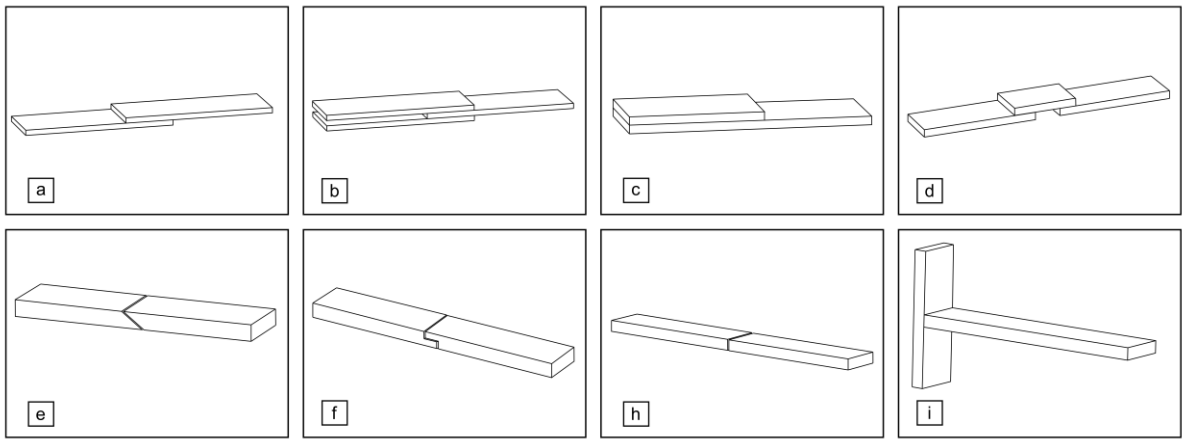

Figure 2.8. Typical joint configurations: (a) single-lap, (b) double-lap, (c) lap-strap, (d) single-strap, (e) scarf, (f) stepped, (g) butt, and (i) tee joints, adapted from [2.1].

Similar to the appearance of structural shapes mimicking other industries, the first and still most used method for connecting pultruded shapes are bolted connections [2.3]. However, while mechanical bolting typically needs drilling operations and often leads to overdesigned GFRP components [2.29, 2.30], adhesively bonding offers more uniform load transfer, being also more material-adapted, as both the substrate and the adhesive are of a polymeric nature [2.31, 2.32]. Moreover, adhesives can be used to increase the ductility of structural joints, compensating the brittle nature of GFRP components [2.33]. Figure 2.9 presents typical examples of bolted, bonded and mixed joints between pultruded GFRP profiles.

Detailed information about the current state of the art on adhesively bonded connections between pultruded FRP components used in civil engineering applications can be found in [2.3], including a thorough analysis of (i) stress states, (ii) influence of adherend and adhesive

mechanical properties, (iii) influence of joint geometry, (iv) stress reduction methods, and (v) failure criteria and design rules.

Figure 2.9. Typical connection types in pultruded GFRP elements; (a) bolted connections from *SATU Oeiras*, (b) bolted connections in Vilamoura water treatment facility, (c) bonded connection of Fiberline FBD 300 bridge deck [2.19], and (d) bonded connections between a GFRP bridge deck panel and steel girders (courtesy of Mário Sá [2.34]).

2.6. Applications of pultruded GFRP profiles in civil engineering

The use of pultruded GFRP profiles in civil engineering started essentially in non-structural applications, where factors such as low specific weight or resistance to more aggressive environments became essential in their choice. In this way, there are several applications of GFRP profiles in water and sewer residual water treatment plants, ports, railway industry and thermoelectric industry [2.3].

Several products produced via GFRP pultruded profiles had applications in these industries, such as, for example, handrails and staircases exposed to aggressive environments, which are quite common in Portuguese water treatment facilities (cf. Figure 2.10). The use of these profiles in these small-scale projects is motivated by the low specific weight and minimum maintenance requires by the GFRP material. Examples of such applications include also entire walkways located in areas with difficult/limited accessibility (Figure 2.11 (a)), or electromagnetic compatibility measuring stations (Figure 2.11 (b)). In the latter type of structures, the use of pultruded GFRP profiles stems from their electromagnetic transparency,

which eliminates electrical interference. For these reasons, the use of non-metallic materials becomes imperative as they could affect test results.

Figure 2.10. Handrails, and walkways made with pultruded GFRP components in Portuguese water treatment facilities (a) all-GFRP walkway, (b)-(c)-(d) handrails and staircases.

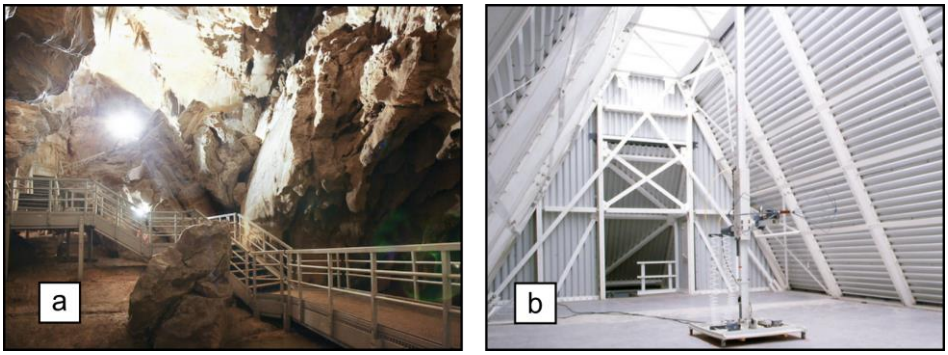

Figure 2.11. (a) 400 m GFRP walkway in Spain (500 m deep excavation), (b) Electromagnetic transparent measuring stations [2.19].

Complex and innovative projects can also illustrate the potential of pultruded GFRP components in bridge applications. There are already several pedestrian and road bridges with a hybrid structure (i.e. where GFRP components are combined with traditional materials) or an all-GFRP structure. Amongst the most well-known examples are the Aberfeldy Bridge (*cf.* Figure 2.12 (a)), the first bridge built with composite materials (1990, United Kingdom). This bridge, which links two golf courses, was designed for pedestrian use and for small vehicles associated with sport and has a length of 113 meters [2.35]. Two other bridges are highlighted, both making use of the low specific weight of these profiles. The Bonds Mill road lift bridge (*cf.* Figure 2.12 (b)) was the first road bridge made with composite materials. The lightness of GFRP was particularly advantageous,

as it allowed considerable savings in the lifting system. The Pontresina pedestrian bridge, located in Switzerland in a harsh Alpine climate (*cf.* Figure 2.12 (c)), consists of two simply supported truss-beams using only GFRP pultruded profiles. The bridge was designed to be removed at the end of the winter before there is risk of flooding due to snow melting and reinstalled afterwards. Another example of the ease of installation of GFRP bridges can be seen in Svendborg Bridge, in Denmark (*cf.* Figure 2.12 (d)), where the entire bridge deck (already with rails) was installed with a moving crane.

Figure 2.12. (a) Aberfeldy Bridge, (b) Bond-Mills Bridge, (c) Pontresina Brigde, (d) Svendborg Bridge [2.7, 2.19].

GFRP profiles have also been used in hybrid bridges. The S. Mateus and S. Silvestre pedestrian bridges are remarkable examples of hybrid applications, comprising pultruded GFRP material in the deck and girders, respectively, allowing for the exploitation of these innovative materials. Those projects resulted from prime examples of collaboration between research groups from the academia and the composites industry, *cf.* Figure 2.13.

Large roofs and buildings structures can also be entirely built with pultruded GFRP materials. Again, factors such as low specific weight and reduced maintenance make these products competitive. An example of such applications can be seen in a suspended train station roof in Copenhagen (Figure 2.14 (a) and (b)), built entirely with pultruded GFRP decks, requiring no supporting beams.

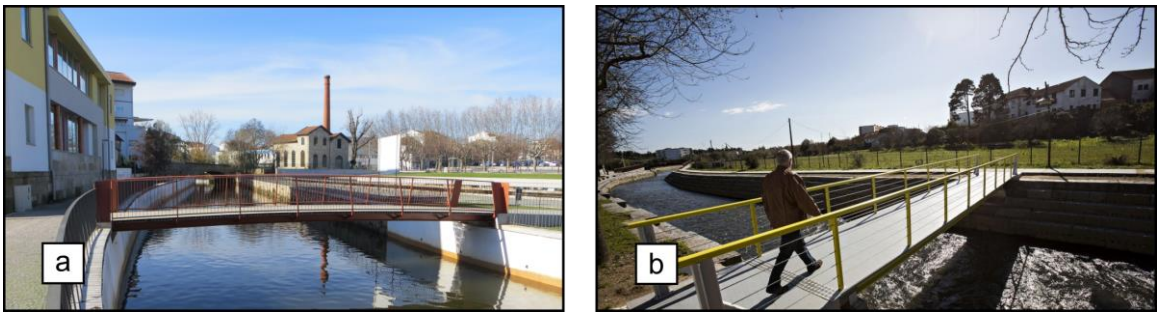

Figure 2.13. (a) S. Mateus, and (b) S. Silvestre pedestrian hybrid composite bridges [2.7, 2.34].

Another remarkable example is the 5-storey building *Eyecatcher*, originally presented at an exhibition in Switzerland, with a main structure made of pultruded GFRP profiles. The main structure of the building comprises three trapezoidal frames, two of which constitute the lateral facades of the building. At the end of the exhibition, the building was dismantled and is now an office building in Basel (Figure 2.14 (c) and (d)).

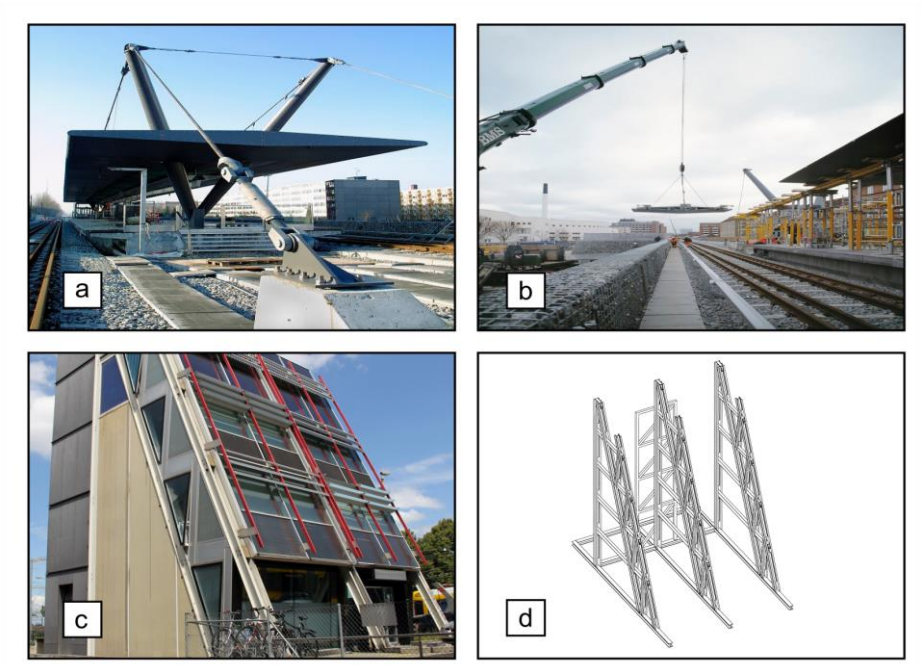

Figure 2.14. Lindevang suspended deck cover: (a) general view, (b) during installation process [2.19]; Eyecatcher building: (c) general view, and (d) sketch of GFRP frame structure [2.31].

2.7. The GFRP and pultruded GFRP market

According to a recent report [2.5], glass fibre reinforced polymers largely govern the composites market, accounting for 95% of its total volume.

In 2017, the GFRP market grew for the fifth consecutive year and increased 2% when compared to 2016. In addition, the volume of European manufactured GFRP is estimated to be about 1118 ktons in 2017 [2.5].

Despite the higher generalised growth of thermoplastic production (primarily for the automobile industry), compared to thermosets, in 2017, the strongest area of growth in production volume was continuous processing, which amounted to 5%, especially the pultrusion process. In terms of production value, a steady growth trend is visible, and production volume is currently not contracting in any European country or region. In particular, the GFRP market has been consolidating in Southern Europe, in countries such as Italy, France, Spain and Portugal. Figure 2.15 shows the total GFRP market in terms of production volume in Europe since 1999 to 2017 [2.5]. Following the decreased production volume during the economic and financial crisis between 2007 and 2009, the GFRP industry is currently presenting a sustained increasing trend.

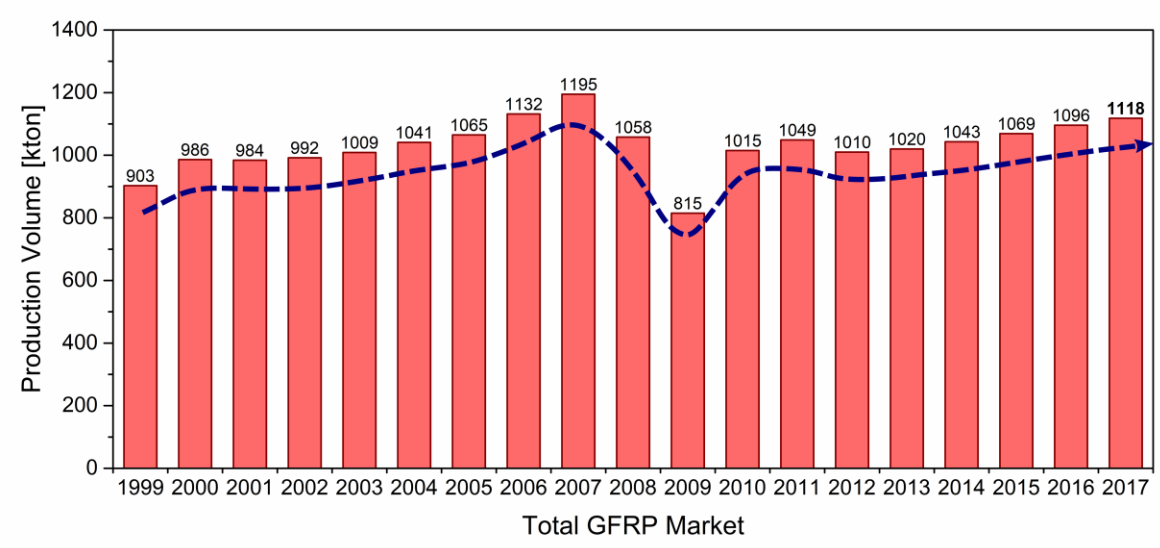

Figure 2.15. GFRP production volume in Europe (1999-2017), adapted from [2.5].

Figure 2.16 depicts the impact of different sectors on the GFRP market [2.5]. The largest sectors using GFRP components are transport and construction. Each of these sectors represent about one third of the total annual production and both play a major role in national economies.

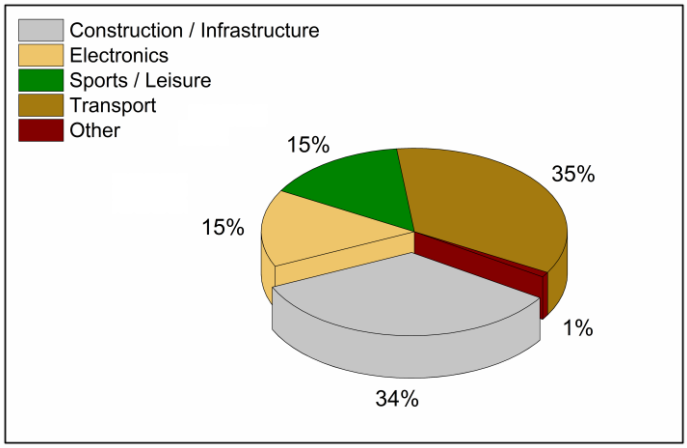

Figure 2.16. GFRP production in Europe as a function of different application sectors in 2017, adapted from [2.5].

Continuous processing techniques, such as pultrusion or filament winding, evidenced the highest growth among all manufacturing techniques, with the total estimated production volume in Europe amounting to 146 000 tons in 2017 [2.5]. Among continuous processing techniques, pultrusion represented the highest increase in market percentage (per individual manufacturing technique), which is estimated to be around 6%, amounting to 53 000 tons in 2017.

In terms of production volume, the pultrusion market is still significantly lower when compared to the two largest manufacturing techniques in terms of production volume: compared to sheet moulding compound (SMC) and hand layup techniques, pultrusion represents about 26% and 38% of the total production volume, respectively [2.5].

Regarding the end users of pultruded components, the construction industry and the consumer/private sector are the larger applications, each with around 20% of the market share. The pultrusion industry is very fragmented, like other composites and GFRP segments. However, despite the existence of about 350 certified pultrusion companies worldwide, the largest companies hold approximately 40% of the market [2.5]

Further opportunities to the pultrusion market are being hindered by legal regulations, or their inexistence, namely the lack of national approval procedures or proper standardisation; efforts are being currently made to overcome this difficulty. In addition, the significant investment by R&D departments of pultrusion companies is allowing further developing newer and improved techniques for the pultrusion process, grating lower production costs and an increasing attractiveness of these solutions [2.3, 2.5].

2.8. Concluding remarks

In the last three decades, the use of pultruded GFRP elements for civil engineering applications has steadily increased (in line with the GFRP market) due to their advantages when compared to conventional solutions. However, the total production volume of these components still has a large room to grow and widespread [2.3, 2.5]. For this to happen, there is a need to overcome the inherent technical difficulties of GFRP materials; to that end, research institutes are essential in providing answers for the current material unknowns and limitations.

Table 2.4 summarizes the main advantages and limitations of pultruded GFRP profiles. There is room for improvement at the different stages of the service life of GFRP constructions, such as (i) manufacturing (*e.g.* minimizing production costs through the increase of pultrusion efficiency), (ii) design (*e.g.* newer and more material adapted structural shapes, improvements in the connection technology systems, or development of specific design codes), and (iii) use

(*e.g.* development of appropriate and specific inspection systems for pultruded GFRP components) [2.3, 2.4, 2.7].

Table 2.4. Advantages and limitations of GFRP pultruded profiles, adapted from [2.3, 2.7]

Advantages	**Limitations**
Low specific weight	High deformability (reduced elasticity and shear moduli)
High strength to weight ratio	Brittle failure
High fatigue strength	Fire behaviour
Ease of application and installation	Lack of specific design codes
High corrosion resistance	Necessity of innovative material adapted structural shapes
Low maintenance costs	Need for improvements in the connection technology
Electromagnetic transparency	Initial costs still not competitive (*vs.* conventional solutions)

In addition to the above-mentioned disadvantages, durability concerns are also extremely relevant for the delay in a more general acceptance of pultruded GFRP materials in civil engineering; in fact, validated long-term data on these "new" materials are still very scarce, regarding both pultruded GFRP elements and adhesively bonded connections between GFRP adherends. The long-term behaviour of GFRP constructions can be considerably influenced by environmental conditions (addressed in Chapter 4) and, in this field, the majority of the research was performed in other industries, such as aerospace and maritime, in which the material requirements are significantly different [2.2]. Gathering a deeper knowledge about the long-term durability of pultruded GFRP profiles and their connections has been pointed out as one of the most relevant factors for the widespread application of these materials in civil infrastructure. In this respect, further investigation [2.2, 2.3, 2.6, 2.36, 2.37] is needed and this is the main motivation of the present thesis.

2.9. References

[2.1] Zoghi M, editor. The international handbook of FRP composites in civil engineering. CRC Press; 2013.

[2.2] Karbhari VM. Durability of Composites for Civil Structural Applications. Boca Raton, Florida: Woodhead Publishing; 2007.

[2.3] Correia JR. GFRP pultruded profiles in civil engineering: hybrid solutions, bonded connections and fire behaviour. PhD Thesis, Instituto Superior Técnico, University of Lisbon, 2008.

[2.4] Correia JR. Pultrusion of advanced composites. Adv. Fibre-Reinforced Polym. Compos. Struct. Appl., 2013.

[2.5] Witten E. The European GRP-market 2017. In: Witten E, Sauer M, editors. Compos. Mark. Rep. 2017, AVK - German professional association for fibre composite plastics/composites; 2017, p. 4–23.

[2.6] Cabral-Fonseca S. Materiais compósitos de matriz polimérica reforçada com fibras usados na engenharia civil – características e aplicações. Laboratório Nac Eng Civil, ICTM 35, Lisboa 2005.

[2.7] Gonilha JA. GFRP–concrete hybrid structural systems. Application to the development of a footbridge prototype. PhD Thesis, Instituto Superior Técnico, University of Lisbon, 2014.

[2.8] Seymor RB. Polymers for engineering applications. 1987.

[2.9] Bank LC. Composites for construction: Structural design with FRP materials. 2006.

[2.10] Groover MP. Fundamentals of modern manufacturing - materials, processes and systems (4ed). 2010.

[2.11] Wallenberder FT, Watson JC, Li H. Glass Fibers. In: Donaldson SL, Miracle DB, editors. ASM Handbook, Vol. 21 Compos. (10th ed), 2004.

[2.12] Keller T. Use of fibre reinforced polymers in bridge construction. Struct Eng Doc IABSE Zurich 2003;vol 7.

[2.13] Chin JW. Durability of composites exposed to ultraviolet radiation. In: Karbhari VM, editor. Durab. Compos. Civ. Struct. Appl., Woodhead; 2007, p. 81–97.

[2.14] Lackey E, Vaughan J. Resin fillers and additives. Compos Fabr 2002;36:12–7.

[2.15] Meyer RW. Handbook of pultrusion technology. 1985.

[2.16] Allnex. Allnex Pultrusion, www.nuplex.com - visited in January 2018.

[2.17] Fibrolux. www.fibrolux.com - visited in January 2018.

[2.18] Geier MH. Quality handbook for composites materials. Kluwer Academic Publishers; 1994.

[2.19] Fiberline Composites. www.fiberline.com - visited in January 2018.

[2.20] Strongwell. www.strongwell.com - visited in January 2018.

[2.21] Keller T. Towards structural forms for composite fibre materials. Struct Eng Int 1999;9:297–300.

[2.22] EN 13706-3. Reinforced plastics composites - Specifications for pultruded profiles - Part 3: Specificic Requirements. Com Eur Norm (CEN), Brussels 2002.

[2.23] EN 13706-2. Reinforced plastics composites - Specifications for pultruded profiles - Part 2: Methods of test and general requirements. Com Eur Norm (CEN), Brussels 2002.

[2.24] ASTM D 198. Standard test methods of static tests of lumber in structural sizes. Am Soc Test Mater 2015.

[2.25] Creative Pultrusions. The Pultex pultrusion design manual of standard and custom fiber reinforced polymer structural profiles 2017.

[2.26] Alto Perfis Pultrudidos Lda. www.alto.pt - visited in January 2018.

[2.27] Clarke JL. Structural Design of Polymer Composites: Eurocomp Design Code and Handbook: Chapman & Hall; 1996.

[2.28] Zhou A, Keller T. Joining techniques for fiber reinforced polymer composite bridge deck systems. Compos Struct 2005;69:336–45.

[2.29] Keller T, De Castro J. System ductility and redundancy of FRP beam structures with ductile adhesive joints. Compos Part B Eng 2005;36:586–96.

[2.30] Keller T, Vallée T. Adhesively bonded lap joints from pultruded GFRP profiles. Part I: Stress-strain analysis and failure modes. Compos Part B Eng 2005;36:331–40.

[2.31] Keller T, Theodorou NA, Vassilopoulos AP, Castro J De. Effect of natural weathering on urability of pultruded glass fiber–reinforced bridge and building structures. J Compos Constr 2015;20:1-9.

[2.32] Gonilha JA, Barros J, Correia JR, Sena-Cruz J, Branco FA, Ramos LF, et al. Static, dynamic and creep behaviour of a full-scale GFRP-SFRSCC hybrid footbridge. Compos Struct 2014;118:496-509.

[2.33] Castro J de, Keller T. Design of robust and ductile FRP structures incorporating ductile adhesive joints. Compos Part B Eng 2010;41:148–56.

[2.34] Sá M. Análise de Painéis de Laje Multicelulares Pultrudidos de GFRP - Aplicação em Pontes Pedonais. PhD Thesis, Instituto Superior Técnico, University of Lisbon (In Portuguese), 2015.

[2.35] Composites and Architecture. www.compositesandarchitechture.com - visited in January 2018.

[2.36] Karbhari VM, Chin JW, Hunston D, Benmokrane B, Jusja T, Morgan R, et al. Durability gap analysis for fiber-reinforced polymer composites in civil infrastructure. J Compos Constr 2003;7:238–47.

[2.37] Cabral-Fonseca S, Correia JR, Rodrigues MP, Branco FA. Artificial accelerated ageing of GFRP pultruded profiles made of polyester and vinylester resins: Characterisation of physical-chemical and mechanical damage. Strain 2012;48:162–73.

Part II

Durability of pultruded GFRP profiles

Preamble

The long-term behaviour of pultruded glass fibre reinforced polymers (GFRP) is an important factor that is hindering their widespread applications in the civil engineering sector. Despite the potential benefits that stem from their several advantages when compared to conventional solutions, these materials are still relatively "innovative" and "recent" in the construction industry. Therefore, it is crucial to obtain reliable information on the effects of several types of possible environmental exposures (which are not always well defined), to develop methodologies that allow understanding the degradation mechanisms that affect those materials, and to predict their long-term behaviour.

Part II of this thesis presents first a detailed literature review of the several factors that affect the durability of FRP composites and pultruded GFRP profiles. Next, results of a comprehensive experimental program carried out in order to assess the influence of hygrothermal, thermal cycling, natural and accelerated outdoor (with UV radiation) ageing are presented; these experiments focused also on possible synergies between those environments and applied loads. The test results were used to implement predictive degradation models, whenever applicable, in an attempt to estimate the long-term mechanical performance of pultruded GFRP material and its general susceptibility to each of the ageing conditions.

Chapter 3.

Literature review on the durability of pultruded GFRP profiles

3.1. Introduction

Pultruded glass fibre reinforced polymer (GFRP) materials applied in civil engineering infrastructure are subjected to several types of exposure environments that may contribute, individually or synergistically, to material degradation. The synergistic interaction may be relevant, since GFRP materials are often exposed to several/simultaneous degradation agents [3.1]. According to Karbhari [3.2], the durability of a material or structure is defined as its ability to resist cracking, oxidation, chemical degradation, delamination, wear and/or the effects of external damage for a specific period of time, under the applicable load conditions, and under specified environmental conditions [3.2, 3.3].

In design, this concept is applied through damage tolerance criteria. Damage tolerance is characterized as the ability of a material or structure to resist failure and to continue performing at prescribed levels of performance in the presence of flaws, cracks or other forms of damage/degradation for a specified period of time under specified environmental conditions [3.4]. The overall concept is shown schematically in Figure 3.1. The use of this concept allows designing a structure using performance values that change with time due to external influences; such performance shall not fall below prescribed minimum levels, thereby accommodating the degradation that is likely to take place with any material system due to mechanical, physical or chemical factors [3.5].

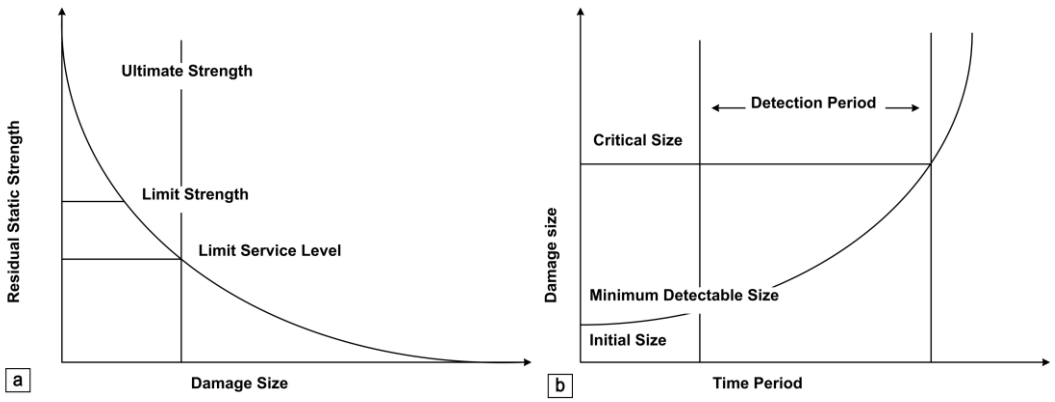

Figure 3.1. Concepts of durability and damage tolerance to design, adapted from [3.5].

Material properties are not constant during service life conditions, even in the absence of visible mechanical degradation. Changes in material properties are usually seen as a measure of the deterioration extent. Nevertheless, not all properties have the same change rate and, as such, the most significant properties to consider need careful consideration [3.1]. It is worth mentioning that the GFRP systems applied in the civil engineering industry have diverse critical differences in terms of loading, exposure environments, constituent materials and/or production processes when compared to the combinations usually applied in other industries, such as marine or aerospace applications. In addition, engineers now aim to design structures with service lives generally above 50 years, thereby requiring design methods that allow predicting the durability and service life of newer GFRP materials used in civil infrastructure [3.2, 3.6, 3.7].

There are several potential causes of degradation and the identification of the most conditioning causes is a complex non-linear process. One of the major issues that contributes to this difficulty is the absence of detailed data about these topics, which can often lead to significant overdesign situations. In addition, this can ultimately compromise the general acceptance and competitiveness of these systems in civil engineering applications when compared to traditional materials (*i.e.* steel and concrete structures), hindering their widespread use in this industry [3.8].

In spite of the above-mentioned difficulty, there has been an increased number of studies and investigations on the durability of GFRP components over the last years [3.2, 3.9-3.16]. In those studies, the following aspects are frequently considered as critical in terms of GFRP materials' durability[2]:

- Moisture and water related effects;
- Thermal effects;
- Ultraviolet radiation;
- Alkaline environments;
- Creep/relaxation;
- Fatigue.

Research about the durability of GFRP composites, in the context of civil infrastructure, aims at analysing the time-dependent changes in material properties and using this information to

[2] The last two aspects have a "mechanical" origin.

efficiently characterize the degradation/deterioration phenomena suffered by these materials. The expected service life of civil infrastructures presents a unique challenge to the issue of durability, where environmental conditions can involve a multitude of exposures [3.6]. In addition, the properties of pultruded products (void content, interface quality, manufacturing process, fibre distribution) and the nature of the aggressive environment can lead to important changes in the behaviour and durability of the final product [3.7].

This chapter reviews the durability issues affecting pultruded GFRP profiles, namely those made of the most used resin matrices, such as unsaturated polyesters, vinylesters and epoxies. Since limited information is available in some cases, the review of some of the following sections may also comprise information about FRP materials in general, since similar or comparable effects are expected to occur when comparing to pultruded GFRP profiles.

As such, an overview of the damage mechanisms of FRP and pultruded GFRP materials associated with each of the relevant environmental conditions is discussed. Discussion about the effects of alkaline environments and fatigue is less detailed, since they were not covered by this thesis.

In the last sections, an overview of analytical diffusion models is provided, being followed by a brief description of the long-term prediction model used to estimate GFRP material level degradation that was considered in Chapter 4 (Experimental Program).

3.2. Review of the durability of FRP/GFRP composites for civil engineering applications

3.2.1 Moisture and water related effects on the durability of GFRP composites

GFRP composites have a long history of use in marine vessels, piping, corrosion equipment and underground storage tanks. Exposure to moisture and aqueous environments include direct contact to rain, humidity, moisture or diffuse solution through other substrates, in addition to immersion in aqueous solutions, as in the case of bridge applications that could have overflow in times of heavy rain.

Limited testing show that they can be applied and have long service life when in contact with moisture and aqueous solution [3.4]. However, moisture diffuses into all organic polymers, leading to changes in physical, mechanical and chemical properties. The primary effect of the absorption is on the resin itself, which may cause both reversible and irreversible changes in the polymer structure. In some cases, the moisture wicks along the fibre-matrix interphase and

has been shown to cause deterioration effects to the fibre-matrix bond, resulting in loss of integrity [3.2]. In the case of glass fibres, moisture and chemicals have also been shown to cause degradation at the fibre level. This degradation is initiated by moisture extracting ions from the fibres, thereby altering their structure. These ions combine with water to form bases, which pit the fibre surface (forming localized cavities in a localized area damaging the fibre surface) and may result in flaws that significantly degrade strength, and can result in premature fracture and failure of the fibres. Basic solutions, when in direct contact with glass fibres, can cause significant pitting and leaching, often resulting in the fibre losing its core over a short period of time with the outer sheath being reactive, thus accelerating the leaching process [3.2, 3.17].

The effect of moisture sorption on the degradation of GFRP materials can be best understood by considering the effect of water on the constituent elements of the system. Thus, the degradation of polymers due to moisture may be broken up into chemical and physical degradation. Physical ageing refers to the reversible alteration of the material properties. The property changes are essentially temperature dependent but can be recovered to some extent upon drying. Chemical ageing occurs with longer exposure duration and mainly involve irreversible degradation of the resin and the fibres, as well as the interface at the molecular level. Chemical degradation mainly includes hydrolysis of the polymer matrix chain, causing chain scission and also affecting the interfacial bond or even cause pitting effects at the fibre level, while physical degradation includes swelling, plasticization and relaxation of the polymer [3.18, 3.19].

Hydrolysis of the ester groups is the primary reason for chemical degradation of the polymer structure [3.20, 3.21]. Hydrolysis typically occurs through the hydrolytic molecular bond cleavage due to exposure to moisture or water molecules, to form water soluble fragments [3.22]. In addition, the alkaline hydrolysis of esters, known as saponification, can also occur in the presence of water and a strong base typically found in alkaline environments. In this reaction, the ester groups may be cleaved back into a carboxylic acid and an alcohol reacting with the hydroxide ions [3.23].

The incorporation of low-molecular weight molecules into a polymer network may act as a diluent or plasticizer, through a mechanism commonly known as plasticization. This physical mechanism occurs without increasing the specific volume, since incorporated molecules fill the empty voids between the polymer macromolecules [3.24]. Swelling describes volumetric changes due to moisture content alone, independent of thermal expansion. Since water is polar, it can form hydrogen bonds with hydroxyl groups. Therefore, interchain hydrogen bonds can be disrupted to increase the inter segmental hydrogen bond length. The swelling volume increase

in polymers is usually lower than the volume of water absorbed. This is due to the fact that when water is absorbed by a polymeric material, the comparatively small water molecules must either occupy the free volume as described above (plasticization) or cause these swelling effects [3.21].

Polymer relaxation usually allows low molecular weight segments to leach out or residual cross linking to occur. This mechanism comprises the redistribution of the voids and free volumes in the polymer network due to swelling effects caused by penetrant molecules, forcing macro-molecular movement - through relaxation more moisture content can be absorbed in the polymer [3.25].

With the described physical and chemical changes, leaching of low molecular weight segments within the polymer matrix can also occur. Water can act as percolating fluid and promote the extraction of low molecular weight degradation products from the polymer matrix, especially at elevated temperatures. Similar residual low molecular weight segments due to the initial polymerization reaction and cure may also be leached out at elevated temperatures, resulting in an apparent weight loss of the polymer [3.26]. These effects can also extend to interface or glass reinforcement, observed through permanent weight loss not observed in the neat resin [3.27].

Mechanical degradation can thus occur due to the combination of different physical and chemical mechanisms, as swelling promotes microcracking in the hydrolysed weakened resin and also debonding effects at the interface [3.28]. An overview of the different moisture induced degradation mechanisms and their classification is presented in Table 3.1.

Table 3.1. Classification of the most relevant moisture induced composite degradation mechanisms [3.17].

Classification	**Degradation mechanism**	**Location**			**Reversibility**
		Fibre	*Matrix*	*Interphase*	
Chemical	Hydrolysis				No
	Chain scission		X		No[a]
	Pitting	X			No[a]
	Debonding			X	No[a]
	Leaching	X	X	X	No
Physical	Plasticization		X	X	Yes[a]
	Swelling		X		Yes[a]
	Relaxation		X		No
a – Processes which have been reported both as irreversible and reversible					

It should be noted that reversible processes will never be fully reversible since the rearrangement of molecules will always lead to increased entropy of the system [3.17]. While hydrolysis is generally considered to be an irreversible degradation mechanism [3.18], there is evidence that hydrolysed bonds can experience a condensation or hydration reaction that can partially reverse the effect of hydrolysis [3.29, 3.30]. Even though a lot of research has been

concentrated on the study of the effects of moisture on composite properties, the mechanisms of water-induced degradation are still not fully understood.

It is possible to protect the reinforcing glass fibres to a significant extent from rapid attack through the selection of appropriate resins systems, processing conditions and the application of gel coats and protective coatings. In general, degradation may be significantly retarded if the resin/composite is completely cured prior to use in a service environment and has not undergone any form of physical/mechanical deterioration.

Since most GFRP composites in civil infrastructure will come in contact with moisture and various solutions during their service life, it is essential that both the short- and long-term effects of these solutions are well understood and documented [3.2].

3.2.1.1 Effects on the polymeric matrix component

The role of the polymer matrix is three-fold. It is used to protect fibres against environmental attack, it serves as a load-transfer medium and it also acts as an energy-dissipation outlet for crack propagation. Hence, it is of crucial importance to determine the effects of water on the resin properties since the absorption of water molecules in the resin may cause a slow but significant degradation of the composite properties.

While an incomplete cross-linking of the resin as well as the presence of a large number of ester links induces low heat stability and greater susceptibility to moisture related degradation [3.20], such as hydrolysis and leaching out of low molecular weight elements, the addition of the styrene monomer in the resin mixture, as its done in unsaturated polyesters and vinylesters, can help improving the hydrolytic stability by increasing the polymer's hydrophobicity [3.31].

Vinylester resins are typically less susceptible to hydrolysis compared to unsaturated polyester resins due to their terminal ester functional groups that are shielded by methyl groups [3.32]. Moreover, it has been shown that vinylester resins absorb less moisture as compared with polyester resins in water immersion at several temperatures [3.11, 3.12, 3.16]. Apicella *et al.* [3.20] observed the opposite at 20 °C; however, the isophthalic polyester resin used in that study exhibited a lower hydrolytic stability, undergoing significant weight loss during exposure, as compared with the vinylester resin. Moreover, according to Ghorbel and Valentin [3.33] results, vinylesters resins had a higher moisture saturation level when compared with unsaturated polyester resins. These contradictory results often stem from significant differences in the chemical formulation of the different polymeric matrixes, the use of additives or other

incorporated substances, as well as dissimilar manufacturing processes, which can induce significant differences in material behaviour [3.12].

It is generally accepted that absorbed moisture can act as a plasticizer, hydrolyser and post-curing promoting agent, increasing or decreasing the mechanical integrity of the ester matrix to a degree dependent upon the exposure temperature [3.20]. At first, water penetration in thermosetting polymers causes physical ageing known as plasticization. As mentioned, plasticization results in an increase in molecular mobility due to small water molecules occupying positions between large polymer chains. This increases the intermolecular distance, thereby decreasing intermolecular cohesive forces. This reversible process primarily results in a decrease in glass transition temperature (T_g) due to the higher molecular mobility [3.33]. In the case of long exposure to water, chemical ageing simultaneously occurs through hydrolysis, with chemical attack on the ester linkages of the resin, which are the reactive groups mostly involved in the breakdown and leaching observed in polyester and vinylester systems [3.20]. Hydrolysis irreversibly affects the chemical structure of the resin and causes a decrease in its T_g [3.33]. The hydrolysis of ester groups results in the formation of carboxyl and hydroxyl groups with the former carboxyl groups being able to auto catalyse further decomposition [3.34, 3.35]. However, chemical ageing can also occur in the form of post-curing, causing T_g to increase. Indeed, ageing in water can lead to further reaction, previously inhibited by the presence of oxygen in the air, increasing the amount of cross-linking of the polymer network [3.36]. Ghorbel and Valentin [3.33] reported that the ageing of neat vinylester and unsaturated polyester resins in water at elevated temperatures was primarily governed by plasticization, with hydrolysis becoming significant for longer exposure time. In addition, and similarly, ageing of glass unsaturated polyester and vinylester composites was initially governed by plasticization effects and later by hydrolysis. Furthermore, chemical ageing of the vinylester composites was counterbalanced by post-curing effects resulting in a substantial final increase in T_g.

3.2.1.2 Effects on glass fibres

It is well known that polymeric resins are sensitive to moisture. However, it should not be overlooked that glass fibres can undergo degradation by moisture too. Two main approaches exist to explain the stress corrosion of glass fibres by water, which can both be related to the Griffith-Irwin-Orowan equation [3.37]. One approach postulates that moisture adsorption causes a decrease in the surface energy of glass fibres, thereby reducing the cohesive strength of the material [3.38]. The second approach attributes the loss of strength of glass fibres in a moisture environment to the slow growth of cracks until a critical size is reached that leads to failure [3.37]. The first corrosion mechanism for glass was proposed by Charles [3.38], who

showed that the corrosion of glass is temperature-dependent with an activation energy of about 20 kcal. The author postulated a mechanism for stress corrosion involving terminal groups in the silica network where the rate of dissolution of the silicate glass is expected to rise with time.

The other theory was proposed by Schmitz and Metcalfe [3.39], which aimed to show how existing structural flaws could serve as a site for hydrolysis and ion exchange reactions, ultimately leading to fibre failure. Their results showed that incubation and flaw growth by corrosion of E-glass fibres involves a two-stage mechanism preceding fracture and that stress corrosion occurs at flaws located at the glass fibres surface. A first incubation period, which extends to 95% or more of the fibre life duration, occurs until the pH reaches the necessary level for corrosion to occur; during this period, the fibres experience no strength loss. Once the critical pH level is reached, subsequent corrosion of the surrounding silica network takes place until a critical size flaw is formed, promoting the occurrence of fracture. In a later study on the mechanism of stress corrosion for E-glass filaments [3.37], the same authors conducted an investigation of the ion exchange involved during immersion of E-glass fibres in various environments, ranging from acidic to alkaline solutions. Ion exchange was found to occur at the glass fibre surface between sodium ions in the glass and hydrogen ions from the surroundings, which occurred in all E-type glass fibres. Three main observations were made in this study [3.37]: (i) if the ion exchange kept occurring, it could lead to a reversal of the initial strength loss; (ii) the maximum strength loss was related to the alkali metal content of glass; (iii) the filaments could crack spontaneously before the residual strength has reached zero. An incubation period was also shown to precede strength loss in static fatigue tests, suggesting that theories involving slow crack growth were not valid for glass fibres. Michalske and Freiman [3.40] have also proposed a similar molecular model for stress corrosion of glasses in which the silicate network (Si-O-Si bond) is destroyed by water molecules.

Bascom [3.41] conducted an extensive review on the adsorption of water into silicate glasses and the subsequent degradation of glass fibres by water, through moisture crack propagation. According to the author, failure is anticipated to begin with the formation of superficial flaws or cracks on glass that will start propagating under an applied stress. The stage of crack growth at which failure occurs will depend on the specimen dimensions and the manner in which load is applied. A crack will tend to propagate when the condition $\delta E_c > \delta\sigma + \delta W$ is observed, where the elastic strain energy due to applied stress (δE_c) needs to be higher than the energy needed to create a new surface ($\delta\sigma$) plus the energy expended in plastic deformation (δW). The decrease in fibre reinforcement strength due to moisture was typically related to reductions in

the surface energy due to the adsorption of moisture onto the glass fibre surfaces as the crack propagated [3.2]. Water could assist failure in other ways, such as the surface corrosion of the glass fibres by water, as well as water condensation into the crack tip, which may increase the capillary pressure and subsequently open flaws [3.41].

3.2.1.3 Effects on the interface

The two previous subsections considered the separate effects of aqueous environments on the fibres and the resin components. However, it is also important to understand the alterations that occur at the interface level between them. Moisture can chemically reduce the bond strength between the fibres and the matrix, by reacting with coupling agents and wicking along the interfaces. In addition, matrix swelling that generally accompanies water absorption can also have negative effects at the interface level. Residual stresses that develop in the matrix during cure of the resin (shrinkage) and cooling down of the composite after cure (for $T < T_g$) are typically tensile, parallel to the fibres, and compressive at the interfaces, due to the typically greater thermal expansion coefficient of the polymer matrix compared to the glass fibres. The moisture related swelling of the resin will reduce these residual stresses and relax the interfacial compressive stress, reducing the interfacial shear strength of the composite [3.2, 3.42].

It is also worth mentioning that the rapid cure and cooling down of the composites during pultrusion result in high resin shrinkage and subsequent microcracking in resin pockets within the composites, which can become sites for accelerated degradation [3.43]. According to Ishai [3.44, 3.45], the fibre/matrix interface region performs a critical role in composites durability in aqueous environments. Fluid attack in the interface region may cause several detachments between fibres and the matrix. Bonding agents (chemical substances that interact with the fibres and the matrix of a composite, and promote a higher bond resistant in the interface [3.46]) tend to delay the interface corrosion process and can minimize mechanical loss. Antoon and Koening [3.18] propose that matrix wearing by fluid absorption reveals itself as a secondary process when compared to the interface region degradation; composite delamination was verified through matrix plasticization combined with detachments at interface regions.

3.2.1.4 Water uptake

Water may penetrate into a polymer resin/composite either by diffusion or capillarity. The generally accepted mechanism for moisture penetration in polymers is an activated absorption/diffusion process [3.47]. The water molecules are first dissolved into the polymer surface and, at the same time as they diffuse through the bulk, they start forming a “solution”

with the polymer. The diffusion mechanism occurs by the direct transport of water molecules in holes of the polymer matrix via random molecular motion and is driven by a concentration gradient [3.48]. The capillarity mechanism involves flow of water molecules along the fibre/matrix interface caused by surface tension. This mechanism depends on the relative magnitude of the cohesive forces between water molecules and adhesive forces of water molecules to the glass fibre surface [3.47].

The diffusion behaviour of moisture in GFRP polymer matrixes predominantly used in civil infrastructure applications, can be classified as follows [3.2, 3.49]: (i) Case I, or Fickian, where the rate of moisture diffusion is much lower than polymer segment mobility; (ii) Case II, where the rate of diffusion is much higher than polymer segment mobility and is strongly dependent on swelling kinetics, and (iii) Case III, or Non-Fickian, where the rate of diffusion is comparable to polymer segment mobility.

It has been shown that moisture sorption can be Fickian by direct diffusion through the polymeric matrix [3.50], non-Fickian by diffusion through existing voids or cracks in the matrix, or capillary by wicking along fibre/matrix interfaces [3.51].

The Fickian diffusion model, derived from the one-dimensional form of Fick's second law, will be addressed in further detail in Section 3.3.1. While Fickian response is often assumed, in reality, various types of sorption curves can be obtained for the immersion of polymer resin and composites in humid or wet environments. The most frequent are indicated in Figure 3.2.

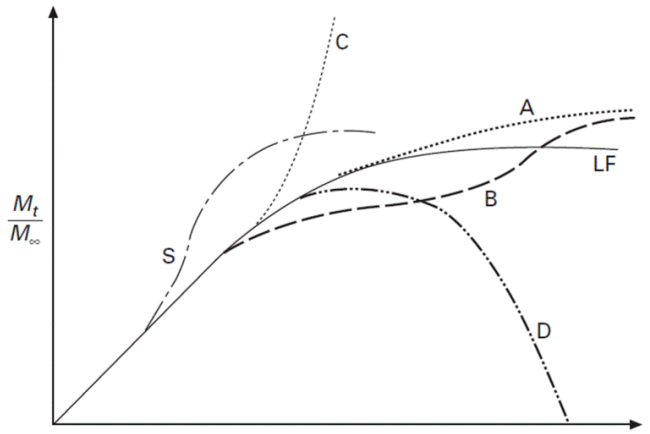

Figure 3.2. Typical range of mass uptake responses (M_t/M_∞, M_t and M_∞ being respectively the mass uptake at time t and mass at saturation), considering Fickian diffusion (A, LF), two-stage Fickian diffusion (B), moving diffusion front (S), and anomalous deviations (C, D) from those responses. [3.2].

The curve LF represents a linear Fickian diffusion behaviour. However, composites usually exhibit one of the other profiles. Curves A, B and S represent anomalous weight gain due to the inherent viscoelastic nature of the polymer matrix, with curve A corresponding to a pseudo-

Fickian behaviour with a continuous gradual increase in weight, curve B to a two-stage diffusion due to relaxation effects, and curve S corresponding to a moving diffusion front. Finally, curves C and D represent profiles where the departure from LF is due to irreversible degradation of the material [3.2, 3.52]. Thermoset resins and glass-fibre reinforced composite systems usually follow Fickian behaviour (curves A or LF), as long as no permanent damage occurs [3.53].

3.2.1.5 Effect of moisture on mechanical and physical properties

The presence of moisture significantly affects the mechanical properties of GFRP composites, as a result of the degradation of the matrix, the fibres and the interfaces. However, degradation is generally less sensitive when compared to neat resins due to the presence of the glass fibres. Still, they are affected by fibre debonding favoured by hydrolysis of the matrix and delamination. Additionally, tensile properties for instance, can be influenced both by plasticization of the matrix, due to water sorption, and by increase in stiffness, due to loss of low-molecular-weight substances from the matrix [3.20, 3.47].

Liao *et al.* [3.11] studied vinylester GFRP composites immersed in deionized water and saline solutions (5% and 10% NaCl) at different temperatures (25 °C and 75 °C). The authors observed degradation of the composite properties in water immersion. However, the presence of salt did not affect the mechanical properties of the materials significantly. They also highlighted the significant fibre wear and the importance of the interface region contribution to environmental degradation. Figure 3.3 presents resin micro fractures observed by Visco *et al.* [3.54] when studying GFRP vinylester and unsaturated polyester composites exposed to salt water immersions.

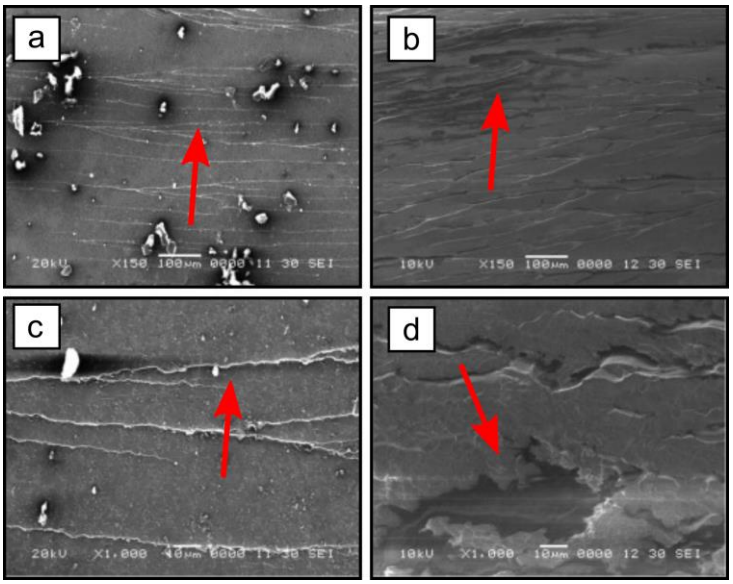

Figure 3.3. SEM micrographs of: (a) vinylester and (b) unsaturated polyester GFRP (150×); (c) vinylester and (d) unsaturated polyester GFRP (1000×) [3.54].

The authors pointed out the higher extent of fractures presented by the unsaturated polyester composite compared to the vinylester one. Reductions in longitudinal and transverse tensile, compressive, shear and flexural properties are frequently observed, as a consequence of fibres, matrix and interface moisture related degradation, [3.11, 3.42, 3.43, 3.54, 3.55].

3.2.1.6 Summary

Although both resins and glass fibres are susceptible to deterioration as a result of hygrothermal exposure, careful material selection, quality control during processing and use of appropriate coatings can result in FRP materials and components that show significantly enhanced durability over conventional materials under these exposure conditions. Karbhari *et al.* [3.4] proposed the following recommendations for aqueous environments:

(i). Since the polymeric resin plays a critical role in protecting the fibres and slowing the diffusion process, preference should be given to the use of appropriate epoxies and vinylesters, in detriment of polyesters.
(ii). In order to decrease the possibility of rapid movement of moisture and chemicals in solution into the bulk composite and towards the fibre surface, it is critical that an appropriate thickness of resin rich surface exists in FRP composites. This effect can be augmented by the use of gel coats and surface scrim layers.
(iii). It is recommended that the resin and the FRP composite system are completely cured prior to use in the field.
(iv). It is emphasized that testing over short periods of time followed by extrapolation of results can lead to erroneous estimates especially for ambient temperature cured systems.
(v). Due to the effect of moisture on T_g, composites must be cured such that the T_g achieved is significantly higher than the maximum service temperature (a minimum margin of 30 °C is recommended).

3.2.2 Effects of alkaline environments on the durability of FRP composites

FRP composites can be exposed to alkaline media though several source interactions, such as alkaline chemicals, soil (solutions that are diffused through it) or concrete. In the last case, GFRP bars used for concrete reinforcement are naturally the most affected GFRP components by this environment, and hence the majority of the available literature is focused on this application [3.2]. However, pultruded GFRP components may also be in contact with concrete in hybrid structural elements [3.56, 3.57] but this contact besides being punctual in the

connection areas, also benefits from the resin rich layers that usually exist in the extremities of the components and that should adequately protect the glass fibres.

The main concerns stem from the potential effects of degradation due to concrete pore water solution, which is known to have a hydrogen ion concentration level as high as 13.5 [3.2]. Bare glass fibres are severely degraded due to a combination of different chemical mechanisms (*e.g.* hydrolysis or leaching). When considering an FRP composite, alkaline solutions can also accelerate the degradation of the resins, especially if not fully cured. However, as aforementioned, the polymeric matrix presence around individual filaments confers some protection to the attack on the fibres [3.58].

Regarding corrosion of glass fibres in alkaline media, the predominant mechanism over pH 10 is the degradation of the silica network. Hydroxide ions of the alkaline solution lead directly to the break-up of Si-O-Si linkages This effect is increased by elevated temperatures and prolonged exposure time [3.59].

3.2.3 Effects of thermal cycles on the durability of FRP composites

Thermal effects are one of the most relevant types of environmental agents that FRP materials are subjected to, namely in outdoor applications. Thermal effects include response changes due to temperatures above the cure temperature, freezing and freeze-thaw conditions, temperature variations and cycles. FRP composites can also be exposed to very high temperatures and fire, but this type of degradation is out of the scope of the present thesis (detailed information in this respect can be found in [3.60, 3.61]).

It is known that not all thermal exposure has a negative effect since in several cases it can foster post-curing phenomena due to additional cross-linking and continuous reticulation of the polymeric matrix [3.62]. It is also acknowledged that polymeric materials soften over a temperature range that increases their viscoelastic response, reducing its mechanical performance (stiffness and strength) and increasing its susceptibility to moisture absorption [3.4, 3.14]. Prior research indicates a wide range of thermal effects in GFRP composites. Sub-zero temperature exposure can result in matrix hardening, microcracking and fibre/matrix bond degradation. Also, freeze-thaw in the presence of salt can result in accelerated degradation due to the formation and expansion of salt deposits in addition to effects of moisture induced swelling and drying. Exposure to temperature above the processing temperature can result in an initial post-cure followed by degradation. In general, polymeric resins have coefficients of thermal expansion at least an order of magnitude greater than those

of the glass fibres [3.4]. Changes in temperature may cause thermal gradients and shrinkage effects in the composite system, which result in the formation of residual stress at the interface between the resin and the fibre. The contraction in the bulk resin is constrained by the stiffer glass fibres [3.63, 3.64].

Although thermal cycles can have a potential deleterious effect in the performance of FRP composites in general and in pultruded GFRP materials in particular, studies reported in the literature are relatively scarce. As discussed later in this section, the materials and exposure conditions used in those studies can vary significantly, which has led to contradictory results.

One of the first studies addressing the effects of thermal cycles on the performance of FRP composites was presented by Dutta and Hui [3.65]. These authors analysed the variation on the flexural properties of two different FRP composites made of isophthalic polyester resin after being exposed to thermal cycles between -60 °C and 50 °C. The first FRP composite, reinforced with E-glass rovings and produced by pultrusion, was subjected to 100 cycles, whereas the second one, reinforced with S2-glass fabric and produced by the vacuum bag technique, was subjected to 250 cycles. The E-glass composite specimens suffered severe degradation after exposure to the thermal cycles, exhibiting extensive cracking in the interior of the material that the authors attributed to the formation of residual stresses from curing. Therefore, no further flexural tests were performed on this material. In opposition, the S2-glass composite specimens showed no visible signs of degradation and their Young's and shear moduli suffered very slight reductions of 6.4% and 6.3%, respectively. Although the performance of the pultruded specimens was unsatisfactory, the authors recognized that the limits of temperatures used in the tests were too extreme and unlikely to be experienced in real applications.

Gomez and Casto [3.66] evaluated the flexural properties of two commercially available GFRP pultruded systems, made of either isophthalic polyester or vinylester resins, after immersion in a 2% sodium chloride solution and subsequently exposed to 300 cycles of freezing and thawing, between -17.8 °C and 4.4 °C (typical of very cold climates). Results obtained showed considerable reductions of both flexural strength and stiffness, which were more pronounced in the vinylester system: flexural strength decreased 19% and 32%, respectively in the unsaturated polyester and vinylester systems, while the corresponding elasticity modulus reductions were 18% and 35%.

Zhang *et al.* [3.67] evaluated the effects of freeze and freeze-thaw exposure on FRP composite systems used in column wrapping. The authors characterized the material response and failure mechanisms through Naval Ordinance Laboratory NOL-ring burst tests, short-beam-shear tests, dynamical mechanical thermal analyses and microscopy. Different systems encompassing a range

of materials, reinforcement forms and processing techniques were investigated. These included E-glass, carbon and aramid fibre types and polyester and epoxy matrices. Several sample specimens were immersed in a 5% NaCl solution for a period of five weeks and later subjected to freeze and freeze-thaw regimes for 90 and 180 cycles (24 hours at -26 °C with 24 hours at 23 °C for six and twelve months). For all composite systems, the authors reported a general decrease in NOL based tensile strength and glass transition temperature levels at 180 cycles (10-16% and 4-13% reductions, respectively). Regarding short beam shear strength, significant reductions were obtained (8-25% reductions) with the exception of one composite system, whose strength increased 2%.

Karbhari *et al.* [3.68] studied the hygrothermal degradation of ambient cured E-glass and carbon reinforced vinylester composites produced by the wet layup process due to exposure to 100 freeze thaw cycles (between -10 °C and 22.5 °C), both in the presence of aqueous solutions (deionized water and salt water) and just ambient humidity. Changes in mechanical (tensile and compressive properties) and thermo-mechanical dynamic characteristics were measured, and short-term effects of environmental exposure were assessed. For both types of composites, the authors reported significant reductions in the mechanical properties due to the exposure to thermal cycles (8-9% and 9-18% reduction of longitudinal tensile and transverse compressive strengths, respectively). These variations increased in the presence of aqueous solutions (14-16% and 30%, respectively) due to moisture diffusion and wicking of NaCl. The values of the glass transition temperature (T_g), determined from both the *tan* δ curve peaks and the *E'* decay curves, were also reduced after freeze-thaw cycles (reductions of 3-7% and 3-10%, respectively in dry and wet conditions).

Tann and Delpak [3.69] reported the influence of freeze and thaw actions on the tensile properties of aramid, carbon and glass FRP fabric strips (unfortunately, the authors did not specify the resin matrix) commonly used in structural strengthening. The material was subjected to freeze thaw cycles (21 cycles between -20 °C and 25 °C) at every three days for a period of nine weeks. The tensile strength of carbon and aramid FRP specimens presented a slight increase of 1.0-1.5%, whereas that of glass FRP suffered a very slight reduction of 1%. The tensile modulus of all FRP systems varied 1.0-2.5%. Given the scatter of the experimental data, the authors concluded that such freeze and thaw actions do not appear to have significant influence on the mechanical properties of common FRP strips used in civil engineering applications.

Haramis *et al.* [3.70] examined the performance in tension (stiffness, strength and failure strain) of pultruded glass-vinylester and glass-epoxy cross-ply laminates in different moisture and freeze-thaw ageing environments. The freeze-thaw conditioning parameters varied between -17.8 °C and 4.4 °C with a ten cycle per day rate (75% cycle time for freezing and 25%

for thawing). One set of samples was previously saturated and remained fully immersed during freeze-thaw cycling and a complementary set remained dry before and during the experiment. Within each set, part of the samples remained unloaded, whereas other samples were loaded in four-point bending (maximum axial strain of 0.55%). Results indicated significant degradation of tensile strength (-40.5%) and no significant degradation of stiffness (+9.8%) for all types of specimens due to saturation. In opposition, freeze-thaw conditioning and loading did not seem to cause any effects on the tensile properties.

Sheikh and Tam [3.71] published an experimental study on the effects of freeze thaw cycles on the tensile properties of two FRP systems, made of epoxy resin reinforced with either E-glass and carbon fibres. In order to understand the effect of the extreme Canadian winter condition, specimens were exposed to either (i) freeze-thaw cycles immersed in water (between -20 °C and 20 °C), (ii) sustained loading and (iii) a combination thereof. The exposure to freeze-thaw cycles and sustained loading caused low to moderate changes in the tensile properties of the materials. For the GFRP specimens, the maximum reduction of tensile strength was only 2.5%, whereas the tensile modulus even increased up to 7.5%. For the CFRP specimens, maximum reductions of tensile strength and stiffness were 12% and 7%, respectively. For both materials, the synergetic effect of sustained loading proved to be reduced or even negligible.

Wu *et al.* [3.72] investigated the effects of freeze-thaw on the flexural properties and glass transition temperature of GFRP multicellular decks used in bridge decks. To this end, laminates made of E-glass fibres and vinylester resin were subjected to thermal cycles between -17.8 °C and 4.4 °C (625 cycles of 2 hours or 250 cycles of 5 hours). This investigation considered the combined effects of exposure to distilled water and salt-water immersion, as well as ambient temperature. In addition, several specimens were subjected to simultaneous environmental exposure and sustained loading up to 25% of the ultimate strain. After thermal cycling, no significant change was found in the flexural strength and storage modulus, as they were within data scatter. The authors presented also small reductions (1%) in the storage modulus of pre-strained specimens subjected to 250 thermal cycles immersed in water.

Kim *et al.* [3.73] studied the degradation of interfacial shear strength of two different (vinylester and modified vinylester) pultruded E-glass composite rods. The specimens were immersed in an alkaline solution (simulating the chemical composition of concrete pores solution) and exposed to 110 thermal cycles varying between -25 °C and 30 °C. In this study, the reductions of the interfacial shear strength caused by the environmental exposure were very significant in one of the reinforcing bars (29%) and reduced in the other (6%). The authors attributed the differences due to the higher chemical resistance properties of the modified vinylester rods.

Li *et al.* [3.74] published an investigation about the freeze-thaw resistance (tensile properties) of unidirectional glass, carbon and basalt fibre reinforced laminates fabricated with epoxy systems using the wet-layup process. The materials were subjected to 90 cycles of 24 hours, including a freezing state (12 hours at -30 °C) and a thawing state (12 hours at 30 °C). The tensile strength and modulus obtained for the glass and basalt composite systems after 90 cycles were within the experimental error, thus indicating a negligible effect of the freeze-thaw cycles. Still, carbon fibre specimens presented reductions of tensile strength and modulus of respectively 16% and 18%.

Aniskevich *et al.* [3.75] conducted experimental investigations regarding the short-term exposure of polyester-based pultruded GFRP to severe freeze-thaw cycles between -30 °C to 20 °C, in both dry and wet condition. Flexural properties and linear thermal expansion coefficient changes were assessed. After 125 cycles, the authors reported an increase of the flexural modulus (14%) and a slight decrease of the flexural strength (13%). No remarkable differences were encountered between dry and wet condition specimens. The T_g suffered a slight decrease (5%).

Overall, the experimental work reported above, regarding the effects of thermal cycles on the physical and mechanical properties of pultruded GFRP composites, is very limited. Moreover, the test methods used in these studies vary considerably, with respect to the constituent materials (fibre and resin nature), manufacturing processes, type (number of cycles and temperature range) and exposure conditions (dry, saturated in different solutions, loaded/unloaded) and characterization techniques. Thus, some results are contradictory and present clearly distinctive degradation magnitudes. It is also worth mentioning that none of the studies reported above provide degradation models able (i) to predict/simulate the effects of thermal cycles on the GFRP physical and mechanical properties and/or (ii) to link experimental laboratory results with actual/field exposure during service life.

3.2.4 Effects of ultraviolet radiation on the durability of FRP composites

Ultraviolet (UV) radiation that reaches Earth's surface comprises about 6% of the total solar radiant flux and has wavelengths between 290 nm and 400 nm. The remainder of the photolytic active solar radiation is composed of visible (52%) and infrared (42%) radiation. UV radiation between 280 nm and 315 nm is commonly called UVB radiation, while the range between 315 nm and 400 nm is called UVA radiation [3.76]. UV radiation is considered to be one of the most critical weathering elements because it initiates photochemical reactions that lead to irreversible material degradation, yet many of its effects on FRP composites are not fully understood. Since the polymeric matrix transfers load to the reinforcing fibres, damage to this

critical component can be detrimental to the overall mechanical properties of the FRP composite and limit its service life [3.77].

3.2.4.1 Ultraviolet radiation effects on polymers

Commercial polymers are susceptible to photodegradation initiated by the UV component of solar radiation. To understand the effects of UV radiation on FRP composites, it is necessary to have a general understanding of the same effect on the polymeric matrix component. Since most polymers have bond dissociation energies on those wavelengths orders, they are greatly affected by exposure to this portion of the solar spectrum [3.77]. The lower the wavelength of the incident radiation, the higher the photon energies and quantum efficiencies, and the more potentially active it is in initiating bond breakage on polymeric materials. Any decrease in the stratospheric ozone column thickness could lead to an increase in the photoactive UVB radiation flux and a corresponding decrease in the photoactive lifetime of polymeric systems used in outdoor applications [3.78].

Of the radiation that is absorbed only a percentage of the absorbed wavelengths are effective in initiating damage [3.79]. When UV radiation is absorbed in the presence of oxygen, a complex series of photochemical reactions are initiated, leading to chemical changes in the material, including the generation of oxygen containing functional groups. Other chemical reactions that may occur in UV-irradiated polymers include chain scission, branching, crosslinking and rearrangement processes [3.80].

Chin *et al.* [3.81] conducted a study about accelerated UV exposure involving cast films of non-UV stabilized vinylester and isophthalic polyester irradiated with a 1000 W xenon arc source for 1200 hours. They reported changes in the surface topography using atomic force microscopy (AFM). Both vinylester and isophthalic polyester specimens showed a substantial degree of cratering and cracking after 1200 hours of UV exposure. No changes in the glass transition temperatures of the exposed specimens were observed following the exposure period. Increases in the surface oxygen concentration indicated the formation of new oxygen-containing functional groups. Due to the fact that absorption of UV radiation diminishes rapidly with depth, these photochemical reactions are generally limited to the topmost several microns to 1 mm [3.82].

Chemical and morphological changes induced by UV exposure are precursors to changes in the physical, mechanical and optical properties of the bulk polymer, ranging from changes in gloss and colour, to extensive mechanical property degradation that severely impacts the service life

of the polymeric component of FRP composites [3.80]. The first signs of UV macro damage usually appear as gloss loss, chalking and yellowing. Gloss loss and chalking are phenomena related to the surface erosion that occur as fragmented polymer chains are removed from the surface of the polymer. For some polymers, yellowing is the result of unreacted double bonds in incompletely cured resins being photo-oxidized to coloured products, or to the formation of conjugated double bonds [3.76]. Polymers containing styrene crosslinks, such as vinylester and isophthalic polyester, are particularly prone to UV-induced yellowing [3.83].

After prolonged periods of exposure, more severe damage in form of surface crazing and cracking may occur. Cracking is often the result of chain scission reactions initiated by UV exposure, in which the fragments resulting from it occupy more volume than the original polymers, causing stresses that lead to crack formation. If the degradation products are volatile or gaseous, pore and pit formation may also occur [3.78, 3.80]. The surface morphological features resulting from UV exposure described above can potentially serve as sites for moisture sorption and fracture initiation that contribute to the degradation of mechanical properties. Signor *et al.* [3.84] carried out a UV exposure study on non-reinforced vinylester matrix resins using a xenon arc lamp source and observed significant decreases in toughness and strain to failure. After 4000 hours of UV exposure, the authors also registered increases in surface hardness and modulus.

3.2.4.2 Ultraviolet radiation effects on FRP composites

As for any polymeric system, the durability, the performance and the rate of degradation of FRP composites are significantly influenced by the material composition and the environmental/climatic conditions to which they are exposed. In general, the variability in weathering behaviour due to temporal changes in temperature, rainfall/relative humidity and UV radiation are not fully understood [3.85]. According to Chin [3.77], UV-induced degradation in FRP composites typically follows the sequence below:

(i). Loss of surface gloss;
(ii). Surface discoloration;
(iii). Chalking;
(iv). Flaking of surface resin;
(v). Pitting;
(vi). Microcracking;
(vii). Blistering;
(viii). Severe loss of resin from outer surface, fibres not yet visible;
(ix). Severe loss of resin from outer surface, fibres visible (blooming);

(x). Fibres visible and loosened from the surface;
(xi). Delamination of topmost ply.

When the polymeric matrix is prone to UV-induced chain-scission reactions, the molecular mass or chain length of the surface polymers will decrease, making it more susceptible to water erosion of the low molecular weight segments. With additional exposure, this degradation by scission will continue to affect the top layers of the FRP composite, until the reinforcing fibres become visible, a mechanism often known as fibre blooming. If the structure of the polymer favours crosslinking reactions, then the increased crosslink density of the surface material may lead to embrittlement and microcracking of the resin matrix [3.85]. As damage progresses, tensile and also impact properties may also decrease as the polymeric matrix and interface region degrades [3.86]. This deterioration of mechanical properties should be related to embrittlement of the matrix or the ingress of moisture into surface microcracks. It is believed that the harshest effects of UV damage, which are limited to the surface region, are not due to direct photolytic UV damage, but to the increased susceptibility for moisture diffusion into fragilized areas [3.77].

Overall, the published literature on the effects of UV radiation on the mechanical properties of FRP composites report contradictory results. However, only minor changes in mechanical properties are usually found after UV exposure. In general, it has been shown that UV radiation effects on mechanical properties are less apparent in thicker specimens, whereas thinner specimens exhibit larger changes in mechanical properties [3.87].

Segovia *et al.* [3.88] observed that glass fibre unsaturated polyester composites exhibited 15% and 20% reductions in elastic modulus and tensile strength, respectively, following 7000 hours of an accelerated laboratory UV exposure. Tensile strain at failure exhibited losses ranging from 20% to 56%, and the majority of the degradation occurred primarily in the surface resin, whereas the glass fibre reinforcement presented no signs of deterioration.

Cabral-Fonseca *et al.* [3.12] studied pultruded GFRP unsaturated polyester and vinylester composites subjected to 3000 hours of artificial accelerated in QUV chamber. The effects of the artificial accelerated QUV ageing were considered to be much less significant when compared to hygrothermal effects on the same materials. After 3000 hours, the tensile and the interlaminar shear strengths of the vinylester profile were marginally affected, while the unsaturated polyester tensile strength suffered a 21% reduction. FTIR analysis evidenced the occurrence of chemical changes at the surface of both materials. The authors also confirmed that the overall effects of UV radiation were confined to the top microns of the superficial

layer, which caused only slight reductions found in mechanical properties. However, UV radiation caused significant aesthetical changes, as the colour and gloss of both profiles were severely affected.

Physical properties of pultruded glass vinylester and unsaturated polyester profiles were evaluated by Bogner and Borja [3.89] following 10000 hours of accelerated laboratory UV exposure and Florida outdoor exposure. After 10000 hours of exposure in a fluorescent device, flexural strength and flexural modulus of both types of FRP profiles were reduced only up to 4% compared to unexposed control specimens. The unsaturated polyester profile retained its performance, but the vinylester profile lost 28% of its initial flexural strength and modulus. In both cases, signs of gloss loss, chalking and surface erosion were evident.

UV testing procedures in FRP composites should be undertaken with caution, whether the testing is carried out outdoor or in a laboratory weathering device. The variability and uncertainty associated with different test methodologies may incur in incomparable results. Outdoor test results are influenced by fluctuations in temperature, moisture and UV irradiation [3.90]. The intensity of UV irradiance changes with the test location, sample orientation, the season and climatological variations. Therefore, results of testing in outdoor environments are seldom reproducible, due to highly variable nature of the weather and associated climatic factors. However, some correlations can be achieved between artificial and natural weathering [3.77].

3.2.4.3 UV protection techniques

Polymer photodegradation due to UV exposure can be hindered or delayed by introducing stabilizers into the polymer matrix or applying gel coats or appropriate paints to the surface of the FRP component.

The concentrations of stabilizers (UV blockers) employed are typically 0.05-2% by mass and their presence should significantly extend the lifetime of a polymer product [3.78]. Stabilizers need to be compatible with the polymer and other additives in order to be effective. Combinations of stabilizers are also often used to protect against more than one mechanism or to provide synergistic protection [3.84]. UV stabilizers function in various ways. Some control the amount of radiation that reaches the polymer and others inhibit chemical reactions initiated by the absorption of the radiation [3.78, 3.86]. UV blockers or absorbers are compounds that function by restricting UV penetration into the topmost surface regions of a polymer and they are effective only if the compound has a larger absorption coefficient than the polymer for the wavelengths of

interest. The greatest effectiveness is found when the blocker/absorber is concentrated on the surface, as in an applied coating or film on the polymeric component [3.91].

Another typical practice, when considering natural ageing conditions, is the application of gel coats or other surface coatings, like paints and varnishes, in order to protect the FRP components surface from direct UV radiation. Gel coats are made of polymeric coatings which can be reinforced or pigmented, as appropriate for each case of application. Note that these coatings are not themselves unaffected by UV radiation, but act as a sacrificial layer, and thus delay the UV degradation of the protected FRP composite [3.77]. This method will require further periodic inspection of the protective layer to ensure that the FRP composite underneath is not in direct contact with UV radiation. The repair of such coats usually involves the application of another new layer [3.78].

3.2.5 Effects of creep and time-dependent effects on the durability of FRP composites

3.2.5.1 Creep and relaxation

Creep is the time-dependent and permanent deformation of materials when subjected to an externally applied load over an extended period of time [3.10]. Stress relaxation is the inverse of creep, corresponding to the stress reduction over time when a material is subjected to a constant strain [3.92].

When unidirectional composites are subjected to a constant load, it is often assumed that the reinforcement fibres display an elastic behaviour, while the polymeric matrix displays viscoelastic behaviour. Creep in FRP composites involves a stress transfer from the matrix to the fibres, causing an increase in the fibres (and composite) strain [3.93].

An idealized creep strain curve is shown in Figure 3.4. The primary phase is characterized by decreasing strain rate over time, progressing towards a stabilization of the strain rate value (secondary phase). In the third creep phase, a significant increase in creep strain rate occurs until fracture or rupture of the FRP component [3.94].

Creep behaviour of FRP composites depends on fibre orientation, fibre volume fraction and structure of the material. However, it will be mainly dependent on the properties of the polymeric matrix [3.10], the main source of creep. In fact, the resin systems typically used in FRP composites are viscoelastic, thus dependent on time and temperature, making time-(temperature)-dependent behaviour of composite materials an important issue that can affect these materials in design stages [3.95]. In addition to the resin matrix viscoelasticity, the

occurrence of creep in FRPs can be attributed to microcracking initiation coupled with residual strain in the matrix, leading to fibre-matrix debonding and cracking, both these mechanisms being time-dependent [3.10].

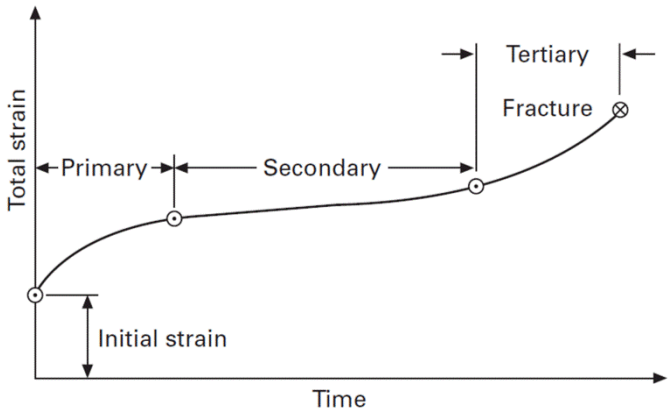

Figure 3.4. Typical creep strain response under constant applied load [3.94].

Microscopic damage in composite materials in the form of microcracking can be a result of several factors that include environmental conditions and loading cycles; it can alter the creep behaviour and shorten the life span of an FRP composite. In addition, FRP composites are more susceptible to creep due to the resins used in their constitution when compared to most traditional materials [3.10]. Thus, there is a need to increase the understanding of the synergistic influence on creep behaviour of several different conditions, such as moisture and temperature, for the design and performance of FRPs in civil engineering applications [3.96].

In terms of durability, creep evaluation of composite materials typically involves the use of isothermal, short-term creep tests, where a constant load is applied for a specific duration of time and for a certain range of temperatures. The loading period is followed by a recovery period where the load is removed and the material returns to its initial state assuming damage has not taken place. The creep strain is modelled using a constitutive law relating time, temperature, and stress to the time-dependent strain response of the material.

The development of such models, used to predict long term creep response of FRP materials, also have to account the effects of moisture and physical ageing on the creep and relaxation behaviour. The development of such models is of utmost importance, since they could potentially enable a more accurate estimate of the structure service life [3.96].

Several analytical models have been developed to model and predict the creep strain response of polymers and polymer composites under the individual and combined influences of stress, temperature and moisture. These constitutive models have been typically based on fundamental

concepts such as energy methods or damage mechanics [3.97]. The most popular analytical models used in the literature to predict long-term creep response are Findley's power law and the Boltzmann superposition principle. More information about these models can be found in [3.95, 3.98, 3.99].

3.2.5.2 Synergistic effects on the time-dependent response

The time-dependent response of FRP materials is a result of complex interactions between the creep behaviour and the environmental conditions affecting a given application. The effects of such interactions on FRP materials are typically related to stiffness degradation, due to time-dependent creep, and modulus and strength deterioration, attributed to damage from the existent environmental factors [3.97].

As discussed in Section 3.2.2, FRP composites are sensitive to temperature. Usually, when exposed to temperatures in the range of their T_g, the mechanical properties of FRPs can be significantly changed [3.100]. A rise in the environmental temperature may cause an increase in creep behaviour over time, due to softening of the polymeric matrix. According to Scott [3.95], increasing temperature also may have the following effects on creep behaviour:

(i). Changes in the linear viscoelastic behaviour of unidirectional FRPs;
(ii). If the FRP is under significant stress at the time of exposure, significant strength reduction may occur;
(iii). Buckling strength reduction;

As discussed in Section 3.2.1, when exposed to water, FRP composites are subjected to several physical and chemical changes [3.97], which may also alter their creep behaviour, similarly to aforementioned effects due to increasing temperature [3.101]. In addition, moisture can have a significant impact on nonlinear viscoelastic due to plasticization effects, and also promote the initial and steady-state creep levels at lower stress values [3.95].

In addition, the interaction of fatigue and creep is also an important consideration that may significantly shorten the life of FRP composites in infrastructure applications due to degradation of strength from cyclic mechanical loading [3.97].

Ellyin and Rohrbacher [3.102] investigated the effects of aqueous environments, temperature and cyclic loading on GFRP epoxy laminates. Several specimens with different fibre configurations were exposed to distilled water immersions, at ambient temperature and at 90 °C, for over four months, followed by cyclic tensile tests. The accumulated cyclic creep strain

of the immersed specimens was characterized by an increase, especially in the early life of the material, being higher in the specimens immersed at 90 °C than in those conditioned at ambient temperature. In addition, immersion at 90 °C resulted in excessive swelling and cracking, and considerable reduction in the fatigue resistance.

The time-dependent response of FRP materials used in civil structural applications needs to be duly considered, especially when dealing with complex interactions, such as creep, fatigue, moisture and temperature [3.96]. However, at present there is no universal or widely accepted creep model to account for the various durability factors that affect the different types of FRP materials.

3.2.6 Effects of fatigue loads on the durability of FRP composites

Fatigue is generally defined as the physical phenomenon that causes damage and failure of material or structural components subjected to several cyclic conditions, even though its level is not high enough to cause failure on the first cycle. Fatigue life is usually measured as the number of cycles to failure for a given applied load level [3.103].

In recent years, the fatigue of FRP materials has been being increasingly focused in theoretical and experimental research, especially considering civil engineering applications, where they could be subjected to several cyclic conditions. Under fatigue loads, FRP materials can be susceptible to microcracking, delamination, fibre fracture, or fibre matrix debonding. These damage modes will accumulate and interact under fatigue load, and subsequently the material will lose resistance that eventually will lead to fracture [3.104].

Several factors may affect the fatigue life of FRPs, including the properties of the constituent materials (fibres and the matrix types), the interface between them, the manufacturing process, the loading parameters (such as frequency, stress range and stress ratio) and the environmental exposure conditions. The latter will have a synergistic effect and may degrade the FRPs properties, generally diminishing fatigue life [3.103].

Loading parameters and the different exposure conditions are the most uncertain factors and still require further research, since they are critical parameters that affect fatigue life. However, the mechanisms of the effects that occur in FRPs, and especially their synergistic interactions, are not fully well understood. In addition, predictions usually rely on extensive laboratory testing, and empirical curve fitting methods. Semi-empirical methods, such as the S-N curves, are more practical and reliable for assessing fatigue performance [3.105].

3.3. Diffusion modelling of pultruded GFRP profiles

As discussed in Section 3.2.1.4, several sorption behaviours can occur in pultruded GFRP profiles. However, the most commonly assumed type of response is Fickian [3.2].

Fick's law characterises the diffusion of a fluid into a distinct absorbing medium from a higher concentration to a lower concentration. His second law makes considerations for a non-steady-state of diffusion, where a concentration profile can be investigated considering the concentration of the sorbate, time and the diffusion coefficient, *D*. The rate of diffusion is given by this coefficient in units of area per time [3.17]. These parameters can be affected by different characteristics of the GFRP profiles, such as their geometry, constitution or manufacturing processes. In addition, Fick's law typically requires an equilibrium content to be reached, where the rate of uptake slows to zero [3.17].

The diffusion coefficient can be assumed to be independent of concentration and time. This coefficient can be determined either by monitoring the concentration profile throughout the volume or via gravimetric measurements [3.106]. Simple geometries are highly desirable for both methodologies. Gravimetric measurements require the weighing of a specimen with known geometry for each step, allowing for the diffusion of the sorbate into a single sorbent specimen to be monitored over time and providing the total weight change due to uptake or loss of the sorbate rather than concentration. Nonetheless, the diffusion coefficient still needs to be calculated according to a theoretical model used to fit the trends of experimental data.

3.3.1 Fickian Diffusion Model

To model moisture diffusion, numerous analytical models exist in the literature. The model most often employed for polymeric materials is the one-dimensional Fickian model, due to its simplicity [3.107]. The one-dimensional case of Fick's second law assumes that the diffusion coefficient is concentration independent,

$$\frac{\partial C}{\partial t} = D\frac{\partial^2 C}{\partial x^2} \tag{3.1}$$

where C is the concentration of sorbate per unit of sorbent, t is time, x is the distance in thickness through the sorbate and D is the Fickian diffusion coefficient.

Additionally, if the diffusion coefficient is independent of time and position, when considering a uniform initial distribution of sorbent (C_0) and a plane plate kept at constant surface

concentration (C_1), the analytical solution of the concentration distribution (C(x,t)) through a polymeric plate with thickness (h) over time is,

$$\frac{C(x,t)-C_0}{C_1-C_0}=1-\frac{4}{\pi^2}\sum_{n=0}^{\infty}\frac{(-1)^n}{(2n+1)}\exp\left[-\frac{Dt}{h^2}\pi^2(2n+1)^2\right]\cos\left[\frac{(2n+1)\pi x}{h}\right] \tag{3.2}$$

where x represents the spatial coordinate measured in parallel to the diffusion direction, from -h/2 to +h/2. The total weight change of substance over time (M_t) can be estimated by integrating the concentration distribution over the thickness,

$$M_t=M_\infty\left\{1-\frac{8}{\pi^2}\sum_{n=0}^{\infty}\frac{1}{(2n+1)^2}\exp\left[-\frac{Dt}{h^2}\pi^2(2n+1)^2\right]\right\} \tag{3.3}$$

where M_∞ is the maximum equilibrium moisture content. The Fickian diffusion model is frequently expressed by plotting the moisture absorption content as a function of the square root of time, as depicted in Figure 3.2, displaying an initial linear trend.

Crank [3.107] provided a linear approximation for Eq. (3.3), for short term periods ($\sqrt{Dt}/h\le 0.2$):

$$M_t=\frac{4M_\infty}{h}\sqrt{\frac{Dt}{\pi}} \tag{3.4}$$

Knowing two points of the linear part at times t_1 and t_2 and considering that M_∞ is also known from gravimetric measurements, it is possible to determine the diffusion coefficient using Eq. (3.4),

$$D=\pi\left(\frac{h}{4M_\infty}\right)^2\left(\frac{M_1-M_2}{\sqrt{t_1}-\sqrt{t_2}}\right)^2\left(1+\frac{h}{l}+\frac{h}{w}\right)^{-2} \tag{3.5}$$

where l and w are, respectively, the length and width of the polymeric plate. As already mentioned, in Eq. (3.5) it is assumed that moisture diffusion uptake occurs predominantly in the through-thickness direction. However, the third parameter in the equation is a correction that accounts for the contribution in moisture absorption through the edges of the material, according to Shen and Springer [3.108]. They also provided an approximation to Eq. (3.3) that can be applied more readily and has been widely used:

$$M_t\approx M_\infty\left\{1-\exp\left[-7.3\left(\frac{Dt}{h^2}\right)^{0.75}\right]\right\} \tag{3.6}$$

Diffusion coefficients may be obtained from Eq. (3.4) for short times or from curve fitting Eq. (3.6).

3.3.2 Two Phase Fickian Diffusion Model

Jacob and Jones [3.109] considered a Fickian-based model, which consists of two phases, where the moisture uptake is a consequence of two independent diffusion phenomena (one phase being denser than the other),

$$\frac{M_t}{M_\infty} = V_d \left\{1 - \exp\left[-7.3\left(\frac{D_d t}{h^2}\right)^{0.75}\right]\right\} + (1 - V_d)\left\{1 - \exp\left[-7.3\left(\frac{D_l t}{h^2}\right)^{0.75}\right]\right\} \tag{3.7}$$

where V_d is the volume fraction of the denser phase, D_d is the diffusion coefficient of the denser phase, and D_l is the diffusion coefficient of the less dense phase.

The model considers that two independent Fickian phases occur, which begin their diffusion at the same time. Consequently, two areas of the moisture uptake curves exist, where sorption is dominated by each phase. When the less dense phase approaches equilibrium, the slope of the uptake curve should be characteristic of diffusion in the denser phase.

Maggana and Pissis [3.110] generalized the more and less dense phases to two arbitrary independent phases. For the two moisture mechanisms with two maximum moisture contents, M_1 and M_2, and two diffusion coefficients, D_1 and D_2, moisture uptake is described by,

$$\begin{aligned} M_t = M_1 \left\{1 - \frac{8}{\pi^2}\sum_{n=0}^{\infty}\frac{1}{(2n+1)^2}\exp\left[-\frac{D_1 t}{h^2}\pi^2(2n+1)^2\right]\right\} + \\ + M_2 \left\{1 - \frac{8}{\pi^2}\sum_{n=0}^{\infty}\frac{1}{(2n+1)^2}\exp\left[-\frac{D_2 t}{h^2}\pi^2(2n+1)^2\right]\right\} \end{aligned} \tag{3.8}$$

Where:

$$M_\infty = M_1 + M_2 \tag{3.9}$$

When exposing a GFRP composite to hygrothermal environments, two water phases can be observed: the first phase sorption is related to the amount of water in the atmosphere and the second phase is related to temperature and time [3.111].

The diffusion coefficients in Eq. (3.7) may be determined from simple linear curve fits of each phase-dominated region, as depicted in Figure 3.5. The initial slope of the uptake curve

provides the approximate diffusion coefficient, D_x, for the bulk after the traditional Fickian approach.

It should be noted that the initial uptake is obtained by adding the uptake of the two phases [3.109],

$$\left[\frac{\partial M_t}{\partial\sqrt{t}}\right]_x = \left[\frac{\partial M_t}{\partial\sqrt{t}}\right]_d + \left[\frac{\partial M_t}{\partial\sqrt{t}}\right]_l \tag{3.10}$$

where the subscripts d and l refer to the more and less dense phases, respectively.

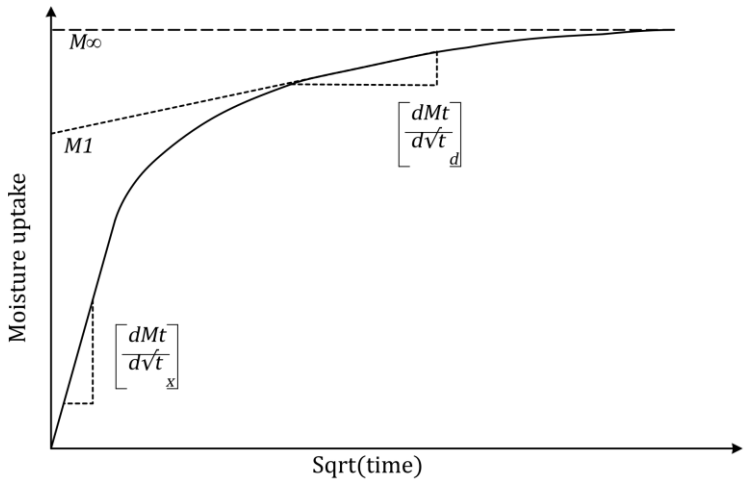

Figure 3.5. Two phase Fickian parameters.

At later durations of hygrothermal exposure, the slope represents the uptake in the denser phase and the uptake in the other approaches equilibrium. By extending a line from the region characterized by sorption of the denser region to the ordinate axis, the equilibrium content for the less dense phase can be determined from the intercept, as depicted in Figure 3.5, allowing for the calculation of the corresponding diffusions coefficients [3.109]. In the case of GFRP composites, not only the bulk material is heterogeneous, but also the resin matrix itself can be considered as a biphasic material, where the total moisture content increases with temperature and the maximum moisture content of those two phases may also vary with temperature at two different rates [3.17].

3.3.3 Thermal dependency of the diffusion coefficient

The diffusion coefficient is typically temperature-dependent and can be used to determine the activation energy for diffusion E_d using an Arrhenius type relationship [3.112],

$$D(t) = D_0 \exp^{\left(\frac{-Ed}{RT}\right)} \tag{3.11}$$

where D_0 is a temperature-independent empirical constant, E_d is the activation energy, R (8.3144 J/mol) is the universal gas constant, T is the temperature in Kelvin and D is the apparent diffusion coefficient. The Arrhenius relation can be used for any diffusion with temperature dependency, where D_0 and E_d are determined for each model, by plotting ln(D) *vs.* the inverse of absolute temperature (1/T).

3.4. Predictive degradation model for GFRP materials

Lifetime prediction studies on polymeric materials rely heavily on the use of accelerated ageing exposures. Failure times or degradation rates are determined at elevated temperatures and these data are used to extrapolate material performance to ambient conditions. The most commonly used methodology for such extrapolations in FRP ageing studies, which is still being used nowadays, is based on the Arrhenius relationship [3.17]. However, linear Arrhenius behaviour is often limited by the availability of experimental data, and the occurrence of only one chemical degradation phenomenon [3.113].

In developing degradation models, a property, P, (*e.g.* tensile or flexural strength) is monitored over a period of environmental exposure. For the purpose of accelerated testing, these environments are usually water immersions, where elevated temperature accelerates the diffusion characteristics and the chemical degradation rate. Prolonged exposure periods over a series of different temperatures usually allows correlating the degradation rate with temperature. As such, it would allow the prediction of the degradation rate at a defined temperature.

There are generally two types of degradation models: (i) the ones that characterize time to failure defined by a material property reaching a critical level and (ii) the ones that predict a property level as a function of time. As this thesis aims to evaluate material degradation applied to civil infrastructure it will focus on the second group of models.

The Arrhenius model, or Arrhenius based models, employ the Arrhenius equation to describe the degradation rate of a material property P, which is assumed to be dependent on temperature [3.114],

$$k = Ae^{\left(\frac{-E_a}{RT}\right)} \tag{3.12}$$

where A is a pre-exponential constant, E_a is the activation energy for the reaction responsible for the degradation, R is the gas constant, T is the absolute temperature in Kelvin, and t is time.

The model also assumes that,

$$t(P)\alpha\left(\frac{dP}{dt}\right)^{-1} \tag{3.13}$$

which implies that:

$$\ln\left[t(P)\right]\alpha\ T^{-1} \tag{3.14}$$

As such, the temporal variation of P can be determined as,

$$P(t) = B\exp\left[\frac{-E_d}{RT}\right]\ln(t) + P_0 \tag{3.15}$$

where B is an integration constant and P_0 is the property at time zero. Eq. (3.15) represents the Arrhenius rate degradation model, and it is usually considered that E_a is well represented by the activation energy for the diffusion process [3.115].

The Arrhenius relationship has been used to predict temperature-accelerated degradation of products used in many fields, including pharmaceuticals, insulation materials, adhesives and batteries. Key assumptions in the simple application of the Arrhenius model are that the same process controls degradation at both elevated and in-service temperatures, and that this single process continues to control degradation throughout the service life of the material. If these assumptions hold, then a value of the activation energy can be determined from experimental and/or service data over a range of temperatures and used to predict degradation or service life at different temperatures [3.116].

It may be possible that the curve(s) $\ln t(P)\ v.\ T^{-1}$ of a certain material demonstrate non-linearity; this means that the rate of degradation in the material is controlled by more than one degradation mechanism [3.114], *i.e.* the above mentioned assumption is not valid.

Other predictive degradation models have been suggested, typically ranging from a simple based parameter in the Arrhenius rate degradation model to more complex models. However, their application is limited and most of them have been specifically adapted to different

materials, other than pultruded GFRP elements. In addition, most of the different degradation models presented assume that Arrhenius model holds, just as for diffusion.

Svetlik [3.17] applied several different modelling and time-temperature superposition and crack propagation models, and these models predicted non-conservative values at early times of environmental exposure. As such, different models other than the typical Arrhenius degradation one will not be implemented in Chapter 4. Detailed information about empirically based alternative models, which also include statistical modelling, can be found in the following references: (i) time-temperature superposition models [3.117, 3.118]; (ii) crack propagation models [3.119, 3.120]; (iii) multicomponent degradation models [3.121-3.123], and (iv) metric based numerical analysis [3.124].

3.5. Concluding remarks

In this chapter, the most relevant critical aspects that affect FRP durability have been reviewed, with a particular emphasis on pultruded GFRP profiles. The general effects of different exposure environments critical for civil engineering applications were presented, their general effects were highlighted, and their potential degradation mechanisms were discussed.

The effects of moisture and water related environments cause physical and chemical changes in pultruded GFRP elements, with plasticization in the short-term and hydrolysis in the long-term being the most common degradation mechanisms. Alkaline environments, briefly described in this chapter, can cause severe corrosion of glass fibres.

Temperature also affects GFRP degradation, especially in what concerns the viscoelasticity of the polymeric matrix and the interface, and can contribute to accelerate the degradation mechanisms if acting synergistically with other exposure agents. In addition, exposure to several thermal cycles may also have a negative influence in the material properties, due to the increase of cumulative residual stresses that stem from the different thermal expansion coefficients of the glass fibres and the polymeric matrix. Solar and most importantly UV radiation can also contribute to GFRP degradation, especially in terms of colour and gloss loss, chalking and fibre blooming.

Prolonged exposure to creep can lead to microcracking initiation and may increase residual strains in the matrix, which in turn can aggravate or induce fibre-matrix debonding and cracking, both these mechanisms being time dependent. Fatigue effects, very briefly abridged in this chapter, can increase the susceptibility of GFRP composites to microcracking, delamination or fibre matrix debonding.

In the final part of this chapter, two typical analytical diffusion models that are used to simulate the sorption behaviour of GFRP materials were described, together with a brief overview of predictive degradation models used to estimate the long-term mechanical response of pultruded GFRP profiles at a material level.

3.6. References

[3.1] Pritchard G. Reinforced Plastics Durability. Kingston University, Surrey: Woodhead Publishing, 1998.

[3.2] Karbhari VM. Durability of Composites for Civil Structural Applications. Boca Raton, Florida: Woodhead Publishing, 2007.

[3.3] Busel JP, Lockwood JD. Product select guide: FRP composite products for bridge application. New York; 2000.

[3.4] Karbhari VM, Chin JW, Hunston D, Benmokrane B, Jusja T, Morgan R, et al. Gap analysis for durability of fiber reinforced polymer composites in civil infrastructure. ASCE J Compos Constr. 2003;7:238-47.

[3.5] Karbhari VM, Chin JW, Reynaud D. Critical gaps in durability data for FRP composites in civil infrastructure. Proceedings of the 45th International Society for the Advancement of Materials and Process Engineering (SAMPE) Symposium and Exhibition. 2000;45:549-63.

[3.6] Lee LS, Estrada H. Part III Externally Bonded FRP Composite Systems for Rehabilitation: 19 - Durability. In: Zoghi M, editor. The International Handbook of FRP Composites in Civil Engineering: CRC Press; 2013. p. 329-41.

[3.7] Robert M, Benmokrane B. Combined effects of saline solution and moist concrete on long-term durability of GFRP reinforcing bars. Constr Build Mater. 2013;38:274-84.

[3.8] Correia JR. Perfis Pultrudidos de Fibra de Vidro (GFRP). Aplicação de Vigas Mistas GFRP-Betão na Construção: Instituto Superior Técnico, Universidade de Lisboa, MSc Dissertation in Construction, 2004.

[3.9] Bank LC, Gentry TR, Barkatt A. Accelerated test methods to determine the long-term behavior of FRP composite structures: Environmental effects. J Reinf Plast Compos. 1995;14:559-87.

[3.10] Liao K, Schultheisz CR, Hunston DL, Brinson LC. Long-term durability of fiber-reinforced polymer-matrix composite materials for infrastructure applications: A review. J Adv Mater. 1998;30:3-40.

[3.11] Liao K, Schultheisz CR, Hunston DL. Effect of environmental aging on the properties of pultruded GFRP. Compos Part B - Eng. 1999;30.

[3.12] Cabral-Fonseca S, Correia JR, Rodrigues MP, Branco FA. Artificial accelerated ageing of GFRP pultruded profiles made of polyester and vinylester resins: Characterisation of physical–chemical and mechanical damage. Strain. 2012;48:162-73.

[3.13] Sousa JM, Correia JR, Cabral-Fonseca S. Durability of glass fibre reinforced polymer pultruded profiles: Comparison between QUV accelerated exposure and natural weathering in a Mediterranean climate. Exp Tech. 2016; 40:207–19.

[3.14] Sousa JM, Correia JR, Cabral-Fonseca S, Diogo AC. Effects of thermal cycles on the mechanical response of pultruded GFRP profiles used in civil engineering applications. Compos Struct. 2014;116:720-31.

[3.15] Grammatikos SA, Jones RG, Evernden M, Correia JR. Thermal cycling effects on the durability of a pultruded GFRP material for off-shore civil engineering structures. Compos Struct. 2016;153:297-310.

[3.16] Grammatikos SA, Evernden M, Mitchels J, Zafari B, Mottram JT, Papanicolaou GC. On the response to hygrothermal aging of pultruded FRPs used in the civil engineering sector. Mater Des. 2016;96:283-95.

[3.17] Svetlik SL. An investigation in the hygrothermal degradation of an E-glass/vinyl-ester composite in humid and immersion environments. PhD Thesis. UC San Diego, 2008.

[3.18] Antoon MK, Koenig JL. The structure and moisture stability of the matrix phase in glass-reinforced epoxy composites. J Macromol Sci Part C. 1980;C19:135-73.

[3.19] Mijovic J, Lin KF. The Effect of hygrothermal fatigue on physical/mechanical properties and morphology of neat epoxy resin and graphite/epoxy composite. J Appl Polym Sci. 1985;30:2527-49.

[3.20] Apicella A, Migliaresi C, Nicolais L, Iaccarino L, Roccotelli S. The water ageing of unsaturated polyester-based composites: influence of resin chemical structure. Composites. 1983;14:387-92.

[3.21] Lee MC, Peppas NA. Water transport in epoxy resins. Prog Polym Sci . 1993;18:947-61.

[3.22] Pickett JE, Coyle DJ. Hydrolysis kinetics of condensation polymers under humidity aging conditions. Polym Degrad Stab. 2013;98:1311-20.

[3.23] Levenson HS, Smith HA. The saponification of ethyl esters of aliphatic acids. J Am Chem Soc. 1940;62:1556-8.

[3.24] Thomson KW, Wong T, Broutman LJ. The plasticization of an epoxy resin by dibutylphthalate and water. Polym Eng Sci. 1984;24:1270-6.

[3.25] Berens AR, Hopfenberg HB. Diffusion and relaxation in glassy polymer powders: 2. Separation of diffusion and relaxation parameters. Polymer. 1978;19:489-96.

[3.26] Lee SB, Rockett TJ, Hoffman RD. Interactions of water with unsaturated polyester, vinyl ester and acrylic resins. Polymer. 1992;33:3691-7.

[3.27] Abeysinghe HP, Edwards W, Pritchard G, Swampillai GJ. Degradation of crosslinked resins in water and electrolyte solutions. Polymer. 1982;23:1785-90.

[3.28] Wood CA, Bradley WL. Determination of the effect of seawater on the interfacial strength of an interlayer E-glass/graphite/epoxy composite by in situ observation of transverse cracking in an Evironmental SEM. Compos Sci Technol. 1997;57:1033-43.

[3.29] Ishida H, Koenig JL. The reinforcement mechanism of fiber-glass reinforced plastics under wet conditions: A review. Polym Eng Sci. 1978;18:128-45.

[3.30] Bunker BC. Molecular mechanisms for corrosion of silica and silicate glasses. J Non Cryst Solids . 1994;179:300-8.

[3.31] Karbhari VM, Zhao L, Murphy K, Kabalnova L. Environmental durability of glass fiber reinforced composites - short term effects. Proceedings of the 1st International Conference on the Durability of Fibre Reinforced Polymer Composites for Construction (CDCC'98). 1998:513-24.

[3.32] Chin JW, Aouadi K, Haight MR, Hughes WL, Nguyen T. Effects of water, salt solution and simulated concrete pore solution on the properties of composite matrix resins used in civil engineering applications. Polym Compos. 2001;22:282-97.

[3.33] Ghorbel I, Valentin D. Hydrothermal effects on the physico-chemical properties of pure and glass fiber reinforced polyester and vinylester resins. Polym Compos. 1993;14:324-34.

[3.34] Magnus G, Dunleavy RA, Critchfield FE. Stability of urethane elastomers in water, dry air, and moist air environments. Rubber Chem Technol. 1966;39:1328-37.

[3.35] Chin JW, Hughes WL, Signor A. Elevated temperature aging of glass fiber reinforced vinyl ester and isophtalic polyester composites in water, salt water and concrete pore solution. American Society for Composites, Proceedings of the 16th Technical Conference. 2001:1-12.

[3.36] Karbhari VM, Zhang S. E-Glass/vinylester composites in aqueous environments - I: experimental results. Appl Compos Mater. 2002;10:19-48.

[3.37] Metcalfe AG, Schmitz GK. Mechanism of stress corrosion in E glass filaments. Glas Technol. 1972;13:5-16.

[3.38] Charles JR. Static fatigue in glass Part I. J Appl Phys. 1958;29:1549-60.

[3.39] Schmitz GK, Metcalfe AG. Stress corrosion of E-glass fibres. Industrial and Engineering Chem Prod Res and Dev. 1966;5:1.

[3.40] Michalske TA, Freiman SW. A molecular mechanism for stress corrosion in vitreous silica. J Am Ceram Soc. 1983;66:284-8.

[3.41] Bascom WD. The surface chemistry of moisture-induced composite failure. In: Interfaces in Polymer Matrix Composites: Academic Press, New York; 1974. p. 79-108.

[3.42] Bradley WL, Grant TS. The effect of moisture absorption on the interfacial strength of polymeric matrix composites. J Mater Sci. 1995;30:5537-42.

[3.43] Phifer SP, Verghese KNE, Lesko JJ. Remaining strength of hygrothermally aged pultruded vinyl ester E-glass laminates. Proceedings of the 3rd International Conference on the Advanced Composite Materials in Bridges and Structures (ACMBS MCAPC). 2000:29-36.

[3.44] Ishai O. Environmental effects on deformation, strength, and degradation of unidirectional glass-fiber reinforced plastics, I. Survey. Polym Eng Sci. 1975;15:486-90.

[3.45] Ishai O. Environmental effects on deformation, strength, and degradation of unidirectional glass-fiber reinforced plastics, II. Experimental Study. Polym Eng Sci. 1975;15:491-9.

[3.46] Dewimille B, Bunsell AR. Accelerated ageing of a glass fibre-reinforced epoxy resin in water. Composites. 1983;14:35-45.

[3.47] Mensitieri G, Nobile MAD, Apicella A, Nicolais L. Moisture-matrix interactions in polymer based composite materials. Revue de l'Institut Français du Pétrole. 1995;50:551-75.

[3.48] Crank J, Park GS. Diffusion in Polymers. Academic Press, New York. 1968.

[3.49] Chin JW, Nguyen T, Aouadi K. Sorption and diffusion of water, salt-water and concrete pore solution in composite matrices. J Appl Polym Sci. 1999;71:483-92.

[3.50] Menges G, Gitschner HW. Sorption behaviour of glass-fibre reinforced composites and the influence of diffusing media on deformation and failure behavior. Proceedings of the 3rd International Conference on Composite Materials (ICCM-3). 1980:25-48.

[3.51] Loos AC, Springer GS. Environmental Effects on Composite Materials. Lancaster, PA: Technomic Publishing Co., 1981.

[3.52] Weitsman YJ. Effects of fluids on polymeric composites - a review. Contract Report for Office of Naval Research. 1995;No. N00014-90-J-1556.

[3.53] Apicella A, Migliaresi C, Nicodemo C, Nicolais L, Iaccarino L, Roccotelli S. Water sorption and mechanical properties of glass-reinforced polyester resin. Composites. 1982;13:406-10.

[3.54] Visco AM, Campo N, Cianciafara P. Comparison of seawater absorption properties of thermoset resins based composites. Compos Part A Appl Sci Manuf. 2011;42:123-30.

[3.55] Nielsen LE, Chen PE. Youngs modulus of composites filled with randomly oriented fibres. J Mater Sci. 1968;64:55-67.

[3.56] Sá M. Análise de Painéis de Laje Multicelulares Pultrudidos de GFRP - Aplicação em Pontes Pedonais. PhD Thesis, Instituto Superior Técnico, University of Lisbon (In Portuguese), 2015.

[3.57] Gonilha JA. GFRP–concrete hybrid structural systems. Application to the development of a footbridge prototype. PhD Thesis, Instituto Superior Técnico, University of Lisbon, 2014.

[3.58] Nkurunziza G, Debaiky A, Cousin P, Benmokrane B. Durability of GFRP bars: A critical review of the literature. Prog Struct Eng Mater. 2005;7:194-209.

[3.59] Benzarti K, Colin X. Understanding the durability of advanced fibre-reinforced polymer (FRP) composites for structural applications. In: Bai J, editor. Advanced Fibre-Reinforced Polymer (FRP) Composites for Structural Applications: Woodhead; 2013. p. 361-439.

[3.60] Mouritz AP, Gibson AG. Fire Properties of Polymer Composite Materials. Dordrecht, The Netherlands: Springer, 2006.

[3.61] Morgado T. Thermal and structural response of GFRP pultruded profiles under fire: PhD Thesis, Instituto Superior Técnico, University of Lisbon, 2018.

[3.62] Karbhari VM, Abanilla MA. Design factors, reliability, and durability prediction of wet layup carbon/epoxy used in external strengthening. Compos Part B - Eng. 2007;38:10-23.

[3.63] Rivera J, Karbhari VM. Cold temperature and simultaneous aqueous environment related degradation of carbon/vinylester composites. Compos Part B - Eng. 2002;33:17-24.

[3.64] Abanilla MA, Li Y, Karbhari VM. Durability characterization of wet layup graphite/epoxy composites used in external strengthening. Compos Part B - Eng. 2006;37:200-12.

[3.65] Dutta PK, Hui D. Low-temperature and freeze thaw durability of thick composites. Compos Part B - Eng. 1996;27:371-9.

[3.66] Gomez JP, Casto B. Freeze-Thaw Durability of Composite Materials. Virginia Transportation Research Council VTRC 96-R25. 1996:1-13.

[3.67] Zhang S, Karbhari VM, Reynaud D. NOL-ring based evaluation of freeze and freeze–thaw exposure effects on FRP composite column wrap systems. Compos Part B - Eng. 2001;32:589-98.

[3.68] Karbhari VM, Rivera J, Zhang J. Low-temperature hygrothermal degradation of ambient cured E-glass/vinylester composites. J Appl Polym Sci. 2002;86:2255-60.

[3.69] Tann DB, Delpak R. Influences of freeze and thaw cycles and elevated temperatures on the properties of FRP composites. ACIC 2004 Conference, University of Surrey. 2004:611-8.

[3.70] Haramis J, Verghese KNE, Lesko JJ, Weyers RE. Characterization of freeze-thaw damage mechanisms in composites for Civil Infrastructure. International Conference on Advanced Composite Materials in Bridges and Structures. 2000:663-70.

[3.71] Sheikh SA, Tam S. Effect of freeze-thaw climatic conditions on long-term durability of FRP strengthening systems. Ministry of Transportation of Ontario HIIFP-037. 2007:1-40.

[3.72] Wu H, Fu G, Gibson R, Yan A, Warnemuende K, Anumandla V. Durability of FRP composite bridge deck materials under freeze-thaw and low temperature conditions. J Bridg Eng. 2006;11:443-51.

[3.73] Kim H-Y, Park Y-H, You Y-J, Moon C-K. Short-term durability test for GFRP rods under various environmental conditions. Compos Struct. 2008;83:37-47.

[3.74] Li H, Xian G, Lin Q, Zhang H. Freeze–thaw resistance of unidirectional-fiber-reinforced epoxy composites. J Appl Polym Sci. 2012;123:3781-8.

[3.75] Aniskevich K, Korkhov V, Faitelsone J, Janson J. Mechanical properties of pultruded glass fiber reinforced plastic after freeze–thaw cycling. J Reinf Plast Compos. 2012;31:1554-63.

[3.76] Davis A, Sims D. Weathering of polymers: Applied Science Publishers, London, 1983.

[3.77] Chin JW. Durability of composites exposed to ultraviolet radiation. In: Karbhari VM, editor. Durability of Composites for Civil Structural Applications: Woodhead; 2007. p. 81-97.

[3.78] Searle ND. Environmental Effects on Polymeric Materials. In: Andrady AL, editor. Plastics and the Environment: John Wiley and Sons, New York; 2003.

[3.79] Martin JW. Quantitative characterization of spectral ultraviolet radiation-induced photodegradation in coating systems exposed in laboratory and the field. Prog Org Coatings. 1993;23:49-70.

[3.80] Kaczmarek H. Changes in polymer morphology caused by U.V. irradiation, 1. Surface damage. Polymer. 2002;37:189-94.

[3.81] Chin JW, Nguyen T, Aouadi K. Effects of environmental exposure on fiber-reinforced plastics (FRP) materials used in construction. J Compos Technol Res. 1997;19:205-13.

[3.82] Schoolenberg GE, P.Vink. Ultra-violet degradation of polypropylene: 1. Degradation profile thickness of the embrittled surface layer. Polymer. 1991;32:432-7.

[3.83] Jian SZ, Lucki J, Rabek JF, Ranby B. Photooxidation and photostabilisation of unsaturated cross-linked polyesters. ACS Symposium Series, Proceedings of the 187th Meeting of the American Chemical Society. 1985.

[3.84] Signor AW, VanLandingham MR, Chin JW. Effects of ultraviolet radiation exposure on vinylester resins: characterization of chemical, physical and mechanical damage. Polym Degrad Stab. 2003;79:359-68.

[3.85] Jones MS. Effects of UV radiation on building materials. Proceedings of Workshop on UV Radiation and its Effects, New Zealand. 2002.

[3.86] Capanescu C, Cincu C. Evaluation of UV inhibitors in polyester gelcoats. Adv Polym Technol. 2003;22:365-72.

[3.87] Hollaway LC. Polymers and Polym Compos in Construction. Thomas Telford Ltd, London1990.

[3.88] Segovia F, Ferrer C, Salvador MD, Amigo V. Influence of processing variables on mechanical characteristics of sunlight aged polyester-glass fibre composites. Polym Degrad Stab. 2001;71:179-84.

[3.89] Bogner BR, Borja PP. Ultraviolet light resistance of pultruded composites. Proceedings of the European Pultrusion Technology Association Conference. 1994.

[3.90] Martin JW. Repeatability and reproducibility of field exposure results. Service Life Prediction: Methodology and Metrologies, ACS Symposium Series 805 (American Chemical Society). 2001.

[3.91] Pickett JE. Calculation of the efficiency of ultraviolet screeners in plastics. J Appl Polym Sci. 1987;33:525-31.

[3.92] Menard KP. Dynamic Mechanical Analysis. Boca Raton: CRC Press, 1999.

[3.93] Kawada H, Kobiki A, Koyanagi J, Hosoi A. Long-term durability of polymer matrix composites under hostile environments. Mater Sci Eng A. 2005;412:159-64.

[3.94] ASTM D2990. Standard test method for tensile, compressive, and flexural creep and creep-rupture of plastics. American Society for testing and materials, Pennsylvania. 2001.

[3.95] Scott DW, Lai JS, Zureick A-H. Creep behavior of fiber-reinforced polymeric composites: A review of technical literature. J Reinf Plast Compos. 1995;14:588-617.

[3.96] Lee LS. Creep and time-dependent response of composites. In: Karbhari VM, editor. Durability of Composites for Civil Structural Applications: Woodhead; 2007.

[3.97] Guedes RM, Morais JJL, Marques AT, Cardon AH. Prediction of long-term behaviour of composite materials. Comput Struct. 2000;76:183-94.

[3.98] Gerdeen JC, Lord HW, Rorrer RAL. Engineering Design with Polymers and Composites. Boca Raton: CRC Press, 2006.

[3.99] Ward IM, Sweeney J. The Mechanical Properties of Solid Polymers. West Sussex: John Wiley & Sons, 2004.

[3.100] Goertzen GK, Kessler MR. Creep behavior of carbon fiber/epoxy matrix composites. Mater Sci Eng A. 2006;421:217-25.

[3.101] Hu H, Sun CT. The equivalence of moisture and temperature in physical ageing of polymeric composites. J Compos Mater. 2003;37:913-28.

[3.102] Ellyin F, Rohrbacher C. The influence of aqueous environments, temperature, and cyclic loading on glass-fibre/epoxy composite laminates. J Reinf Plast Compos. 2003;22:615-36.

[3.103] Zhou A, Post N, Pingry R, Cain J, Lesko JJ, Case SW. Durability of composites under fatigue load. In: Karbhari VM, editor. Durability of Composites for Civil Structural Applications: Woodhead; 2007. p. 127-49.

[3.104] Reifsnider KL. Damage and damage mechanisms. In: Reifsnider KL, editor. Fatigue of Composite Materials. New York: Elsevier Science; 1991. p. 11-77.

[3.105] Keller T, Tirelli T, Zhou A. Tensile fatigue performance of pultruded glass fibre reinforced polymer profiles. Compos Struct. 2005;68:235-45.

[3.106] Marshall JM, Marshall GP, Pinzelli RF. The diffusion of liquids into resins and composites. Polym Compos. 1982;3:131-7.

[3.107] Crank J. The Mathematics of Diffusion: Oxford University Press: New York, 1970.

[3.108] Shen CH, Springer GS. Moisture absorption and desorption of composite materials. J Compos Mater. 1976;10:2-20.

[3.109] Jacobs PM, Jones FR. Diffusion of moisture into two-phase polymers. Part 1. J Mater Sci. 1989;24:2331-6.

[3.110] Maggana C, Pissis P. Water sorption and diffusion studies in an epoxy resin system. J Polym Sci. 1999;37:1165-82.

[3.111] Zhou J, Lucas JP. Hygrothermal effects of epoxy resin. Part II: Variations of glass transition temperature. Polymer. 1999;40:5513-22.

[3.112] Karbhari VM, Chin JW, Hunston D, Benmokrane B, Juska T, Morgan R, et al. Durability gap analysis for fiber-reinforced polymer composites in Civil Infraestructure. J Compos Constr. 2003;7:238-47.

[3.113] Celina M, Gillen KT, Assink RA. Accelerated aging and lifetime prediction: Review of non-Arrhenius behaviour due to two competing processes. Polym Degrad Stab. 2005;90:396-404.

[3.114] Litherland KL, Oakley DR, Proctor BA. The use of accelerated ageing procedures to predict the long term strength of GRC composites. Cem Concete Res. 1981;11:455-66.

[3.115] Phani KK, Bose NR. Temperature dependence of hydrothermal ageing of CSM-laminate during water immersion. Compos Sci Technol. 1987;29:79-87.

[3.116] Purnell P. Interpretation of climatic temperature variations for accelerated ageing models. J Mater Sci. 2004;39:113-8.

[3.117] Nakada M, Miyano Y, Kinoshita M, Koga R, Okuya T, Muki R. Time-temperature dependence of tensile strength of unidirectional CFRP. J Compos Mater. 2003;36:2567-81.

[3.118] Halpin JC, Kopf JR, Goldberg W. Time dependent static strength and reliability for composites. J Compos Mater. 1970;4:461-74.

[3.119] Purnell P, Short NR, Page CL. A static fatigue model for the durability of glass fibre reinforced cement. J Mater Sci. 2001;36:5385-90.

[3.120] Matthewson MJ, Kurkjian CR. Environmental effects on the static fatigue of silica optical fiber. J Am Ceram Soc. 1988;71:177-83.

[3.121] Barbero EJ, Damiani TM. Phenomenological prediction of tensile strength of E-glass composites. J Reinf Plast Compos. 2003;22:373-94.

[3.122] Gao SL, Mäeder E, Abdkader A, Offerman P. Environmental resistance and mechanical performance of alkali-resistant glass fibers with surface sizings. J Non Cryst Solids . 2003;325:230-41.

[3.123] Brown EN, Davis AK, Jonnalagadda KD, Sottos NR. Effect of surface treatment on the hydrolytic stability of E-glass fiber bundle tensile strength. Compos Sci Technol. 2005;65:129-36.

[3.124] McManus HL, Foch BJ, Cunningham RA. Mechanism-based modeling of long-term degradation. J Compos Technol Res. 2000;22:146-52.

Chapter 4.

Hygrothermal ageing of pultruded GFRP profiles

4.1. Introduction

Currently, the number of research studies about the long-term behaviour of fibre reinforced polymer (FRP) composites in civil engineering applications is increasing, since many knowledge "gaps" need to be fulfilled in this industry. Results obtained in studies conducted in other industries (*e.g.* aerospace or naval), where more documentation and a better understanding were already obtained [4.1], show that several competitive mechanisms may affect the FRP durability during exposure to hygrothermal ageing conditions: (i) additional cross-linking due to residual curing of the polymeric resin; (ii) secondary cross-linking between polymer chains and water molecules; (iii) swelling; (iv) micro-cracking; (v) plasticization; (vi) hydrolysis; (vii) leaching of low molecular weight segments, and (viii) relaxation phenomena [4.2–4.6].

In the specific case of pultruded GFRP profiles, comprehensive and validated data on their durability is still limited and there is a lack of understanding about the ageing and degradation mechanism suffered by GFRP materials when subjected to different service conditions found in civil engineering applications. Since the required service life for most structures is usually above 50 years and there is a typical lack of routine inspections and maintenance found in this industry when compared to the aerospace and marine sectors, the availability of such information is of extreme importance. In addition, some limitations or particularities of previous studies (*cf.* Chapter 3) make it difficult to draw general conclusions about the durability of pultruded GFRP materials in civil engineering applications, namely when considering hygrothermal (moisture and temperature) ageing. In fact, the test methods, exposure conditions and characterisation techniques often vary considerably, which can lead to contradictory results. Moreover, even considering the same manufacturing technique (pultrusion), the final GFRP element can have different fibre and void contents, matrix/fibre combinations, or reinforcement architecture (*e.g.* the number of mats, unidirectional rovings and/or surface veils and their positioning in the cross section). Experiments under accelerated conditions are rarely longer than one year and only a few studies compare alternative resin systems. No systematic information is available regarding the "dry state" behaviour of pultruded GFRP profiles (*i.e.* after a desorption period up to constant mass, following hygrothermal ageing), which is paradoxical since most of civil engineering applications (apart from submersed elements) are not typically in permanent contact with aqueous solutions during their service life, and are

often subjected to 'dryer' periods, during the warmer seasons, especially in mild Mediterranean climates, such as Portugal. Finally, very little information is available on the effects of hygrothermal ageing on the in-plane shear properties; according to the author's best knowledge, no long-term estimates are available for such properties, which are frequently very relevant for the design of GFRP structures, which exhibit limited shear strength and significant shear deformations.

Due to the aforementioned reasons, an extensive experimental programme was carried out in the present thesis to investigate the effects of hygrothermal ageing on the durability performance of two commercial GFRP profiles made of two alternative resin systems – unsaturated polyester and vinylester (both comprising the same fibre content and architecture). Specimens of the two types of profiles were subjected to different ageing environments, namely immersion in demineralised and salt water at three different temperatures (20 °C, 40 °C, and 60 °C) and continuous condensation at 40 °C for up to two years, and were tested after a desorption period, thus including the potential property recovery after drying to constant mass due to the reversibility nature of some physical degradation mechanisms [4.7]. The performance of both profiles was analysed and compared regarding their physical, viscoelastic and mechanical responses, after subjected to hygrothermal ageing. Finally, long-term prediction models (Arrhenius based) were implemented, when applicable.

4.2. Experimental programme

4.2.1 Materials

For this experimental study, two types of "off-the-shelf" pultruded GFRP profiles (3 m long) were manufactured by *ALTO Perfis Pultrudidos*. The profiles had 33 × 5 mm^2 of rectangular cross section and comprised E-glass unidirectional rovings with linear density of 4800 tex (typically corresponding to a filament diameter of ≈24 μm) in the core region, and two outer continuous strand mats (CSM) with a weight of 450 g/m^2, embedded in either unsaturated polyester (UP profile) or vinylester (VE profile) resins.

The pultruded profiles were produced by pulling the fibres with a silane sizing through a bath of resin, at an average speed of 0.25 m/min, passing through a heated die, where temperatures ranged between 130 °C and 165 °C.

The criteria for choosing the different resin matrixes were as follows: UP resin was selected, since this polymeric matrix is used in most structural applications when there are no requirements in terms of environmental harshness; on the other hand, the VE resin was chosen

as it is often selected for applications in relatively harsh or corrosive environments. Both profiles had the same glass fibre content and architecture, thus allowing for a direct comparison of the durability performance of their resins. Figure 4.1 (a) illustrates the pultruded GFRP profiles, and Figure 4.1 (b) depicts the cross section of a representative UP profile. Figure 4.1 (c) and (d) presents different amplifications for the cross section: 50× amplification of the whole section and 220× amplification of the central part of the cross section. These images were acquired through a *Dino-Lite Premier* digital microscope (some glass fibres can be easily identified as the black dots with a very different gloss, probably due to charring during the cutting process).

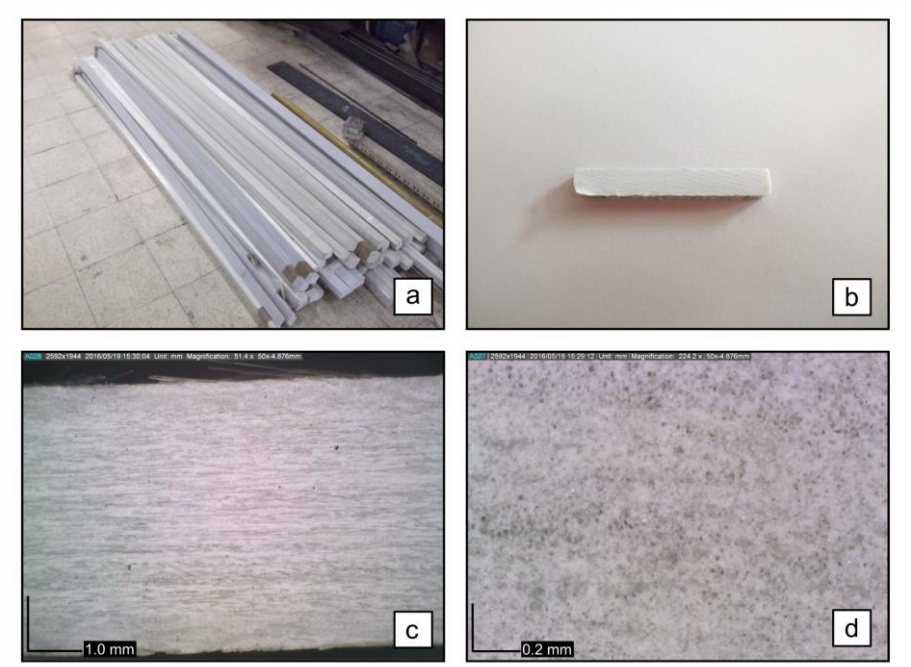

Figure 4.1. Pultruded GFRP profiles: (a) 3 m long (as received), (b) cross section, (c) 50× and (d) 220× magnification (core region).

4.2.2 Ageing environments

Different ageing environments were chosen to evaluate the susceptibility to degradation of pultruded GFRP profiles typical of civil engineering applications. In particular, the degradation effects of such exposure can be related to wet environments, coastal areas and outdoor conditions, as they are typical for GFRP structures, which are often selected due to their improved performance in relatively harsh environments.

Taking these factors into consideration, specimens of both types of profiles were subjected to the following environments, as shown in Table 4.1: (i) immersion in demineralized water at 20 °C, 40 °C and 60 °C; (ii) immersion in salt water at the same temperatures, and (iii) continuous condensation at 40 °C.

Immersion ageing in the above mentioned media was based on ISO 175 standard [4.8], while the salt water concentration was selected as indicated in ASTM D 1141 standard [4.9]. The 20 °C temperature was set as normal room temperature, corresponding to typical average temperatures encountered in mild climates, such as southern European countries.

Table 4.1. Ageing environments conditions

Ageing environments	**Label**	**Duration [months]**	**Conditions** [(a)]
Immersion in demineralised water	W20	0, 3, 6, 9, 12, 18, 24	T: 20 ± 3 °C
	W40		T: 40 ± 2 °C
	W60		T: 60 ± 2 °C
Immersion in salt water	S20	0, 3, 6, 9, 12, 18, 24	T: 20 ± 3 °C; 35 g/l NaCl
	S40		T: 40 ± 2 °C; 35 g/l NaCl
	S60		T: 60 ± 2 °C; 35 g/l NaCl
Continuous condensation	C40	0, 3, 6, 9, 12	T: 40 ± 2 °C; RH: 100%

[(a)] *Temperature (T); Relative Humidity (RH)*

Higher temperatures of 40 °C and 60 °C were selected to accelerate the diffusion process and to promote the hygrothermal degradation mechanisms; these values were carefully set, taking into account the need to remain well below the GFRP glass transition temperature (T_g), which was in the range of 106-112 °C for both UP and VE profiles (taken from onset of the E' modulus curve obtained from DMA tests, *cf.* Section 4.3.1), in order to avoid or limit any additional degradation mechanisms that occur when such temperature is approached or exceeded [4.6, 4.10].

The continuous condensation environment was provided by a condensation chamber that combines the effects of moisture and temperature. Specimens were hanged inside the chamber, not contacting with the chamber walls. Temperature and relative humidity (RH) values were defined according to ISO 6270-1 standard [4.11]. The considered ageing environments (appropriate chambers and containers) are depicted in Figure 4.2.

Prior to ageing, only longitudinal cuts were made in the GFRP material, using a water-cooled diamond saw blade; those cuts included 20 mm gaps for each side of the profile (as depicted in Figure 4.3 for tensile and flexural specimens), in order to accurately represent the bulk material and to minimize the cut sections, which are preferable points for water ingress. In other words, specimens were aged with the biggest geometry possible, instead of ageing small scale specimens (with geometries set by the standards corresponding to the different tests). After executing the longitudinal cuts, the profiles (33×340 mm^2) were preconditioned until constant weight in a ventilated chamber at 80 °C, according to ASTM D 5229 standard [4.12], before exposure to the different ageing environments.

At predefined exposure times, specimens were removed from the ageing environments, and then cut with the same diamond saw, in appropriate dimensions for characterisation testing

(described in the next section). In addition, later they were subjected to a desorption period, through conditioning until constant weight, through the same method described above, guaranteeing the aforementioned "dry-state".

Figure 4.2. Ageing environments: (a) containers for immersions at 20 °C; (b) and (c) chambers used for immersions at 40 °C and 60 °C; (d) condensation chamber.

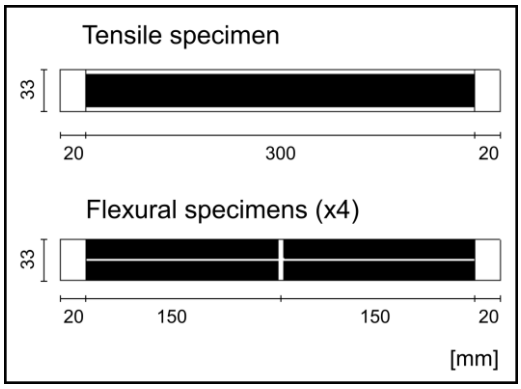

Figure 4.3. Specimen geometry during ageing (33 × 340 × 5 mm^3).

Finally, the specimens were placed in hermetically closed polyethylene recipients for transportation purposes and tested without further conditioning at controlled room temperature (20 ± 2 °C).

4.2.3 Characterisation methods

Both UP and VE profiles were subjected to different characterisation tests in order to determine their physical, viscoelastic and mechanical response when subjected to hygrothermal ageing, namely: (i) media diffusion, through gravimetric changes; (ii) thermo-mechanical behaviour,

through dynamic mechanical analysis (DMA); and (iii) mechanical behaviour, by means of tensile, flexural, and in-plane and interlaminar shear tests. Characterisation tests were conducted on each batch of test specimens after predetermined periods (*cf.* Table 4.1).

The mass variations during the hygrothermal ageing were assessed by means of gravimetric measurements. Specimens with $5 \times 15 \times 60$ mm^3 of geometry were periodically removed from the recipients and, after wiping the superficial water from all surfaces, were immediately weighted using a Mettler analytical balance to determine the percentage of absorbed water, according to ASTM D 5229 standard [4.12]. Subsequently, the specimens were immediately returned to the recipient. Two specimens per ageing condition were considered, as preliminary tests provided very consistent measurements (insignificant error margin).

The temperature-dependent behaviour and glass transition temperature (T_g) of the materials was assessed through dynamic mechanical analysis (DMA), according to parts 1 and 5 of ISO 6721 standard [4.13], using a DMA analyser from *TA instruments*, model *Q800*. GFRP specimens with geometry of $5 \times 15 \times 60$ mm^3 were tested in a three-point bending configuration at a constant frequency of 1 Hz and strain amplitude of 15 μm, from room temperature to 200 °C (in air), at a rate of 2 °C/min. The T_g was determined from the peak of the loss factor (tan δ) curve and from the storage modulus (E') curve as the extrapolated onset of its sigmoidal change, per the definition of ASTM E 1640 standard [4.14]. Three specimens per ageing condition and duration period were tested. Unfortunately, the results obtained from DMA tests for the last two batches of the UP specimens (*i.e.* at 18 and 24 months of ageing) were anomalous. Figure 4.4 illustrates the DMA equipment.

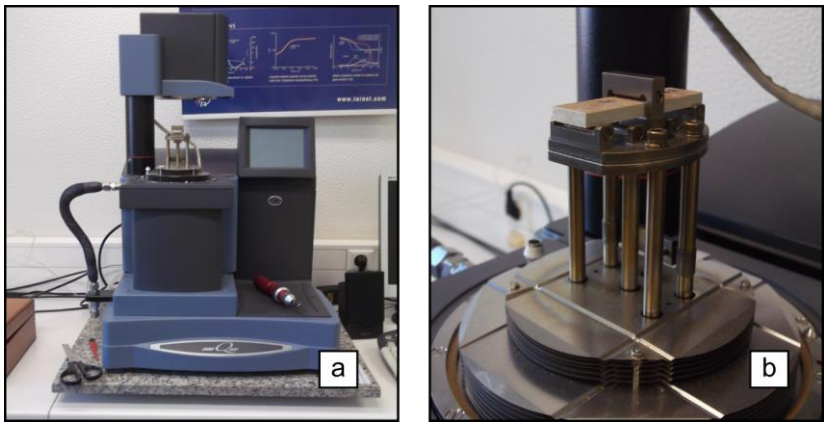

Figure 4.4. DMA equipment: (a) general view; (b) three-point bending configuration.

As mentioned, the mechanical properties were determined through (i) tensile, (ii) flexural, (iii) in-plane shear and (iv) interlaminar shear tests. At least five specimens were tested for each material and type of test.

The tensile properties of the GFRP laminates were determined according to parts 1 and 4 of ISO 527 standard [4.15] in rectangular specimens with 5 × 25 × 300 mm^3, without end tabs; tests were carried out in an *Instron 4803* universal testing machine (UTM) with 100 kN of load capacity, under displacement control, at a speed of 2 mm/min. The longitudinal strains were measured with an Instron 2630-112 clip-on extensometer, with a gauge length of 50 mm.

The flexural properties of the GFRP laminates were assessed according to ISO 14125 standard [4.16] in rectangular test specimens with 5 × 15 × 150 mm^3; specimens were tested in a three-point bending configuration in a 100 mm span using a *Seidner Form* testing machine with 10 kN of load capacity, under displacement control, at a speed of 2 mm/min.

The in-plane shear properties were determined from V-notched beam tests according to ASTM D 5379/D 5379 M standard [4.17]. The geometry of the specimens was 5 × 20 ×50 mm^3 for the GFRP laminates, comprising a 4 mm deep notch on both sides. Specimens were tested under displacement control, at a speed of 0.5 mm/min, using an *Instron 4803* UTS, integrating a 10 kN load cell and the Iosipescu apparatus. Shear strains at the notch were measured with a video extensometer constituted by a high definition *Sony XCG 5005E* video camera coupled with *Fujinon Fujifilm HF50SA-1* lens, which continuously monitored the position of target dots marked at the notched centre of the test specimens. Eight target dots were marked on each specimen, forming two square grids with size of 6 mm and 10 mm, at an equal distance from the specimen centre. The variation of their coordinates was used to calculate the shear strains.

The interlaminar shear strength of the GFRP laminates was determined in accordance to ASTM D 2344 standard [4.18] in specimens with 5 × 15 × 30 mm^3, tested in a 20 mm span. Tests were carried under displacement control at a speed of 1 mm/min, with the above-mentioned *Seidner Form* system.

The fixtures used for the mechanical tests are shown in Figure 4.5. For all the mechanical characterisation tests, at least five specimens per ageing condition and duration period were tested (ten for the unaged material).

Moreover, additional chemical and physical tests were performed to fully characterise the unaged materials, namely: (i) chemical composition, through Fourier Transform Infrared (FTIR) spectroscopy; (ii) constituent materials proportion, through calcination; and (iii) density, through the immersion method.

Infrared spectra of both profiles were assessed for initial characterisation by means of Fourier Transform Infrared (FTIR) spectroscopy in the 450–4000 cm^{-1} region. For these measurements,

powder samples, scraped from the surfaces of test specimens, were mixed with dry spectroscopic grade potassium bromide and pressed into pellets. 32 scans were collected and averaged at a spectral resolution of 4 cm^{-1} in a *Bruker Tensor 27* spectroscope, according to ASTM E 1252 standard [4.19]. This technique was used to provide initial detailed data on the surface constituents of the GFRP material.

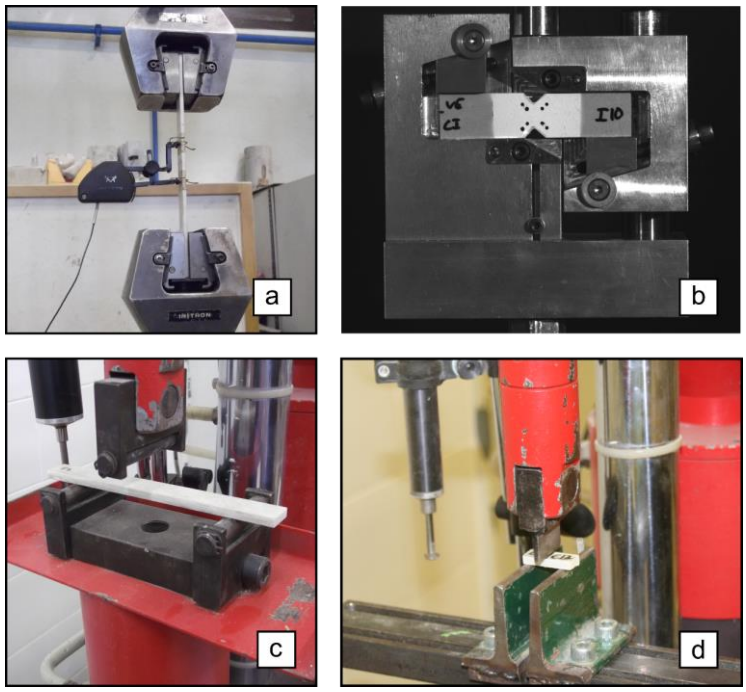

Figure 4.5. Mechanical tests: (a) tensile; (b) in-plane shear; (c) flexural, and (d) interlaminar shear.

The glass fibre content was determined by the calcination method, described in ISO 1172 standard [4.20], in three specimens with 20 × 10 × 5 mm^3, and the density of the materials was determined in accordance with method A of ISO 1183 (Part 1) standard [4.21], in three 0.5 mm^3 cubic specimens with 0.1 mg. Figure 4.6 illustrates the furnace as well as the remaining glass fibres (after calcination) in a representative specimen, where the CSM is easily identified above the unidirectional rovings.

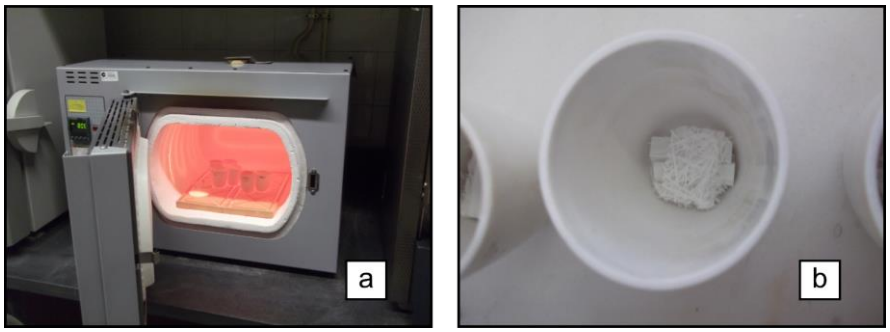

Figure 4.6. (a) Furnace; (b) remaining glass fibres after calcination.

4.3. Experimental results and discussion

4.3.1 Characterisation of reference GFRP materials (unaged)

The experimental results of physical-chemical characterisation of both profiles before ageing are listed in Table 4.2 (average ± standard deviation values are listed, where applicable).

Table 4.2. Physical and chemical properties of the unaged GFRP profiles.

Property	**Method**		**UP profile**	**VE profile**
Chemical composition	FTIR	FTIR spectra consistent with unsaturated polyester or vinylester, with presence of calcium carbonate and silica		
Glass fibre content	Calcination	[%]	65.3 ± 1.8	67.9 ± 1.8
Density	Immersion	[g/cm^3]	1.92	1.96
T_g	DMA	T_g (E'_{onset}) [°C]	112.3 ± 3.6	106.6 ± 1.3
		T_g (tan δ) [°C]	136.6 ± 0.4	124.1 ± 0.3
Mechanical properties	Tensile response	σ_{tu} [MPa]	479.5 ± 28.9	430.0 ± 33.8
		E_t [GPa]	37.4 ± 2.3	39.2 ± 0.5
		ε_{tu} [-]	0.014 ± 0.001	0.012 ± 0.001
	Flexural response	σ_{fu} [MPa]	552.6 ± 40.2	561.1 ± 16.8
		E_f [GPa]	21.4 ± 2.3	23.0 ± 0.8
		ε_{fu} [-]	0.024 ± 0.003	0.021 ± 0.001
	In-plane shear	τ_{max} [MPa]	53.7 ± 1.9	67.6 ± 2.1
		G [GPa]	3.0 ± 0.5	3.8 ± 0.6
		γ_u [-]	0.035 ± 0.006	0.035 ± 0.005
	Interlaminar shear	σ_{sbs} [MPa]	34.7 ± 4.5	37.8 ± 1.7

The chemical composition of both materials, determined by FTIR spectroscopy, was fairly similar and is illustrated in Figure 4.7.

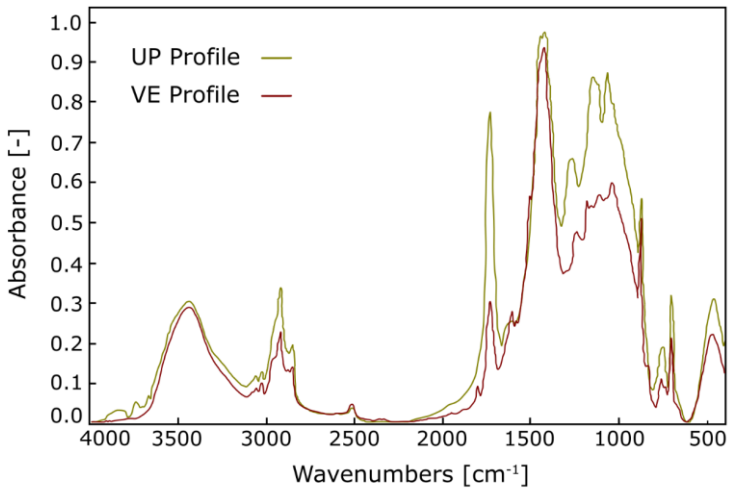

Figure 4.7. FTIR spectra of unaged UP and VE profiles.

The peaks' intensity and localisation confirmed the presence of the ester group, as well as aromatic and aliphatic molecular structures, usually common in both unsaturated polyester

and vinylester polymers. The FTIR spectra also show the presence of calcium carbonate (filler) and silica (from E-glass fibres). However, comparing both spectra it is possible to observe that the C=O peak located at 1730 cm^{-1} is more intense in the UP profile, which is indicative of the higher amount of ester groups present in unsaturated polyester in their chemical composition, as depicted in Figure 4.8.

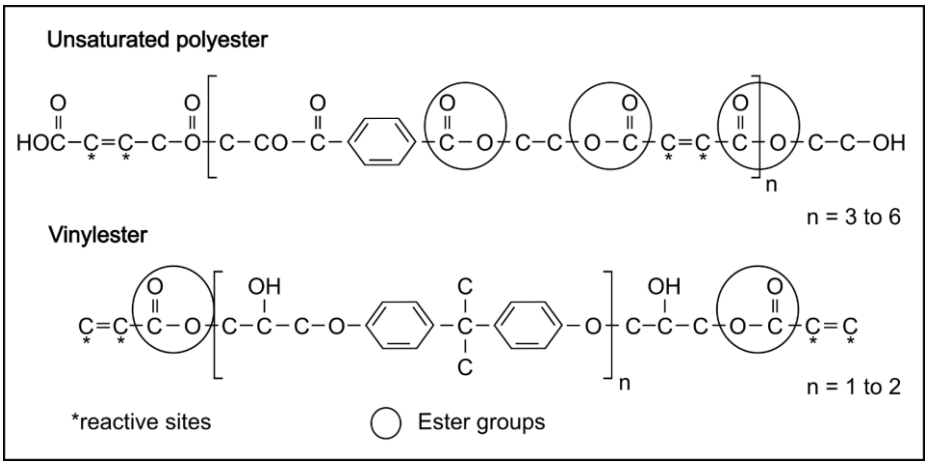

Figure 4.8.Chemical structure of UP and VE resins (adapted from [4.22]).

The glass fibre content and density of the UP profile were slightly lower when compared with the VE profile. The values obtained for both these physical properties are in the typical range for this type of materials, being consistent with previous works on these materials [4.5].

Figure 4.9 presents representative DMA curves (storage modulus, E', left axis - dashed lines and loss factor, tan δ, right axis - continuous lines).

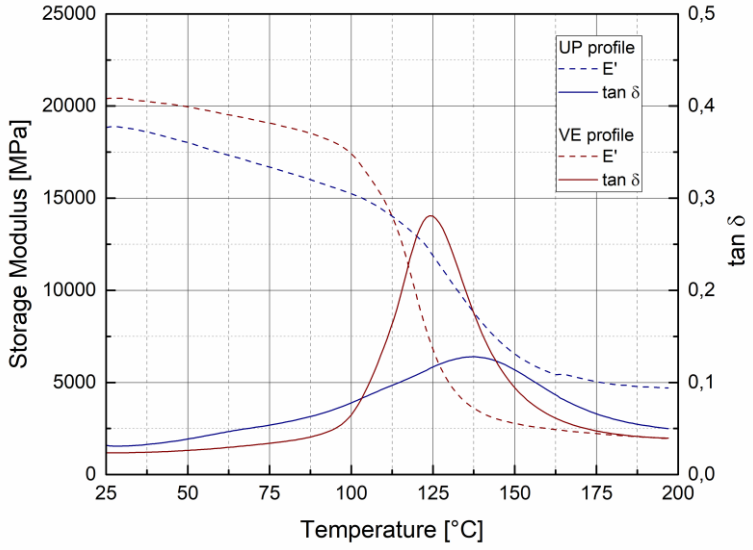

Figure 4.9. DMA experimental curves for unaged UP and VE profiles.

The E' curves presented the typical sigmoidal shape usually found in polymers and fibre reinforced polymer structures, with the onset of the reduction of E' occurring at 112 °C and 107 °C for the UP and VE profiles, respectively. From a mechanical point of view, these temperatures correspond to the beginning of a steep reduction in the profiles flexural stiffness. Moreover, the VE profile depicted higher values of the initial E' modulus, which should be related to the higher flexural stiffness when comparing both profiles (*cf.* Table 4.2), as well as a steeper drop in this curve, compared to the UP profile.

In a less conservative approach, the tan δ curve exhibited peaks at a higher temperature range of 124-137 °C, and the curve peak value was lower for the VE profile. The T_g values obtained from both the tan δ curve and the onset of the E' curve were slightly higher in the UP profile. Moreover, the tan δ peak value was significantly lower in the UP profile; this fact stems from the denser molecular arrangement of the ester groups in the polymeric chain of the UP profile, making it less sensitive to molecular rearrangements due to temperature [4.5].

Figure 4.10 presents representative stress *vs.* strain curves (stress *vs.* displacement in the interlaminar shear test) obtained from the different mechanical tests.

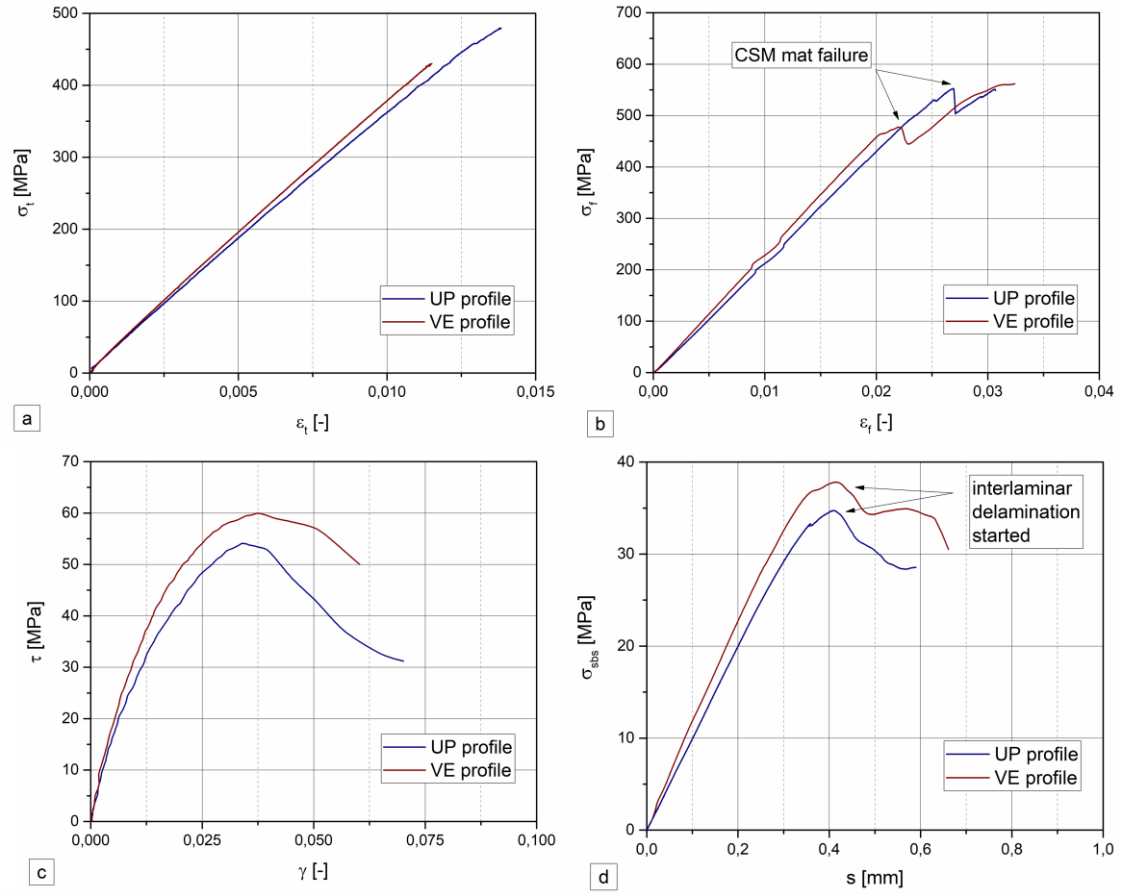

Figure 4.10. Representative experimental curves for different mechanical properties: (a) tensile; (b) flexural; (c) in-plane shear; (d) interlaminar shear.

In general, as expected, the mechanical tests indicated linear elastic behaviour until rupture, for both profiles; the single exception was the in-plane shear tests, where the material presented a progressive stiffness reduction (non-linear behaviour) after an initial linear response. The average mechanical properties obtained for both profiles are listed in Table 4.2. Overall, the VE profile presented higher elastic properties (stiffness), which is visible in Figure 4.10. Regarding the flexural, in-plane, and interlaminar shear strength, the two profiles presented similar values, slightly higher in the VE profile. However, the UP profile disclosed superior performance regarding the tensile strength properties, when compared to the VE profile.

Figure 4.11 illustrates the typical failure modes observed in the mechanical tests, which were as expected and quite similar for both profiles. Tensile failure (Figure 4.11 (a)) started with rupture of the CSM outer layers, followed by progressive rupture of the unidirectional glass fibres. Flexural failure started in the lower outer layer (*cf.* Figure 4.11 (b)), where tensile stresses are maximum, and progressed to the upper part of the section, causing rupture in the longitudinal fibres. In-plane shear failure (Figure 4.11 (c)) was characterised by vertical cracking between the notched edges of both the matrix and fibres (in the transverse direction). Finally, the interlaminar shear test caused failure to occur in the matrix at the central part of the specimen, and the consequent interlaminar delamination (*cf.* Figure 4.11 (d)). It is also worth mentioning that the failure modes were unaffected by hygrothermal ageing, while the mechanical properties suffered considerable variations.

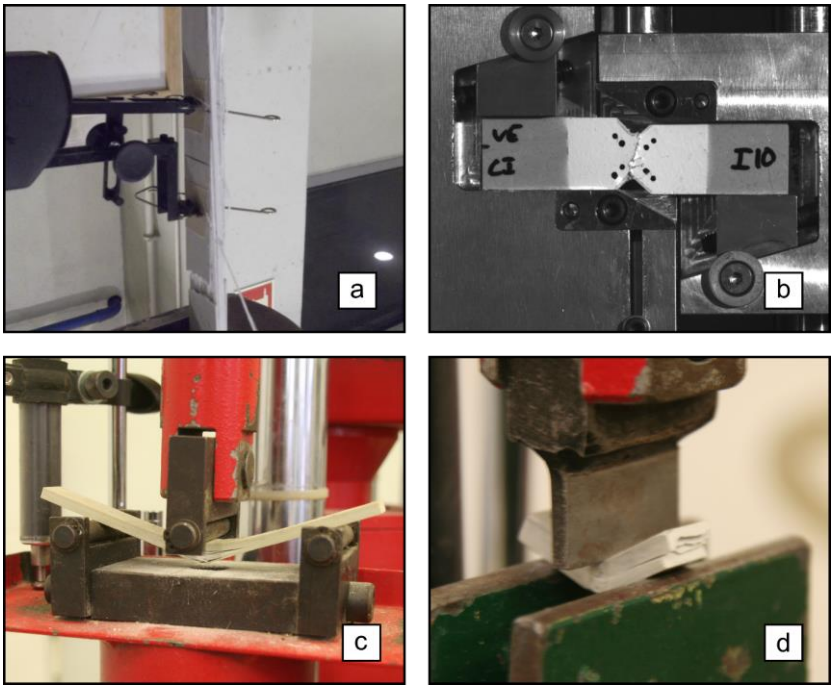

Figure 4.11. Typical failure modes in different mechanical tests: (a) tensile; (b) in-plane shear; (c) flexural; (d) interlaminar shear.

4.3.2 Sorption behaviour

Figure 4.12 shows the mass variation (experimental curves) as a function of the square root of the exposure time, for the different hygrothermal environments – immersions in demineralized and salt water at different temperatures (20, 40 and 60 °C) and continuous condensation at 40 °C, for both profiles.

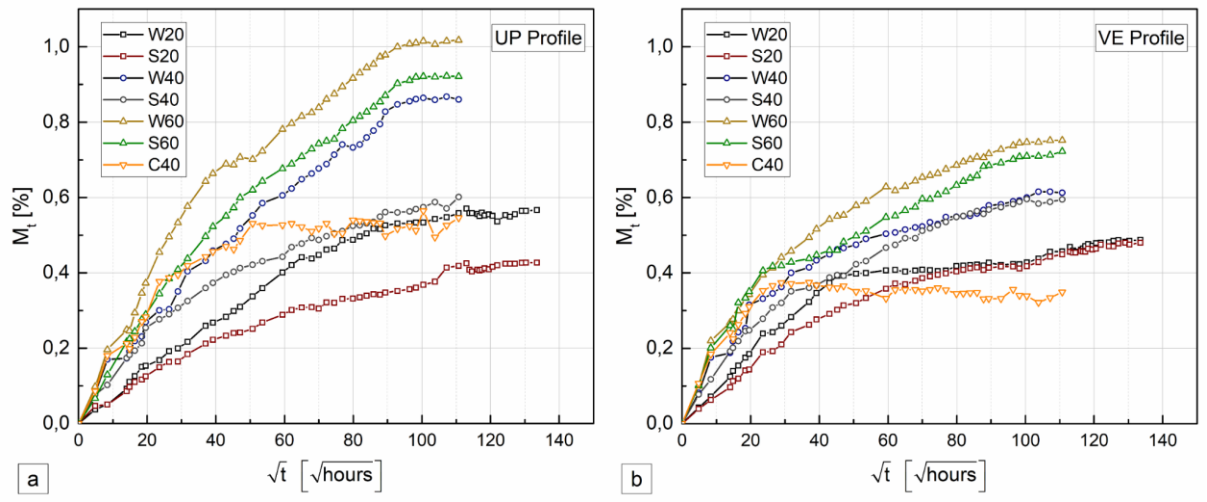

Figure 4.12. Mass uptake during hygrothermal ageing for (a) UP and (b) VE profiles.

Overall, mass uptake in the different ageing conditions showed a roughly approximated Fickian response. In fact, for both profiles water diffusion was significantly higher in earlier periods and approximated to nearly constant values at the later periods. However, as discussed in Chapter 3, water uptake can deviate from purely Fickian behaviour when considering longer exposure periods, where effects such as polymer relaxation may occur, causing differences from the theoretical response, as seen for some of the exposure environments, especially at higher temperatures (*e.g.* W60 and S60). In such cases, the water content is seemingly absorbed by the resin due the redistribution of voids and free volumes in the polymer network that are created through swelling effects caused by penetrant molecules. In addition, these molecules can force macro-molecular movement, causing even more water absorption by the polymer [4.23, 4.24].

In general, as expected, the UP profile had higher mass uptake in almost all ageing environments (excluding S20), when compared to the VE profile, due to the chemical nature of both matrix polymers, as pointed out by Chin *et al.* [4.25] and Cabral-Fonseca *et al.* [4.5]. According to those authors, moisture diffusion into the polymeric matrix occurs in different ways, in terms of moisture profile throughout the thickness, water uptake capacity and moisture ingress rate, and depend upon several microstructural and molecular aspects (*i.e.* molecular structure polarity and degree of cross-linking). These higher UP sorption parameters

are evident in Table 4.3, where the maximum experimental weight gain content (M_{max}) measured for each environment and respective time (t) are listed.

A clear and consistent temperature effect was noted in the experimental results for both profiles, where higher immersion temperatures corresponded progressively to higher water uptake, which is consistent with results reported in several previous works [4.2, 4.4-4.6].

Table 4.3. Maximum experimental weight changes.

Profile		**W20**	**S20**	**W40**	**S40**	**W60**	**S60**	**C40**
UP	M_{max} [%]	0.57	0.43	0.87	0.60	1.02	0.92	0.56
	t [days]	532	743	479	511	511	479	420
VE	M_{max} [%]	0.49	0.48	0.62	0.60	0.75	0.72	0.37
	t [days]	743	743	449	420	511	511	57

For instance, considering the VE profiles (*cf.* Figure 4.12 (b)), water uptake at 111 h^{-1} was 0.46%, 0.61% and 0.75% respectively for W20, W40, and W60 environments. However, higher temperatures can revert mass uptake, which is attributed to mass loss by extraction of low molecular weight segments. This effect, expected to increase with temperature, was found at 80 °C in a recent study concerning pultruded GFRP profiles with polyester matrix [4.6], and has also been reported to occur up from 60 °C in pultruded GFRP materials [4.5, 4.26, 4.29]. However, these effects were not found during the present experimental campaign.

For both profiles, when comparing both water and salt water at the same temperatures, it can be seen that the mass uptake is higher in the former medium. According to Jones [4.28], this effect can be attributed to the cross-linked polymeric matrix behaviour, enabling water movements and haltering large inorganic ions, thus acting as a semipermeable membrane. Previous studies [4.5, 4.31] also reported that the presence of salts such as NaCl in immersion media result in a reduction of the saturation value.

Continuous condensation at 40 °C, when compared to water immersions at the same temperature, involved a levelling off, with a saturation stage being reached clearly at lower exposure periods (around 50 and 25 h^{-1} for both UP and VE profiles, respectively) and for lower water uptake values (0.55% and 0.35%, respectively). However, in the earlier periods, during which higher diffusion rates were observed, the absorption for continuous condensation was comparable to that in water and salt-water immersion. These results are in accordance with Svetlik [4.4] findings, when comparing saturated to fully immersed environments. However, a contrary trend was reported in another study regarding the same materials [4.5], with higher initial rate of water absorption in the saturated environments.

Concerning the modelling of the diffusion process, both Fickian and two-phase Fickian diffusion models, explained in detail in Chapter 3, were implemented. Both models were fitted to the experimental data through a nonlinear curve fit, using an orthogonal distance regression iteration algorithm, available in the commercial software package *OriginPro* that retrieved the diffusion parameters of such models. Figure 4.13 depicts the comparison between the experimental results and the analytical models. Table 4.4 shows the moisture diffusion coefficients and the mean absolute percentage errors (MAPE) obtained.

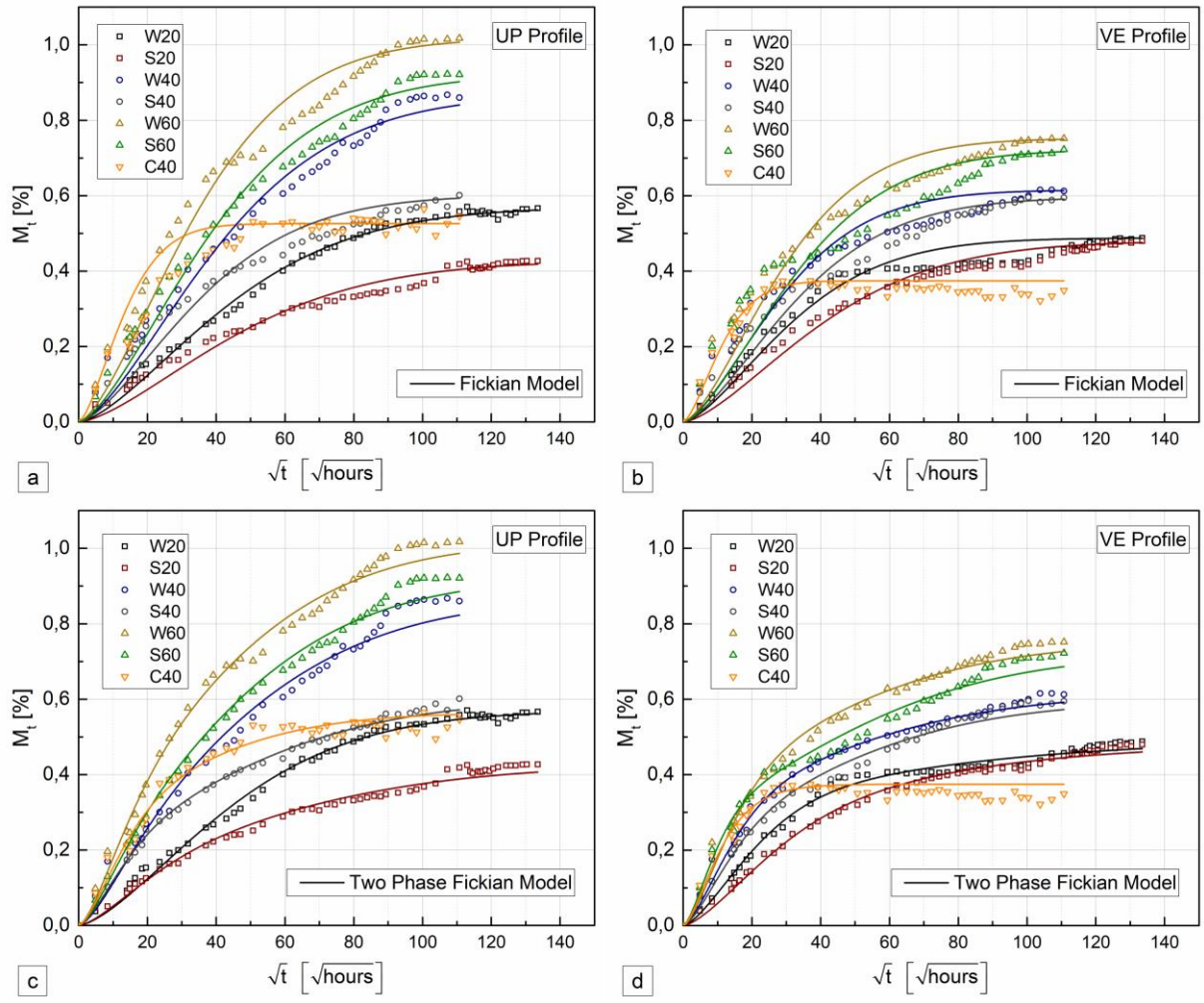

Figure 4.13. Diffusion models: (a) and (b) Fickian approach for UP and VE profiles; (c) and (d) two-phase Fickian approach for UP and VE profiles.

Overall, both models provided good fitting to the test data, which is reflected in the general low values of the MAPE. However, the two-phase Fickian diffusion model provided better agreement for both UP and VE profiles, with the MAPE ranging from 2.9% to 7.4%. The relative differences between the models should be due to the deviation of the experimental test data to a theoretical Fickian behaviour. Moreover, the diffusion coefficients obtained reflected the expected temperature-dependence of the GFRP profiles, increasing with temperature in

both water and salt water immersions. Comparing the different environments, there are no substantial differences in the quality of the estimates obtained for lower and higher temperature immersion results, and almost every estimate provided a good fit, which increases the method reliability. However, some difficulties were found in the C40 environment, in which higher MAPE values were obtained (8-17% in the Fickian diffusion model in both profiles). In addition, significantly high covariance values can be identified for the diffusion coefficients, proving to be somewhat inaccurate in this environment. This issue was also found when estimating the D_1 coefficient for the two-phase Fickian model in the same environment (VE profile). Another discrepancy was found in the S60 environment (VE profile) concerning the Fickian diffusion model. In this case, the MAPE is relatively higher (16%) than that obtained for the remaining environments for both profiles. Nonetheless, the diffusion coefficient has an acceptable covariance value (9%).

Table 4.4. UP and VE profiles diffusion properties.

Profile	**Model**	**Coefficients**	**W20**	**S20**	**W40**	**S40**	**W60**	**S60**	**C40**
UP	Fickian	M_∞ [%]	0.57	0.43	0.87	0.60	1.02	0.92	0.53
		D [$\times 10^{-7}$ mm^2/s]	1.87	1.45	2.84	2.10	3.02	2.39	20.4
		Cov. D [$\times 10^{-7}$ mm^2/s]	0.03	0.07	0.08	0.17	0.15	0.09	16.3
		MAPE [%]	5.4	10.5	10.3	12.5	10.0	9.5	17.4
VE	Fickian	M_∞ [%]	0.49	0.48	0.62	0.60	0.75	0.72	0.37
		D [$\times 10^{-7}$ mm^2/s]	2.85	2.17	4.09	3.26	4.82	3.73	27.7
		Cov. D [$\times 10^{-7}$ mm^2/s]	0.23	0.08	0.32	0.20	0.30	0.31	2.89
		MAPE [%]	9.3	8.6	11.9	11.9	11.4	15.6	7.5
UP	Two Phase Fickian	M_1 [%]	0.14	0.15	0.19	0.22	0.30	0.19	0.29
		M_2 [%]	0.43	0.28	0.68	0.38	0.72	0.73	0.27
		D_1 [$\times 10^{-7}$ mm^2/s]	1.87	9.03	14.8	21.9	19.9	22.8	22.9
		Cov. D_1 [$\times 10^{-7}$ mm^2/s]	0.29	1.18	2.72	1.65	2.82	4.53	3.36
		D_2 [$\times 10^{-7}$ mm^2/s]	1.87	0.98	1.52	1.41	1.84	1.72	2.57
		Cov. D_2 [$\times 10^{-7}$ mm^2/s	0.10	0.04	0.07	0.03	0.06	0.05	0.25
		MAPE [%]	5.4	5.7	6.4	2.9	4.7	3.4	6.0
VE	Two Phase Fickian	M_1 [%]	0.33	0.28	0.32	0.25	0.38	0.30	0.21
		M_2 [%]	0.16	0.20	0.30	0.35	0.37	0.42	0.16
		D_1 [$\times 10^{-7}$ mm^2/s]	8.69	5.50	19.4	20.1	19.9	43.9	43.7
		Cov. D_1 [$\times 10^{-7}$ mm^2/s]	0.45	0.27	1.38	2.24	1.62	6.41	20.5
		D_2 [$\times 10^{-7}$ mm^2/s]	0.72	0.84	1.38	1.50	1.50	1.33	16.9
		Cov. D_2 [$\times 10^{-7}$ mm^2/s	0.04	0.03	0.06	0.07	0.07	0.06	7.53
		MAPE [%]	3.6	3.9	3.7	4.7	3.9	4.4	7.4

4.3.3 Characterisation of the thermo-mechanical response

Figure 4.14 shows representative DMA curves (storage modulus, E', left axis - dashed lines and loss factor, tan δ, right axis – continuous lines) obtained for unaged and aged profiles subjected to the different ageing environments for the selected periods. Note that salt water and continuous condensation environments are not represented; in fact, in both UP and VE profiles

their behaviour was fairly similar when compared to water immersion environments at the same temperature.

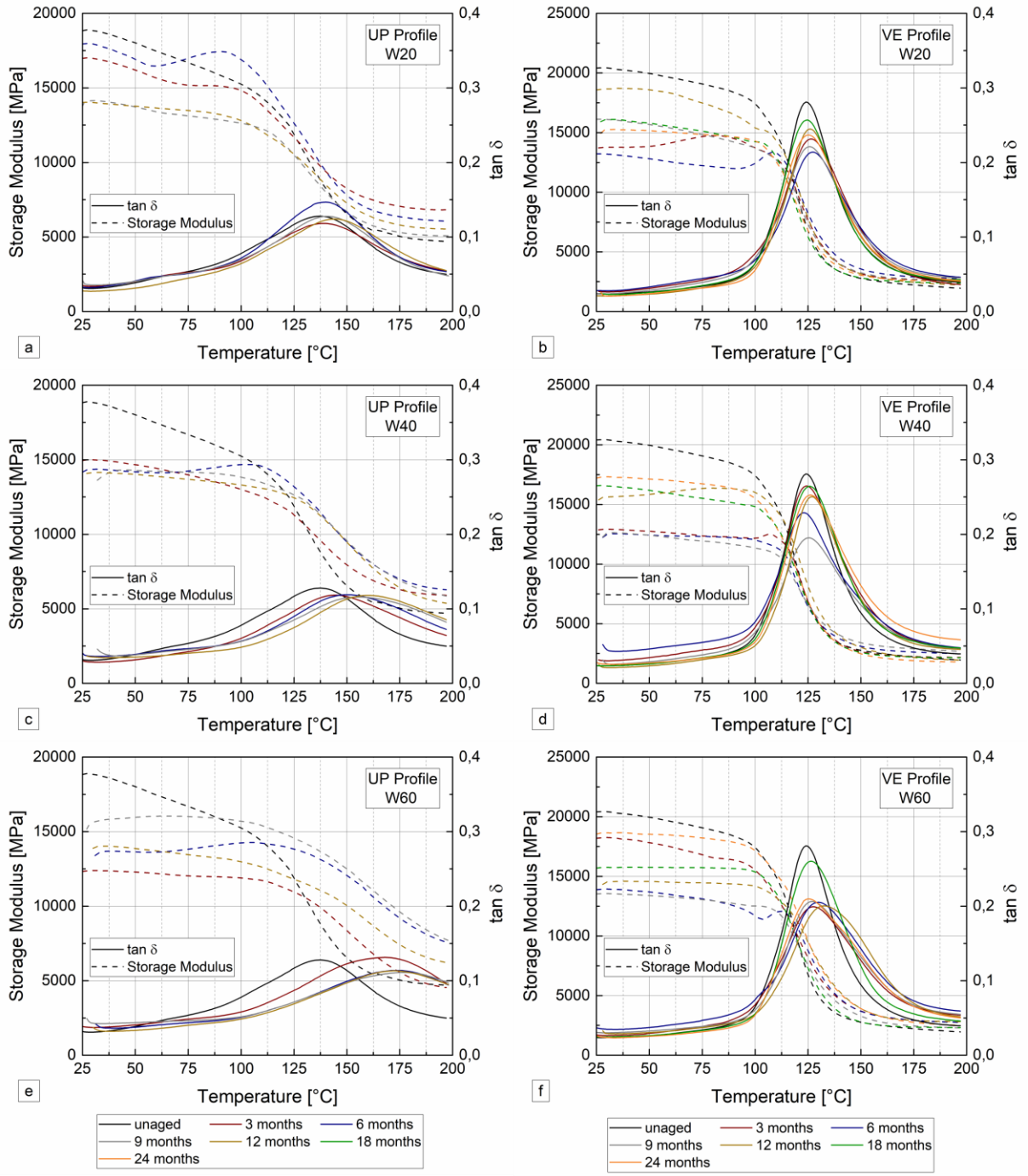

Figure 4.14. DMA curves for water immersion at distinct temperatures and periods of time: at 20 °C for (a) UP and (b) VE profiles; at 40 °C for UP (c) and VE (d) profiles; at 60 °C for UP (e) and VE (f) profiles.

Concerning water immersion in both profiles, regardless of the immersion time and temperature, the E' curves present the typical sigmoidal shape of these materials: after a glassy plateau, the storage modulus drops (more steeply for the VE profile, and more softly for the UP profile) up to approximately 10-20% of the initial values. The curve shape reflects mainly

the changes in the viscoelastic polymer matrix (progressing from a glassy to an elastomeric state), since the glass fibres do not suffer stiffness reduction in this temperature range [4.5] and did not seem to be affected by ageing; some deviations occurred (*e.g.* Figure 4.14 (a) E' curve at 6 months), which consisted of two inflexion changes before the curve drop, first decreasing and subsequently increasing the storage modulus values. It is important to add that this deviation occurred only in just a few specimens and periods of time.

Nonetheless, this fact should stem from residual water molecules that were still trapped inside the specimens (even considering the drying process), since it occurred somewhat close to 100 °C. Considering 25 °C as a representative temperature of the glassy plateau, an initial decrease can be identified in both profiles. This decrease was softer for the UP profile at W20, where a progressive lowering can be seen up to 12 months of ageing, followed by a later stabilisation in the subsequent periods. This effect was more pronounced at higher temperatures and can be attributed to the remaining absorbed water acting as a plasticizer [4.7]. As for the VE profile, this decrease was harsher right after 2 months of ageing regardless of the exposing temperature. Grammatikos *et al.* [4.6] observed this tendency for pultruded UP profile at lower temperatures (20 °C). However, at 40 °C an initial drop was reported followed by an increase that exceeded the unaged values; while at 60 °C the increase occurred right after 28 days and this trend continued for the remainder of the studied period. These differences should stem from the different "dry" *vs.* "wet" conditioning. However, Cabral-Fonseca *et al.* [4.5] studied similar profiles in a wet condition and reported in general similar trends for the E' curve.

In addition, concerning the UP profile, the tan δ curve presented a right shift, that occurred progressively up to 12 months. This shift was significantly temperature-dependent and consequently increased the T_g. Similar effects have been reported in previous works, but only for higher temperatures [4.5] or lower exposure times [4.7], and have been attributed to post-curing phenomena. However, the main difference between the studies lies in the drying procedure, that should contribute to accentuate the post-curing effects, while attenuating some physical degradation (plasticization) that the specimens might have suffered, both effects contributing positively to this change. Post-cure is bound to happen during hygrothermal ageing of GFRP profiles, especially at higher temperatures, and is well documented [4.5, 4.7, 4.10, 4.30]. The tan δ curves also presented some widening of the base, which seemed to increase with temperature, and suggested that some changes occurred at the molecular structure.

Concerning the VE profile, little changes occurred in the tan δ curve, except some progressive lowering of the curve height, which was also more noticeable at higher temperatures; this suggests the occurrence of post-cure phenomena, also reported by Karbhari [4.7]. The results for salt water immersion and continuous condensation were very similar to those discussed above, regarding the main trends of variation and the corresponding T_g values (described next).

Figure 4.15 present the changes in T_g estimates (average ± standard deviation) obtained from the two alternate methods described in Section 4.2.3: (i) the peak of the tan δ curve ($T_{g,\,\tan\delta}$), and (ii) the onset of the drop in the E' curve ($T_{g,\,\text{E'onset}}$).

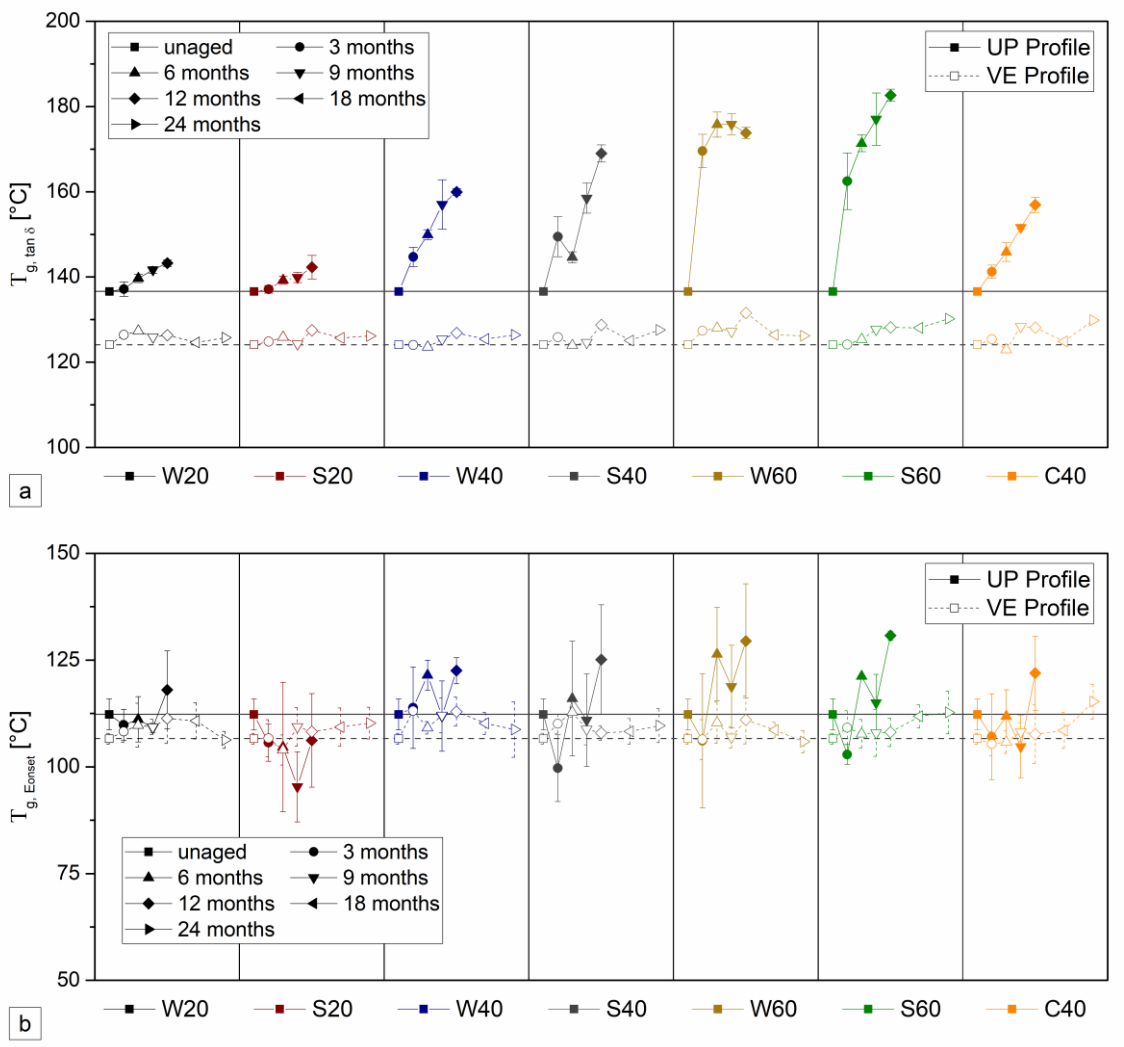

Figure 4.15. Variations of the glass transition temperature for the different ageing environments and profiles: (a) $T_{g,\tan\delta}$, and (b) $T_{g,\text{E'onset}}$.[3]

[3] As mentioned above, it was not possible to obtain estimates of the T_g of the UP profile after 18 and 24 months of ageing.

For the UP profile, water immersion showed a general increasing trend of T_g from the unaged values up to 12 months, which was accentuated with temperature. This effect was clearer in $T_{g,\,\tan\delta}$, which showed increases of 5%, 17% and 27% for W20, W40 and W60 environments, respectively.

Since the material could have not been fully cured, the degradation suffered by the ageing mechanisms may have resulted in a competing process with post-curing phenomenon. In fact, the higher temperature may have also contributed to these post-curing effects, attenuating and even compensating the overall degradation. These findings are consistent with the parallel study performed on polymeric adhesives for similar periods, presented in Chapters 8 and 9.

Salt water and continuous condensation showed the exact same trends when compared to immersion at the same temperature (slightly higher increase of T_g for S40 and S60, compared to W40 and S60, respectively). Moreover, the same overall trend of increasing T_g (with some fluctuations for the salt water immersions) can also be found in the $T_{g,\,\text{E'onset}}$ for the UP profile, although with slightly less increases (5%, 9% and 16% for W20, W40 and W60 at 12 months, respectively) and coupled with some irregular drops. This non-monotonic pattern of variation of the T_g has also been reported elsewhere [4.7].

Regarding the VE profile, little changes occurred in $T_{g,\,\tan\delta}$, with some insignificant increases at the higher temperatures (maximum of 4%) for the later exposure periods. The variation was less dependent from the immersion temperature, and less significant when compared to the UP profile, which is in accordance with previous investigations [4.5]. The consistency of the results obtained for water, salt water and continuous condensation is also observed, including for the different temperatures (in case of immersions). The $T_{g,\,\text{E'onset}}$ presented similar variation compared to the $T_{g,\,\tan\delta}$ (*i.e.* small variations). Comparing with the results obtained for the UP profile, the nature of VE polymer (less ester groups, positioned in the extremities of the molecular structure, and a tougher chain) makes it less susceptible to water degradation by hydrolysis [4.22], and also more resistant to the above-mentioned plasticization mechanisms [4.5]. As such, the same positive effects due to drying resulted in a very stable T_g performance, even at higher temperatures (up to 60 °C).

In summary, in the present study, less overall degradation on T_g has been found for both profiles when comparing to other investigations [4.4-4.7, 4.25]. As already discussed, this was most likely due to the drying process, which allowed to attenuate some degradation mechanisms and fomented a competing post-curing effect. Altogether, this resulted in fluctuations in the T_g as a function of the exposure period, which was more evident in the UP profile.

4.3.4 Characterisation of the tensile response

All tensile tests were conducted up to the specimen failure. The failure mode (*cf.* Section 4.3.1) was the same throughout the different ageing periods. However, hygrothermal ageing affected both tensile strength (σ_t) and modulus (E_t). Figure 4.16 depicts the stress *vs.* strain curves for representative specimens of both profiles subjected to one of the ageing environments (W60 - the harsher), as an example, where the ageing effects on both properties are evident.

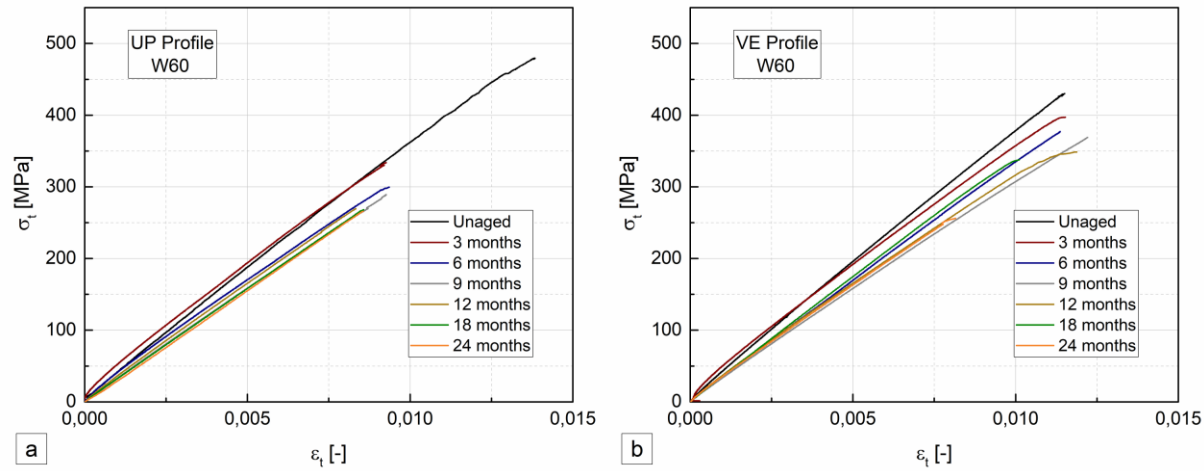

Figure 4.16. Tensile stress *vs.* strain curves at different ageing times for immersion in water at 60 °C: (a) UP and (b) VE profiles.

The effects of hygrothermal ageing on the tensile strength and modulus of the UP and VE profiles for all ageing environments (average ± standard deviation) are shown in Figure 4.17.

Regarding the **UP profile**, the global negative effect of water uptake on the tensile properties was more evident in the tensile strength. General progressive reductions occurred for both properties and they were clearly temperature dependent. The results obtained indicate that irreversible degradation took place. In addition, the tensile strength of the UP profile presented a higher initial reduction at 3 months, corresponding to the initial period where higher water uptake also occurred. Reductions between 8-12%, 18-21%, and 21-28% occurred for immersions at 20 °C, 40 °C, and 60 °C, respectively. Afterwards, it increased (as mentioned) or stabilised for W20 and S20, respectively, which most likely stemmed from the desorption period that should have attenuated some reversible degradation, and possibly increased the post curing effects. However, the decreasing trend was still noted at the remaining ageing environments, although at a lower rate, suggesting that the high temperatures continued to promote irreversible degradation mechanisms, such as hydrolysis. These competing degradation mechanism have already been reported in previous works [4.2, 4.4, 4.7, 4.10, 4.25, 4.28].

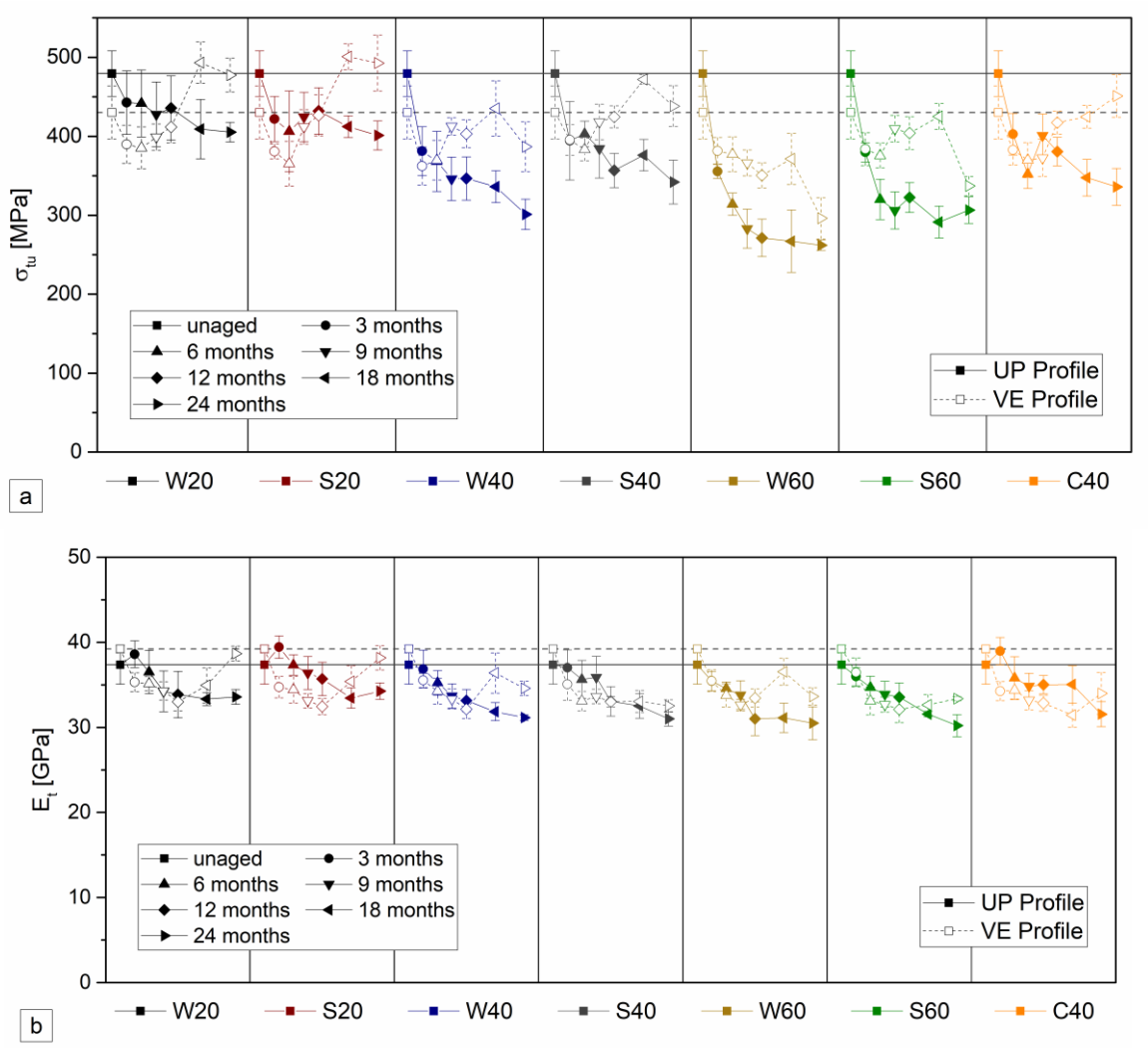

Figure 4.17. Variations of tensile (a) strength and (b) modulus, for both profiles, during the different ageing environments.

In agreement to the water uptake behaviour, salt water environments caused similar changes when compared to water at the same temperature, although indicating less overall degradation (especially at higher temperatures). In addition, the continuous condensation environment also presented similar trends when compared to immersions at the same temperature.

After 24 months of hygrothermal ageing, reductions in tensile strength of 15-16%, 29-37%, 36-45% and 30% were observed for immersions at 20 °C, 40 °C, 60 °C, and C40, respectively.

The tensile modulus of the UP profile was less affected - despite not showing a higher initial drop (observed in the tensile strength), it presented a general decaying trend over the time of exposure, with a monotonic/steady reduction trend with almost no signs of recovery (apart from 3 months at W20, S20, and C40, for which the tensile modulus was 3-5% higher than that of unaged specimens). Although the reduction of tensile modulus was more pronounced for higher temperatures, this effect was not so evident when compared to tensile strength. Salt

water immersions had roughly the same effects as water immersions and the same can be said for C40 compared to immersion at 40 °C.

After 24 months of exposure, the tensile modulus reduced by 8-10%, 16-17%, 18-19%, and 16% for immersions at 20 °C, 40 °C, 60 °C, and C40, respectively.

Different effects were found in the **VE profile**. In fact, apart from immersions at 60 °C (W60 and S60), in all ageing environments the tensile strength presented an early decrease up to 9 months, which was of the same order of magnitude for the 20 °C and 40 °C immersions (10-15%, 11-14% reductions, respectively), and was followed by a progressive increase up to 24 months of exposure, even exceeding the unaged values for some environments. This increase probably stemmed from the already mentioned residual curing competing mechanisms, and seemed to be more significant in the lower temperature environments. In the last exposure period at W40 this increase was not observed, with tensile strength presenting a slight reduction. C40 presented similar changes when compared to W40 and S40. Immersions at 60 °C caused the highest degradation in tensile strength: for W60 there was an almost monotonic decrease during the whole exposure period and for S60 a general reduction trend took place (with a slight increase from 12 to 18 months), suggesting that irreversible degradation occurs and is more relevant at higher temperatures. After 24 months of hygrothermal ageing, the tensile strength increased by 11-15%, 2% and 5% for the 20 °C immersions, S40, and C40 respectively. On the other hand, reductions of 10%, 31% and 22% were observed for W40, W60 and S60 environments at the same period. Overall, compared to the UP profiles, the tensile strength of the VE profile was less affected. Even considering that the VE profile had lower initial tensile strength, it was less susceptible to hygrothermal degradation effects.

The tensile modulus of the VE profile presented an initial higher drop at 3 months of ageing for all environments, a subsequent lower reduction throughout the exposure time, and then tended to a plateau at later stages of exposure. The 20 °C immersions and W40 also showed some property recovery up from 12 months. In this case, the temperature dependency of the tensile modulus variation was not evident, *i.e.* this property exhibited similar degradation levels for lower and higher temperatures of immersion (despite the last periods at 20 °C). Similarly, the tensile strength (and tensile properties of the UP profile), as expected, salt water and continuous condensation had the same correlations with immersion in water at the same temperatures. At 24 months, the tensile modulus presented reductions of 1-3%, 12-17%, 14-15%, and 13% for immersions at 20 °C, 40 °C, 60 °C, and C40, respectively.

The same degradation mechanisms that were referred to affect the tensile properties of the UP profile should have also affected the VE profile. The differences between the magnitudes and trends of the degradation experienced by their tensile properties should stem from (i) the higher chemical resistance of the VE profile, together with (ii) the reduction of the physical degradation mechanisms due to the drying process, which made the post-curing phenomena more relevant, since it had less "competition" in the VE profile.

These results are consistent with findings reported in previous works on the tensile properties of similar pultruded profiles [4.5, 4.6, 4.27]. However, the degradation levels in the present study were lower, and the performance increase exhibited by the VE profile was higher, and this should be attributed to the desorption period before testing the specimens. Chu *et al.* [4.2] also studied pultruded vinylester-GFRP and reported similar decaying trends, which were also more significant at early stages, in agreement with the results obtained here. However, despite the occurrence of post-curing, noted in DMA tests, its effects were not visible in the retention of tensile properties. It is also worth mentioning that the desorption period used in that study did not cause significant differences in tensile properties retention. These differences to the present study may be due to dissimilarities in specimen thickness (only 1.6 mm in [4.2]).

4.3.5 Characterisation of the flexural response

As for the tensile tests, all specimens were tested monotonically in bending until rupture. Despite maintaining the same failure mechanisms throughout the ageing periods, flexural properties were also affected by hygrothermal ageing. Figure 4.18 depicts experimental stress *vs.* strain curves for representative specimens of both profiles exposed to one of the ageing environments (W60), as an example of the changes in flexural strength (σ_f) and stiffness (E_f).

A generalised reduction of flexural strength can be identified with the increase of exposure time, while stiffness presented irregular (non-monotonic) variations with some sign of recovery. It is also interesting to note that the constitutive behaviour in the brink of collapse changed during ageing: while for unaged specimens and for shorter ageing durations, there was some stress recovery after the tensile failure of the lower CSM, for the latter periods of exposure, where higher degradation effects are bound to occur, the flexural stress did not increase after the failure of the lower CSM; this is indicative of degradation of the unidirectional rovings and of the interfaces between layers of fibre reinforcement.

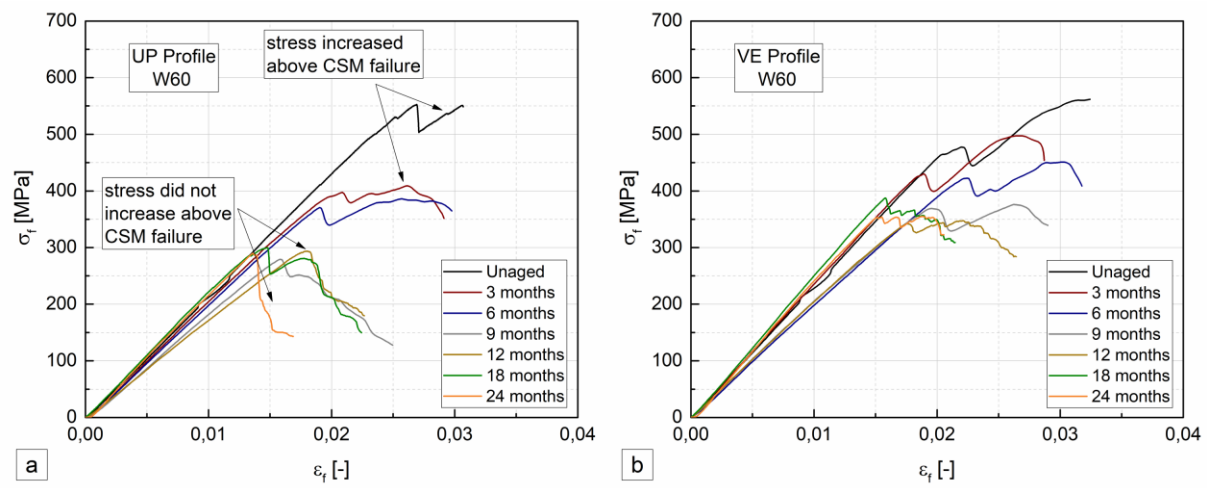

Figure 4.18. Flexure stress-strain curves at different ageing times for immersion in water at 60 °C: (a) UP and (b) VE profiles.

The effects of all types of hygrothermal ageing environments on the flexural strength and modulus of the UP and VE profiles (average ± standard deviation) are shown in Figure 4.19.

In general, as for the tensile strength, for both profiles the level of degradation in flexural strength increased with the temperature of the immersion media, being maximum at 60 °C. Both profiles exhibited similar behaviour when comparing immersions at 20 °C, with an initial gradual and progressive reduction, followed by a stabilisation trend after 12 months of ageing. Similar trends are observed for the higher temperature environments, however with a steeper and more pronounced initial reduction. In the 40 °C and 60 °C ageing environments similar effects were found for both profiles, consisting of a higher initial reduction of flexural strength up to 9 months (27-31%) and then a slower (but yet monotonic) reduction up to 24 months.

Unlike the tensile tests, no apparent recovery was found, even in the VE profile, which should stem from the higher influence of the polymer matrix and interface properties in the flexural tests, when compared to tensile tests (more fibre-dominated). These trends are in accordance with previous results [4.5]. In any case, as expected, the VE profile exhibited less reduction in flexural strength than the UP profile, especially at 40 °C and 60 °C.

After 24 months, the flexural strength of the UP profile presented reductions of 9-15%, 23-24%, 39-48%, and 30% for immersions at 20 °C, 40 °C, 60 °C, and C40, respectively, while those figures were 9-10%, 18-20%, 23-37%, and 16% in the VE profile.

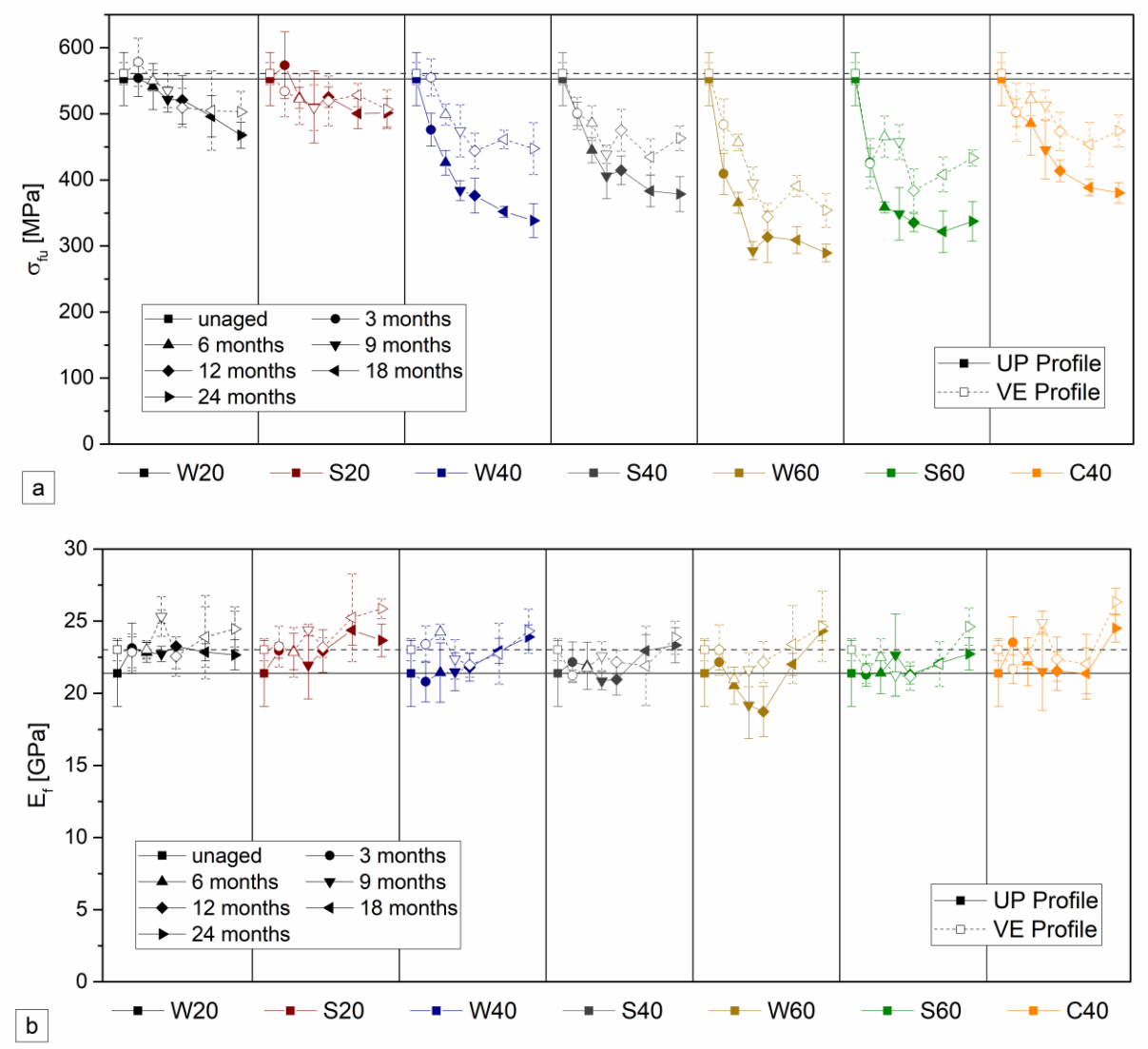

Figure 4.19 Variations of (a) flexural strength, and (b) modulus, for both profiles, during the different ageing environments.

The variation following exposure to continuous condensation was again roughly similar to that in immersion environments at the same temperature, and the flexural strength after water immersions were usually slightly higher when compared to salt water immersions. However, Liao et *al.* [4.33] reported different results when studying effects of saline environment. In previous studies [4.5, 4.26, 4.27, 4.34] that analysed the flexural properties of GFRP profiles made of UP and VE resins, in which a desorption period was not considered, higher overall reduction was found due to hygrothermal aging, especially in the VE profile. This fact should be attributed to the drying effects already mentioned in the tensile properties that have been confirmed to contribute to attenuate and eventually recover some of the physical degradation mechanisms, such as plasticization [4.7].

Regarding flexural modulus, much alike the tensile modulus, a more irregular variation (non-monotonic) was found for both profiles. Overall, the VE profile displayed better performance and presented usually higher stiffness values than the PU profile. However, since the unaged flexural modulus was also higher, the moduli retentions were similar. Again, similarly to the tensile modulus, temperature did not seem to have a significant effect in the flexural modulus of both profiles. After 9 months, some property recovery can be identified, which should be associated with the aforementioned post-cure effects. This recovery is more evident in the UP profile, being consistent with the DMA test results. After 24 months of hygrothermal ageing, the flexural modulus of the UP profile presented 6-11%, 9-11%, 6-13% and 15% increase when compared to the unaged values, for immersions at 20 °C, 40 °C, 60 °C, and C40, respectively. The same figures for the VE profile were 6-12%, 4-6%, 7% and 14% (increase). These irregular trends in flexural modulus variation associated with post-curing were also reported by Visco *et al.* [4.34] (VE profiles), being also in agreement with Cabral-Fonseca *et al.* [4.5]. These effects were attributed to the possible development of residual stresses in the cross-section due to differential moisture uptake throughout the specimen's cross section.

4.3.6 Characterisation of the in-plane shear response

As for the other mechanical tests, all specimens were tested monotonically in shear until rupture. Figure 4.20 depicts the in-plane shear stress *vs.* strain behaviour of one representative specimen of both profiles for one of the ageing environments (W60), as an example of the changes exhibited by the in-plane shear strength (τ) and stiffness (G).

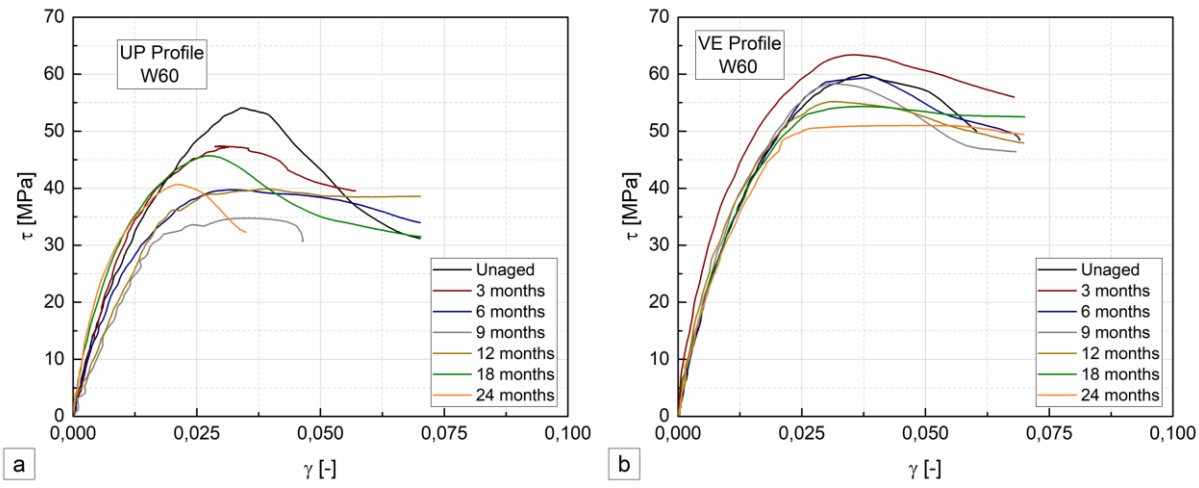

Figure 4.20. In-plane shear stress *vs.* strain curves at different ageing times for immersion in water at 60 °C: (a) UP and (b) VE profiles.

The variations in both properties are evident with the ageing time, especially in what concerns the maximum shear stress (τ_{max}) that specimens could resist. In this test, the much better

performance of the VE profile is clearer than in the previous tests, as the shear properties are more matrix-dependent, highlighting the differences in short- and long-term performance of both types of polymer matrixes.

Figure 4.21 summarizes the effects of hygrothermal ageing on the shear modulus and strength (average ± standard deviation) of the UP and VE profiles for all ageing environments.

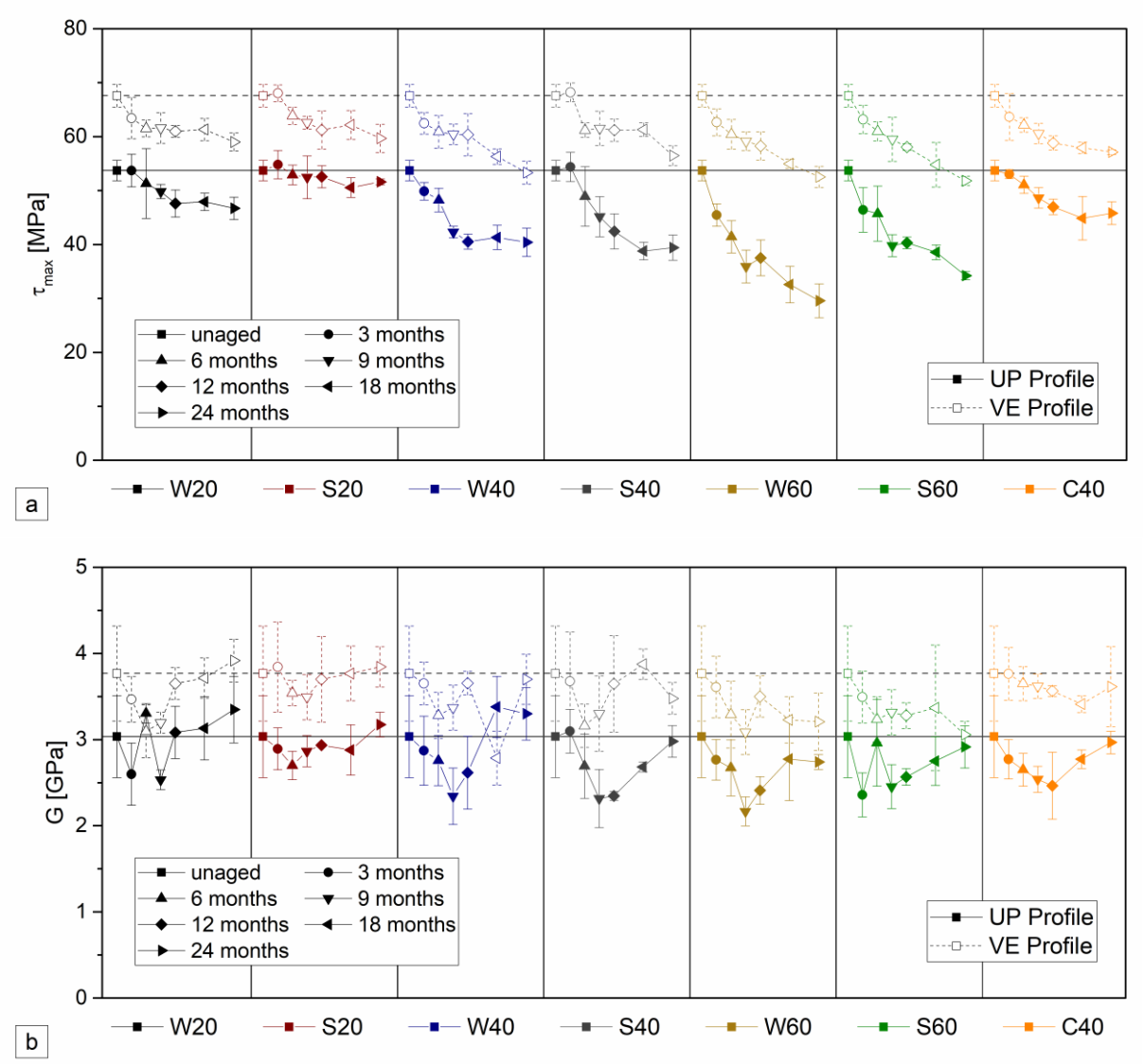

Figure 4.21. Variations of (a) in-plane shear strength and (b) modulus, for both profiles, during different ageing environments.

The general effects of hygrothermal ageing on the in-plane shear strength corresponded to a general monotonic degradation trend, with a clear strength reduction with increasing time and temperature of exposure. These effects are usually attributed to plasticization of the polymer matrix and other degrading mechanisms, such as micro-cracking, that can contribute to the reduction of the shear properties [4.31].

As mentioned above, the VE resin afforded superior performance in all ageing environments, and even at the latter exposure periods, the VE profile still exhibited higher shear strength when compared to that of the unaged UP profile.

For the 20 °C and 40 °C immersions, a gradual reduction of in-plane shear strength is noted up to 9 months, which then progressed to a stabilization plateau, analogously to the flexural strength. For the 60 °C immersions, reductions of in-plane shear strength occurred in a more continuous way – a stabilization plateau was not visible throughout the whole ageing period. For both profiles, no apparent recovery was found for this property, which should stem from the higher chemical degradation undergone by the polymer matrixes when compared to that experienced by the glass fibres; this explanation is supported by the differences encountered between the tensile and flexural tests, that were even more significant in the shear tests. After 24 months of exposure, the in-plane shear strength of the UP profile presented reductions of 4-13%, 25-27%, 36-45%, and 15% for immersions at 20 °C, 40 °C, 60 °C, and C40, respectively, while those figures were 12-13%, 17-21%, 22-23%, and 15% for the VE profile. These values are consistent with results of similar tests conducted by Grammatikos *et al.* [4.31]. These authors studied the in-plane shear properties of a pultruded unsaturated polyester GFRP flat sheet. Despite the similarities in terms of temperature dependence of the shear strength reduction, the authors also reported evidence of strength increase due to additional cross-linking associated with post-curing effects in the matrix, after 112 days, which were not seen in the present research. These differences should stem from the shorter exposure periods (maximum of 6 months) used in their tests, which did not allow to promote the effects that occur at longer exposure periods, as well as the lower fibre glass content in the studied sheet, causing higher amounts of resin and thus increasing the susceptibility of the GFRP sheet to post-curing effects.

Regarding the in-plane shear modulus, an apparent monotonic reduction is noted up to 9 months for most of the ageing environments, followed by a significant recovery up to 24 months. Temperature dependence is also noted, however to a lesser extent compared to shear strength. As for the other elastic properties, the variation pattern of shear modulus was more irregular and had higher scatter compared to shear strength. The highest reductions were found at 9 months and at the higher temperature environments, ranging from 20-28% in the UP profile and 12-18% in the VE profile. For this particular property, the effects of hygrothermal ageing at the latter exposure periods were more pronounced in the VE profile, especially for the higher immersion temperature; this is attributed to the susceptibility of the UP resin to post-curing effects, as reported in the DMA tests.

At the end of the experiments, the in-plane shear modulus of the UP-profile presented a 5-10% increase in the 20 °C immersion environments. For immersion at 40 °C, the shear modulus increased 8% in W40, while it presented a minute reduction of 2% in S40. In W60, S60 and C40 environments, the shear modulus presented reductions of 10%, 4% and 2%, respectively. As for the VE profile, similar results were obtained, with increases of 2-4% in the 20 °C immersions. For the remaining environments, reductions of 2-7%, 15-18% and 4% were observed for immersions at 40 °C and 60 °C, and C40, respectively. The main trends of these results are quite similar to those obtained in the previously described work [4.31]. However, compared to that study, due to the desorption period, now the early monotonic reduction was attenuated and the property recovery was slightly higher, which is consistent with the other mechanical properties characterised so far.

4.3.7 Characterisation of the interlaminar shear response

Interlaminar shear strength (σ_{sbs}) provides insightful information about the degradation effects at the matrix-reinforcement interface. Figure 4.22 presents the stress *vs.* midspan displacement behaviour of representative specimens from both UP and VE profiles subjected to the W60 environment.

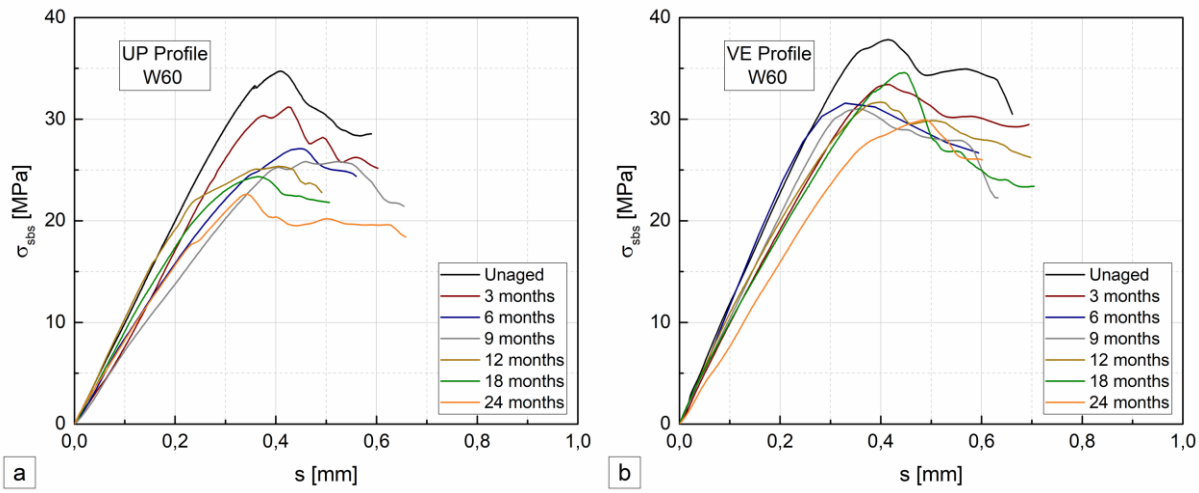

Figure 4.22. Interlaminar shear stress *vs.* midspan displacement curves at different ageing times for immersion in water at 60 °C: (a) UP and (b) VE profiles.

Even maintaining an approximately linear behaviour, hygrothermal ageing caused a significant effect in the interlaminar shear strength of both profiles, which was more evident in the UP profile. Figure 4.23 plots the variation of the interlaminar shear strength of the UP and VE profiles (average ± standard deviation) for all the ageing environments.

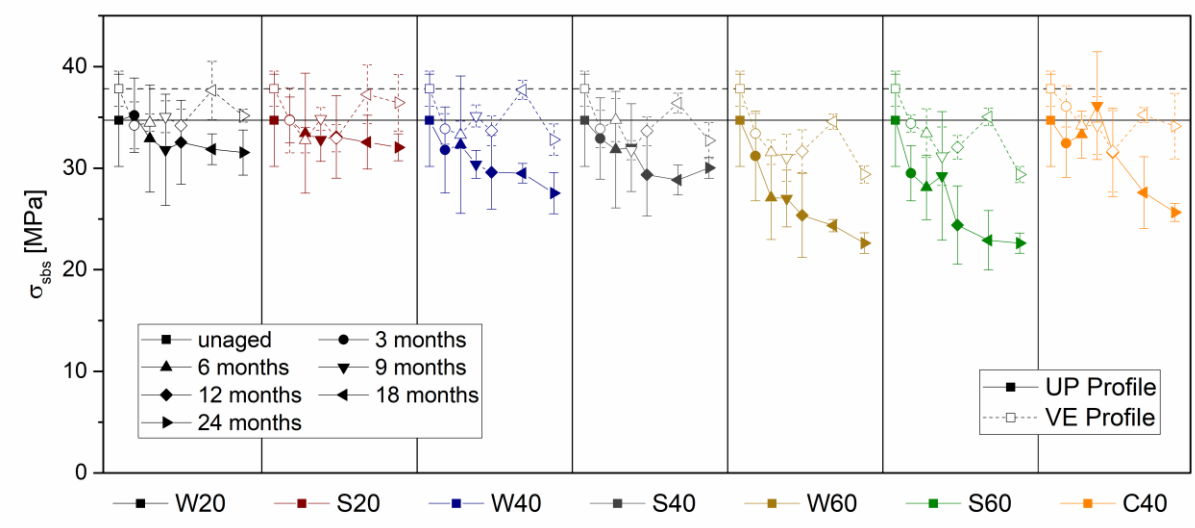

Figure 4.23. Variation of interlaminar shear strength, for both profiles, exposed to the different ageing environments.

Figure 4.23 shows that the interlaminar shear strength of both profiles exhibited a general reduction trend with the ageing period, more or less continuous up to 9 months in all environments. Moreover, the strength reductions were more pronounced with increasing temperature, which is in agreement with other strength properties measured in this study and also with results reported earlier by Kharbari [4.35] and Cabral-Fonseca *et al.* [4.5]. However, in the latter study, after an initial and harsher reduction of interlaminar shear strength, a stabilisation plateau was attained. In the present thesis, the interlaminar shear strength of the UP profile gradually decreased, while that of the VE profile presented some recovery after 9 months, especially in the immersions at 20 °C; this non-monotonic variation is also consistent with the aforementioned occurrence of post-curing effects, also identified in the flexural properties. Kharbari [4.35] also identified this increase in a VE-GFRP profile. The author attributed the higher degradation suffered at higher exposure temperatures not only to plasticization and hydrolysis effects, but also to interface debonding and microcracks coalescence to form transverse cracks, which result in greater propensity for wicking of moisture. In addition, according to that author, long exposure periods (above 12 months) may cause degradation at the fibre level, through pitting, cracking and fibre dissolution [4.36]. It is also worth highlighting the overall good agreement between the variation of flexural and interlaminar shear strengths (also reported in [4.5]), most likely due to the influence of the resin matrix on both properties.

After 24 months of hygrothermal ageing, the UP profile presented interlaminar shear strength reductions of 8-9%, 14-21%, 34-35%, and 21% for immersions at 20 °C, 40 °C, 60 °C, and C40,

respectively; for the VE profile, those figures were significantly lower, 4-7%, 13-14%, 21-22%, and 9%.

It is interesting to note that salt water immersions followed closely the water immersions at the same temperature. In this case, and differently from other mechanical properties (*e.g.* flexural strength), salt appeared to have no evident effect on hindering hygrothermal deterioration. Yet, continuous condensation produced comparable effects to water immersion at 40 °C, as for all the other mechanical properties. The superior durability performance of the VE profile compared to the UP profile in terms of resistance to interlaminar shear failure is attested by (i) the higher strength in unaged condition and (ii) the consistently lower strength reduction when subjected to the various hygrothermal ageing environments.

4.4. Long-term performance

One significant challenge for pultruded GFRP composites in civil infrastructure is the prediction of long-term effects and service life based on (limited) experimental data currently available, especially because a full understanding of the degradation mechanics underwent by these materials when subjected to several possible exposure conditions is still lacking [4.3]. Arrhenius type models, as described in Chapter 3, are often used in these cases to represent first-order effects in material properties. This section presents the application of these modelling tools to the data obtained in the experimental campaign.

4.4.1 Activation energy and apparent diffusion coefficient

The activation energy for diffusion, E_d, provides an indication of the energy barrier that must be overcome for diffusion of moisture to take place, and can be determined using the following Arrhenius type relationship [4.35],

$$D = D_0 e^{\left(\frac{-E_d}{RT}\right)} \tag{4.1}$$

where D_0 is a constant coefficient, R is the universal gas constant (8.3144 J/mol), D is the apparent Fickian diffusion coefficient and T is the absolute temperature. Since the apparent diffusion coefficients have already been calculated (*cf.* Table 4.4), by plotting ln(D) *vs.* the inverse of absolute temperature (1/T), as depicted in Figure 4.24, values of the activation energy for both UP and VE profiles can be determined.

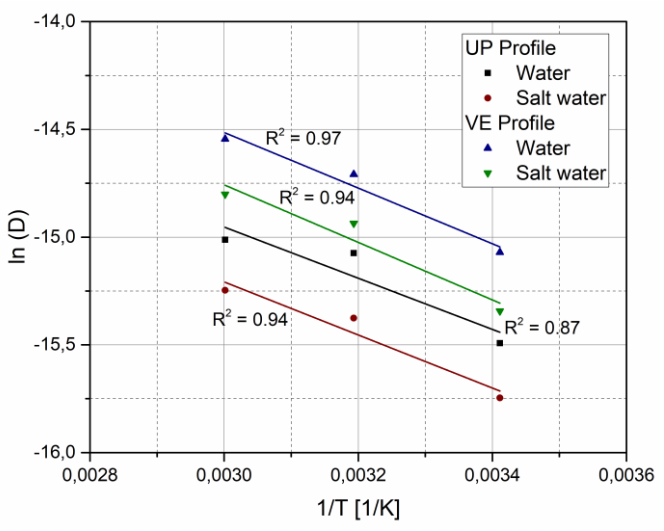

Figure 4.24. Determination of activation energy for both profiles in water and salt water immersions.

The activation energy for the UP profile in water and salt water immersions were determined as 9.9 kJ/mol and 10.2 kJ/mol, respectively. The same figures for VE profile were 10.7 kJ/mol and 11.1 kJ/mol. The (slightly) lower activation energy of water compared to salt water immersions for both profiles indicates a weaker diffusion barrier and consequent higher absorption, which is logical and consistent with the absorption experimental results described in Section 4.3.2. In addition, the same observation can be made when comparing both profiles, with the UP profile showing higher overall water intake when compared to the VE profile, also in line with the experimental results.

The results obtained are in accordance to those of Kharbari [4.35], who reported activation energies between 9.8-10.6 kJ/mol for VE-GFRP subjected to water immersions. Carra and Carvelli [4.27] reported higher values (approximately twice) for both UP- and VE-GFRP profiles, with the VE profile presenting higher energy values than the UP profile (as in the present study). This increasing trend in activation energy for resin matrixes with lower water absorption provides a good indication of their lower susceptibility to hygrothermal degradation, being also in agreement with the results obtained from mechanical characterisation tests where the VE profiles generally outer-performed the PU profiles.

4.4.2 Prediction of long-term effects

The long-term mechanical performance of the pultruded GFRP profiles can be estimated assuming that the Arrhenius principle applies. As described in Chapter 3, according to such principle, the rate at which chemical degradation occurs is dependent on temperature,

$$k = Ae^{\left(\frac{-E_a}{RT}\right)} \tag{4.2}$$

where k is a variable representing the rate of degradation of a given phenomenon, A is a pre-exponential factor characteristic of the failure mechanism and test conditions, E_a is the activation energy, R is the universal gas constant and T is the absolute temperature. The primary limitation of these models is the assumption that the material is subjected to one degradation mechanism that does not change with time and temperature, but is accelerated by temperature increase [4.26, 4.35]. The main limitations and concerns about the accuracy of this simulation approach stems from the consideration of the effects of a single degradation mechanism (*i.e.* additional degradation mechanisms and competing post-curing phenomena, which were seen to affect composite materials, are not considered), which potentially makes them less reliable in capturing time-dependent changes due to various degradation mechanisms, especially related to damage progression at the fibre-matrix interface and fibre levels [4.4]. However, using these models for extrapolation of short-term data to larger time scales provides a useful tool, namely for comparative purposes, considering a representative or standardized service life [4.35].

Following the model specifications proposed by Bank *et al.* [4.37], the experimental data can be plotted in a logarithmic time scale as a function of normalized performances. If the results present a good linear fit in such scale, the performance or time curves *vs.* the inverse of absolute temperature (Arrhenius plots) can be constructed and used to predict long-term behaviour at a given temperature.

The primary basis of Arrhenius procedures is uniformity of degradation mechanisms over time for a given exposure temperature; significantly high R^2 values in the approximations are required. For a regression to be deemed as acceptable, the authors recommended such value to be at least 0.8; this was the baseline used in the present investigation to apply the model to the experimental data [4.37]. In the present study, predictions of material performance were obtained by employing this method for a service life time of up to 100 years, for the following three exposure temperatures: (i) 10 °C, to characterise low temperature environments; (ii) 23 °C, as a typical ambient temperature; and (iii) 35 °C, representative of high temperature exposures.

It is important to highlight the fact that the predictions of degradation suffered by the elastic and strength related properties of UP and VE profiles refer to fully immersed material, which typically presents relatively high degradation rates [4.37]. The degradation that is likely to

occur under natural weathering conditions (assessed in Chapter 5) is expected to be significantly lower.

4.4.3 Tensile properties

Concerning tensile properties, both strength and stiffness of the UP profile verified the initial assumption for the application of the Arrhenius model (*i.e.*, at least an $R^2 = 0.8$). However, the convergence criteria for the VE profile was not observed (low R^2 values), which was attributed to the effect of visible competing post-curing phenomena that affected the tensile properties of the VE profile throughout the ageing period. The strength and modulus retention values for the UP profile as a function of time are plotted in Figure 4.25 for both water and salt water immersions.

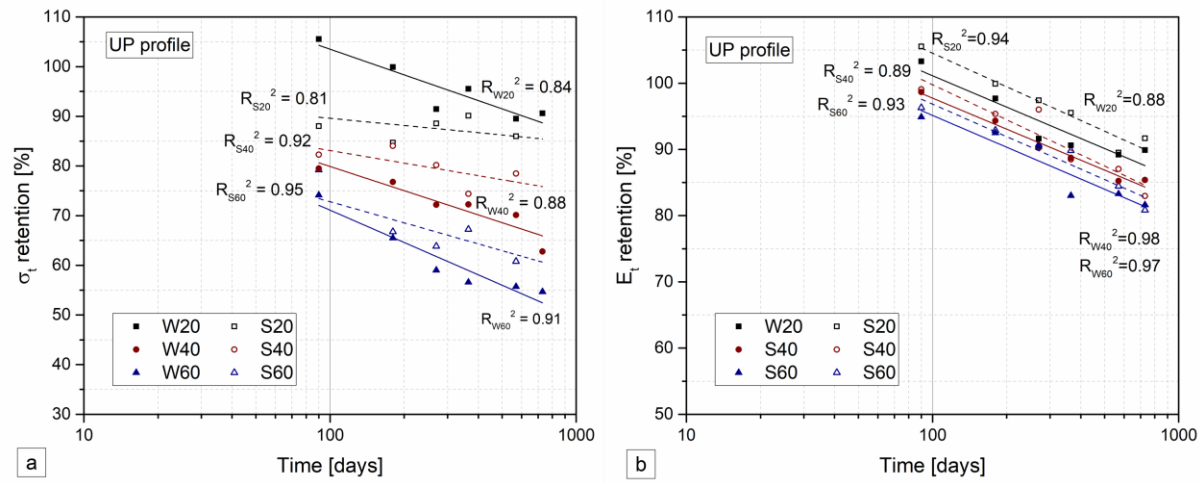

Figure 4.25. Retention of tensile (a) strength and (b) modulus *vs.* logarithm of exposure time to different types of immersion (media and temperature), for the UP profile.

Figure 4.25 shows that the R^2 values obtained from the different regressions were above the proposed minimum threshold for the implementation of the method. The Arrhenius plots, in Figure 4.26, were constructed according to the second method proposed by Bank *et al.* [4.37], by setting the property retention as a function of the inverse absolute temperature for several lifetimes.

Based on these results, it is then possible to predict the tensile strength and modulus retentions for the selected lifetimes at the predefined temperatures. Figure 4.27 presents the prediction curves, displaying the retention of both strength and modulus as a function of time at 10 °C, 23 °C and 35 °C.

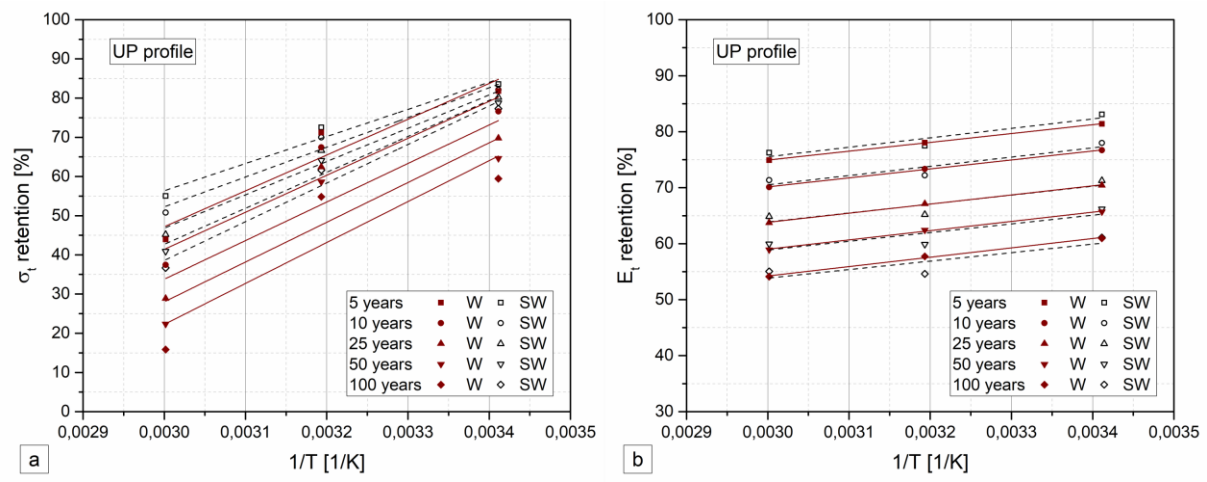

Figure 4.26. Arrhenius plots of retention of tensile (a) strength and (b) modulus, for the UP profile in water (W) and salt water (SW).

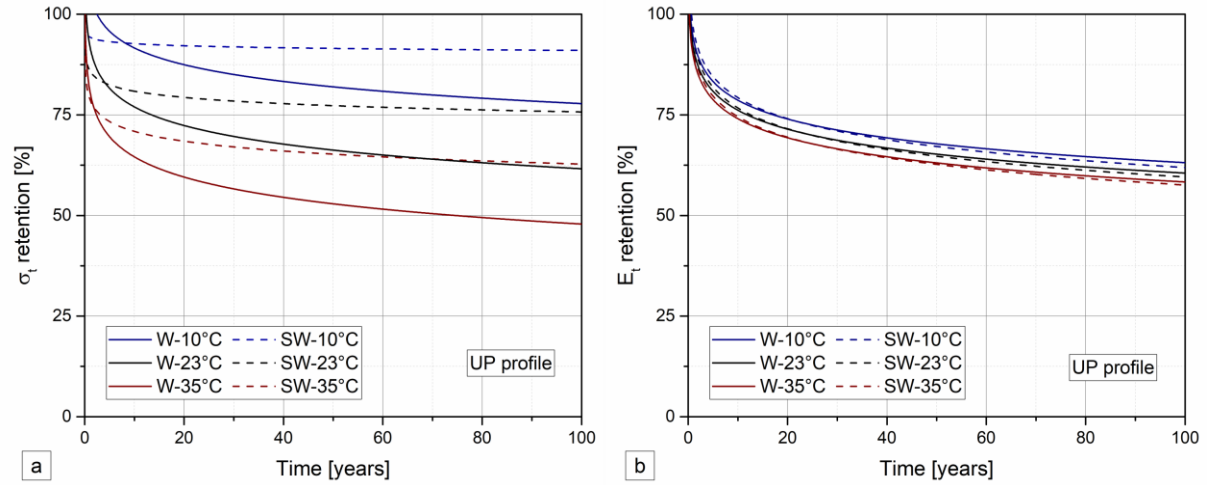

Figure 4.27. Predicted tensile (a) strength and (b) modulus, at reference temperatures, for the UP profile in water (W) and salt water (SW).

Concerning the tensile strength of the UP profile, for both immersion media and for all temperatures, the predicted tensile strength presents a faster reduction in the initial years, with the degradation rate being progressively reduced; this overall trend of the predicted curves is consistent with the assumed Fickian behaviour for the GFRP profiles. In addition, the degradation is higher with increasing temperature, which is also logical. It is interesting to note that, in the experiments, salt water led to significantly higher initial reductions, followed by a more noticeable stabilisation plateau; this trend was well captured by the prediction model. On the other hand, immersion in demineralised water produced a more gradual degradation, which, after a short period, started diverging considerably and becoming more pronounced than that of salt water. At the end of the 100-year period, predicted tensile strength retentions in water immersion were 78%, 62% and 48% for 10 °C, 23 °C, and 35 °C, respectively, while for salt water immersion those figures were 91%, 76%, and 63%.

These overall trends are in agreement with those presented by Chu *et al.* [4.2] for immersion in demineralised water; however, these authors predicted higher degradation values at 23 °C (below 50% at 50 years, for 23 °C), which should stem from differences in material constitution and manufacturing methods.

The tensile modulus of the UP profile was significantly less affected by temperature compared to the tensile strength, which is consistent with the experimental data obtained. Also in agreement with test data, predictions of tensile modulus in water and salt water immersion were very similar. During the initial periods, salt water immersion led to slightly lower reductions of tensile modulus when compared to water immersion, and after approximately 25 years the tensile modulus reduction was approximately the same for both immersion media. Afterwards, salt water immersion corresponded to slightly higher reduction values. The predicted retention values of tensile modulus after 100 years of immersion in water were 63%, 61%, and 58% for 10 °C, 23 °C, and 35 °C, respectively; for salt water immersion these figures were 62%, 60%, and 58% for the same temperatures.

4.4.4 Flexural properties

The same method was implemented to predict the long-term flexural properties, when applicable. In this case, a sufficiently strong correlation criterion was met for the flexural strength of both UP and VE profiles; on the other hand, for the flexural modulus of both profiles such correlation was low, emphasizing the significant property recovery this property showed during the experimental programme.

Figure 4.28 plots the flexural strength retention values for the UP and VE profiles as a function of time for both water and salt water immersions. In a similar way as for the tensile properties, the Arrhenius plots are presented in Figure 4.29, and the predicted values are shown in Figure 4.30.

Overall, the predicted flexural strength of the UP profile was more affected by hygrothermal ageing than its predicted tensile strength – this result is due to the higher matrix and interfacial degradation (more relevant for the flexural strength) compared to the fibre degradation (more important for tensile strength). Compared to the VE profile, as expected the predicted degradation for the flexural strength of the UP profile was higher. In addition, the prediction models capture the significant effect of elevated temperature in accelerating degradation. As in the experiments, immersion in salt water produced lower degradation compared to water; this

effect is more visible in the VE profile (as seen in the UP tensile strength), where a harsher initial reduction is followed by a flatter stabilisation period.

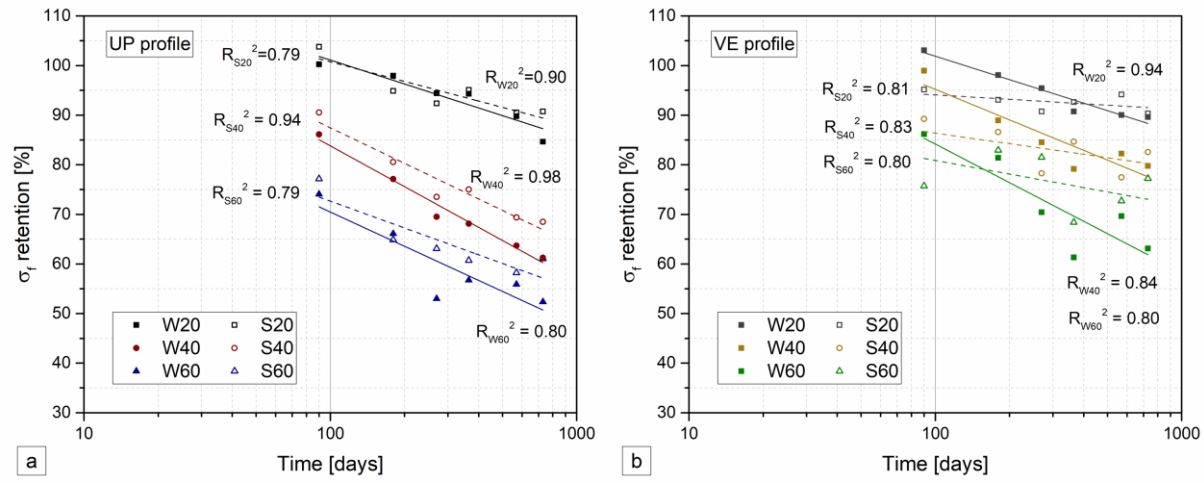

Figure 4.28. Flexural strength retention *vs.* logarithm of exposure time for (a) UP and (b) VE profiles.

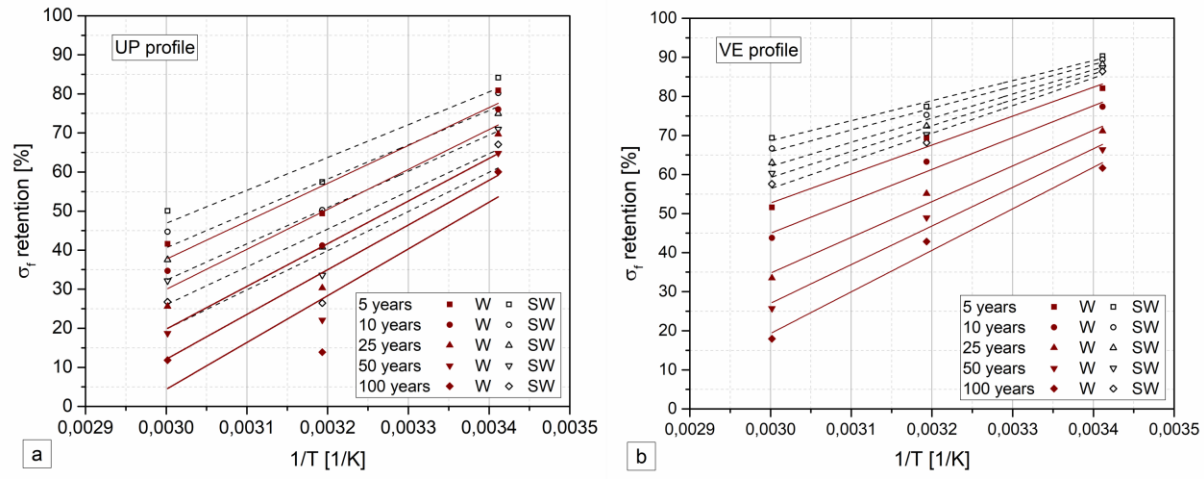

Figure 4.29. Flexural strength Arrhenius plots for (a) UP and (b) VE profiles.

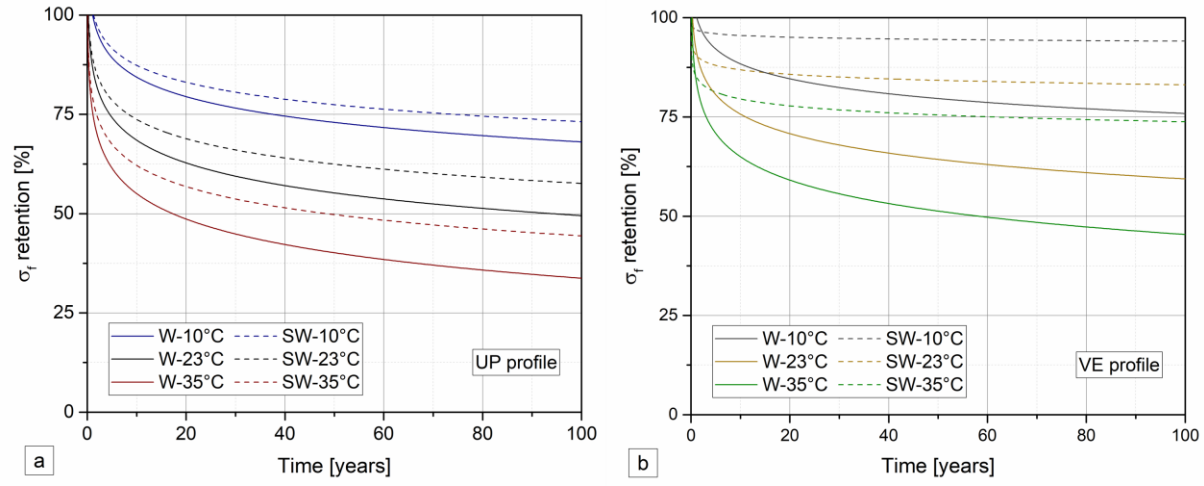

Figure 4.30. Predicted flexural strength, at the reference temperatures, for (a) UP and (b) VE profiles.

After 100 years, the predicted values for the flexural strength retention of the UP profile were 68%, 49%, and 34% for water immersion at 10 °C, 23 °C, and 35 °C, respectively, while in salt water these figures were 73%, 58%, and 44%. As for the VE profile, for the same temperatures, it exhibited strength retentions of 76%, 59% and 45% in water immersion and of 94%, 83% and 74% in salt water immersion, respectively. Carra and Carvelli [4.27] predicted higher retention values for the flexural strength of both pultruded UP and VE profiles at 100 years (66% and 70% at 23°C for 100 years). This better durability performance is consistent with the significantly lower sorption characteristics reported for those materials, which resulted in higher activation energy and less overall predicted degradation values.

4.4.5 In-plane shear properties

This subsection presents the implementation of the Arrhenius principle to the in-plane shear properties, when applicable. Much like the flexural properties, which are significantly influenced by the matrix, only the shear strength could be predicted through this method.

In-plane shear strength retention values for the UP and VE profile as a function of time are plotted in Figure 4.31, for both water and salt water immersions. The Arrhenius plots are presented in Figure 4.32 and the predicted strength retention values are shown in Figure 4.33.

Overall, the same remarks made with respect to the flexural strength retention can be made when assessing the overall predicted behaviour for the in-plane shear strength of both materials. The VE profile was significantly less affected compared to the UP profile. As in the experiments, the overall superior performance of the VE profiles is quite clear, as this specific property is very much dependent on the properties of the polymer matrix.

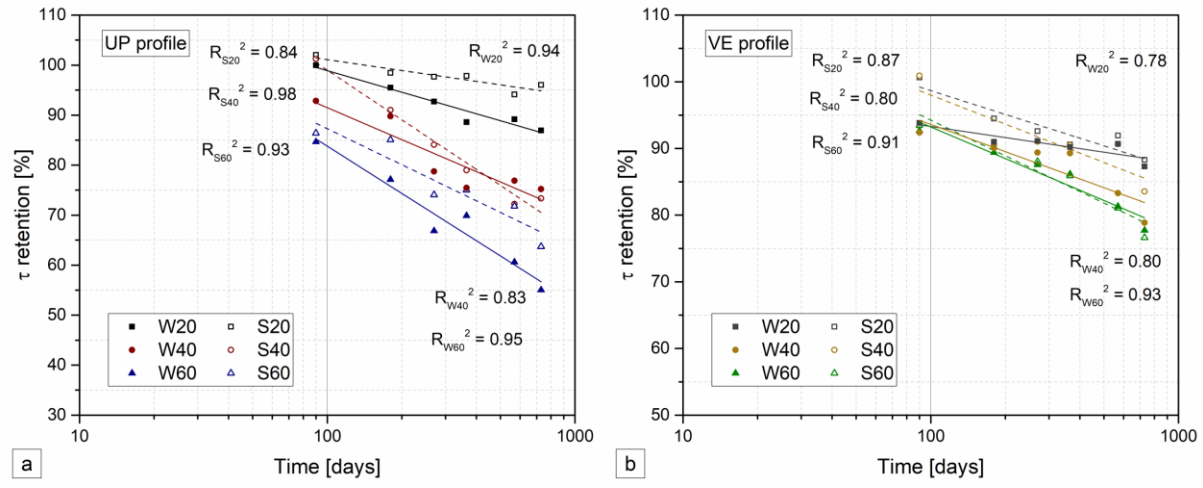

Figure 4.31. In-plane shear strength retention *vs.* logarithm of exposure time for (a) UP and (b) VE profiles.

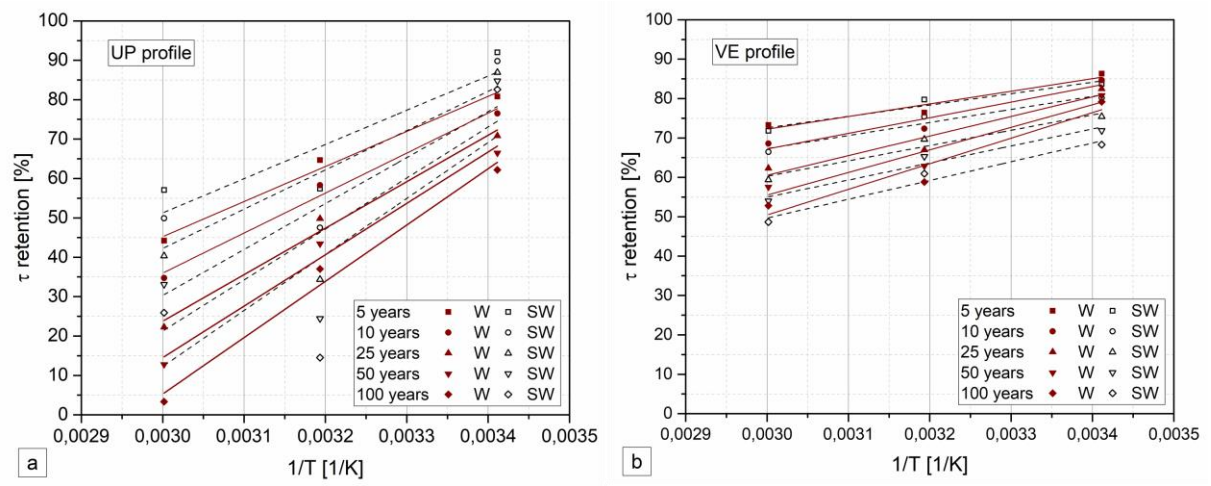

Figure 4.32.In-plane shear strength Arrhenius plots for (a) UP and (b) VE profiles.

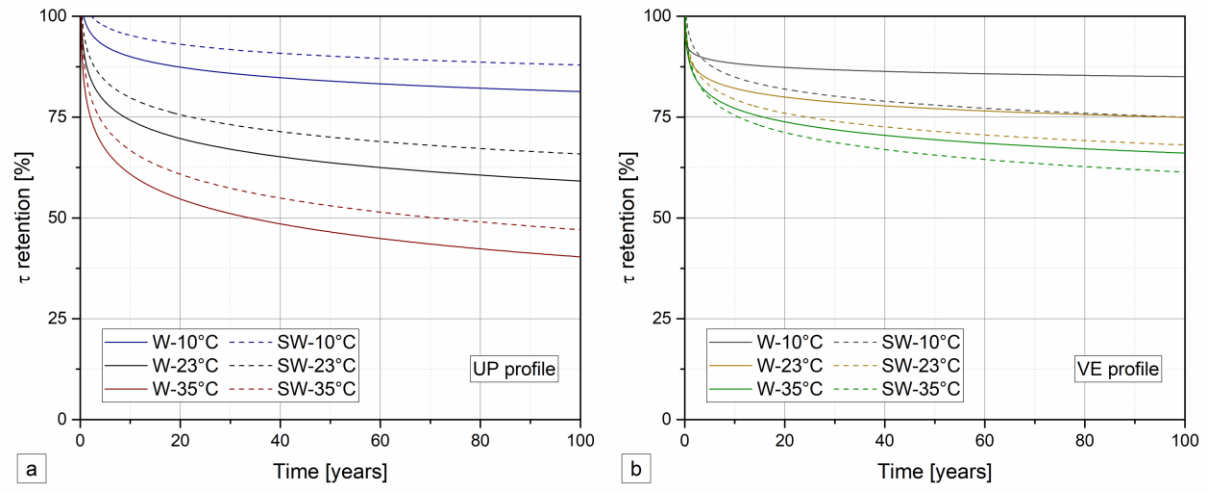

Figure 4.33. Predicted in-plane shear strength, at the reference temperatures, for (a) UP and (b) VE profiles.

For the UP profile, the predictions of in-plane shear strength retentions in salt-water immersion were higher compared to water immersion at the same temperature. However, the opposite was predicted for the VE profile apart from a short initial period, which is in agreement with the experimental results. As for the previous properties, the effect of temperature in accelerating degradation of both profiles was quite clear. In the case of the UP profile, this property presented higher reductions when compared to tensile strength at the same temperatures.

After 100 years the predicted values for the in-plane shear retention of the UP profile were 81%, 59%, and 40% for water immersion at 10 °C, 23 °C, and 35 °C, respectively, while in salt water immersion these figures were 88%, 66%, and 47%. As for the VE profile, it exhibited in-plane shear strength retentions of 85%, 75% and 66% in water immersion and 75%, 68% and 61% in salt water immersion, for the same temperatures.

4.4.6 Interlaminar shear properties

In the case of the interlaminar shear strength, the convergence criteria for the implementation of the Arrhenius principle was only possible for the UP profile.

Interlaminar shear strength retention values for the UP profile as a function of time are plotted in Figure 4.34 (a) for both water and salt water immersions. The corresponding Arrhenius plots are presented in Figure 4.34 (b), and the predicted strength retention values are shown in Figure 4.35.

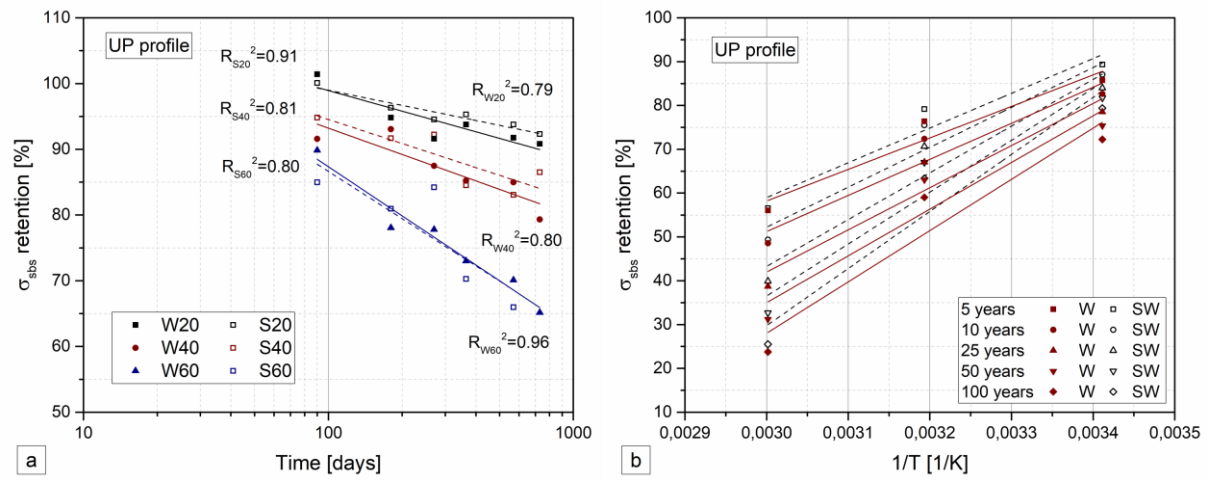

Figure 4.34. (a) Interlaminar shear strength retention *vs.* logarithm of exposure time and (b) Arrhenius plots, for the UP profile.

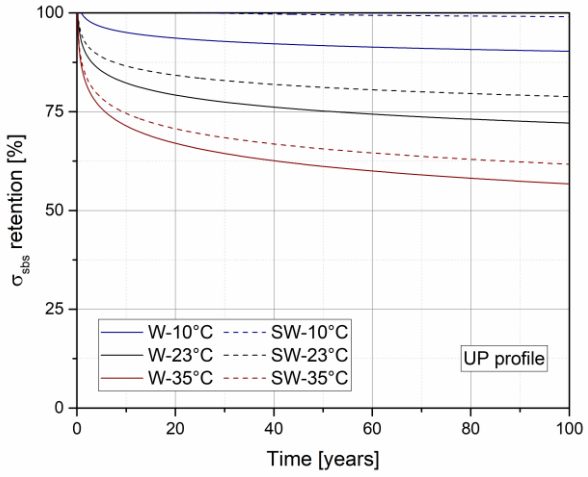

Figure 4.35. Predicted interlaminar shear strength, at the reference temperatures, for the UP profile.

As expected, the predicted interlaminar shear strength of the UP profile was very sensitive to temperature effects. In addition, and also in line with the experiments, salt water immersion caused less degradation when compared to water immersion, especially at lower temperatures (*e.g.* at 10 °C salt water immersion was predicted to cause very little reduction of performance

in terms of interlaminar shear strength). After 100 years the predicted values of interlaminar shear strength retention for the UP profile were 90%, 72%, and 57% for water immersion at 10 °C, 23 °C, and 35 °C, respectively, while in salt water immersion these figures were 99%, 79%, and 62%.

Kharbari [4.35] predicted 59% of interlaminar shear strength retention for a VE-GFRP profile subjected to water immersion at the reference temperature of 23 °C after 50 years. In spite of the general better durability performance of VE resins, this value is 15% lower than that reported above for the UP-profile (for the same period) tested in this thesis. The differences should stem from the desorption period that our specimens underwent and the resin infusion manufacturing process used to produce the specimens tested in [4.35], which also resulted in a lower fibre content (50%) of the composite material compared to our pultruded profiles.

Overall, the predicted values for the interlaminar shear strength of the UP profile after 100 years of ageing remained above 50%, even in water immersion at 35 °C, which is a quite harsh environment. Although it was not possible to predict the long-term performance of the VE profile, based on the experimental results (and the data available in the literature), it is expected to present an even better performance throughout time.

4.5. Summary

Tables 4.5 and 4.6 list the retention values for the predicted mechanical properties of the UP and VE profiles that were possible to model after respectively 50 and 100 years.

The figures listed in this table reflect (i) the better overall performance of the VE resin system; (ii) the higher degradation of mechanical properties that are more matrix-governed; (iii) the higher speed of degradation at elevated temperature; and (iv) the lower overall degradation in salt-water immersion compared to water immersion.

Table 4.5. Retention values for predicted mechanical properties of the UP and VE profiles after 50 years.

Media	Temperature [°C]	Profile	σ_t [%]	E_t [%]	σ_f [%]	τ [%]	σ_{sbs} [%]
Water	10	UP	82.0	67.8	73.0	83.9	91.7
		VE	-	-	79.6	86.0	-
	23	UP	66.2	65.2	55.2	63.7	75.2
		VE	-	-	64.3	77.1	-
	35	UP	52.9	63.1	40.2	46.5	61.1
		VE	-	-	51.3	69.6	-
Salt Water	10	UP	91.5	67.1	77.4	90.1	99.5
		VE	-	-	94.5	78.0	-
	23	UP	77.3	64.7	62.5	70.1	81.2
		VE	-	-	84.2	71.3	-
	35	UP	65.2	62.7	49.8	53.0	65.6
		VE	-	-	75.5	65.6	-

Table 4.6. Retention values for predicted mechanical properties of the UP and VE profiles after 100 years.

Media	Temperature [°C]	Profile	σ_t [%]	E_t [%]	σ_f [%]	τ [%]	σ_{sbs} [%]
Water	10	UP	77.8	63.1	68.1	81.3	90
		VE	-	-	75.9	85.0	-
	23	UP	61.6	60.5	49.5	59.1	72
		VE	-	-	59.4	74.9	-
	35	UP	47.9	58.3	33.7	40.3	57
		VE	-	-	45.4	66.4	-
Salt Water	10	UP	91.0	61.9	73.2	87.9	99.0
		VE	-	-	94.1	75.0	-
	23	UP	75.7	59.6	57.6	65.9	78.8
		VE	-	-	83.1	67.6	-
	35	UP	62.8	57.6	44.4	47.1	61.7
		VE	-	-	73.8	61.3	-

4.6. Concluding remarks

This chapter presented the results of comprehensive experimental investigations about the effect of hygrothermal ageing on the physical, viscoelastic and mechanical properties of two pultruded GFRP profiles with UP and VE matrix used in civil engineering applications. The results obtained following a desorption period prior to characterisation allow drawing the following main conclusions:

1. The sorption behaviour in the immersion environments – water and salt water - was approximately Fickian; indeed, after an initial higher absorption, water uptake progressed to lower absorption rates and nearly constant values at the later periods of exposure. However, some deviations from pure Fickian behaviour occurred. For both profiles, higher temperature increased the diffusivity of both profiles, and the presence of salt seemed to hinder water uptake to some extent in both profiles. Continuous condensation presented early saturation when compared to immersion, and overall the VE profile presented lower water uptake comparing to the UP profile. Both considered analytical models provided overall good fitting to the test data; however, the two-phase Fickian diffusion had better correlation with test data, as expected.

2. Concerning DMA results, an initial decrease of the storage modulus followed by a stabilization of the glassy plateau was identified in both profiles; these changes, coupled with some widening of the tan δ curves base suggests the occurrence of plasticization effects, although to a small extent. The tan δ curve had an overall right shift in the UP profile, coupled with lowering of the curve peak, and this could be related to post-curing phenomena effects in the polymeric matrix. The changes in the polymeric structure had a positive effect in the T_g of the UP profile up to 12 months, which was temperature dependent; subsequently, significant

reductions (10%) associated with long term hydrolysis occurred up to 24 months. The T_g of the VE profile was not significantly affected throughout the ageing period with maximum variations of 4%, regardless of the temperature.

3. Regarding mechanical characterisation, salt water caused similar (though slightly lower) detrimental effects when compared to water immersion at the same period, due to osmotic effects that hindered diffusion in this media. In addition, the continuous condensation environment led to fairly similar changes when comparing to immersion in water at the same temperature, despite the sorption differences observed in sorption behaviour. The VE profile had overall better performance than the UP profiles in all mechanical tests, especially when considering in-plane and interlaminar shear strength; these properties, being more matrix-dependent, highlight more clearly the better durability performance of VE resin.

4. Hygrothermal ageing negatively affected the tensile properties of the UP profile: the tensile strength reduction was higher at initial periods of exposure, consistent with the higher initial water uptake, while the modulus reduction was more gradual. After 12 months, the degradation effects were attenuated, presenting lower reductions, albeit still revealing detrimental effects. After an initial reduction in both strength and modulus, some property recovery was observed at 20 °C and 40 °C. After 24 months, the highest reductions in strength occurred for water immersion at 60 °C - 45% and 33% for the UP and VE profiles, respectively.

5. Flexural strength was also affected by hygrothermal ageing. As expected, the degradation levels were higher in the UP profile when compared to the VE profile; the latter profile also presented property recovery after 12 months. In a similar way as tensile strength, higher initial reductions occurred in strength, while reductions in modulus were lower. In fact, flexural modulus seemed to follow the trends of flexural strength, but at slower rates and with no evidence of temperature dependency. The highest reductions in flexural strength were 48% and 37% for the UP and VE profiles, respectively.

6. Overall, in-plane shear strength showed an overall reduction with time for all ageing conditions, that was increased with higher temperature exposure, for both profiles. After 24 months, the in-plane shear strength of the UP profile had a maximum reduction of 45%, while that figure was only 23% for the VE profile. The in-plane shear strength of the VE profile seemed to be much more resistant to hygrothermal exposure, due to the nature of this test, which makes more use of the polymeric matrix. The shear modulus showed irregular variations, with initial reductions for both profiles at higher temperatures, followed by property increase, consistent with the existence of post-curing effects affecting the polymeric matrixes. The variation of the interlaminar

shear strength followed the general trends of the in-plane shear strength, although after 12 months of exposure the VE profile exhibited some property recovery.

7. In the final part of the chapter, based on the test data gathered in the experiments, the Arrhenius model was implemented to predict the long-term mechanical properties of both profiles. In line with the tests, the VE profile revealed an overall better performance in comparison to the UP profile, which is also consistent with the higher activation energy and lower susceptibility to water incorporation. The predicted tensile strength and modulus retention for the UP profile after 100 years of water immersion at 23 °C was approximately 60%. In addition, flexural strength retention after the same period and temperature was 50% in the UP profile and 59% in the VE profile. For the same conditions and periods, the predicted in-plane shear strength retention was 59% and 75% for the UP and VE profiles, respectively, reflecting the overall superior performance of the VE polymeric matrix. Overall, for water immersion at the reference temperature of 23 °C, none of the estimated properties fell below 50% after 100 years.

4.7. References

[4.1] Karbhari VM, Chin JW, Hunston D, Benmokrane B, Jusja T, Morgan R, et al. Durability gap analysis for fiber-reinforced polymer composites in civil infrastructure. J Compos Constr 2003;7:238–47.

[4.2] Chu W, Wu L, Karbhari VM. Durability evaluation of moderate temperature cured E-glass/vinylester systems. Compos Struct 2004;66:367–76.

[4.3] Karbhari VM. Durability of Composites for Civil Structural Applications. Boca Raton, Florida: Woodhead Publishing; 2007.

[4.4] Svetlik SL. An investigation in the hygrothermal degradation of an E-glass/vinyl-ester composite in humid and immersion environments. PhD Thesis. UC San Diego, 2008.

[4.5] Cabral-Fonseca S, Correia JR, Rodrigues MP, Branco FA. Artificial accelerated ageing of GFRP pultruded profiles made of polyester and vinylester resins: Characterisation of physical-chemical and mechanical damage. Strain 2012;48:162–73.

[4.6] Grammatikos SA, Evernden M, Mitchels J, Zafari B, Mottram JT, Papanicolaou GC. On the response to hygrothermal aging of pultruded FRPs used in the civil engineering sector. Mater Des 2016;96:283–95.

[4.7] Karbhari VM. dynamic mechanical analysis of the effect of water on E-glass vinylester composites. J Reinf Plast Compos 2006;25:631–44.

[4.8] ISO 175. Methods of test for the determination of the effects of immersion in liquid chemicals. Int Organ Stand 1999.

[4.9] ASTM D 1141. Standard practice for the preparation of substitute ocean water. Am Soc Test Mater 2008.

[4.10] Karbhari VM, Zhang S. E-glass/vinylester composites in aqueous environments – I: Experimental results. Appl Compos Mater 2003;10:19–48.

[4.11] ISO 6270. Paints and varnishes. Determination of resistance to humidity. Part 2: Continuous condensation (in-cabinet exposure with heated water reservoir). Int Organ Stand 2017.

[4.12] ASTM D 5229. Standard test method for moisture absorption properties and equilibrium conditioning of polymer matrix composite materials. Am Soc Test Mater 2014.

[4.13] ISO 6721. Plastics - Determination of dynamic mechanical properties - Part 1: General principles. Part 5: Flexural vibration - non-resonance method. Int Organ Stand 1996.

[4.14] ASTM E 1640. Standard test method for assignment of the glass transition temperature by dynamic mechanical analysis. Am Soc Test Mater 1999.

[4.15] ISO 527. Plastics - Determination of tensile properties. Int Organ Stand 2009.

[4.16] ISO 14125. Fiber-reinforced plastic composites - Determination of flexural properties. Int Organ Stand 1998.

[4.17] ASTM D 5379 / D 5379M. Standard test method for shear properties of composite materials by the V-notched beam method. Am Soc Test Mater 2011.

[4.18] ASTM D 2344. Standard test method for short-beam strength of polymer matrix composite materials and their laminates. Am Soc Test Mater 2000.

[4.19] ASTM E 1252. Standard practice for general techniques for obtaining spectra for qualitative analysis. Am Soc Test Mater 2007.

[4.20] ISO 1172. Textile-glass-reinforced plastics – Prepegs, moulding compounds and laminates – Determination of the textile-glass and mineral-filler content – Calcination methods. Int Organ Stand 1996.

[4.21] ISO 1183. Plastics – Methods for determining the density of non-cellular plastics. Part 1: Immersion method, liquid pyknometer and titration method. Int Organ Stand 2004.

[4.22] SP Systems. Guide to Composties. GTC-1-1908 n.d.

[4.23] Bao LR, Yee AF, Lee CYC. Moisture absorption and hygrothermal aging in a bismaleimide resin. Polymer 2001;42:7327–33.

[4.24] Jiang X, Kolstein H, Bijlaard FSK. Moisture diffusion in glass-fiber-reinforced polymer composite bridge under hot/wet environment. Compos Part B Eng 2013;45:407–16.

[4.25] Chin JW, Nguyen T, Aouadi K. Effects of environmental exposure on fiber-reinforced plastic (FRP) materials used in construction. J Compos Technol Res 1997;19:205–13.

[4.26] Bazli M, Ashrafi H, Oskouei AV. Effect of harsh environments on mechanical properties of GFRP pultruded profiles. Compos Part B Eng 2016;99:203–15.

[4.27] Carra G, Carvelli V. Long-term bending performance and service life prediction of pultruded glass fibre reinforced polymer composites. Compos Struct 2015;127:308–15.

[4.28] Jones F. Durability of reinforced plastics in liquid environments. In: Pritchard G, editor. Reinf. Plast. Durab., Woodhead Publishing, Cambridge; 1999, p. 70–110.

[4.29] Karbhari VM, Rivera J, Zhang J. Low-temperature hygrothermal degradation of ambient cured E-glass/vinylester composites. J Appl Polym Sci 2002;86:2255–60.

[4.30] Aniskevich K, Aniskevich A, Arnautov A, Jansons J. Mechanical properties of pultruded glass fiber-reinforced plastic after moistening. Compos Struct 2012;94:2914–9.

[4.31] Grammatikos SA, Zafari B, Evernden MC, Mottram JT, Mitchels JM. Moisture uptake characteristics of a pultruded fibre reinforced polymer flat sheet subjected to hot/wet aging. Polym Degrad Stab 2015;121:407–19.

[4.32] Kim H-Y, Park Y-H, You Y-J, Moon C-K. Durability of GFRP composite exposed to various environmental conditions. KSCE J Civ Eng 2006;10:291–5.

[4.33] Liao K, Schultheisz CR, Hunston DL. Effect of environmental aging on the properties of pultruded GFRP. Compos Part B Eng 1999;30.

[4.34] Visco AM, Campo N, Cianciafara P. Comparison of seawater absorption properties of thermoset resins based composites. Compos Part A Appl Sci Manuf 2011;42:123–30.

[4.35] Karbhari VM. E-glass/vinylester composites in aqueous environments : effects on short-beam shear strength. J Compos Constr 2004;8:148–56.

[4.36] Ishai O. Environmental effects on deformation, strength, and degradation of unidirectional glass-fiber reinforced plastics. II. Experimental study. Polym Eng Sci 1975;15:491–9.

[4.37] Bank LC, Gentry TR, Thompson BP, Russell JS. A model specification for FRP composites for civil engineering structures. Constr Build Mater 2003;17:405–37.

Chapter 5.

Natural weathering and QUV ageing of pultruded GFRP profiles

5.1. Introduction

Due to the present limitations of pultruded GFRP profiles, discussed in Chapters 2 and 3, most of their applications in civil construction are still concerned with non-structural elements or secondary structures, particularly in industries with specific performance requirements in terms of durability [5.1]. In spite of practical evidence of improved performance under harsh environments, namely when compared with more traditional materials, comprehensive and validated data on the durability of FRP materials is still relatively scarce. Furthermore, there is a lack of understanding concerning the ageing and degradation mechanisms suffered by FRP materials for the different service conditions they are likely to be subjected to in civil engineering applications.

In light of the relatively long service life periods typically required for civil structures, performing comprehensive initial material characterization tests and assessing the durability and damage tolerance of GFRP materials are of utmost importance. Until recently, environmental effects on composites have often been considered to be of secondary importance, mainly due to significant overdesign [5.2]. A significant amount of attention is now being paid to this aspect, including the development and validation of accelerated test methods for the assessment of long-term durability. In the interim, structures are being designed using conservative principles [5.3]. However, the use of inordinately high safety factors on this account cannot be easily justified and there is an urgent need to deepen the understanding about the environmental degradation mechanisms of composites. Since structural composites will be exposed to several conditions through their service design, the determination of the mechanics of degradation and levels of performance retention are critical for designers [5.4, 5.5].

Reviews about the durability of FRP materials [5.6-5.8] reveal that methodologies used in experimental studies vary considerably, results are sometimes contradictory, experiments under accelerated conditions are performed for maximum durations that are rarely longer than 12 months and only a few studies compare the performance of alternative resin systems.

Pultruded GFRP profiles used in outdoor applications are, at least, exposed to UV radiation from the sun, temperature and moisture. All these agents are known to affect the material

performance, namely the UV radiation, which promotes photochemical degradation reactions [5.2]. Even though UV light constitutes just 5% of the sunlight, these short wavelengths are responsible for considerable amounts of damage to organic materials [5.9]. UV radiation, in combination with oxygen, may cause some breaks in existing chemical bonding and start oxidation reactions that can affect material degradation or at least cause its discoloration [5.2, 5.10], making their aesthetics less appealing. UV radiation exposure is normally confined to the surface and occurs in a relatively reduced thickness, about 10 microns. However, this superficial degradation may affect the polymer mechanical properties not proportionally due to localized stress accumulation and to the fact that crack development may occur for lower stress values [5.11]. In addition, the surface degradation of pultruded composites due to UV exposure tends to expose the fiberglass reinforcements, often referred to as fibre blooming, which over the long-term can cause more serious structural damage. In the short-term, the protruding glass fibres are unattractive and cause skin irritation to users, this being particularly true for handrails and fiberglass safety ladders, where the glass fibres can chafe the users' hands [5.12].

This chapter presents results of an experimental study about the environmental degradation of commercial pultruded GFRP profiles made of two alternative resin systems - unsaturated polyester and vinylester - both comprising identical fibre content and reinforcement architecture [5.13]. In order to complement Chapter 4 and study other possible degradation factors that may occur in pultruded GFRP profiles, specimens from the two types of profiles were subjected to two types of environmental ageing, namely: (i) artificial accelerated ageing in a QUV chamber (simulating outdoor weathering with alternating cycles of UV light and moisture at controlled elevated temperature) for up to 3000 hours; and (ii) natural ageing in the city centre of Lisbon, a Mediterranean exposure, for up to 102 months (8.5 years). The performance of both profiles following such ageing environments was analysed and compared regarding their physical, viscoelastic and mechanical responses, as well as their chemical changes. The main objectives of this study were two-fold: (i) to study the environmental degradation of GFRP profiles in a Mediterranean environment; and (ii) to evaluate the possibility of correlating such degradation with that caused by artificial accelerated ageing in a QUV chamber.

5.2. Experimental programme

5.2.1 Materials

For the purposes of the current study E-glass vinylester and polyester composites were obtained from two commercial pultruded GFRP profiles with square tubular cross-section ($50 \times 50 \times 5$ mm^3), produced by *ALTO Perfis Pultrudidos Lda., Portugal*. The materials are very similar to those studied in Chapter 4. However, they resulted from a different batch of pultruded tubular sections, that were manufactured earlier.

Similarly to the pultruded profiles subjected to hygrothermal ageing, the tubular sections used now consisted of alternate layers of unidirectional E-glass fibre rovings and strand mats embedded in either isophthalic unsaturated polyester resin (UP) or vinylester resin (VE). Pultruded profiles were produced by pulling the E-glass fibres with a silane sizing through a bath of resin, at an average speed of 0.25 m/min. The tubular sections were produced in a heated die, where temperatures vary between 130 °C (entrance) and 165 °C (exit).

The same polymeric matrixes that were chosen in the previous chapter were selected in this experimental programme for the sake of consistency. Both profiles have the same glass fibre content and architecture, as shown in Figure 5.1, thus allowing for a direct comparison of the durability performance of their resins.

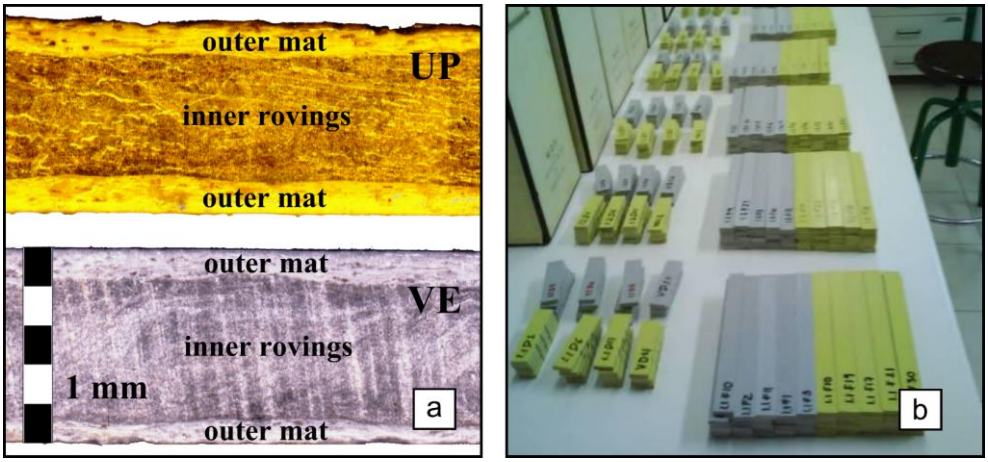

Figure 5.1. UP and VE profiles: (a) cross sections, divided by outer mats and inner rovings; (b) specimens general view.

5.2.2 Ageing environments

In order to adequately assess the changes in the characteristics of the composites, as well as the mechanisms of degradation of the two types of profiles due to natural weathering and artificial accelerated ageing with ultraviolet radiation, small-scale coupons of both GFRP

profiles were prepared and exposed to the two following environments: (a) natural weathering exposure (NE) and (b) QUV accelerated weathering fluorescent UV light apparatus (QUV), as shown in Figure 5.2.

Figure 5.2. Ageing environments: (a) natural weathering, and (b) artificial accelerated ageing in a QUV chamber.

The natural weathering consists of exposure to Lisbon city centre urban environment, in the roof of the National Laboratory of Civil Engineering (LNEC) main building, located at latitude of 38.77° North, longitude of 9.13° West and 100 m above the sea level. The samples were attached to a metallic structure with plastic rails, oriented towards South (in plan) and at a 45° angle with the vertical surface. The atmospheric conditions near the specimens were continuously monitored with a weather station, which includes a combined temperature and RH sensor from *Thies* and two pyranometers from *Kipp & Zonen* that measured the global and UV solar radiation (with the same 45° incidence angle as the specimens), and is depicted in Figure 5.3.

Figure 5.3. National Laboratory of Civil Engineering weather station.

Batches of test specimens (*cf.* Section 5.2.3) were exposed to natural weathering for 12, 24, 42, and 102 months (1, 2, 3.5, and 8.5 years), between October 2008 and April 2017. Figure 5.4

plots the average curves (minimum, medium and maximum values) of (a) air temperature and (b) relative humidity variations, for this period.

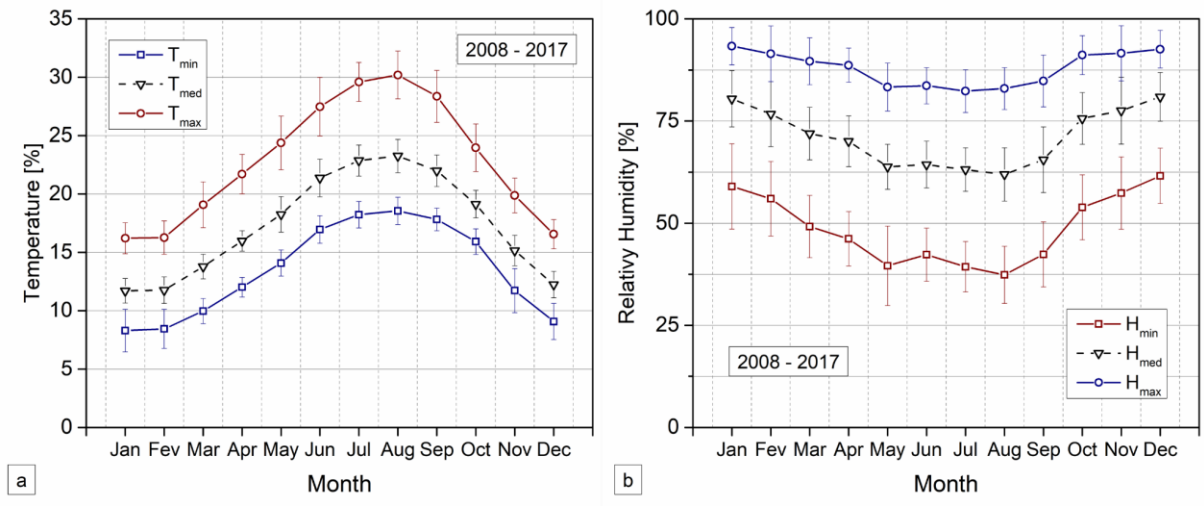

Figure 5.4. Monthly variation of (a) air temperature and (b) relative humidity between 2008 and 2017.

Between 2008 and 2017, the monthly average air temperature ranged between 11.7 °C (Winter) and 23.3 °C (Summer), while the monthly average relative humidity ranged between 80.9% (Winter) and 61.9% (Summer). In what concerns global and UV radiation, average monthly results are shown in Table 5.1, whereas the total global radiation varied between 335 786 kJ/m^2 and 698 937 kJ/m^2, while the UV component variation ranged between 9 451 kJ/m^2 and 28 570 kJ/m^2.

Table 5.1. Monthly solar radiation and UV component values [2008-2017]

Month	**Solar Radiation [kJ/m²] – 2008-2017**					
	Global value			**UV component [300-400 nm]**		
	Total	Min.	Max.	Total	Min.	Max.
January	370 024	577	23 864	10 472	61	580
February	367 808	2 001	24 643	12 042	151	697
March	548 558	2 798	27 102	19 538	189	905
April	580 372	8 099	26 528	22 626	385	973
May	607 818	6 317	25 611	25 524	344	1 024
June	584 454	6 243	23 922	25 401	320	1 027
July	676 759	11 931	24 451	28 570	564	1 018
August	698 937	8 754	25 676	26 960	405	1 000
September	641 802	7 821	26 019	22 836	349	936
October	536 982	4 000	25 601	17 618	238	814
November	437 245	1 570	23 355	12 570	121	636
December	335 786	894	21 333	9 451	92	481

The QUV chamber used was an artificial accelerated weathering equipment, allowing to expose materials to alternating cycles of UV radiation and moisture. The laboratory simulation of the damaging effects of sunlight was provided by fluorescent UV lamps, which alternated with

exposure to moisture caused by constant condensation of de-ionized water at 50 °C. Cycling sets were prepared according to parts 1 and 3 of ISO 4892 standard [5.14], alternating 4 hours with UV radiation at 50 °C (dry cycle) and 4 hours without UV radiation at 60 °C and moisture (wet cycle). The fluorescent lamps used in the QUV chamber were UVA-340 type, providing an irradiance of 0.77 W/(m^2.nm) at 340 nm, which reproduces the most relevant part of the Sun's spectrum, between 290 - 350 nm. Batches of specimens were prepared for 1000, 2000 and 3000 hours of QUV exposure.

5.2.3 Characterisation methods

Specimens with appropriate dimensions (for physical-chemical and mechanical characterisation) were cut from the 5 mm thick walls of both tubular profiles in the longitudinal direction, using a water-cooled diamond saw blade. After pre-conditioning until constant weight (in a ventilated chamber at 50 °C, without relative humidity control), specimens were exposed to the two ageing environments.

At predefined times, batches of test specimens used for physical, chemical, aesthetical and mechanical characterisation, were (i) removed from the previously mentioned exposure environments, (ii) stored in polyethilene hermetically closed recipients, and then (iii) placed inside a room with temperature controlled at 20 (±2) °C. Prior to testing, specimens were removed from the polyethylene recipients and immediately tested without any further conditioning.

Environmental degradation in both environments was assessed through the evaluation of changes in physical-chemical and mechanical properties during ageing, namely: (a) colour and gloss variations; (b) viscoelastic response, evaluated by means of dynamic mechanical analysis (DMA); (c) mechanical response in tension, bending and interlaminar shear; and (d) chemical changes, assessed through infrared spectroscopy (FTIR).

Regarding aesthetical characterization, colour changes were evaluated in specimens with geometry of $5 \times 25 \times 300$ mm^3 tested in accordance with parts 1 and 2 of ISO 7724 standard [5.15], using the colour space CIE L*a*b* 1976, illustrated in Figure 5.5 (a). Tests were carried out using a *Macbeth Coloreye 3000* colorimeter (*cf.* Figure 5.5 (b)). The same specimens were tested also for gloss variation according to ISO 2813 standard [5.16]. Gloss was measured at 20°, 60° and 85° incidence angles using a *Novo-Gloss Statistical Glossmeter* (*cf.* Figure 5.5 (c)).

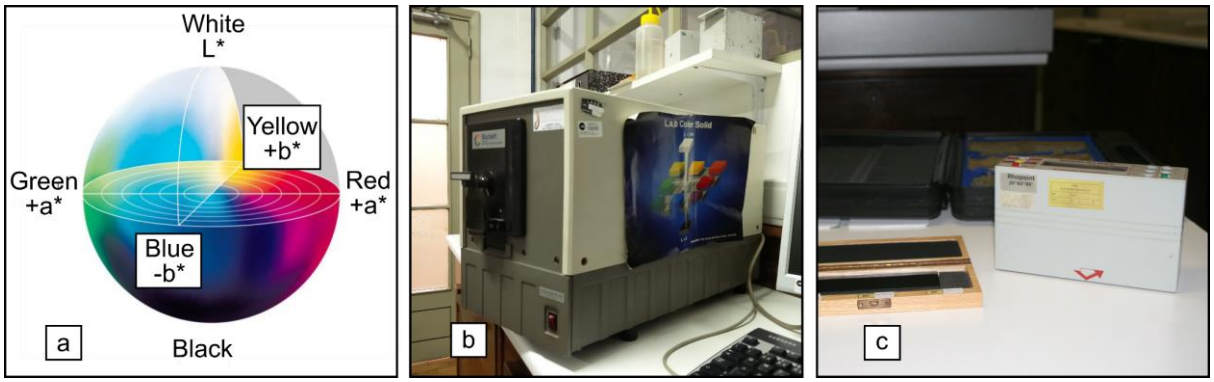

Figure 5.5. (a) CIE L*a*b* colour space, (b) Colorimeter;(c) Glossmeter.

The DMA, FTIR and mechanical tests, were performed using the same equipment, test fixtures and specifications as described in Section 4.2.3.

5.3. Experimental results and discussion

For clarity in discussion, results are presented as related to the characterisation method used. However, wherever possible or relevant effects are cross-referenced.

5.3.1 Characterisation of reference GFRP materials (unaged)

The results of initial characterisation for both UP and VE profiles before natural and artificial ageing are listed in Table 5.2 (average ± standard deviation values are shown, where applicable).

Table 5.2. Physical and chemical properties of the unaged GFRP profiles.

Property	**Method**		**UP profile**	**VE profile**
Chemical composition	FTIR	FTIR spectra consistent with unsaturated polyester or vinylester, with presence of calcium carbonate and silica		
Glass fibre content	Calcination	[%]	68.4 ± 1.1	68.7 ± 0.4
Density	Immersion	[g/cm^3]	1.87	2.03
T_g	DMA	E'$_{onset}$ [°C]	107.9 ± 10.8	98.6 ± 7.0
		tan δ [°C]	146.0 ± 2.3	126.9 ± 2.3
Mechanical properties	Tensile response	σ_{tu} [MPa]	406.2 ± 31.1	393.3 ± 51.2
		E_t [GPa]	37.6 ± 2.6	38.9 ± 4.1
		ε_{tu} [-]	0.011 ± 0.001	0.010 ± 0.001
	Flexural response	σ_{fu} [MPa]	472.2 ± 76.4	537.2 ± 73.1
		E_f [GPa]	22.6 ± 4.4	28.4 ± 3.4
		ε_{fu} [-]	0.020 ± 0.002	0.018 ± 0.003
	Interlaminar shear	σ_{sbs} [MPa]	38.5 ± 2.7	39.2 ± 4.2

Chemical composition, determined by FTIR spectroscopy, showed little differences between the two materials analysed. In fact, the spectra of both profiles are quite similar. Peaks' localizations and intensities confirm the presence of ester, as well as aromatic and aliphatic

structures, which are in the molecular structure of both unsaturated polyester and vinylester resins. FTIR spectra also disclosed the existence of calcium carbonate (filler) and silica (from E-glass fibres), and was fairly similar to both pultruded GFRP profiles studied in Chapter 4.

The glass fibre content was determined by the calcination method, and the density was determined by the immersion method described in Section 4.2.3. Those physical properties are slightly higher for the VE profile compared to the UP profile.

However, glass transition temperature (obtained from the peak of the loss factor curve, tan δ, and from the beginning of the decay of the storage modulus curve, $E'_{initial}$) is lower in the VE profile. Mechanical performance loss for UP and VE profiles starts above 108 °C and 99 °C, respectively. Although maintaining roughly the same differences between UP and VE profiles, the obtained average values were lower in comparison to the profiles studied in the last chapter, but within the scatter range. Both E' and tan δ presented very similar shape and behaviour as already seen in Figure 4.8 (Section 4.3.1).

All mechanical tests (flexural, tensile and interlaminar shear) showed linear elastic behaviour until rupture of both profiles, typical of FRP materials. Regarding tensile properties (strength, σ_t, and stiffness, E_t) and interlaminar shear strength (σ_{sbs}), both profiles present similar behaviour. However, concerning flexural behaviour, the VE profile presents higher performance in terms of both flexural strength (σ_f) and stiffness (E_f). The failure modes were as expected and similar to those already described in Section 4.3.1.

5.3.2 Colour and gloss characterisation

Table 5.3 lists the values of colour space system coordinates including their overall colour variation ΔE*. After environmental exposure, both profiles presented significant colour changes, which was easily identifiable with the naked eye. The progression of parameter ΔE* (traducing the overall colour change) as a function of time for both exposure environments is shown in Figure 5.6. The variations of L* (black-white axis), a* (green-red axis) and b* (blue-yellow axis) parameters show that both profiles became more yellow, and darker.

Overall, the UP profile presented more global colour variation as a function of time, with higher changes of ΔE*, around 18. The corresponding variation of the VE profile was 13. Results suggest that colour changes tend to increase with ageing, observed throughout the natural ageing. QUV seemed to stabilise at a plateau, especially at the later stages of exposure.

Table 5.3. Values of colour coordinates after natural exposure (NE) and QUV ageing, for UP and VE profiles.

Material	Ageing and duration	L*	a*	b*	ΔL*	Δa*	Δb*	ΔE*
UP	Unaged	75.8	0.5	57.6				
	24 months NE	74.5	0.3	43.6	-1.3	-0.2	-14.1	14.2
	42 months NE	73.7	0.9	51.8	-2.1	0.4	-6.0	6.2
	102 months NE	70.5	0.2	40.8	-5.3	-0.3	-16.9	17.7
	1000 h QUV	76.3	0.4	51.0	0.4	-0.1	-7.9	7.9
	2000 h QUV	77.0	0.2	45.3	1.0	-0.3	-13.5	13.5
	3000 h QUV	76.6	0.0	45.9	0.7	-0.5	-13.0	13.0
VE	Unaged	74.2	-0.9	1.1				
	24 months NE	72.3	-1.7	7.9	-1.9	-0.8	6.8	7.1
	42 months NE	68.8	-1.7	9.7	-5.4	-0.8	8.6	10.1
	102 months NE	65.4	-1.8	10.3	-8.7	-0.9	9.2	12.7
	1000 h QUV	72.5	-1.9	9.3	-1.8	-0.9	8.6	8.8
	2000 h QUV	72.5	-1.6	9.4	-1.8	-0.6	8.8	8.9
	3000 h QUV	73.0	-1.3	11.9	-1.3	-0.2	11.3	11.3

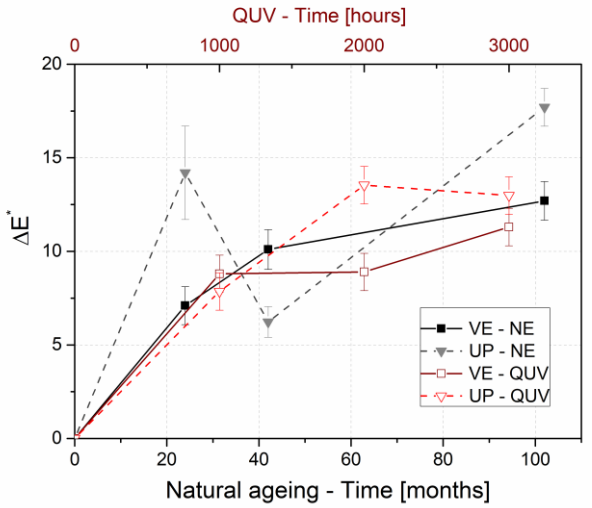

Figure 5.6. Colour changes as a function of time and ageing environment, for UP and VE profiles.

A good correlation between QUV and natural ageing is noticed up to 42 months and is more noticeable in the VE profile (*cf.* Figure 5.6). Similar changes were reported by Bogner and Borja [5.12].

Regarding gloss changes, Figure 5.7 presents results at the recommended 60° incidence angle, with results at both 20° and 85° having followed the same tendencies. Gloss values measured at all incidence angles are shown in Table 5.4.

Table 5.4. Gloss at 20°, 60° and 85° incidence angles after natural exposure (NE) and QUV ageing, for UP and VE profiles.

Ageing and duration	**UP profile**			**VE profile**		
	20°	60°	85°	20°	60°	85°
Unaged	3.5	22.3	31.8	4.3	27.7	27.4
24 months NE	0.9	3.2	6.2	0.9	2.0	1.4
42 months NE	0.7	1.1	1.1	0.8	1.2	1.2
102 months NE	0.3	0.6	0.9	0.4	0.8	0.9
1000 h QUV	4	23.7	23.1	3.8	24.3	18
2000 h QUV	1.9	8.4	6.4	0.8	2.6	1.2
3000 h QUV	1.0	2.0	2.8	0.7	1.4	0.9

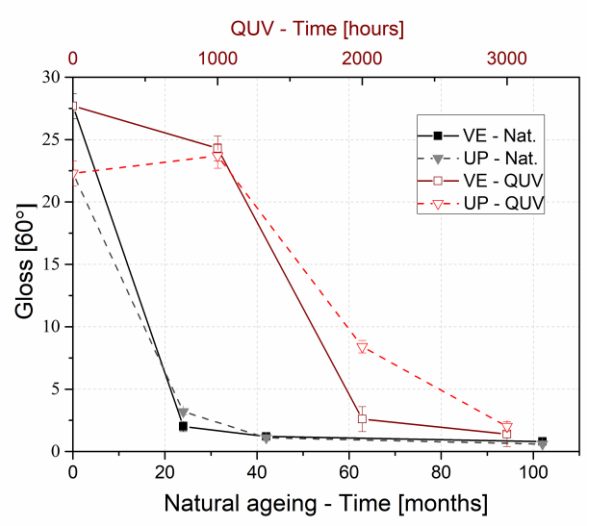

Figure 5.7. Gloss changes as a function of time and ageing environment, for UP and VE profiles.

Both profiles suffered significant gloss loss - both surfaces retained only approximately 3-5% of their initial gloss at final stages of exposure - again, correlation between QUV ageing and natural exposure was quite significant, although initially there was a relative delay in the QUV chamber. A steep gloss reduction occurs between 1000 and 2000 hours of QUV, as well as in the first 20 months of natural ageing, both progressing towards almost null values, afterwards.

In addition to the aforementioned changes in colour and gloss, visible fibre content (fibre blooming) due to the polymeric matrix photo-chemical degradation was observed in all specimen This phenomenon was evident after 6 months of natural ageing and 1000 hours of QUV ageing for both profiles and kept increasing with exposure time in both QUV and natural ageing. A good correlation between 42 months and 3000 hours QUV was observed, in agreement with colour and gloss changes. Figure 5.8 exemplifies the fibre blooming observed, as well as visible changes in colour, and the presence of small debris and dirt incrusted in the matrix and

fibres due to 102 months of natural ageing. Appropriate protection should be considered (*i.e.* application of surface veils, gel coating or paint) in order to avoid this effect.

Figure 5.8. (a) Fibre blooming effect after 102 months of natural exposure; (b) VE profile 50× magnification; (c) UP profile 220× magnification.

5.3.3 FTIR spectroscopy characterisation

The FTIR spectra performed on material obtained from the surface of test specimens exposed to UV radiation during 3000 hours of QUV, and 42 and 102 months of natural ageing, are shown in Figure 5.9 for both VE and UP profiles. The absorbance intensity increase of wavenumber 1636 cm^{-1} presented after 3000 hours of QUV for both profiles can be related to the formation of double bonds C=C, that explains the yellowness observed in the materials' surface.

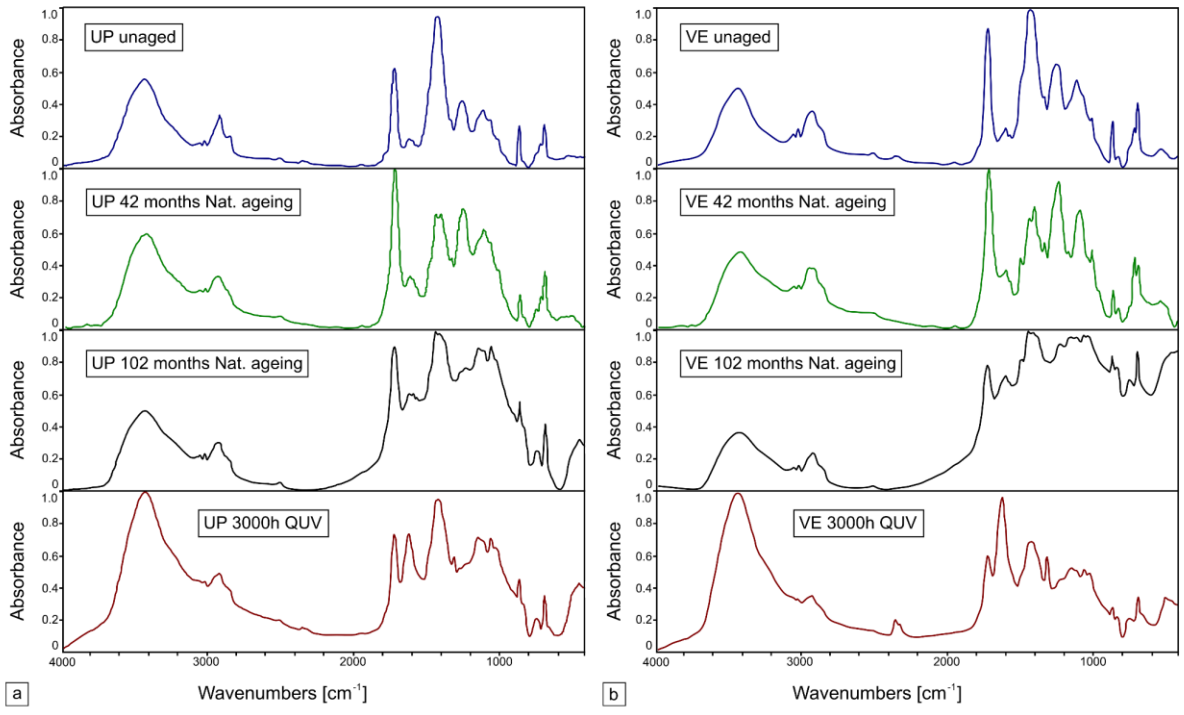

Figure 5.9. FTIR spectra of surface material after natural exposure and QUV ageing of (a) UP and (b) VE profiles.

Naturally aged samples showed similar peak increase in wavenumbers around 1300 cm^{-1} for 42 and 102 months of exposure, which can produce accentuated colour degradation and yellowness.

The latter result is confirmed by colour and gloss changes measured. The chemical damage mechanism in the surface of the resin, with loss of material, causes some glass fibres to be more directly exposed to the environmental degradation. This fact is confirmed in the FTIR spectra of aged materials by the presence of peaks that disclose the existence of silica.

5.3.4 Characterisation of the thermo-mechanical response

Since the results of FTIR analysis suggest resin and interface level degradation that may not be directly characterised by mechanical tests, dynamic mechanical analysis (DMA) was used as a tool to assess changes at this level. These tests also provide distinct advantages over other forms of characterisation. Their ability to assess the effects of subtle physical and chemical changes in the polymeric matrix, and hence also in the composite, allows the evaluation of its viscoelastic nature contribution to the behaviour and durability of the composite when exposed to environmental degradation.

Water uptake by unsaturated polyester and vinylester composites is known to cause plasticisation in the short term and hydrolysis over the long term through attack of the ester linkages [5.17]. Since the ester group is located in the middle of the molecular structure of polyester, and in the ends of the molecular structure of vinylester, in principle, the latter resin is more resistant to the above-mentioned plasticisation mechanisms. Both these phenomena induce higher levels of molecular mobility resulting in consequent decreases in glass transition temperature [5.13, 5.18]. However, some competing post-curing mechanism can occur due to additional cross-linking and further polymerization of the polymeric matrix, which has been already identified and discussed in Chapter 4.

Figure 5.10 (a) shows DMA experimental curves (storage modulus, E', left axis - dashed lines and loss factor, tan δ, right axis - continuous lines) for UP and VE profiles after their environmental ageing (one sample representative curve for both QUV accelerated ageing and natural ageing is plotted): E' curves present the characteristic slope in the glass transition region, being represented in the left axis of the graph; tan δ curves indicate as well a maximum peak in the same region, being plotted in the right axis. The progression of *E'* curve in the glass transition region suggests essentially alterations in the polymeric matrix, which changes from a glassy to an elastomeric state, due to its viscoelastic nature. In fact, the glass reinforcement does not present stiffness loss in this temperature range. However, degradation of the fibre-matrix interphase quality can be reflected through changes in DMA results.

The height of the tan δ curve peak progressed towards a decrease with ageing, while the storage modulus values increased in the glassy plateau (25 °C). These changes were similar as seen for the exposure at higher immersion temperatures during hygrothermal ageing (*cf.* Chapter 4) and should be associated with the existence of post-curing phenomena, due to further polymerization of the resin matrix, attributed to the higher temperatures during warmer seasons for natural ageing, and part of the QUV cycle, at 50 °C. However, this effect was negligible in affecting the T_g, especially as obtained through the tan δ curve, which had low variation.

A progression of change in T_g as a function of artificial ageing and natural exposure durations is shown in Figure 5.10 (b). Both profiles presented slight increases in T_g values obtained from the peak of the loss factor curve as well as in the glassy storage modulus, which suggests the existence of post-curing effects induced by the UV radiation, increased temperature and moisture. The higher T_g variations were obtained after 2000 hours of QUV exposure and were roughly around 4% for both UP and VE profiles.

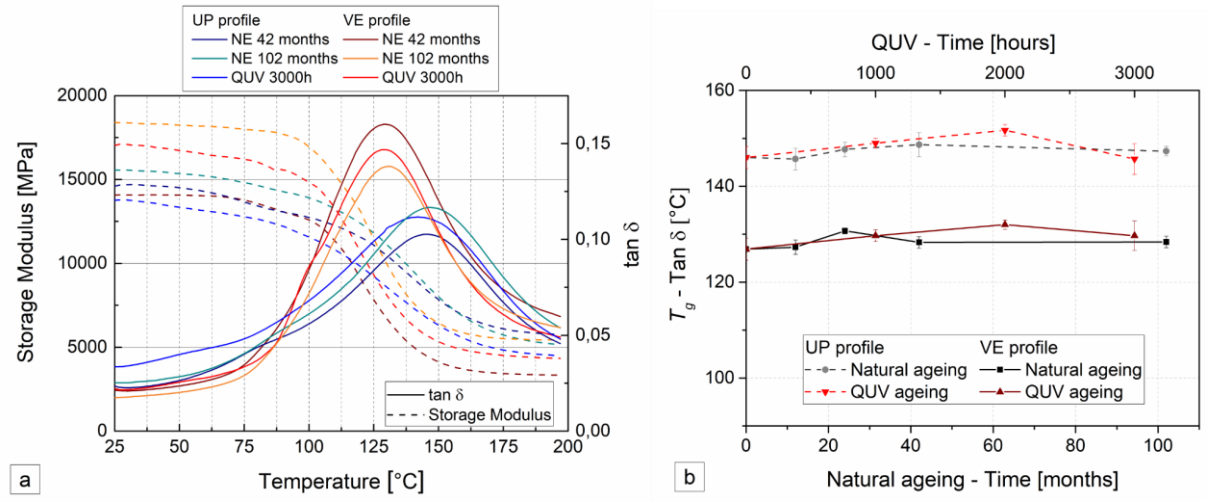

Figure 5.10. DMA results as a function of time and ageing environment for UP and VE profiles: (a) experimental curves; (b) *Tg* variations.

According to Chin *et al.* [5.10], these small variations are expected for the two different resins analysed. The UP profile presented higher T_g values compared with the VE profile during the entire experimental procedure, with relative differences ranging between 16 °C to 20 °C. In what regards the correlation between both environments, the evolution of T_g with the exposure period was fairly similar.

These changes in T_g were less significant when compared to accelerated hygrothermal ageing on the UP profile (*cf.* Chapter 4). In fact, the effect of the different immersion environments

caused significant increases (up to 27%) of the UP T_g. Regarding the VE profile, little changes occurred when compared to results obtained for hygrothermal ageing (described in the previous chapter), even considering higher temperature immersions, which should stem from the higher chemical stability of the VE resin when compared to the UP resin. However, when not considering a drying period, these differences can be higher, as seen in [5.13].

5.3.5 Characterisation of the tensile response

Figure 5.11 shows the variation of tensile strength and modulus as a function of the ageing duration (natural exposure and QUV ageing), for UP and VE profiles. It can be seen that the tensile strength presents a slight reduction tendency through time. Overall, the UP profile suffered more degradation than the VE profile, with minimum tensile strength retention being 79% and 84% after 3000 hours of QUV exposure and 102 months of natural ageing, respectively.

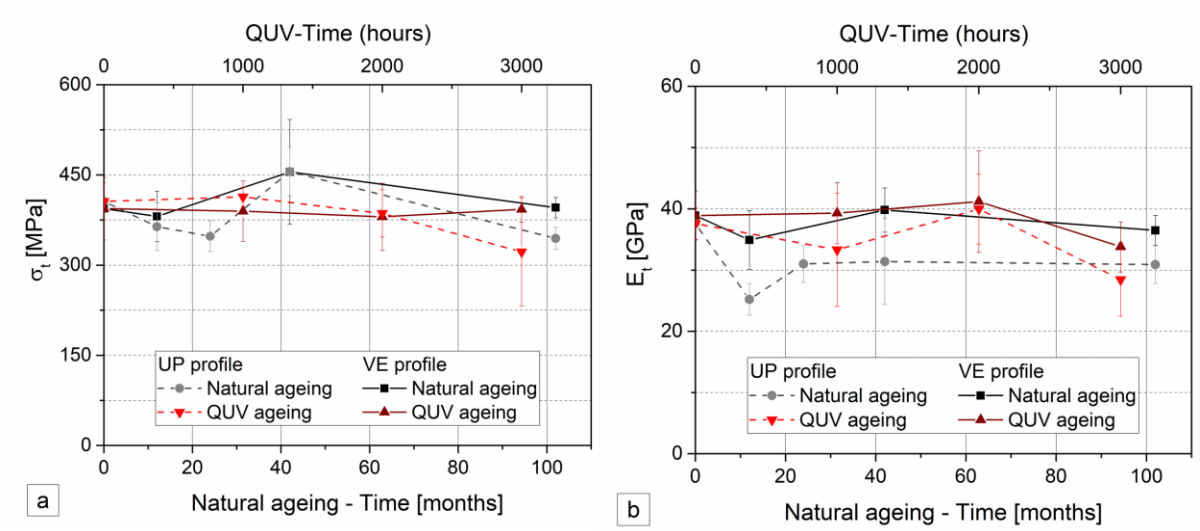

Figure 5.11. Variation of (a) tensile strength and (b) modulus, for both profiles, during exposure to the different ageing environments.

The highest variation suffered by the VE profile corresponded to a 97% strength retention, with only slight changes having occurred throughout the investigation, some of them even indicating property gain. These results are consistent with post-curing effects being more accentuated in the VE profile. These effects were also reported by Merah *et al.* [5.19], who studied the natural exposure of GFRP made of vinylester matrix and obtained an increasing trend in the tensile strength up to 12 months of exposure, with this property remaining higher than that of the as received samples.

Tensile modulus presents analogous results, although a higher degradation level was observed compared to strength (67% and 76% of minimum moduli retention for UP and VE profiles,

respectively). Segovia *et al.* [5.20] reported reductions of 15% and 20% in the elastic modulus and tensile strength of GFRP made of unsaturated polyester matrix, respectively, after 7000 hours of accelerated laboratory UV exposure. Overall, results indicate that the retention of tensile strength and modulus of the VE profile are higher, this profile being more stable to degradation than the UP profile.

In this case, QUV accelerated results are more difficult to correlate with natural ageing, most likely due to the post-curing phenomena being different in the two ageing environments. Despite the relatively high scatter, for the maximum durations of testing in both environments, tensile strength retention in natural ageing is higher than in QUV. However, concerning tensile modulus, the general variation trend consisted of an initial drop, followed by a post-curing stage, and afterwards progressing to a stable plateau. This trend can be identified for both materials and both types of ageing. In addition, at 102 months, the effects were roughly similar on both tensile strength and modulus changes, when compared to QUV ageing after 3000 hours. After 102 months of natural exposure, tensile strength retentions were 101% and 85% for the VE and UP profiles, respectively. Regarding tensile modulus, these figures were 94% and 82%.

Significant differences can be found when comparing the effects of hygrothermal ageing presented in the previous chapter. Both the UP and VE profiles exhibited lower tensile strength (up to 28% and 31% reductions were observed in the UP and VE profiles, respectively, at the higher immersion temperatures) as a consequence of the ageing effects. In terms of modulus, similar observations can be made, with the exception of natural weathering effects on the UP profile, which had considerable reductions, of the same magnitude as those observed during hygrothermal degradation.

5.3.6 Characterisation of the flexural response

The variation of flexural strength and modulus as a function of the ageing duration (natural exposure and QUV ageing) for UP and VE profiles is shown in Figure 5.12.

The VE profile suffered a decrease in flexural strength throughout exposure to both QUV and natural ageing. This decrease was more pronounced in natural ageing - flexural strength retentions were 78% and 87% after 42 months (natural) and 3000 hours (QUV), respectively. However, at the latter stages of natural ageing, flexural strength recovery could be observed, and should be related to the aforementioned post-curing effects. Flexural modulus showed higher levels of degradation, generally decreasing with time; the same non-monotonic behaviour was noticed for both QUV and natural ageing, evidencing flexural modulus recovery.

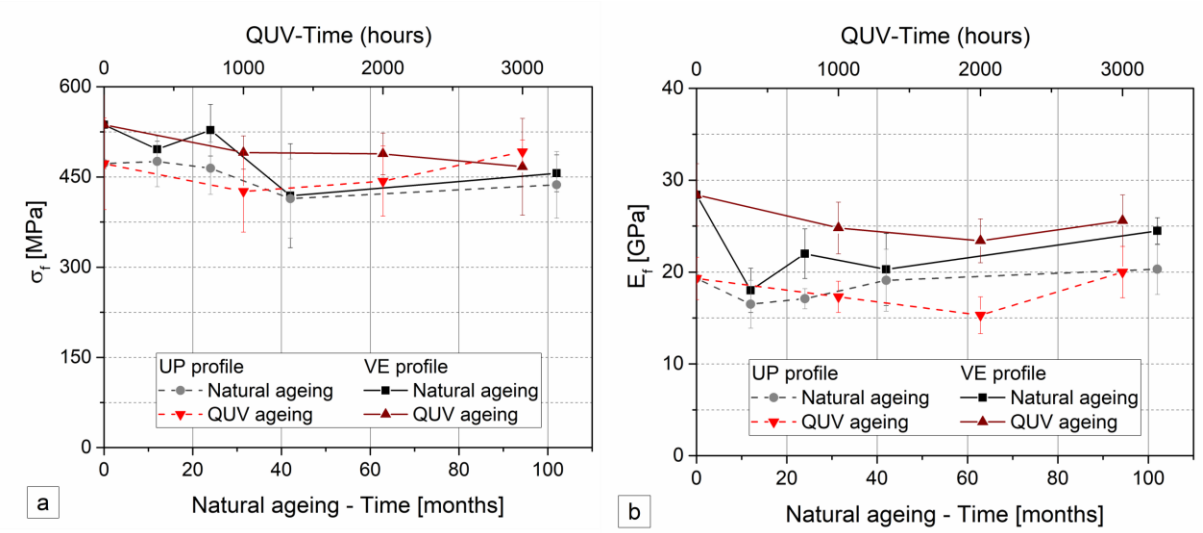

Figure 5.12. Variations of (a) flexural strength and (b) modulus, for both profiles, during exposure to the different ageing environments.

The UP profile showed lower overall degradation than the VE profile, even presenting property gains (especially noted at latter stages of QUV and natural ageing), which is consistent with the existence of post-curing effects and is in agreement with results reported earlier by Bogner and Borja [5.9] and Correia *et al.* [5.21]. However, flexural strength and modulus variations on the VE profile were not that significant.

The UP profile presented flexural strength retentions of 93% and 112% (12% gain) after 102 months (natural) and 3000 hours (QUV) of exposure, respectively. Nevertheless, as illustrated in Figure 5.12, the VE profile still presented higher absolute values for both flexural properties when compared to the UP profile. In opposition to tensile properties, the variation of both flexural strength and modulus in natural and QUV environments are roughly similar. This better correlation, when compared to tensile properties, probably stems from the fact that flexural properties are more influenced by surface degradation mechanisms.

The effects of hygrothermal ageing on the flexural properties were harsher for both profiles. As mentioned in Chapter 4, reductions in flexural strength as high as 48% and 37% were observed at the higher immersion temperatures. As for the flexural modulus, these figures reached 15% and 14%. In this regard, the VE profile did not present an evident better performance compared to the UP profile, despite always having higher absolute stiffness values.

5.3.7 Characterisation of the interlaminar shear response

Short-beam-shear (SBS) tests are often used to assess interlaminar shear strength and to compare the relative effects of environmental exposure, especially considering interfacial

degradation between the matrix and the glass fibres. Figure 5.13 indicates the progression of change in interlaminar shear strength as a function of exposure time.

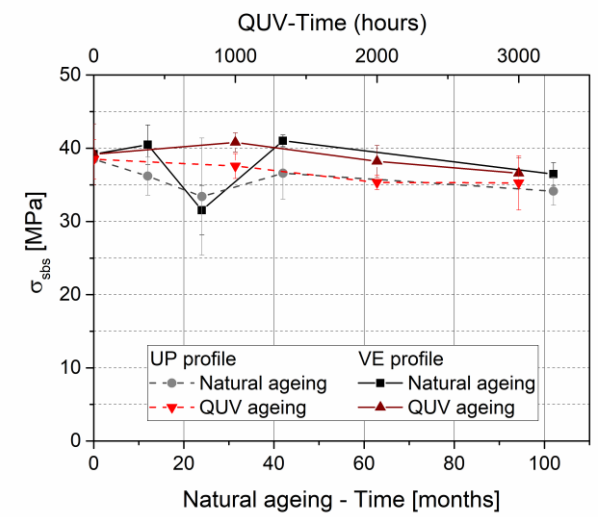

Figure 5.13. Variation of interlaminar shear strength, for both profiles, during exposure to the different ageing environments.

Interlaminar shear strength shows a general decreasing tendency for both profiles. However, at some point, both profiles presented interlaminar shear strength recovery, indicating again the existence of post-curing phenomena. This effect was more evident under natural ageing conditions. It is shown that both profiles presented approximately similar levels of degradation and interlaminar shear strength values. The UP profile presented 93% and 91% strength retention, respectively, after 102 months and 3000 hours of QUV exposure, whereas those figures were 89% and 93% for the VE profile. It is worth mentioning that the 42 months of natural exposure batch showed significant property recovery in both profiles, and later progressed to a similar slight degradation trend, in agreement with QUV ageing. Interlaminar shear strength degradation was much lower than that presented by the same GFRP profiles when exposed to hygrothermal ageing [5.4, 5.5], in which short-beam-strength retention after saturation was lower than 50%. With the exception of the results for 24 months in natural ageing, the variation of interlaminar shear strength under QUV and natural exposures are of the same orders of magnitude, and both degradation trends and values correlate extremely well between both types of ageing.

Much alike flexural strength, the hygrothermal ageing described in the previous chapter produced much higher degradation in the interlaminar shear strength of both profiles (maximum of 35% and 22% for the UP and VE profiles, respectively), which were not noticeable during both QUV and natural weathering. This indicates that interfacial matrix damage is

significantly more sensitive to that type of ageing environment than to natural or outdoor ageing.

5.4. Concluding remarks

This study allowed evaluating and correlating the degradation suffered by two types of GFRP profiles made of unsaturated polyester and vinylester resins after exposure to QUV artificial accelerated ageing and natural exposure. The results obtained allow drawing the following main conclusions:

1. For both QUV artificial accelerated and natural exposure, gloss and colour presented very significant changes, mainly due to UV exposure. Both UP and VE profiles presented yellowness, darkening, extremely low gloss retention and visible fibre content (fibre blooming) due to resin photo-chemical degradation. These considerable changes in aesthetical properties caused by UV radiation must be duly considered in outdoor applications.

2. FTIR analysis confirmed the above mentioned chemical changes and, together with mechanical testing, showed that the effects of UV exposure are mainly confined to the top few microns of the surface, leading to much smaller changes in mechanical properties when compared to hygrothermal ageing. In fact, it seems that the most damaging effects on GFRP composites by UV radiation are not due to the direct exposure to sunlight. However, this direct exposure can accelerate degradation by other agents, namely moisture.

3. DMA analysis showed slight changes in glass transition temperature for both QUV artificial accelerated and natural ageing but, at some point, it also indicated the existence of post-curing effects due to moisture and high temperature exposure, which is confirmed by mechanical testing. Compared to hygrothermal ageing, little changes occurred in the VE profile under both types of ageing. The UP profile also presented lower changes when comparing the effects of natural weathering with the effects of hygrothermal ageing reported in the previous chapter, where significant T_g increase had been observed during hygrothermal ageing.

4. In all mechanical tests both profiles exhibited linear elastic material behaviour until rupture. Tensile, flexural and interlaminar shear strength presented some changes throughout the exposure time, which at some point seem to have been affected by the post-curing phenomena. Flexural strength was the most affected resistance property (22% loss for the VE profile). Tensile and flexural modulus showed higher signs of degradation,

which was maximum in the UP profile (33% and 37% loss for tensile and flexural modulus, respectively). Interlaminar shear strength presented overall degradation for both profiles; however, significant property gain was reported at some point. Overall, between 42 and 102 months of natural ageing, mechanical property recovery was observed, or at most the degradation effects were insignificant. Compared to hygrothermal effects, natural weathering and QUV ageing produced in general significantly less reduction of both profiles' mechanical properties.

5. In general, the VE profile presented higher mechanical properties and stability to outdoor degradation compared with the UP profile, which is consistent with the findings reported in Chapter 4 concerning hygrothermal ageing. However, such better performance was not observed in terms of glass transition temperature variation, which may also be due to differences in the initial curing degree of both resins, and is also consistent with the materials studied in Chapter 4.

6. Overall, QUV artificial accelerated and natural ageing could be correlated, particularly in what concerns colour and gloss changes, and interlaminar shear strength – 2000 to 3000 hours of QUV exposure caused similar aesthetic degradation to 30 to 40 months of natural ageing in Lisbon city centre. In general, it was also possible to correlate physical (T_g) and mechanical changes after exposure to those two environments – properties are of the same order of magnitude and exhibit comparable variation trends. For tensile strength, such correlation was not so strong, most likely due to the influence of post-curing phenomena caused by those two environments being different. However, for interlaminar shear strength, the results of QUV and natural ageing have a considerably good correlation.

5.5. References

[5.1] Correia JR. GFRP pultruded profiles in civil engineering: hybrid solutions, bonded connections and fire behaviour: Instituto Superior Técnico, 2008.

[5.2] Karbhari VM. Durability of Composites for Civil Structural Applications. Boca Raton, Florida: Woodhead Publishing, 2007.

[5.3] Karbhari VM, Seible F. Fiber reinforced composites – Advanced materials for the renewal of civil infrastructure. Appl Compos Mater. 2000;7:95-124.

[5.4] Sousa JM. Durability of GFRP pultruded profiles made of vinylester resin. Lisbon: Instituto Superior Técnico, Technical University of Lisbon, 2011.

[5.5] Karbhari VM, Zhang S. g-Glass/vinylester composites in aqueous environments – I: Experimental results. Appl Compos Mater. 2003;10:19-48.

[5.6] Schuttle CL. Environmental durability of glass-fiber composites. Materials Science and Engineering. 1994;13:265-323.

[5.7] Liao K, Schultheisz CR, Hunston DL, Brinson LC. Long-term durability of fiber-reinforced polymer matrix composite materials for infrastructure applications: A review. J Adv Mater. 1998;30:3-40.

[5.8] Karbhari VM, Chin JW, Hunston D, Benmokrane B, Juska T, Morgan R, et al. Durability gap analysis for fiber-reinforced polymer composites in civil infrastructure. J Compos Constr. 2003;7:238-47.

[5.9] Bogner BE, Borja PP. Strength retention of pultruded composites after exposure to ultra-violet (UV) light. Research Report. Naperville, Illinois: BP Amoco Research Center; 1997.

[5.10] Chin JW, Nguyen T, Aouadi K. Effects of environmental exposure on fiber-reinforced plastic (FRP) materials used in construction. Journal of Composites, Technology and Research. 1997;19:205-13.

[5.11] Bank LC, Gentry TR, A. Barkatt. Accelerated test methods to determine the long-term behaviour of FRP Compos Struct: Environmental effects. J Reinf Plast Compos. 1995;14:559-87.

[5.12] Bogner BE, Borja PP. Ultra-violet light resistance of pultruded composites. European Pultrusion Technology Association. Venice, Italy1994. p. 1-18.

[5.13] Cabral-Fonseca S, Correia JR, Rodrigues MP, Branco FA. Artificial accelerated ageing of GFRP pultruded profiles made of polyester and vinylester resins: Characterisation of physical–chemical and mechanical damage. Strain. 2012;48:162-73.

[5.14] ISO 4892. Plastics. Methods of exposure to laboratory light sources. Part 1: General guidance; Part 3: Fluorescent UV lamps. Int Organ Stand, 2016.

[5.15] ISO 7724. Paints and varnishes. Colorimetry. Part 1: Principles; Part 2: Colour management. Int Organ Stand, 1984.

[5.16] ISO 2813. Paints and varnishes. Determination of specular gloss of non-metallic paint films at 20^{o}, 60^{o}, 85^{o}. Int Organ Stand, 2014.

[5.17] Chu W, Karbhari VM. Effect of water sorption on performance of pultruded E-glass/vinylester composites. Journal of Materials in Civil Engineering. 2005;17:63-71.

[5.18] Correia JR, Cabral-Fonseca S, Costa R, Carreiro A, Rodrigues MP, Eusébio MI, et al. Environmental degradation of GFRP pultruded profiles made of polyester and vinylester resins. In: Ferreira AJM, editor. 15th International Conference on Compos Struct. FEUP, Porto2009. p. 1-17.

[5.19] Merah N, Nizamuddin S, Khan Z, Al-Sulaiman F, Mehdi M. Natural weathering and sea water effects on the durability of glass fiber reinforced vinylester: Fractographic analysis. Appl Compos Mater. 2010;17:363-72.

[5.20] Segovia F, Ferrer C, Salvador MD, Amigo V. Influence of processing variables on mechanical characteristics of sunlight aged polyester-glass fibre composites. Polym Degrad Stab. 2001;71:179-84.

[5.21] Correia JR, Cabral-Fonseca S, Branco FA, Ferreira JG, Eusébio MI, Rodrigues MP. Durability of pultruded glass-fiber-reinforced polyester profiles for structural applications. Mechanics of Composite Materials. 2006;42:325-38.

Chapter 6.

Effects of thermal cycles on pultruded GFRP profiles

6.1. Introduction

As discussed in preceding chapters, in spite of anecdotal evidence of improved durability, the widespread acceptance of GFRP profiles for civil engineering structural applications is being delayed by the lack of comprehensive and validated data about their durability. In fact, although there is a wealth of information available concerning their short-term behaviour, their durability has not yet been investigated to an extent that provides enough confidence to construction agents, namely when compared with traditional materials. The need to document, evaluate and quantify the durability performance of GFRP profiles is particularly relevant for civil engineering structural applications, as the majority of the projects are developed considering relatively long service lives, often higher than 50 years [6.1, 6.2].

Thermal cycles are one of the most relevant types of environmental agents that FRP materials are subjected to, namely in outdoor applications. The concerns regarding thermal cycles are related not only with the exposure to sub-zero temperatures, but also to the thermal variations (amplitude and heating or cooling rates). There is anecdotal evidence that exposure of FRP composites to sub-zero temperatures can cause matrix hardening and microcracking, as well as fibre-matrix debonding [6.2]. The exposure to thermal variations can also promote fibre-matrix debonding due to the different coefficients of thermal expansion of the fibres and the matrix and the consequent build-up of internal stresses. Although thermal cycles can have a potential deleterious effect in the performance of FRP materials, studies reported in the literature are relatively scarce. As discussed in Chapter 3, the materials and exposure conditions used in those studies can vary significantly. Furthermore, in general, few properties were assessed in each of those studies.

Overall, the experimental work reviewed in Chapter 3, regarding the effects of thermal cycles on the physical and mechanical properties of pultruded GFRP composites, is very limited. Moreover, the test methods used in these studies vary considerably, with respect to the constituent materials (fibre and resin nature), manufacturing processes, type (number of cycles and temperature range) and exposure conditions (dry, saturated in different solutions, loaded/unloaded) and characterization techniques. Thus, some results are contradictory and present clearly distinctive degradation magnitudes. It is also worth mentioning that none of the reported studies provide degradation models able (i) to predict/simulate the effects of thermal cycles on the GFRP

physical and mechanical properties and/or (ii) to link experimental laboratory results with actual/field exposure during service life.

This chapter presents results of an experimental study about the degradation of two commercial GFRP profiles - identical to those used in the investigations presented in Chapters 4 and 5 -, made of two alternative resin matrix systems - unsaturated polyester (UP) and vinylester (VE) - both comprising identical fibre content and reinforcement architecture, after being exposed to thermal cycles, with limit characteristic temperatures of Mediterranean mild climates. The performance of both profiles following such exposure conditions was analysed and compared regarding their physical, viscoelastic and mechanical responses. Complementary data provided by scanning electron microscopy (SEM) analysis was also gathered.

6.2. Experimental programme

6.2.1 Materials

The materials used in the experimental study consist of two square tubular section ($50 \times 50 \times 5$ mm^3) *off-the-shelf* pultruded GFRP profiles, manufactured and supplied by *ALTO Perfis Pultrudidos.* Both profiles comprise alternating layers of E-glass unidirectional rovings and strand mats embedded in either unsaturated polyester resin (UP profile) or vinylester resin (VE profile). These materials were obtained from the same batch used in the investigations reported in Chapter 5 (please refer to that chapter for the detailed properties of unaged material).

In addition to those reference materials, batches from the UP and VE profiles used in the experiments described in Chapter 4 were also considered; this material was used as a second test series, subjected to a larger number of thermal cycles, as described in the next section.

6.2.2 Ageing environments

In order to adequately assess (i) the changes in the physical and mechanical properties of the GFRP composites, as well as (ii) the mechanisms of degradation as a result of thermal cycles, specimens from the material used in Chapter 5 (Batch 1) were subjected to three sets of cycles (70, 120 and 190 cycles) in a conditioning chamber from *Aralab*, model *Fitoclima 300 EDTU*, depicted in Figure 6.1 (a). Each thermal cycle had a total duration of 14 hours, with 6 hours at -5 °C, 6 hours at 40 °C and 2 hours of continuous heating or cooling between those two reference temperatures, as illustrated in Figure 6.1 (b). Because there is no information on the literature or in test standards specifying the minimum number of thermal cycles GFRP

materials must resist for a given service life and climate, existing specifications for other construction materials (*e.g.*, ASTM D 6944 [6.3], EN 1504-2 [6.4], EN 1504-3 [6.5], EN 1504-4 [6.6] and EN 539-2 [6.7]) were considered.

Most of the mentioned documents refer to coatings and non-structural materials (generally designed for service lives that do not exceed 25 years), specifying no more than 50 thermal cycles. Therefore, about 200 cycles should be a reasonable figure for pultruded GFRP profiles used in structural applications (generally, with a service life of 50 years), particularly for a Mediterranean (mild) climate. However, it was decided to make a further effort to deepen the understanding of the effects of thermal cycles, and therefore a second batch of specimens used in the tests described in Chapter 4 (Batch 2) was subjected for 200, 400 and 600 cycles (similar to those used for Batch 1).

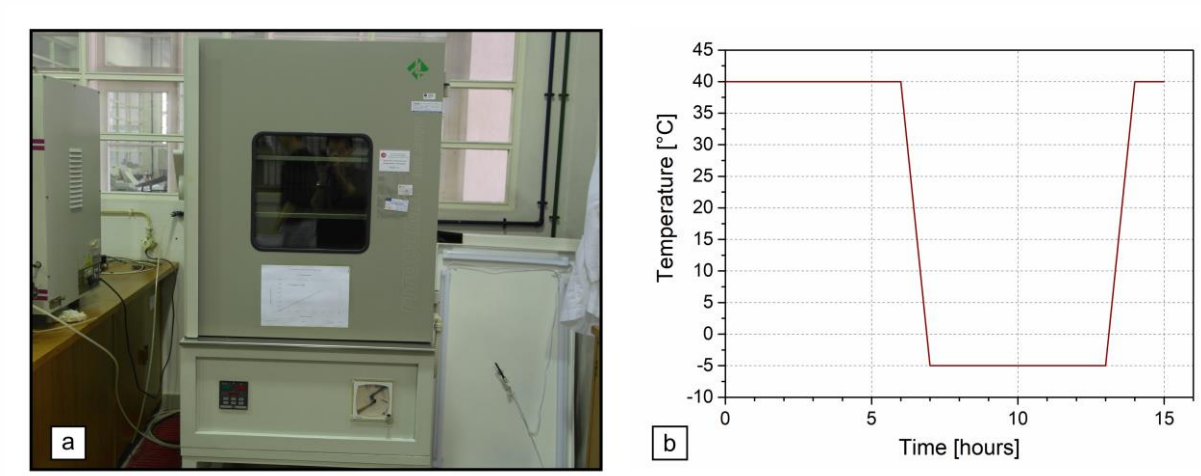

Figure 6.1. (a) Thermal cycling chamber; (b) thermal cycle sequence.

6.2.3 Characterisation methods

Specimens with appropriate dimensions (for physical-chemical and mechanical characterisation, detailed below), were cut from the 5 mm thick walls of both tubular (Batch 1) and flat (Batch 2) profiles in the longitudinal direction, using a water-cooled diamond saw blade. After pre-conditioning until constant weight (in a ventilated chamber at 50 °C), specimens were exposed to the referred thermal cycles.

At predefined times, batches of test specimens used for physical and mechanical characterisation were (i) removed from the previously mentioned conditioning chamber, (ii) stored in polyethylene hermetically closed recipients, and then (iii) placed inside a room with temperature controlled at 23 (±2) °C. Prior to testing, specimens were removed from the polyethylene recipients and immediately tested without any further conditioning.

Thermal cycling effects was assessed through the evaluation of changes in physical-chemical and mechanical properties during ageing, namely: (a) dynamic mechanical analyses (DMA), to assess the viscoelastic behaviour; (b) tensile, flexural, interlaminar shear, and in-plane shear tests, to evaluate the mechanical properties; and (c) scanning electron microscopy (SEM), to monitor the potential changes in the microstructure due to the degradation (if any) caused by the thermal cycles, as well as the possible changes into the main mechanisms of fracture.

Both DMA and all of the mechanical tests were performed as described in Section 4.2.3. SEM analysis was performed in the two following electron microscopes: (i) *Hitachi S-2400 Scanning Electron Microscope* with a tungsten thermionic emission gun and elemental analysis (Bruker), equipped with an Energy Dispersive Spectrometer (EDS) and a digital image acquisition and analysis feature, with maximum accelerating voltage of 25 kV and resolution of 5 nm at 25 kV (maximum magnification = 3×10^5 ×); (ii) *JEOL JSM-7001F Scanning Electron Microscope*, with a Schottky emission gun, elemental and diffraction pattern analysis (*Oxford INCA 250*), equipped with secondary and backscattered electron detectors, EDS with light elements detector, a system for detecting and processing electron backscattered diffraction patterns and a digital image acquisition and analysis feature, with maximum accelerating voltage of 30 kV and resolution of 1.2 nm at 30 kV (maximum magnification = 10^6 ×). In the SEM experiments, the surface of the specimens has been sputter coated with either a gold layer or a gold/palladium layer, using standard procedures. All the SEM observations reported were performed on the crack surfaces of the specimens after mechanical rupture, in three different testing geometries: tensile, bending and interlaminar shear modes. Both unaged specimens and aged specimens from Batch 1 (190 thermal cycles) were considered. SEM has been widely used in fibre-reinforced composite materials to identify the following failure mechanisms by detailed analysis of fracture specimens [6.8-6.13]: delamination, interlaminar matrix cracking, longitudinal matrix splitting, fibre-matrix debonding, fibre pull-out and fibre fracture.

6.3. Experimental results and discussion

For clarity of the discussion, the results are presented and analysed as related to the method of characterisation used. However, wherever relevant, results of different tests are cross-referenced. The results obtained in this study are also benchmarked with those obtained in studies reported in the literature that are comparable with ours in terms of fibre reinforcement and resin system.

6.3.1 Characterisation of reference GFRP materials (unaged)

The initial characterisation results for both UP and VE profiles before exposure to thermal cycles are described and listed in Section 5.3.1 (Batch 1) and Section 4.3.1 (Batch 2).

6.3.2 Characterisation of the thermo-mechanical response

Figure 6.2 shows representative DMA curves (storage modulus, E', left axis and loss factor, tan δ, right axis) for UP and VE profiles, from both batches before and after exposure to different numbers of thermal cycles (for each set of cycles, one representative curve among three replicates is presented).

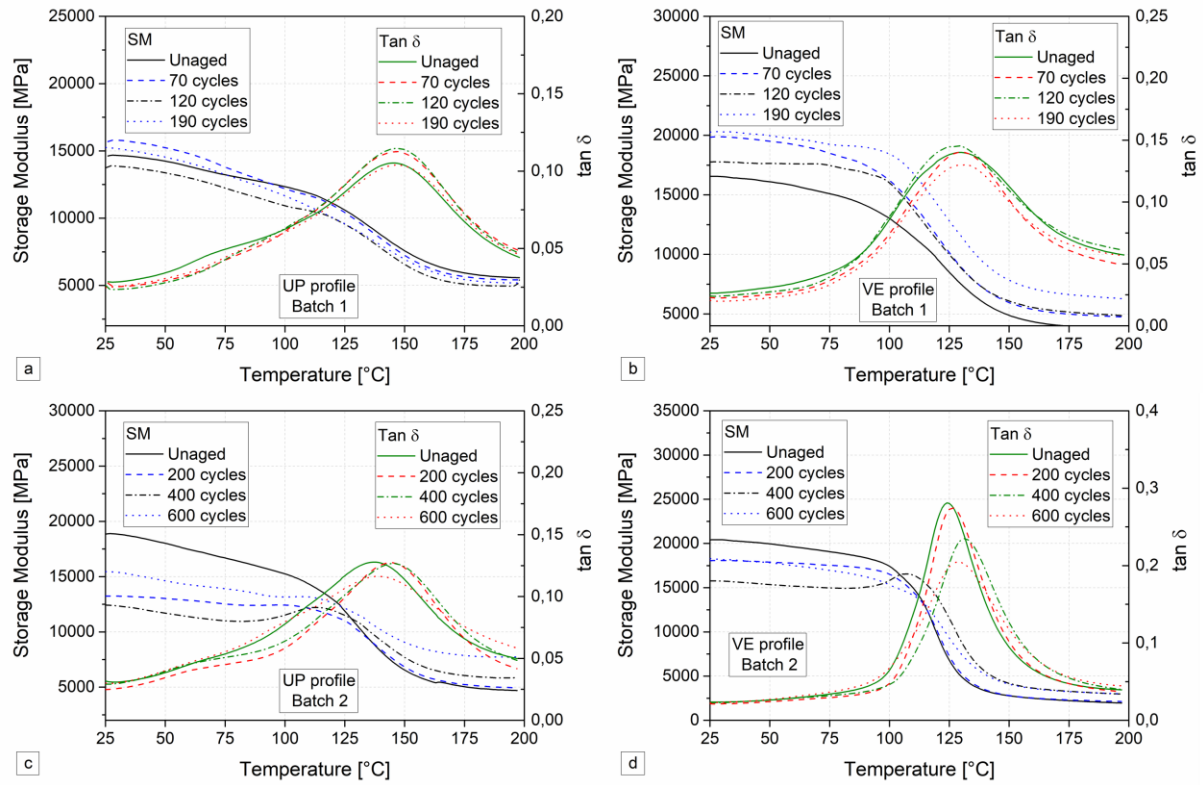

Figure 6.2. DMA curves of (a) Batch 1 - UP, (b) Batch 1 - VE, (c) Batch 2 - UP, and (d) Batch 2 - VE profiles, before and after different number of thermal cycles.

The storage modulus (E') curves represented in the left axis of the graphs present the characteristic slope in the glass transition region. The loss factor (tan δ) curves plotted in the right axis indicate the typical maximum peak in the same region. The pattern of the E' curves in the glass transition region reflect essentially modifications in the polymeric matrix, which changes from a glassy to an elastomeric state, due to its viscoelastic nature. In fact, the reinforcing material (glass fibres) does not present stiffness loss for this temperature range. However, as already mentioned, degradation of the matrix-fibre interphase quality can influence DMA results.

Figures 6.2 (a) and 6.2 (b) show that, in general, following the exposure to the thermal cycles, the progression of the E' and tan δ curves exhibited by both materials of Batch 1 was kept constant, indicating that no significant changes occurred in their viscoelastic properties up to 200 cycles. For more than 200 cycles (Figures 6.2 (c) and 6.2 (d)), similar results were obtained for Batch 2. Although some lowering of the storage modulus curve in the glassy area (*i.e.* around 25-50 °C) was observed comparing to the unaged values of the profiles, the overall reduced values are in agreement with the results from Batch 1. In addition, slight but progressive decreases in the height of the tan δ curves peak are also observed as the number of thermal cycles increase. Both these effects have been reported to be related to the existence of post-curing phenomena (*cf.* Chapter 4), probably associated with residual curing of the polymeric matrixes during the longer periods of exposure to higher temperature.

Figure 6.3 plots for both profiles the changes in T_g, determined from both *E'* (taken as the extrapolated onset of its sigmoidal change, according to the definition of ASTM E 1640 standard [6.14]) and tan δ curves, as a function of the number of thermal cycles for both batches of pultruded GFRP profiles.

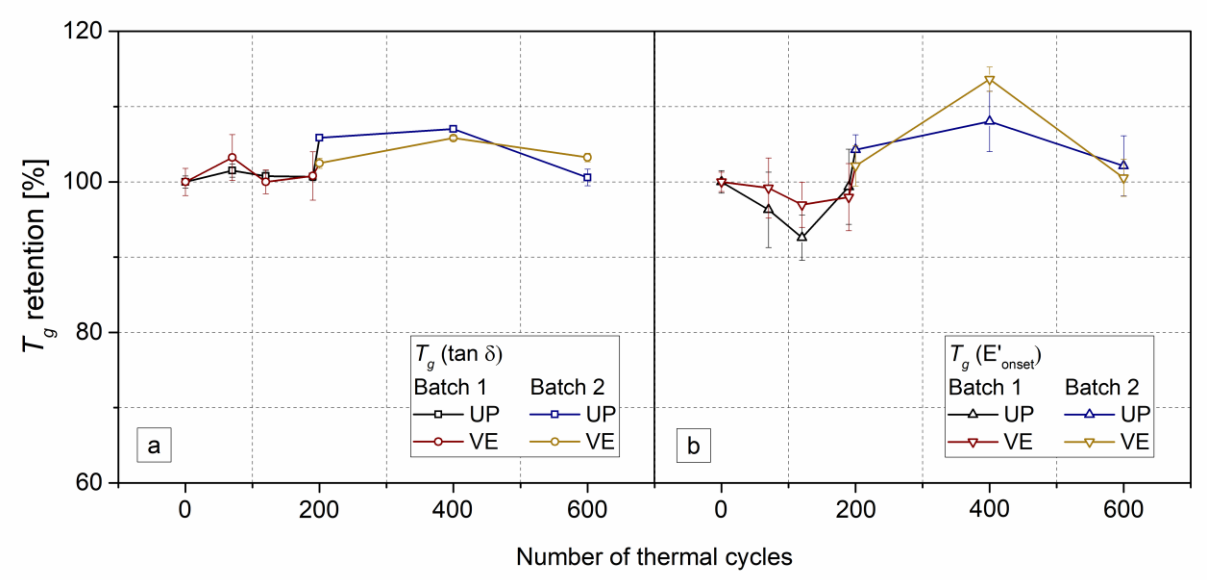

Figure 6.3. Retention of T_g as a function of the number of thermal cycles for UP and VE profiles: (a) T_g (tan δ); (b) T_g (E'$_{onset}$).

It can be seen that both profiles present a very slight increasing pattern in the T_g defined from the tan δ curve peak and a slight initial decreasing pattern in the T_g defined from the *E'* decay curve, more pronounced in the UP profile, which exhibited a maximum reduction of 7% after 120 cycles. After 190 cycles, the reduction in the T_g of both profiles defined from *E'* was less than 2%, which is almost negligible and well within the experimental uncertainty. However, from 200 to 400 cycles small increases in T_g are observed, more evident in the values taken

from the onset of the storage modulus curve, up to a maximum of 7-8% in the UP profile and 6-14% for the VE profile, which are consistent with the existence of the aforementioned post-curing effects (negligible up to 190 cycles). The increasing pattern was slight in terms of absolute values (never exceeding a 13% increase), being more evident in the UP profile. After 600 thermal cycles the T_g values were significantly close to the unaged values for both profiles. These results indicate that changes in T_g due to thermal cycles are not relevant, being much less significant when compared to those caused by accelerated hygrothermal ageing [6.15].

Despite some differences (in terms of materials, manufacturing process, and/or test conditions) between the present study and those performed by Karbhari *et al.* [6.16] and Aniskevich *et al.* [6.17], the range of variation in DMA results obtained here was similar to that reported by those authors.

6.3.3 Characterisation of the tensile response

Figure 6.4 plots for both profiles and batches the variation of the tensile strength and modulus, respectively, as a function of the number of thermal cycles.

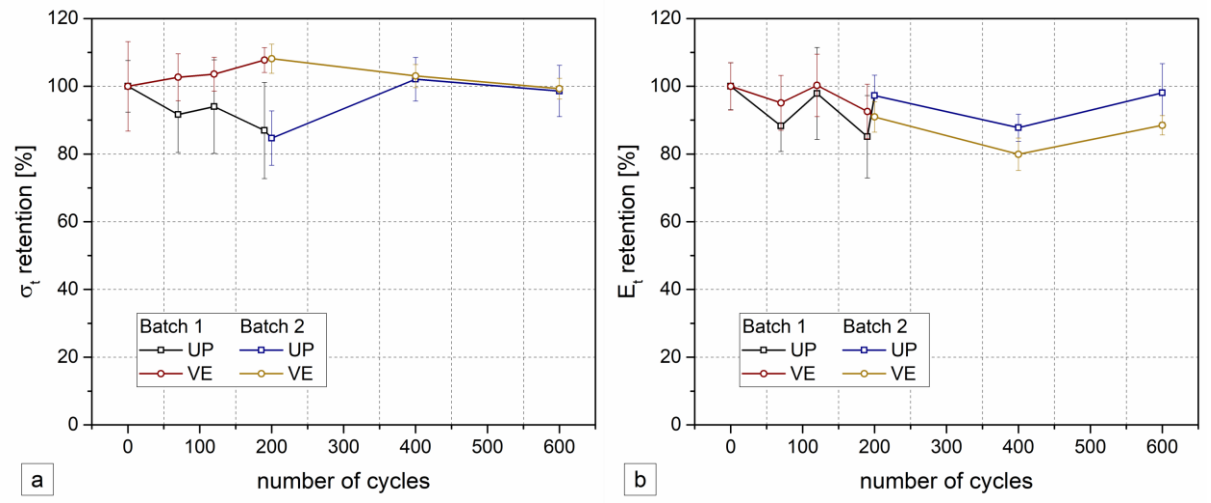

Figure 6.4. Tensile properties retention as a function of the number of thermal cycles for UP and VE profiles: (a) strength and (b) modulus.

For the UP profile, in spite of the scatter in the experimental data, it can be seen that there is a general decreasing trend of the tensile strength with the increase in the number of thermal cycles up to 190 cycles. The tensile strength retention of the UP profile was 92%, 94% and 87% after respectively 70, 120, and 190 cycles. However, after 200 cycles some property recovery was noted up to 400 cycles, which stabilised in values similar to those of the unaged material. This non-monotonic variation should be related to the post-curing effects, described in Chapter 3, and also relevant in different ageing environments (*cf.* Chapters 4 and 5). After 600

cycles, the tensile strength of the UP profile was 99%. The VE profile exhibited an opposite variation trend, with tensile strength increasing 3%, 4% and 8% after respectively 70, 120 and 190 cycles, and subsequently decreasing, again reaching retention values close to the unaged values. After 600 cycles, the VE tensile strength retention was 99%. It is interesting to note that besides evidencing property recovery/loss at different times, both values for the UP and VE profiles were very similar after 400 and 600 cycles, regarding tensile strength. However, the VE profile seemed to be more stable to thermal cycles, since it never lowered below the unaged values.

In what concerns stiffness, the tensile modulus of both profiles presented a general, although irregular, decreasing tendency up to 400 cycles. Afterwards, both profiles exhibited a moderate increase at 600 cycles. The lower tensile modulus retentions were 85% and 80% for both UP (200 cycles) and VE (400 cycles) profiles, respectively. After 600 cycles, these figures were 98% and 88% for UP and VE profiles, respectively.

As already mentioned, thermal cycles (and freeze-thaw exposure) may cause fibre-matrix debonding and matrix microcracking, leading to a reduction in both tensile strength and modulus. The UP profile exhibited an early decrease in both tensile strength and modulus, which seems to indicate that the above-mentioned mechanisms were effectively caused by the thermal cycles. The increasing trend of both strength and modulus, which was evident between 200 and 600 cycles, should stem from post-curing effects, due to the higher range of exposure temperature (40 °C) during the hot part of the thermal cycle. In what concerns the VE profile, it is again likely that the higher range of temperature exposure increased the degree of matrix reticulation, thereby contributing to the slight increase of tensile strength (up to 200 cycles) and modulus (between 400 and 600 cycles), which is in agreement with the DMA results, where the occurrence of such effects is also suggested. In general, tensile strength of the VE profile did not present any significant degradation when compared to the unaged results during the globality of the thermal cycles, while the tensile modulus presented some changes (maximum reduction of 20%).

Karbhari *et al.* [6.16] reported reductions in the tensile strength of an E-glass vinylester composite. Despite some differences to our study, which may be explained by the differences in the test programme (manufacturing process, temperature ranges and duration), it is worth mentioning that the magnitude of tensile strength variations was similar (although of different signs), whereas the tensile modulus variation was very similar when compared with that of the VE profile. Tann and Delpak [6.18] observed no significant influence of freeze-thaw cycles, which is most likely related with the very reduced number of cycles used in this study. In the

experimental program performed by Haramis *et al.* [6.19], similar results were obtained on glass-vinylester composites: the authors reported a slight increase in tensile strength, which was not affected by the application of sustained (flexural) loading, and attributed such increase to material desiccation during conditioning. In the work reported by Sheikh and Tam [6.1], the tensile properties of a glass-epoxy composite system suffered also very little changes.

The comparison of the results obtained in the present study with the ones reported in the literature that are more comparable shows that, despite some differences in the manufacturing processes, resin matrixes and thermal cycles (number and duration of cycles, minimum and maximum temperatures), there is an overall general agreement between the test data, indicating that the tensile properties of GFRP composites suffer only slight changes due to thermal cycles (lower than 15%).

6.3.4 Characterisation of the flexural response

Figure 6.5 illustrate for the UP and VE profiles the variation in flexural strength and modulus, respectively, both as a function of the number of thermal cycles.

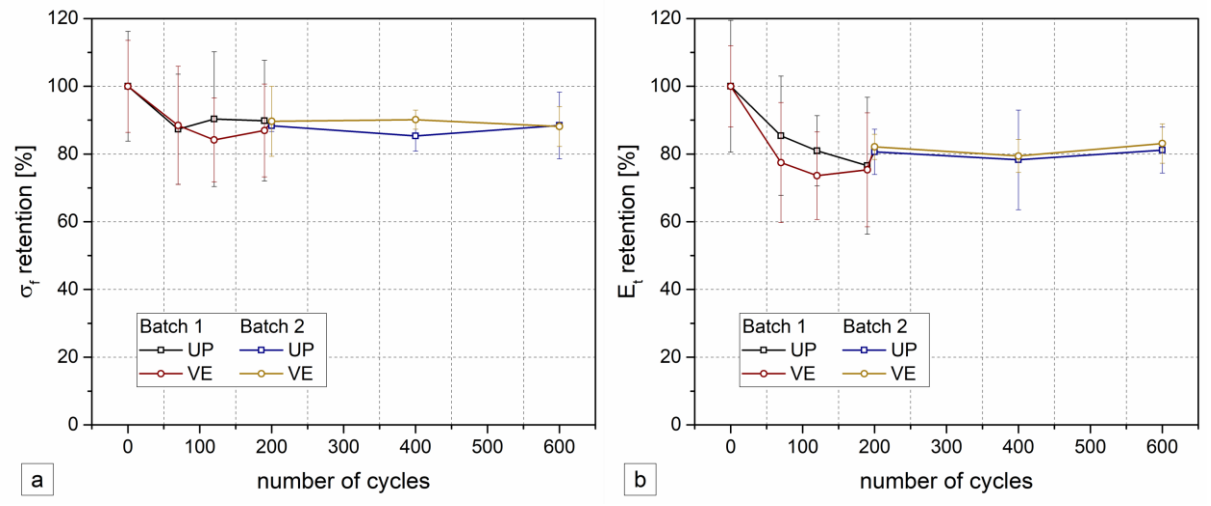

Figure 6.5. Flexural properties retention as a function of the number of thermal cycles for UP and VE profiles: (a) strength and (b) modulus.

Although the scatter of the results obtained is rather significant, it seems clear that the flexural strength and modulus of the Batch 1 profiles are negatively affected by the exposure to the thermal cycles. In addition, the overall trends of variation exhibited by the flexural strength and modulus curves seem to indicate that those parameters are stabilizing for increasing thermal cycles, i.e. the degradation is more important during the first cycles. Concerning the Batch 2, both UP and VE profiles seemed to maintain the level of degradation, progressing

towards a stabilization plateau with a generalised reduction of around 10% in strength and 20% in modulus for both profiles.

Regarding the material from Batch 1, in terms of flexural strength, the UP profile exhibited retentions of 87% (minimum value), 90% and 89% after respectively 70, 120 and 190 thermal cycles. The VE profile experienced slightly higher strength degradation, with the previous figures being respectively 88%, 84% and 87%. In terms of flexural modulus, the performance reduction caused by the thermal cycles was higher than that of flexural strength: flexural modulus retentions after 70, 120 and 190 cycles were respectively 86%, 81% and 76% for the UP profile, and 78%, 74% and 75 % for the VE profile.

In Batch 2, the results obtained for both flexural strength and modulus progressed to a stabilisation plateau, for around 80% retention values. In terms of flexural strength, the UP profile exhibited retentions of 88%, 85%, and 87%, after respectively 200, 400 and 600 cycles. The VE profile presented slightly higher values, with the previous figures being respectively, 89%, 90%, and 88%. The flexural modulus of this batch followed the same trend as strength with higher level of degradation. Flexural modulus retentions after 200, 400, and 600 cycles were respectively 81%, 78%, and 82% for the UP profile, and 82%, 79%, and 83% for the VE profile. This stabilisation of retention, compared to Batch 1, should be related to the occurrence of the aforementioned post-curing effects (*i.e.* prolonged exposure at the higher temperatures of 40 °C during cycling promoted further crosslinking and polymerization of the resin matrix, *cf.* Chapter 4), and were also visible in the other properties; these phenomena should have had a competing effect with the degradation mechanisms caused by the temperature cycles.

In the study performed by Dutta and Hui [6.20], the pultruded E-glass fibre unsaturated polyester system (more similar to the material tested in our study) presented extensive visible degradation and cracks after 100 cycles. In opposition, the S2-glass reinforced polyester composite system did not show signs of significant flexural modulus variation. Gomez and Casto [6.21] also reported considerable reductions of flexural strength and stiffness of both isophthalic polyester or vinylester resins, particularly for the latter resin, which is in accordance with our results. The flexural strength results reported by Aniskevich *et al.* [6.17] are in general agreement with our test data, in opposition to the flexural modulus which contrasts with our results; differences may be due to post-curing phenomena and matrix hardening caused by the exposure to low temperatures.

In general, the results obtained in the present study together with "more comparable" data reported in the literature show that exposure to thermal cycles likely to be observed in civil

engineering applications negatively affects the flexural properties of glass-reinforced polymer composites (more intensely than the tensile properties), particularly the flexural modulus. Such increased magnitude should be caused by the stronger dependency of flexural properties on the resin matrix and the fibre-matrix interphase (compared to tensile properties that are more fibre-dependent), which are believed to be more affected by the thermal cycles.

6.3.5 Characterisation of the in-plane shear response

Figure 6.6 plots for both profiles the variation of the in-plane shear strength and modulus, respectively, as a function of the number of thermal cycles. This characterisation was made only for specimens from Batch 2 (200 to 600 cycles).

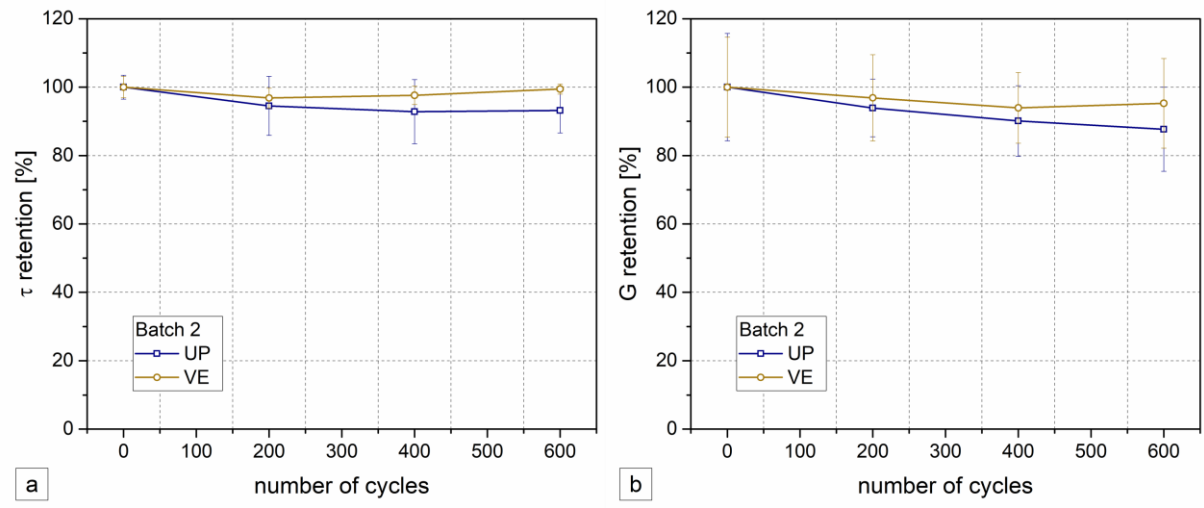

Figure 6.6. Retention of in-plane shear properties as a function of the number of thermal cycles for UP and VE profiles (Batch 2): (a) strength; (b) modulus.

Overall, the in-plane shear strength and modulus of both UP and VE profiles suffered little variations. Regarding the in-plane shear strength, the UP profile suffered a slight progressive reduction (7%) up to 400 cycles and seemed to progress towards a stable retention value at 600 cycles. Meanwhile, the VE profile had less overall degradation, which is in agreement with the other mechanical properties. After an initial reduction at 200 cycles (3%), the average values presented property recovery up to 600 cycles, very close to the unaged values. This non-monotonic (and low) variation should be related to the existence of the aforementioned post-curing effects and, possibly, to the intrinsic variability associated to the experiments. After 600 cycles, the interlaminar shear strength retention was 93 and 99% for the UP and VE profile, respectively.

Concerning the in-plane shear modulus, similar trends are observed despite the higher scatter values associated; however, this property seemed to be slightly more affected by thermal cycling, in a similar way as what was observed in flexural properties. The UP profile presented a continuous reduction, while the VE showed the same property recovery signs, at some point. After 600 cycles, the in-plane shear modulus retention was 88% and 95% for the UP and VE profiles, respectively.

Grammatikos *et al.* [6.22] studied the in-plane shear properties of pultruded polyester GFRP specimens up to 300 thermal cycles with 90 minutes duration with a softer amplitude configuration (-10 °C to 20 °C). The in-plane shear properties obtained here are in agreement with the results reported by those authors, which also showed very little changes due to thermal cycles. However, the reported changes were slightly lower than ours, which should stem from the lower duration of their experiments and also the lower temperature gradients, which should have less impact in the pultruded GFRP material.

6.3.6 Characterisation of the interlaminar shear response

Figure 6.7 illustrates the variation of the interlaminar shear strength of both profiles as a function of the number of thermal cycles.

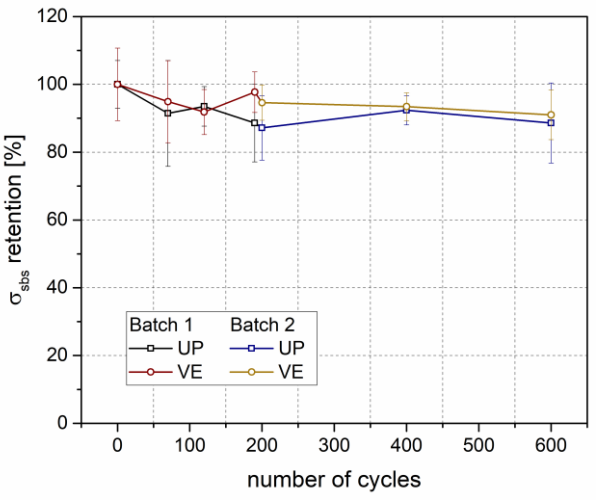

Figure 6.7. Interlaminar shear strength retention as a function of the number of thermal cycles for UP and VE profiles.

The curves plotted in Figure 6.7 for specimens from Batch 1 show that the interlaminar shear strength of both profiles suffered little variation due to the exposure to thermal cycles. The interlaminar shear strength of both profiles presents a general decreasing trend, with similar (and reduced) levels of degradation and short-beam-shear strength values. For the UP profile, the interlaminar shear strength variation was more consistent, with strength retentions of 91%,

94% and 89% after 70, 120 and 190 thermal cycles, respectively. For the VE profile those figures are respectively 95%, 92% and 98%.

Extending the number of thermal cycles in Batch 2, the results seem to progress towards a stabilisation plateau, much alike the flexural properties. The degradation levels of the interlaminar shear strength were low, suggesting that the interface between the polymeric matrix and the glass fibres was not significantly affected due to thermal cycling. For the UP profile, maximum reductions were around 8-12%. The VE profile seemed to be more resistant to thermal cycling, presenting reductions around 5-9%, which is in agreement with the remaining experimental results. After 600 thermal cycles, the interlaminar shear strength retentions was 88% and 91% for the UP and VE profiles, respectively.

In the study of Kim *et al.* [6.23], despite the important differences compared to our experimental work (namely in terms of typology and geometry of the composite system, as well as fibre architecture, and immersion in an alkaline solution), the E-glass vinylester system presented similar behaviour when compared to our VE profile. Regarding the study of Zhang *et al.* [6.24], although there were also evident experimental differences, the obtained interlaminar shear strength variation when compared to our unsaturated polyester profile was fairly similar.

It is relevant to note that the degradation pattern in the interlaminar shear strength caused by the exposure to thermal cycles illustrated in Figure 6.6 is much lower than that caused by the exposure to hygrothermal ageing, described in Chapter 4, for which short-beam-strength retention was as low as 50%.

6.3.7 SEM characterisation

The SEM characterisation reported here was performed on the fracture surface of both UP and VE pultruded specimens from Batch 1, after mechanical testing. As mentioned, three different testing geometries were considered for GFRP material from Batch 1: tensile, bending and interlaminar shear. For each of type of pultruded material, both aged (190 cycles) and unaged samples were assessed.

Figures 6.8 and 6.9 display low magnification SEM micrographs of bending cracked unaged UP and VE specimens, respectively. Figures 6.10 and 6.11 display high magnification SEM micrographs of, respectively, unaged and aged (190 cycles) UP pultruded specimens, after bending tests. Figures 6.12 and 6.13 display similar SEM micrographs for unaged and aged (190 cycles) VE pultruded specimens, also after bending tests.

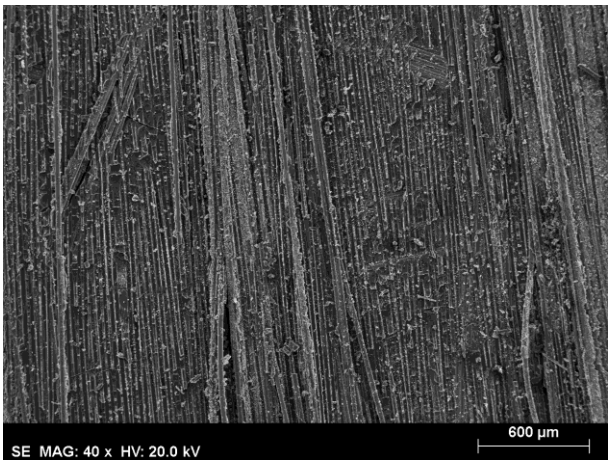

Figure 6.8. SEM micrograph of unaged UP profile after bending test (cracked surface).

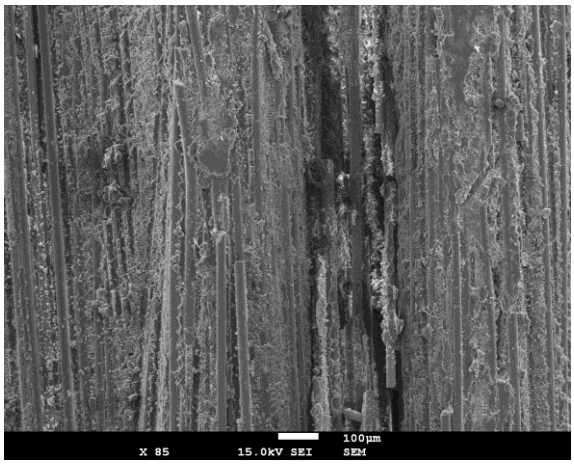

Figure 6.9. SEM micrograph of unaged VE profile after bending test (cracked surface).

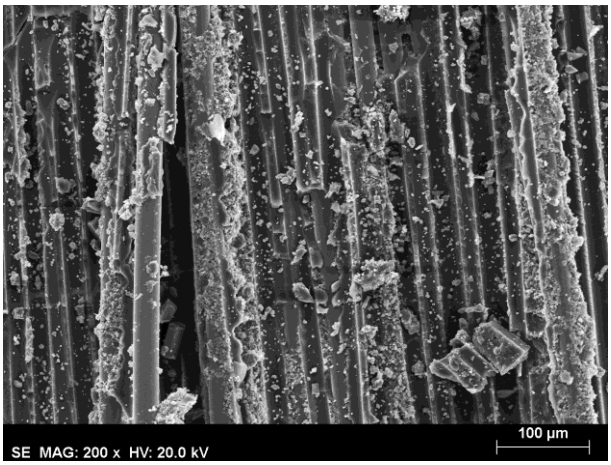

Figure 6.10. SEM micrograph of unaged UP profile, after bending test (higher magnification).

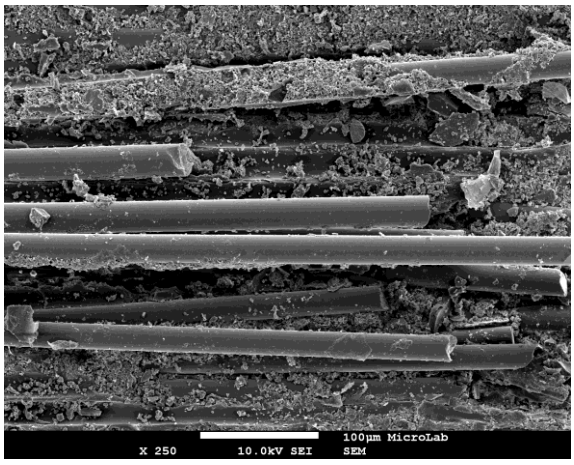

Figure 6.11. SEM micrograph of aged UP profile (190 cycles), after bending test (higher magnification).

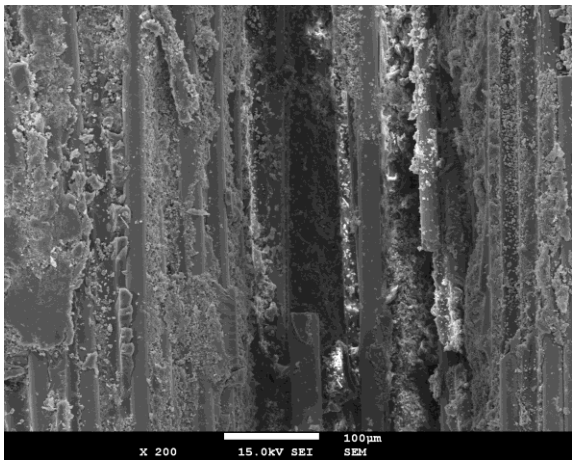

Figure 6.12. SEM micrograph of unaged VE profile, after bending test (higher magnification).

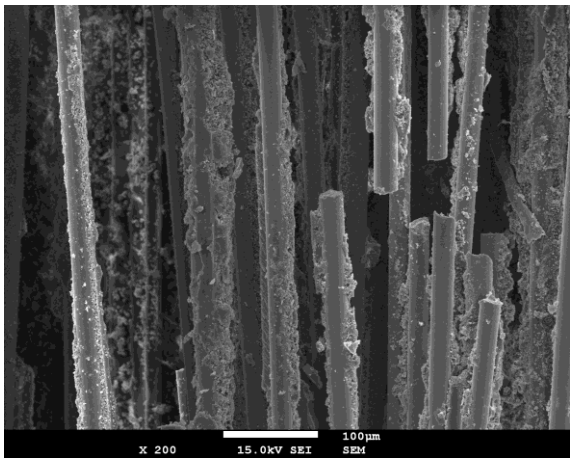

Figure 6.13. SEM micrograph of aged VE profile (190 cycles), after bending test.

For unaged UP pultruded composites (Figures 6.8 and 6.10), both cohesive rupture and adhesive rupture can be observed, the latter appearing to be the (slightly) dominant mechanism. Adhesive rupture occurs at the fibre-matrix interface and, as a result of the fibre-matrix debonding, both the fibre surface and the matrix surface look shiny. Cohesive rupture occurs in the matrix, in the bulk. Crack propagation occurs at the matrix around the fibres, but since the volume fraction of the matrix is relatively small, it is expected that cracks with origin in the matrix may also include the matrix-fibre interface in some part of their way. Consequently, isolated fibres appear coated by the matrix; they do not look fully coated because the tight packing of glass fibres makes it difficult for the propagation of cracks to occur exclusively in the matrix. Therefore, fibres isolated by cohesive rupture appear as partially coated by the matrix.

Both cohesive rupture and adhesive rupture can also be observed in unaged VE profile (Figures 6.9 and 6.12). In this case, cohesive rupture appears to be the dominant mechanism, as a consequence of better adhesion between the VE matrix and the glass fibres. The same patterns are observed for cracked samples after tensile or shear testing.

Figures 6.10 (unaged) and 6.11 (190 cycles) show that thermal cycles ageing has two main consequences in UP pultruded specimens: (i) some degradation of the fibre-matrix interface, increasing the relative weight percentage of fibre-matrix debonding, and (ii) some degradation of the matrix itself, evidenced by matrix cracking debris of micron size. Crack propagation in a degraded matrix originates secondary cracks (crack multiplication is easier as degradation proceeds).

As compared to UP resins, VE resins are expected to present better resistance to thermal cycles degradation and this is the case, as illustrated in Figures 6.12 (unaged) and 6.13 (190 cycles). Less adhesive debonding in both figures is associated to improved resistance of the fibre-matrix interface. On the other hand, no evidence of extensive microcracking was found in the VE matrix: cohesive rupture is not associated to extensive microcracking, as it is observed in UP (cured) matrix.

6.4. Concluding remarks

This chapter presented an experimental study about the effects of thermal cycles likely to be experienced in Mediterranean mild climates by pultruded GFRP profiles made of unsaturated polyester and vinylester resins. The results obtained allow drawing the following conclusions:

1. In general, both types of GFRP profiles presented low to moderate degradation of their mechanical properties due to thermal cycles, particularly when compared to the hygrothermal degradation experienced by those same materials.

2. DMA analysis indicates no evident structural changes in the resin matrix as well as at the fibre-matrix interphase, showing only slight variations in the glass transition temperature of both profiles. In addition, for both profiles, results suggest the existence of post-curing effects due to the higher temperature exposure ranges, especially when the number of cycles is higher, *i.e.* between 200 and 600 cycles. In addition, after 600 thermal cycles, the viscoelastic properties were very similar w.r.t those of the unaged specimens.

3. In terms of tensile properties, both types of GFRP profiles suffered small changes. The tensile strength of the UP profile decreased 13% up to 190 cycles, while for the VE profile it presented an overall increasing trend with a maximum increase of 8%. However, between 200 and 600 cycles, an opposite trend was evident, with signs of post-curing effects in the UP profile. After 600 cycles, the values of those properties were very similar to the unaged specimens (1% difference) for both profiles. Considering tensile modulus, both profiles presented an irregular decreasing pattern up to 400 cycles, during which the highest reductions were 15% and 20% for the UP and VE profiles, respectively. After 600 cycles, only slight changes (2%) were observed in the UP profile w.r.t. the unaged specimens, while in the VE profile this difference was of 12%.

4. Regarding the flexural properties, they were negatively and more considerably affected in both types of GFRP profiles. The degradation of flexural properties was more pronounced in the first set of cycles and it tended to stabilize for increasing thermal cycles. After 190 cycles, the flexural strength decreased 11% and 13% for the UP and VE profiles, respectively, whereas their flexural modulus was reduced by as much as 24% and 25%, respectively. Afterwards, both flexural properties seemed to have stabilised at a plateau that was nearly constant between 200 and 600 cycles. At the highest number of cycles, flexural strength decreased 13% and 12% for the UP and VE profiles, respectively, whereas their flexural modulus was reduced by as much as 18% and 17%. Such increased magnitude (namely, when compared to tensile properties) is deemed to have been caused by the stronger dependency of flexural properties on the resin matrix and the fibre-matrix interphase.

5. Concerning the in-plane shear strength and modulus, both UP and VE profiles suffered slight changes; overall, the UP profile was more affected than the VE profile. After 600 cycles, the in-plane shear strength was reduced by 7% and 1% for the UP and VE profiles, respectively.

The in-plane shear modulus presented similar trends, although with higher reductions of 12% and 5% for the UP and VE profiles, respectively, after 600 thermal cycles.

6. In terms of interlaminar shear properties, both types of GFRP profiles suffered slight changes. Both profiles presented a generalised decreasing trend with reduced levels of degradation and similar short beam shear strength values. The highest level of degradation was 11% for the UP profile and 8% for the VE profile and occurred at 120 and 190 cycles, respectively. Considering the extended cycles from batch 2, the degradation seemed to progress towards a stabilisation plateau, in the same way as what was observed in the flexural properties. The observed results suggest that thermal cycles (with the temperature amplitude used herein) do not significantly affect the interface between the polymeric matrix and the glass fibres.

7. SEM observations on crack surfaces provide evidence that two main processes are involved in crack initiation: adhesive rupture (fibre debonding) and cohesive rupture (matrix cracking). VE resins show better fibre-matrix adhesion and improved interphase resistance, as compared to UP resins. Also, the VE matrix resisted better to the thermal cycles than the UP matrix: in the former pultruded composite fibre-matrix debonding occurs in less extent, and matrix microcracking is scarcely present.

8. Globally, the VE profile presented better mechanical performance when compared to the UP profile, particularly in what concerns the tensile and interlaminar shear properties. Given the same fibre content and architecture of those profiles, such improved performance stems from the improved durability of the vinylester matrix system, together with the above-mentioned post-curing phenomenon.

9. Overall, thermal cycling affected the mechanical properties of both pultruded profiles to a lesser extent when compared to the other ageing factors considered in the previous chapters, especially in what concerns hygrothermal ageing.

6.5. References

[6.1] Sheikh SA, Tam S. Effect of freeze-thaw climatic conditions on long-term durability of FRP strengthening systems. Ministry of Transportation of Ontario HIIFP-037. 2007:1-40.

[6.2] Karbhari VM, Chin JW, Hunston D, Benmokrane B, Juska T, Morgan R, et al. Durability gap analysis for fiber-reinforced polymer composites in Civil Infraestructure. J Compos Constr. 2003;7:238-47.

[6.3] ASTM D 6944. Standard practice for resistance of cured coatings to thermal cycling. West Conshohocken, PA2009.

[6.4] EN 1504-2. Products and systems for the protection and repair of concrete structures. Definitions, requirements, quality control and evaluation of conformity - Part 2: Surface protection systems for concrete. Brussels: European Committee for Standardization; 2006.

[6.5] EN 1504-3. Products and systems for the protection and repair of concrete structures. Definitions, requirements, quality control and evaluation of conformity - Part 3: Structural and non-structural repair. Brussels: European Committee for Standardization; 2006.

[6.6] EN 1504-4. Products and systems for the protection and repair of concrete structures. Definitions, requirements, quality control and evaluation of conformity - Part 4: Structural bonding. Brussels: European Committee for Standardization; 2006.

[6.7] EN 539-2. Clay roofing tiles for discontinuous laying - Detemination of physical characteristics - Part 2: Test for frost resistance. 2007.

[6.8] Adams DF, Miller AK. An analysis of the impact behavior of hybrid composite materials. Mater Sci & Engineering. 1975;19:245-60.

[6.9] Elber W. Failure mechanics in low velocity impact on thin composite plates. NASA Technical Paper 2152. 1983.

[6.10] Cantwell JW. Impact damage in carbon fibre composites: PhD thesis, University of London, 1985.

[6.11] Vedula M, Koezak MJ. Impact resistance of cross-plied polyphenylene sulfide composites. Proc Fourth Japan-US Conf on Composite Materials. 1988:72-81.

[6.12] Clark G. Modelling of impact damage in composite laminates. Composites. 1989;20:209-14.

[6.13] Cantwell WJ, Morton J. The impact resistance of composite materials – a review. Composites. 1991;22:347-62.

[6.14] ASTM E 1640. Standard test method for assignment of the glass transition temperature by Dynamic Mechanical Analysis. West Conshohocken, PA American Society for Testing and Materials; 1999.

[6.15] Correia JR, Cabral-Fonseca S, Branco FA, Ferreira JG, Eusébio MI, Rodrigues MP. Durability of pultruded glass-fiber-reinforced polyester profiles for structural applications. Mech Compos Mater. 2006;42:325-38.

[6.16] Karbhari VM, Rivera J, Zhang J. Low-temperature hygrothermal degradation of ambient cured E-glass/vinylester composites. J Appl Polym Sci. 2002;86:2255-60.

[6.17] Aniskevich K, Korkhov V, Faitelsone J, Janson J. Mechanical properties of pultruded glass fiber reinforced plastic after freeze–thaw cycling. J Reinf Plast Compos. 2012;31:1554-63.

[6.18] Tann DB, Delpak R. Influences of freeze and thaw cycles and elevated temperatures on the properties of FRP composites. ACIC 2004 Conference, University of Surrey. 2004:611-8.

[6.19] Haramis J, Verghese KNE, Lesko JJ, Weyers RE. Characterization of freeze-thaw damage mechanisms in composites for Civil Infrastructure. Advance Composite Materials in Bridges and Structures -International Conference. 2000:663-70.

[6.20] Dutta PK, Hui D. Low-temperature and freeze thaw durability of thick composites. Compos Part B - Eng. 1996;27:371-9.

[6.21] Gomez JP, Casto B. Freeze-thaw durability of composite materials. Virginia Transportation Research Council VTRC 96-R25. 1996:1-13.

[6.22] Grammatikos SA, Jones RG, Evernden M, Correia JR. Thermal cycling effects on the durability of a pultruded GFRP material for off-shore civil engineering structures. Compos Struct. 2016;153:297-310.

[6.23] Kim H-Y, Park Y-H, You Y-J, Moon C-K. Short-term durability test for GFRP rods under various environmental conditions. Compos Struct. 2008;83:37-47.

[6.24] Zhang S, Karbhari VM, Reynaud D. NOL-ring based evaluation of freeze and freeze–thaw exposure effects on FRP composite column wrap systems. Compos Part B - Eng. 2001;32:589-98.

Chapter 7.

Synergistic effects of different ageing environments and sustained loading on pultruded GFRP profiles

7.1. Introduction

Several factors can affect the service life of pultruded glass fibre reinforced polymer (GFRP) profiles in civil engineering applications; they may cause detrimental effects at both material and structural levels. The most relevant factors that affect the durability of these materials have been thoroughly described in Chapter 3.

Besides acting isolated, these factors may act synergistically (*i.e.*, simultaneously) and further affect pultruded GFRP structures during their service life. This complex combination of several ageing factors, that in some cases are not always easy to define, constitutes an additional challenge in obtaining reliable information for the assessment and in-depth understanding of the overall long-term behaviour of pultruded GFRP elements.

Since civil engineering structures are generally subjected to sustained loads, either static, cyclic or dynamic, the synergistic effects between mechanical loading and environmental exposure has a large significance in the context of pultruded GFRP applications in this sector. However, limited investigations are available in the literature regarding this particular topic [7.1], especially in what concerns pultruded components, and this is the main motivation of the present chapter.

Buck *et al.* [7.2] studied the effects of exposure to demineralised water under sustained tension of infused glass vinylester composites. The specimens were immersed and subjected to 30% of their ultimate tensile strength for 700 hours. Results indicated that sustained load only slightly affected the strength loss of specimens under immersion. Additional scanning electron microscopy (SEM) data corroborated the results, since no cracking was observed in the coupons before testing.

Hebling and Karbhari [7.3] studied the sorption and tensile response of pultruded E-glass vinylester GFRP composites (squared plate specimens) subjected to hygrothermal exposure and sustained bending strain (30% and 45% of the specimens' ultimate load) for up to two years. Four ageing environments were considered: three immersion exposures at three different temperatures (22 °C, 44 °C, and 60 °C), and a reference environment at 22 °C and 60% relative

humidity (RH). Gravimetric measurements had anomalous responses in specific conditions, namely for long exposure times at high temperature and strain levels; moreover, the higher applied strain levels (45%) at 40 °C and 60 °C led to premature failure during the test procedure. The premature failure was attributed to hydrolysis and extraction of low molecular weight segments, which caused interfacial debonding and delamination at the central part of the specimens (load application area). Tensile strength decreased with increasing temperature and immersion time, with high sustained strain levels having a harsher detrimental effect at higher temperatures (over 60% reductions). It is worth referring that the stress/strain levels used in this study are way beyond the typical stress levels of GFRP structures in service conditions (generally limited to 20% of the material strength).

Wang *et al.* [7.4] studied the combined effects of moisture and sustained load in the tensile properties of vacuum infused GFRP sheets made of isophthalic polyester resin. Specimens were exposed to 0%, 10%, and 20% of their ultimate tensile load and simultaneously to immersion in tap water and salt water at room temperature, for up to 1 year. The water uptake was not influenced by the loading level. However, a slight increase in the diffusion coefficient for the higher strain levels was observed. All tested specimens registered an initial increase in tensile strength and modulus, which was attributed to post-curing phenomena, followed by a steady decrease. After one year, small reductions (7%, 5% and 2% for applied loads of 20%, 10%, and 0%, respectively) were observed for immersion in tap water. Slightly higher degradation was found in salt water immersion (around 14%), with relative differences between sustained load levels being similar to those measured after tap water immersion.

Ghaz *et al.* [7.1] evaluated the tensile strength and modulus of pultruded vinylester and unsaturated polyester GFRP specimens after 1000 and 2000 hours of exposure to simultaneous mechanical (10%, 20% and 30% of the specimens ultimate tensile strength) and environmental loading (fresh water and salt water immersions). The authors did not find any significant correlation between the sustained stress level and the rate of degradation of the mechanical properties of both composites. However, the evidence of post-curing effects and degradation due to hygrothermal ageing was observed, with tensile strength presenting reductions up to 15-18% after 2000 hours of conditioning.

The studies reported above, apart from that by Hebling and Karbhari [7.3] (where very high stress levels were used), although providing useful information, did not consider prolonged exposure periods, during which further detrimental and synergistic effects may occur; they therefore make it difficult to predict the long-term effects in these materials. In addition, very limited studies concern pultruded GFRP profiles, and none of the studies above consider the

effects of natural weathering or saturated environments (only immersion environments are considered). Moreover, longer exposing periods are also unavailable for unsaturated polyester GFRP profiles. Finally, none of these studies addressed the influence of synergistic effects on the flexural properties of these materials, which further limits the understanding of this loading condition pultruded parts may be subjected to.

Due to the aforementioned limitations, this chapter presents an experimental investigation concerning the flexural properties of two types of pultruded GFRP profiles, made of vinylester (VE) and unsaturated polyester (UP) resins, which aimed at obtaining a better understanding about the synergistic effects of sustained loading and exposure to different ageing environments for up to two years: (i) natural weathering in Lisbon, Portugal, (ii) continuous condensation, and (iii) controlled indoor environmental exposure. It is worth referring that the stress levels considered for the sustained loading are within the range of variation for typical service conditions.

7.2. Experimental programme

7.2.1 Materials

The materials used in the experimental investigation were the same as described in Chapter 4 and consisted of pultruded GFRP profiles with 33 × 5 mm^2 of cross section and 3 m of length, manufactured by *ALTO Perfis Pultrudidos*. The plates consist of E-glass fibres (with a silane sizing), namely unidirectional rovings in the core region and two outer chopped strand mats (CSM) at the upper and lower parts of the section, all embedded in unsaturated polyester or vinylester resin matrices[4].

7.2.2 Ageing environments

A total of three different ageing environments typical of civil engineering applications, as detailed in Table 7.1, were selected to analyse the flexural properties of two types of pultruded GFRP profiles, which consisted of: (i) natural weathering, (ii) continuous condensation at 20 °C, and (iii) a controlled indoor ageing environment at 23 °C and relative humidity (RH) of 60%. Since composites for civil engineering applications are typically designed for a maximum of 20% of their strength [7.1] in service limit states (SLS) conditions, load levels of 10% and

[4] Further information about the GFRP materials and their initial properties can be found in Chapter 4.

20% of the ultimate flexural strength were applied simultaneously to the environmental exposure.

The natural weathering consisted of the same previous exposure conditions described in Chapter 5, during the same periods, up to 24 months[5]. The continuous condensation exposure was performed using a large scale wet chamber (often use to cure concrete specimens), which permanently maintained RH levels over 95% at 20 °C. Finally, the last environment comprised a room with controlled conditioning, where the (room) temperature is set at 23 °C and RH is permanently at 50 ± 10%.

Table 7.1. Ageing environmental conditions.

Ageing environments	**Label**[(a)]	**Duration [months]**	**Conditions** [(b)]
Natural weathering environment	NE-10% NE-20%	0, 3, 6, 12, 18, 24	T, RH and UV radiation continuously monitored
Continuous condensation	CC-10% CC-20%	0, 3, 6, 12, 18, 24	T = 20 ± 2 °C, RH over 95%,
Controlled environment	CE-10% CE-20%	0, 3, 6, 12, 18, 24	T = 23 ± 2 °C, RH = 50 ± 10%

(a) *10% and 20% labels refer to the loading conditions of 10% and 20% of the ultimate flexural strength.*
(b) *Temperature (T); Relative Humidity (RH); Ultraviolet (UV) radiation.*

Both temperatures used in the continuous condensation (CC) and controlled environment (CE) were selected around 20 °C as they represent the typical average temperature in mild climates, such as Portugal. The 10% and 20% loading conditions were also selected to represent usual loading conditions of pultruded GFRP structural elements in service conditions (*i.e.* the typically recommended maximum stress value for GFRP composites is 20% of their ultimate tensile strength [7.1]).

7.2.3 Experimental procedures and characterisation methods

GFRP test frames were specially designed for these experiments, namely to support the GFRP specimens under sustained loading. A total of six framed fixtures comprising squared and I-sections GFRP pultruded profiles and stainless-steel rods were built as shown in Figure 7.1 (a) – two fixtures were used for each type of ageing environment. Small scale specimens with rectangular section (5 × 15 × 150 mm^3) were cut from the pultruded GFRP profiles and simply supported in the stainless steel rods in a span of 100 mm. The specimens were subjected to the same drying

[5] The exposure period occurred together with the adhesive specimens from Chapter 8 and 9 natural weathering. Detailed information about the monitoring of this ageing is detailed in Chapter 8 (*i.e.* average monthly temperatures, humidity, and ultraviolet radiation).

procedure before exposure (*i.e.* the specimens were preconditioned until constant mass in a ventilated chamber at 80 °C as described in Chapter 4, according to ASTM D 5229 standard [7.5]).

Concrete prisms were used as dead weights, suspended to the GFRP specimens, guaranteeing the specified loading levels. The load was applied at the mid span of each simply supported GFRP specimen (*c.f.* Figure 7.1). At the predefined durations defined in Table 7.1 the specimens were removed, placed in hermetically closed polyethylene recipients for transportation purposes, and subjected to flexural tests without further conditioning at controlled room temperature (23 ± 2 °C). Similar to the hygrothermal ageing in GFRP specimens described in Chapter 4, the specimens subjected to the continuous condensation environment (saturated) were subjected to a desorption period up to constant mass in a chamber at 80 °C before testing. The other ageing environments did not follow this procedure.

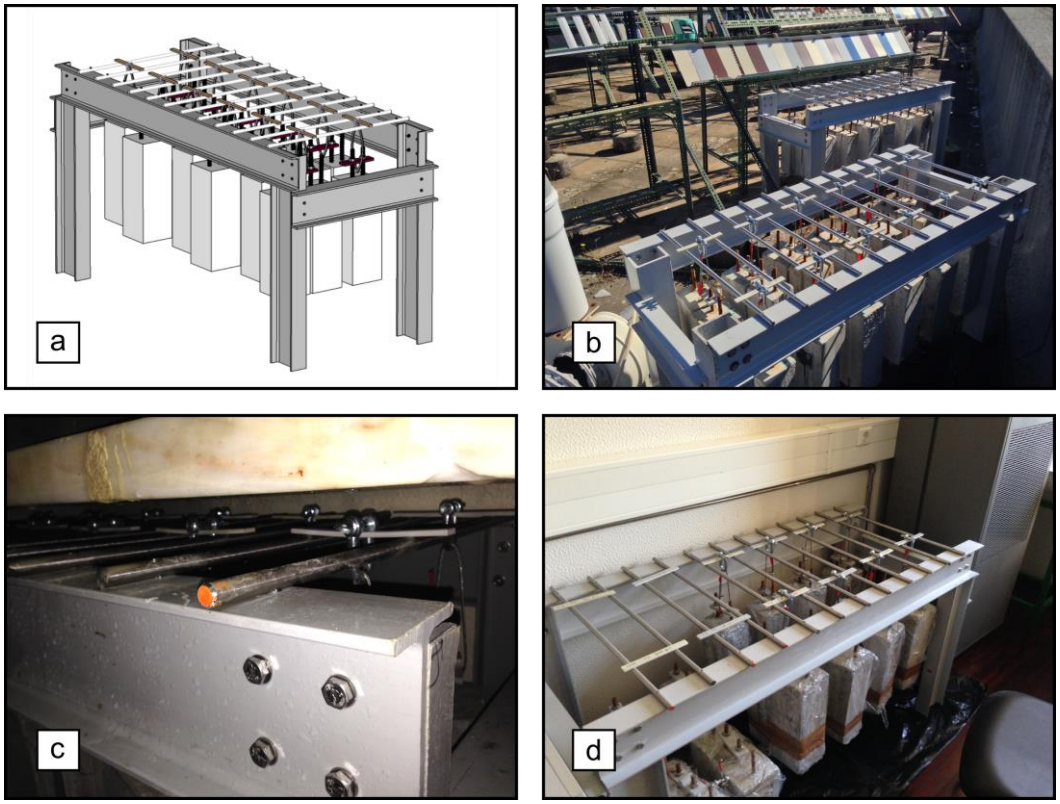

Figure 7.1. Test fixture and setup: (a) schematic, (b) natural weathering, (c) continuous condensation chamber, and (d) controlled environment.

Both UP and VE specimens (with 5 × 15 × 150 mm^3) were subjected to flexural tests according to ISO 14125 [7.6] standard. Specimens were tested in a three-point bending configuration in a 100 mm span using a *Seidner Form* testing machine with 10 kN of load capacity, under displacement control, at a speed of 2 mm/min. Figure 4.5 (c) depicts the flexural test setup. The specimens' flexural strength and stiffness were monitored throughout the whole

experimental programme. A total of 3 specimens were considered for each period and environmental exposure.

7.3. Experimental results and discussion

The unaged properties of the reference GFRP specimens, resulting from the initial characterisation tests, are detailed in Section 4.3.1. All pultruded GFRP specimens were tested monotonically until rupture. The failure mechanisms (*c.f.* Figure 4.10 (c)) were found to be the same throughout the ageing process, despite the flexural properties being affected by the different exposures Figure 7.2 depicts the stress *vs.* strain curves for representative specimens of both profiles subjected to the different ageing conditions.

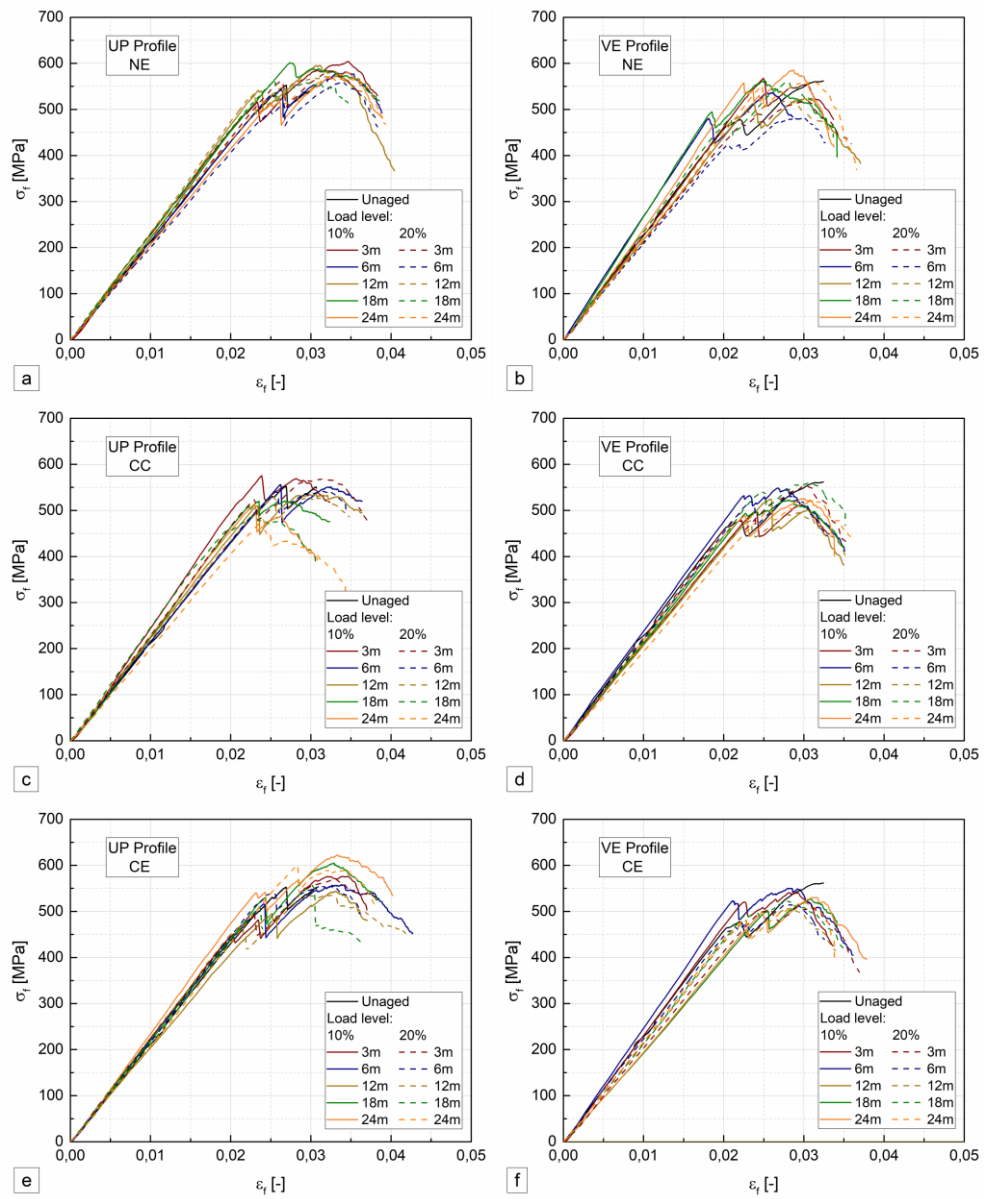

Figure 7.2. Representative flexural stress *vs.* strain curves at different loading levels and for different ageing periods under: (a) and (b) natural weathering; (c) and (d) continuous condensation; (e) and (f) controlled environment, for UP and VE profiles, respectively.

Despite some qualitative changes in the ultimate flexural strength and flexural modulus, no significant differences were observed on the overall shape of the bending stress *vs.* strain curves. Moreover, as mentioned, the failure modes did not change due to the applied loading conditions. In any case, it is noticeable that overall the higher load level (20%) caused higher detrimental effects, especially in the VE profile for the CE environment (*i.e.* the dashed lines). The same qualitative observations also apply to the other two environments, as illustrated in Figure 7.2 (c)-(f).

The effects of the different ageing environments coupled with sustained loading on the flexural strength (average ± standard deviation) of the UP and VE profiles are shown in Figure 7.3. In addition, the most comparable results obtained from this thesis regarding an unloaded condition, *i.e.* natural weathering from a different GFRP material batch (NE – Chapter 5), demineralised water immersion at 20 °C (W20 – Chapter 4) and a remaining material batch that was kept in controlled conditioning for 3 years (CE), are shown in Figure 7.4.

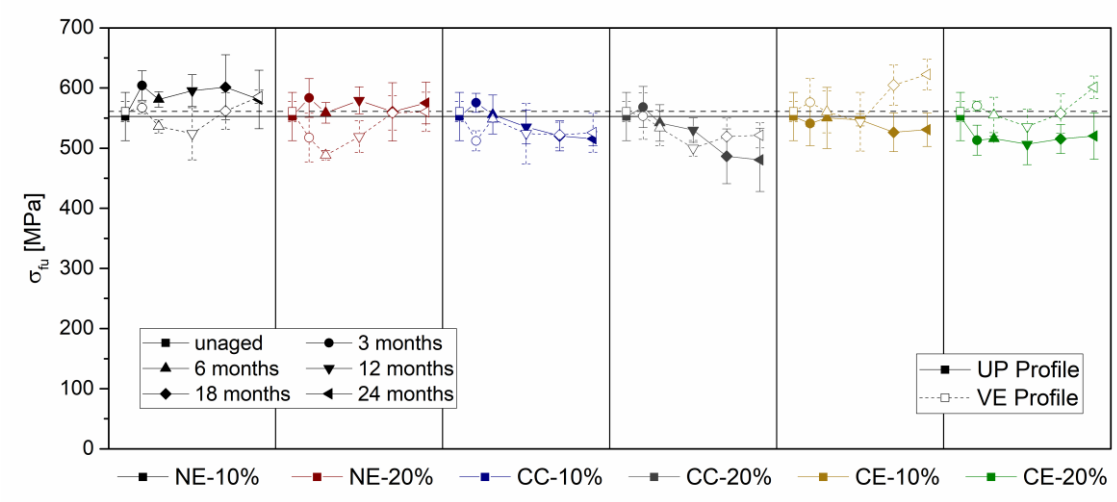

Figure 7.3. Flexural strength variation during ageing for both profiles and loading conditions.

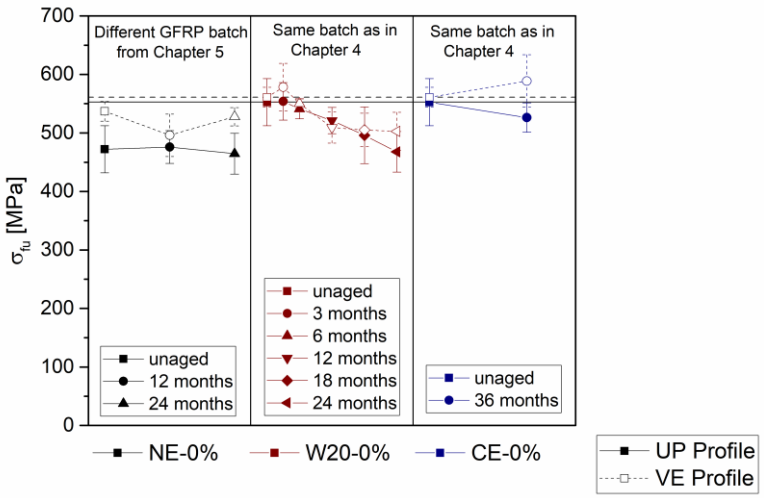

Figure 7.4. Flexural strength variation during ageing for comparable unloaded conditions.

To complement the results shown above, Figures 7.5 to 7.7 depict the flexural strength retention as a function of time for each ageing environment.

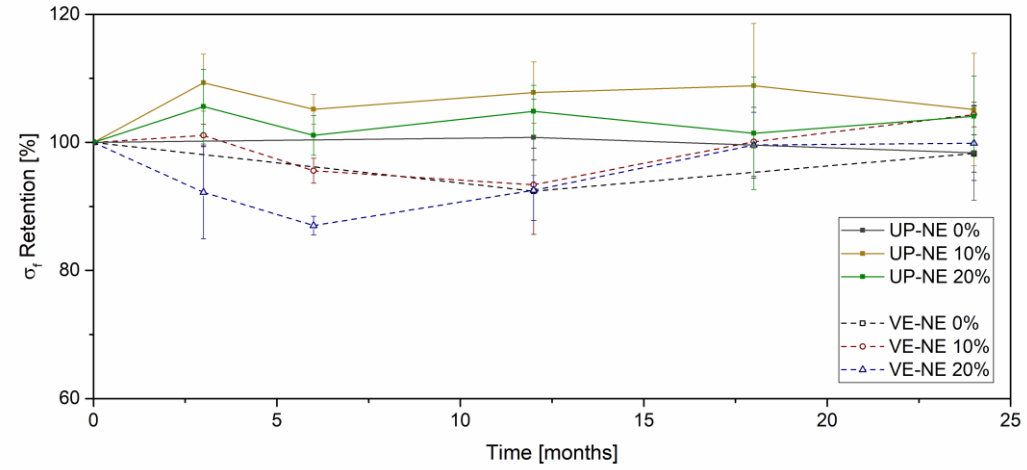

Figure 7.5. Flexural strength retention for both profiles exposed to natural weathering for each loading condition, *vs.* exposure time.

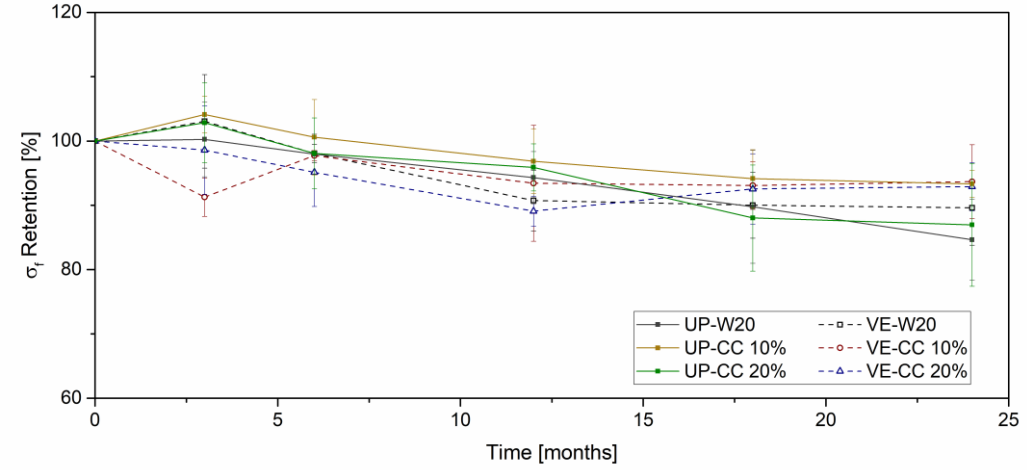

Figure 7.6. Flexural strength retention for both profiles exposed to continuous condensation for each loading condition, *vs.* exposure time.

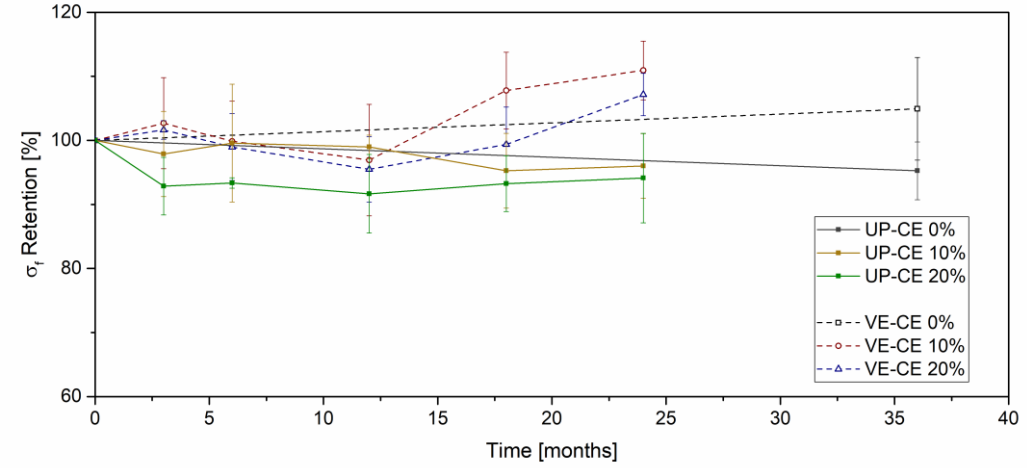

Figure 7.7. Flexural strength retention for both profiles exposed to the controlled environment for each loading condition, *vs.* exposure time.

The flexural strength of the UP profile was not significantly affected during **natural weathering** during the ageing period. In fact, some increase in flexural strength can be observed, which is consistent with the results of natural ageing in unloaded specimens reported in Chapter 5; moreover, the variations are within the standard deviation. As already mentioned, GFRP profiles are susceptible to post-curing effects, which in turn compete with the degradation, masking it and resulting in insignificant strength changes. Albeit small, there was a consistent influence of the loading level, with the 20% loading level corresponding to slightly lower flexural strength, compared to the 10% level - after 24 months of natural weathering ageing, the flexural strength of the UP profile increased 8% and 4% for the 10% and 20% load levels, respectively. Compared to unloaded specimens (*cf.* Section 5.3.6), the loading conditioning did not seem to aggravate the flexural properties of the UP profiles compared to the unloaded profiles. In this case, despite the lower unaged properties, flexural strength seemed to have insignificant variation during 24 months, and did not show any increases.

Regarding the VE profiles, after an initial reduction of flexural strength (7% and 12% of maximum reduction for the 10% and 20% load levels, respectively), a consistent increase occurred up to 24 months. The same aforementioned post-curing effects should have been responsible for this increase. After 24 months of natural weathering, the flexural strength increased 4% under the load level of 10%, while for the 20% load level the flexural strength virtually matched that of the unaged material. The results obtained for the VE profile were also consistent with those of the unloaded specimens in terms of overall trend, as seen in Figure 7.4. Although the UP profile seemed more susceptible to earlier post-curing effects, at the end of the experimental programme, its flexural strength became fairly similar to that of the VE profile for both 10% and 20% loading levels.

Regarding the **continuous condensation** environment, after an initial increase at 3 months, the flexural strength of the UP profile specimens loaded in bending monotonically decreased up to 24 months. A similar qualitative behaviour could be observed for the specimens exposed to 10% and 20% load levels at all periods; however, the higher load level produced more intense degradation, suggesting that the loading condition affected the flexural properties when acting together with the hygrothermal degradation mechanisms (discussed in Chapter 3). Comparing the results with unloaded specimens subjected to immersion at the same temperature (*cf.* Figure 7.4 – W20 curve), the same generalised reduction trend is evident, which is consistent with the results obtained now. The maximum reduction of flexural strength for the unloaded specimens fully immersed at 20 °C was 15% at 24 months, and in this experimental programme

reductions of 7% and 13% were obtained for 10% and 20% load levels. At least to some extent, the lower changes in flexural strength for the loaded specimens should stem from the fact that the latter were not fully immersed, but rather subjected to a continuous condensation environment. In any case, these results indicate that the load level did not remarkably affect the flexural strength.

The flexural strength of the VE profile was even less affected by sustained load, namely when comparing the results obtained for the 10% and 20% load levels, which presented fairly similar values during the ageing period, and less overall reduction of flexural strength. Comparing the obtained results for the unloaded and fully immersed VE specimens, described in Chapter 4 (*cf.* Figure 7.4 – W20 curve), all the results tended to stabilise at later stages of the ageing period. The differences in flexural strength found in the fully immersed and saturated UP profiles were also observed for the VE profiles: the flexural strength of fully immersed specimens exhibited 10% reduction at 24 months, while for saturated specimens under 10% and 20% loading levels those reductions were 6% and 7%, respectively, being slightly lower despite the loading. Similar results (*i.e.* low degradation levels at 20 °C hygrothermal ageing under similar loading conditions) were reported by Ghaz *et al.* [7.1] and Hebling and Karbhari [7.3]. However, both works only considered the tensile properties of the profiles.

The **controlled environment** (CE) aimed to isolate the effects of the load levels, without any further relevant "external" environmental degradation factors. Compared to natural weathering, similar increasing trends of flexural strength were observed for the VE profile at 18 and 24 months, with higher strength values in the CE environment, possibly due to the absence of UV and moisture related degradation. The remaining periods showed small changes for both loading conditions. At 24 months, the flexural strength increased 8% and 10%, for load levels of 20% and 10%, respectively. The UP profile seemed to be more prone to changes due to the loading conditions in this environment. In fact, the 20% loading level caused an initial drop of flexural strength (around 9%) at 3 months, which subsequently remained relatively unchanged up to 24 months. For the 10% loading conditions, the flexural strength presented insignificant changes with a maximum reduction of 5%. In addition, specimens were also tested after 36 months of ageing in a controlled environment without any applied loading (Figure 7.4 – CE 0%). The same trends could be observed, since a 5% reduction of the UP profile flexural strength occurred (comparable to that corresponding to the 10% and 20% loading conditions at 24 months), reflecting that the loading condition did not seem to significantly affect the degradation caused by this environment. Similarly, for the VE profile comparable results were obtained to those corresponding to the 10% and 20% loading

conditions at 24 months; results for the unloaded VE specimens after 36 months evidenced a 5% increase of flexural strength.

Globally, the results obtained from all ageing environments with sustained loading and the comparison with the results obtained from the isolated ageing effects suggest that the load levels representative of service conditions, although noticeable, had little effect on the flexural strength changes of both profiles.

The effects of the different ageing environments on the flexural modulus of the UP and VE profiles (average ± standard deviation) for all ageing environments are shown in Figure 7.8. In the same way as shown for the flexural strength, the most comparable flexural modulus results are shown in Figure 7.9.

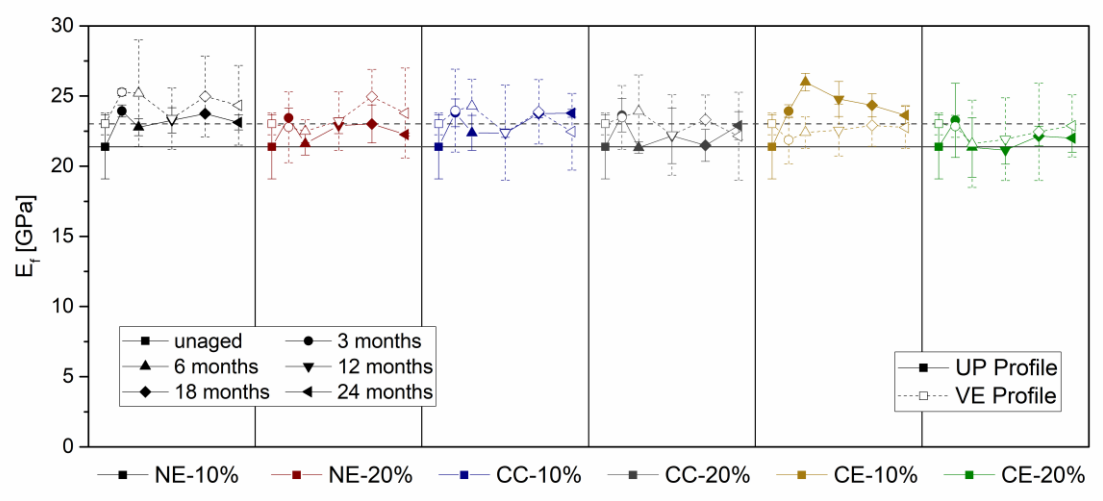

Figure 7.8. Flexural modulus variation during ageing for both profiles and loading conditions.

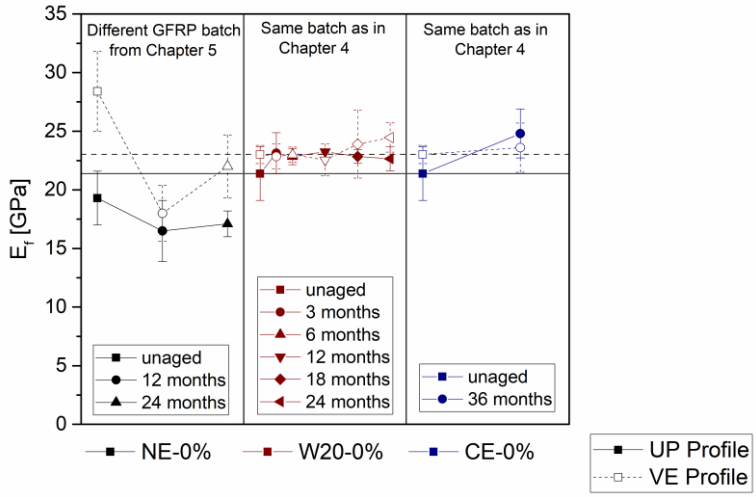

Figure 7.9. Flexural modulus variation during ageing for comparable unloaded conditions.

Similarly to the flexural strength property, to complement the results shown above, Figures 7.10 to 7.12 depict the flexural modulus retention as a function of time for each ageing environment.

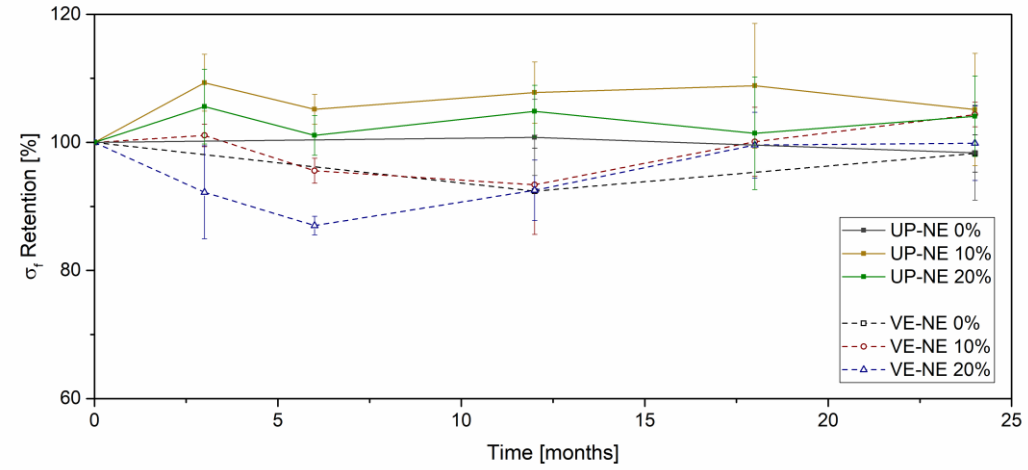

Figure 7.10. Flexural modulus retention for both profiles exposed to natural weathering for each loading condition, *vs.* exposure time.

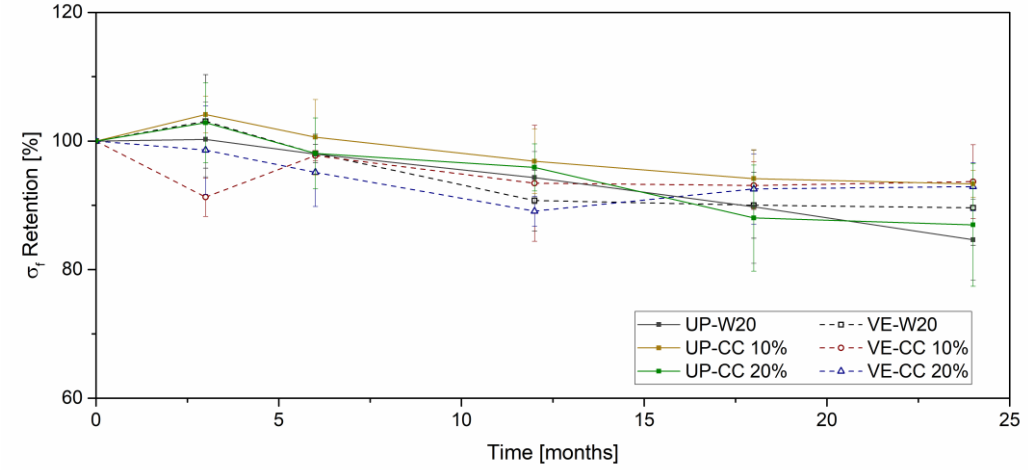

Figure 7.11. Flexural modulus retention for both profiles exposed to continuous condensation for each loading condition, *vs.* exposure time.

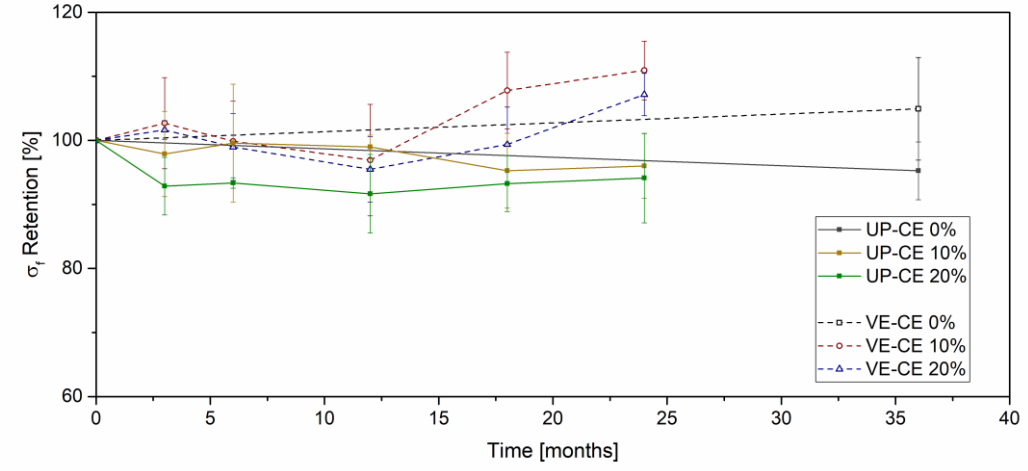

Figure 7.12. Flexural modulus retention for both profiles exposed to the controlled environment for each loading condition, *vs.* exposure time.

Similarly to the results presented in Chapter 4, for the variation of the flexural modulus due to hygrothermal ageing, the flexural stiffness determined in these experiments presented irregular variations (non-monotonic) in both profiles. In general, for both profiles the different loading levels produced very similar trends of changes in flexural stiffness.

Considering **natural weathering**, comparable trends can be found in the UP and VE profiles. For both profiles, a generalised increase in flexural modulus was observed, compared to the unaged results, with the VE profile presenting overall higher values.

No differences can be identified between results obtained for the 10% and 20% loading conditions: after 24 months, the flexural modulus of the UP profile increased by 10% and 3% for the 10% and 20% loading levels, respectively; for the VE profile, those figures were 6% and 3%, respectively.

Comparing to the naturally aged unloaded specimens (Figure 7.6), some differences can be noted, which could be due to the effects of UV radiation and exposure to moisture in natural ageing. In fact, for natural ageing, the unloaded UP specimens presented insignificant changes up to 24 months, but their flexural stiffness did not increase. In addition, an opposite behaviour was found for the VE profile, whose flexural stiffness after 24 months was reduced by 12%. However, the results have in common the overall higher performance (in terms of absolute values of E_f) of the VE profile, compared to the UP profile.

For the **continuous condensation** environment, the flexural modulus of the UP and VE profiles also presented an irregular variation trend, with slight overall changes during the ageing period. These results are consistent with those corresponding to immersion at 20 °C, presented in Figure 7.6, where higher flexural stiffness w.r.t. the unaged values was found for both profiles. In fact, the same occurred now for the UP profile, while the VE profile presented overall insignificant and irregular changes always around the baseline value. After 24 months of continuous condensation, the flexural modulus of the VE profile was reduced by 2% and 4% for the 10% and 20% load levels, respectively. On the contrary, the flexural modulus of the UP profile increased 11% and 7% for the same loading conditions. No evident correlation could be found between the load level (10% and 20% of the ultimate flexural strength) and the variation of flexural modulus; however, for both profiles, the stiffness values were consistently and systematically (slightly) lower for the specimens subjected to highest load level during the entire ageing period.

Finally, in the **controlled environment**, the VE profile presented insignificant changes when subjected to the 10% load level throughout the 24 months of ageing. When subjected to a load level of 20%, the flexural modulus presented a 6% reduction at 6 months, which was followed by a slight recovery (consisted with post-curing effects), and at 24 months the flexural stiffness was again similar to that of the unaged material. The UP profile exhibited an initial increase of 20% (maximum variation) after 6 months when subjected to the 10% loading level; for this environment and loading condition the same increasing trend was found for the flexural strength, although to a smaller extent; afterwards, a progressive reduction of flexural modulus occurred up to 24 months. However, that property was still 10% higher compared to the unaged material. For the 20% loading level, this significant increasing trend was not observed: with the exception of an 8% increase at 3 months, insignificant changes occurred during the ageing period, much like the VE profile. Considering the results obtained for specimens tested after 36 months of ageing in a controlled environment without any applied loading (Figure 7.6 – CE 0%), it can be seen that the same increase in the flexural modulus of the UP profile occurred, with an increase of 15% w.r.t. the unaged material (comparable to the 10% and 20% loading conditions at 24 months). In the VE profile, small changes (2% increase) in the flexural modulus were observed after this period. Much like in flexural strength, the overall results of the unloaded specimens in a controlled environment suggest that the loading conditions did not seem to significantly affect the flexural modulus of both profiles.

7.4. Concluding remarks

This chapter presented experimental investigations about the synergistic effects of sustained loading representative of service conditions and different ageing environments, typical of civil engineering applications, on the flexural properties of two pultruded GFRP profiles made of UP and VE matrices. The results obtained allow drawing the following main conclusions:

1. In general, when compared to unloaded specimens subjected to comparable ageing environments, the loading conditions did not seem to thoroughly aggravate the effects caused by different ageing environments on the flexural properties of pultruded GFRP profiles.

2. Regarding flexural strength, for all ageing environments, the average flexural strength of specimens subjected to a load level of 20% was lower than that of specimens subjected to a load level of 10%; however, the differences were always relatively small and often within the experimental scatter.

3. For specimens subjected to natural weathering and the controlled environment, increases in the flexural strength of both profiles were found, at different periods, which were in agreement with the results obtained for unloaded specimens, reported in Chapter 5; such increases should be attributed to post-curing effects.

4. For the continuous condensation environment, considerable degradation was observed at later stages of exposure, especially for the UP profile. Once more, similar changes could also be found between the specimens exposed to continuous condensation in these experiments and those immersed in demineralised water at 20 °C (*cf.* Chapter 4).

5. The specimens of the UP profile subjected to a controlled environment evidenced small flexural strength reductions, while the VE profile evidenced increase in flexural strength of as much as 10%. Compared to unloaded specimens aged for 36 months, similar results were observed.

6. The flexural modulus presented non-monotonic and small variations in all environments during the 24 months of ageing. As for the flexural strength, the loading level did not seem to have significant influence in the changes shown by the flexural modulus of both types of profiles.

7.5. References

[7.1] Pour-Ghaz M, Miller BLH, Khalaf Alla O, Rizkalla S. Do mechanical and environmental loading have a synergistic effect on the degradation of pultruded glass fiber reinforced polymers? Compos Part B Eng 2016;106:344–55.

[7.2] Buck SE, Lischer DW, Nemat-Nasser S. The durability of E-glass/vinyl ester composite materials subjected to environmental conditioning and sustained loading. J Compos Mater 1998;32:874–92.

[7.3] Helbling CS, Karbhari VM. Investigation of the sorption and tensile response of pultruded E-glass/vinylester composites subjected to hygrothermal exposure and sustained strain. J Reinf Plast Compos 2008;27:613–38.

[7.4] Wang J, GangaRao H, Liang R, Zhou D, Liu W, Fang Y. Durability of glass fiber-reinforced polymer composites under the combined effects of moisture and sustained loads. J Reinf Plast Compos 2015;34:1739–54.

[7.5] ASTM D 5229. Standard test method for moisture absorption properties and equilibrium conditioning of polymer matrix composite materials. Am Soc Test Mater 2014.

[7.6] ISO 14125. Fiber-reinforced plastic composites - Determination of flexural properties. Int Organ Stand 1998.

Part III

Durability of structural adhesives for civil engineering applications

Preamble

There is a growing interest in adhesive bonding in the construction sector as it offers more uniform load transfer compared to traditional bolting. Bonding operations in building and bridge construction are often performed outdoors, sometimes involving large bonding areas. This explains why ambient cured thermosetting resins, such as epoxies and polyurethanes, are usually selected for this purpose. Moreover, polyurethanes may be selected to increase the ductility of joints between brittle adherents, such as GFRP. In spite of the above-mentioned interest, the use of adhesive bonding in civil engineering operations entails several challenges, some of which are related to the adhesives themselves and their durability, as the joint durability is very much dependant on the bonding agent. Moreover, the current information about the long-term behaviour of bonded joints in building and bridge constructions is limited.

Part III of this thesis presents first a literature review about the effects of hygrothermal and natural weathering on structural cold-curing epoxies and polyurethanes. Next, results of an experimental program carried out in order to assess the influence of such long-term exposures on those types of adhesives is presented and their performance is compared.

Chapter 8.

Hygrothermal ageing and natural weathering of a cold curing epoxy adhesive

8.1. Introduction

Bonding operations in building and bridge construction are often performed outdoors, sometimes involving large bonding areas. This explains why ambient cured thermosetting resins, namely epoxies, are generally selected as adhesives for this purpose [8.1]. The increasing interest in epoxy adhesives also stems from the many formulations available, which provide a wide range of properties (before and after curing) that make them suitable for bonding different substrate materials in a broad variety of applications and conditions; the usual range of operating temperatures and the limited cure shrinkage of epoxies also favour their use in civil engineering [8.2, 8.3].

However, the use of adhesive bonding in civil engineering entails several challenges, some of which are related to the adhesives themselves and their durability, as the joint reliability is very much dependent on the bonding agent [8.4]. The effects of environmental agents on structural adhesives, such as moisture and temperature, have been considered as the most relevant factors concerning their long-term performance [8.3, 8.5, 8.6]. In fact, in several civil engineering applications, bonded joints can be exposed to moisture or humid environments [8.7].

As mentioned, the exposure temperature is an important environmental factor that limits the application range of structural adhesives. Temperatures that approach or exceed the glass transition temperature (T_g) of the adhesive promote significant changes in the material behaviour, which may change from hard to rubbery, thus limiting its applicability [8.8]. The temperature during the application is also very relevant for the curing degree and mechanical properties attained by structural adhesives. In fact, exposure to low or elevated temperature (the first typically delays curing, while the latter is often used to accelerate it) can cause positive or negative changes in strength and stiffness, depending on the magnitude and duration of the temperatures experienced by the adhesive [8.9, 8.10].

Another important factor is concerned with moisture. Water diffusion in adhesives, which is intrinsically related to their polymeric structure, can be influenced by their chemical composition [8.11], topology, polarity and molecular motions [8.12], with water molecules being

usually classified into free water (isolated) and bound water (*i.e.*, linked to the epoxy [8.13]). Once absorbed by epoxy, water can change its properties through plasticization (reversible), hydrolysis, cracking or crazing (irreversible) [8.1]. The physical and chemical transformations experienced by epoxies in the presence of water cause detrimental effects, namely reductions of the T_g and of the mechanical strength [8.14].

The information about the long-term behaviour of bonded joints in building or bridge construction is limited, and the same applies to the durability of epoxy adhesives, revised in the next section. The availability of such information is of paramount importance, since the required service life for most civil engineering applications is generally above 50 years. This lack of experimental data about the durability of joints and adhesives (needed for design) is one of the aspects that is hindering the widespread dissemination of this connection technology.

Other industries, such as aerospace and electronics, have longer experience in studying the effects of ageing on epoxy adhesives [8.3, 8.15]. However, the results obtained are hardly useful for civil engineering applications, given the many differences between those industries, namely (i) the loading conditions, (ii) the types of environmental exposure, (iii) the substrate materials and manufacturing processes and (iv) the service life requirements.

To address these issues, this chapter aims at assessing the influence of different ageing conditions, representative of civil engineering environments, on the durability of a commercial epoxy adhesive used in structural applications. In particular, the effects of immersion in water and salt-water at 20 °C and 40 °C, continuous condensation at 40 °C and natural weathering for up to two years on the physical, viscoelastic and mechanical properties of the adhesive were determined.

8.2. Literature review on the durability of structural epoxy adhesives

This section presents a literature review of previous studies about the effects of hygrothermal and natural weathering on epoxy adhesives. The review, summarized at the end of this section in Table 8.1, focused on how different types of hygrothermal and natural ageing environments affect the properties of epoxy adhesive systems[6] likely to be used in civil engineering structural applications. However, it is worth referring that the formulation of the adhesives used in the

[6] This review focused only on epoxy adhesive systems, excluding adhesives with other material combinations (*e.g.*, reinforced polymer matrixes).

studies may differ, as well as the curing/conditioning conditions employed before testing, and such differences can influence their behaviour and susceptibility to external factors.

8.2.1 Hygrothermal ageing

Zhou and Lucas [8.16, 8.17] investigated the nature of absorbed water and the hygrothermal effects in the T_g of three different thermoset epoxy systems immersed in water at different temperatures (45 °C to 90 °C). The authors concluded that changes in the T_g did not depend only on the water content, but also on the hygrothermal history of the polymers (both time- and temperature-dependent). After an initial reduction, the T_g began to gradually recover with time after reaching the saturation stage, with higher immersion periods and temperatures resulting in higher recovery values. However, the residual T_g after immersion still showed a significant reduction compared to the unaged condition - at 45 °C it ranged from 54% to 65%, at 60 °C it was around 43% to 57%, and at 90 °C it varied between 28% and 48% for the three epoxy systems.

Nogueira *et al.* [8.18] studied the effect of water sorption at 100 °C in an amine-cured epoxy system and noticed that the T_g continuously decreased as the absorbed water increased - reductions of 16% and 6% (depending on the pre-curing conditions) were noted on fully saturated specimens, which were much lower than those reported in the study by Zhou and Lucas [8.17] for a similar duration and temperature of immersion. Mechanical properties were also affected: the tensile strength exhibited a global decreasing trend, especially in the earlier stages of diffusion, with a 33% reduction for the last immersion period (55 days); after an initial increase, the tensile modulus also showed a general reduction trend, yet with a much lower magnitude - 5% reduction at the later stages.

Frigione *et al.* [8.19] obtained similar results in another particular epoxy system. The specimens were immersed in water and subjected to water vapour (100% relative humidity, RH) for 28 days (about half of the time of the previous studies) at 23 °C (lower than in earlier studies). Both types of hygrothermal ageing caused moderate to low reductions in performance: 14% (water vapour) and 16% (water immersion) in flexural modulus; 1% and 4% in flexural strength, and 1% and 5% in T_g, respectively. The authors highlighted that the 28 days exposure period was too short to induce irreversible degradation to the adhesive; in any case, unlike the previous work [8.18], the modulus seemed to be more affected than strength. In this study, specimens were also exposed to 50 °C for 28 days: the thermal exposure led to a 15% increase of the T_g, due to density increase of crosslinking. For this exposure the flexural strength

increased 32% (due to the same effect), but the flexural modulus was reduced by 19%, which was attributed to a detrimental effect (not specified) of the post curing process.

Yang *et al.* [8.20] assessed the response of an ambient cured epoxy adhesive when exposed to a variety of immersion environments over 24 months: (i) deionized water immersion at 23 °C, 38 °C and 60 °C, (ii) salt-water (5% NaCl) immersion at 23 °C, and (iii) alkaline immersion at 23 °C. Regarding the viscoelastic response of the adhesive, specimens immersed at 23 °C registered small reductions in T_g for the first 6 months, after which only insignificant changes were reported. For the 38 °C and 60 °C immersions, a 9% increase in T_g was observed in the same period, which was then levelled off after very small reductions; in addition, for higher immersion temperatures the loss factor curves showed a split in the tan δ peaks. The authors concluded that the initial post-cure due to elevated temperatures dominated over the plasticization. The immersion in deionized water caused a significant decrease in tensile properties. After 24 months at 23 °C, 38 °C and 60 °C, the tensile strength and the tensile modulus exhibited reductions of respectively 43%, 44% and 69% (strength), and 36%, 40%, and 68% (modulus). Samples immersed in salt water (at 23 °C) showed less degradation in the earlier stages, but comparable effects were reported after 12 months of exposure; alkali immersion (at 23 °C) led to higher degradation levels when compared to water or salt-water immersions at the same temperature.

Cabral-Fonseca *et al.* [8.6] presented a further effort in this field; the authors investigated the durability of three commercial epoxy adhesives, subjected to immersion in demineralised water, salt-water and an alkaline solution at three different temperatures – 23 °C, 40 °C and 60 °C. A clear dependence of immersion media and temperature was observed in the mechanical properties of all adhesives and the same general effects were found.

Silva *et al.* [8.21] characterised a commercial epoxy adhesive after 8 and 16 months of hygrothermal ageing, that included water and salt water immersions and wet-dry cycles at 20 °C. The authors concluded that no visible chemical changes were registered comparing to the reference specimens. The T_g values showed general decreasing trends for all ageing environments, and the harsher effects (21% reduction) were due to salt water immersion for 8 months. Regarding mechanical properties, tensile strength and modulus exhibited a general decreasing trend, with reductions up to 47% and 38%, respectively, after 16 months of water immersion. Salt water immersion also caused a reduction in mechanical properties, although to a smaller extent.

More recently, Savvilotidou *et al.* [8.22] investigated the behaviour of a post-cured and a cold cured epoxy adhesive for 24 months. The post-cured specimens were immersed in demineralised

water and an alkaline solution at three temperatures (13 °C, 30 °C, and 50 °C), while the cold cured specimens were only subjected do demineralised water immersion at 13 °C. Regardless of the immersion temperature, the post-cured specimens presented a decrease (23%) of T_g, which was attributed to plasticization effects; yet, as expected, this decrease was faster at higher immersion temperatures, which led to higher diffusivity properties. The mechanical properties of the post-cured specimens were significantly affected after 150 days, with higher immersion temperatures promoting higher degradation: after 2 years, the E-modulus reduction was around 20%, 30% and 47% for water immersion at 13 °C, 30 °C and 50 °C, respectively; the tensile strength followed the same trend, with reductions of 18%, 24%, and 37%. Plasticization induced by water uptake also affected the stress-strain response.

Other studies focused on the effects of high humidity environments, showed that they cause similar effects when compared to immersion regarding the diffusion processes and temperature dependence. For example, Lettieri and Frigione [8.1] addressed the effects of humid environments on the properties of a cold cured epoxy, previously studied in [8.19]. Similar replicates were exposed to controlled humidity levels (55%, 75%, and 100% RH) or immersed in distilled water, at a constant temperature of 23 °C for up to 28 days. In terms of absorption, the 100% RH environment led to the highest uptake, followed closely by water immersion. Regarding the changes in T_g and mechanical properties, the environments with lower RH (50% and 75%) did not have significant influence in the adhesive; the 100% RH environment produced similar results compared to water immersion – reductions of respectively 13% and 15% in T_g, 2% and 1% in tensile strength and 13% and 15% in tensile modulus. Similar observations were also noticed by Cabral-Fonseca *et al.* [8.6] when comparing immersion in water and 100% RH both at 40 °C. Other investigations in epoxy adhesives under high humidity/thermal exposures [8.23-8.25], also summarised in Table 8.1, showed similar degradation mechanisms compared to what has been reported for immersion in aqueous solutions.

8.2.2 Natural weathering

Some other investigations focused on the effects of natural weathering on epoxy adhesives in relatively mild climates, where climatic changes (RH and temperature) as well as ultraviolet (UV) radiation can affect the adhesive properties. Frigione *et al.* [8.26, 8.27] studied the effects of different environmental conditions on the curing behaviour and flexural properties of two commercial cold curing epoxy systems with different viscosities. Both adhesives were cured at room temperature for 10 days before ageing, and then exposed for 24 months to (i) -20 °C and (ii) 18-26 °C in a dark room without ultraviolet (UV) radiation; in parallel, some samples were

aged outdoors, in Salerno - Italy, for a period of 3 years. Both epoxies showed similar curing behaviour to similar material cured at high-temperature; however, the T_g attained by both epoxies was lower than that of similar heat-cured specimens. When exposed to -20 °C and to the 18-26 °C conditioning, both adhesives showed an increase of strength and stiffness and lower strain at failure. Natural weathering (with UV radiation / temperature variations) caused cyclic changes in both physical and mechanical properties, but these did not substantially differ from the initial values.

More recently, Lettieri and Frigione [8.28] investigated the artificial and natural weathering of three commercial cold cured epoxy systems for 42 months. Artificial weathering was conducted in a climatic chamber at 70 °C and 75% RH up to 34 days. With regards to natural ageing, one system was placed outdoor (A1 - in Lecce, Italy) after 4 months of curing at room temperature, while the other two were placed outdoors (A2 and A3 - in Salerno, Italy) after curing for 10 days at ambient temperature. The artificial ageing led to different effects compared with the outdoor environment, being more severe for epoxies A2 and A3. The natural ageing produced T_g reductions in epoxies A2 and A3 that showed to be reversible to some extent; the variation was attributed to plasticization effects due to water uptake during outdoor ageing. In the warmer periods, post-cure effects took place and some T_g increases were registered. The epoxy A1 showed an overall increasing trend of T_g, which was attributed to post-cure phenomena. Natural weathering significantly affected the performance of epoxy A1 - after 42 months, the flexural modulus and strength were reduced by 35% and 60%, respectively. These marked decreases, which started after 1 year, were attributed to a strong effect of water incorporation due to a rainy period, in accordance with gravimetric measurements. An opposite trend was noted for epoxies A2 and A3, with increases in flexural modulus and strength of respectively 7% and 6% (A2) and 9% and 7% (A3).

8.2.3 Summary and research significance

The experimental work discussed above, although providing useful information about the effects of hygrothermal ageing and natural weathering on the behaviour of epoxy adhesives, presents some limitations and makes it difficult to draw general conclusions about the durability of epoxy adhesives currently used in civil engineering applications.

In fact, although highlighting the main degradation mechanisms, changes in the physical and mechanical properties of epoxy adhesives reported in the above-mentioned studies vary considerably and sometimes the results obtained are contradictory.

Table 8.1. Summary of previous studies concerning hygrothermal and natural weathering of epoxy systems.

Author	**Applications**	**Chemical composition**	**Pre-conditioning**	**Ageing**			**Property variation [%]**	
				Type	**Temperature [°C]**	**Duration [days]**		
Zhou and Lucas [8.16,8.17]	High performance FRPs	DGEBA + mDPA TGDDM + DDS TGDDM + DDS + additives	110 °C for 24 h	Water immersion	45[a]; 60[b]; 75[c]; 90[d]	64	T_g	-54[a]; -43[b]; -34[c]; -29[d] -65[a]; -57[b]; -53[c]; -48[d] -60[a]; -51[b]; -48[c]; -42[d]
Nogueira *et al.* [8.18]	Composite matrices; general adhesives	TGDDM + EPN + DDS	Cure 2 system + drying at 50 °C Cure 3 system + drying at 50 °C	Water immersion	100[a] 100[b]	~55	T_g E_t σ_t T_g	-16[a] -5[a] -33[a] -6[b]
Frigione *et al.* [8.19]	FRP matrix system; bonding adhesive for external strengthening systems	DGEBA + PEI-MXD-NPE	23 °C and 50% RH for up to 24 months + desiccator drying up to constant mass	Thermal treatment[a]; Water vapour (100% RH)[b]; Distilled water immersion[c]	50[a]; 23[b c]	28[a b c]	T_g E_f σ_f	+15[a]; -1[b]; -5[c] -19[a]; -14[b]; -16[c] +32[a]; -1[b]; -4[c]
Yang *et al.* [8.20]	FRP strengthening of concrete	AH + AA	23 °C for 30 days	Water immersion[a, b, c]; 5% NaCl immersion[d]; alkaline immersion[e]; unexposed[f]	23[a d e f]; 38[b]; 60[c]	730	T_g E_t σ_t	-5[a]; +8[b]; +9[c]; -4[d]; -5[e]; +6[f] -36[a]; -40[b]; -68[c]; -30[d]; -50[e]; +17[f] -43[a]; -44[b]; -69[c]; -36[d]; -53[e]; +7[f]
Silva *et al.* [8.21]	FRP strengthening applications	DGEBA + BED + AA	22 °C (55% RH) for 1 year	Water immersion[a]; salt water immersion[b]; wet/dry salt water cycles[c];	20	482	T_g E_t σ_t	-14[a]; -16[b]; -6[c] -47[a]; -35[b]; -22[c] -38[a]; -28[b]; -21[c]
Savvilotidou *et al.* [8.22]	FRP strengthening systems	BPA + AA + IF	21 °C (40% RH) for 7 days + 60 °C for 3 days[a b c d e f]; 13 °C for 2 days[g h]	Water immersion[a b c g]; alkaline solution[d e f]; unexposed[h]	13[a d g]; 30 [o b e]; 50[c f]	740[a]; 737[b]; 557[c]; 726[d]; 730[e]; 684[f]; 754[g]	T_g E_t σ_t	-20[a]; -20[b]; -21[c]; -18[d]; -19[e]; -24[f]; +33[g]; +50[h] -20[a]; -30[b]; -38[c]; -16[d]; -25[e]; -46[f]; +7[g]; +31[h] -17[a]; -25[b]; -33[c]; -13[d]; -17[e]; -36[f]; +31[g]; +48[h]
Lettieri and Frigione [8.1]	Rehabilitation or renewal of civil infrastructures	DGEBA + PEI-MXD-NPE	23 °C (50% RH) for 10 days + 23 °C (15% RH) for 3 months	Water immersion[a]; water vapour (100% RH)[b] , (75% RH)[c]; (55% RH)[d];	23	28	T_g E_f σ_f	-9[a]; -13[b]; -10[c]; -9[d] -15[a]; -13[b]; -5[c]; -8[d] -2[a]; -1[b]; +1[c]; +5[d]

Table 8.1. Summary of previous studies concerning hygrothermal and natural weathering of epoxy systems (cont).

Cabral-Fonseca *et al.* [8.6]	CFRP repair and strengthening of concrete	DGEBA based + AA (60% IF)	24 days at room temperature	Water immersion[a b c]; salt water immersion[d e f]; alkaline solution[g h i]; continuous condensation[j]	23[a d g]; 40[b e h j]; 60[c f i]	548	T_g	-1[a]; -15[b]; -17[c]; -11[d]; -10[e]; -4[f]; -8[g]; +2[h]; -15[i]; -6[j]
							E_t	-48[a]; -15[b]; -58[c]; -12[d]; -4[e]; -57[f]; -67[g]; -92[h]; NA[i]; -35[j]
							σ_t	-43[a]; -39[b]; -60[c]; -43[d]; -25[e]; -64[f]; -64[g]; -85[h]; NA[i]; -58[j]
							E_f	-10[a]; -11[b]; -45[c]; -8[d]; -16[e]; -33[f]; -50[g]; -84[h]; -86[i]; -30[j]
							σ_f	-41[a]; -36[b]; -60[c]; -36[d]; -25[e]; -39[f]; -54[g]; -78[h]; -91[i]; -46[j]
		DGEBA based + AA (88% IF)					T_g	+16[a]; +54[b]; +66[c]; +38[d]; +86[e]; +79[f]; +43[g]; +94[h]; +78[i]; +97[j]
							E_t	+103[a]; +150[b]; +112[c]; +110[d]; +231[e]; +202[f]; +69[g]; +5[h]; NA[i]; +150[j]
							σ_t	+8[a]; +28[b]; +20[c]; +8[d]; +32[e]; +26[f]; +1[g]; -1[h]; NA[i]; +7[j]
							E_f	+82[a]; +71[b]; +22[c]; +110[d]; +139[e]; +112[f]; +53[g]; -5[h]; -43[i]; +41[j]
							σ_f	+16[a]; +26[b]; +7[c]; +20[d]; +62[e]; +48[f]; +13[g]; -9[h]; -33[i]; +17[j]
		DGEBA based + AA (55% IF)					T_g	-12[a]; +1[b]; -4[c]; -7[d]; +4[e]; 0[f]; -4[g]; +8[h]; -8[i]; +5[j]
							E_t	+42[a]; +46[b]; +34[c]; +61[d]; +59[e]; +53[f]; +49[g]; -9[h]; NA[i]; +57[j]
							σ_t	-5[a]; +5[b]; -11[c]; -2[d]; +2[e]; +4[f]; +5[g]; -21[h]; NA[i]; +17[j]
							E_f	-18[a]; -23[b]; -44[c]; -18[d]; -28[e]; -26[f]; -34[g]; -43[h]; -76[i]; -20[j]
							σ_f	-27[a]; -13[b]; -21[c]; -23[d]; -11[e]; -17[f]; -28[g]; -31[h]; -66[i]; -9[j]
Lettieri and Frigione [8.1]	Rehabilitation or renewal of civil infrastructures	DGEBA + PEI-MXD-NPE	23 °C (50% RH) for 10 days + 23 °C (15% RH) for 3 months	Water immersion[a]; water vapour (100% RH)[b] , (75% RH)[c]; (55% RH)[d];	23	28	T_g	-9[a]; -13[b]; -10[c]; -9[d]
							E_f	-15[a]; -13[b]; -5[c]; -8[d]
							σ_f	-2[a]; -1[b]; +1[c]; +5[d]

Table 8.1. Summary of previous studies concerning hygrothermal and natural weathering of epoxy systems (cont.).

Lapique and Redford [8.23]	Aviation industry; GFRP structures	2C thixotropic resin - unspecified	64 °C for 4 h	Water vapour (~100% RH)	40	36	E_t σ_t	-35 -45
Lin and Chen [8.24]	Adhesives; laminates and composites; microelectronic packaging	DGEBA + DDA	Kept in a desiccator for 10 days	Hygrothermostat at 85% RH[a]; vacuum drying[b]	85[a b c]	65[a]; 30[b]; 13[c]	E_t σ_t	-30[a]; -9[b]; -43[c] -29[a]; -11[b]; -54[c]
Goglio and Rezaei [8.25]	Structural bonding - metals, ceramics and rigid plastics	2C thixotropic resin - unspecified	23 °C (50% RH) for 1 day + 2h at 80 °C	Climatic chamber (100% RH)	50	35	E_t σ_t	-20 -75
Frigione *et al.* [8.26,8.27]	Concrete repairing, or mortars, applications	DGEBA based + AA DGEBA + 40% IF + AA	20 days at room temperature	Low temperature[a]; dark and inert conditions[b]; outdoor exposure (Salerno, Italy)[c]	-20[a];18-26[b]; variable[c]	730[a b]; 1095[c]	T_g E_f σ_f T_g	-7[a]; +4[b] +4[c]; +47[a]; +53[b]; +59[c] +48[a]; +70[b]; 0[c] -8[a]; +6[b]; -5[c]
Lettieri and Frigione [8.28]	Rehabilitation or renewal of civil infrastructures and cultural heritage	DGEBA + PEI-MXD-NPE BPA + IPDA BPA + IPDA + IF	4.5 months[a b] 4.5 months[a]; 10 days[b]	Artificial weathering (75% RH)[a]; natural weathering[b]	70 [a]; variable[b]	34[a];1290[b] 34[a];1080[b]	T_g E_f σ_f T_g E_f σ_f T_g E_f σ_f	+9[a]; +26[b] -31[a]; -35[b]; -31[a]; -60[b] -24[a]; +4[b] +50[a]; +50[b] -6[a]; -2[b] -20[a]; +8[b] -3[a]; +21[b] -14[a]; +7[b]

Acronyms:
Aliphatic amines (AA); Aromatic hydrocarbon (AH); Bisphenol-A (BPA); 1,3-bis(2,3-epoxypropoxy)-2,2-dimethylpropane (BED); Carbon fibre reinforced polymer (CFRP); 4,4'-diaminodiphenyl sulfone (DDS); Dicyandiamide (DICY or DDA); Diglycidyl ether of bisphenol-A (DGEBA); Flexural modulus (E_f); Flexural strength (σ_f); Glass transition temperature (T_g); Inorganic fillers (IF); 3-aminomethyl-3,5,5-trimethyl cyclohexylamine (IPDA); Metaphenylene diamine (mDPA); M-xylenediamine (MXD); Nonylphenol (NPE); Not available (NA); Polyethylenimine (PEI); Sodium Chloride (NaCl); Tensile modulus (E_t); Tensile strength (σ_t); Tetraglycidyl-4,4'-diaminodiphenyl (TGDDM); Tetraglycidylmethylene dianiline (TGMDA);
[a-h] The lettered footnotes match the different pre-conditioning procedures, ageing conditions, and property variation.

This may be explained by the differences in several factors that considerably affect the durability of epoxy adhesives: chemical formulation, manufacturing process (*i.e.*, curing conditions), pre-conditioning environment, temperature range, exposure conditions, duration times, and characterisation techniques – in fact, these factors vary considerably among the different investigations reported above (*cf.* Table 8.1). Another limitation is that most previous studies on hygrothermal ageing characterised the sorption behaviour of epoxy adhesives for very limited periods.

Finally, although in civil engineering applications adhesives are mostly subjected to shear stresses, none of the studies reviewed investigated the influence of hygrothermal ageing and natural weathering on the in-plane shear properties of epoxy adhesives.

8.3. Experimental programme

8.3.1 Materials

The adhesive selected for this investigation was a commercial cold curing epoxy, because it is being frequently used in several civil engineering structural applications, namely for bonding CFRP strips to existing structures. This material consists of a thixotropic, solvent-free, bi-component epoxy based adhesive and is depicted in Figure 8.1, as well as the specimens' appearance after demoulding.

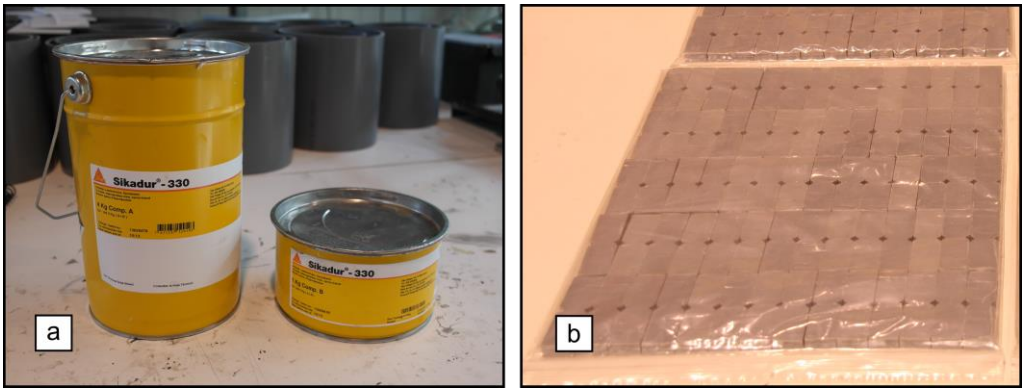

Figure 8.1. Material: (a) epoxy adhesive; (b) specimens' appearance after demoulding.

The chemical structure comprises a bisphenol-A based epoxy resin and aliphatic amines as hardeners, with small amounts of silica-based fillers. A mix ratio of 4:1 (resin to hardener in weight) was used, as recommended by the supplier.

The adhesive was produced under laboratory conditions at room temperature (23 ± 2 °C and 50 ± 10% RH). The mixing and fabrication operations were manual to represent typical *in situ* conditions in structural applications. Specific polyethylene moulds were used to produce the

test specimens. The specimens were cured for 24 hours at room temperature before removal from the moulds. Subsequently, the specimens were cured for another 24 hours period in a ventilated chamber at 50 °C prior to initial characterisation and consequent exposure to the ageing environments; this pre-conditioning provided a higher curing degree. According to Savvilotidou *et al.* [8.7], the same epoxy presents a continuous curing in dry environments and it can take about 300 days to achieve full cure at 20 °C. However, a similar pre-conditioning to that used in our study guaranteed a curing degree of at least 94% after 5 days.

8.3.2 Ageing environments

Although bonded joints in civil structural applications are typically prevented from direct exposure to moisture (if appropriately sealing is provided) or UV radiation, exposure to those agents is bound to happen for long service life periods, especially outdoors (*e.g.*, bridge applications). In addition, defective sealing can also promote premature contact with those environmental agents. Moreover, even if sealed, FRP adherends absorb water through diffusion [8.14], which can later affect the adhesive layer. Therefore, exposure to water and UV radiation need to be duly considered, as these agents are known to affect the stability of polymers, promoting chemical and physical degradation mechanisms [8.5]. In this context, the following six ageing environments, depicted in Table 8.2, were considered: immersion in demineralized water and salt water at 20 °C and 40 °C for up to 2 years; continuous condensation at 40 °C and natural exposure for up to 1 year.

Table 8.2. Summary of ageing environments conditions.

Ageing environments	**Label**	**Duration [months]**	**Conditions** [(a)]
Immersion in demineralised water	W20	0, 2, 4, 6, 9, 12, 18, 24	T = 20 ± 3 °C
	W40	0, 2, 4, 6, 9, 12, 18, 24	T = 40 ± 2 °C
Immersion in salt water	S20	0, 2, 4, 6, 9, 12, 18, 24	T = 20 ± 2 °C; 35 g/l NaCl
	S40	0, 2, 4, 6, 9, 12, 18, 24	T = 40 ± 2 °C; 35 g/l NaCl
Continuous condensation	C40	0, 2, 4, 6, 9, 12	T = 40 ± 2 °C; 100% RH
Outdoor exposure	NE	0, 2, 4, 6, 9, 12	T, RH and UV radiation continuously monitored

(a) *Temperature (T); Relative Humidity (RH); Ultraviolet (UV).*

The temperature of 20 °C was defined as normal room temperature level, corresponding to the average temperatures encountered in mild climates, such as southern European countries. The temperature of 40 °C was selected to accelerate diffusion and promote polymer deterioration; this value was set taking into account the need to remain well below the T_g of the adhesive (60 ± 0.1 °C, from the onset of the E' modulus curve obtained from DMA tests, *cf.* Section 8.4.1). This option aimed at limiting additional degradation mechanisms that occur when such temperature is approached or exceeded [8.22, 8.29]. The immersion ageing was based

on ISO 175 standard [8.30] and the salt water sodium concentration of 35 g/l was defined according to ASTM D 1141 standard [8.31].

The continuous condensation environment was provided by a condensation chamber that combines the effects of moisture and temperature. Specimens were hanged inside the chamber, not contacting with the chamber walls. Temperature and RH values were defined according to ISO 6270-2 standard [8.32].

The natural exposure was performed in Lisbon, Portugal (-38.77°N, 9.13°W, 100 m above seawater), at the rooftop of the main building of the National Civil Engineering Laboratory (LNEC). The specimens were inserted in plastic railings, at a 45° angle with the roof floor, facing southwest. A weather station constituted by two *Kipp & Zonen* pyranometers and a *Thies* combined sensor measured the global and UV solar radiation, as well as temperature and RH, respectively. The specimens were aged during the period of February 2016 to January 2017. The average RH ranged between 83% (Winter) and 58% (Summer) and the average monthly temperature ranged between 11 °C and 24 °C, respectively. The total global sun radiation varied between 385966 kJ/m^2 and 675583 kJ/m^2 and the UV component variation ranged between 10428 and 27690 kJ/m^2. Batches were exposed to a total of 226917 kJ/m^2 of UV radiation throughout the whole year. Figure 8.2 displays the weather station information gathered during that period.

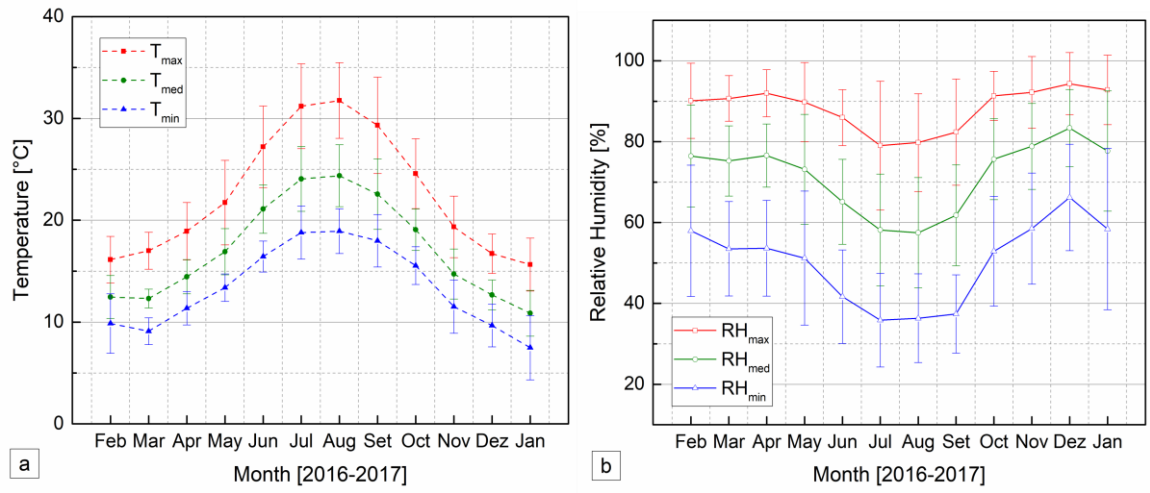

Figure 8.2. Monthly variations of (a) air temperature and (b) relative humidity during the exposure period.

At predetermined exposure times, specimens were removed from the ageing environments and were subjected to a desorption period, being dried for at least 30 days at room temperature (23 ± 2 °C and 60 ± 10 %RH); this aimed at characterising the adhesive in a "dry" state and assess the potential property recovery. The desorption time was defined as the average period

needed for specimens to achieve constant mass, according to ASTM D 5229 standard [8.33]. Afterwards, the specimens were placed in hermetically closed polyethylene recipients for transportation purposes and tested without further conditioning.

8.3.3 Characterisation methods

Similar to Part II chapters, analogous characterisation methods were employed to both unaged and aged adhesives, with some differences in test procedures, and are described listed in Table 8.3.

Table 8.3. Experimental methods and durations of ageing environments.

Method	**Duration of ageing environments [months]**		
	W20, W40, S20, S40	**C40**	**NE**
DMA	0, 2, 4, 6, 12, 18, 24	0, 2, 4, 6, 12	12
Flexure properties			-
In-plane shear properties	0, 3, 6, 9, 12	-	0, 3, 6, 9, 12
Water sorption	periodic monitoring		-

Thermogravimetric analysis (TGA) of the epoxy was conducted to quantify the percentage of its constituent materials. Tests were performed in a *Setaram TGA 92* analyser according to ISO 11358 standard [8.34]. Specimens (65 mg) were heated from 25 °C to 800 °C in air at a rate of 10 °C/min.

Fourier Transform Infrared spectroscopy (FTIR) spectra of the epoxy were also obtained, to assess the chemical nature of the material. Powder samples, scraped from the specimens' surface were mixed with dry spectroscopic grade potassium bromide and pressed into pellets. 32 scans were collected at 0.6 cm/s using a *Bruker Tensor 27* spectroscope, in the 4000-450 cm^{-1} region, and averaged at a spectral resolution of 4 cm^{-1}, according to ASTM E 1252 standard [8.35]. The infrared (IR) spectra observed were compared to with spectra available in spectral libraries.

The density of the epoxy was determined according to method A of ISO 1183-1 standard [8.36], Three unaged cubic specimens (with 0.5 mm and 0.1 mg) were analysed according to method A of ISO 1183-1 [8.36], an immersion method for non-cellular plastic materials in solid state.

The weight variations of the adhesive during the hygrothermal ageing - immersion in demineralised water and salt water and continuous condensation - were assessed by means of gravimetric measurements. Specimens with $4 \times 10 \times 60$ mm^3 were periodically removed from the recipients and, after wiping the superficial water, were immediately weighted using a *Mettler* analytical balance to determine the percentage of absorbed water, according to ASTM D5229 [8.33]. Subsequently, the specimens were immediately returned to the recipient. One sample per ageing condition was considered, as preliminary tests performed in three similar specimens for 45 days provided very consistent measurements.

The viscoelastic temperature-dependent behaviour of the unaged and aged adhesive, as well as the changes in the loss modulus (tan δ) and storage modulus (E') curves and in the T_g were assessed through DMA. The analysis was performed in accordance with parts 1 and 5 of ISO 6721 [8.37]. Prismatic specimens with $4 \times 10 \times 60$ mm^3 were tested in a dual cantilever configuration at a constant frequency of 1 Hz and a maximum deformation of 15 μm, using a *TA Instruments Q800* dynamic mechanical analyser. The tests were conducted in air atmosphere from 25 °C to 150 °C, at a rate of 2 °C/min. For each ageing condition and duration, three replicates were tested. The T_g was determined from the peak of the tan δ curve, and also from the E' curve, taken as the extrapolated onset of its sigmoidal change, as per the definition of ASTM E 1640 [8.38].

Concerning the adhesive mechanical properties characterisation test were made to it tensile properties (unaged only), and also flexural and in-plane shear properties (unaged and aged). The tensile properties of the unaged adhesive were determined according to ISO 527-2 standard [8.39], only for initial characterisation purposes. Five 115 mm long dog-boned shaped specimens were produced with a 10×4 mm^2 cross section in the central part. Tests were carried out using an *Instron 4803* universal testing machine (UTS) at a cross-head loading rate of 1 mm/min. The longitudinal strain was measured with an *Instron* 2630-112 clip-on extensometer, with a gauge length of 50 mm; the tensile modulus was determined from the slope of the stress *vs.* strain curve, for strains ranging between 0.05% and 0.25%.

The initial flexural properties of the adhesive and the effects of ageing on those properties were measured by means of three-point bending tests, according to ISO 178 standard [8.40]. Tests were carried out in $4 \times 10 \times 80$ mm^3 specimens (64 mm of span) at a loading rate of 2 mm/min, using an *Instron 4803* UTS. Five replicates were tested for each ageing condition and period.

The in-plane shear response of the adhesive and the influence of the ageing environments on such response was assessed by means of *Iosipescu* (V-notched beam) tests, performed according to ASTM D5379/D 5379M standard [8.41]. Although this method applies to laminated composites, it has been recently applied to assess the shear properties of softer materials [8.42, 8.43]. Tests were performed in specimens with $8 \times 20 \times 50$ mm^3, comprising a 4 mm deep notch on both sides, loaded at rate of 0.5 mm/min using an *Instron 4803* UTS, integrating a 10 kN load cell and the Iosipescu test apparatus. Shear strains at the notch area were measured with a video extensometer, comprising a high definition video camera from *Sony XCG 5005E* with a *Fujinon Fujifilm HF50SA-1* lens integrated with specific *LabView* data

acquisition software, that monitored the displacements at different specimen points. Four target dots were marked on each specimen, forming a square grid with a size of 6 mm, at an equal distance from the specimen centre. The variation of their coordinates was used to calculate the shear strains. The shear modulus was determined within the initial linear trend of the curves, in the 0.0025-0.008 shear strain range. Despite the different geometry and thickness of the shear specimens, they were subjected to a controlled and uniform manufacturing procedure and curing conditions. In this regard, due to the relatively long curing and ageing periods, little differences are expected to occur in terms of the specimens' degree of cure, T_g, and defects.

Regarding mechanical tests, five specimens were tested for each ageing condition and duration, while 10 specimens were used for unaged characterisation.

8.4. Experimental results and discussion

In this section, the experimental results obtained in the different tests are presented and analysed. Whenever relevant, results of different tests are cross referenced and compared to similar studies in the literature.

8.4.1 Reference epoxy adhesive specimens (unaged)

The physical, chemical and mechanical properties of the adhesive obtained in the initial characterisation tests (*i.e.*, before ageing) are listed in Table 8.4 (average ± standard deviation, when applicable).

Table 8.4. Physical and chemical properties of the epoxy adhesive*.

Characteristic	**Method**	**Property**	**Result**
Constituent materials	TGA	M [%]	67% epoxy resin, 11% calcium carbonate, 22% silica-based filler
Chemical nature	FTIR		Spectra consistent with epoxy peaks. Presence of calcium carbonate and silica-based peaks
Density	Immersion	ρ [g/cm^3]	1.36
Glass transition temperature	DMA	$T_{g,\ E'onset}$ [°C]	59.5 ± 0.10
		$T_{g,\ \tan\delta}$ [°C]	78.2 ± 0.10
Mechanical properties	Tensile	σ_{tu} [MPa]	33.8 ± 1.30
		E_t [GPa]	4.5 ± 0.30
		ε_{tu} [%]	0.79 ± 0.15
	Flexure	$\sigma_{f\ max}$ [MPa]	71.7 ± 7.90
		E_f [GPa]	3.9 ± 0.20
		ε_{fu} [%]	1.74 ± 0.22
	In-plane shear	τ_{max} [MPa]	28.3 ± 4.01
		G [GPa]	1.8 ± 0.37
		γ_u [%]	1.9 ± 0.34

* 24 h of curing at room temperature plus 24 h of curing at 50 ^{o}C

The thermogram obtained from the TGA analysis is illustrated in Figure 8.3. Mass loss started at 150 °C and an abrupt drop occurred at approximately 350 °C, which can be attributed to the decomposition of organic material (67% content). Calcium carbonate decomposed from 600 °C to 730 °C and the 22% residual mass was attributed to the presence of silica-based fillers.

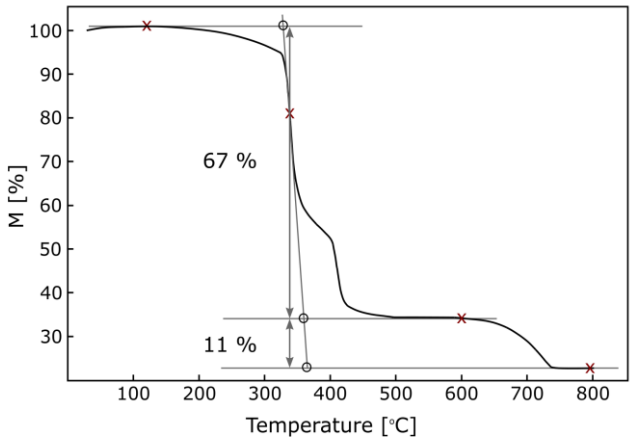

Figure 8.3. Thermogram of the epoxy adhesive.

The FTIR spectra, depicted in Figure 8.4, showed consistent peak characteristics of an epoxy resin (E) and calcium carbonate (C). It was also possible to identify bands that refer to silica-based fillers marked with (S).

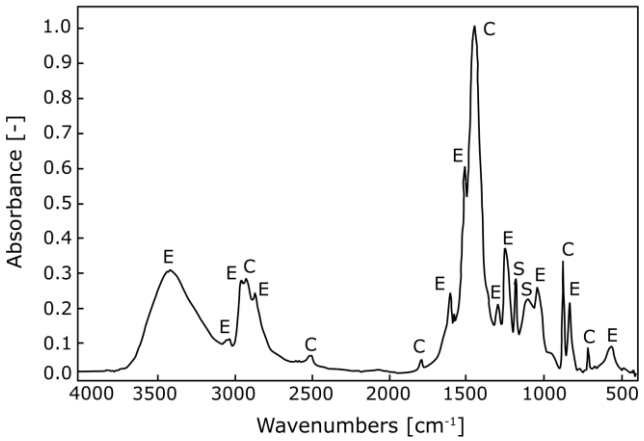

Figure 8.4. FTIR spectra of the reference specimens.

Figure 8.5 presents the DMA curves (storage modulus, E', left axis - dotted line and loss factor, tan δ, right axis - straight line) of the epoxy.

The E' curve presented the typical sigmoidal shape often representative of polymeric materials and started to exhibit significant reductions at around 60 °C, while the tan δ curve exhibited a peak near 78 °C, that corresponded to both T_g of the adhesives.

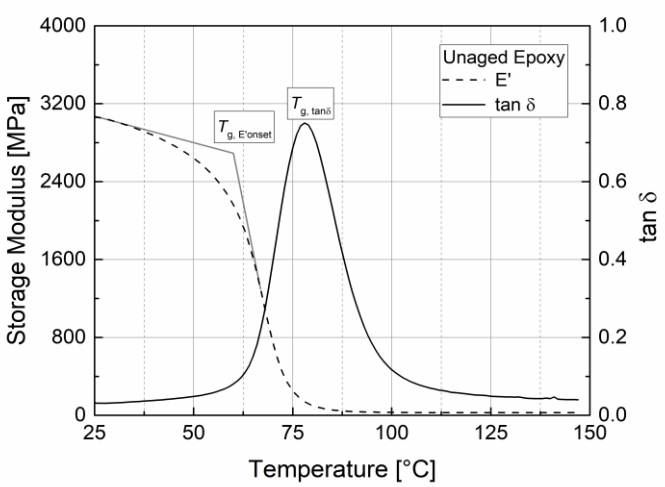

Figure 8.5. DMA experimental curves of the epoxy adhesive.

Figure 8.6 illustrates the mechanical behaviour, in tensile, flexure and shear of the epoxy adhesive, along with the error envelope (standard deviation of the experimental curves).

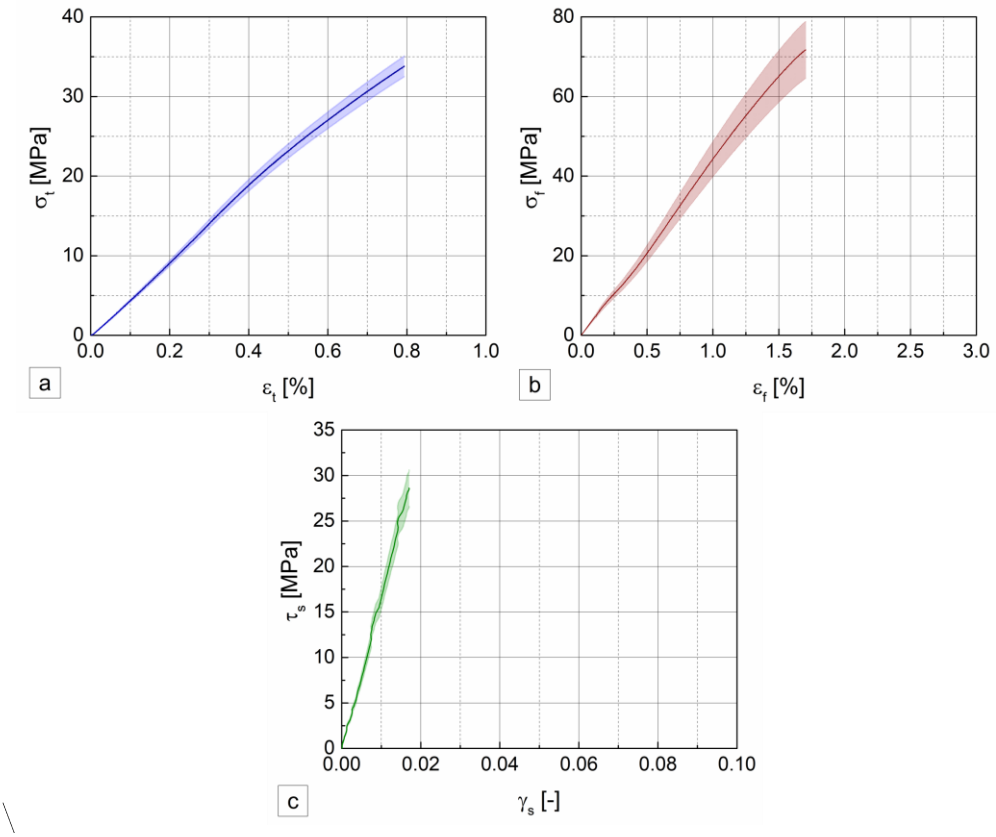

Figure 8.6. Mechanical behaviour of the epoxy adhesive in (a) tensile, (b) flexure and (c) shear.

For the three types of mechanical tests, the epoxy adhesive showed an almost linear behaviour until rupture, typical of most epoxies. The average mechanical properties of the unaged material are listed in Table 8.4.

8.4.2 Sorption behaviour

Figure 8.7. depicts the mass changes as a function of the square root of time for the different hygrothermal environments – immersion and continuous condensation. Two different non-linear fit models described below are plotted together with the test data.

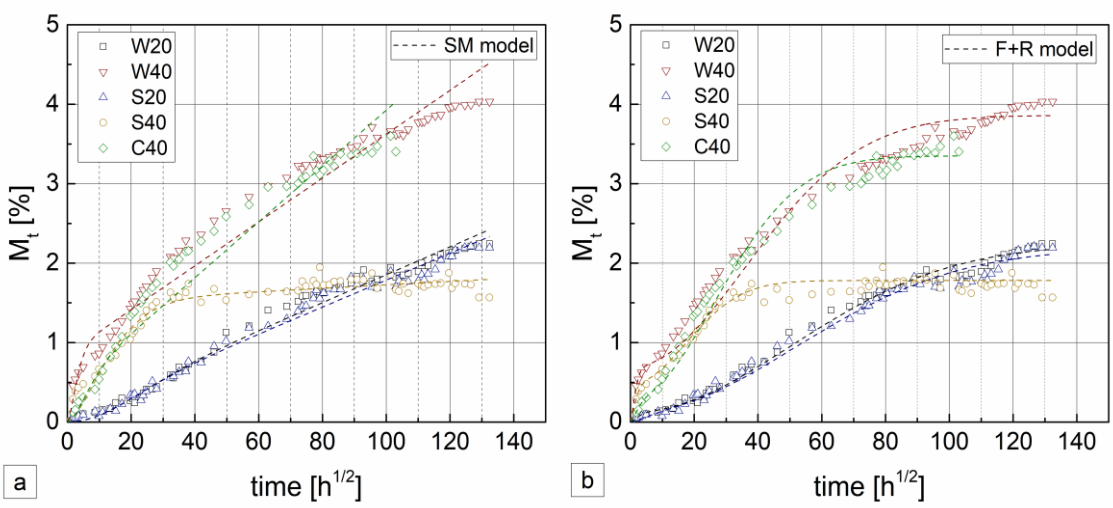

Figure 8.7. Mass uptake during hygrothermal ageing of epoxy adhesive and analytical diffusion models: (a) SM; (b) F+R.

For all types of hygrothermal exposure, mass increased throughout the exposure period. For the higher temperature environments (W40, C40 and S40) the absorption rate in the early stages was considerably higher compared to room temperature, and then the water uptake continued but at a slower pace. For the S40 environment an equilibrium plateau seems to have been achieved after ~80 $h^{1/2}$, while for the other environments a fully saturated state was not clearly attained; it is likely that more time would be needed to attain such a condition.

At the higher immersion temperature, salt water inhibited/delayed the mass uptake and reduced the sorption rate. This effect, already reported in earlier investigations [8.14, 8.44], should be attributed to the cross-linked behaviour of this type of polymers, enabling water movements and haltering large inorganic ions, thus acting as a semipermeable membrane [8.45]. However, somehow these differences were not clear at the lower immersion temperature, for which the mass uptake in salt water was only slightly lower than in demineralized water; this suggests that the above-mentioned effect is also influenced by temperature. Nevertheless, it is also worth mentioning that at later stages of the experiments the water uptake in S40

environment was lower than in both immersions at 20 °C. This seems to indicate that mass loss by extraction of low molecular components during immersion at higher temperatures may have occurred, resulting in a potential mass loss; this degradation mechanism was also identified in previous works [8.14]. In this case, such effect may have competed with the moisture uptake.

The mass changes in the continuous condensation environment were similar (slightly lower) to those in water immersion at the same temperature of 40 °C.

Regarding the modelling of the absorption behaviour, both Fickian and non-Fickian responses have been observed in polymeric adhesives [8.20, 8.46-8.49]. In the latter case, after an initial stage where the diffusion rate and water incorporation is well described by the traditional Fick's second law, deviations from that law occur and they have been attributed to polymer relaxation processes. Voids and free volumes redistribution in the polymer network due to swelling effects caused by penetrant molecules force macro-molecular movement and more moisture content is seemingly absorbed by the resin [8.47, 8.49].

The experimental curves depicted in Figure 8.7 indicate that Fickian diffusion models are not able to represent the test data. In fact, significant water uptake (relaxation effect) was still observed at the end of the experiments, especially at higher temperatures. Yang *et al.* [8.20] also reported this phenomenon in an epoxy adhesive tested for long exposure times.

Therefore, two more versatile models for polymeric materials, were used as an alternative, and are depicted in Figure 8.8.

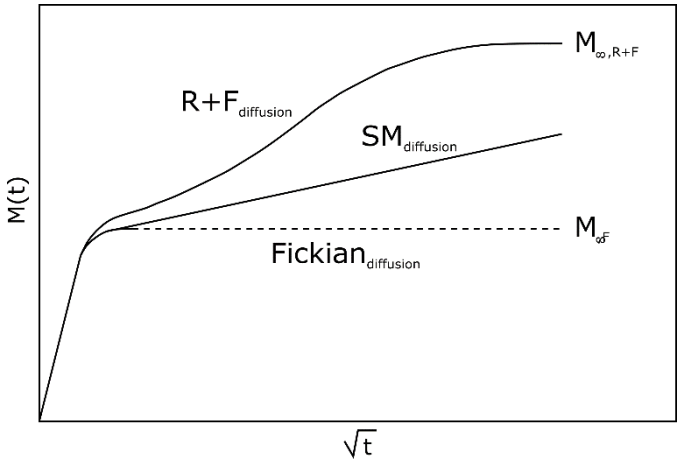

Figure 8.8. Fickian diffusion and both alternative diffusion models considered.

The first model, presented by Bao *et al.* [8.47], accounts for structural modification (SM) of the polymer. Because an equilibrium level uptake was not reached in their experiments, the authors proposed a two-stage relaxation model that allows simulating increasing moisture

uptake over time. The first stage exhibits a typical Fickian diffusion trend. The second stage simulates the relaxation of the polymer, presenting a relaxation asymptote as an increasing linear function of $t^{1/2}$. The mass uptake (M_t) as a function of time (t) is defined as,

$$M_t = M_{0\infty}(1+k\sqrt{t})\left\{1-\exp\left[-7.3\left(\frac{Dt}{h}\right)^{0.75}\right]\right\} \tag{8.1}$$

where $M_{0\infty}$ is the pseudo-equilibrium moisture content, k is a relaxation coefficient, D is the diffusion coefficient and h is the specimen thickness.

The Fickian and relaxation model (F+R), proposed by Berens and Hopfenberg [8.46], also accounts for polymeric relaxation. The authors suggested a linear superposition of two independent contributions, one accounting for Fickian diffusion and the other for relaxation processes. The Fickian diffusion takes part in the most initial stages of water uptake and after a first stabilization level, relaxation takes control of the intake process. The mass uptake can be calculated from,

$$M_t = M_{\infty,F}\left\{1-\exp\left[-7.3\left(\frac{Dt}{h}\right)^{0.75}\right]\right\} + M_{\infty,R}\left[1-\exp(-kt)\right] \tag{8.2}$$

where $M_{\infty,F}$ is the Fickian asymptote and $M_{\infty,R}$ is the amount of absorption due to relaxation.

The two models described above were fitted to the test data through a nonlinear curve fit, that applied an orthogonal distance regression iteration algorithm, available with the commercial software package *OriginPro*. that retrieved the diffusion parameters in Eq. (8.1) and Eq. (8.2). Table 8.5 shows the moisture diffusion, relaxation coefficients, and mean absolute percentage error (MAPE) obtained. Figure 8.7 depicts the comparison between the experimental results and analytical models.

Table 8.5. Moisture diffusion and relaxation coefficients for the epoxy adhesive.

Model	**Coefficients**	**W20**	**W40**	**S20**	**S40**	**C40**
SM	D [×10^{-6} mm^2/s]	0.84	27.2	0.95	1.34	6.86
	k [×10^{-3} s^{-1}]	2.84	0.53	3.08	0.03	1.43
	$M_{0\infty}$ [%]	0.10	0.86	0.09	1.51	0.41
	MAPE	14.4	9.6	13.6	9.0	13.4
F+R	D [×10^{-5} mm^2/s]	2.81	9.44	0.64	4.26	3.81
	k [×10^{-8} s^{-1}]	5.52	0.11	5.27	863	0.20
	$M_{\infty,F}$ [%]	0.12	0.69	0.14	0.48	0.32
	$M_{\infty,R}$ [%]	2.12	3.17	2.06	1.30	3.03
	MAPE	6.9	8.1	11.68	4.6	7.9

Overall both models provided good fitting to the test data reflected in the general low values of the MAPE, which ranged from 9-14% in the SM model, and between 5-12% in the F+R model (better approximations). The relative differences between both models should be due to the non-linearity of the experimental results in the relaxation dominated part, where the SM model assumes a linear trend (an intrinsic limitation of the model) and the F+R tends to a plateau. Analysing the different environments, the SM models presented higher relative errors values at lower immersion temperatures and continuous condensation when compared to higher immersion temperatures. Apart from the W20 environment, the same was observed for the F+R model.

The diffusion coefficients obtained for the Fickian dominated period reflect the expected temperature-dependence of polymeric adhesives: this parameter increased with temperature, especially in demineralised water immersion. Lower diffusion parameters were obtained for salt water immersion, which is also logical.

8.4.3 Characterisation of the thermo-mechanical response

Figure 8.9 shows representative DMA curves (storage modulus, E', left axis - dotted lines and loss factor, tan δ, right axis - straight lines) for unaged and aged epoxy adhesive subjected to the different ageing environments for various periods of time.

Regarding immersion in demineralised water (Figure 8.9 (a) and (b)), for both unaged and aged epoxy and regardless of the immersion temperature, the E' curves present the typical slope of polymeric materials: after a glassy plateau at 20-25 °C, the storage modulus drops sharply and becomes practically null. Considering 25 °C as a representative temperature of the glassy plateau, an initial increase in the storage modulus was visible after 4 months in W20 and 2 months in W40 environments. Subsequently, a general decreasing trend is observed for up to 24 months, which was more pronounced at the higher temperature. This can be attributed to the absorbed water acting as a plasticizer of the epoxy adhesive [8.20]; this seems to be supported by the comparison of the E' values at both temperatures, which are generally higher for W20 (for the same immersion duration). Moreover, for both immersion temperatures, the drop in E' progressively occurs at lower temperatures, reflecting a general decreasing trend of the $T_{g,onset}$ of the epoxy adhesive.

Regarding the tan δ curve, its variation over time may be influenced by many factors, such as the leaching out of low molecular weight content due to prolonged immersion periods, overall material degradation, cure progression, and moisture induced plasticization [8.20, 8.50, 8.51]. Three main changes due to immersion can be identified in the tan δ curve, which are described next.

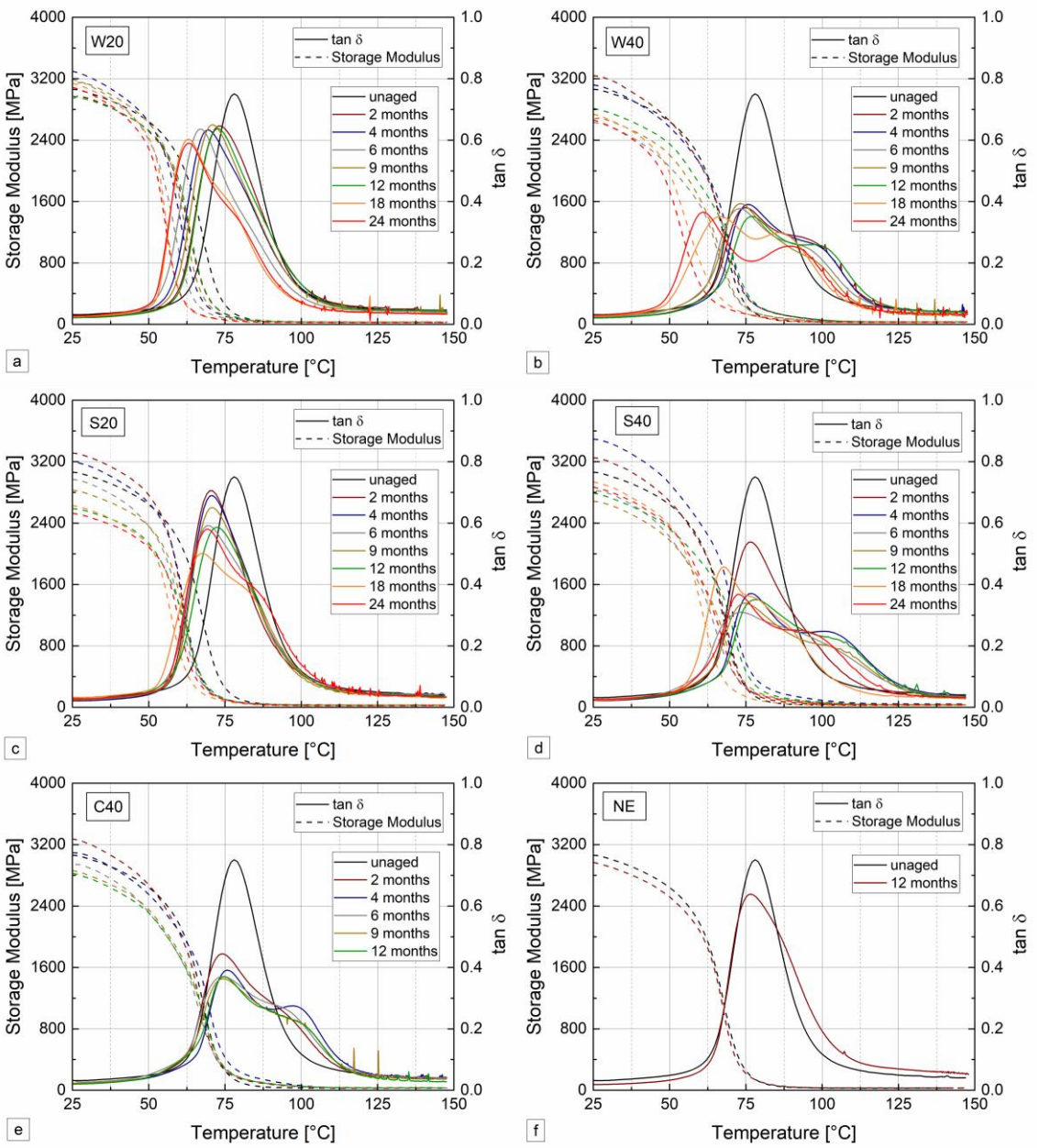

Figure 8.9. DMA curves for different exposure times of epoxy adhesive in water immersion at (a) 20 ºC and (b) 40 ºC; salt water immersion at (c) 20 ºC and (d) 40 ºC; (e) continuous condensation and (f) natural exposure.

The first change consists of a progressive decrease of the tan δ peak height, with (i) reductions being more pronounced for the higher immersion temperature and (ii) the highest reduction occurring after only 2 months of immersion at both temperatures. This early reduction should be related to the higher diffusivity (noticed in the gravimetric measurements) during the first stage of the immersion period, where the adhesive incorporated higher amounts of water.

During that initial period, the tan δ peak was reduced by about 40% at 40 °C and 15% at 20 °C. These results are in agreement with several previous works on epoxy

adhesives [8.1, 8.6, 8.20-8.22]. Subsequently, the tan δ peak continued to decrease, but at a much lower rate and eventually stabilized at the end of the ageing period.

The second main change corresponds to the widening of the base of the tan δ curve, coupled with the appearance of another peak, thus splitting the curve in two peaks. This latter change is more noticeable at 40 °C, for which the split formation occurs progressively with ageing. In fact, at 20 °C, only a widening of the right side of the curve (where the splitting should occur) is noticed after 18 and 24 months of exposure. In opposition, at 40 °C the widening is very clear already after 2 months, and after 12 months of ageing the second peak is easily recognised. This phenomenon (splitting of tan δ peaks) has been reported in other investigations about the hygrothermal ageing of polymeric adhesives and FRP composites [8.6, 8.18, 8.20, 8.29, 8.51], and attributed to the heterogeneous plasticization or to the drying effect caused by the DMA test procedure (involving heating). Yang *et al.* [8.20] noticed that the upper peak was very similar to values obtained from vacuum dried specimens after ageing; in addition, the authors associated the lower and upper peaks respectively to the water-plasticized and dried fractions of the adhesive.

The third main change is the general shifting of the tan δ curve towards lower temperatures, and the consequent reduction of T_g. Similar effects have been reported in previous works [8.6, 8.14, 8.20, 8.29]. It is of interest to note that after 12 months of immersion, the desorption period was not enough to dry the adhesives. Even after achieving constant mass, water molecules were still trapped inside the specimens; this is reflected in the fluctuations of the tan δ curves when approaching and exceeding 100 °C. This also corroborates the relation between the lower peak in the tan δ curve and the water-plasticized fraction of the adhesive.

The results obtained for salt water immersion (Figure 8.9 (c) and (d)) and continuous condensation (Figure 8.9 (e)) were very similar to those discussed above for demineralised water immersion, regarding the main trends of variation in the storage modulus and loss factor curves and the corresponding T_g values. In other words, the presence of salt did not significantly affect the performance of the epoxy adhesive.

One year of exposure to natural exposure (Figure 8.9 (f)) caused little changes in the thermomechanical response of the epoxy adhesive. Regarding the tan δ curve, a 10% reduction in the peak values occurred, as well as the widening of its base; a slight reduction of the E' value at the glassy state was also noted. These small differences may be related to UV exposure, also reported in other investigations [8.19, 8.28].

The effects of the different ageing environments on T_g (average ± standard deviation values), obtained from the two alternative methods described in Section 3.3.5: (i) the peak of the tan δ curve ($T_{g,\ tan\ \delta}$), and (ii) the onset of the drop in the E' curve ($T_{g,\ E'onset}$), are shown in Figure 8.10. For the tan δ curve, in cases where splitting occurred, the water plasticized fraction was considered (*i.e.*, the lower peak).

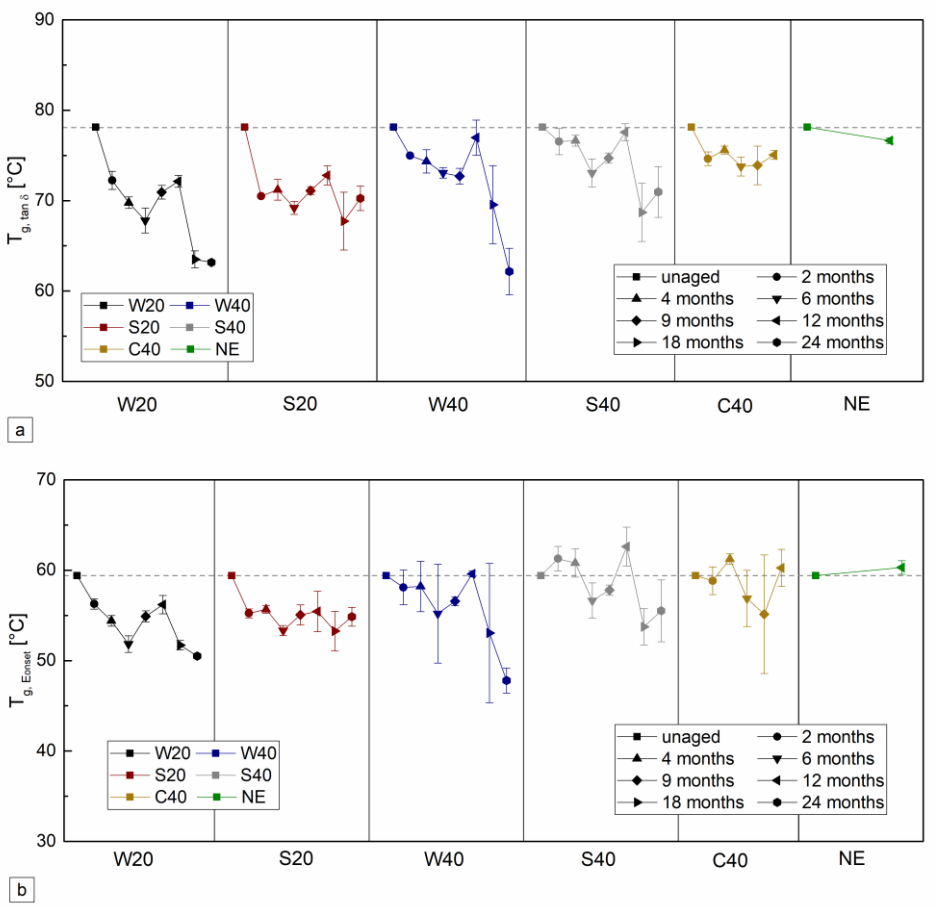

Figure 8.10. Variations of the glass transition temperature for the different ageing environments: (a) $T_{g,\ tan\ \delta}$; (b) $T_{g,\ E'onset}$

For hygrothermal environments, the T_g estimated from both methods showed a general decreasing trend over time. This effect was more clear in the tan δ curves, which showed significant reductions after 2 years (around 20% for W20 and W40, and 10% for S20 and S40). Reductions of T_g are usually attributed to plasticization and hydrolysis that occur in long immersion periods and induce high level of molecular mobility [8.14]. However, an increasing trend is consistently noted between 6 and 12 months, although the T_g never attained the initial value. The desorption period must have contributed to attenuate some reversible degradation effects (*i.e.*, the plasticization phenomenon) in that period. This non-monotonic pattern of variation of the T_g of adhesives during immersion has also been reported elsewhere [8.22]. Since the adhesive could have been not fully cured, the degradation suffered by the physical aging

may have resulted in a competing process with post-curing phenomenon. In fact, the higher temperature may have also contributed to these post-curing effects, attenuating the overall degradation, which is quite evident until 12 months of immersion. In the C40 environment, the T_g also showed little variations throughout the ageing process (from the tan δ curve, 4% reduction after 12 months), despite the evident changes in the DMA curves. As mentioned above, the effects of salt water immersion in the changes of T_g were very similar to those of immersion in demineralised water.

As for outdoor ageing, negligible changes in the T_g value occurred after 12 months (2% reduction from the tan δ curve), attesting the stability of the adhesive for this type of exposure. In any case, since there is evidence that the adhesive was not fully cured, it is likely that the outdoor exposure promoted the further reticulation of the epoxy polymer, which may have contributed to a potential increase of T_g [8.28]. The small changes in T_g can be explained by the structural modifications caused by the environmental agents (reflected by the DMA curves, *cf.* Figure 8.9 (f)), such as UV exposure and moisture, which may have compensated the former effect.

8.4.4 Characterisation of the flexural response

All flexural tests were conducted up to the adhesive failure at midspan section, depicted in Figure 8.11, which was brittle and sudden; the failure mode was consisted throughout the ageing periods.

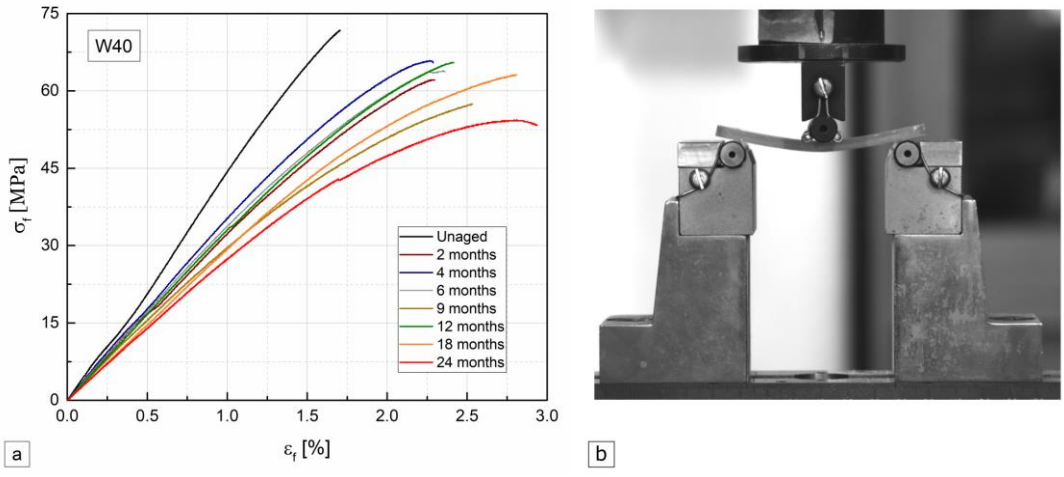

Figure 8.11. (a) Flexural stress-strain curves at different ageing times for immersion in water at 40 ºC; (b) deformed shape of a test specimen in the brink of rupture

Plasticization and relaxation mechanisms promoted by the water absorption also affected the stress *vs.* strain responses, with increasing values of strain at rupture being observed during ageing for all exposure conditions. In addition, irreversible degradation mechanisms also

affected the aged epoxy specimens, lowering their flexural properties especially at higher temperatures. Figure 8.11 (a) illustrates this effect, by depicting representative stress *vs.* strain curves for one of the exposure conditions (W40) and presenting the deformation of an aged specimen prior to failure (Figure 8.11 (b)).

The effect of hygrothermal ageing on the flexural modulus and strength of the epoxy adhesive is shown in Figure 8.12 (average ± standard deviation values).

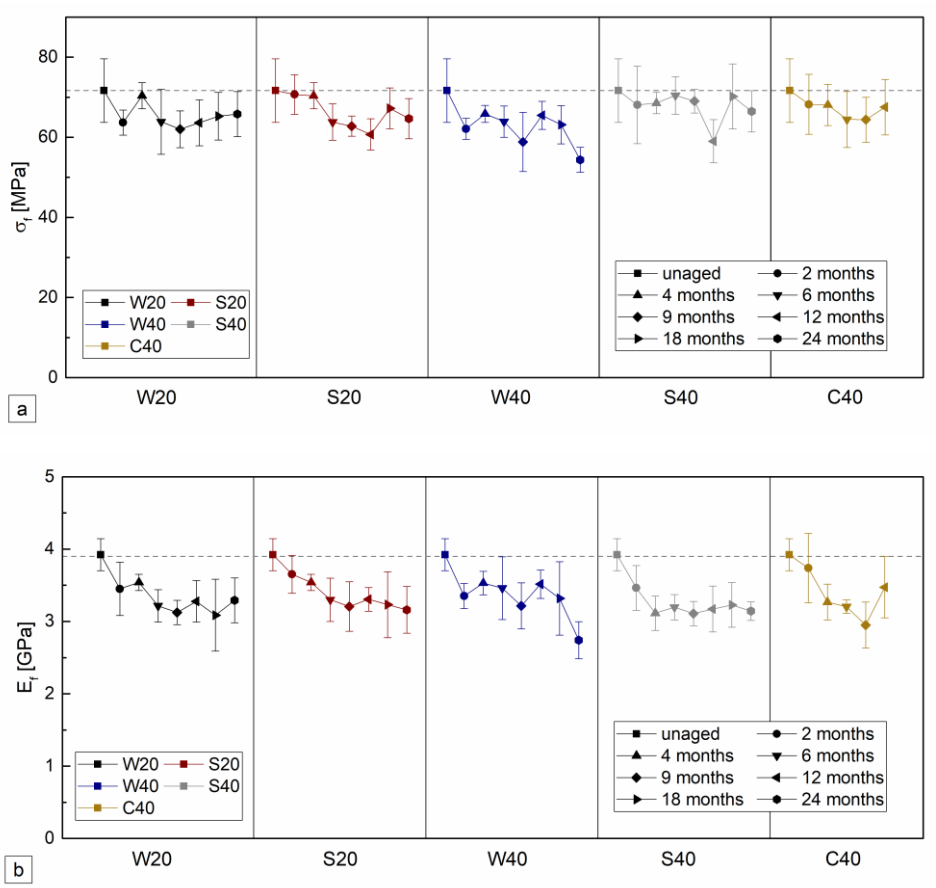

Figure 8.12. Variation of (a) flexural strength and (b) modulus, during the different ageing environments.

Water uptake had a global negative effect on the flexural properties of the epoxy adhesive, which was more accentuated in the flexural modulus. The results obtained indicate that irreversible degradation took place, in spite of the desorption period. After an initial (mostly linear) reduction, flexural properties tended to stabilize, with much less changes occurring in the later exposure periods. These results are in agreement with previous studies about the tensile behaviour of epoxy adhesives [8.7, 8.29, 8.52]. It is worth noting that for some periods the scatter in the experimental data is significant, which should be probably due to voids in

the adhesive caused during the manufacturing process[7]. In terms of flexural strength, the same general trends were observed, yet the performance reduction was smaller.

The highest reductions in flexural properties occurred in the W40 environment: after 2 years of ageing, the flexural modulus and strength were reduced by 30% and 24%, respectively; these changes are consistent with the T_g reduction observed for the same ageing conditions. The reduction of flexural properties in the 40 °C environments was only slightly higher than that at 20 °C – elevated temperature did not globally affect the flexural properties of the epoxy adhesive. The lowest reductions in flexural properties after 2 years of ageing occurred in the C40 environment, with the flexural modulus and strength decreasing 11% and 6%, respectively.

When assessing the property variations as a function of time, some increases can be identified in average values, which are in agreement with the DMA results. Once more, this result points out to the occurrence of post-cure phenomena, which, together with the desorption period, attenuated the material degradation. In previous investigations on the flexural properties of different epoxy systems [8.1, 8.6], comparable results were reported and the degradation effects were attributed to plasticization and hydrolysis mechanisms.

8.4.5 Characterisation of the in-plane shear response

The effect of ageing on the shear stress *vs.* strain response of the epoxy adhesive is shown in Figure 8.13 (a). For most exposure conditions, as for the flexural tests, specimens exhibited brittle behaviour up to failure; nevertheless, at the later stages, for all conditions except for outdoor ageing several specimens started to accommodate higher levels of shear strain before failing, exhibiting an increased non-linear behaviour. This was attributed to the aforementioned plasticization effects in the epoxy adhesive.

The typical (shear) failure mode is illustrated in Figure 8.13 (b) and was due to the development of cracks between the notches at a 45° angle. In the "more brittle" specimens, cracks propagated almost instantaneously, while in the "softer" specimens (more prolonged exposure, especially at higher temperature), the same failure mechanism occurred but at a much slower rate. The failure mode was not the same as for the GFRP laminates and raises some concerns about the internal stresses in the specimen.

[7] Manufacturing was mostly manual, *i.e.* it was not automatically controlled or vacuum assisted, in order to replicate real application conditions.

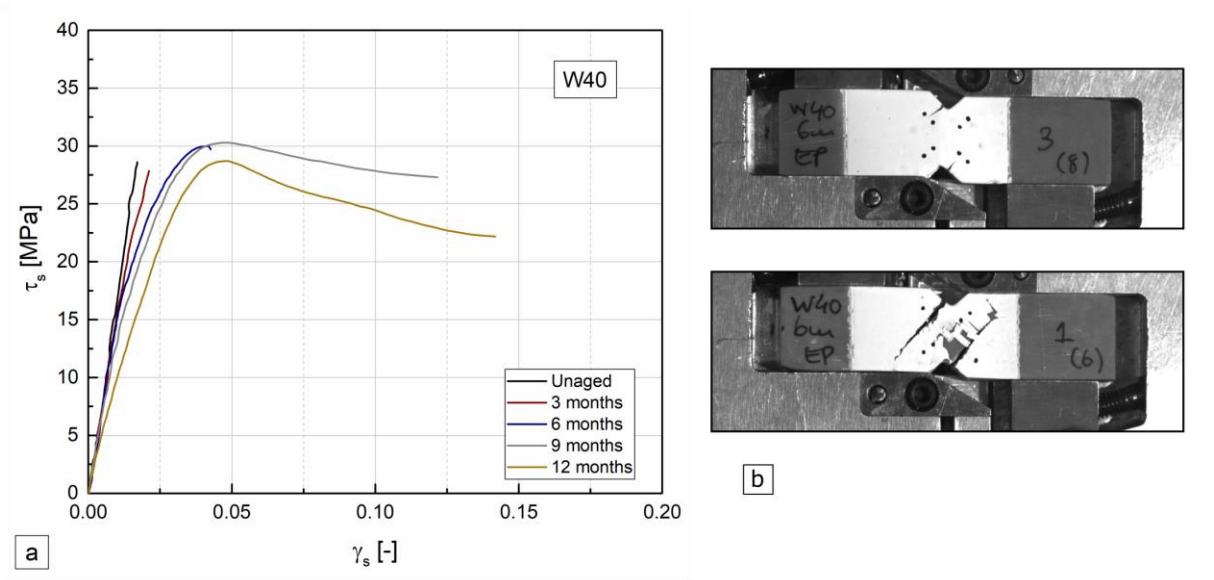

Figure 8.13. (a) In plane shear stress-strain curves at different ageing times for immersion in water at 40 ºC; (b) typical failure modes in shear.

The effect of ageing on the shear modulus and strength of the epoxy adhesive is shown in Figure 8.14 (average ± standard deviation values).

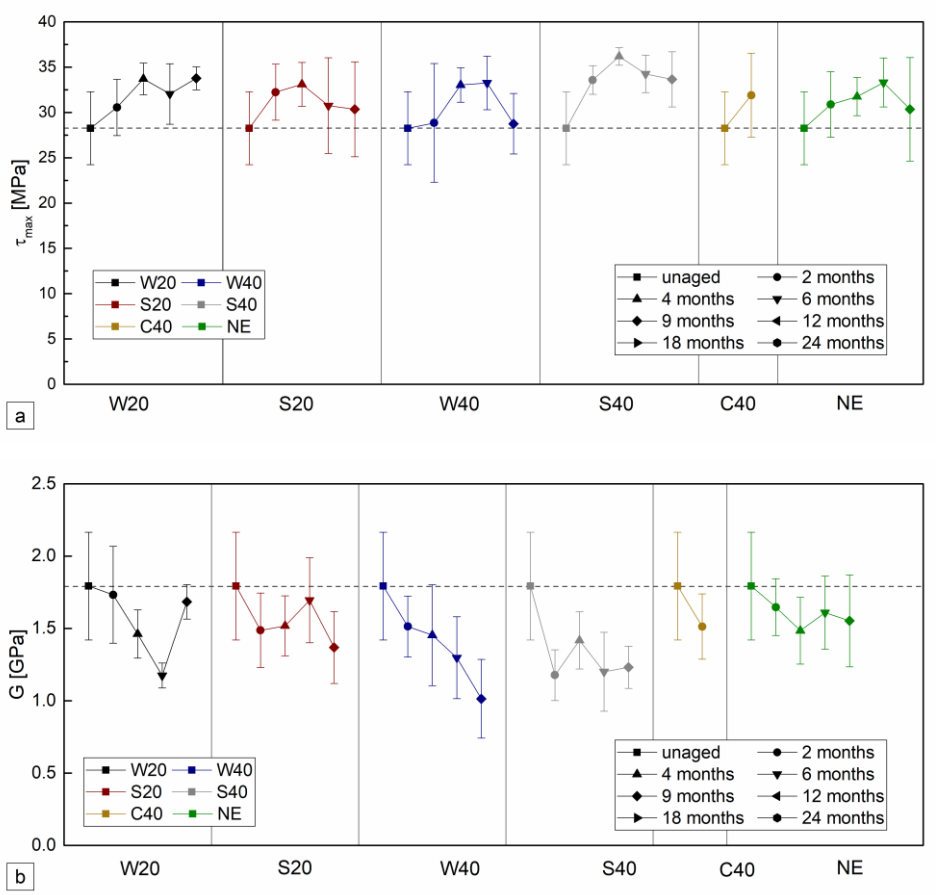

Figure 8.14. Variation of (a) in-plane shear strength and (b) modulus, during exposure to different ageing environments.

Although the scatter in the experimental data was relatively high (which can be attributed to the reasons mentioned before), the negative effect of water uptake on the shear modulus of the epoxy adhesive is very clear. Once more this reflects the irreversible degradation that took place in the material in spite of the desorption period. Exposures W40 and S40 were relatively harsher when compared to the same immersions at 20 °C, with the highest reduction in the shear modulus being measured after 12 months for W40 exposure (43%).

On the other hand, the shear strength exhibited an increasing trend for all hygrothermal environments. The highest shear strength was measured in S40 exposure after 9 months (28% increase). At the later stages, a slight tendency for shear strength reduction was noted, especially for W40, C40 and S20 environments; the overall trend seems to indicate that an inflexion point in the shear strength *vs.* time curve occurred, suggesting that such property would further decrease for longer exposure periods. The early increasing stage could be related to post cure phenomena, which is in agreement with the results of flexural properties and test data obtained in other investigations about tensile properties [8.22, 8.53].

The exposure to natural ageing led to similar qualitative changes in the shear properties of the epoxy adhesive, but the magnitude of the variations was lower: after 12 months, the shear modulus decreased 13% and the shear strength increased 7%.

8.5. Concluding remarks

This chapter presented experimental investigations about the effects of hygrothermal and outdoor ageing on the physical and mechanical properties of a structural epoxy adhesive used in civil engineering applications. The results obtained allow drawing the following main conclusions:

1. The sorption behaviour in the immersion environments was not Fickian; indeed, after 2 years, water molecules were still being incorporated, in most cases causing significant mass gain, which was attributed to relaxation effects in the polymeric structure. For both immersion media, as expected, higher temperature increased the diffusivity coefficients. In general, the (non-Fickian) analytical models used provided an overall good fitting to the test data.

2. Concerning the DMA results, generalised reductions in the glassy plateau of the storage modulus were visible and could be related to water plasticization effects; this result is in agreement with increasing fluctuations in the tan δ peak curve after 100 °C, suggesting that the desorption period was not enough to fully remove the water content from the adhesive. In the tan δ curve the height of the peak progressively decreased for all ageing conditions; in

addition, at higher conditioning temperature, the original peak of the tan δ curve was split in two, which occurred together with the widening of the curve. The changes in the polymer structure also had a detrimental effect on the T_g values, which decreased ~20% and 10% in water and salt water immersion, respectively, regardless of the temperature. The continuous condensation and outdoor ageing caused only negligible changes in T_g.

4. The flexural strength and modulus were affected due to ageing environments. Both properties had an initial and steeper decay and tended to stabilize at later periods. The highest reductions (30% in modulus and 24% in strength) were observed in the W40 environment after 2 years. Water-induced plasticization and relaxation also affected the stress-strain behaviour of the adhesive, with increasing values of strain at failure with the exposure period. In any case, post-cure phenomena were also identified at some periods, when those properties showed some gains. The continuous condensation environment showed similar results when compared to water immersions at the same temperature, in line with the sorption behaviour.

5. The same plasticization effects were noted in the mechanical behaviour in shear of specimens subjected to hygrothermal ageing, which exhibited a more non-linear response than unaged specimens and a more progressive (less sudden) failure. These differences were more pronounced for higher temperatures and longer conditioning periods. In terms of shear properties, opposite trends were found for the shear modulus and shear strength - the shear modulus showed decreasing trends, with the highest reduction (43%) occurring for W40 after 1 year; while the shear strength presented an overall increase. Outdoor ageing caused similar changes in shear properties, but the magnitude of the changes was lower (13% reduction of shear modulus after 1 year).

8.6. References

[8.1] Lettieri M, Frigione M. Effects of humid environment on thermal and mechanical properties of a cold-curing structural epoxy adhesive. Constr Build Mater 2012;30:753–60.

[8.2] The Institution of Structural Engineers. Guide to the structural use of adhesives. London: 1999.

[8.3] Abbey KJ. Advances in epoxy adhesives. Adv. Struct. Adhes. Bond., Woodhead Publishing Limited; 2010, p. 20–34.

[8.4] Cabral-Fonseca S, Correia JR, Custódio J, Silva HM, Machado AM, Sousa JM. Durability of FRP - concrete bonded joints in structural rehabilitation: a review. Int J Adhes Adhes Accept Publ n.d.

[8.5] Bowditch MR. The durability of adhesive joints in the presence of water. Int J Adhes Adhes 1996;16:73–9.

[8.6] Cabral-Fonseca S, Nunes JP, Rodrigues MP, Eusébio MI. Durability of epoxy adhesives used to bond CFRP laminates to concrete structures. Proc. 17th Int. Conf. Compos. Mater. - ICCM 17, Edinburgh, UK: 2009, p. 1–8.

[8.7] Savvilotidou M, Vassilopoulos AP, Frigione M, Keller T. Effects of aging in dry environment on physical and mechanical properties of a cold-curing structural epoxy adhesive for bridge construction. Constr Build Mater 2017;140:552–61.

[8.8] Michels J, Widmann R, Czaderski C, Allahvirdizadeh R, Motavalli M. Glass transition evaluation of commercially available epoxy resins used for civil engineering applications. Compos Part B Eng 2015;77:484–93.

[8.9] Michels J, Sena-Cruz J, Christen R, Czaderski C, Motavalli M. Mechanical performance of cold-curing epoxy adhesives after different mixing and curing procedures. Compos Part B Eng 2016;98:434–43.

[8.10] Moussa O, Vassilopoulos AP, Keller T. Effects of low-temperature curing on physical behavior of cold-curing epoxy adhesives in bridge construction. Int J Adhes Adhes 2012;32:15–22.

[8.11] Grave C, McEwan I, Pethrick RA. Influence of stoichiometric ratio on water absorption in epoxy resins. J Appl Polym Sci 1998;69:2369–76.

[8.12] Soles CL, Yee AF. Discussion of the molecular mechanisms of moisture transport in epoxy. J Polym Sci Part B Polym Phys 2000;38:792–802.

[8.13] Maxwell ID, Pethrick RA. Dielectric studies of water in epoxy-resins. J Appl Polym Sci 1983;28:2363–79.

[8.14] Cabral-Fonseca S, Correia JR, Rodrigues MP, Branco FA. Artificial accelerated ageing of GFRP pultruded profiles made of polyester and vinylester resins: Characterisation of physical-chemical and mechanical damage. Strain 2012;48:162–73.

[8.15] Pethrick RA. Design and ageing of adhesives for structural adhesive bonding - A review. J Mater Des Appl 2015;229:349–79.

[8.16] Zhou J, Lucas JP. Hygrothermal effects of epoxy resin. Part I: The nature of water in epoxy. Polymer 1999;40:5505–12.

[8.17] Zhou J, Lucas JP. Hygrothermal effects of epoxy resin. Part II: Variations of glass transition temperature. Polymer 1999;40:5513–22.

[8.18] Nogueira P, Ramírez C, Torres A, Abad MJ, Cano J, López J, et al. Effect of water sorption on the structure and mechanical properties of an epoxy resin system. J Appl Polym Sci 2001;80:71–80.

[8.19] Frigione M, Lettieri M, Mecchi AM. Environmental effects on epoxy adhesives employed for restoration of historical buildings. J Mater Civ Eng 2006;18:715–22.

[8.20] Yang Q, Xian G, Karbhari VM. Hygrothermal ageing of an epoxy adhesive used in FRP strengthening of concrete. J Appl Polym Sci 2008;107:2607–17.

[8.21] Silva P, Fernandes P, Sena-Cruz J, Xavier J, Castro F, Soares D, et al. Effects of different environmental conditions on the mechanical characteristics of a structural epoxy. Compos Part B Eng 2016;88:55–63.

[8.22] Savvilotidou M, Vassilopoulos AP, Frigione M, Keller T. Development of physical and mechanical properties of a cold-curing structural adhesive in a wet bridge environment. Constr Build Mater 2017;144:115–24.

[8.23] Lapique F, Redford K. Curing effects on viscosity and mechanical properties of a commercial epoxy resin adhesive. Int J Adhes Adhes 2002;22:337–46.

[8.24] Lin YC, Chen X. Moisture sorption-desorption-resorption characteristics and its effect on the mechanical behavior of the epoxy system. Polymer 2005;46:11994–2003.

[8.25] Goglio L, Rezaei M. Variations in mechanical properties of an epoxy adhesive on exposure to warm moisture. J Adhes Sci Technol 2014;28:1394–404.

[8.26] Frigione M, Naddeo C, Acierno D. Cold-curing epoxy resins: aging and environmental effects. II - Mechanical Properties. J Polym Enginnering 2001;21:349–68.

[8.27] Frigione M, Naddeo C, Acierno D. Cold-curing epoxy resins: aging and environmental effects I: Thermal Properties. J Polym Enginnering 2001;21:23–52.

[8.28] Lettieri M, Frigione M. Natural and artificial weathering effects on cold-cured epoxy resins. J Appl Polym Sci 2011;119:1635–45.

[8.29] Xian G, Karbhari VM. DMTA based investigation of hygrothermal ageing of an epoxy system used in rehabilitation. J Appl Polym Sci 2007;104:1084–94.

[8.30] ISO 175. Plastics. Methods of test for the determination of the effects of immersion in liquid chemicals. Int Organ Stand, 2010.

[8.31] ASTM D 1141. Standard practice for the preparation of substitute ocean water. Am Soc Test Mater, 2013.

[8.32] ISO 6270. Paints and varnishes.Determination of resistance to humidity. Part 2: Continuous condensation (in-cabinet exposure with heated water reservoir). Int Organ Stand, 2017.

[8.33] ASTM D 5229. Standard test method for moisture absorption properties and equilibrium conditioning of polymer matrix composite materials. Am Soc Test Mater, 2014.

[8.34] ISO 11358. Plastics.Thermogravimetry (TG) of polymers. Part 1: General principles. Int Organ Stand, 2014.

[8.35] ASTM E 1252. Standard practice for general techniques for obtaining infrared spectra for qualitative analysis. Am Soc Test Mater, 2013.

[8.36] ISO 1183. Plastics.Methods for determining the density of non-cellular plastics. Part 1: immersion method, liquid pyknometer and titration method. Int Organ Stand 2004.

[8.37] ISO 6721. Plastics. Determination of dynamic mechanical properties.Part 1: General principles; Part 5: Flexural vibration - non-resonance method. Int Organ Stand, 1996.

[8.38] ASTM E 1640. Standard test method for assignment of the glass transition temperature by dynamic mechanical analysis. Am Soc Test Mater, 2013.

[8.39] ISO 527. Plastics.Determination of tensile properties. Part 1: General principles; Part 2: Test conditions for moulding and extrusion plastics. Int Organ Stand, 2012.

[8.40] ISO 178. Plastics.Determination of flexural properties. Int Organ Stand, 2010.

[8.41] ASTM D 5379 / D 5379M. Standard test method for shear properties of composite materials by the V-notched beam method. Am Soc Test Mater, 2012.

[8.42] Osei-Antwi M, De Castro J, Vassilopoulos AP, Keller T. Shear mechanical characterization of balsa wood as core material of composite sandwich panels. Constr Build Mater 2013;41:231–8.

[8.43] Garrido M, Correia JR, Keller T. Effects of elevated temperature on the shear response of PET and PUR foams used in composite sandwich panels. Constr Build Mater 2015;76:150-7.

[8.44] Karbhari VM, Rivera J, Zhang J. Low-temperature hygrothermal degradation of ambient cured E-glass/vinylester composites. J Appl Polym Sci 2002;86:2255–60.

[8.45] Jones F. Durability of reinforced plastics in liquid environments. In: Pritchard G, editor. Reinf. Plast. Durab., Woodhead Publishing, Cambridge; 1999, p. 70–110.

[8.46] Berens AR, Hopfenberg HB. Diffusion and relaxation in glassy polymer powders: 2. Separation of diffusion and relaxation parameters. Polymer 1978;19:489–96.

[8.47] Bao LR, Yee AF, Lee CYC. Moisture absorption and hygrothermal aging in a bismaleimide resin. Polymer 2001;42:7327–33.

[8.48] Mubashar A, Ashcroft I, Critchlow G, Crocombe A. Moisture absorption-desorption effects in adhesive joints. Int J Adhes Adhes 2009;29:751–60.

[8.49] Jiang X, Kolstein H, Bijlaard FSK. Moisture diffusion in glass-fiber-reinforced polymer composite bridge under hot/wet environment. Compos Part B Eng 2013;45:407–16.

[8.50] Fraga AN, Alvarez VA, Vazquez A, Osa O De. Relationship between dynamic mechanical properties and water absorption of unsaturated polyester and vinyl ester glass fiber composites. J Compos Mater 2003;37:1553–74.

[8.51] Karbhari VM. Dynamic mechanical analysis of the effect of water on E-glass-vinylester composites. J Reinf Plast Compos 2005;25:631–44.

Chapter 9.

Effects of hygrothermal ageing and natural weathering on a structural polyurethane adhesive

9.1. Introduction

In recent years, the use of adhesives in the construction sector increased. Although bolted connections are still the most frequent, bonded connections offer significant advantages, namely the reduction of stress concentrations in the vicinity of bolts and the inexistence of holes [9.1]. For fibre reinforced polymer (FRP) adherends, further advantages stem from the compatibility between the polymer matrix and the adhesive. However, among other concerns (*e.g.*, the behaviour at elevated temperature), a wider use of bonded joints is pending on obtaining a better understanding of their long-term behaviour [9.2].

Nowadays, a wide range of adhesives are available to bond structural components made of different materials. Some industries, such as aerospace, naval and automotive, provide anecdotal evidence of good durability properties of bonded joints. However, limited comprehensive data is usually available regarding their long-term performance [9.3]. Moreover, as discussed in the previous chapter, structural adhesive bonding in civil engineering applications has very diverse requirements compared to those industries, namely different (longer) design service lives and exposure environments. In order to reliably design structural adhesive joints, such information is needed to reliably consider the environmental degradation underwent by the adhesive (and the adherends) throughout the service life [9.4].

Among the different adhesives used in civil engineering applications, structural polyurethane (PUR) adhesives are being considered with increasing interest [9.5]. This is due to the possibility of designing bonded joints with ductile behaviour, making use of their non-linear constitutive behaviour [9.6] to join brittle elements, such as FRPs. The creep behaviour of this type of adhesives also needs to be duly accounted for. As for other adhesives, little information is available on the effects of different environmental agents on their mechanical properties [9.3]. Moreover, these particular adhesives present a wide range of chemical and structural variations; as discussed ahead, this makes it difficult to compare results obtained in different studies, since ageing effects may vary and often show different results.

This chapter presents experimental investigations on the durability of a two-component structural polyurethane adhesive exposed to immersion in water, salt-water and continuous

condensation, and outdoor ageing at different temperatures for up to two years. Due to the post-conditioning drying procedure used in the experiments, the results obtained did not reproduce the worst-case scenario of real life conditions, as part of the changes underwent by the adhesive were reverted. Indeed, the main goal was to focus on the irreversible changes caused by the different environmental conditions. The influence of such exposure on the adhesive performance was evaluated regarding (i) the water diffusion process, (ii) the viscoelastic behaviour and (iii) the flexural and in-plane shear properties.

9.2. Literature review on the durability of structural polyurethane adhesives

Polyurethane (PUR) adhesives contain several urethane groups in their molecular structural backbone. They are obtained by step-growth polymerization (polyaddition) from three main components: (i) isocyanates, (ii) polyols or prepolymers (active hydrogen compounds) and (iii) small molecular weight chain extenders or cross-linkers (diamines or diols) [9.7]. In addition, catalysts (such as tertiary amines), and additives (*e.g.* drying agents, antioxidants, UV inhibiters, fillers or colorants), can also be added, thus contributing to significant differences between several types of PUR products. Several isocyanates (aromatic and aliphatic) can be used to react with active hydrogen compounds, in which toluene diisocyanate (TDI) or methylene diphenyl isocyanate (MDI) are the most commonly used, thus resulting in the diversity of polyurethanes. In addition, several polyols can also be incorporated, such as polyether and polyester polyols, among others; depending on their molecular weight, chemical type, functionality and chain structure they can confer more rigid and flexible properties to the resulting polyurethane [9.8]. They can also be tailored to the desired application by changing the formulation and stoichiometry of the components and they can be produced in many forms (usually one component or two component systems) [9.7].

Hollingsworth *et al.* [9.9] studied the hardness and the tensile properties of commercial polyurethanes adhesives used in a wide range of applications (solid tyres, seals) after accelerated ageing for up to two years, namely demineralised immersion and conditioning in a dry chamber at 40 °C, 70 °C and 90°C. Most of the adhesives slowly deteriorated when subjected to hot/dry conditions for long periods. When immersed in water or in contact with moisture at elevated temperatures, the polyester urethanes showed very high degradation rates - several adhesives even became too deteriorated for testing and several others showed 80% tensile strength reduction. The results obtained revealed the effects of plasticization and swelling during ageing, showing that the degradation rate is very much temperature dependent.

Buchman *et al.* [9.5] studied the effects of thermal ageing on three different elastomeric polyurethane adhesives usually applied in bonded joints for electric circuits. The adhesives were pre-cured at 55 °C for 24 hours and then post-cured before ageing. The ageing was carried out at 40 °C, 55 °C and 70 °C, at 50% of relative humidity (RH), from 20 days to 18 months. The polyurethane adhesives were characterized through tensile tests. The three adhesives showed crosslinking effects that were promoted through post-curing at elevated temperatures. However, three different behaviours over time were registered for each of the polyurethane adhesive types: (i) minimal property reductions, (ii) pronounced changes in tensile properties, due to extraction of gel molecules and embrittlement and (iii) severe deterioration, with steep reductions in all properties tested. The authors attributed these differences to the different chemical structure of the elastomers.

Davies and Evrard [9.10] studied the effect of salt water environments at 50 °C and 100 °C for periods up to two years on two different polyether based polyurethanes (one rigid and one flexible, differing in chemical composition) for marine applications. In parallel, they also subjected them to immersion in Brest Estuary sea for up to five years. The authors monitored the changes in tensile properties, in wet and dry conditions. Both adhesives showed the same trends, and ageing for up to two years resulted in stiffness and strength drops in the wet state at different temperature ranges. However, improved mechanical properties were noted after drying, for all ageing conditions. In addition, some deterioration that occurred in wet conditions, due to plasticization effects, could be reverted. Regarding the sea water tests, after 5 years of immersion the mechanical properties of both adhesives were not significantly affected.

Aglan *et al.* [9.11] studied the effect of ultraviolet (UV) radiation and hygrothermal ageing on the performance of a polyurethane elastomer, used in several industries (*e.g.*, forklift tires, seals). Different samples were conditioned in a UV chamber and a hygrothermal chamber. Tensile properties and dynamic mechanical analysis (DMA) changes were determined for up to 5 months of exposure in each condition. Significant changes in the UV exposed specimens (75% ultimate strength reduction) were found, in comparison with the negligible changes in the hygrothermal ageing (2% reduction). DMA analysis indicated significant reductions in the storage modulus of the adhesive due to UV exposure. In addition, a phase separation of the soft segments was also noted, due to urethane bond breaking. Unlike the hygrothermal weathering, UV exposure severely degraded the polyurethane elastomer.

Boubraki *et al.* [9.12] also studied the hygrothermal ageing of a thermoplastic polyurethane adhesive, usually applied in the manufacture of cables, adhesives and seals. The adhesive was immersed at 70 °C for up to 6 months and tested for water absorption behaviour, physical and

mechanical properties. The diffusion behaviour during the initial immersion was Fickian, being followed by a saturation stage. The glass transition temperature of the adhesive decreased with the ageing process, and indicated plasticization mechanisms. However, the most noticeable degradation after ageing was found in the tensile stress and modulus, with reductions of ~30% in stress level at 200% strain and 20% in modulus. A complementary investigation was made, which showed that the degradation underwent by the polyurethane adhesive was mostly irreversible. The authors also studied the influence of UV-ageing [9.13], reporting changes in mechanical properties and material structure; after an initial decrease, the glass transition temperature (T_g) exhibited an increasing trend with UV exposure, and the tensile stress and modulus showed the same trend – these changes were attributed to the competing effects of chain scission and increase in crosslinking density.

Le Gac *et al.* [9.14] studied a commercial polyether based polyurethane widely used for passive thermal insulation in offshore applications. The ageing was conducted in natural sea water at different temperature ranges (25 °C to 120 °C) for up to 18 months. In addition, for temperatures above 95 °C, ageing procedures were performed under a hydrostatic pressure of 100 bar. Concerning water diffusion, mass changes exhibited Fickian behaviour, except for temperatures above 80 °C. Tensile tests were performed, indicating large modifications in the adhesive behaviour: a decrease of tensile modulus was reported and attributed to polymer chain breakage; moreover, higher temperatures promoted the degradation kinetics and the stress at failure decreased noticeably when hydrolysis occurred.

Oliveira *et al.* [9.15] characterised a polyurethane elastomer for offshore applications. The material was exposed to outdoor environment and artificial seawater for up to 12 months. Although physical testing did not show significant material changes on the polyurethane chemical structure, the tensile properties were affected: the strength and modulus of the outdoor-aged samples exhibited an increasing trend (7% and 6%, respectively) and the authors attributed this to the additional crosslinking provided by the oxidation process. Nevertheless, for the specimens exposed to artificial seawater at 60 °C, a significant reduction of tensile properties (50% and 70%, respectively for strength and modulus) occurred and was attributed to plasticization.

Overall, the previous studies mentioned above besides being limited (in number) are difficult to compare – this is due to the wide variety of polyurethane adhesive formulations w.r.t. the constituent materials. Furthermore, the ageing conditions and durations and the characterisation methods used in these studies often have considerable differences. This may explain to some extent why some results are contradictory and different degradation

mechanisms are reported. In spite of such differences, the previous studies show that polyurethane ageing results from complex physical, chemical and mechanical processes; several factors seem to influence their performance, namely UV light, moisture and heat, and the most common degradation mechanisms affecting polyurethane adhesives under hygrothermal and natural ageing include hydrolysis [9.5, 9.10, 9.12, 9.14], crosslinking [9.5, 9.10, 9.13, 9.15], chain scission [9.5, 9.11, 9.13, 9.14] and plasticization [9.9, 9.10, 9.12, 9.15].

Concerning the influence of fillers in the adhesives ageing mechanisms, Torró-Palau *et al.* [9.16]. observed an increase in viscosity, imparted thixotropy and pseudoplasticity of filled polyurethane adhesives, as well as in the storage and loss moduli values. The filler content may also affect the adhesive water sorption. In fact, there is evidence of deviations from the usual Fickian behaviour in large particle filled adhesives [9.17, 9.18]. In those studies, the amount of water uptake in the adhesive increased with filler concentration [9.18], which in turn affected the hygrothermal ageing history, the T_g, and swelling. Moreover, in the presence of water, the bond between some fillers and the adhesive may not remain thermodynamically stable. Such water can displace the adhesive from the fillers, causing interfacial debonding and act as nucleus for hydrogen-bonded cluster formation [9.17].

None of the studies discussed above refer to civil engineering applications, where the service life is generally much longer, often set as 50 years. In addition, such studies vary significantly in terms of the polyurethane formulations and products and the ageing conditions, which can considerably affect the test results. Therefore, comprehensive information about the long-term behaviour of PUR structural adhesives used in this industry is needed to more reliably design and apply adhesively bonded joints. For instance, the vast majority of experimental data presented in the literature refers to the tensile properties of PUR adhesives; to the best of the author's knowledge, no information is available about their shear properties, although this stress state is the most relevant in many applications.

9.3. Experimental programme

9.3.1 Materials

The material used in this study is an *off-the-shelf* fast curing 2C adhesive (mixed in a 1:1 ratio in volume), based on filled polyols (A - resin) and unfilled isocyanates derivates (B - hardener), provided by *Sika Portugal S.A* (*SikaForce* 7888 L10), displayed in Figure 9.1.

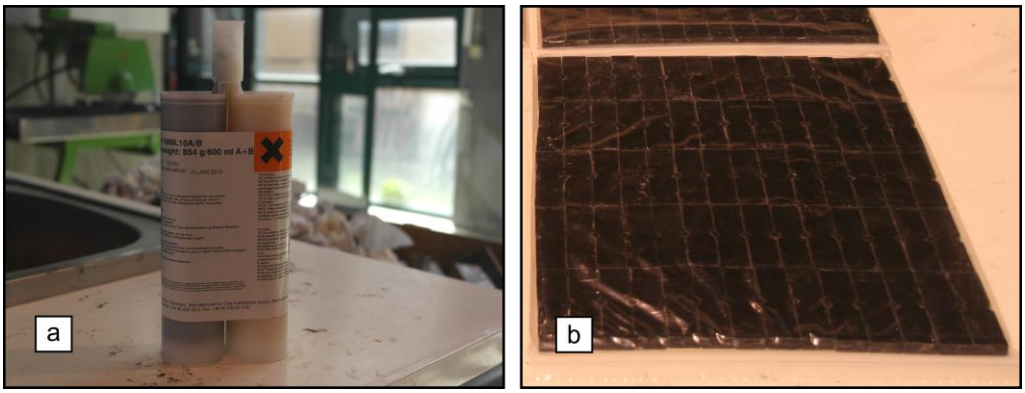

Figure 9.1. Material: (a) polyurethane adhesive; (b) specimens' appearance after demoulding.

The curing mechanism that occurs in this adhesive is polyaddition. According to the manufacturer, the adhesive T_g is approximately 40 °C, obtained from an internal test procedure (reference CPQ 509-1). This type of polyurethane adhesive is well suited for adhesive bonding of large components and assemblies; it can also be applied with different substrate materials, such as plastics, metals, and FRPs, namely glass-FRP (GFRP). The application process was performed using an adequate compressed air gun, which minimized the presence of defects in the bulk of the adhesive. Figure 9.2 depicts the quality of the adhesive; only small defects, such as superficial voids, were observed in a very limited number of specimens.

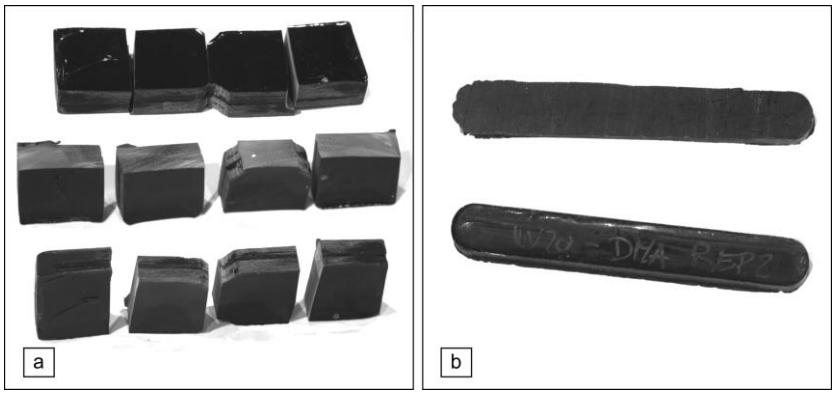

Figure 9.2. Images of polyurethane specimens: (a) shear specimens (after testing), and (b) flexural specimens.

9.3.2 Ageing environments

Different ageing environments were selected considering typical exposures likely to be found in civil engineering applications. According to Bowditch [9.19], the presence of moisture or water is usually critical to the stability of polymeric adhesives; although some adhesives are formulated to minimise hydrolysis effects, changes will always occur. Increasing temperature can also contribute to accelerate the diffusion progress, thus promoting further degradation. Many civil engineering structures comprising adhesively bonded members can be installed in

wet environments, coastal areas and outdoor conditions. This is the case of FRP structures, which are often selected due to their improved performance in relatively aggressive environments.

Taking these factors in consideration, the same four ageing environments that were selected for the exposing conditions in Chapter 8 were selected, as shown in Table 9.1: (i) immersion in demineralized water at 20 °C and 40 °C; (ii) immersion in salt water at the same temperatures; (iii) continuous condensation at 40 °C and (iv) natural exposure. The four immersion conditions were monitored up to two years of ageing, while for the remaining the maximum exposure duration was one year. The main objectives were to assess and compare the effects of these ageing environments in the performance of the polyurethane adhesive after being turned to its dry state, as described next in Section 9.3.3.

Table 9.1. Ageing environments conditions.

Ageing environments	**Label**	**Duration [months]**	**Conditions** [(a)]
Immersion in demineralised water	W20	0, 2, 4, 6, 9, 12, 18, 24	T = 20 ± 3 °C
	W40	0, 2, 4, 6, 9, 12, 18, 24	T = 40 ± 2 °C
Immersion in salt water	S20	0, 2, 4, 6, 9, 12, 18, 24	T = 20 ± 2 °C; 35 g/l NaCl
	S40	0, 2, 4, 6, 9, 12, 18, 24	T = 40 ± 2 °C; 35 g/l NaCl
Continuous condensation	C40	0, 2, 4, 6, 9, 12	T = 40 ± 2 °C; 100% RH
Outdoor exposure	NE	0, 2, 4, 6, 9, 12	T, RH and UV radiation continuously monitored

(a) *Temperature (T); Relative Humidity (RH); Ultraviolet (UV).*

The 20 °C temperature used in the immersions was set as the normal room temperature level; moreover, it is a good representation of the typical average temperature verified in mild Mediterranean countries such as Portugal. A higher temperature of 40 °C was selected to accelerate the diffusion process, as explained above. Figure 9.3 illustrates the different ageing environments.

Figure 9.3. Ageing environments: (a) condensation chamber, (b) chamber used for immersions; (c) natural exposure in LNEC's roof.

The specimens were placed inside appropriate recipients and stored in controlled chambers. Immersion ageing in the mentioned media was based on ISO 175 standard [9.20]. For the salt

water immersions, a sodium chloride concentration of 35°g/l was used in accordance to ASTM D 1141 standard [9.21].

The condensation chamber combined the effects of moisture and temperature. The specimens did not have any contact with the interior chamber walls, being suspended as illustrated in Figure 9.2 (a), thus ensuring a complete exposure to the saturated environment. The 40 °C temperature and the 100% RH were defined according to part 2 of ISO 6270 standard [9.22].

The natural exposure was performed on the rooftop of LNEC main building, located at latitude of 38.77°N, longitude of 9.13°W and 100 m above the sea level in Lisbon, Portugal. The samples were attached to a metallic structure with plastic rails, at a 45° angle with the vertical surface. The atmospheric conditions were monitored near the specimens with a weather station, which includes a combined temperature and RH sensor from *Thies* and two pyranometers from *Kipp & Zonen* that measured the global and UV solar radiation. Batches of specimens were exposed from the beginning of February 2016 until January 2017, and the temperature, relative humidity and radiation values were already described in Section 8.3.2.

9.3.3 Characterisation methods

The characterisation methods used in the experimental programme and the corresponding durations of different ageing environments are listed in Table 9.2.

Table 9.2. Experimental methods and durations of ageing environments.

Method	**Duration of ageing environments [months]**		
	W20, W40, S20, S40	**C40**	**NE**
DMA	0, 2, 4, 6, 12	0, 2, 4, 6, 12	12
Flexure properties	0, 2, 4, 6, 12, 18, 24		-
In-plane shear properties	0, 3, 6, 9, 12	-	0, 3, 6, 9, 12
Water sorption	periodic monitoring		-

Small scale coupons of the polyurethane adhesive were manufactured using three different types of polyethylene moulds, allowing to produce different specimens' geometries in accordance to the dimensions required for the physical-chemical and mechanical characterisation tests described below. The specimens were allowed to cure for 24 hours before being removed from the moulds. Furthermore, since the curing process of polyurethane adhesive at room temperature conditions (23 °C and 50% RH) may be relatively long, this process was accelerated by preconditioning the samples at 50 °C in a ventilated chamber for 24 hours, and stored in polyethylene bags for seven days at room temperature, before ageing. This procedure was conducted before exposing the specimens to the ageing environments as well as before any experimental characterisation tests.

The methods used to characterise the polyurethane adhesive were similar to those used in the characterisation of the epoxy adhesive, described in the preceding chapter: (i) Fourier Transform Infrared (FTIR) spectroscopy, according to ASTM E 1252 standard [9.23], (ii) thermogravimetric analysis (TGA), as described in ISO 11358 standard [9.24], (iii) density tests, according to method A of method A of ISO 1183-1 standard [9.25], (iv) water diffusion, through gravimetric measurements ASTM D 5229 standard [9.26], (v) DMA tests, in accordance with parts 1 and 5 of ISO 6721 standard [9.27] and (vi) mechanical characterisation of tensile (ISO 527-2 standard [9.28]), flexural (ISO 178 standard [9.29]), and in-plane shear (ASTM D 5379/D 5379M standard [9.30]) properties. These tests were already described in Section 8.3.3. However, since the inherent differences between adhesives are evident, some differences in test procedures were adopted, which are described next.

The DMA tests were conducted from -50 °C to 150 °C, at a rate of 2 °C/min. The low temperatures were reached with the use of liquid nitrogen. After the first initial tests, it was noticed that the relative differences in T_g values and curve shapes were insignificant. Therefore, a single specimen was tested for each set of ageing conditions up to 6 months, and two specimens were tested afterwards (up to 1 year). In addition, the in-plane shear response of the adhesive also had a different displacement control speed of 0.5 mm/min, instead of 1 mm/min in order to fulfil the testing time requirements proposed in the ASTM standard.

At predefined times, indicated in Table 9.2, batches of test specimens used for physical and mechanical characterisation were removed from the different ageing environments, and stored inside a room with temperature controlled at 23 ± 2 °C for a desorption period of at least 30 days, which was the average time required to observe constant mass, according to ASTM D 5229 standard [9.26]. This process had the objective of studying the adhesive in a dry (and controlled) state. The specimens were then placed in polyethylene hermetically closed recipients for transportation purposes and tested without any further conditioning.

9.4. Experimental results and discussion

This section presents the results and discussion. First, the results of initial characterisation tests of the polyurethane adhesive are presented, which served as reference. Next, the influence of exposure to the different ageing environments is presented, concerning each characterisation method separately; whenever relevant, results of different tests are cross-referenced.

9.4.1 Reference polyurethane adhesive specimens (unaged)

The several methods described above were used to thoroughly characterise the properties of the unaged adhesive. Table 9.3 summarizes the results obtained in those tests (average ± standard deviation, when applicable).

Table 9.3. Physical and chemical properties of the unaged polyurethane adhesive.

Characteristic	Method	Property	Result
Constituent materials	TGA	M [%]	64% polyurethane resin, 10% calcium carbonate, and 26% mineral filler (silicates)
Chemical nature	FTIR	-	FTIR spectra consistent with polyurethane peaks, and presence of calcium carbonate
Density	Immersion	ρ [g/cm^3]	1.37
Glass transition temperature	DMA	$T_{g,\,\text{E'onset}}$ [°C]	9.0 ± 0.3
		$T_{g,\,\tan\delta}$ [°C]	49.8 ± 1.1
Mechanical properties	Tensile	σ_{tu} [MPa]	16.5 ± 1.6
		E_t [GPa]	1.1 ± 0.2
	Flexure	$\sigma_{f\,max}$ [MPa]	30.6 ± 2.1
		E_f [GPa]	1.3 ± 0.2
	Shear	τ_{max} [MPa]	24.7 ± 1.42
		G [GPa]	0.84 ± 0.14

Figure 9.4 illustrates the thermogram obtained by the TGA analysis. Mass loss started at approximately 150 °C, and there was a significant variation at around 350 °C. Organic material decomposition (polyurethane resin) corresponded to 64% mass loss. Considering that calcium carbonate deteriorates between 600-800 °C, results indicates a content of about 10% of this compound. The material remaining for temperatures above 800 °C suggests the presence of another mineral filler, with a content of around 26%. filler (silicates), with a content of around 26%.

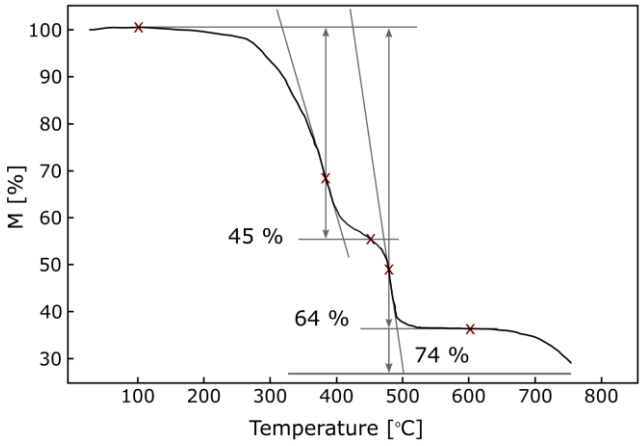

Figure 9.4. Thermogram of the polyurethane adhesive

Figure 9.5 illustrate the morphology of remaining filler content and residues after calcination.

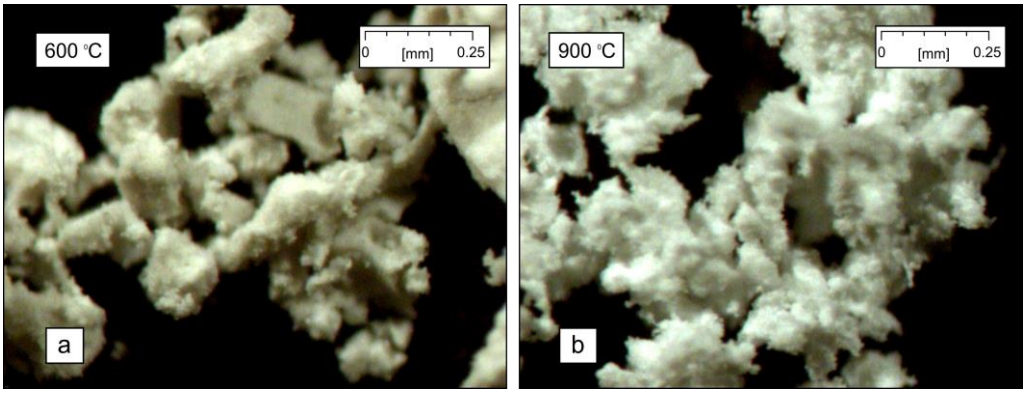

Figure 9.5. Residues of adhesive after calcination at (a) 600 °C, and (b) 900 °C.

The FTIR spectra is illustrated in Figure 9.6. The absorbance spectrum presented consistent peaks, typical of PUR resin (P), and also fillers (F) such as calcium carbonate and silicates. It was also possible to identify bands that refer to the aliphatic nature of the resin. However, the isocyanate derivate groups could not be identified, suggesting that this component fully reacted.

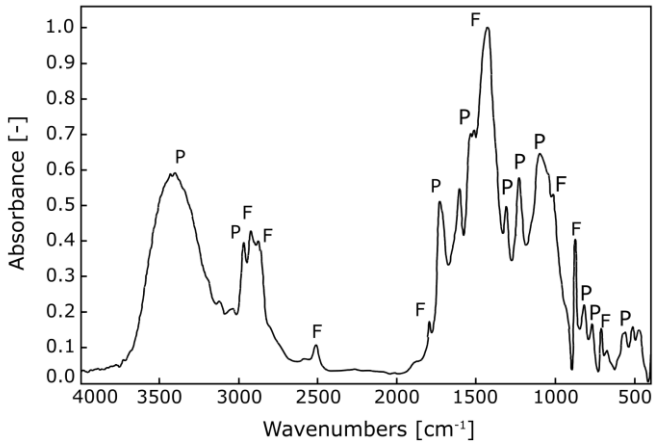

Figure 9.6. FTIR spectra of the polyurethane adhesive.

DMA analysis allowed assessing the glass transition temperature and viscoelastic behaviour of the adhesive. The results obtained are presented ahead in Figure 9.7, where the storage modulus and tan δvalues are presented in the left and right axes, respectively. The T_g was determined from the loss factor (tan δ) curve and the storage modulus (E') curve, taken as the extrapolated onset of its sigmoidal change, as per the definition of ASTM E 1640 standard [9.31].

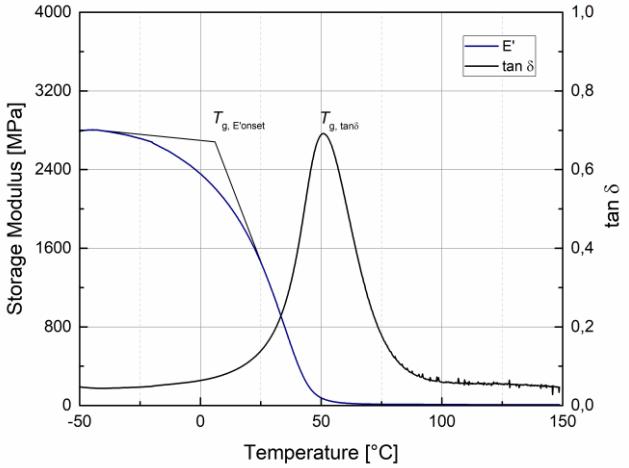

Figure 9.7. DMA experimental curves of the polyurethane adhesive.

Overall, the E' curves presented a sigmoidal shape, typical of polymeric materials, and started to exhibit a steep reduction at significantly lower temperatures (~10 °C) when compared to that corresponding to the loss factor peak (~50 °C). The storage modulus curve format at the transition region indicates changes in polymeric viscoelastic behaviour, progressing from a more "glassy" state to an elastomeric state, according to Cabral-Fonseca [9.32]. Therefore, this adhesive showed a wide region of glass transition. Note that despite the aforementioned steep reduction of the E' curve values for relatively low temperatures, the main goal of using this particular adhesive in civil engineering applications is precisely to exploit its deformation capacity to design flexible joints. To that end, its rubbery behaviour at service temperatures needs to be accounted and used in a range of E' values lower than those in the glassy state.

Figure 9.8 illustrates the mechanical behaviour, in tensile, flexure and shear of the polyurethane adhesive, along with the error envelope (standard deviation of the experimental curves).

Average values of the mechanical properties obtained are presented in Table 9.3. All mechanical tests (tensile, flexural and shear) reflected a nonlinear material behaviour and high deformation capacity of the adhesive, consistent with the viscoelastic nature of polyurethane. In tension, the resin presented an average strain at failure around 31% and a yielding stage with some hardening (stress increase). Flexural and shear tests were performed up to the maximum cross-head displacement allowed by the test fixture, without causing the collapse of the specimens. Yet, in these tests it was possible to register the peak values of flexural and shear stresses; indeed, in the flexural tests, after the peak value, stress continuously (and non-linearly) decreased, while in the shear tests, it tended to a plateau after a first initial reduction.

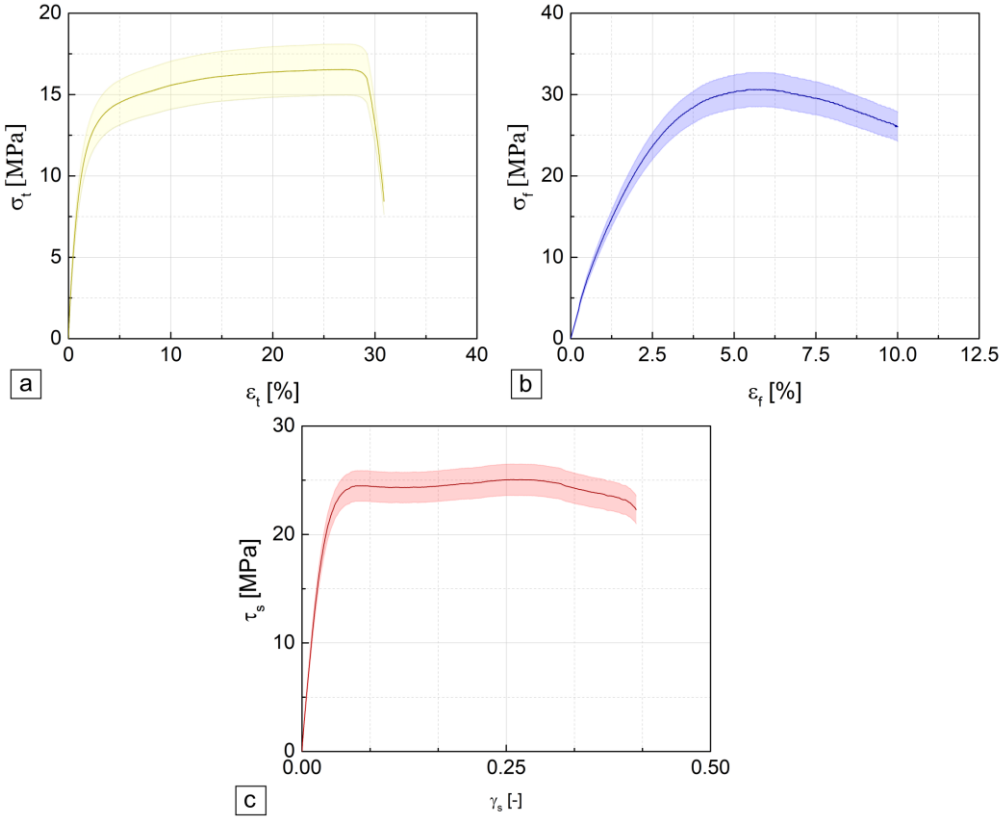

Figure 9.8. Mechanical behaviour of the polyurethane adhesive in (a) tensile, (b) flexure, and (c) shear.

9.4.2 Sorption behaviour

Figure 9.9 shows the experimental curves of mass variation as a function of the square root of time, exhibited by the polyurethane adhesive for the different immersion media and the continuous condensation exposures. Experimental data are plotted together with two diffusion models, described ahead.

For all hygrothermal environments, the adhesive showed a high absorption rate in the early stages and then continued to incorporate water at a smaller rate. Only the condensation environment (C40) showed a different transition between these phases, where the absorption rate was fairly similar in both phases, with a smoother transition period. W40 and C40 exposures showed the highest water uptake throughout the 2 years of exposure, with weight gains of 9.2% and 6.5%, respectively. It was interesting to note that this difference was significantly higher than that corresponding to the lower temperature – 3.6% of maximum weight gain for the W20 environment.

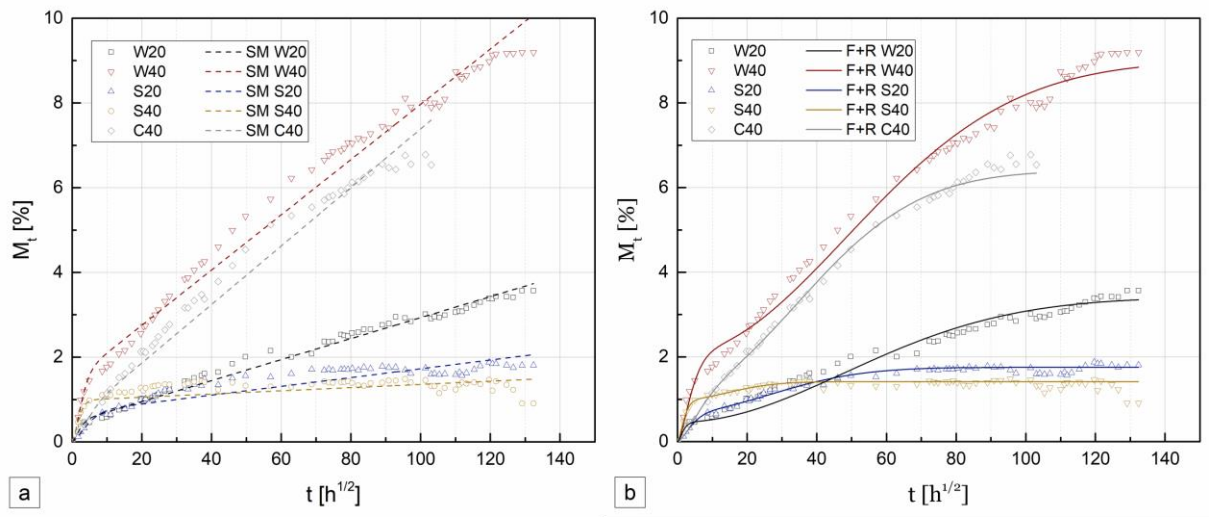

Figure 9.9. Mass uptake during hygrothermal ageing of polyurethane adhesive and analytical diffusion models: (a) SM; (b) F+R.

Similar results at a 40 °C immersion were obtained by Jiang *et al.* [9.33]. However, in that study the exposure times were not long enough ($\approx 50h^{1/2}$) to adequately assess the saturation water uptake level at this temperature. In fact, results show that, by that time, the adhesive continued incorporating water. As expected, higher temperatures promoted the diffusion process, even when the specimens were not fully immersed and just exposed to a saturated environment. Nevertheless, immersion medium led to higher mass changes when compared to continuous condensation at the same temperature.

Salt water immersion led to similar qualitative trends to demineralised water immersion: after an initial higher absorption stage, water continued to be incorporated; however, during this second stage, the absorption capacity was much smaller and a fully saturated state seems to have been reached at relatively short exposure times. Quantitatively, the water uptake in these environments was significantly lower than that observed in demineralized water (Figure 9.9), as expected. Cabral-Fonseca *et al.* [9.32] reported that the presence of salts in aqueous solutions results in in a lower equilibrium content, by virtue of its lower chemical activity. This effect can be attributed to the cross-linked behaviour of these polymers, enabling water movements and haltering large inorganic ions, thus acting as a semipermeable membrane. Jones [9.34] also adds that these ions could then function as osmotic centres.

S40 showed a higher initial absorption rate and a lower final saturated value, when compared to S20 (1.4% and 1.8% of maximum mass variation, respectively). In this case, there was no clear correlation between the immersion temperature and the level of mass uptake. This phenomenon may be attributed to mass loss by extraction of low molecular components during immersion, resulting in a potential mass loss by degradation mechanisms. According to

Cabral-Fonseca *et al.* [9.32], this effect competes with the moisture uptake and, as a result, weight changes reflect a balance between both effects.

Regarding modelling the diffusion process, and as already detailed in Chapters 3 and 8, under long immersion periods and at high temperatures, *i.e.* for harsh environmental conditions, deviations from the classical Fickian model can be found due to intrinsic chemical changes in the materials [9.33, 9.35, 9.36]. Berens [9.35] stated that polymer relaxation and incomplete adhesive curing can contribute to these deviating effects, allowing low molecular weight segments to leach out or residual cross linking to occur. This mechanism comprises the redistribution of the voids and free volumes in the polymer network due to swelling effects caused by penetrant molecules, forcing macro-molecular movement - through relaxation more moisture content can be absorbed in the adhesive.

Due to this limitation of the general Fickian diffusion model, two more versatile models for polymeric materials (both based on Fick's model) were considered (*cf.* Section 8.4.2.).

The first accounts for structural modification (SM) of the polymer and was presented by Bao *et al.* [9.36]. The authors noted that no equilibrium level uptake was reached in their experiments and proposed a two-stage relaxation model. The second model - Fickian and relaxation model (F+R) - also accounts for polymeric relaxation. This model, was proposed by Berens and Hopfenberg [9.35], who suggested a linear superposition of two independent contributions – one accounting for relaxation ($M_{t,R}$) and the other for Fickian diffusion ($M_{t,F}$).

Both alternative diffusion models were fit to the experimental data using Eq. (8.1) and Eq. (8.2), through a nonlinear curve fit, using an orthogonal distance regression iteration algorithm, available with the commercial software package *OriginPro*. The moisture diffusion and relaxation coefficients obtained are listed in Table 9.4, as well as the saturation values and the mean absolute percentage error (MAPE).

Table 9.4. Moisture diffusion and relaxation coefficients for the polyurethane adhesive.

Model	**Coefficients**	**W20**	**W40**	**S20**	**S40**	**C40**
SM	D [$\times 10^{-5}$ mm^2/s]	3.89	6.17	1.18	5.85	1.80
	k [$\times 10^{-4}$ s^{-1}]	9.00	7.50	2.50	0.70	24.0
	$M_{0\infty}$ [%]	0.46	1.44	0.69	0.98	0.48
	MAPE [%]	6.0	5.9	11.7	11.7	8.9
F+R	D [$\times 10^{-5}$ mm^2/s]	1.48	9.65	1.33	5.80	0.54
	k [$\times 10^{-8}$ s^{-1}]	6.08	5.97	20.00	71.10	11.60
	$M_{\infty,F}$ [%]	0.46	2.07	0.69	0.98	1.25
	$M_{\infty,R}$ [%]	2.95	6.92	1.06	0.44	5.15
	MAPE [%]	11.1	6.0	4.6	5.5	4.5

Results clearly reflect the typical effects on the diffusion coefficient of polymeric material of (i) elevated temperature and (ii) salt water. Indeed, elevated temperatures led to higher diffusion coefficients, whereas salt water caused lower diffusion coefficients compared to demineralized water.

The SM model presented better results for the water immersions, comparing to the salt water immersions, in terms of MAPE – the variation ranged between 5.9-11.7%. Overall, the F+R model provided lower MAPE values, which apart from the W20 curve (11.1% error), ranged between 4.5-6.0%. Overall both models provided good agreement with the experimental data (*cf.* Figure 9.9). However, in general, the F+R model allowed achieving better approximations.

In spite of the general good agreement, both models also have some limitations: (i) in the F+R model, the initial part of the relaxation phase showed some deviations to the test data for the water immersion environments and (ii) the SM model does not converge to a final saturation state, which seems to be suggested by the final test data. Experimental results also indicated that higher temperature highly promotes the relaxation effects (disregarding the S40 ageing condition due to the presence of NaCl). In fact, after the initial Fickian response, high amounts of water uptake could still be accommodated; although at a slower rate, mass gain proceeded almost until the end of the test, becoming 3.4 and 4.1 times higher than the Fickian saturation level, for W40 and C40 environments, respectively. Jiang *et al.* [33] reported similar observations, and suggested that the microstructure of polyurethane adhesives can exist in a relatively large scale, allowing higher water uptake. The authors also suggested that the differences between the higher mass changes for immersion, when compared to a humid environment, are related the higher pressures experienced by the specimens when immersed, which could force the water molecules to diffuse into the polymeric material during relaxation stages.

The desorption period underwent by the PUR adhesive after 9 months of hygrothermal ageing is depicted in Figure 9.10 as an example.

The desorption process was qualitatively similar in all the remaining periods; even considering a higher or lower initial amount of incorporated water, the remaining water content was in the following ranges: of 0.57-0.66% for W20, 0.45-0.50% for S20, 1.60-1.65% for W40, 0.28-0.31% for S40, and 1.46-1.54%. Overall, a good agreement with the corresponding absorption curves was observed, and the specimens did not fully recover the initial "dry" values. As expected, the remaining water content could be related to the degree of water uptake. As such, ageing environments such as W40 and C40 had the highest remaining water content, while in the salt water environments the opposite was observed.

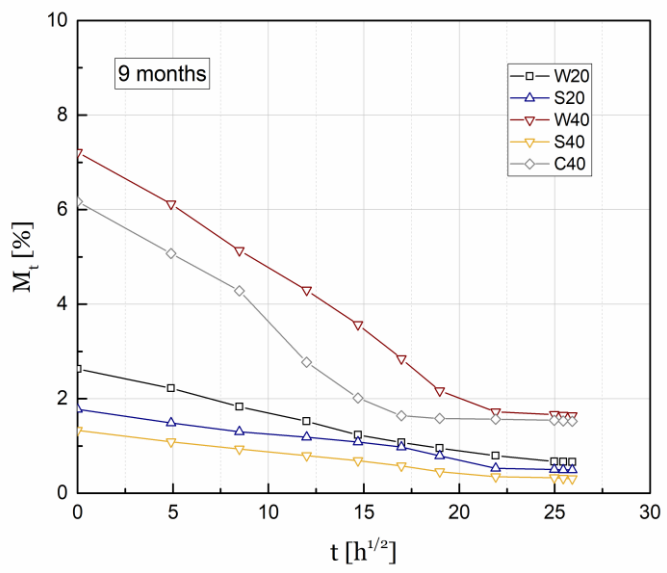

Figure 9.10. Desorption curves for 9 months of hygrothermal ageing.

9.4.3 Characterisation of the thermo-mechanical response

Figure 9.11 shows representative DMA curves (storage modulus, E', left axis - dotted lines and loss factor, tan δ, right axis - straight lines) for unaged and aged polyurethane subjected to the different ageing environments) for various periods of time.

Overall, both curves maintained their shape throughout all the ageing conditions. However, a significant difference in the E' curve can be found after only 2 months of ageing for all ageing environments. The beginning of the decay (onset) of this curve started to occur for significantly higher temperatures. This observation could be attributed to a non-fully cured state of the unexposed specimens (in spite of the pre-conditioning procedure), where the amount of crosslinking effects still continued to occur, contributing to this increase, and were more noticeable at the higher temperature environments (W40, S40 and C40).

Regarding the E' values, a general early increase up to 4 months is noted, followed by a subsequent decrease up to 12 months. The tan δ curve exhibited two general differences throughout the ageing process, for most of the ageing environments: (i) the lowering of the maximum peak after some initial fluctuations is clearly evident after 6 months of exposure (apart from S40) and (ii) a general curve shifting to the right side, again more pronounced after 6 months, that indicated an increase in the peak temperature.

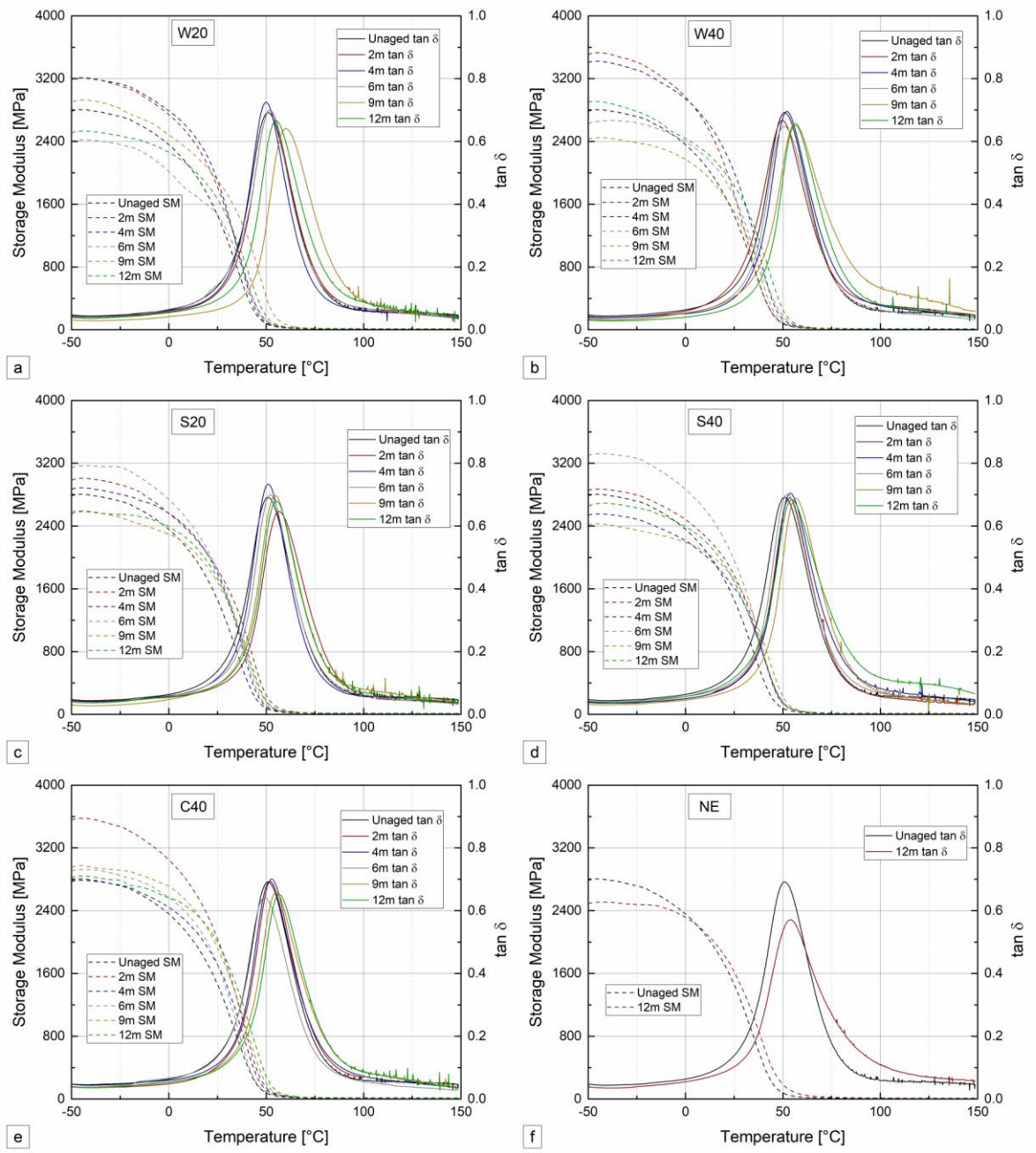

Figure 9.11. DMA curves for different exposure times of polyurethane adhesive in water immersion at (a) 20 °C and (b) 40 °C; salt water immersion at (c) 20 °C and (d) 40 °C; (e) continuous condensation at 40 °C; and (f) natural exposure.

Although the specimens went through a desorption period before testing, it is possible that water molecules were still trapped inside the polymer chains even after constant mass was reached. This fact can be observed in Figure 9.10 and 9.11. In the latter, at temperatures of about 100 °C some fluctuations occurred. The fact that the specimens exhibited higher water uptake at later exposures times also seems to confirm this, as the above-mentioned fluctuations are noticeably higher in the environments at higher temperature. Still, this period had a positive effect in reversing possible plasticization and relaxation effects suffered during ageing, resulting from the physical interaction between the polymer and water molecules, which acted as

plasticizer and promoted molecular mobility. This effect, which often translates into the widening of the peak base in the tan δ curve [9.32], was not particularly significant in the hygrothermal ageing environments, but could be identified after outdoor ageing. In addition, the E' and tan δ exhibited lower values after 12 months of exposure. In this case, exposure to UV radiation may have promoted structural modifications in the specimens, as reported in Aglan *et al.* [9.11], and also by Boubraki *et al.* [9.13] in their works.

The effects of the different ageing environments on T_g, obtained from the two alternative methods described in Section 3.3.5: (i) the peak of the tan δ curve ($T_{g,\ tan\ \delta}$), and (ii) the onset of the drop in the E' curve ($T_{g,\ E'onset}$), are shown in Figure 9.12.

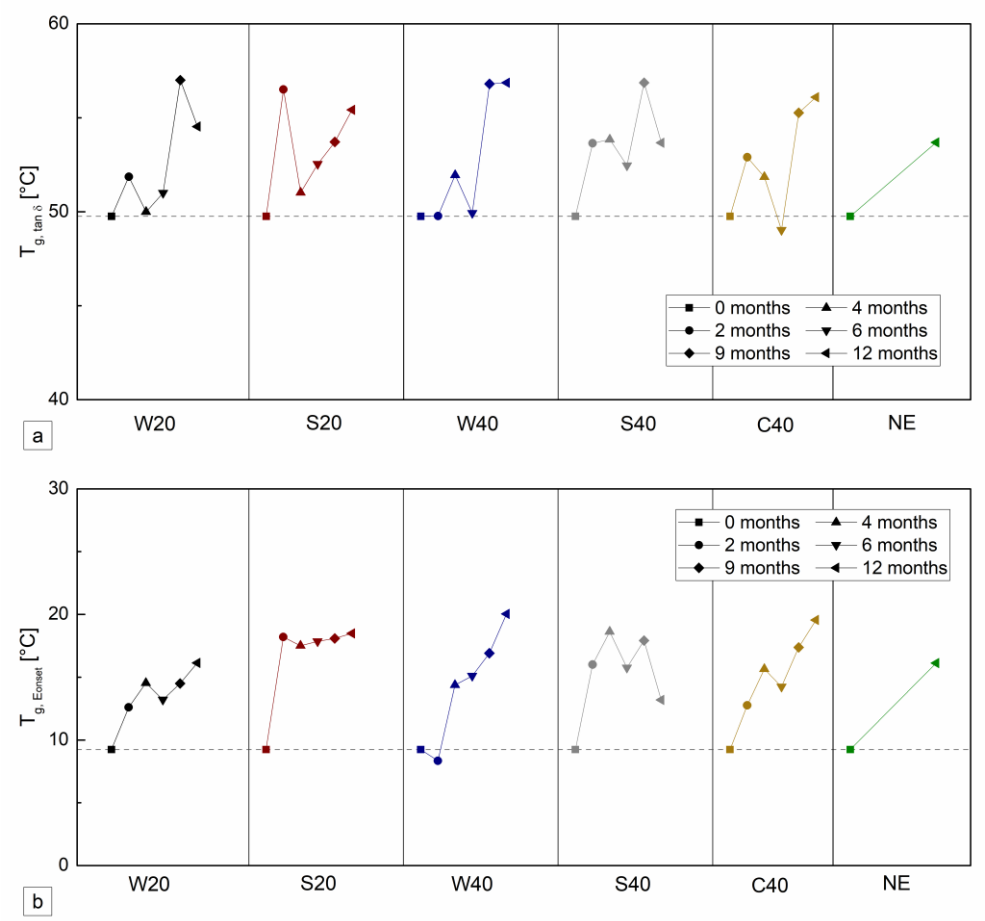

Figure 9.12. Variation of the glass transition temperature for the different ageing environments: (a) $T_{g,\ tan\ \delta}$; (b) $T_{g,\ E'onset}$.

In general, in most environments the adhesive T_g showed a slightly increasing trend. This effect seemed to be more noticeable in the environments at higher temperatures. After 12 months of W40 and C40 ageing, the T_g from the tan δ peak curve increased 7.1 °C and 10.8 °C, respectively; when measured from the onset of the E' curve, those figures are 6.3 °C and 10.3 °C (note that the initial T_g value taken from E' is much lower than that estimated from tan δ).

In general, a significant increase in T_g from the E' curve was noticed already after 2 months of ageing (in W40 it was only observed after 4 months). These results suggest once more that the specimens used in the initial characterisation tests were not in a fully cured state and that post-curing of the polymer occurred during the ageing period. Similar behaviour has been reported in the literature and attributed to early oxidative or post-curing effects that enhance the crosslinking density of the adhesive [9.10, 9.12, 9.15].

Phenomena that induce high level of molecular mobility, such as hydrolysis or plasticization, normally result in a decrease in the T_g over time, although this decrease can often be masked by residual curing of resins in aqueous immersions. Moreover, the desorption period in these experiments may have contributed to reverse some of the physical degradation that occurred, explaining the general increasing trend.

The presence of NaCl in the salt water environments did not significantly affect the changes in the adhesive's thermo-mechanical behaviour; indeed, the changes in the T_g were very similar to those caused by immersion in demineralized water. The continuous condensation environment also showed similar results to immersion.

In what concerns specimens exposed to outdoor ageing for 12 months, similar changes in T_g occurred in comparison to the other ageing environments for similar exposure (immersion) period. The mild air temperatures registered during 2016-2017 together with the solar radiation most likely contributed to post-curing the polyurethane adhesive and therefore increasing this property; similar results were reported by Boubraki *et al.* [9.13].

9.4.4 Characterisation of the flexural response

For all ageing environments and durations, the flexural tests were performed until the maximum cross-head displacement of the UTS was reached, without occurrence of specimens' collapse, similarly to the unaged specimens. In addition, local indentation was never observed.

Figure 9.13 (a) shows the flexural stress *vs.* strain curves obtained for W40 environment (the harshest one). It can be seen that at the end of the tests, the specimens exhibited very significant deformations. This is depicted in Figure 9.13 (b), which shows the deformation of a specimen aged during 18 months in W40 at different stages of the flexural test; after being unloaded, the extent of permanent deformations (4.4-4.8% of flexural strain) was about 42% w.r.t. maximum deformations.

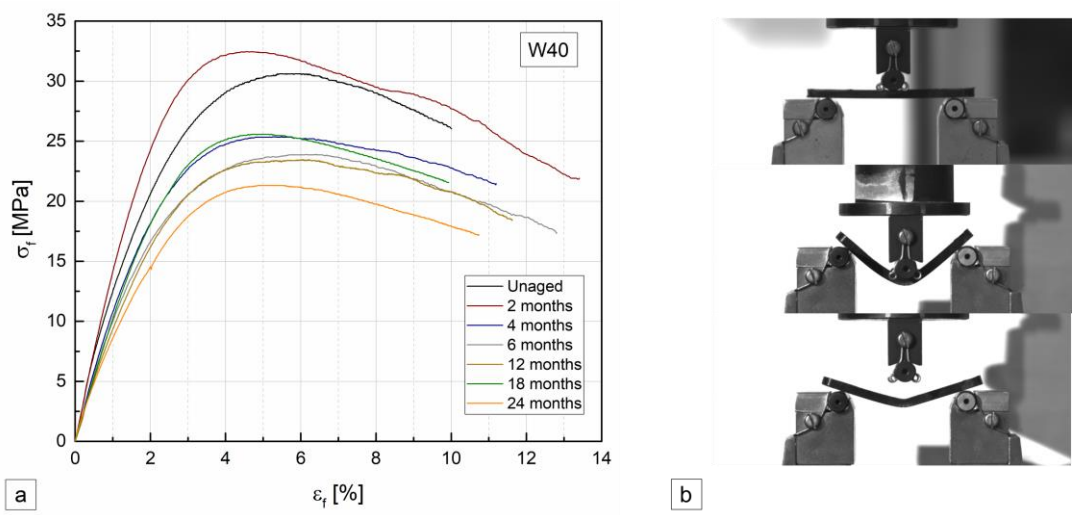

Figure 9.13. (a) Flexural stress-strain curves at different ageing times for immersion in water at 40 °C; (b) deformation during different stages of the test after 18 months (initial, at maximum deformation, after unloading) the same environment.

The results indicate that significant irreversible degradation took place in the polyurethane adhesive, affecting the overall flexural stress *vs.* strain response, namely its stiffness and strength. In the W40 environment, significant changes took place after only 2 months of ageing, when an increase of both flexural strength and modulus were observed (this initial trend was not observed in the other environments). Afterwards, immersion at 40 °C caused a globally decreasing trend in the flexural properties, which somewhat tended to a stable plateau, with reductions of flexural strength and modulus of respectively 30% and 36%.

For the other ageing environments, the stress *vs.* strain curves obtained were similar, with the exception of the aforementioned performance increase after 2 months. Figure 9.14 shows, for all ageing environments, the overall variation of the flexural strength and modulus as a function of the exposure time.

Although presenting a significant scatter (possibly due to manufacturing flaws, not possible to prevent), the flexural strength and modulus showed an overall decaying trend throughout the course of the exposure time for most ageing environments.

For hygrothermal ageing (immersion and continuous condensation), both flexural modulus and strength presented some level of degradation, which was more pronounced at the higher temperature environments. As expected, the temperature increase promoted irreversible degradation, with differences over time being more significant in the flexural modulus than in the flexural strength.

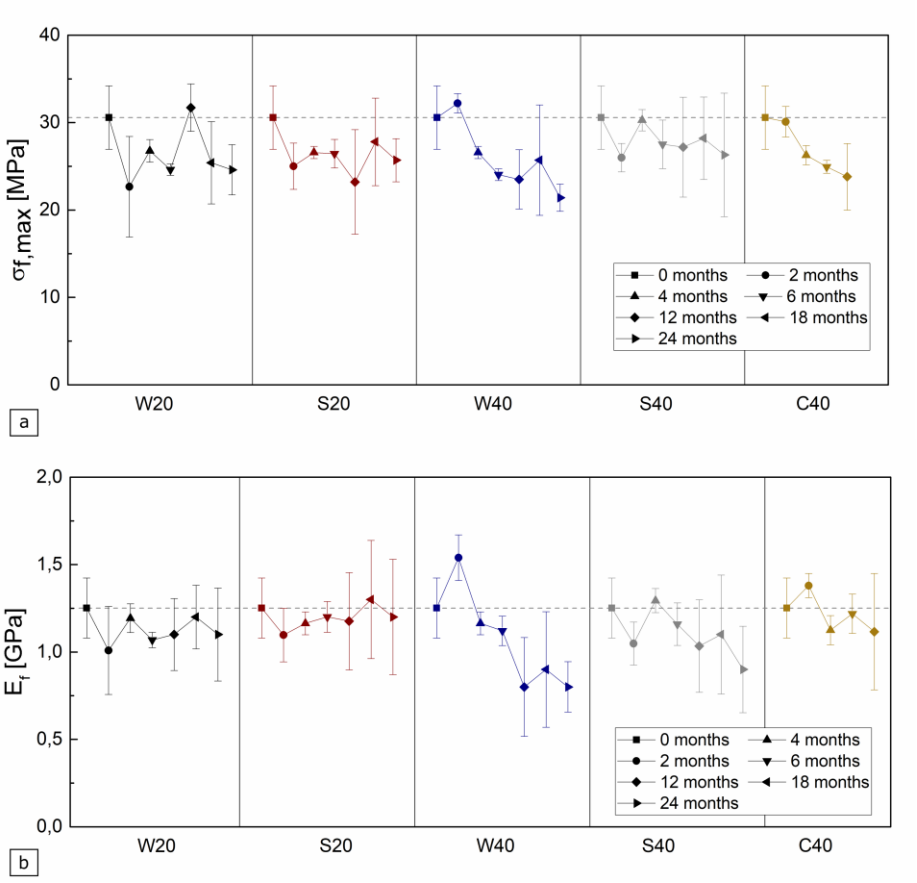

Figure 9.14. Variations of (a) flexural strength and (b) modulus during exposure to the different ageing environments.

For the 20 °C and 40 °C environments, similar trends of flexural strength reduction were observed at the same exposure time, suggesting that physical degradation was reversed during the desorption period (plasticization effects), which would be more pronounced in the higher temperature environments due to higher water uptake values. In addition, the post-curing effects attenuated the chemical degradation experienced by the polyurethane adhesive and also contributed to minimize such differences. These results are corroborated by the DMA analysis and are consistent with experimental data reported for the mechanical properties of other types of polyurethane adhesives [9.5, 9.13, 9.15].

Regarding the flexural modulus, after an initial reduction in the first exposure periods, it tended to a stable plateau. For the lower immersion temperature of 20 °C, the initial degradation was not significant and next there was even an increasing trend in the flexural modulus. In opposition, the higher temperature of 40 °C, which led to more incorporated water in the polyurethane adhesive, caused higher levels of degradation.

After 2 years of exposure, the water immersion environments W20 and W40 caused reductions of 20% and 30% in the flexural strength and of 12% and 36% in the flexural modulus, respectively.

As expected, the salt water environments caused less reduction in these properties, which is in agreement with the diffusion results. The C40 exposure (monitored only up to 12 months) caused similar and comparable effects to the W40 environment, causing slightly lower degradation.

9.4.5 Characterisation of the in-plane shear response

The in-plane shear tests were performed until the maximum cross-head displacement allowed by the Iosipescu text fixture was reached. For most ageing environments, the adhesive specimens exhibited very significant (non-linear) deformations and did not present any noticeable failure mechanism – Figure 9.15 (a) (note that the cracks observed only affected the thin layer of paint used to set the video extensometer targets, *i.e.* the bulk of the polyurethane specimen did not fail). As for the flexural tests, after testing the specimens exhibited very significant permanent deformations. However, some of the specimens exposed to outdoor ageing (OA) failed abruptly after a short yielding stage (when compared to the other specimens), with cracks developing between the notches at an angle of about 45° along the entire width of the specimens, typical of shear failure – Figure 9.15 (b).

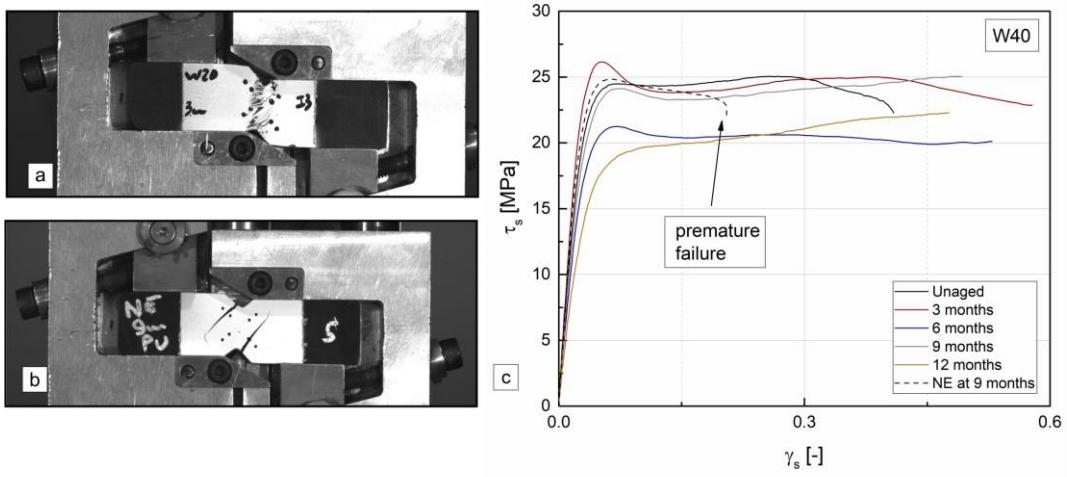

Figure 9.15. (a) typical final deformation of test specimen; (b) premature failure mode in natural ageing environment; (c) stress-strain curves at different ageing times in water at 40 °C.

Considering Figure 9.15 (c), irreversible degradation mechanisms seemed to be responsible for the (significant) decrease of shear strength after 6 and 12 months of ageing; it should be noted that some of the physical degradation mechanisms should have been attenuated during the drying period. A competing post-cure process also seems to occur (already noticed w.r.t. DMA and flexural tests), explaining the performance increase noticed at 3 and 9 months of exposure (compared to the corresponding preceding periods). It is also worth mentioning that the initial

strength peak, prior to the softening plateau, started to become less visible throughout the ageing period. This effect was more evident in the later exposure periods, with this peak no longer being noticeable after 12 months; in fact, for this period during the non-linear stage of the stress *vs.* strain response, the shear stress continuously increased until the end of the test. It is also worth mentioning that specimens which collapsed (before attaining the maximum deformation allowed by the Iosipescu test fixture) accommodated less than half of the maximum deformation reached by the other replicates/specimens.

In the other environments, the same overall trends were generally observed. Figure 9.16 depicts the global variation of the maximum shear stress and shear modulus in the different test conditions.

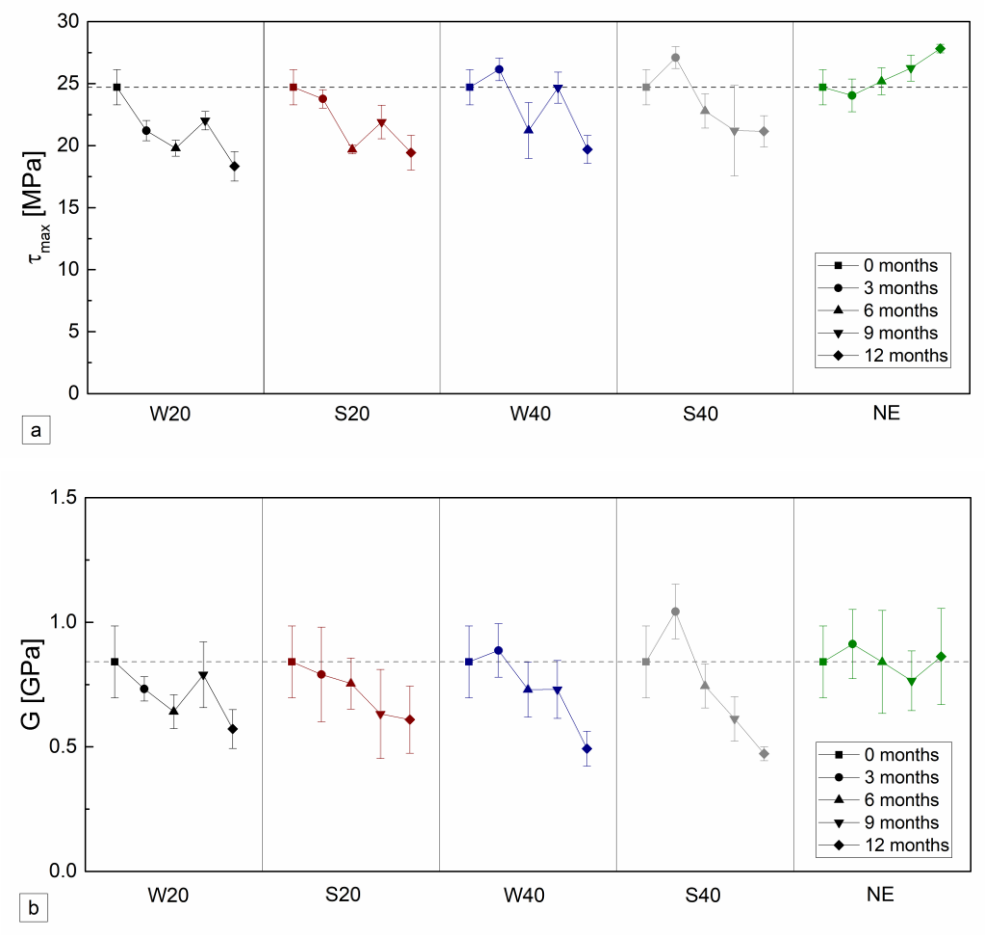

Figure 9.16. Variations of (a) shear strength and (b) modulus during exposure to the different ageing environments.

An overall degradation trend of the shear strength (Figure 9.16 (a)) is evident for all immersion environments. For all conditions, the minimum shear strength corresponds to 12 months of exposure, with the following reductions compared to the unaged state: (i) 26% for W20;

(ii) 21% for S20; (iii) 20% for W40 and (iv) 15% for S40. The degradation underwent in the hygrothermal environments at 40 °C (closer to the T_g) were lower than at 20 °C, and this may be explained by higher post curing effects at the former temperature. This can be noticed when comparing the peak stresses for W20 and W40 immersions after 3 months (21.2 MPa *vs.* 26.1 MPa) and 9 months (22.0 MPa *vs.* 24.6 MPa), respectively. Overall, the salt water immersion had similar effects to the immersion in demineralized water; hence, in this case, the presence of NaCl was not relevant.

Unlike hygrothermal ageing, specimens subjected to natural exposure presented a general increasing trend in the shear strength. It seems that the solar radiation together with the mild or warm temperatures promoted significant post-cure, which completely compensated for any irreversible degradation that may have occurred. After 12 months of natural exposure, the shear strength increased 13% in comparison to unaged specimens. In what concerns the shear modulus (Figure 9.16 (b)), for the hygrothermal ageing it presented a similar decreasing trend of variation to that exhibited by the shear strength. Nevertheless, from a quantitative point of view, the magnitude of the degradation presented by the shear modulus was higher and it seemed to be more affected by irreversible degradation mechanisms, especially for the higher temperature environments. After 12 months of ageing, the shear modulus presented reductions of 32% and 41% in demineralized water immersion at 20 °C and 40 °C, respectively. As for the shear strength, the presence of salt did not affect the degradation of the shear modulus when compared to demineralized water – in this case, after 12 months the shear modulus exhibited reductions of 28% and 44% at 20 °C and 40 °C, respectively. The natural exposure did not cause significant changes in the shear modulus of the polyurethane adhesive. As described above, the combined effects of post-curing and UV degradation seemed to have affected only the viscoelastic behaviour of the polyurethane adhesive, causing some specimens to have a premature failure for a much lower strain at failure. Similar results were reported by Boubakri *et al.* [9.12] and de Oliveira *et al.* [9.15] in other studies, while harsher effects of UV radiation were also reported by Aglan *et al.* [9.11].

9.5. Concluding remarks

This chapter presented an experimental study about the effects of hygrothermal and outdoor ageing on a structural polyurethane adhesive used in different civil engineering applications, namely to join FRP components. Based on the results obtained, the following main conclusions are drawn:

1. In general, the polyurethane adhesive suffered irreversible degradation mechanisms, even in the presence of competing post-cure phenomena; the effects of degradation were more noticeable in its mechanical properties.

2. In terms of water diffusion, the general adhesive behaviour was not purely Fickian. A long relaxation period was noticed and water molecules were continuously incorporated in the adhesive. The highest weight gains were observed for the W40 and C40 environments, where the higher temperatures strongly promoted diffusion (9.2% and 6.5% mass increases, respectively). The water uptake in the salt immersions was significantly lower and reached a fully saturated state for shorter time periods. The desorption period was insufficient to remove all the absorbed water and the remaining water content ranged between 0.6-1.7%. Two analytical models were considered to describe the diffusion process, and provided good agreement with the experimental data. As expected, higher diffusion coefficients were obtained for water immersion, when compared to salt water.

3. In the DMA analysis slight changes in the shapes of both E' and tan δ curves were noted, indicating the occurrence of some modifications in the material structure. Furthermore, post-cure phenomena were noticed in all ageing environments. The T_g showed a global increasing trend, which was more noticed on the E' values, but was also visible in tan δ values. The outdoor environment specimens showed a widening of the tan δ peak curve base, which suggested molecular structural modification that was attributed to UV radiation. Despite the overall low values of T_g obtained from the E'_{onset} curves, the changes in the viscoelastic properties of the PUR adhesive when subjected to both hygrothermal and outdoor ageing seem compatible with its structural use.

4. In terms of flexural properties, both flexural strength and modulus showed degradation signs, that were not attenuated during the desorption period. Similar trends of strength reduction were noticed for 20 °C and 40 °C environments, suggesting that plasticization mechanisms were reverted to some extent. However, the final flexural properties were considerably affected: 20-30% strength reduction and 12-36% modulus reduction, for W20 and W40 exposures, respectively, after 24 months. Salt water immersion caused less reduction in the flexural properties when compared to demineralized water immersion, which is in line with the diffusion results. The C40 environment caused comparable degradation to the immersion environments at the same temperature.

5. The shear strength showed a general decaying trend over the exposure time in hygrothermal environments, whose magnitude was comparable to that of the flexural strength at lower

temperatures, but more pronounced at higher temperatures: 26% and 20% reduction in W20 and W40 environments, respectively, after 12 months. For outdoor ageing, the shear strength showed an increasing trend, which was attributed to post-curing effects stemming from the mild to elevated temperatures and the UV radiation. In what concerns the shear modulus, in hygrothermal environments, more significant reductions (compared to shear strength) were noticed, especially for the higher temperature environments: after 12 months, the shear modulus was reduced 40% and 44% in W40 and S40 environments, respectively. For outdoor ageing, although several specimens presented much less deformation capacity (collapsing prematurely), the shear modulus showed negligible signs of degradation.

6. The magnitude of the changes observed in the PUR adhesive seems to be compatible with their application in bonded joints for durable civil engineering structures. Nevertheless, some attention is required for outdoor ageing exposure, as a consequence of direct UV exposure, since the shear deformation capacity can be significantly lowered.

7. 'Softer' PUR adhesives typically have lower elastic moduli when compared to other structural adhesives used in civil engineering applications (such as epoxies) and are used due to their higher deformation capacity. Compared to the results obtained from the previous chapter, the PUR adhesive presented higher water absorption properties (around 1.5-2 times higher) when compared to the epoxy adhesive. In what concerns the thermal and mechanical properties considered, generalised degradation trends occurred for both adhesives. Despite the similar magnitude of the degradation observed in both adhesives, in some environments the reduction of performance was higher in the epoxy adhesive. However, even accounting for the degradation effects, the epoxy adhesive still showed higher performance compared to the PUR adhesive.

9.6. References

[9.1] Zhou A, Keller T. Joining techniques for fiber reinforced polymer composite bridge deck systems. Compos Struct 2005;69:336–45.

[9.2] Custódio J. Structural adhesives. In: Gonçalves MC, Margarido F, editors. Mater. Constr. Civ. Eng. Sci. Process. Des., Springer International Publishing; 2015, p. 717–71.

[9.3] Pethrick RA. Design and ageing of adhesives for structural adhesive bonding - A review. J Mater Des Appl 2015;229:349–79.

[9.4] Hutchinson AR, Hollaway LC. 6 – Environmental durability. Strength. Reinf. Concr. Struct., 1999, p. 156–82.

[9.5] Buchman A, Holdengraber Y, Dodiuk H, Kenig S. Durability of polyurethanes elastomers. Polym Adv Technol 1991;2:137–47.

[9.6] Castro J De, Keller T. Design of robust and ductile FRP structures incorporating ductile adhesive joints. Compos Part B 2010;41:148–56.

[9.7] Janik H, Sienkiewicz M, Kucinska-Lipka J. Polyurethanes. In: Dodiuk H, Goodman SH, editors. Handb. thermoset Plast. (3rd ed.), Elsevier; 2014, p. 253–89.

[9.8] Petrie E. Handbook of adhesives and sealants. McGraw-Hill; 2007.

[9.9] Hollingsworth B, Ledbury K, Stokoe A. The accelerated ageing of some Commercial Polyurethane Rubbers. Waltham Abbey, Essex: 1967.

[9.10] Davies P, Evrard G. Accelerated ageing of polyurethanes for marine applications. Polym Degrad Stab 2007;92:1455–64.

[9.11] Aglan H, Calhoun M, Allie L. Effect of UV and hygrothermal aging on the mechanical performance of polyurethane elastomers. J Appl Polym Sci 2008;108:558–64.

[9.12] Boubakri A, Elleuch K, Guermazi N, Ayedi HF. Investigations on hygrothermal aging of thermoplastic polyurethane material. Mater Des 2009;30.

[9.13] Boubakri A, Guermazi N, Elleuch K, Ayedi HF. Study of UV-aging of thermoplastic polyurethane material. Mater Sci Eng A 2010;527:1649–54.

[9.14] Le Gac PY, Choqueuse D, Melot D. Description and modeling of polyurethane hydrolysis used as thermal insulation in oil offshore conditions. Polym Test 2013;32:1588–93.

[9.15] de Oliveira GL, Ariza Gomez AJ, Caire M, Vaz MA, da Costa MF. Characterization of seawater and weather aged polyurethane elastomer for bend stiffeners. Polym Test 2017;59:290–5.

[9.16] Torró-Palau A, Fernández-García J, Orgilés-Barceló A, Pastor-Blas M, Martín-Martínez J. Comparison of the properties of polyurethane adhesives containing fumed silica or sepiolite as filler. J Adhes 1997;61:195–211.

[9.17] Fernández-Garcia M, Chiang MYM. Effect of hygrothermal aging history on sorption process, swelling, and glass transition temperature in a particle-filled epoxy-based adhesive. J Appl Polym Sci 2002;84:1581–91.

[9.18] Tai RCL, Smialowska S. Effect of fillers on the degradation of automotive epoxy adhesives in aqueous solutions. J Mater Sci 1993;28:6199–204.

[9.19] Bowditch MR. The durability of adhesive joints in the presence of water. Int J Adhes Adhes 1996;16:73–9.

[9.20] ISO 175. Plastics. Methods of test for the determination of the effects of immersion in liquid chemicals. Int Organ Stand 2010.

[9.21] ASTM D 1141. Standard practice for the preparation of substitute ocean water. Am Soc Test Mater 2013.

[9.22] ISO 6270. Paints and varnishes. Determination of resistance to humidity. Part 2: Continuous condensation (in-cabinet exposure with heated water reservoir). Int Organ Stand 2017.

[9.23] ASTM E 1252. Standard practice for general techniques for obtaining infrared spectra for qualitative analysis. Am Soc Test Mater 2013.

[9.24] ISO 11358. Plastics. Thermogravimetry (TG) of polymers. Part 1: General principles Int Organ Stand 2014.

[9.25] ISO 1183. Plastics. Methods for determining the density of non-cellular plastics. Part 1: immersion method, liquid pyknometer and titration method. Int Organ Stand 2004.

[9.26] ASTM D 5229. Standard test method for moisture absorption properties and equilibrium conditioning of polymer matrix composite materials. Am Soc Test Mater 2014

[9.27] ISO 6721. Plastics. Determination of dynamic mechanical properties. Part 1: General principles; Part 5: Flexural vibration - non-resonance method. Int Organ Stand 1996.

[9.28] ISO 527. Plastics. Determination of tensile properties. Part 1: General principles; Part 2: Test conditions for moulding and extrusion plastics. Int Organ Stand 2012.

[9.29] ISO 178. Plastics. Determination of flexural properties. Int Organ Stand 2010.

[9.30] ASTM D 5379 / D 5379M. Standard test method for shear properties of composite materials by the V-notched beam method. Am Soc Test Mater 2012:1–13.

[9.31] ASTM E 1640. Standard test method for assignment of the glass transition temperature

by dynamic mechanical analysis. Am Soc Test Mater 2016.

[9.32] Cabral-Fonseca S, Correia JR, Rodrigues MP, Branco FA. Artificial accelerated ageing of GFRP pultruded profiles made of polyester and vinylester resins: Characterisation of physical-chemical and mechanical damage. Strain 2012;48:162–73.

[9.33] Jiang X, Kolstein H, Bijlaard FSK. Moisture diffusion in glass-fiber-reinforced polymer composite bridge under hot/wet environment. Compos Part B Eng 2013;45:407–16.

[9.34] Jones F. Durability of reinforced plastics in liquid environments. In: Pritchard G, editor. Reinf. Plast. Durab., Woodhead Publishing, Cambridge; 1999, p. 70–110.

[9.35] Berens AR, Hopfenberg HB. Diffusion and relaxation in glassy polymer powders: 2. Separation of diffusion and relaxation parameters. Polymer (Guildf) 1978;19:489–96.

[9.36] Bao LR, Yee AF, Lee CYC. Moisture absorption and hygrothermal aging in a bismaleimide resin. Polymer (Guildf) 2001;42:7327–33.

Part IV

Durability of adhesively bonded joints between pultruded GFRP profiles

Preamble

The connection technology for pultruded GFRP profiles also presents challenges due to the brittle and anisotropic nature of the material. While adhesively bonded connections are relatively better suited to join GFRP adherends, since they are more material-adapted and offer a more uniform load transfer, a wider use of bonded joints is pending on obtaining a better understanding of their long-term behaviour. The gap of current knowledge on the long-term performance of adhesively bonded GFRP joints is currently pointed out as one of the factors that needs to be overcome in order to further enable the use of these solutions in civil engineering applications.

Part IV of this thesis first presents a literature review of the effects of hygrothermal ageing, natural weathering, and thermal cycles on adhesively bonded joints between GFRP adherends. Next, results of experimental and numerical investigations carried out in order to assess the influence of such long-term exposures are presented and discussed.

Chapter 10.

Durability of adhesively bonded joints between pultruded GFRP adherends under hygrothermal and natural ageing

10.1.Introduction

As mentioned in Chapter 2, the connection technology for pultruded GFRP profiles presents challenges due to the brittle and anisotropic nature of the material. GFRP profiles are usually connected via bolting and/or adhesive bonding. While mechanical bolting typically needs drilling operations and often leads to overdesigned GFRP components [10.1, 10.2], adhesively bonding offers more uniform load transfer, being also more material-adapted, as both the substrate and the adhesive are of a polymeric nature [10.3, 10.4].

Despite the potential benefits of adhesively bonding pultruded GFRP components, there are concerns about the long-term performance and durability of such bonded joints. These concerns stem from (i) the potential influence of environmental conditions on both the adhesives and the GFRP adherends, which may affect the stiffness, strength and deformation capacity of bonded joints [10.5, 10.6], and (ii) the lack of systematic and comprehensive studies on the durability of bonded joints between pultruded GFRP adherends, as discussed in Section 11.2.

This chapter presents experimental and numerical investigations about the effects of hygrothermal and natural ageing on the performance of single lap joints (SLJs) between pultruded GFRP adherends for civil engineering structural applications, bonded with either epoxy or polyurethane adhesives. All the constituent materials were previously subjected to similar hygrothermal and natural weathering (*cf.* Chapters 4, 5, 8, and 9). Likewise, SLJ specimens were exposed to different hygrothermal conditions and Lisbon outdoor environment for up to 2 years. Tensile tests were used to assess the effects of ageing on the stiffness, strength and deformation at failure of the joints. In parallel with the experimental campaign, numerical simulations of the tests on SLJ specimens were performed, in order to obtain further insights, namely about the effects of hygrothermal ageing of the constituent materials on the load transfer mechanisms in the SLJs.

10.2.Literature review

Previous studies [10.6–10.9] have shown that the main environmental agents that affect the durability of adhesively bonded joints for civil engineering applications are moisture and temperature, especially when combined. In addition, ultraviolet (UV) radiation, relevant in outdoor applications, can also affect adhesively bonded joints, although to a smaller extent. The general information available about their effects and the main research needs that motivated the present chapter are described next.

The influence of moisture on FRP bonded joints depends on several parameters, namely the adherend and adhesive materials, the bonding method, the curing degree, the surface preparation, and the exposure conditions and duration [10.10]. In such joints, the adhesive and the polymeric matrix of FRP adherends are the constituents most affected by moisture; both can be altered through plasticization, cracking, swelling and hydrolysis; in FRP adherends, moisture can also cause deleterious effects due to damage at the fibres-matrix interface and fibres degradation [10.7, 10.8]. Those mechanisms may reduce the glass transition temperature (T_g) and also the elastic modulus and strength of both adhesive and adherends. In FRP bonded joints, moisture may also affect the stability of the interfacial adhesion, this being very relevant for long-term durability; indeed, interfacial degradation is usually more relevant than that underwent by the adhesive or the adherends [10.8]. In addition, moisture uptake can also influence the joint failure mode, typically changing from cohesive (within the adhesive or the adherends), to adhesive (in the interfaces or their vicinity), leading to irreversible changes as a result of weakened inter-molecular forces [10.7]. However, some physical degradation mechanisms that occur in the presence of moisture, such as plasticization, are found to be reversible to some extent after drying [10.20].

The presence of salts in aqueous solutions usually results in a lower equilibrium moisture content, by virtue of the lower chemical activity of such solutions. This effect stems from the polymers' cross-linked behaviour, which may act as semipermeable membrane, enabling water movements and haltering large inorganic ions [10.11]. The effects of salt water can thus result in less absorbed water content and are usually less aggressive when compared to demineralised water [10.11, 10.12].

In what concerns the influence of temperature, when FRP bonded joints are subjected to a wide range of temperatures, their stiffness and strength are generally affected by (i) cure shrinkage of both the adhesive and the polymer matrix of FRP adherends, (ii) their different coefficients of thermal expansion (CTE) and also (iii) the changes in material properties with temperature [10.8]. The influence of temperature on the physical and mechanical properties of adhesives is usually the

most important factor when designing a bonded joint [10.7], as the exposure to very high or very low temperatures has generally significant degradation effects in the joint performance: while high temperatures (usually above the adhesive T_g) cause significant reductions in the adhesive properties (modulus and strength), low temperatures cause high thermal stresses and material embrittlement [10.10].

The combined effects of moisture and temperature (hygrothermal ageing) are often more damaging than those caused by each individual agent. For instance, the moisture diffusion at elevated temperature is significantly accelerated, thus increasing the degradation of bonded joints [10.10]. Although the separate effects of temperature and moisture on bonded joints have been thoroughly studied, recent reviews [10.7, 10.8] point out that limited research is available on their combined effects, especially in what concerns pultruded GFRP bonded joints for civil engineering applications. Very limited information is also available on the effects of outdoor ageing on such type of joints. The few studies on the durability of bonded joints involving pultruded GFRP adherends are described in the next paragraphs.

Zhang *et al.* [10.13] studied the influence of environmental effects on the fatigue behaviour of adhesively bonded joints between pultruded GFRP laminates and epoxy. The joints were manufactured and cured for 10 days at 23 °C and 50% relative humidity (RH) and then tested in the following conditions (in an environmental chamber): (i) -35 °C (RH not measured), (ii) 23 °C and 50% RH, (iii) 40 °C and 50% RH, and (iv) 40 °C and 90% RH. The latter specimens were also previously immersed in water at 40 °C for 70 days, to reach saturation. The fatigue behaviour of the joints was significantly affected by the test environment, with increasing temperature and humidity levels shortening the fatigue life. Specimens that were immersed at 40 °C exhibited the lowest fatigue resistance (from the S-N fatigue curves). Higher temperature and humidity levels (the latter increased due to immersion) progressively increased the stiffness reduction. Increasing moisture also caused a shift in the failure mode, from cohesive (in the adherend) to interfacial.

Stazi *et al.* [10.5] studied the durability of pultruded GFRP-vinylester single lap (SLJ) and butt (BJ) joints, bonded with six different adhesives (two epoxies, one acrylic, one methacrylate and two polyurethanes, with T_gs ranging from -40 °C and 70 °C), subjected to two types of environmental ageing. In the first type, the specimens were subjected to the following 14 cycles (2 weeks) of varying temperature and RH: (i) 16 hours at 40 °C and 100% RH, (ii) 4 hours at -40 °C (RH unspecified), and (iii) 4 hours at 70 °C and 50% RH. In the second type of ageing, specimens were exposed for 1000 hours to fluorescent ultraviolet (UV) lamps at 23 °C and 30% RH. For all environmental conditions, the behaviour of SLJs was similar to that of BJs in

terms of load-joint elongation response. The two artificial ageing conditionings had similar influence on the specimens' behaviour: (i) slightly higher average failure loads, which was attributed to further polymerization, achieved due to exposure to either elevated temperature or UV radiation; (ii) higher elongations at failure, and (iii) significantly lower joint stiffness (70-90%), which were attributed to the softening of the adhesives, as their T_g range was reached and exceeded during thermohygrometric cycles, and to UV exposure, which promoted dissociation of chemical bonds (even affecting the colour of one of the adhesives). Noticeable changes were also found in the failure modes, which changed from mixed failure (a combination of two or more modes) in the unaged specimens to mainly adhesive failure after exposure to hygrothermal ageing and UV radiation. Among the adhesives tested, the best mechanical performance was provided by epoxies, for both unaged and aged specimens.

Giampaoli *et al.* [10.14] investigated the performance of SLJs between pultruded GFRP profiles and steel bonded with three different epoxy adhesives. Small-scale SLJ specimens were subjected to two different artificial ageing procedures: (i) continuous condensation (CC) at 40 °C and 100% RH for 6 months; and (ii) artificial ultraviolet (AUV) exposure at 26 °C and 33% RH for 1000 hours. Additional specimens (only for two epoxies) were also exposed to a combination of both types of ageing. Exposure to CC caused very significant stiffness reduction (~90%), increase of elongation at failure and 20% reduction in ultimate load. AUV exposure caused moderate stiffness reduction (~30%), attributed to the polymer bond dissociation due to the UV wavelength radiation, and an increase of load carrying capacity (~15-20%), attributed to additional cross-linking promoted by radiation heating. When subjected to a combination of both types of ageing, the performance of the SLJs improved, with increases in stiffness and average ultimate load up to 20% and 36%, respectively, which were attributed to the same possible beneficial effects of UV radiation.

Heshmati *et al.* [10.15] studied the durability of GFRP-steel double lap joints bonded with epoxy subjected to hygrothermal ageing for up to 18 months: immersion in distilled and salt water at 20 °C and 45 °C. Ageing caused corrosion in the steel plates, more severe for immersions at 45 °C. After 12 months, some specimens presented cracks in the adhesive layer, next to the GFRP adherend (before testing); this was attributed to the non-uniform moisture distribution in the adhesive layer, which could lead to swelling in specific parts, introducing shear stresses. The primary failure mode, consisting of interlaminar delamination of the GFRP, changed to the adhesive layer close to the GFRP adherend, *i.e.* cohesive failure, after 18 months at 45 °C in water and after only 6 months in salt water at the same temperature. After 12 months of immersion at 45 °C in salt and distilled water, joint stiffness presented significant

reductions of respectively 26% and 34% (much higher when compared to lower temperatures), which were attributed to the higher moisture content in the adhesive and the GFRP material; from 12 to 18 months, stiffness did not change for distilled water immersion at 45 °C, while a sharp reduction occurred in salt water, which was attributed to the effects of steel corrosion (more severe in this medium). In terms of joint strength, after 12 months of immersion in distilled water at 20 °C and 45° C, the ultimate load decreased 20% and 41%, respectively; immersion in salt water produced similar degradation; from 12 to 18 months, the failure load decreased further 20% for the immersions at 45°C, which was attributed to the above-mentioned change in failure mode.

Keller *et al.* [10.3] conducted a comprehensive assessment of the Pontresina bridge and of the Eyecacther building, respectively 17 and 15 years after construction. Both structures comprise adhesively bonded joints, which were visually inspected. Small cracks and local adhesive debonding were detected in some profiles of the bridge. On the other hand, the building joints showed no signs of damage, which was attributed to the less aggressive environmental exposure.

The studies described above, which are the most relevant in the context of the durability of bonded joints between pultruded GFRP components for civil engineering applications, although providing useful information about hygrothermal and natural ageing, encompass the following shortcomings: (i) two of the studies [10.14, 10.15] refer to GFRP-to-steel joints and these have important differences compared to all-GFRP joints (namely the influence of steel corrosion) and another one [10.13] addresses a very specific aspect of the joint response (fatigue behaviour); (ii) there is no information on the response of all-GFRP bonded joints subjected to immersion; (iii) no quantitative and in general limited information is also available on the influence of natural weathering, which is of paramount importance to provide realistic data that can be used to validate accelerated procedures; (iv) in the single study on all-GFRP bonded joints [10.5], the ageing periods were very limited (maximum of 2 weeks of hygrothermal cyclic ageing and 1.5 months of artificial UV ageing). In this context, the study presented in this chapter aims at addressing the above mentioned gaps, pursuing previous studies on the effects of hygrothermal or outdoor ageing on adhesives [10.12, 10.16, 10.17] and pultruded GFRP laminates [10.11, 10.18].

10.3.Experimental programme

10.3.1 Materials

The materials used in the experimental investigations comprised pultruded GFRP profiles with 33×5 mm^2 of cross section and 3 m of length, manufactured by *ALTO Perfis Pultrudidos*. The profiles consist of the same materials used in Chapter 4[8], although only unsaturated polyester resin was selected for the matrix, since it is the most commonly used in civil structural applications when there are no particular requirements in terms of environmental harshness.

The two commercial, bi-component structural adhesives used in Chapters 8 and 9[9] were used as bonding agents between the GFRP adherends: the first is a thixotropic, solvent-free, cold curing epoxy based adhesive (EP), frequently used in civil structural applications, namely for bonding FRP strips to different substrates; the second is a bi-component polyurethane adhesive (PUR), based on filled polyols and unfilled isocyanates derivates.

10.3.2 Material characterisation tests

The initial (unaged) properties of the GFRP laminate (*cf.* Chapter 4) and of both adhesives (*cf.* Chapter 8 and 9) were characterised based on the following chemical, thermo-physical and mechanical techniques: Fourier Transformed Infrared Spectroscopy (FTIR); density measurements; thermogravimetric analysis (TGA); Dynamic Mechanical Analysis (DMA); tensile tests; flexural tests; in-plane shear tests; and interlaminar shear tests (only for GFRP). Table 10.1 presents a summary of the procedures and results obtained in each test that were explained in detail in the aforementioned chapters.

In order to review and compare the differences between all three constituent materials, Figure 10.1 presents the normalized values (w.r.t. ambient temperature for the epoxy adhesive and GFRP, and -50 °C for the polyurethane adhesive) of the storage modulus (E') and loss factor (tan δ) as a function of temperature for the GFRP laminate and both adhesives.

[8] Further information about the GFRP material is detailed in Section 4.2.1

[9] Further information about the EP and PUR adhesives are detailed in Sections 8.3.1 and 9.3.1, respectively.

Table 10.1. Results obtained from material characterisation tests on GFRP laminate and epoxy and polyurethane adhesives (average ± standard deviation).

Test method		**Standard**	**Specifications**	**Property**	**GFRP**[a]	**Epoxy**[b]	**Polyurethane**[c]
Chemical composition	FTIR	ASTM E1252 [10.19]	32 scans Range: 4000-450 cm^{-1} Spectral resolution: 4cm^{-1}		Unsaturated polyester peaks; presence of calcium carbonate	Epoxy peaks; presence of calcium carbonate and silica based peaks	Polyurethane peaks; presence of calcium carbonate
Constituent materials	TGA	ISO 11358 [10.20]	Range: 23-800 °C; Rate: 10 °C/min	M [%]	28% unsaturated polyester resin, 65% glass fibres, 7% calcium carbonate	67% epoxy resin, 11% calcium carbonate, 22% silica based filler	64% polyurethane resin, 10% calcium carbonate, 26% mineral filler
Density	Immersion	ISO 1182-1 [10.21]	0.5 mm^3; 0.1 mg	ρ [g/cm^3]	1.92	1.36	1.37
Glass transition temperature	DMA	ISO 6721 [10.22]	Geometry: 5×15×60 $mm^{3\ a}$ Geometry: 4×10×60 $mm^{3\ b,c}$ Frequency 1 Hz; Strain amplitude: 15 μm; Rate: 2 °C/min; Range: 25-150 °C[a,b] (air); Range: -50-150 C[c] (nitrogen) Clamp: 3-point bending[a]; Clamp: Dual cantilever[b,c]	E'_{onset} [°C]	112.3 ± 3.6	59.5 ± 0.10	9.0 ± 0.3
				tan δ [°C]	136.6 ± 0.4	78.2 ± 0.10	49.8 ± 1.1
Mechanical properties	Tension	ISO 527 [10.23]	Geometry:5×25×300 $mm^{3\ a}$; Speed: 2 mm/min[a]; Specimen: dog boned (115×10×4 mm^3)[b,c]; Speed: 1 mm/min[b,c]	σ_{tu} [MPa]	479.5 ± 28.9	33.8 ± 1.30	16.5 ± 1.6
				E_t [GPa]	37.4 ± 2.3	4.5 ± 0.30	1.1 ± 0.2
	Flexure	ISO 14125[a] [10.24]; ISO 178[b,c] [10.25]	Geometry:5×15×150 $mm^{3\ a}$; Speed: 2 mm/min[a]; Specimen: 4×10×80 $mm^{3\ b,c}$; Speed: 1 mm/min[b,c]	$\sigma_{f\ max}$ [MPa]	552.6 ± 40.2	71.7 ± 7.90	30.6 ± 2.1
				E_f [GPa]	21.4 ± 2.3	3.9 ± 0.20	1.3 ± 0.2
	In-plane shear	ASTM D5379 [10.26]	Geometry:5×20×50 $mm^{3\ a}$; Speed: 0.5 mm/min[a,b]; Specimen: 8×20×50 $mm^{3\ b,c}$; Speed: 1 mm/min[c]	τ_{max} [MPa]	53.7 ± 1.9	28.3 ± 4.01	24.7 ± 1.42
				G [GPa]	3.0 ± 0.5	1.8 ± 0.37	0.84 ± 0.14
	Interlaminar shear	ASTM D2344 [10.27]	Geometry:5×15×30 $mm^{3\ a}$; Speed: 1 mm/min[a,b];	σ_{sbs} [MPa]	34.7 ± 4.5	-	-

[a–c] The footnotes match different procedures specifications with the different materials.

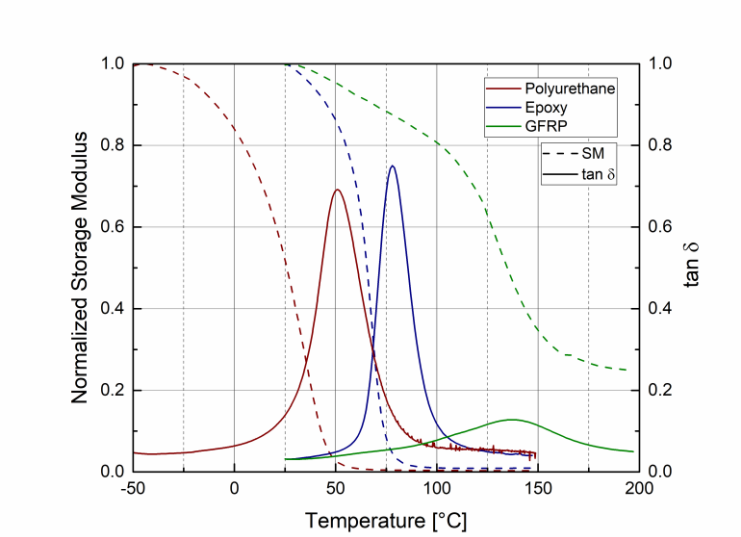

Figure 10.1. DMA curves of unaged epoxy, polyurethane and GFRP laminate.

The shape of the normalized E' curve of epoxy is similar to that of polyurethane; however, in polyurethane the transition from the glassy state to the leathery state occurs at a considerably lower temperature. The tan δ curves also reflect this difference, with peaks depicting a relative difference of 18 °C. For GFRP, the typical sigmoidal change of the E' curve takes place at much higher temperature compared to both adhesives; this is also reflected in the tan δ curve, whose peak is also much lower than that of the adhesives – this is ascribed to differences in the constituent polymers (and curing temperature) and especially the contribution of glass fibres.

In a similar way as the DMA tests, Figure 10.2 presents average stress *vs.* strain curves obtained from the various mechanical tests in the different materials, as well as the error envelopes (standard deviation of the experimental curves). In the different tests the epoxy adhesive showed an almost elastic behaviour and brittle failure. In comparison, the polyurethane adhesive presented lower stiffness and strength and higher deformability; after an initial elastic behaviour, this adhesive presented non-linear behaviour (for flexural and in-plane shear tests, the maximum cross-head displacement of the test machine was reached prior to specimens' failure). As expected, the GFRP laminates generally presented linear elastic behaviour up to failure (slightly more non-linear in shear and with progressive failure in bending) and much higher mechanical properties compared to the adhesives.

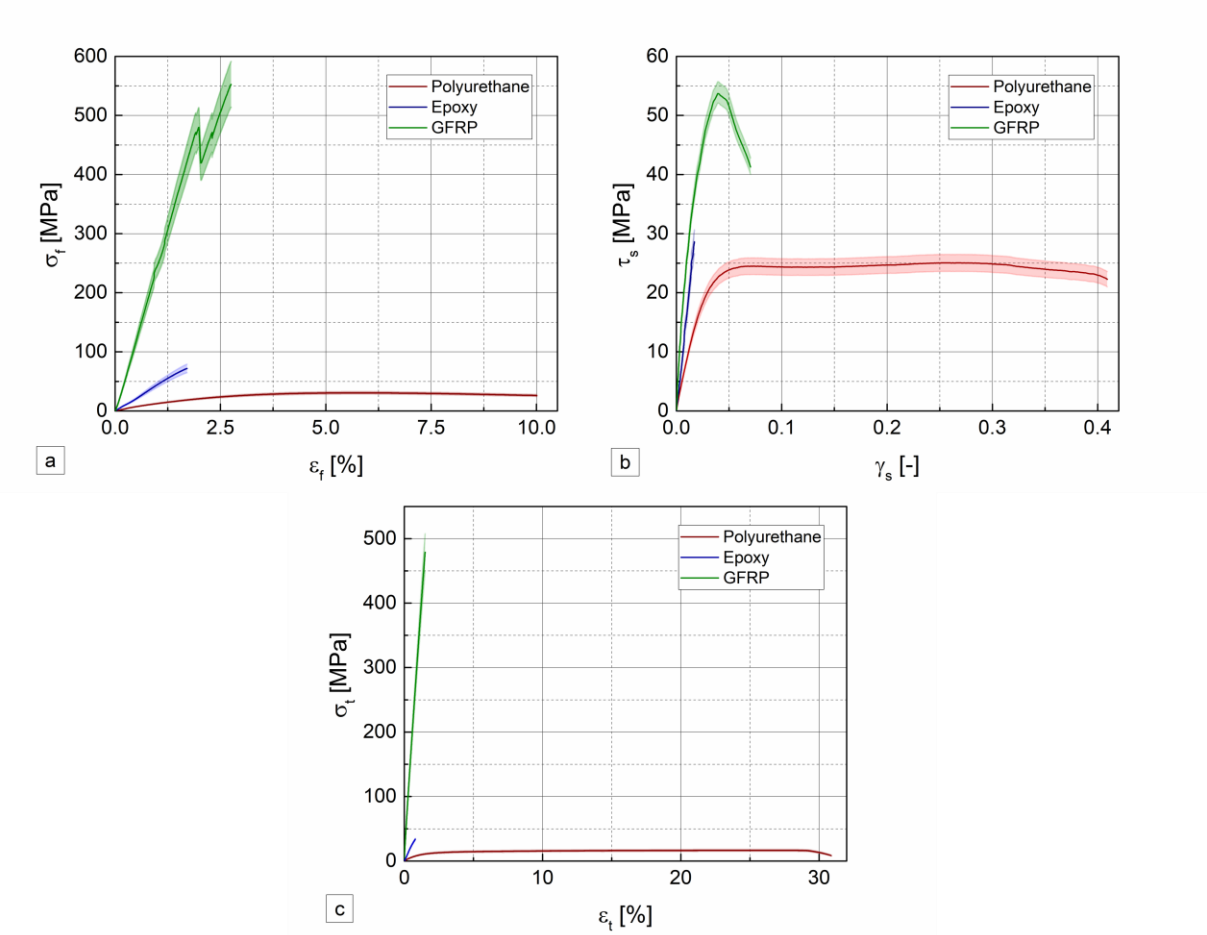

Figure 10.2. Stress *vs.* strain curves obtained for GFRP and both adhesives in the different mechanical tests: (a) flexure, (b) in-plane shear, and (c) tension.

10.3.3 Tests on lap joints

SLJ specimens were manufactured from the pultruded GFRP laminates and one of the adhesives. Figure 10.3 depicts the geometry of the epoxy (EP-GFRP) or polyurethane (PUR-GFRP) bonded specimens. The GFRP laminates were 33 mm wide, 180 mm long and 5 mm thick. The overlap length was 60 mm and the adhesive thickness was 1 mm, with a fillet radius of 1 mm at the ends of the overlap (*cf.* Figure 10.3 (b)).

The surfaces of the laminates' bonding areas were mechanically abraded with a P80 sandblasting paper, and degreased with acetone. To guarantee the predetermined bondline thickness, three metallic 1 mm thick spacers were used in predetermined positions, fixed with liquid cyanoacrylate adhesive. A specific wooden frame was designed and used to guarantee a correct alignment of the GFRP adherends. The SLJ specimens were produced in a controlled environment at 23 ± 2 °C and 50 ± 10% RH. After 24 hours, the specimens were removed

from the frame and cured at ambient conditions for 20 days, before ageing. Five SLJ specimens were fabricated for each ageing environment/period (see next section).

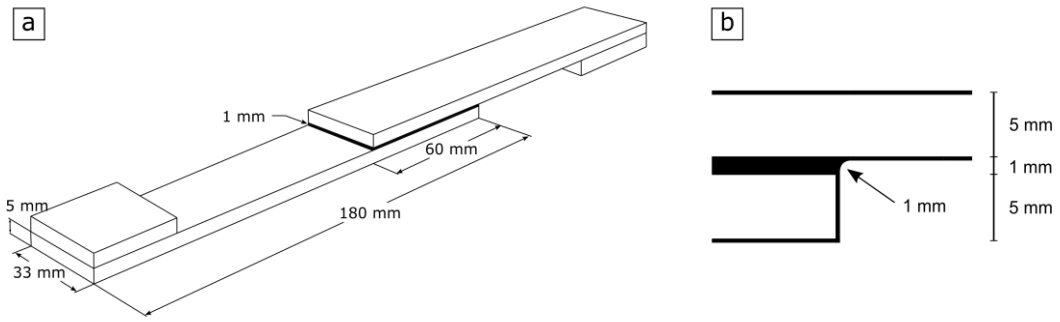

Figure 10.3. SLJ specimen geometry; and (b) detail of the overlap end.

The SLJ tests were performed according to ASTM D 1002 [10.28] and ASTM D 5868 [10.29] standards. The SLJ specimens were monotonically loaded up to failure, under displacement control, at a rate of 2 mm/min, in an Instron *4803* test machine with 100 kN of load capacity. GFRP end tabs were used to avoid misalignment between the load application plane and the adhesive layer, and also to balance and improve the efficiency of the gripping. Specimen elongation was recorded from the cross-head displacement of the test machine. The results of these measurements are not shown ahead, as they were affected by non-quantifiable slippage in the grips. Thus, for some test conditions (unaged, immersion and natural weathering for 18 and 24 months) videoextensometry was used to monitor the deformations in the bonded area. Figure 10.4 illustrates the position of the 56 dots marked in the specimens to assess the global deformed shape of the SLJ and also the local deformations of the overlap area.

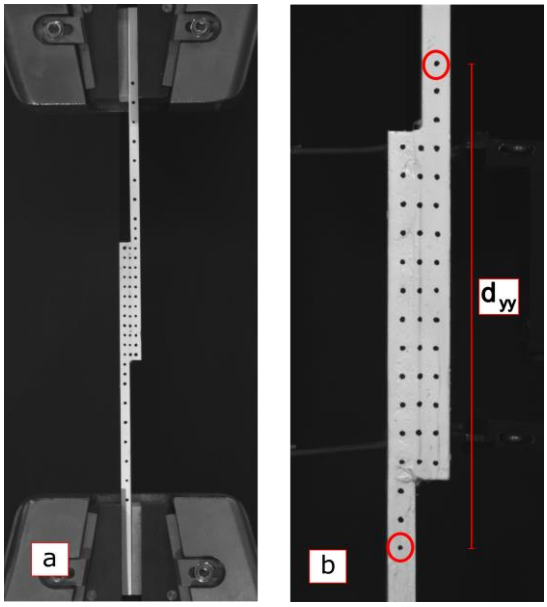

Figure 10.4. Setup used in the tensile tests of the SLJ specimens, with position of dots for videoextensometer: (a) general view and (b) detailed view of overlap zone.

Readings obtained from the videoextensometer were validated from data measured by a clip-on extensometer attached to one of the GFRP adherends.

10.3.4 Ageing conditions

In civil structural applications, direct exposure of bonded joints to external aggressive agents (such as UV radiation and moisture) is usually prevented by proper sealing techniques. However, for long service life periods, exposure to those agents is bound to occur especially in outdoor applications, such as bridges or roofs. Furthermore, premature contact with those agents can also occur due to defective sealing; GFRP components can also incorporate water through diffusion processes, which at some point can affect bonded joints [10.11]. Therefore, the following ageing environments, described in Table 10.2 and depicted in Figure 10.5, were considered: immersion in (i) water and (ii) salt water at 20 °C and 40 °C; (iii) natural weathering; (iv) continuous condensation at 40 °C, and (v) salt fog spray.

Table 10.2 Ageing environments, conditioning, and exposure durations.

Ageing environment	**Label**	**Duration]**	**Conditioning**[(a)]
Immersion in demineralised water	W20 W40	0, 2, 4, 6, 9, 12, 18, 24 months	T: 20 ± 3 °C T: 40 ± 2 °C
Immersion in salt water	S20 S40	0, 2, 4, 6, 9, 12, 18, 24 months	T: 20 ± 3 °C; 35 g/l NaCl T: 40 ± 2 °C; 35 g/l NaCl
Continuous condensation	C40	0, 2, 4, 6, 9, 12 months	T: 40 ± 2 °C; RH: 100%
Salt fog spray	SF35	0, 500, 1000, 2000 hours	T: 35 ± 2 °C; RH: 100%; Salinity: 50 ±5 g/l; pH: 6.9;
Natural weathering exposure	NE	0, 2, 4, 6, 9, 12, 18, 24 months	T, RH and UV radiation continuously monitored

(a) *Temperature (T); Relative Humidity (RH); Ultraviolet (UV).*

Immersion ageing was based on ISO 175 standard [10.30], while the salt water concentration was defined as indicated in ASTM D 1141 [10.31]. The 20 °C temperature was selected as normal room temperature, while 40 °C was selected to accelerate diffusion and promote the degradation mechanisms.

The continuous condensation and salt fog spray ageing were performed in specific chambers that combine the effects of moisture, temperature and salinity. In the first environment, specimens were hanged inside the chamber not contacting its walls, and temperature and RH values were selected according to ISO 6270 [10.32]. In the second environment, a similar chamber was used, containing a reservoir with a NaCl concentration of 50 g/l that assured the salinity of the inner environment, by aspersion of that solution into the inner chamber, as per ISO 9227 [10.33]. The latter exposure to the salt fog environment occurred continuously.

Figure 10.5. Ageing environments: (a) immersions, (b) continuous condensation, (c) natural ageing, (d) salt fog spray.

Natural ageing was performed in Lisbon, on the rooftop of the National Laboratory of Civil Engineering (LNEC), located at 38.77°, 9.13°W (Lisbon, Portugal), 100 m above the sea level. The samples were attached to a metallic structure with plastic rails, oriented towards South and at a 45° angle with the horizontal surface. The atmospheric conditions were monitored with a weather station located near the specimens, where the UV and solar radiation were measured at the same angle with the horizontal surface as the specimens. RH ranged between 84.2% and 61.7%, and the average monthly temperatures varied between 11.6 °C and 23.4 °C, considering winter and summer seasons, respectively. The global solar radiation varied between 3.5×10^5 kJ/m^2 and 6.6×10^5 kJ/m^2, while the UV component ranged between 9.4×10^3 kJ/m^2 and 26.9×10^3 kJ/m^2. The specimens were exposed to a total of 4.5×10^5 kJ/m^2 UV radiation throughout the whole exposure period (Jan/2015 – Dec/2016). Figure 10.6 displays average, maximum and minimum values of RH and temperatures, as well as radiation, monitored during the exposure period.

At predetermined exposure times, specimens were removed from the ageing environments and were subjected to a desorption period, being dried for at least 30 days at room temperature (at 23 ± 2 °C and 50 ± 5 %RH); this aimed at characterising the specimens in a dry state, considering the potential performance recovery. The desorption time was defined as the average period needed for specimens to achieve constant mass, according to ASTM D 5229 [10.34] (relative difference between consecutive mass measurements lower than 0.01%). Afterwards, the SLJ specimens were placed in polyethylene hermetically closed recipients for transportation purposes, and tested without further conditioning.

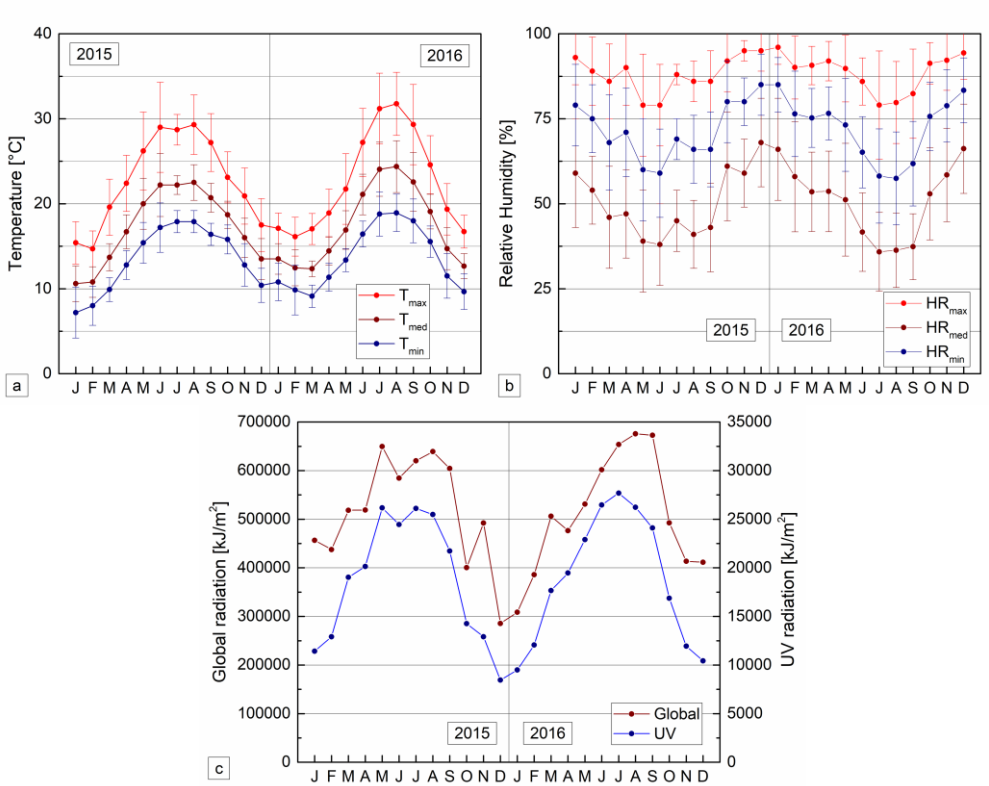

Figure 10.6. Outdoor environmental conditions in Lisbon during the exposure period: (a) temperature, (b) relative humidity, and (c) solar radiation.

10.4.Experimental results and discussion

10.4.1 Failure load behaviour

Figures 10.7 plots the average failure load (F_u) of EP-GFRP specimens as a function of the ageing period for the different environments.

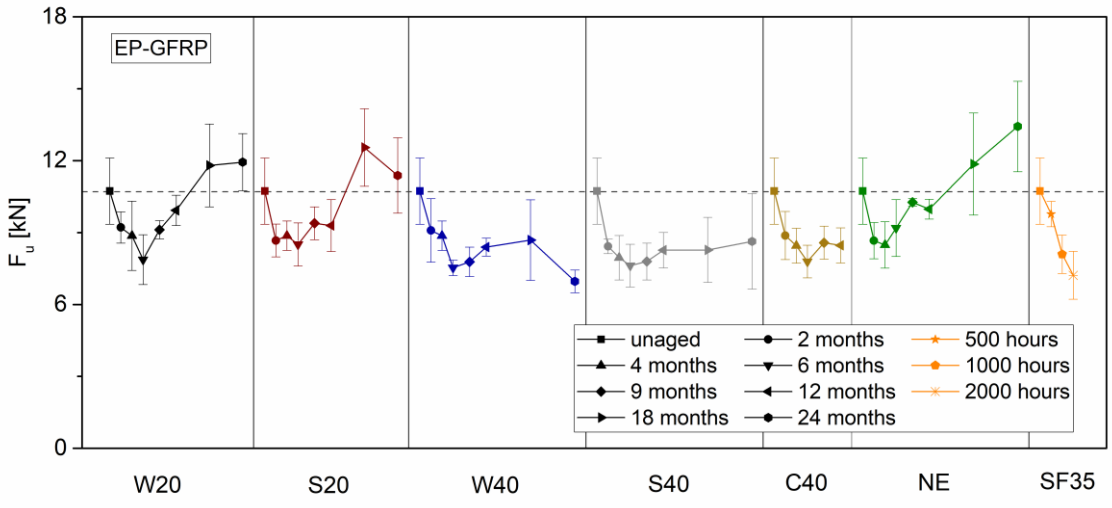

Figure 10.7. Failure load (average ± standard deviation) of EP-GFRP specimens, subjected to the different ageing environments.

In the immersion environments, the failure load of EP-GFRP specimens continuously decreased up to 6 months of exposure; at this stage, the strength degradation ranged from 21%-27%, with the higher reductions corresponding to immersions at 40 °C (W40 and S40). Subsequently, different behaviours were observed depending on the immersion temperature. At 40 °C the failure load tended to stabilize, with final reductions after 24 months of 20% and 35% in salt-water (S40) and demineralized water (W40), respectively. On the other hand, at 20 °C the failure load progressively increased in the 6-12 months period; subsequently, in W20 it tended to stabilize, while in S20 it exhibited a slight decrease, with final increases after 24 months of 11% and 6%, respectively.

The non-monotonic variation of failure load seems to be related to (i) the occurrence of post-curing phenomena, which affect both the GFRP and the adhesives (even at lower temperatures), and (ii) the desorption period prior to mechanical testing, which contributes to revert part of the degradation. Both effects compete with the irreversible degradation mechanisms experienced by the materials and bonded interfaces. Note that the degradation suffered by the stiffness of the adhesive may contribute to increase the strength of the bonded joints, as it promotes smoother stress distributions at the end of the overlaps; this effect, numerically investigated in further depth in Section 10.5.2, also counterbalances the potential strength degradation of the materials and interfaces. Furthermore, the desorption period, although guaranteeing constant mass (as per [10.34]), is not long enough to remove all the bounded water from the joint, especially in the epoxy adhesive, as seen in Chapter 9.

The results obtained suggest that reversible degradation mechanisms (*e.g.*, plasticization) are predominant at 20 °C; in opposition, at 40 °C (closer to the adhesives' T_g) irreversible degradation mechanisms (*e.g.*, hydrolysis) seem to be more relevant. The influence of such mechanisms on GFRP and adhesives exposed to these types of environments is well documented in the literature (*e.g.*, [10.11, 10.15, 10.17, 10.35]). Stazi *et al.* [10.5] also reported post-curing effects on pultruded GFRP joints bonded with epoxy adhesives subjected to hygrothermal ageing. It is also worth mentioning that for 12 months of immersion at 20 °C, the variations of failure load are comparable with those obtained by Heshmati *et al.* [10.15]; for immersion at higher temperature, the magnitude of the reduction was lower than that reported by those authors, due to the change in failure mode caused by steel corrosion (increasing the overall joint degradation). For hygrothermal ageing at 40 °C, the performance reduction was similar to that reported by Zhang *et al.* [10.13].

Continuous condensation at 40 °C (C40) produced similar trends to immersion at 40 °C: after 12 months, the ultimate load was reduced by 21% (C40) and 22% (W40). SF35 had similar

effects to C40 until 6 months, *i.e.*, an almost linear decaying trend; however, after 2000 hours, the ultimate load was more affected (30% reduction). The failure load reductions obtained here in continuous condensation environments were similar to those reported by Giampaoli *et al.* [10.14] up to 6 months (maximum tested period).

Natural weathering exposure (NE) caused an initial reduction of failure load (~20%) up to 4 months; this initial trend should stem from the lower temperatures and high RH level (*cf.* Figure 10.4) registered during this period of higher precipitation (winter), promoting higher moisture ingress in the specimens. Subsequently, a progressive growing trend was observed, with the failure load increasing 45% after 24 months. This increase, considerably higher than that observed in environments W20 and S20, can also be attributed to post-curing effects underwent by the GFRP and epoxy adhesive, especially during the warmer seasons. Such seasonal effects on epoxy adhesive subjected to natural ageing had already been reported in Chapter 9. It is worth referring that the slight reduction of failure load between 9 to 12 months (2%, irrelevant for the overall increasing trend) occurred during a period of lower temperature and higher precipitation, which is also consistent with the explanation presented above.

In what concerns PUR-GFRP specimens, with the exception of some slight differences (discussed ahead), the overall magnitude of the ultimate load variation (Figure 10.8) was similar compared to that of EP-GFRP specimens subjected to the same ageing condition.

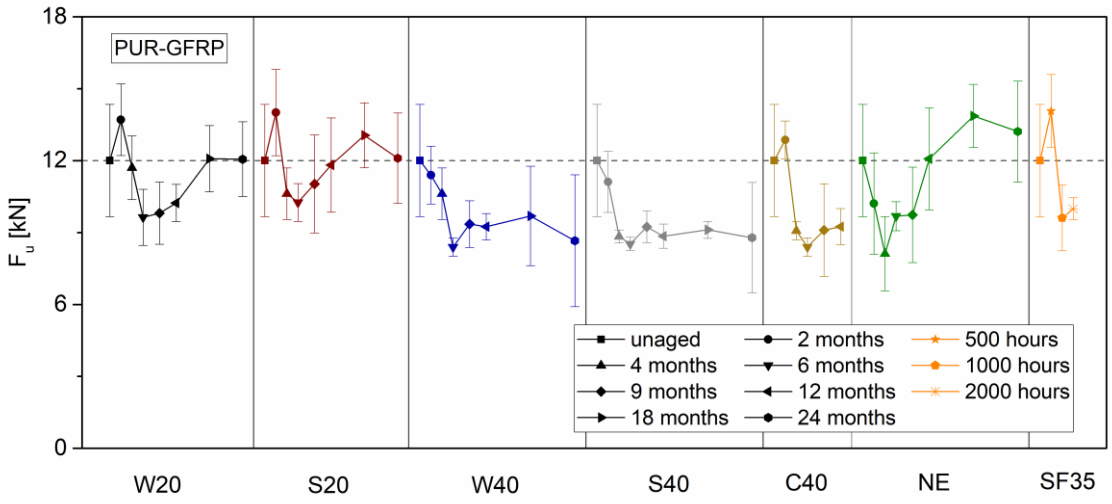

Figure 10.8. Failure load (average ± standard deviation) of PUR-GFRP specimens, subjected to the different ageing environments.

For immersion environments, as for EP-GFRP specimens, an initial decrease is noted, followed by either an increasing trend at 20 °C or a stabilization plateau at 40 °C. The main differences compared to EP-GFRP specimens included (i) a failure load increase (14-17%) after 2 months

of immersion at 20 °C, and (ii) a lower failure load reduction after 2 months of immersion at 40 °C. These (slight) differences should be related with the procedure used to condition the joint specimens prior to ageing, which seems to have been less effective in the PUR adhesive, possibly due to its lower T_g; in other words, PUR-GFRP specimens may have attained a higher level of post-curing during this initial ageing period. After 24 months of immersion at 20 °C (W20 and S20), the failure load roughly matched the initial value. For immersion at 40 °C, after an initial drop (in line with that observed for EP-GFRP specimens), the ultimate load tended to a plateau after 9 months, and after 24 months it presented reductions of 28% and 27% for W40 and S40 conditioning, respectively.

Continuous condensation at 40 °C (C40) caused the same effects on the ultimate load of PUR-GFRP specimens compared to immersion at 40 °C (W40 and S40), also in line with the results obtained for EP-GFRP specimens. However, the PUR-GFRP specimens exhibited the same initial post-cure effects seen in the immersion environments. After 12 months of C40 ageing, the ultimate load decreased 23% (identical to W40 for the same period). For SF35 the overall performance reduction was similar to that caused by C40 (slightly less severe) - after 3000 hours, the ultimate load decreased 17%.

NE produced similar effects in the failure load of PUR-GFRP specimens compared to EP-GFRP specimens: an initial reduction of 20% after 4 months, and an increase of 25% after 24 months of exposure. These figures confirm the outdoor seasonal effects mentioned above, namely higher degradation in wetter and colder periods and the occurrence of post-cure phenomena, especially in warmer periods.

10.4.2 Overall deformation and local stiffness

As mentioned, the local deformations of the SLJ joints were measured (using videoextensometry) to assess the overall deformation of the specimens and their local deformability in the overlap area. This had the main goal of obtaining further information about the behaviour of the joints and experimental data not affected by the effects of slippage in the grips.

Figure 10.9 depicts the global deformed shape of a typical SLJ specimen (unaged GFRP-EP joint) for different load levels. Note that the longitudinal deformations (x_l) were amplified 3 times to provide a better readability.

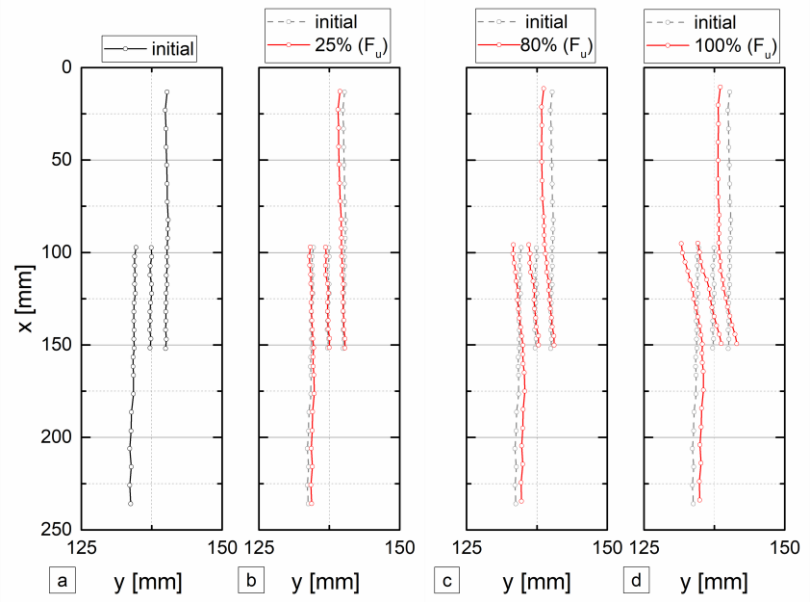

Figure 10.9. Deformed configuration of SLJ specimen at different fractions of the failure load.

In a first stage, for relatively low loads, up to about 2.0-2.5 kN (approximately 25% of F_u, Figure 10.9 (b), the specimens presented much higher deformations at the GFRP adherends near the grips of the test machine (top and bottom part of Figure 10.9 (b) than at the bonded central part – this shows the occurrence of slipping/adjustments in the grips at this stage. Subsequently, with increasing load, the bending of the specimens progressively became more pronounced, due to the eccentricity of the load path. At some point, due to a combination of peeling (out of plane tension) and shear stresses (*cf.* Section 10.5), brittle and sudden failure occurred.

Figure 10.10 shows representative curves of the load *vs.* (local) deformation in longitudinal direction (d_{yy}) of SLJ joints for three different conditions where videoextensometry was used: unaged and aged (immersions and natural ageing) for 18 and 24 months. The local deformation was computed based on the relative distance between points initially distanced by 85 mm (see Figure 10.4 (b); it was not possible to obtain fully accurate measurements at a distance of 60 mm, due to the adhesive residues that had been wiped out during bonding operations).

Both EP-GFRP and PUR-GFRP specimens presented the same qualitative behaviour: an initial non-linear (toe) behaviour that progressed to a stiffer linear response up to 90-100% of the ultimate load; in the brink of collapse, the response became non-linear, with stiffness reduction, and this was seen to correspond to the progression of a crack within the overlap (see Figure 11.11).

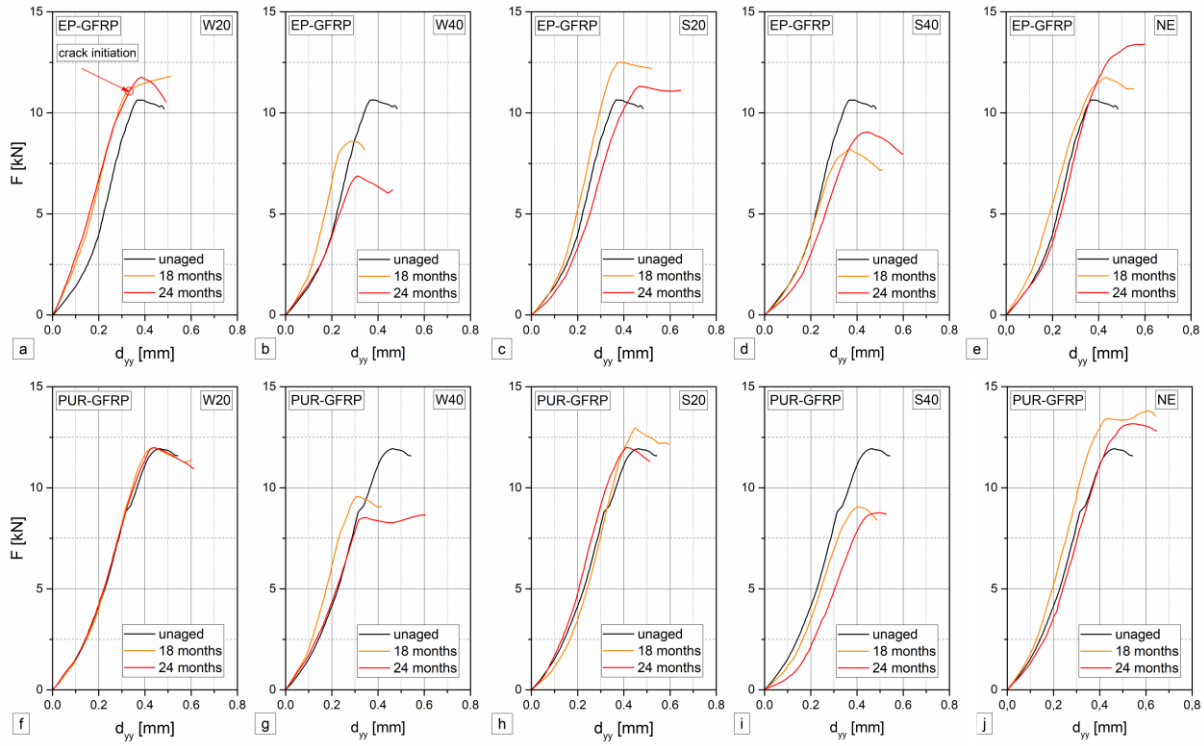

Figure 10.10. Load vs. local relative displacement of bonded joints throughout different ageing/time conditionings for EP-GFRP (a to e) and PUR-GFRP (f to j) joints.

Based on the slope of the linear branch of the load *vs.* local relative displacement curves in the longitudinal direction, the local stiffness of the bonded joints was computed (K_{local}) - Table 10.3 presents the results obtained for EP-GFRP and PUR-GFRP joints subjected to different ageing conditions.

Table 10.3 Local stiffness of EP-GFRP and PUR-GFRP joints K_{local} subjected to hygrothermal and natural ageing for 18 and 24 months and difference compared to unaged joints (Δ).

Environment	**Period [months]**	**EP-GFRP**		**PUR-GFRP**	
		K_{local} [kN/mm]	Δ [%]	K_{local} [kN/mm]	Δ [%]
Unaged specimen	0	41.8 ± 4.7	-	39.2 ± 3.9	-
W20	18	43.9 ± 6.8	+5	46.4 ± 6.0	+18
	24	40.9 ± 7.4	-2	41.2 ± 2.7	+5
W40	18	39.4 ± 4.0	-6	38.3 ± 5.1	-2
	24	30.7 ± 4.2	-26	36.2 ± 7.4	-8
S20	18	45.3 ± 8.4	+8	46.2 ± 4.2	+18
	24	43.2 ± 7.3	+3	44.7 ± 3.1	+14
S40	18	41.3 ± 7.5	-1	36.1 ± 4.6	-8
	24	36.3 ± 8.2	-13	34.8 ± 4.7	-11
NE	18	43.6 ± 5.8	+4	43.6 ± 4.3	+11
	24	44.5 ± 1.2	+6	41.0 ± 0.9	+5

For the unaged condition, the local stiffness of PUR-GFRP joints was 6% lower when compared to EP-GFRP ones - this difference is attributed to the lower modulus of polyurethane adhesive compared to epoxy. Regarding the influence of immersion, although the scatter of experimental results is relatively high, at 20 °C the local stiffness did not seem to be detrimentally affected;

in fact, in salt-water there was a trend for increasing local stiffness for both EP-GFRP (3-8%) and PUR-GFRP joints (14-18%). At 40 °C, the local stiffness clearly and progressively decreased, with maximum reductions of 26% (W40) and 11% (S40), respectively for EP-GFRP and PUR-GFRP joints. Natural ageing caused an increasing trend in the local stiffness of both types of joints, similarly to the variation of failure load described in the preceding section; accordingly, the performance increase of PUR-GFRP specimens (5-11%), where post-curing effects were more relevant, was higher than that of EP-GFRP joints (4-6%).

10.4.3 Failure modes

Figure 10.11 shows the typical failure of the SLJ specimens tested in this investigation. For both types of adhesives and regardless of the ageing process, failure was triggered by the initiation of a crack (exemplified in Figure 10 (a) at 24 months) at the end of the overlap, within one of the GFRP adherends, next to the bondline [10.2]. The crack propagated mainly in the GFRP adherend (where it initiated), next to the bondline, until the full debonding of that adherend. During the crack propagation process, another crack initiated at the other GFRP adherend. The ageing environments did not seem to affect this failure mode, also reported in several previous works (*e.g.* [10.15]).

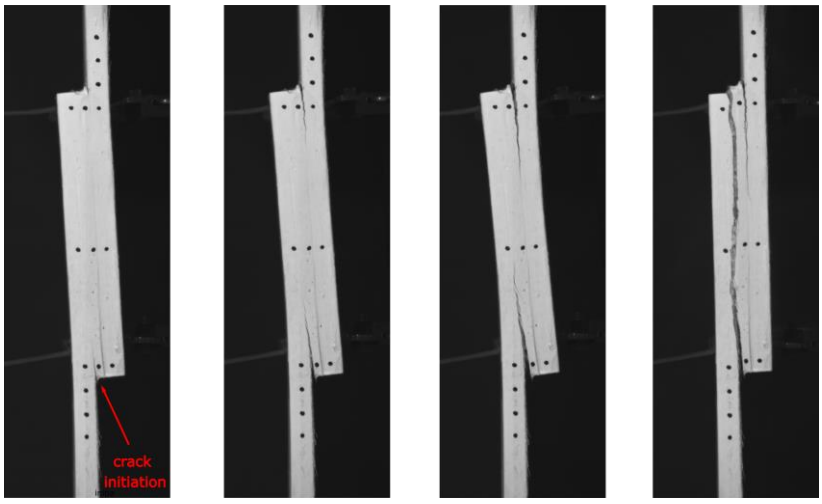

Figure 10.11. Single lap bonded joint specimen failure mechanism for both adhesives.

Based on the visual observation of the specimens bonded area, the following three failure modes could be distinguished according to ASTM D5573 [10.36] standard: adhesive, light fibre tear, and fibre tear (Figure 10.12). Fibre tear failure was typically located in the outer fibre-mat region of the GFRP adherend(s). Cohesive failure was never observed.

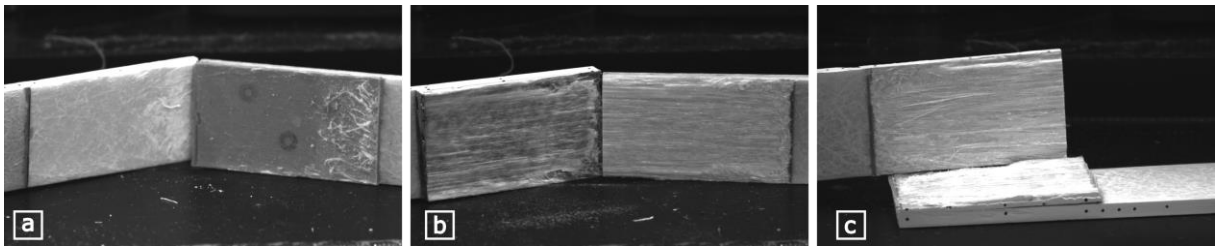

Figure 10.12. Failure modes: (a) adhesive, (b) light fibre tear, and (c) fibre tear.

In the vast majority of SLJ specimens, a single failure mode did not occur in the bonded area. In fact, specimens usually presented mixed failure modes, involving a combination of two or even the three modes described above. In this context, the percentage of the bond area featuring each type of failure mode was carefully measured. The results obtained from this assessment are presented in Figures 10.13 and 10.14, respectively for the EP-GFRP and PUR-GFRP specimens, subjected to the different ageing conditions.

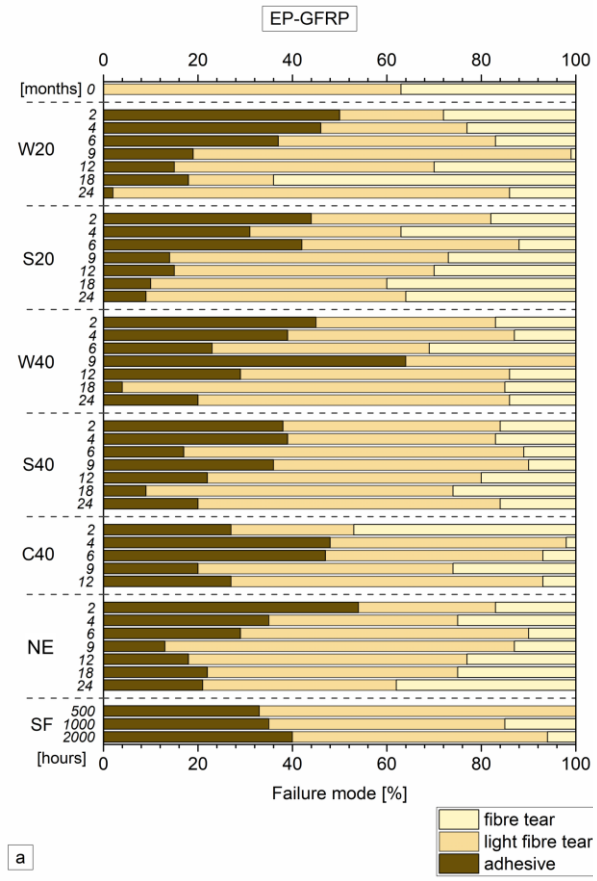

Figure 10.13. Average percentage of bonded area where each failure mode was observed, for EP-GFRP joints subjected to different ageing conditions.

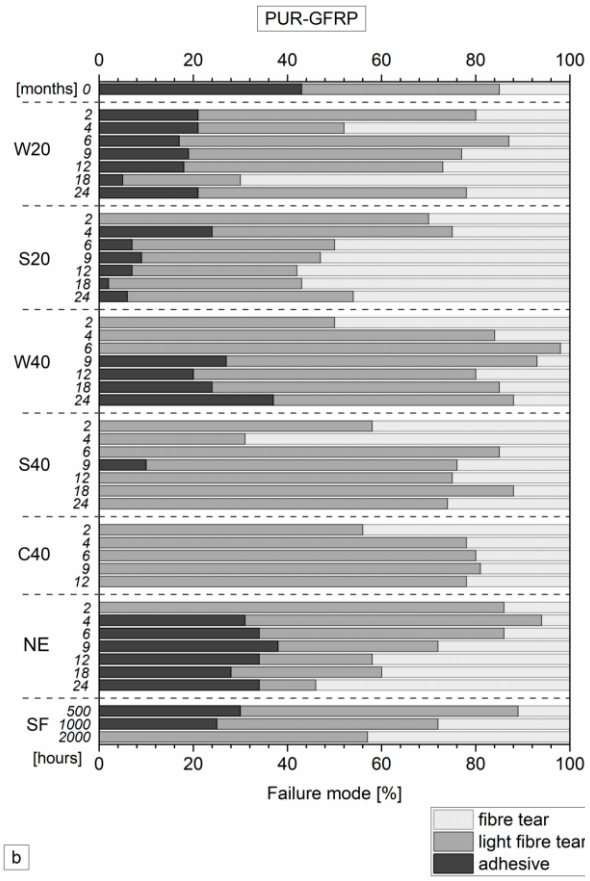

Figure 10.14. Average percentage of bonded area where each failure mode was observed, for PUR-GFRP joints subjected to different ageing conditions.

Overall, the various ageing processes did not seem to have influenced the types of failure modes observed nor the fracture initiation; however, they did affect the relative variation of the failure modes along the bonded area.

Regarding the EP-GFRP joints (Figure 10.13), before ageing no adhesive failure was observed throughout the bonded area, which attests the good material compatibility and effectiveness of the adhesion process. At the earlier stages of hygrothermal ageing (2 months), the frequency of adhesive failure increased, negatively affecting the EP-GFRP specimens, which is consistent with the overall initial reduction of ultimate load (this increase in adhesive failure was reported in the literature for similar (short) ageing periods [10.5]). Next, a decreasing trend of adhesive failure was noted in most ageing environments, especially at later stages and for lower temperatures, together with a corresponding increasing trend in fibre tear (and light-fibre tear) failure; this can be associated to the existence of post-curing phenomena (promoting the adhesion), being in agreement with the increasing trend exhibited by ultimate load. For instance, in environment W20, the proportion of the bonded area with adhesive failure decreased from 50% (2 months) to only 2% (24 months). For the higher immersion temperature and C40, the same general trend occurred (although with a more irregular pattern). As for stiffness and ultimate load, the failure modes for salt fog ageing correlated well with those in C40 up to 6 months (~40% adhesive failure). For natural weathering, a decreasing trend in adhesive failure (and increasing trend in light fibre tear failure) was observed, also possible to relate with the post-curing effects, not so evident due to the cyclic nature of this type of ageing.

Unaged PUR-GFRP specimens (Figure 10.14), in opposition to EP-GFRP ones, exhibited significant percentage (43%) of adhesive failure throughout the bonded area. At early stages of ageing, adhesive failure became less frequent, most likely due to post-curing phenomena, which were more relevant with PUR adhesive (an opposite trend was reported in [10.5], which should be attributed to differences between the PUR adhesives used and the type of hygrothermal conditioning, more severe in [10.14]). For immersion at 20 °C, after 24 months, the percentage of adhesive failure was reduced to 22% in W20 and 6% in S20. For immersion and continuous condensation at 40 °C and salt fog at 35 °C, although the overall mechanical performance of PUR-GFRP joints decreased, the percentage of bonded area with adhesive failure was significantly reduced or even eliminated; the only exception was immersion in demineralized water at 40 °C, for which adhesive failure started to be observed again after 9 months, showing an increasing trend up to 24 months (20-40%). Natural weathering did not cause significant changes in the percentage of bonded area with adhesive failure (~30% for most periods); however, fibre tear failure became progressively more frequent.

10.5.Numerical Study

10.5.1 Objectives and model description

In order to assess the evolution of the internal stresses developed in the SLJs due to the effects of hygrothermal ageing and, therefore, to obtain a better understanding of the evolution of the load-transfer mechanisms of these joints, three-dimensional (3D) FE models of the joints described in the previous sections were developed using the commercial package *ABAQUS* [10.37]. These models aimed at simulating the elastic response (load-transfer) of the joints, therefore no damage or failure initiation and propagation criteria were considered for the constituent materials and interfaces. The following paragraphs provide a brief description of the models and of the main assumptions considered.

The complete geometry of the SLJs was considered in the FE models, as depicted in Figure 10.15, including the fillets (*cf.* Figure 10.3). The model was developed with 8-node solid elements with reduced integration (C3D8R), with the exception of the adhesive fillets, which where modelled with 20-node solid elements (C3D20). The mesh of the GFRP laminates had a maximum size of 1 mm, while the mesh of the adhesive layer had maximum sizes of 0.2 mm and 0.5 mm in the through-thickness and remaining directions, respectively. Furthermore, the mesh was refined around the fillets, where stress peaks were expected to occur. A perfect bond was assumed in the GFRP-adhesive interfaces.

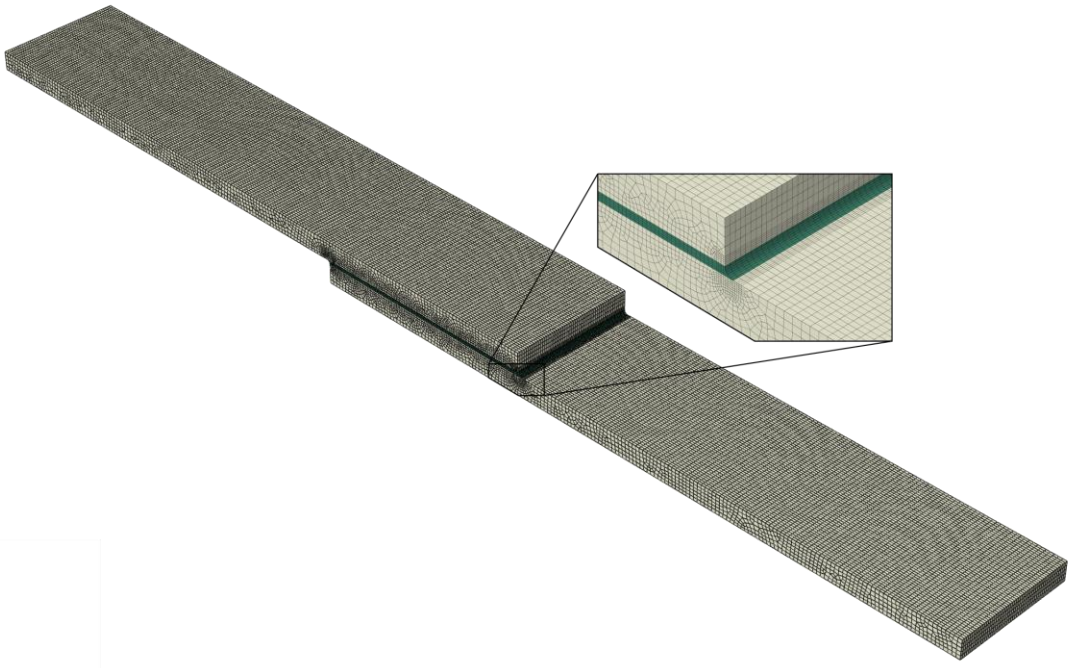

Figure 10.15. Overall view of the FE mesh and detailed view of the fillet.

Since the objective of the models was to simulate the elastic response of the joints, all materials were modelled as linear-elastic. The GFRP material was modelled as linear elastic and orthotropic, while the adhesives were modelled as linear elastic and isotropic. The elastic constants used in the FE models are listed in Table 10.4, where 1, 2 and 3 stand for the longitudinal, transverse and through-thickness directions. These properties were, when possible, derived from experimental testing performed by the author: most un-aged properties of the constituent materials are summarized in Table 10.1, while their aged properties are given in detail in Chapters 4, 8 and 9. The simulations were conducted for both adhesives with reference to the un-aged specimens and those subjected to 12 months (longest period for which the adhesive material shear properties were available) of water immersion at 40 °C (W40), which was the ageing medium that produced the most deleterious effects (*cf.* Section 10.4).

Table 10.4 Elastic properties of the materials used in the FE models (from [10.12] and Chapter 4).

Environment	**Material**	E_1 **[GPa]**	E_2 / E_3 **[GPa]**	G_{12} / G_{13} / G_{23} **[GPa]**
Unaged specimens	GFRP	37.4	8.3	3.0
	EP	4.5	-	1.8
	PU	1.1	-	0.8
W40 – 12 months	GFRP	33.1	4.0	2.6
	EP	2.6	-	1.0
	PU	0.65	-	0.5

In order to evaluate the elastic stresses developed in the SLJs, namely the effects of materials degradation, geometrical non-linear analysis was conducted. One free-end of the specimens was fixed, while at the opposite end a unit load (1 kN) was applied in the laminates' longitudinal direction, with the out-of-plane displacements being restrained.

10.5.2 Numerical results

The evolution of the internal stresses was investigated along a path located at the centreline of the specimens, as shown in Figure 10.16, and aligned with their longitudinal direction. The path was set within the laminate at a depth of 1 mm with reference to the interface, where failure initiation was typically observed in the experimental tests (*cf.* Section 10.4.3).

The longitudinal out-of-plane shear (S13) and peeling (S33) stresses along the aforementioned path are presented in Figures 10.17 and 10.18 for the EP-GFRP and PU-GFRP joints, respectively. The results show a reduction of 10% and 11% on the maximum shear stresses after an ageing period of 12 months, for joints with EP and PU adhesives, respectively. A similar trend was obtained for the peeling stresses, with reductions of 22% and 21%, respectively.

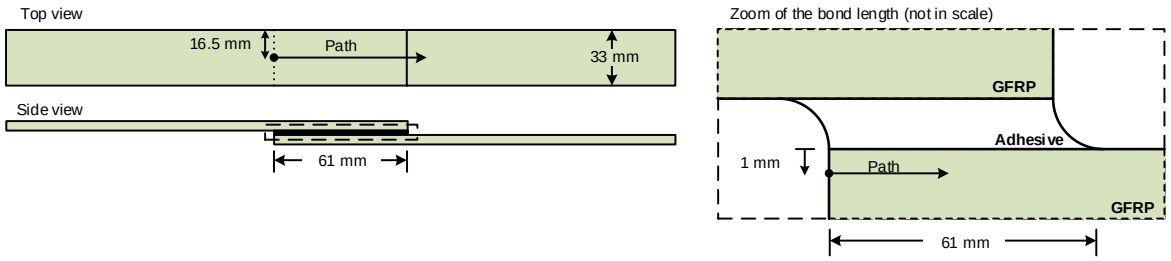

Figure 10.16. Location of the path in the FE models.

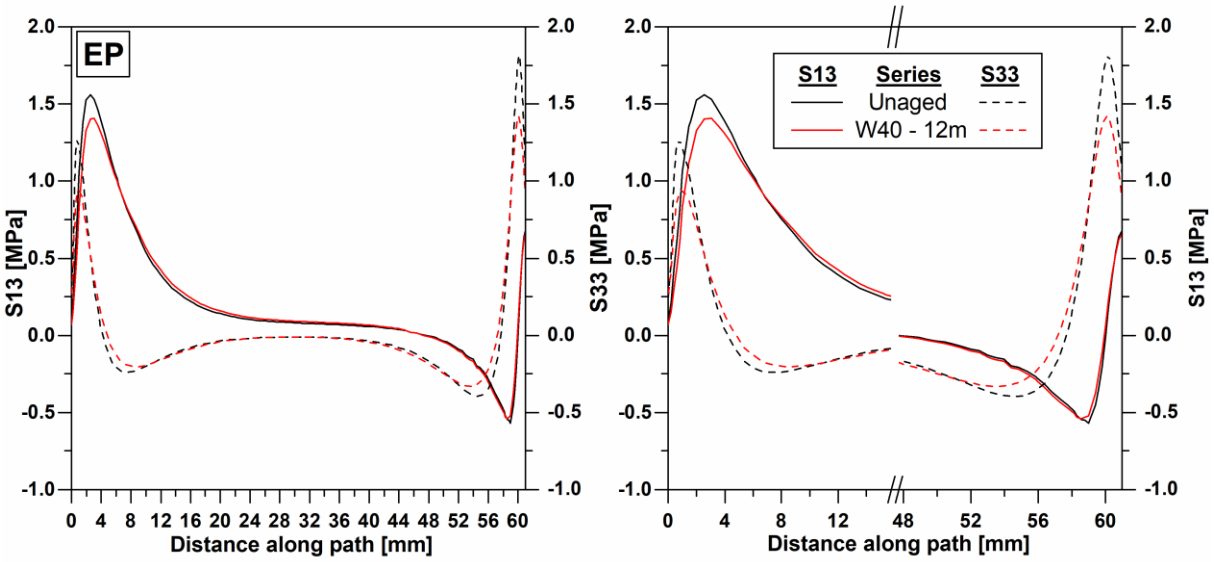

Figure 10.17. Stresses along the path for the EP adhesive: full path (left-hand side) and detail of peak zones (right-hand side).

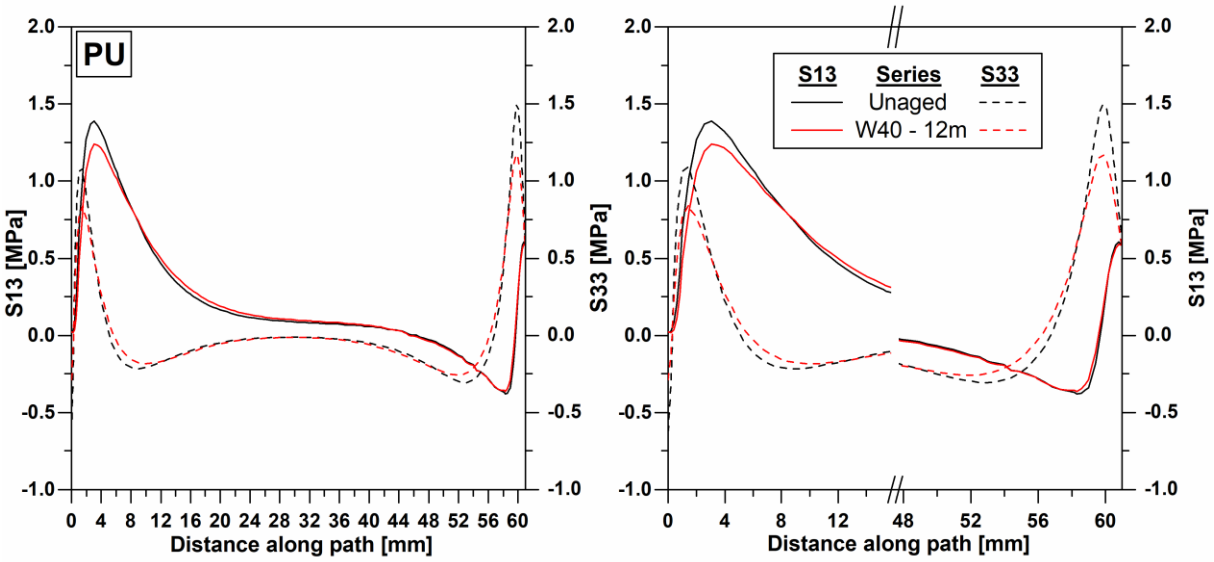

Figure 10.18. Stresses along the path for the PU adhesive: full path (left-hand side) and detail of peak zones (right-hand side).

These results confirm that the degradation of the elastic moduli of the constituent materials of the SLJs lead to a smoother stress distribution on the overlap area, consequently reducing the

peak stresses at the extremities of the overlap, especially the peeling stresses. This effect delays the failure initiation, (partly) counterbalancing the material strength degradation, as indicated in Section 10.4.1. Note that the analysis presented above does not account for material non-linearity, namely for the PU adhesive: compared to a linear elastic behaviour, such progressive stiffness reduction for increasing loads (more relevant for the PU adhesive) would lead to a further reduction of stress peaks at the overlap ends [10.38].

10.6. Concluding remarks

This chapter presented experimental and numerical study about the effects of hygrothermal and natural ageing on the behaviour of single lap bonded joints between pultruded GFRP laminates and two structural adhesives, epoxy and polyurethane. Based on the results obtained, the following main conclusions are drawn:

1. In spite of the intrinsic differences between the two adhesives (higher stiffness and strength (and T_g) of epoxy, higher deformation capacity of polyurethane), the mechanical performance of unaged EP-GFRP and PUR-GFRP single lap joint specimens was comparable: the local joint stiffness of PUR-GFRP specimens was 6% lower, and the ultimate load was 12% higher than that of EP-GFRP ones.

2. Hygrothermal ageing significantly affected the mechanical response (local stiffness and ultimate load) of both EP-GFRP and PUR-GFRP bonded joints, especially at higher temperatures. The immersion medium (demineralized water or salt water) did not have significant effects in the overall degradation of the joints. At lower immersion temperature, increasing trends were found at some stages, which could be related to the occurrence of post-curing phenomena. For immersion at 20 °C, the maximum reductions of ultimate load during the ageing period were 27% (EP-GFRP) and 20% (PUR-GFRP), but after 24 months the initial ultimate load was re-attained or even slightly exceeded. For hygrothermal ageing at 40 °C, maximum reductions of ultimate load were 35% (EP-GFRP) and 28% (PUR-GFRP), while for local stiffness those figures were 26% (EP-GFRP) 11% (PUR-GFRP). Continuous condensation and salt fog spray ageing caused very similar effects, which were comparable to those due to immersion at 40 °C.

3. Natural weathering did not cause significant changes in the mechanical performance of bonded joints made of both types of adhesives: stiffness exhibited little and increasing variations (6% for EP-GFRP and 5% for the PUR-GFRP); changes in ultimate load were

moderate and cyclic (matching the seasonal cycles), comprising a general increasing trend for both adhesives - after 24 months, it increased 25% (EP-GFRP) and 10% (PUR-GFRP).

4. For both adhesives and regardless of the ageing process, failure always initiated in one of the GFRP adherends, next to the extremity of the overlap. In unaged specimens, the types of failure modes throughout the bonded area were seen to depend on the adhesive: in EP-GFRP specimens only light-fibre tear and fibre tear failure was observed (reflecting the quality of the adhesion), while in PUR-GFRP specimens adhesive failure also occurred (quite frequently). During the ageing process, the percentage of the different failure modes changed and to some extent this could be correlated with the changes in the mechanical performance of the bonded joints.

5. Numerical investigations highlighted the effects of the degradation of the elastic moduli of the laminates and adhesives in the reduction of the peak stresses in the overlap area, (partly) counterbalancing the strength degradation of those materials in terms of failure initiation.

10.7. References

[10.1] Keller T, De Castro J. System ductility and redundancy of FRP beam structures with ductile adhesive joints. Compos Part B Eng 2005;36:586–96.

[10.2] Keller T, Vallée T. Adhesively bonded lap joints from pultruded GFRP profiles. Part I: Stress-strain analysis and failure modes. Compos Part B - Eng 2005;36:331–40.

[10.3] Keller T, Theodorou NA, Vassilopoulos AP, Castro J De. Effect of natural weathering on durability of pultruded glass fiber–reinforced bridge and building structures. J Compos Constr 2015;20:1–9.

[10.4] Gonilha JA, Barros J, Correia JR, Sena-Cruz J, Branco FA, Ramos LF, et al. Static, dynamic and creep behaviour of a full-scale GFRP-SFRSCC hybrid footbridge. Compos Struct 2014;118:496–509.

[10.5] Stazi F, Giampaoli M, Rossi M, Munafò P. Environmental ageing on GFRP pultruded joints: Comparison between different adhesives. Compos Struct 2015;133:404–14.

[10.6] Mays GC, Hutchinson AR. Adhesives in Civil Engineering. Cambridge University Press; 2005.

[10.7] Budhe S, Banea MD, de Barros S, da Silva LFM. An updated review of adhesively bonded joints in composite materials. Int J Adhes Adhes 2017;72:30–42.

[10.8] Heshmati M, Haghani R, Al-Emrani M. Environmental durability of adhesively bonded FRP/steel joints in civil engineering applications: State of the art. Compos Part B Eng 2015;81:259–75.

[10.9] Marques EAS, da Silva LFM, Banea MD, Carbas RJC. Adhesive joints for low- and high-temperature use: An overview. J Adhes 2015;91:556–85.

[10.10] Banea MD, da Silva LFM. Adhesively bonded joints in composite materials: An overview. J Mater Des Appl 2009;223:1–18.

[10.11] Cabral-Fonseca S, Correia JR, Rodrigues MP, Branco FA. Artificial accelerated ageing of GFRP pultruded profiles made of polyester and vinylester resins: Characterisation of physical-chemical and mechanical damage. Strain 2012;48:162–73.

[10.12] Sousa JM, Correia JR, Cabral-Fonseca S. Durability of an epoxy adhesive used in civil structural applications. Constr Build Mater 2018;161:618–33.

[10.13] Zhang Y, Vassilopoulos AP, Keller T. Environmental effects on fatigue behavior of adhesively-bonded pultruded structural joints. Compos Sci Technol 2009;69:1022–8.

[10.14] Giampaoli M, Terlizzi V, Rossi M, Chiappini G, Munafò P. Mechanical performances of GFRP-steel specimens bonded with different epoxy adhesives, before and after the aging treatments. Compos Struct 2017;171:145–57.

[10.15] Heshmati M, Haghani R, Al-Emrani M. Durability of bonded FRP-to-steel joints: Effects of moisture, de-icing salt solution, temperature and FRP type. Compos Part B Eng 2017;119:153–67.

[10.16] Cabral-Fonseca S, Nunes JP, Rodrigues MP, Eusébio MI. Durability of epoxy adhesives used to bond CFRP laminates to concrete structures. Proc. 17th Int. Conf. Compos. Mater. - ICCM 17, Edinburgh, UK: 2009, p. 1–8.

[10.17] Savvilotidou M, Vassilopoulos AP, Frigione M, Keller T. Development of physical and mechanical properties of a cold-curing structural adhesive in a wet bridge environment. Constr Build Mater 2017;144:115–24.

[10.18] Sousa JM, Correia JR, Cabral-Fonseca S. Durability of glass fibre reinforced polymer pultruded profiles: comparison between QUV accelerated exposure and natural weathering in a mediterranean climate. Exp Tech 2016;40:207–19.

[10.19] ASTM E 1252. Standard practice for general techniques for obtaining infrared spectra for qualitative analysis. Am Soc Test Mater 2007.

[10.20] ISO 11358. Plastics - Thermogravimetry (TG) of polymers. Int Organ Stand 1997.

[10.21] ISO 1183. Plastics – Methods for determining the density of non-cellular plastics. Part 1: Immersion method, liquid pyknometer and titration method. Int Organ Stand 2004.

[10.22] ISO 6721. Plastics - Determination of dynamic mechanical properties - Part 1: General principles. Part 5: Flexural vibration - non-resonance method. Int Organ Stand 1996.

[10.23] ISO 527. Plastics - Determination of tensile properties. Int Organ Stand 2009.

[10.24] ISO 14125. Fiber-reinforced plastic composites - Determination of flexural properties. Int Organ Stand 1998.

[10.25] ISO 178. Plastics - Determination of flexural properties. Int Organ Stand 2001.

[10.26] ASTM D 5379 / D 5379M. Standard test method for shear properties of composite materials by the V-notched beam method. Am Soc Test Mater 2011.

[10.27] ASTM D 2344. Standard test method for short-beam strength of polymer matrix composite materials and their laminates. Am Soc Test Mater 2000.

[10.28] ASTM D 1002. Standard test method for apparent shear strength of single-lap joint adhesively bonded metal specimens by tension loading (metal-to-metal). Am Soc Test Mater 2004.

[10.29] ASTM D 5868. Standard test method for lap shear adhesion for fiber reinforced plastic (FRP) bonding. Am Soc Test Mater 2008.

[10.30] ISO 175. Methods of test for the determination of the effects of immersion in liquid chemicals. Int Organ Stand 1999.

[10.31] ASTM D 1141. Standard practice for the preparation of substitute ocean water. Am Soc Test Mater 2008.

[10.32] ISO 6270. Paints and varnishes. Determination of resistance to humidity. Part 2: Continuous condensation (in-cabinet exposure with heated water reservoir). Int Organ Stand 2017.

[10.33] ISO 9227. Corrosion tests in artificial atmospheres – Salt spray tests. Int Organ Stand 2009.

[10.34] ASTM D 5229. Standard test method for moisture absorption properties and equilibrium conditioning of polymer matrix composite materials. Am Soc Test Mater 2014.

[10.35] Grammatikos SA, Evernden M, Mitchels J, Zafari B, Mottram JT, Papanicolaou GC. On the response to hygrothermal aging of pultruded FRPs used in the civil engineering sector. Mater Des 2016;96:283–95.

[10.36] ASTM D5573. Standard practice for classifying failure modes in fiber-reinforced-plastic (FRP). Am Soc Test Mater 2012:3–5.

[10.37] SIMULIA. ABAQUS 6.11 - Analysis User's Manual. Dassault Systèmes, Maastricht 2011.

[10.39] Castro J, Keller T, "Ductile double-lap joints from brittle GFRP laminates and ductile adhesives, Part II: Numerical investigation and joint strength prediction", Compos Part B Eng 2008; 39(2); 282-291.

Chapter 11.

Effects of thermal cycles on adhesively bonded joints between pultruded GFRP adherends

11.1.Introduction

Pultruded glass fibre reinforced polymer (GFRP) profiles are usually connected by means of bolting and/or adhesive bonding, as discussed in Chapter 2. While mechanical bolting involves drilling operations and often leads to overdesign of GFRP components [11.1, 11.2], adhesively bonded joints lead to a more uniform load transfer, being more material-adapted, as both the adherends and the adhesive are of a polymeric nature, thus providing better compatibility [11.3, 11.4]. Some adhesives can also be chosen to increase the ductility of bonded joints [11.5], namely to guarantee load redistribution in redundant structures and/or energy dissipation under seismic loads. In addition to these advantages, sections assembled by means of adhesive bonding may also benefit the construction process by reducing installation times [11.6].

In spite of their potential benefits, as discussed in the preceding chapter, there are concerns about the durability and long-term performance of adhesively bonded joints between GFRP components. In fact, both the adhesives and the adherends can be influenced by environmental conditions, which may affect the stiffness, strength and deformation capacity of bonded joints [11.7, 11.8].

Temperature variations are among the most important environmental factors that may affect the durability of adhesively bonded joints for civil engineering applications [11.8–11.10]. In addition to the detrimental effects caused by exposure to extreme (low and high) temperatures on the constituent materials themselves – the adhesive and the adherends – the concerns with thermal cycles also stem from the thermal deformations of the adherends and the potential dissimilarity between the coefficients of thermal expansion (CTE) of the adherends and the adhesive, which may lead to the development of interfacial internal stresses at the bonded joint and eventually lead to micro-cracks at the interfaces or even premature debonding failure [11.11].

In what concerns the effects of thermal cycles on polymeric adhesives and GFRP adherends, there is already some information available in the literature. For most typical adhesives used in civil structural applications, previous studies [11.10, 11.12, 11.13] have shown that internal

stresses are developed during thermal cycles: tensile stresses due to thermal expansion can be found when temperature increases, while compression stresses (shrinkage) occur when temperature decreases. Moreover, the cyclic change in stress state and temperature can lead to shrinkage, embrittlement, hardening and microcracking of the adhesives. Regarding pultruded GFRP adherends, the research described in Chapter 6, in addition to other earlier works [11.13, 11.14], has shown that thermal cycles may lead to fibre-matrix interface failure (due to different CTEs of the fibre and the matrix, and the consequent increase of internal stresses), microcracking and matrix hardening. Further degradation may occur when thermal cycles are combined with moisture, due to the development of internal stresses caused by the expansion of the trapped water inside the composite at lower temperatures. Results presented in Chapter 6 have also shown that in mild climates the degradation in the physical and mechanical properties of pultruded GFRP profiles is low.

As for adhesive joints, exposure to thermal cycles generally causes a decrease in strength. According to Humfeld and Dillard [11.15], raising the temperature of the joint induces residual thermal stresses due to the CTE mismatch between the adhesive and the adherends. The higher temperatures facilitate polymer chain mobility and lead to some degree of relaxation of these stresses. However, when cooling the joint, the stress relaxation is reflected in an increased interfacial stress between the substrate and the adhesive layer. In addition, the lower temperature reduces the polymer chain mobility, and these tensile stresses cannot be relaxed at the same degree (initial stress state) until the next cycle starts, resulting in accumulating low temperature thermal stresses within each cycle. This cumulative effect repeats each cycle, leading to residual stress increase that can eventually promote failure.

As discussed below, in spite of its importance, there is very limited information available about the effects of thermal cycles on the long-term performance of adhesively bonded joints between pultruded GFRP components used in civil engineering applications. Most previous studies on bonded joints between composites refer to different adherend/adhesive systems used in other industries [11.7, 11.16], or focus on a different combination of substrates, namely FRP-to-concrete (*e.g.*, [11.17]), FRP-to-metal (*e.g.*, [11.18, 11.19]) or metal-to-metal (*e.g.*, [11.9]). To the best of the author knowledge, the only studies about the effects of thermal cycles on bonded joints between GFRP adherends are the ones by Stazi *et al.* [11.7] and Lopez-Anido *et al.* [11.20], which are summarized next.

Stazi *et al.* [11.7] studied the environmental ageing of joints between pultruded GFRP (glass-vinylester) adherends bonded with six different types of adhesives (two epoxies, one acrylic, one methacrylate, and two polyurethanes). The authors considered single lap and butt

joint configurations and subjected them to two types of artificial ageing, one of which comprised hygrothermal cycles, where temperature (and relative humidity) were varied in three stages: (i) 16 hours at 40 °C and 100% RH; (ii) 4 hours at -40 °C; (iii) 4 hours at 70 °C and 50% RH. The specimens were aged for 2 weeks, being exposed to a total of 14 thermal cycles. For most adhesives ultimate loads slightly increased, except for one epoxy (12.5% reduction) and the methacrylate adhesive in the single lap configuration (60% reduction due to premature failure); this generalised increase was attributed to the completion of the polymerization process of the adhesives after the first cycle at high temperatures (w.r.t. the unaged specimens). Joint elongation at failure increased very considerably, while the stiffness of the joints was reduced (70-90%) compared to that of the corresponding unaged specimen; these changes were attributed to the softening of the adhesives, as their glass transition temperature range was reached and exceeded. The failure modes were also largely affected, changing from mixed failure (combination of two or more modes) to mainly adhesive failure (especially in the epoxy adhesives). It is worth noting that the degradation/changes reported in this study were due to the combined effects of thermal cycles and relative humidity.

Lopez-Anido *et al.* [11.20] studied the freeze-thaw resistance of single lap bonded joints between GFRP composites (glass-epoxy-based vinylester), produced by vacuum assisted resin transfer moulding (VARTM), and an underwater curing epoxy adhesive. After fabrication, specimens were immersed in tap water at 38 °C to allow the epoxy adhesive to cure in an underwater environment. After 2 weeks, the control samples were removed and tested in a dry condition, while the specimens subjected to thermal cycles were removed after 3 weeks. The freeze-thawing exposure consisted of 20 cycles characterised by (i) 8 hours at -18 °C, and (ii) 16 hours of tap water immersion at 38 °C. The apparent bond strength of the specimens was very sensitive to freezing and thawing, suffering a 43% reduction after exposure. The authors suggested that the reduction in the bond strength was mainly due to increased moisture ingress in voids present in the adhesive layer that resulted from the fabrication process (uneven spreading and absence of proper clamping). The void content was affected during the freezing period due to water expansion, which generated cracks and degraded the epoxy adhesive bond line; the failure mode was also affected, changing from predominantly adhesive to a combination of adhesive and cohesive. Similarly to the previous study, the degradation experienced by the joints was due to several factors: water immersion, thermal cycles, and freeze-thaw.

The two studies reported above, although providing useful information, make it difficult to predict the long-term response of bonded joints between pultruded GFRP components in relatively mild climates, a limitation that is delaying their widespread use [11.21, 11.22]. Indeed,

the extreme temperatures and the thermal amplitude used were quite high compared to normal outdoor exposure in those climates. In addition, the number of cycles considered in both studies was quite limited, taking into account the typical service life of civil engineering structures (generally, 50 years or higher). Finally, it is also worth noting that the durability behaviour of FRP components and joints depends on the following aspects (which varied in those studies): (i) the manufacturing process, (ii) the test protocol, namely the type of conditioning during exposure to thermal cycles (either saturated or dry condition), (iii) the moisture level during mechanical testing, and (iv) the type of adhesive.

In order to obtain a better understanding about the long-term durability of adhesively bonded joints between pultruded GFRP adherends, this chapter presents experimental and numerical investigations about the effects of thermal cycles on the mechanical response of single lap bonded joints between pultruded glass-unsaturated polyester laminates. GFRP adherends were bonded with two commercial adhesives – epoxy and polyurethane (the same bonded joints that were used in the previous chapter) - and were exposed to a mild (Mediterranean) range of thermal variations (-5 °C to 40 °C) for up to 350 cycles, in a dry condition. Single-lap joint tests were then performed at predetermined times to assess the effect of thermal cycles in overall joint performance, in terms of load *vs.* elongation response, joint stiffness, bond strength and failure modes. Three-dimensional (3D) finite element (FE) models were developed using the commercial package ABAQUS to assess the magnitude of the thermal stresses caused by the mismatch of the coefficients of thermal expansion (CTE) of the GFRP and the adhesives.

11.2.Experimental programme

11.2.1 Materials

The materials used in the experimental investigations comprised pultruded GFRP profiles with 33×5 mm^2 of cross section and 3 m of length, manufactured by *ALTO Perfis Pultrudidos*. The profiles consist of the same materials used in Chapter 4[10]. As in the previous chapter, unsaturated polyester resin was selected for the matrix of the GFRP profiles, since it is the most commonly used in civil structural applications when there are no particular requirements in terms of environmental harshness.

[10] Further information about the GFRP material is detailed in Section 4.2.1

The two commercial, bi-component structural adhesives used in Chapters 8 and 9[11] were used as bonding agents to join the GFRP adherends: the first is a thixotropic, solvent-free, cold curing epoxy based adhesive (EP), frequently used in civil structural applications, namely for bonding FRP strips to different substrates; the second is a bi-component polyurethane adhesive (PUR), based on filled polyols and unfilled isocyanates derivates.

11.2.2 Material characterisation tests

Several tests were carried out to characterise the initial physical and mechanical properties of the three materials – pultruded GFRP profiles and EP and PUR adhesives. These tests and the corresponding procedures are described in Chapter 4 for the GFRP and in Chapters 8 and 9 for the EP and PUR adhesives, respectively. Section 10.3.2 summarizes and compares the initial tests for the three materials.

11.2.3 Tests on lap joints

Single lap joints were manufactured from the pultruded GFRP plates and one of the adhesives; this specimen geometry was selected as it is the most widely used method to assess the shear strength of adhesively bonded joints [11.7]. Figure 11.1 depicts the geometry of lap specimens bonded with epoxy (EP-GFRP) and polyurethane (PUR-GFRP) adhesives. The adherends (GFRP laminates) had cross-section of 33 × 5 mm^2 (width × thickness) and 180 mm of length. The overlap length was 60 mm and the adhesive thickness was set as 1 mm, representative of several civil engineering applications, where relatively large tolerances need to be considered when designing bonded joints. The adhesive layer was manufactured with a fillet radius of approximately 1 mm (*cf.* Figure 11.1).

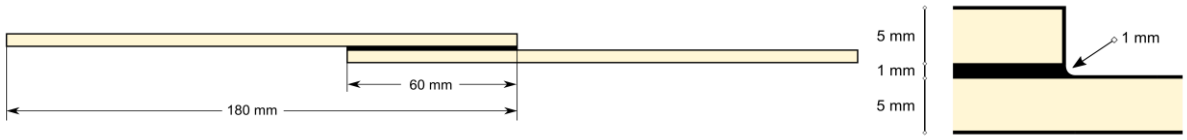

Figure 11.1. Single lap joint specimen geometry

All specimens were fabricated under laboratory conditions (23 ± 2 °C / 50 ± 5% RH) and the manufacturing procedure is described in the previous chapter.

[11] Further information about the EP and PUR adhesives is provided in Sections 8.3.1 and 9.3.1, respectively.

To assess the changes in the mechanical behaviour of the single lap bonded specimens, as well as the mechanisms of degradation due to thermal cycles, the specimens were subjected to three set of cycles (150, 250 and 350 cycles) in a conditioning chamber from *Aralab*. Each thermal cycle had a total duration of 14 hours, with 6 hours at -5 °C, 6 hours at 40 °C, and 2 hours of continuous heating or cooling between the referred temperatures, as depicted in Figure 11.2.

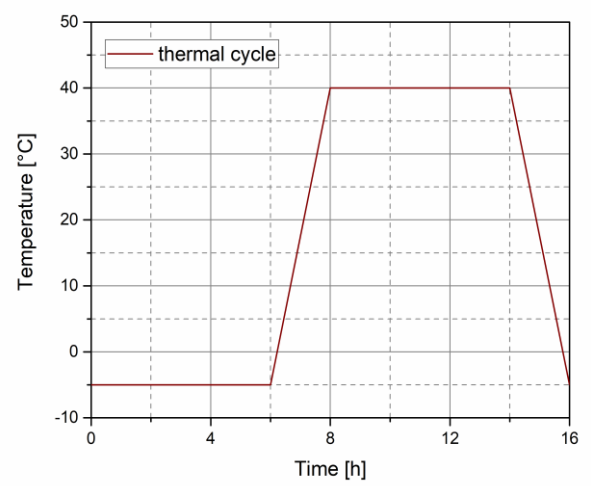

Figure 11.2. Thermal cycle profile.

Due to the lack of information in the literature or in test standards about the minimum number of thermal cycles representative of a certain service life (and climate), based on previous works on the effects of thermal cycles on pultruded GFRP profiles [11.14, 11.23] (and in Chapter 6[12]), about 350 cycles were considered to be reasonable to characterize the long-term performance of the bonded joints, particularly for a mild Mediterranean climate. Note that this number of cycles is at least 20 times higher than that used in previous studies on this topic [11.7, 11.20].

At predetermined times, batches of test specimens were removed from the thermal cycle chamber, stored in polyethylene hermetically closed recipients, and placed in a controlled room at 23 ± 2 °C, until testing.

The single lap shear tests were performed according to ASTM D 1002 [11.24] and ASTM D 5868 [11.25] standards in an *Instron 4803* UTM with 100 kN of load capacity. Specimens were monotonically loaded up to failure, under displacement control, at a rate of 2 mm/min. GFRP end tabs were used in all specimens (*cf.* Figure 11.3), in order to avoid misalignment of the load application plane with the centre of the bonded joint and to guarantee

[12] Where no significant differences were found in the pultruded GFRP materials from 400 to 600 cycles.

the balance and efficiency of the gripping. Specimen elongation was recorded from the cross-head displacement of the testing machine. In all tests, the ultimate load and the overall stiffness (measured from the linear branch of the load *vs.* elongation curves, after the initial adjustments due to slipping effects at the clamps, which generally corresponded to minimum elongations of 2.0 to 2.5 mm, and up to 60% of the ultimate load) were registered and the failure modes were carefully assessed.

Figure 11.3. Single lap shear test setup.

11.3.Experimental results and discussion

11.3.1 Experimental load *vs.* displacement response

The load (F) *vs.* (cross-head) displacement (d) response of the EP-GFRP and PUR-GFRP joints, both unaged and subjected to different thermal cycles, is shown in Figure 11.4.

All curves show a similar qualitative development: (i) there is an initial non-linear branch up to a load of about 2 kN, due to adjustments in the test setup, namely in the gripping system; (ii) then, the response becomes close to linear, yet with a slight and progressive stiffness increase, most likely due to the (geometrically non-linear) effects associated to the bending of the specimens (*cf.* Figure 11.5); (iii) the final branch of the curves correspond to the brittle rupture of the joints (*cf.* Section 11.3.2), which caused an abrupt load reduction after the maximum value was attained.

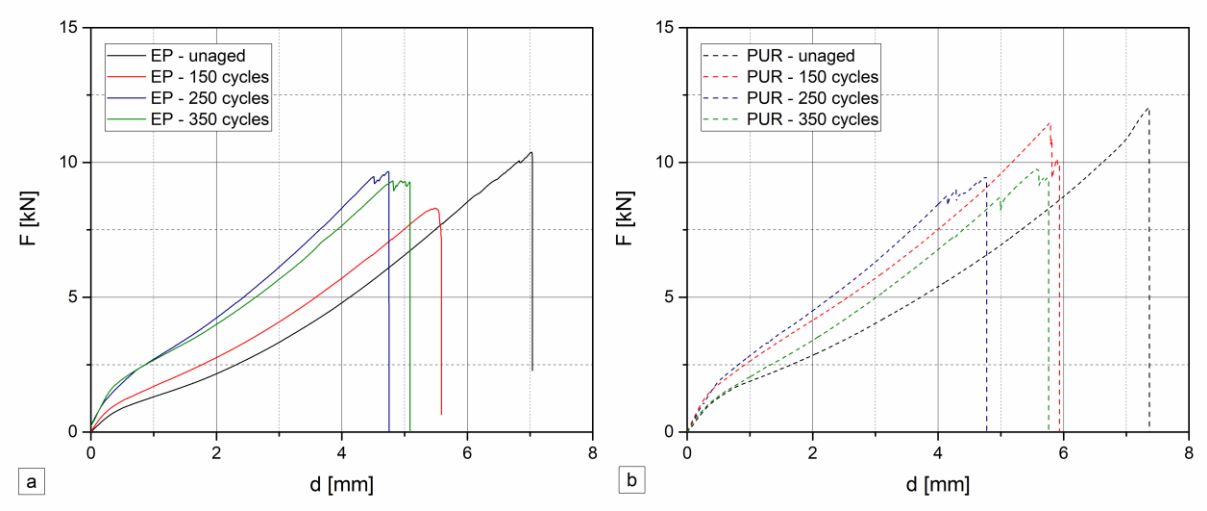

Figure 11.4. Load *vs.* displacement response of representative specimens (a) EP-GFRP; (b) PUR-GFRP.

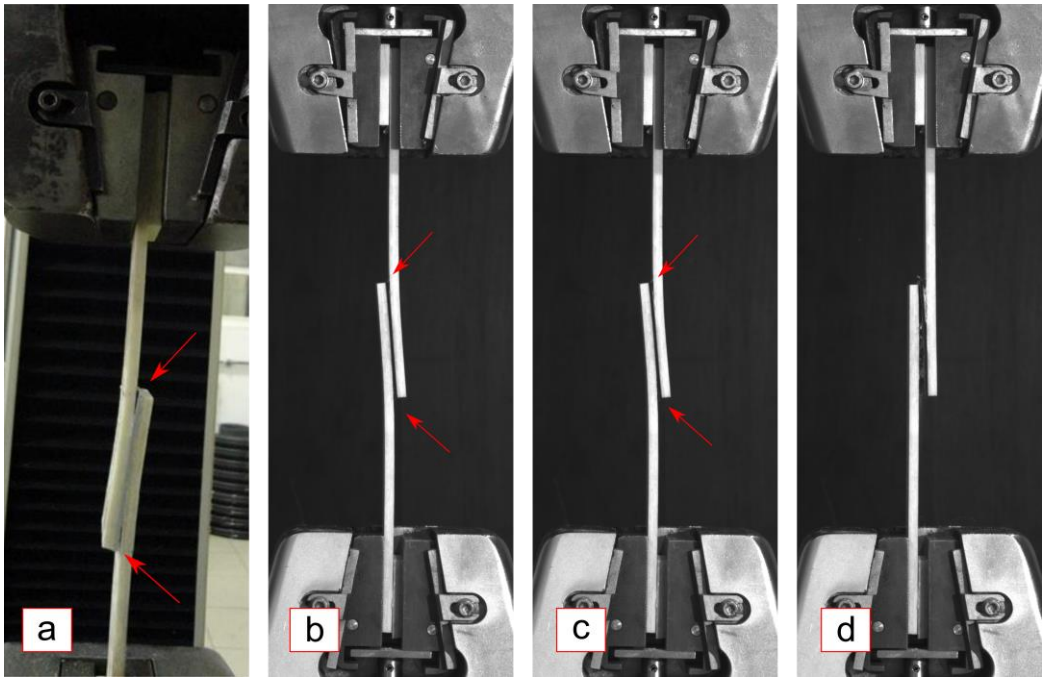

Figure 11.5. Deformed configuration of the single lap joint: (a) cracking in a EP-GFRP joint; (b) and (c) cracking in a PUR-GFRP joint; (d) PUR-GFRP joint failure.

Table 11.1 presents, for both types of joints, the retention (*w.r.t.* unaged specimens) of ultimate load (F_u) and overall stiffness (K), computed in the linear branch of the load *vs.* cross-head displacement curves.

Figure 11.6 plots the average ultimate load and the overall stiffness as a function of the number of thermal cycles for both types of joints.

Table 11.1. Property retention [%] for both joint types.

Property	Joint type	Unaged	Thermal cycles		
			150	250	350
Ultimate load (F_u)	EP-GFRP	100 ± 11.9	82 ± 8.5	90 ± 1.7	86 ± 9.1
	PUR-GFRP	100 ± 14.5	98 ± 5.5	81 ± 5.2	83 ± 2.2
Stiffness (K)	EP-GFRP	100 ± 9.5	78 ± 8.7	91 ± 1.4	81 ± 8.9
	PUR-GFRP	100 ± 15.7	97 ±13.4	89 ± 4.1	93 ± 9.4

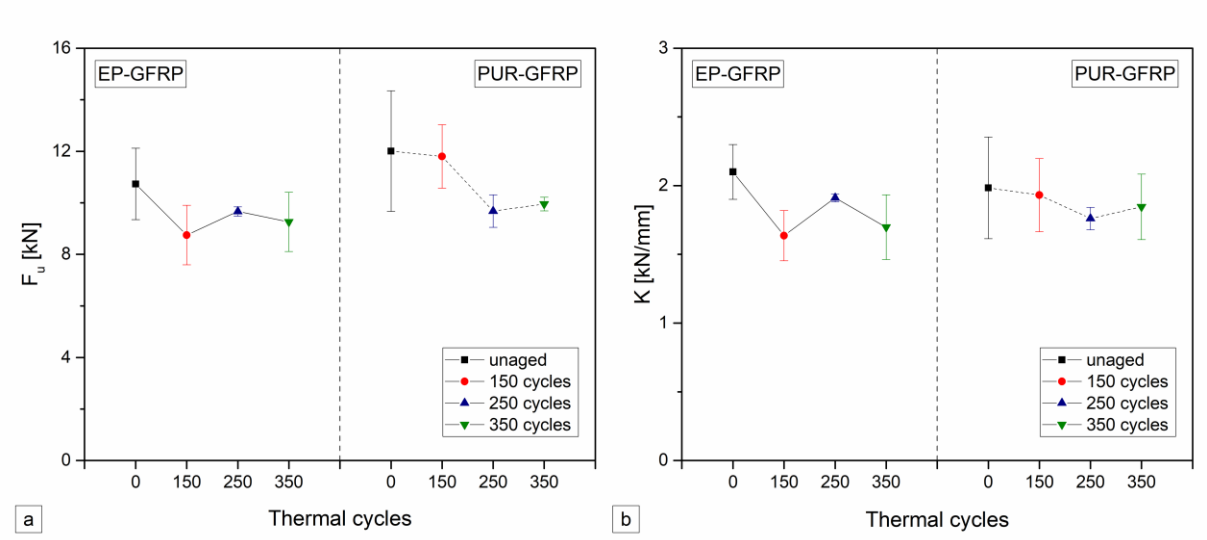

Figure 11.6. Effects of thermal cycles on: (a) failure load, and (b) stiffness (average value ± standard deviation).

Considering the unaged bonded joints, PUR-GFRP specimens presented higher ultimate load (12%) and elongation at failure (16%) and lower overall stiffness (6%) when compared to the EP-GFRP specimens. The lower stiffness of PUR-GFRP joints should stem from the lower shear modulus of the polyurethane adhesive, compared to the epoxy one (*cf.* Table 10.1). Taking into account the failure modes observed (*cf.* Section 11.3.2), the higher ultimate load obtained with the PUR-GFRP joints can be due to the lower stress peaks in the GFRP adherends at the overlap ends provided by the softer polyurethane adhesive.

Thermal cycles caused detrimental effects in the mechanical response of the bonded joints made of both adhesives, in terms of average failure load, stiffness and elongation at failure. In general, for both types of joint specimens, the average failure load and stiffness followed the same overall trends throughout the number of thermal cycles; as discussed below, the main differences are related with the magnitude of the initial performance reduction.

Regarding the EP-GFRP specimens, detrimental effects in the joint behaviour due to thermal cycles were maximum after 150 cycles: 18% and 22% in F_u and K, respectively. Between 150 and 250 cycles, both properties even presented some limited increase. This effect should be associated to the occurrence of post-cure phenomena during the cycles at higher temperature that is known to occur in both the GFRP [11.26, 11.27] and the adhesive [11.28, 11.29], which competed against

the degradation effects caused by the temperature variations *per se*. However, these effects are expected to have more influence in the epoxy (and polyurethane) adhesive than in the GFRP adherends; in fact, in a previous study on pultruded GFRP profiles where similar thermal cycles were used, insignificant viscoelastic and T_g changes were obtained, as well as very limited reduction of mechanical properties [11.23]. The reductions of average bond strength and stiffness experienced by the EP-GFRP specimens after 350 cycles were similar to those obtained after 150 cycles. Stazi *et al.* [11.7] reported a similar effect of post-curing in EP bonded adhesive joints subjected to thermal and moisture variations; however, this effect seemed to affect only the ultimate load of the joints, as their stiffness was much more severely affected, with reductions close to 70% for both epoxy adhesives. Lopez-Anido *et al.* [11.20] reported harsher effects on epoxy-GFRP bonded joints (compared to the present chapter) with an average reduction of 43% of the average bond strength. This discrepancy should be related to the combined effects of water immersion, thermal cycling, and freeze-thaw, that the specimens were subjected to and also the higher temperature amplitude used in the thermal cycles.

In what concerns the PUR-GFRP specimens, unlike the ones bonded with EP adhesive, after 150 thermal cycles they presented negligible changes in joint strength and stiffness. This much more limited reduction of performance may be attributed to a higher level of curing attained during the first thermal cycles underwent by the PUR adhesive; in other words, it is likely that the procedure used to condition the joint specimens prior to the thermal cycles was more effective in the epoxy adhesive, which is consistent with its higher T_g. In this case, the maximum reduction in joint performance was observed after 250 thermal cycles, with reductions of 19% and 11% in F_u and K, respectively. Afterwards, from 250 to 350 cycles, both properties exhibited some slight increase, that could be attributed to the same phenomena mentioned above for the EP-GFRP joints. Stazi *et al.* [11.7] reported quite different results on PUR bonded specimens: very significant stiffness reduction (77%) and a significant increase in the ultimate load (35%). These very considerable differences to our results should stem from the much higher temperatures (-40 to 70 °C) and relative humidity used in those experiments.

Comparing the EP-GFRP and PUR-GFRP specimens tested in the present chapter, although thermal cycles seemed to have affected the epoxy bonded joints at an earlier stage, similar maximum and final reductions of F_u were obtained. In terms of stiffness, the PUR-GFRP specimens showed better overall performance, with significantly lower maximum and final reductions than the EP-GFRP joints; this better performance of the PUR-GFRP specimens should be due to post-curing effects in the PUR adhesive and their influence in the adhesive shear modulus and hence in the joint stiffness.

11.3.2 Failure modes

For both adhesives, and regardless of the exposure to thermal cycles, the failure mechanism involved the initiation and very fast propagation of a crack at the extremity of one of the GFRP adherends, next to or at the interface (*cf.* Figures 11.5 (b) to Figure 11.5 (d)). The crack propagation occurred along the interface, until one preferential plane completely debonded, typically the side where the first cracks initiated. It is worth mentioning that due to the geometry of the bonded joint specimens, the eccentricity of the load path (not possible to fully prevent with the end tabs) leads to the development of a combination of shear and peeling (out-of-plane tensile) stresses at the extremities of the overlaps; these concomitant stress peaks were the cause of crack initiation and propagation.

After testing, the specimens were carefully assessed and the following three types of failure modes were observed, classified according to ASTM D5573 standard [11.30]: adhesive failure, light fibre tear failure, and fibre tear failure (Figure 11.7). The fibre tear failure modes occurred in the outer fibre-mat region. No cohesive failure modes were observed.

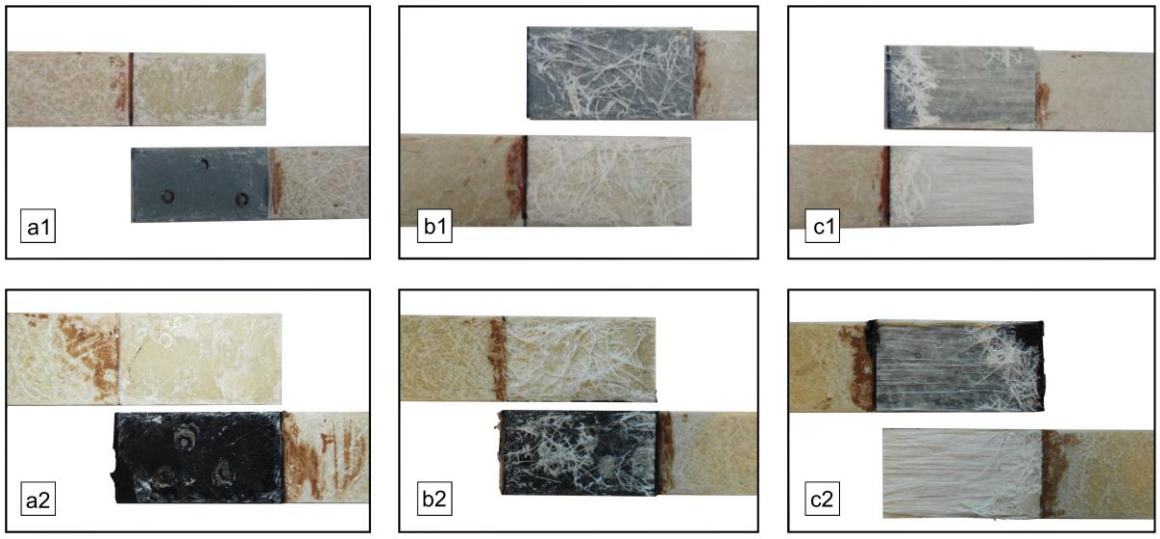

Figure 11.7. Failure modes of (1) EP-GFRP and (2) PUR-GFRP joints: (a) adhesive failure, (b) light fibre tear failure, and (c) fibre tear failure.

The majority of EP-GFRP and PUR-GFRP joint specimens presented mixed failure modes, *i.e.*, each specimen exhibited more than one type of failure throughout the bonded area. Figure 11.8 depicts the average percentage of bonded area where each failure mode was observed, for both adhesives and for all exposure periods.

After the different thermal cycles experienced by the test specimens, the dominant failure modes were light fibre tear and fibre tear, which together (considering all specimens tested)

corresponded to around 80-90% of the cases. Overall, this figure reflects an effective adhesion and good material compatibility between the adhesives and the GFRP adherends for both types of joints. The only series where such an effective adhesion did not prevail was the one of the unaged PUR-GFRP specimens, where adhesive failure occurred in almost half of the specimens' bonded area.

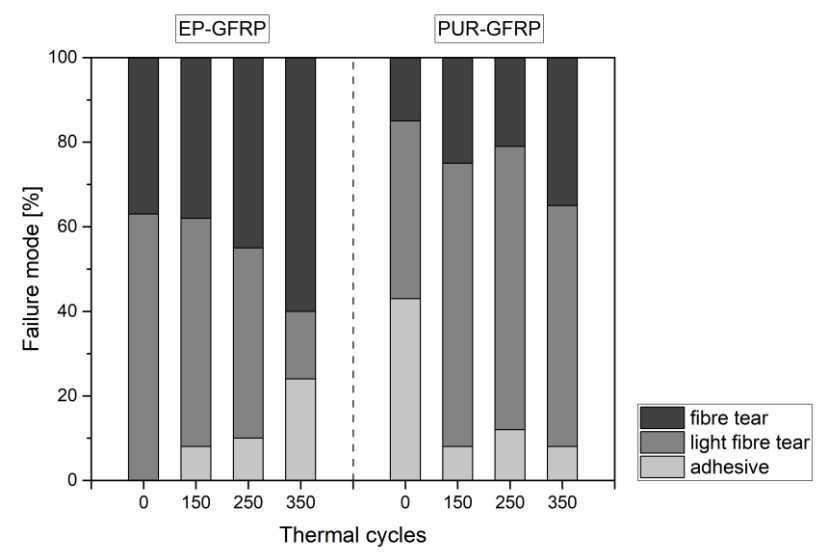

Figure 11.8. Average percentage of bonded area where each failure mode was observed, for both adhesives and for all exposure periods.

In general, the exposure to thermal cycles did not affect the types of failure modes identified in the joint specimens, but affected the relative frequency of their occurrence. In this respect, two distinct trends can be noticed when assessing the behaviour of both types of joints.

For the EP-GFRP joints the adhesive failure became more frequent (as well as the fibre tear failure), with a relative frequency of 24% after 350 cycles; this figure indicates that the exposure to the thermal cycles negatively affected the adhesion between the EP adhesive and the GFRP adherends. A similar trend was also noted by Stazi *et al.* [11.7] for epoxy adhesives, where the frequency of adhesive failure increased very considerably (much more than in the present chapter), which should be attributed to the already referred harsher ageing conditions. Lopez-Anido *et al.* [11.20] reported different changes in the failure modes of epoxy joints exposed to freeze-thaw cycling, which progressed from predominantly adhesive to a combination of adhesive and cohesive failure.

For the PUR-GFRP joints, the adhesive failure mode became progressively less frequent at the expense of more frequent light fibre tear and fibre tear modes; in fact, the relative frequency of the former mode decreased from 43% (unaged specimens) to 8% after 350 cycles. The better

performance of the PUR-GFRP bonded joint specimens could be attributed to (i) the above-mentioned post-curing effects, which must have been more relevant in the PUR adhesive than in the EP one, and (ii) the lower shear modulus of PUR, which was able to accommodate more easily the relative deformations imposed by the thermal cycles.

11.4.Numerical Study

11.4.1 Description of the finite element model

Three-dimensional (3D) FE models of the single lap joints described in the previous section were developed using the commercial package *ABAQUS* in order to assess the magnitude of the internal stresses developed in the materials during the thermal cycles, and thus obtain a better understanding of the effects caused by those thermal variations. It is worth mentioning that the models only simulated the elastic response of the joints during the thermal exposure - no damage or failure initiation and propagation criteria were considered for the constituent materials and interfaces. The following paragraphs provide a brief description of the models and of the main assumptions considered.

The 3D FE models simulated the complete geometry of the bonded joints, including the fillets, which were modelled as manufactured (radius of 1 mm, *cf.* Figure 11.1). For the GFRP laminates, 8-node solid elements with reduced integration (C3D8R) were used (maximum size of 1 mm). The adhesive layer was modelled using the same element type (maximum size of 0.2 mm through-thickness and 0.5 mm in the remaining directions), with the exception of the fillets, where 20-node solid elements (C3D20) were adopted; the mesh was refined around the fillets, where stress variations were expected to increase. Figure 11.9 shows an overall view of the FE mesh adopted, as well as a detailed view of the volume around one of the fillets. A perfect bond between the adhesives and the adherends was assumed.

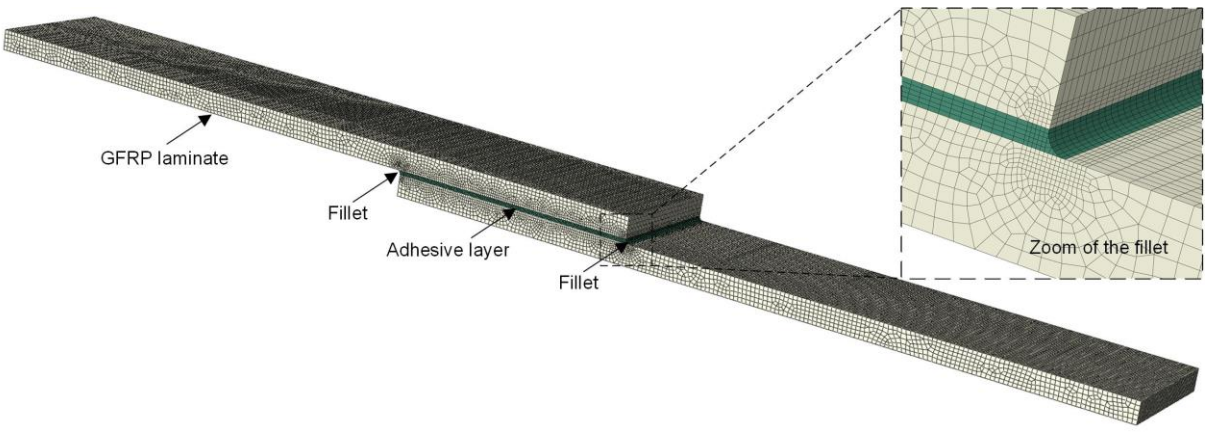

Figure 11.9. Overall view of the FE mesh and detailed view of the fillet.

The GFRP material was modelled as orthotropic accounting for the elastic properties derived from experimental characterization tests performed at ambient temperature, most of them summarized in Table 10.1; a Poisson ratio of 0.27 was used for the in-plane direction, whereas a value of 0.11 was assumed in the other planes, based on [11.31]. With the exception of the shear modulus, all elastic properties of the GFRP material were considered to be temperature-independent – for the temperature range adopted in the thermal cycles (from -5 °C to 40 °C) the variations reported in the literature are low; for the shear modulus a reduction of 15% at 40 °C (when compared to that at ambient temperature) was assumed based on different experimental tests [11.32]; for temperatures below 20 °C, that property was considered unaffected. Regarding the CTE, the following values (temperature-independent) were used for the longitudinal (α_{long}) and transverse (α_{trans}) directions of the GFRP laminates, $\alpha_{long} = 6.7\times10^{-6}$ and $\alpha_{trans} = 22.0\times10^{-6}$, according to the values reported in the literature [11.31, 11.33].

Both adhesives were modelled as isotropic materials, with their elastic properties at ambient temperature also derived from the material characterization tests (*cf.* Table 10.1). Due to lack of information in the literature regarding the temperature dependence of these properties (and also due to a wide variety of adhesive formulations available in the construction industry), it was assumed that both the tensile and shear modulus followed the variation with temperature of the storage modulus curves obtained from DMA tests (*cf.* Table 11.2). It is worth mentioning that for the epoxy adhesive, the properties for temperatures lower than 25 °C were extrapolated from the storage modules curve (as mentioned in Chapter 8, the DMA tests on this adhesive were performed from 25 °C to 150 °C). For the CTE of the epoxy adhesive, a value of $\alpha_{EP} = 26.0\times10^{-6}$ /°C (constant with temperature) was considered according to the experimental tests performed by Klamer [11.34] on a similar adhesive (from the same manufacturer). For the polyurethane adhesive, due the high variability of the CTE reported in the literature (*e.g.* [11.35]), two different values were considered (both constant with temperature): $\alpha_{PUR} = 40\times10^{-6}$ /°C and $\alpha_{PUR} = 240\times10^{-6}$ /°C; this wide range of CTE corresponds to the lower and higher values reported by polyurethane manufacturers [11.36], and, consequently will allow to define a range of the thermal stresses that are expected to be developed in these joints. All the above-mentioned material properties were assumed as time-independent; with this simplification, the possible cumulative effect of the residual thermal stresses was not simulated.

For simulating the stresses developed during a thermal cycle, the numerical analysis comprised two main steps, in which, the following temperature variations were uniformly[13] imposed to the specimens' models: (i) from ambient temperature (20 °C) to -5 °C, to simulate the first cooling phase; and (ii) from -5 °C to 40 °C, corresponding to the heating phase of the thermal cycle (*cf.* Figure 11.2).

Table 11.2. Material properties of the adhesives considered in the FE models.

Adhesive	$\mathbf{E_{t,T}/E_{t,20\,°C}}$ **and** $\mathbf{G_T/G_{20\,°C}}$			**CTE** $[\times 10^6]$
	-5 °C	**20 °C**	**40 °C**	
Epoxy	1.12	1.0	0.94	2.6
Polyurethane	1.43	1.0	0.23	40 or 240

Note 1: $E_{t,20\,°C}$ and $G_{20\,°C}$ are the tensile modulus and shear modulus at ambient temperature (Table 10.1);
Note 2: $E_{t,T}$ and G_T are the tensile modulus and shear modulus at the temperature T.

11.4.2 Numerical results

The development of the thermal stresses was investigated along the two paths depicted in Figure 11.10, both located at the central line of the specimen and aligned with their longitudinal direction: Path A was set in the adhesive at a depth of 0.5 mm and intercepts the entire bond length (including the fillets at that depth); path B is located at a depth of 0.5 mm within the GFRP laminates. The positioning of these paths was defined based on the most frequent failure surfaces observed in the single lap shear tests (*cf.* Section 11.3.2).

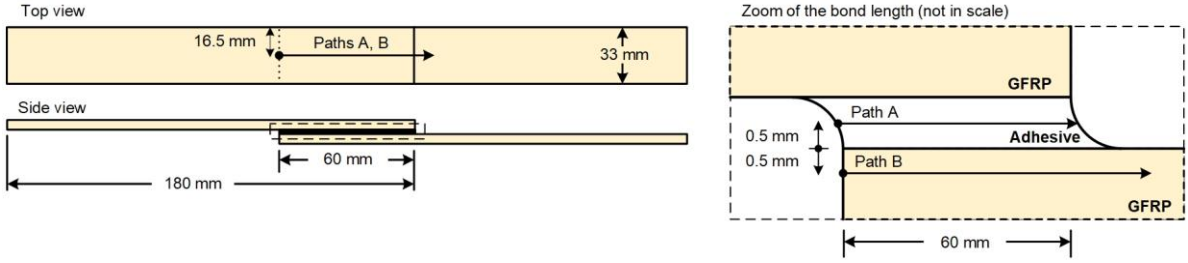

Figure 11.10. Location of the investigated paths in the FE models.

Figure 11.11 shows the calculated normal (Figure 11.11 (a)) and shear stresses (Figure 11.11 (b)) obtained for the EP-GFRP joints at the end of the above mentioned steps, *i.e.*, at -5 °C and at 40 °C. Analogous results for the PUR-GFRP specimens are shown in Figures 11.12 and 11.13, where the influence of the CTE of the polyurethane adhesive

[13] Due to the relatively low thickness of the specimens and the low heating and cooling ratios during the thermal cycles (+0.38 ºC/min and -0.38 ºC/min, respectively), a uniform temperature distribution was assumed.

($\alpha_{PUR} = 40\times10^{-6}$ *vs.* $\alpha_{PUR} = 240\times10^{-6}$) can be evaluated; it is worth reminding that due to the uncertainty about the CTE of the PUR adhesive, these figures depict the lower (for $\alpha_{PUR} = 40\times10^{-6}$) and upper (for $\alpha_{PUR} = 240\times10^{-6}$) limits of the thermal stresses that are expected to develop in these joints.

Regarding the normal stresses in the adhesive at -5 °C (*cf.* path A in Figure 11.11 (a) and Figure 11.12), a symmetric profile was obtained for both joints, increasing from the beginning of the path towards a flat plateau and then decreasing to zero at its end (at around 60 mm, which corresponds to the end of the overlap). At 40 °C, a similar profile was obtained, but with negative normal stresses (*i.e.* compression) and, as expected, presenting a lower magnitude than that of at -5 °C, due to the stiffness reduction (softening) underwent by the adhesive.

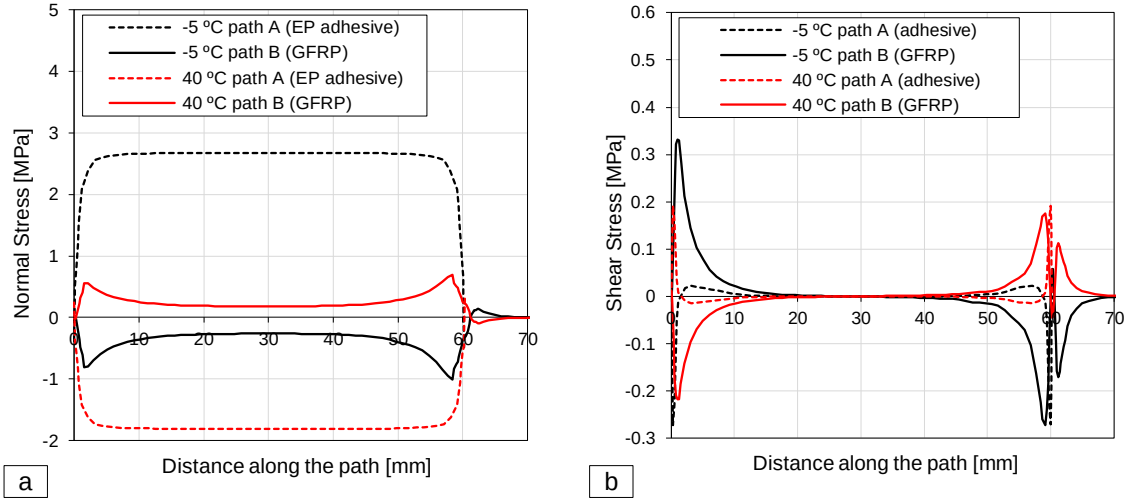

Figure 11.11. Numerical thermal stresses along the paths in the EP-GFRP joints: (a) normal stresses, (b) shear stresses.

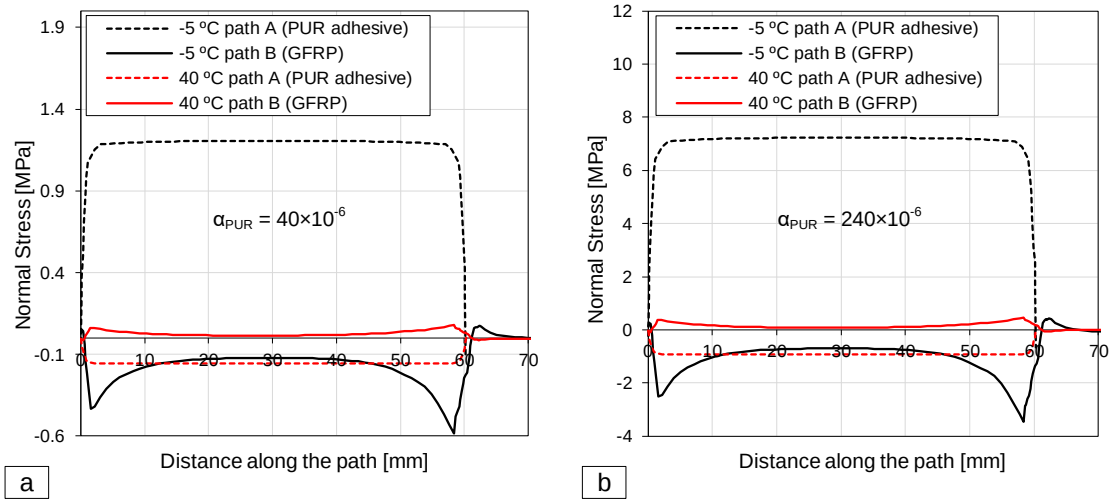

Figure 11.12. Numerical thermal stresses along the paths in the PUR-GFRP joints: (a) normal stresses for $\alpha_{PUR} = 40\times10^{-6}$; (b) normal stresses for $\alpha_{PUR} = 240\times10^{-6}$.

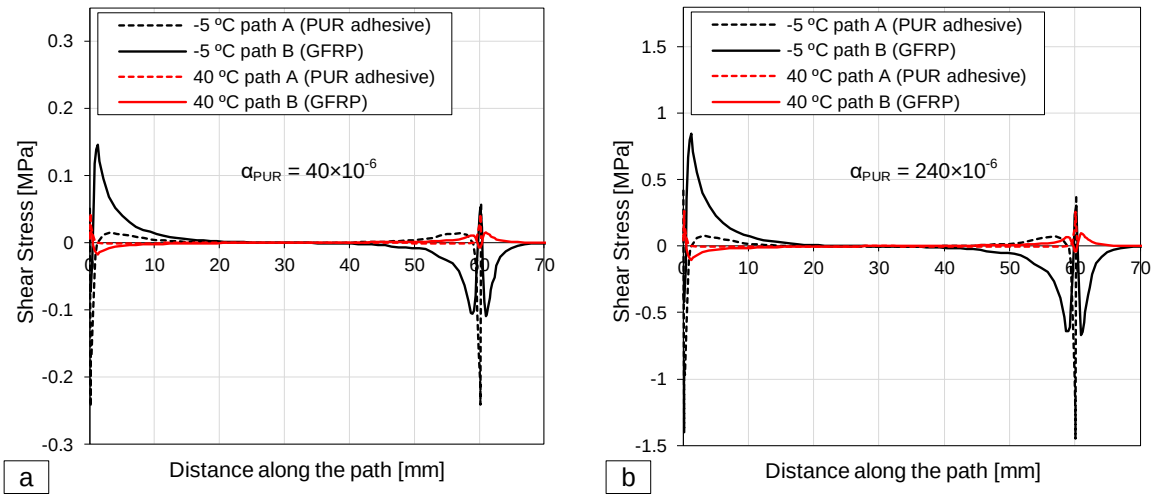

Figure 11.13. Numerical thermal stresses along the paths in the PUR-GFRP joints: (a) shear stresses for $\alpha_{PUR} = 40\times10^{-6}$; (b) shear stresses for $\alpha_{PUR} = 240\times10^{-6}$.

The normal stresses in the GFRP (*cf.* path B in Figure 11.11 (a) and Figure 11.12) exhibit opposite signs in both steps (*i.e.* compression at -5 °C and tension at 40 °C) and a different profile – a first peak at the beginning of the overlap, followed by a gradual stress reduction (in absolute value) towards a plateau at the middle of the overlap and a second (and higher) peak at the end of the joint. These results show that for the thermal variations used in the present chapter, the magnitude of the normal stresses developed in the materials are very low (when compared to the mechanical properties listed in Table 10.1): for the EP-GFRP joints, 2.7 MPa[14] in the EP adhesive and -1.0 MPa in the GFRP adherend; for the PUR-GFRP joints, from 1.2 MPa ($\alpha_{PUR} = 40\times10^{6}$) to 7.2 MPa ($\alpha_{PUR} = 240\times10^{-6}$) in the PUR adhesive and from -0.6 MPa ($\alpha_{PUR} = 40\times10^{-6}$) to -3.4 MPa ($\alpha_{PUR} = 240\times10^{-6}$) in the GFRP adherend.

The shear stresses plotted in Figure 11.11 (a) and Figure 11.13 exhibit a similar qualitative development along the bond length for both adhesives and GFRP adherend – very pronounced and opposite peaks at the extremities of the overlap (*i.e.* at 0 mm and around 60 mm) and negligible stresses at the middle portion of the joint (specially between 20 mm and 40 mm). As for the normal stresses, the magnitude of the shear stresses developed in the materials are very low: for the EP-GFRP joints, -0.3 MPa[15] in the EP adhesive and 0.3 MPa in the GFRP

[14] This stress level corresponds to only 15% of the expected tensile strength of the epoxy adhesive at 40 ºC (in a recent experimental study [52], the tensile strength of a similar epoxy adhesive was reduced by 40% at that temperature).

[15] This stress level corresponds to only 2% of the expected shear strength of the epoxy adhesive at 40 ºC (in a recent experimental study [52], the shear strength of a similar epoxy adhesive was reduced by 30% at that temperature).

adherend; for the PUR-GFRP joints, from -0.2 MPa ($\alpha_{PUR} = 40\times10^{-6}$) to -1.4 MPa ($\alpha_{PUR} = 240\times10^{-6}$) in the PUR adhesive and from 0.1 MPa ($\alpha_{PUR} = 40\times10^{-6}$) to 0.8 MPa ($\alpha_{PUR} = 240\times10^{-6}$) in the GFRP adherend.

These numerical results, in particular the relatively low magnitude of the thermal stresses, seem to indicate that, for the joint geometry and materials considered, the variations of bond strength after thermal cycles should be mainly related to the detrimental effects on the mechanical properties of the materials (especially the adhesives) and interfaces, and not to the severity of the stresses developed due to CTE mismatch between the adhesives and the GFRP adherends. As pointed out by Humfeld and Dillard [11.21], additional detrimental effects may stem from (thermal) stress fatigue, not considered in the present numerical study.

11.5. Concluding remarks

This chapter presented experimental and numerical investigations about the effects of thermal cycles typical of mild climates on the mechanical behaviour of lap joints between pultruded GFRP adherends and two structural adhesives. Based on the results obtained, the following main conclusions are drawn:

1. Thermal cycles had detrimental effects in the mechanical response of both EP-GFRP and PUR-GFRP bonded joints, causing low to moderate reduction of their average failure load and stiffness. For the conditions used in the present chapter, the magnitude of the strength reduction of the bonded joints between pultruded GFRP adherends due to thermal cycles seems to be compatible with their use in civil engineering structures.

2. The maximum performance reduction of EP-GFRP joints occurred after 150 thermal cycles, when the ultimate load and stiffness decreased by 18% and 22%, respectively. Little changes occurred with additional thermal cycles, which was partly attributed to the occurrence of post-cure phenomena in the EP adhesive during exposure at higher temperatures.

3. The PUR-GFRP specimens only showed signs of degradation after 250 cycles, when the ultimate load and stiffness were reduced by 19% and 11%, respectively, which were the maximum performance reductions registered in the experiments. The delayed performance reduction compared to EP-GFRP joints was attributed to a higher level of post-curing during the first thermal cycles in the PUR adhesive, whose T_g is much lower than that of the EP adhesive.

4. In spite of the significant differences between EP and PUR adhesives properties, the mechanical behaviour of both types of joints presented the same overall trends with increasing number of cycles, with maximum performance reductions of the same order of magnitude: maximum decreases in load capacity were fairly similar; in terms of stiffness, the PUR adhesive seemed to be less susceptible to degradation, which was also attributed to a higher level of post-curing during thermal ageing.

5. Thermal cycles also influenced the failure modes of the bonded joints and such influence depended on the type of adhesive: in EP-GFRP specimens, adhesive failure progressively became more frequent (from 0% in unaged specimens to 24% after 350 cycles), highlighting the detrimental effects of thermal cycles on the adhesion between EP and the GFRP adherends; on the other hand, in the PUR-GFRP specimens, the prevalence of adhesive failure decreased from 40% (unaged specimens) to 8% (after 350 cycles). The higher degree of post-cure experienced by the PUR adhesive together with its lower shear modulus and T_g (allowing more polymer chain mobility at the lower temperature cycles) may have contributed to the improved adhesion performance of the PUR-GFRP bond.

6. The numerical results showed that the stresses developed during the thermal cycles due to CTE mismatch between the adhesive and the adherends are of relatively low magnitude – this may indicate that the variations on bond behaviour of the joints observed in the single lap shear tests are mainly related to the effects of the thermal cycles on the mechanical properties of the materials (especially the adhesives, and including also competing post-curing phenomena) and interfaces (namely, for EP-GFRP joints), and not to the severity of the thermal stresses.

11.6. References

[11.1] Keller T, De Castro J. System ductility and redundancy of FRP beam structures with ductile adhesive joints. Compos Part B Eng 2005;36:586–96.

[11.2] Keller T, Vallée T. Adhesively bonded lap joints from pultruded GFRP profiles. Part I: Stress-strain analysis and failure modes. Compos Part B - Eng 2005;36:331–40.

[11.3] Keller T, Theodorou NA, Vassilopoulos AP, Castro J De. Effect of natural weathering on durability of pultruded glass fiber–reinforced bridge and building structures. J Compos Constr 2015;20:1–9.

[11.4] Gonilha JA, Barros J, Correia JR, Sena-Cruz J, Branco FA, Ramos LF, et al. Static, dynamic and creep behaviour of a full-scale GFRP-SFRSCC hybrid footbridge. Compos Struct 2014;118:496–509.

[11.5] Castro J de, Keller T. Design of robust and ductile FRP structures incorporating ductile adhesive joints. Compos Part B Eng 2010;41:148–56.

[11.6] Lee SW, Hong KJ, Park S. Current and future applications of glass-fibre reinforced polymer decks in Korea. Struct Eng Int 2010;20:405–8.

[11.7] Stazi F, Giampaoli M, Rossi M, Munafò P. Environmental ageing on GFRP pultruded joints: Comparison between different adhesives. Compos Struct 2015;133:404–14.

[11.8] Mays GC, Hutchinson AR. Adhesives in Civil Engineering. Cambridge University Press; 2005.

[11.9] Hu P, Han X, Da Silva LFM, Li WD. Strength prediction of adhesively bonded joints under cyclic thermal loading using a cohesive zone model. Int J Adhes Adhes 2013;41:6–15.

[11.10] Li H, Xian G, Lin Q, Zhang H. Freeze-thaw resistance of unidirectional-fiber-reinforced epoxy composites. J Appl Polym Sci 2012;123:3781–8.

[11.11] Marques EAS, da Silva LFM, Banea MD, Carbas RJC. Adhesive joints for low- and high-temperature use: An overview. J Adhes 2015;91:556–85.

[11.12] Grabovac I, Mestan SA, Morris CEM. The effect of freeze–thaw cycling on some structural film adhesives. J Appl Polym Sci 1984;29:4407–10.

[11.13] Heshmati M, Haghani R, Al-Emrani M. Environmental durability of adhesively bonded FRP/steel joints in civil engineering applications: State of the art. Compos Part B Eng 2015;81:259–75.

[11.14] Grammatikos SA, Jones RG, Evernden M, Correia JR. Thermal cycling effects on the durability of a pultruded GFRP material for off-shore civil engineering structures. Compos Struct 2016;153:297–310.

[11.15] Humfeld RG, Dillard DA. Residual stress development in adhesive joints subjected to thermal cycling. J Adhes 1998;65:277–306.

[11.16] Zhang Y, Vassilopoulos AP, Keller T. Environmental effects on fatigue behavior of adhesively-bonded pultruded structural joints. Compos Sci Technol 2009;69:1022–8.

[11.17] Green MF, Bisby LA, Beaudoin Y, Labossière P. Effect of freeze-thaw cycles on the bond durability between fibre reinforced polymer plate reinforcement and concrete. Can J Civ Eng 2000;27:949–59.

[11.18] Giampaoli M, Terlizzi V, Rossi M, Chiappini G, Munafò P. Mechanical performances of GFRP-steel specimens bonded with different epoxy adhesives, before and after the aging treatments. Compos Struct 2017;171:145–57.

[11.19] Heshmati M, Haghani R, Al-Emrani M. Durability of bonded FRP-to-steel joints: Effects of moisture, de-icing salt solution, temperature and FRP type. Compos Part B Eng 2017;119:153–67.

[11.20] Lopez-Anido R, Michael AP, Sandford TC. Freeze-thaw resistance of fiber-reinforced polymer composites adhesive bonds with underwater curing epoxy. J Mater Civ Eng 2004;16:283–6.

[11.21] Turvey GJ. 13 - Testing of pultruded glass fibre-reinforced polymer (GFRP) composite materials and structures. Woodhead Publ. Ser. Civ. Struct. Eng., 2013, p. 440–508.

[11.22] Karbhari VM, Chin JW, Hunston D, Benmokrane B, Jusja T, Morgan R, et al. Durability gap analysis for fiber-reinforced polymer composites in civil infrastructure. J Compos Constr 2003;7:238–47.

[11.23] Sousa JM, Correia JR, Cabral-Fonseca S, Diogo AC. Effects of thermal cycles on the mechanical response of pultruded GFRP profiles used in civil engineering applications. Compos Struct 2014;116:720–31.

[11.24] ASTM D 1002. Standard Test Method for apparent shear strength of single-lap joint adhesively bonded metal specimens by tension loading (metal-to-metal). Am Soc Test Mater 2004.

[11.25] ASTM D 5868. Standard test method for lap shear adhesion for fiber reinforced plastic (FRP) bonding. Am Soc Test Mater 2008.

[11.26] Grammatikos SA, Evernden M, Mitchels J, Zafari B, Mottram JT, Papanicolaou GC. On the response to hygrothermal aging of pultruded FRPs used in the civil engineering sector. Mater Des 2016;96:283–95.

[11.27] Sousa JM, Correia JR, Cabral-Fonseca S. Durability of glass fibre reinforced polymer pultruded profiles: comparison between QUV accelerated exposure and natural weathering in a Mediterranean climate. Exp Tech 2013;40:207–19.

[11.28] Savvilotidou M, Vassilopoulos AP, Frigione M, Keller T. Effects of aging in dry environment on physical and mechanical properties of a cold-curing structural epoxy adhesive for bridge construction. Constr Build Mater 2017;140:552–61.

[11.29] Yang Q, Xian G, Karbhari VM. Hygrothermal Ageing of an Epoxy Adhesive Used in FRP Strengthening of Concrete. J Appl Polym Sci 2008;107:2607–17.

[11.30] ASTM D5573. Standard practice for classifying failure modes in fiber-reinforced-plastic (FRP). Am Soc Test Mater 2012:3–5.

[11.31] Bank LC. Composites for Construction: Structural design with FRP materials. 2006.

[11.32] Rosa IC, Morgado T, Correia JR, Firmo JP, Silvestre N. Shear behaviour of GFRP composite materials at elevated temperature. (accepted for publication). J Compos Constr 2018.

[11.33] Morgado T, Silvestre N, Correia JR. Simulation of fire resistance behaviour of pultruded GFRP beams – Part I: Models description and kinematic issues. Compos Struct 2018;187:269–80.

[11.34] Klamer E. Influence of temperature on concrete beams strengthened in flexure with CFRP. PhD thesis in Civil Engineering, Eindhoven University of Technology, Eindhoven, Netherlands, 2009.

[11.35] The Institution of Structural Engineers. Guide to The structural use of adhesives. London: 1999.

[11.36] BASF. Thermoplastic Polyurethane Elastomers – Elastollan – Material Properties. Thecnical data sheet. 2018.

Part V

Natural weathering performance of a GFRP structure

Preamble

The correlation between the effects of natural weathering on pultruded GFRP structures with the effects of artificial environmental laboratory ageing is not an easy task. The environmental aggression is not always easy to quantify and numerous parameters that present complex interactions may influence the material and structural behaviour. In this context, natural weathering studies are needed to understand in further depth the long-term behaviour of GFRP components used in civil engineering applications and to provide reliable results about the durability in real service conditions.

Part V of this thesis presents a comprehensive assessment of a GFRP structure subjected to natural weathering after 11 years in service conditions. The study comprised (i) a detailed visual inspection, as well as (ii) material and (iii) structural characterisation tests, of both unaged and aged components, in order to quantify and assess the performance of the pultruded GFRP material and structural components under natural ageing and service conditions.

Chapter 12.

Natural weathering of a GFRP structure: *SATU Oeiras*

12.1.Introduction

The need to increase the speed of construction in civil engineering applications and the durability problems presented by traditional building materials have fostered the development of new constructive solutions and the use of innovative structural materials. In addition, most international regulations reflect growing concerns with durability, setting increasing demands about the required service life for civil engineering structures [12.1].

In this context, in the construction of structures such as buildings or bridges, glass fibre reinforced polymer (GFRP) materials can have significant advantages when compared to traditional materials (steel or concrete), such as high mechanical strength, low specific weight, corrosion resistance and reduced maintenance requirements [12.2, 12.3]. Notwithstanding these advantages and the fact that there are already several GFRP constructions in service, in some cases installed several years ago, studies regarding their in-service performance are still limited today [12.4]. This way, it becomes crucial to identify and evaluate the anomalies and the degradation suffered by this type of materials and constructions.

Nowadays, pultruded GFRP profiles are being more commonly used as structural components in bridges and building [12.4]. As mentioned above, GFRPs are typically associated with high performance in terms of durability [12.5]. Nevertheless, the durability of GFRPs in a given environment depends heavily on the matrix type. Typically, in pultruded profiles used in structural applications, unsaturated polyester or vinylester matrices are used along with E-glass fibres, with epoxies matrices being used less frequently. The durability of this combination of materials will depend on the environmental conditions in which they are inserted and their harshness, with humidity, thermal cycles and ultraviolet (UV) radiation being three of the factors normally associated with degradation processes [12.6].

The degradation processes generally take place slowly. Thus, it may take several years or even decades for relevant degradation in structures to develop. This way, accelerated experimental tests are often used to simulate long-term degradation. However, the results of this type of approach are very dependent on the tests themselves and sometimes contradictory results are obtained [12.5]. Extrapolation of short-term results over longer periods (several decades) has

limitations, since a consistent and comprehensive correlation between accelerated artificial ageing and natural ageing has not yet been developed. The large number of parameters involved in natural ageing and their complex interactions makes it difficult to simulate and predict them. For example, Chapter 5 attempted to compare accelerated ageing of pultruded GFRP profiles exposed to UV radiation, temperature and humidity cycles (in a QUV chamber) for 3000 hours and 102 months of natural ageing in Lisbon. The results indicated that despite similar general behaviour, it was not possible to identify a clear and strong correlation between the two types of ageing.

These limitations reinforce the importance of studies about the effects of natural ageing on structures with GFRP components. However, very little information is still available at this level, as described in the following paragraphs.

Alampalli [12.7] performed load tests and a visual inspection of a FRP bridge after a period of 4 years of use in New York. The results of the load tests indicated that the structure showed good performance, with displacements and deformations lower than those foreseen in design. The author concluded that the design of the deck could have been optimised to guarantee a reduction of costs. With visual inspection, some delamination was observed at the bottom of the bridge deck and damage to the surface coating. Farhey [12.8] continuously monitored, for 4 years, a fully composite bridge in Ohio. The deformations monitored at various points of the bridge were satisfactory, not revealing degradation. In general, the structural behaviour over time was consistent and within the design parameters. No visible signs of degradation were observed on the exposed surfaces during the visual inspection. Reising *et al.* [12.9] compared the performances of four different FRP bridge deck panels after two years of monitoring, and reported satisfactory results, despite some delamination in the decks due to traffic. The authors also noted that pultruded decks had the most accurate panel dimensions and were less vulnerable to the occurrence of delamination.

All case studies described above included a too short period of observation to draw conclusions about the behaviour of the respective constructions during their entire service life.

Nishizaki *et al.* [12.10] carried out a study on the durability of pultruded GFRP slabs with three different laminate systems with variable percentage of longitudinal reinforcement fibres (12%, 26% and 43%). The authors measured differences in tensile performance of specimens removed from the plates at the end of 1 and 10 years of exposure to natural ageing in Tsukuba, Japan. After 10 years, the two systems with the lowest fibre content presented reductions of about 17% in tensile strength and increases of about 4% in the tensile modulus. On the other

hand, the specimens with higher percentage of longitudinal fibres presented increases in tensile strength and modulus of 7% and 29%, respectively. The changes after 1 year were not significant.

Klamer *et al.* [12.11] observed the effects on 13-year GFRP plates exposed to outdoor humidity and water conditions in Werkendam, the Netherlands. The authors characterised plates placed on a pontoon, submerged and above the water level. Not having specified the manufacturing process, the authors reported a relatively low fibre content compared to pultrusion. The plates that were exposed above water level, therefore not subject to degradation by direct contact with water, were the ones that presented less degradation. Nonetheless, except for interlaminar shear strength, all mechanical properties decreased after exposure. The tensile strength showed reductions between 16% and 33% for the plates above and below the water level, respectively. The tensile modulus showed smaller variations, between 7% and 10% for the same type of plates.

Keller *et al.* [12.4] evaluated the natural ageing in pultruded GFRP components of a building structure and a pedestrian bridge after 15 and 17 years of service, respectively. A detailed inspection (to both structures) was performed, accompanied by full-scale tests representative of in service conditions, and coupon tests for mechanical characterisation (for the bridge only). The bridge, located in Pontresina, is exposed to the aggressive environment of the Swiss Alps and the building (*Eyecatcher*) is situated in Basel, Switzerland. The authors observed that the mechanical performance of the bridge profiles was significantly affected by the combined presence of thermal cycling and strong UV radiation, especially in the profiles' upper flange - 32% (flange) and 17% (web) tensile strength reductions. Still, the tensile modulus showed small variations - 2% in the flanges and 5% in the web. UV radiation was also responsible for the appearance of fibre on the surface (fibre blooming). In the building structure, colour changes were identified near the bolted connections of the profiles, related to the increased sensitivity of these zones to water and humidity incorporation. In both structures, both serviceability and structural safety levels were not compromised, and should not become critical in the near future. Based on the results obtained, the authors recommended the use of surface protection systems in GFRP structures exposed to adverse environmental conditions.

In this Chapter, the durability of the GFRP components installed in a case study - *the Urban Automated Transportation System (SATU) in Oeiras, Portugal* - after 11 years of service is examined. The investigation included a detailed inspection of the structure and the analysis of the structural, mechanical, physical and aesthetic performance of the pultruded GFRP components, comparing it with that of unaged material and the performance after 7 years of

exposure, which had also been examined. In addition, some of the results obtained in the present study were also compared with those obtained in accelerated ageing tests presented in preceding chapters.

12.2.Description of building site and inspection of the structure

SATU Oeiras was an urban, unmanned passenger transportation system installed in the municipality of Oeiras, which linked the train station of *Paço de Arcos* to the *Oeiras Parque* Shopping Center. It was inaugurated in 2004 and shut down in 2015. The relevant components for this study are part of the substructure supporting the board of the railway viaduct. This sub-structure (Figure 12.1) allows pedestrian access to the top of the bridge deck and consists of different GFRP elements: (i) moulded GFRP gratings and two types of pultruded unsaturated polyester GFRP profiles, placed in the longitudinal (I100) and transverse directions (I150).

Figure 12.1. *SATU Oeiras* structure.

All material was supplied by the *Sociedade Técnica de Estruturas Pultrudidas* (STEP) and was produced by *Nantong Shirui* (grates) and *TOP GLASS* (profiles) companies. The connections between the profiles, grates and the concrete structure were made through steel bolted connections and GFRP angle profiles. A visual inspection of the GFRP components was carried out and 6 elements (3 beams of each typology, I100 and I150) were subsequently removed for structural characterisation and evaluation of the material properties, and replaced by new elements.

In February 2016, a visual inspection of the *SATU Oeiras* bridge deck was carried out, in particular the track closest to Paço de Arcos. This portion of the track is closer to the sea, and therefore more prone to be influenced by a marine environment. Some anomalies were detected in some of the GFRP elements, as illustrated in Figure 12.2.

Among the anomalies observed, the most prominent were superficial marks, mostly caused during the installation stage and the remaining from the use stage. Biological colonisation and corrosion of metallic bolting elements was also detected in some areas of the structure. Punctually, some stain marks and indentations were detected, and they were caused during the installation phase.

Figure 12.2. Anomalies: (a) surface marks; (b) biological colonisation and corrosion of metallic elements in the connections; (c) indentation in a transverse profile.

The loss of gloss and fibre blooming, which are frequent anomalies in GFRP structures [12.4], and can subsequently justify the need for additional maintenance operations, such as the use of appropriate coatings in the affected areas, were not detected during the inspections. The profiles were installed in the lower part of the deck, thus being protected from direct sun exposure (the main factor of degradation responsible for the appearance of these anomalies) by the gratings.

In general, the elements presented non-mechanical anomalies with little relevance and a good state of conservation. Therefore, only minor maintenance interventions should be required.

12.3.Characterisation of the GFRP beams structural behaviour

12.3.1 Tested elements

The structural characterisation of GFRP components included bending tests of pultruded beams with different I cross sections with nominal heights (H) of 100 mm (I100) and 150 mm (I150) and lengths (L) of 2.40 m (I100) and 3.60 m (I150). The dimensions of the cross sections of the six beams tested (3 per cross section) are shown in Table 12.1, where e is the thickness of the web, and B and t correspond respectively to the width and thickness of the flanges. The dimensions of the beams were measured using a manual measuring tape (in mm) and a Mitutoyo digital Caliper, model CD-15D, with resolution of 0.01 mm.

Table 12.1. Dimensions of the tested beams.

Beam	L [m]	H [mm]	e [mm]	Upper Flange		Lower Flange	
				B [mm]	t [mm]	B [mm]	t [mm]
I100-V1	2.41	100.52	6.16	50.08	6.77	50.02	6.83
I100-V2	2.43	100.69	6.21	50.14	6.73	50.23	6.89
I100-V3	2.45	100.11	6.30	50.04	6.96	50.04	6.78
I150-V1	3.68	149.72	9.10	75.33	8.36	75.45	8.54
I150-V2	3.73	150.14	8.39	75.00	8.62	74.97	8.76
I150-V3	3.68	150.22	8.09	75.34	8.15	75.19	8.15

12.3.2 Test methodology

Bending tests were performed in the two types of beams, monotonically until rupture, in accordance with Annex D of the EN 13706-2 [12.12] standard. The test setup is shown in Figure 12.3. The beams were simply supported at both ends (one of the supports allowing for longitudinal sliding) and subjected to a concentrated load, P, applied at mid-span using a hydraulic jack mounted on a closed metallic frame.

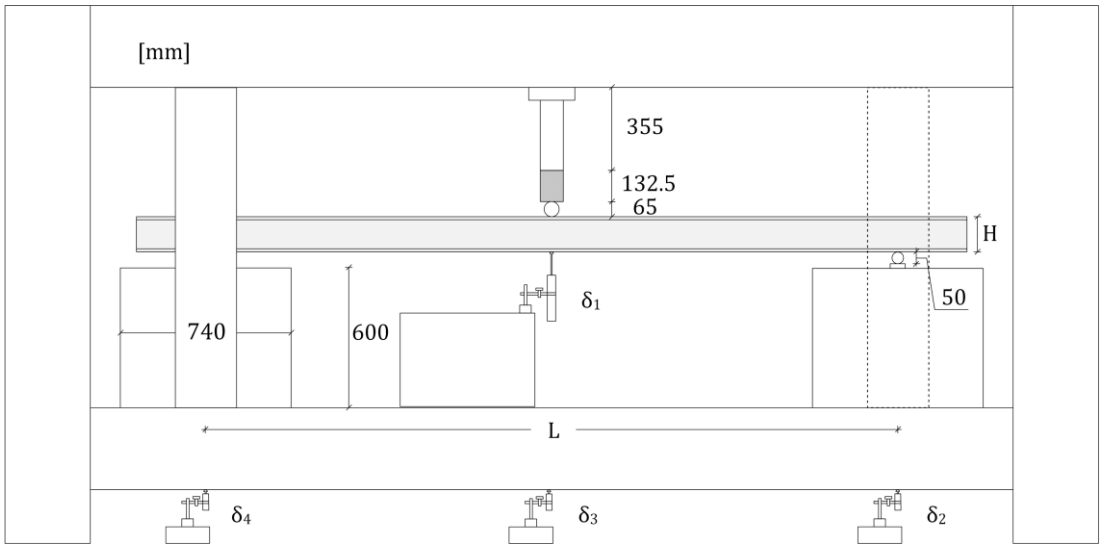

Figure 12.3. Representation of the test setup used for beams testing.

A bracing system was used in the support areas, comprising vertical elements that prevented lateral displacements and torsional rotations at the ends of the beams (*c.f.* Figure 12.3). This system was used to make these tests consistent and comparable with those conducted in the same type of beams in unaged conditions and 7 years after construction. The tests of the beams were carried out with control of the vertical displacement at midspan, s, until global failure of the beams. The average duration of the tests was about 6 minutes in the beams I150 and 4 minutes in the beams I100. The tests were performed using a *Novatech* load cell, with a capacity of 200 kN. For the application of the load, an *Enerpac* hydraulic jack, with 300 kN of capacity and 125 mm of stroke was used. Three displacement *TML* transducers with 10 mm of stroke

(to monitor possible deformations in the metallic frame) and another *TML* transducers with 100 mm of stroke (to measure the midspan displacements of the beams) were used. An *HBM* data acquisition system, model *Quantum X*, was used to gather the force and displacement values throughout the test.

The I150 beams were also subjected to the test indicated in Annex G of the aforementioned standard [12.12], which allowed determining the effective full-section flexural and shear moduli of the beams, assuming an equivalent isotropic behaviour of the GFRP material. This test, being non-destructive, was carried out prior to the rupture test. In accordance with this method, flexural tests were carried out on simply supported beam elements with variable span, where the force and the displacement were gathered at half span. Five spans were tested for each of the three I150 beams (1.20 m, 1.80 m, 2.40 m, 3.00 m, and 3.40 m), two of them longer and two of them shorter than the estimated critical span, for which the shear deformations correspond to 12% of the total deformation. Three cycles of loading/unloading were considered up to the standard displacement values [12.12].

12.3.3 Results and discussion

Figure 12.4 presents the results obtained from the variable span flexural tests according to Annex G of EN 13706-2 [12.12] and the cyclic test results obtained for beam I150-V1, when tested in a span of 1.20 m. Only beam I150-V1 is shown, as a representative beam, since the results were very similar for the other two beams.

The test comprised three cycles of loading and unloading each beam up until the suggested displacement values (within the linear elastic branch), as suggested by the standard. Note that an initial apparent non-linearity occurred due to accommodation of the test fixture, in the loading point and the supports; this toe region of the curves was not considered for calculation purposes. The values for the third cycle were used to determine the slope (P/s) in Figure 12.4 (b), which had a significantly high coefficient of correlation (R^2 was in the 0.99-1.00 range). These results allowed plotting Figure 12.4 (c) and (d), and thus determine the effective flexural and shear stiffness, according to [12.12]. The effective values obtained for each beam are listed in Table 12.2, which has a global summary of all test results.

After the variable span tests, all beams were subjected to monotonic tests until rupture. Figure 12.5 presents the applied force, P, as a function of the vertical displacement, s, obtained in those tests for the I100 and I150 beams.

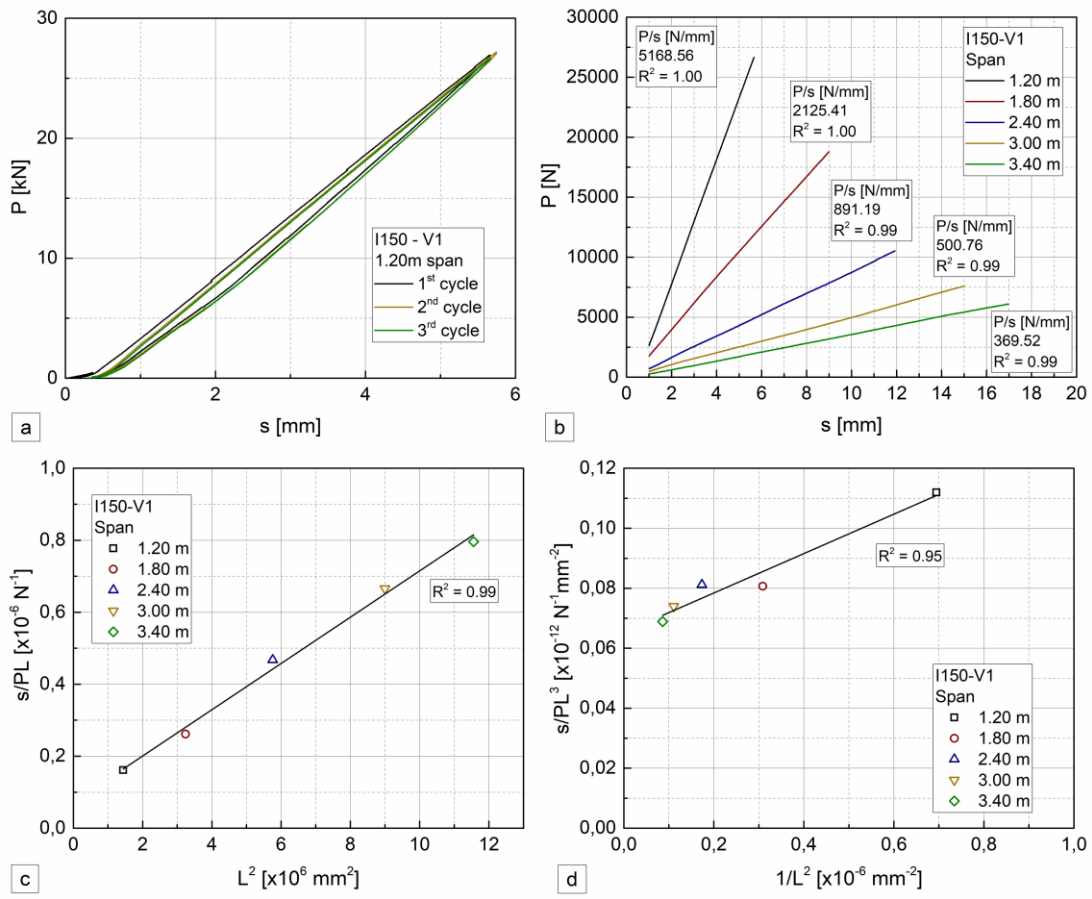

Figure 12.4. Variable span test for I150-V1 beam: (a) cyclic test for 1.20 m span, (b) third cycle considered for all spans, (c) s/PL *vs.* L^2, and (d) s/PL^3 *vs.* 1/L^2.

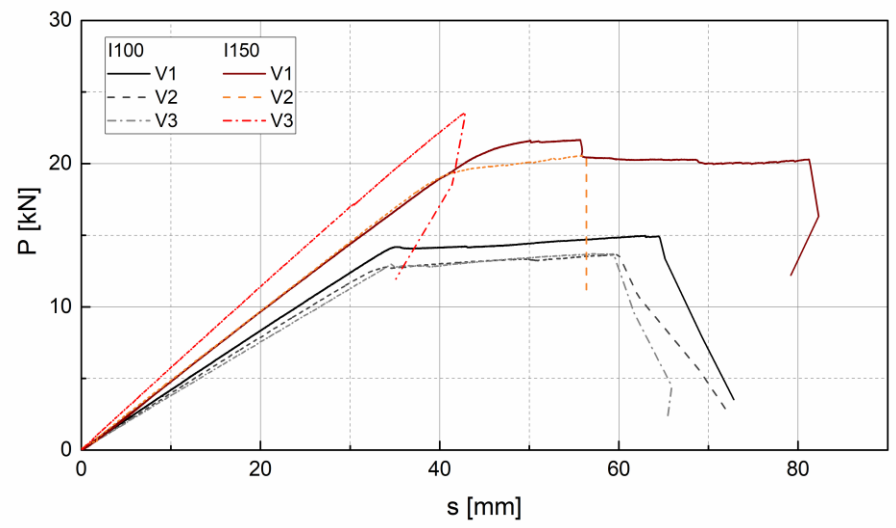

Figure 12.5. Loads *vs.* midspan deflection curves from flexural tests until rupture for both I150 and I100 beams.

The three I100 beams showed a similar behaviour until rupture, namely linear behaviour until the occurrence of lateral-torsional instability. The I100-V1 beam had a higher initial stiffness, and also a higher value of maximum strength when compared to the others. In this beam, it is

also interesting to note that a small reduction of force occurred for a displacement value of about 35 mm, before the occurrence of lateral instability; this corresponded to a small crushing in the load application zone.

The I150 beams displayed a similar overall behaviour, although beam I150-V3 was somehow stiffer and presented higher maximum force. Nevertheless, in terms of lateral instability, the three beams revealed slightly different behaviours. The beam I150-V3 did not present an approximately constant vertical displacement plateau, exhibiting a fragile rupture. On the other hand, in beam I150-V1 there was a relatively high vertical plateau due to the high rotations exhibited in the midspan section, while the beam I150-V2 showed an intermediate behaviour. It should also be noted that there was a marginal loss of force in beam I150-V1, which corresponded to the occurrence of cracking in the upper flange at a distance of about 35 cm from the midspan area.

Regarding the failure modes, depicted in Figure 12.6, the I100 beams failed by a lateral-torsional bending mechanism (*cf.* Figure 12.6 (a)). This instability mechanism involves high rotations in the central part of the beams, resulting from their lateral bending and torsion. The consequent high deformations caused crushing of the compressed upper flange, with interlaminar delamination occurring in these zones (in the three beams). In addition, the profile's web also presented cracking oriented at approximately 45° with the horizontal surface, at a distance of 22.5 cm to 32.5 cm from the load application point.

In the I150-V1 beam (Figure 12.6 (b)) it was possible to observe clearly that the high rotations in the midspan section, due to the lateral instability phenomenon, caused an eccentricity of the load application point, which resulted in a shear-related web-flange failure mode in the longitudinal direction at the same zone. The occurrence of cracks at half height of the upper flange caused by delamination was also observed. The beam I150-V2 exhibited a similar failure mode, albeit for smaller section rotations. The beam I150-V3 (Figure 12.6 (c)), did not seem to instabilise, and presented a failure mode by crushing of the compressed upper flange, causing cracking in the web-flange connection zone. Overall, the failure modes observed in the present tests were consistent with the results of tests performed previously on profiles of the same type [12.13].

Table 12.2 includes the main values obtained from the failure tests on the beams: the apparent flexural modulus of elasticity, E_{app}, the maximum load recorded, P_{max}, and the associated vertical displacement, d_{max}. In addition, the effective modulus of elasticity and distortion obtained from the variable span tests, E_{eff} and G_{eff}, respectively, are also presented.

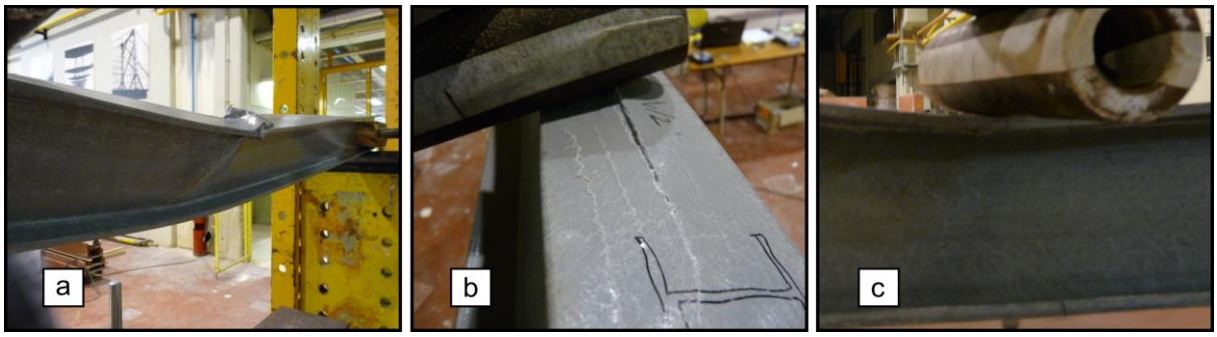

Figure 12.6. Failure modes: (a) I100 beams, (b) I150-V1/V2 beam, and (c) I150-V3 beam.

Table 12.2. Flexural test results for all beams.

Beam	**E_{app} [GPa]**	**P_{max} [kN]**	**d_{max} [mm]**	**E_{eff} [GPa]**	**G_{eff} [GPa]**
I100-V1	39.8	15.0	62.9		
I100-V2	37.9	13.7	59.9		
I100-V3	36.5	13.7	59.3		
I100-V_{avg}	38.0 ± 1.6	14.1 ± 0.7	60.7 ± 1.9		
I150-V1	35.6	21.7	55.1	39.7	3.0
I150-V2	34.8	20.6	59.7	37.9	3.9
I150-V3	43.3	23.6	42.8	43.4	3.5
I150-V_{avg}	37.9 ± 4.7	21.9 ± 1.5	52.5 ± 8.7	40.3 ± 2.8	3.5 ± 0.4

All values were calculated according to EN 13706-2 [12.12]. It should be noted that E_{app} corresponds to the value of the modulus of elasticity obtained from the slope of the force-displacement curve considering only the flexural deformability, plus a factor of 1.05, to consider, in a simplified way, the effect of shear deformability (as per the standard).

The analysis of the results obtained for the I100 beams shows that the values of the apparent flexural modulus presented a relatively low scatter (maximum coefficients of variation around 5%). The figures listed in the table reflect the above-mentioned difference in flexural behaviour presented by beam I100-V1 (compared to the other two of the same series), with higher values of maximum applied force and flexural stiffness.

In what concerns the beams I150, the values of apparent flexural stiffness showed a more significant dispersion; this should be due to beam I150-V3, which did not present lateral instability and presented higher stiffness values. As expected, the values obtained for the effective flexural modulus E_{eff} were slightly higher than those of the apparent flexural modulus (with the exception of beam I150-V3), such difference resulting from the methods used for the calculation of those parameters (Thimoshenko beam theory in the case of E_{eff} and Euler-Bernoulli beam theory in the case of E_{app}).

According to the results obtained and cross-referencing them with previously performed tests in similar profiles by Sá [12.14] and the structural department (NCE) of the Laboratório

Nacional de Engenharia Civil (LNEC) [12.13, 12.15], it was possible to analyse the change in the properties of these profiles over in-service time. These values are shown in Table 12.3 and Figure 12.7.

Table 12.3. Mechanical properties of the beams as a function of time.

Beam	**Property**	**Time**	**unaged**	**7 years**	**11 years**
		Ref.	NCE [12.13]	NCE [12.15]	-
I100	P_{max} [kN]		13.4 ± 0.6	13.8 ± 0.3	14.1 ± 0.7
	E_{app} [GPa]		33.2 ± 0.3	33.5 ± 0.5	38.1 ± 1.6
I150	P_{max} [kN]		16.3 ± 0.7	17.0 ± 1.2	21.9 ± 1.5
	E_{app} [GPa]		31.1 ± 1.4	33.9 ± 0.8	37.9 ± 4.7
		Ref.	Sá [12.14]		-
I150	E_{eff} [GPa]		32.4		40.3 ± 2.8
	G_{eff} [GPa]		2.3		3.5 ± 0.4

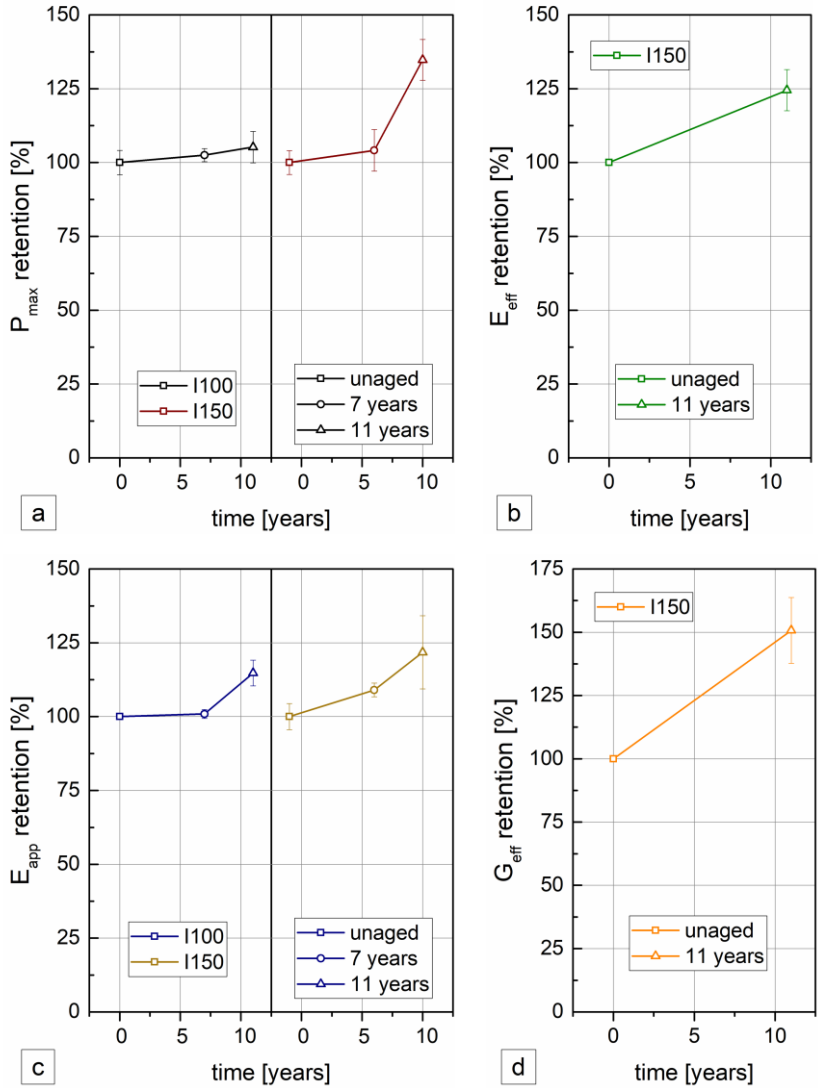

Figure 12.7. Property retention: (a) P_{max}, (b) E_{ff}, (c) E_{app}, and (d) G_{eff}, as a function of time.

By analysing the results listed in Table 12.3 and illustrated in Figures 12.7 it is possible to verify that the mechanical properties of both types of beams under analysis showed an overall good performance over 11 years of use in service conditions.

In fact, for the I100 beams there was an increasing trend in both monitored properties (P_{max} and E_{app}), which presented maximum values for the last period, and with the largest difference recorded in this last testing period, where values increased by 5% and 15%, respectively, w.r.t. the unaged values. Comparing the same properties for the I150 beams, one can see the same growing trend, but in a more expressive way. In this case, the variation observed for the values of P_{max} and E_{app} was 35% and 22%, respectively. The results of the effective flexural and shear stiffness, compared with the results obtained by Sá [12.14], also reflected the same growing trend, with increases of 25% and 50% for the E_{eff}, and G_{eff}, respectively.

This performance improvement should be associated to the occurrence of post-cure phenomena, due to the additional crosslinking suffered by the polymeric materials that constitute the matrix of these profiles, which has already been identified and discussed in Chapter 5, regarding natural ageing of GFRP profiles. Thus, these phenomena not only compete against the degradation effects on the composite material, but in this case, they even contributed to an increase in mechanical performance. These post-cure processes were also well identified in several investigations on materials similar to those tested in the present study [12.6]. It should also be noted that there was a greater scatter in the results obtained for longer service periods (11 years).

Keller *et al.* [12.4] also reported consistent results, concluding that the structural serviceability properties (especially the system stiffness) of the footbridge subjected to the harsh alpine climate was not affected after 17 years of use; this is in agreement with the overall results obtained in the present study.

12.4. Characterisation of the GFRP material properties

Samples with appropriate dimensions were cut from the webs of the I150 GFRP profiles using a water-cooled diamond saw, and were later subjected to mechanical, physical and aesthetical characterisation. Note that the test methods were the same as those used to test unaged samples 11 years before, for proper comparison. These tests were carried out in the Materials Department of LNEC [12.16].

12.4.1 Methods

The mechanical characterisation was carried out in the longitudinal direction through: (i) tensile tests, and (ii) flexural tests. The tensile properties were determined according to ISO 527 - parts 1 and 4 [12.17], on rectangular test specimens measuring 250 mm × 20 mm × 8 mm. The tests were carried out on an Instron universal test machine with load capacity of 100 kN, under displacement control at a speed of 2 mm/min. The flexural tests were performed according to ISO 14125 [12.18] on rectangular test specimens measuring 164 mm × 15 mm × 8 mm, with a 128 mm span (16 times the thickness value). The testing equipment and speed was the same as in the previous test.

The physical characterisation was performed through the Charpy impact test, according to the method described in ISO 179-1 [12.19]. A pendulum shock test machine with capacity of 50 J and a Charpy hammer with 15 J capacity was used. The specimens were cut to the dimensions of 12 mm × 106 mm × 8 mm and the test span was 66 mm. The impact velocity was 3.8 m/s.

Considering the aesthetic characterisation, colour changes were evaluated on specimens with the same dimensions as those used for the determination of tensile properties, according to parts 1 and 2 of the ISO 7724 standard [12.20] using the CIEL*a*b* 1976 system. The tests were performed on a *Macbeth Coloreye 3000* colorimeter, as already described in Chapter 5.

12.4.2 Results and discussion

Figure 12.8 shows the failure modes observed in the tensile and flexural tests. In all tests the material showed linear elastic behaviour until failure, as expected.

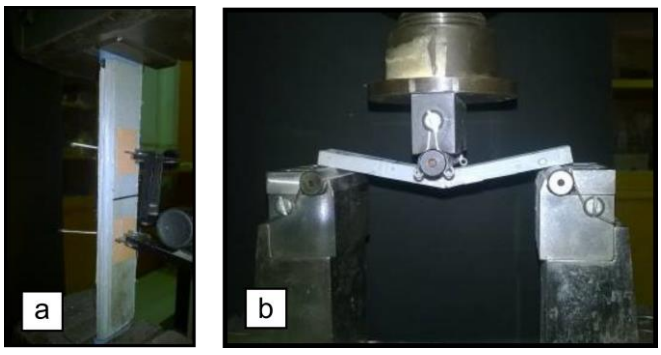

Figure 12.8. Failure modes: (a) tensile test, and (b) flexural test.

Tensile failure started with rupture of the outer CSM layers, followed by a progressive rupture of the unidirectional glass fibres. As for the flexural failure, it started in the lower outer layer, and progressed to the upper part of the section, causing rupture in the longitudinal fibres.

These results were consistent with the failure modes reported in Chapters 4 and 5, although the material was obtained from a different supplier.

Table 12.4 presents the results of the mechanical characterisation tests after 11 years of natural ageing and their comparison with the initial results, as well as after 2000 hours of accelerated ageing in QUV and Xenon arc chambers, as described in [12.16][16]. In this table, σ_{tu} is the tensile strength, ε_{tu} is the strain at failure, and E_t is the tensile modulus. The remaining properties are analogous to those reported for the tensile test, but for flexural properties.

Table 12.4. Tensile and flexural properties of the pultruded GFRP profile.

Property	**Time**	**unaged**	**QUV 2000 h**	**Xenon 2000 h**	**11 years**
	Ref.	**NMPC [12.16]**	**NMPC [12.16]**	**NMPC [12.16]**	**-**
σ_{tu} [MPa]		431.6 ± 14.9	412.6 ± 28.8	375.0 ± 10.8	385.3 ± 10.8
ε_{tu} [-]		0.013 ± 0.001	0.013 ± 0.001	0.012 ± 0.001	0.012 ± 0.001
E_t [GPa]		34.2 ± 1.4	34.8 ± 1.0	32.9 ± 0.6	34.2 ± 0.6
σ_{fu} [MPa]		511.4 ± 7.2	496.4 ± 28.4	491.8 ± 15.1	471.5 ± 15.9
ε_{fu} [-]		0.023 ± 0.001	0.022 ± 0.001	0.022 ±0.001	0.021 ± 0.001
E_f [GPa]		23.7 ± 1.0	23.2 ± 1.0	23.7 ± 0.6	23.3 ± 0.2

Analysing Table 12.4, it is evident that tensile and flexural strengths have experienced some reduction, of 10.7% and 7.8%, respectively. This fact should stem from material degradation mechanisms that are likely to occur in environments with high humidity, namely next to the sea, which could have affected the GFRP components [12.6].

However, both stiffness values presented insignificant changes. These differences should be related to the same competing phenomena between the aforementioned post-curing effects, and the degradation mechanisms, which have also been identified in Chapters 4 and 5. Similar trends were reported by Keller *et al.* [12.4] concerning the tensile strength and stiffness from specimens obtained from pultruded elements of the Pontresina bridge. However, the harsher Alps environment (presence of snow, thermal cycles, and UV radiation) had a more negative impact in these properties (around 10% higher), comparing specimens obtained from the profiles' webs. Regarding tensile material stiffness, the authors also referred that 17 years of ageing did not affect this property.

[16] The initial results corresponding to unaged material were obtained during the construction phase, to fulfil acceptance criteria requirements for the materials used in the construction site, as defined in the construction tender.

Comparing the results obtained now after 11 years of use with results from accelerated ageing tests [12.16], it can be seen that the strength degradation suffered by ageing in a Xenon arc chamber for 2000 hours resulted in degradation levels that are similar to those obtained after 11 years of natural ageing. In general, the changes observed in this type of characterisation were very reduced to moderate.

Concerning physical properties, Figure 12.9 presents a typical partially failed specimen subjected to the Charpy shock test. The unaged samples described in [12.16] presented the same failure mode.

Figure 12.9. Partial failure modes observed in the Charpy shock test.

Table 12.5 shows the results of the Charpy shock test and the comparison with the unaged results.

Table 12.5. Charpy test results.

Property	**unaged**	**11 years**
	Ref	**NMPC [12.16]**	**-**
Energy [J]	26.73 ± 2.69	14.86 ± 1.42
Type of rupture	partial	partial
Shock resistance [kJ/m^2]	315 .1± 34.0	144.7 ± 11.5

Analysis of the results presented in Table 12.5 shows a loss of more than half (54%) of the value of the shock resistance of the aged material under service conditions, which was the highest reduction observed in the all the characterisation tests. This indicates that the shock properties of the beams were significantly affected during these 11 years of ageing near a maritime environment. However, despite the reduced scatter values, only five specimens were tested and this characterisation test is very dependent on specimen geometry, as well as the part of the beam they were cut from. These may have been taken from a more brittle/weaker zone, thus influencing the results.

Regarding the aesthetical properties, Table 12.6 shows the results of the colour test for determining differences of the materials after 11 years and accelerated ageing.

The results presented in Table 12.6 show that the artificial ageing was more aggressive and affected more significantly the colour of the profiles than natural ageing for 11 years. Although the profiles exposed to natural ageing conditions presented similar trends in all of the colour axes w.r.t. artificial ageing, presenting yellowing and greener colour, their variation was more moderate (globally around 2 times less difference in colour when compared to 2000 hours of QUV ageing). Despite being less pronounced, the colour variation observed in the profiles after 11 years of natural ageing was already perceptible by visual observation.

Table 12.6. Colour properties of the pultruded GFRP profiles, after artificial and natural ageing.

Property	**Time Ref.**	**unaged NMPC [12.16]**	**QUV 2000 h NMPC [12.16]**	**Xenon 2000 h NMPC [12.16]**	**11 years -**
L*		62.48	68.67	70.19	64.72
a*		-2.01	-3.52	-3.30	-2.7
b*		-3.2	8.71	5.41	2.7
ΔE*			13.23	10.53	6.31

12.5. Concluding remarks

The experimental work presented in this chapter aimed at contributing to increase the knowledge of the durability of pultruded GFRP profiles under service conditions. After 11 years of service, a detailed inspection of a load-bearing substructure of a bridge deck composed of pultruded GFRP profiles was performed accompanied by full-scale and destructive specimen testing. The structure was exposed to a mild Mediterranean climate under the influence of a saline environment. The results obtained allow drawing the following main considerations:

1. In general, the GFRP components, after 11 years of environmental exposure under conditions of service, subjected to a climate with maritime influence, presented very low to moderate degradation of their mechanical properties and structural performance, except for the Charpy shock resistance.

2. Through the bridge deck inspection, it was possible to detect the existence of surface marks quite frequently and also the punctual existence of biological colonisation and corrosion of metallic elements. Based on the inspection results, only minor maintenance operations should be required in the near future, opposite to what has been found when in direct contact with solar radiation, which typically promotes the appearance of fibre blooming.

3. In the structural characterisation of the elements tested, no degradation was observed in the monitored properties. In fact, the flexural and shear stiffness, as well as the ultimate load, showed an increasing trend over time, and as such they were not negatively affected after 11

years of use close to a maritime environment. This fact should be associated with post-curing phenomena of the polymer matrix, well known in these materials.

4. In the characterisation of the GFRP material, the mechanical properties indicated degradation levels between 8 and 10% in flexural strength and tensile strength. However, the remaining material properties, namely the stiffness-related ones were unaffected after 11 years of use.

5. The resistance to Charpy shock showed very significant degradation to about 54% of the initial value. However, further testing is suggested in order to validate/confirm these results, which are largely inconsistent with those obtained from the remaining material and structural characterisation tests.

6. As far as the aesthetic properties are concerned, there was a moderate variation of colour, which, in the future, may justify the maintenance of the profiles. However, since the profiles of this structure were protected from direct exposure to UV solar radiation, fibre blooming did not occur.

7. Considering the overall results obtained in this study, it is reasonable to conclude that the structural safety of the pultruded GFRP substructure inspected is presently largely fulfilled, especially taking into account the generally very conservative values of safety factors included in design manuals; moreover, its structural safety should not become critical in the near future.

12.6. References

[12.1] Keller T. Recent all-composite and hybrid fibre-reinforced polymer bridges and buildings. Prog Struct Eng Mater 2001;3:132–40.

[12.2] Sobrino J, Pulido M. Towards advanced composite material footbridges. Struct Eng Int 2002;12:84–6.

[12.3] Keller T. Towards structural forms for composite fibre materials. Struct Eng Int 1999;9:297–300.

[12.4] Keller T, Theodorou NA, Vassilopoulos AP, Castro J De. Effect of natural weathering on durability of pultruded glass fiber–reinforced bridge and building structures. J Compos Constr 2015;20:1–9.

[12.5] Karbhari VM. Durability of Composites for Civil Structural Applications. Boca Raton, Florida: Woodhead Publishing; 2007.

[12.6] Cabral-Fonseca S, Correia JR, Rodrigues MP, Branco FA. Artificial accelerated ageing of GFRP pultruded profiles made of polyester and vinylester resins: Characterisation of physical-chemical and mechanical damage. Strain 2012;48:162–73.

[12.7] Alampalli S. Field performance of an FRP slab bridge. Compos Struct 2006;72:494–502.

[12.8] Farhey DN. Long-Term Performance Monitoring of the Tech 21 All-Composite Bridge. J Compos Constr 2005;9:255–62.

[12.9] Reising RMW, Shahrooz BM, Hunt VJ, Neumann AR, Helmicki AJ. Performance Comparison of Four Fiber-Reinforced Polymer Deck Panels. J Compos Constr 2004;8:265–74.

[12.10] Nishizaki I, Sakuraba H, Tomiyama T. Durability of pultruded GFRP through ten-year outdoor exposure test. Polymers (Basel) 2015;7:2494–503.

[12.11] Klamer E, Boer A, Nijssen R. Long-term effects of wet and outdoor conditions on GFRP. IABSE Conf - Struct Eng Provid Solut to Glob Challenges 2015:1591–8.

[12.12] EN 13706-2. Reinforced plastics composites - Specifications for pultruded profiles - Part 2: Methods of test and general requirements. Com Eur Norm (CEN), Brussels 2002.

[12.13] NT-NCE 17/04. Estudo experimental das características resistentes de vigas e grelhas em plástico reforçado com fibra de vidro. Laboratório Nac Eng Civ (LNEC), Núcleo Comport Estruturas 2004:1–14.

[12.14] Sá M. Comportamento Mecânico e Estrutural de FRP - Elementos Pultrudidos de GFRP. Dissertação de Mestrado, Instituto Superior Técnico, Lisboa, 2007.

[12.15] NT-DE/NCE 75/10. Avaliação experimental da resistência de vigas e grelhas de plástico reforçado com fibra de vidro. Laboratório Nac Eng Civ (LNEC), Núcleo Comport Estruturas 2010:1–14.

[12.16] R125-DM/NMPC. Caracterização de materiais compósitos de matriz polimérica reforçados com fibras de vidro. Laboratório Nac Eng Civ (LNEC), Núcleo Mater Plásticos e Compósitos 2004:1–50.

[12.17] ISO 527. Plastics - Determination of tensile properties. Int Organ Stand 2009.

[12.18] ISO 14125. Fiber-reinforced plastic composites - Determination of flexural properties. Int Organ Stand 1998.

[12.19] ISO 179-1. Plastics – Determination of Charpy impact properties. Part 1: Non-instrumented impact test. Int Organ Stand 2010.

[12.20] ISO 7724. Paints and varnishes - Colorimetry Part 1: Principles; Part 2: Colour measurement. Int Organ Stand 1997.

Part VI

Conclusions and future developments

Preamble

Part VI of this thesis presents the main conclusions drawn from parts II, III, IV, and V of the thesis, namely about (i) the durability of pultruded GFRP profiles, (ii) the durability of structural adhesives, (iii) the durability of adhesively bonded joints between pultruded GFRP profiles, and (iv) the natural weathering performance of a GFRP structure in outdoor service conditions. In addition, future developments related to the aforementioned subjects are pointed out.

Chapter 13.

Conclusions and future developments

13.1. Conclusions

Recent reports [13.1] show that the market of glass fibre reinforced polymer (GFRP) composites is steadily growing, with increasing emphasis on pultruded products for the construction industry. Several advantages such as light weight, high strength and ease of installation are contributing to a progressive increase in structural applications of these materials when compared to conventional solutions.

However, the global production volume of pultruded components for construction is still small compared to other products, and presently it still corresponds to niche applications [13.1], such as water waste treatment facilities (at least in Portugal); therefore, there is a significant room for growth. Current disadvantages of these materials, such as the relatively high initial costs, the high deformability, the brittle failure or the lack of widely accepted design codes and guidelines (such as Eurocodes) are factors that hinder the widespread application of pultruded GFRP products.

The issue of the durability of these alternative solutions is another critical factor that can be added to the above-mentioned limitations. Despite practical evidence of their high durability performance, there are still several uncertainties about the long-term behaviour and durability of pultruded GFRP components and their connections, namely those made of polymeric adhesives. In this context, the main objectives set for this thesis were to provide further insights about these topics, namely to obtain a better understanding of the different degradation mechanisms, and the effects of typical ageing environments experienced by civil engineering constructions made of pultruded GFRP profiles and their adhesively bonded connections. Thereafter, the research presented in this document was developed in four specific parts: (i) the effects of different ageing environments on the durability of pultruded GFRP profiles; (ii) the durability of two different structural adhesives for bonding GFRP components; (iii) the durability of adhesively bonded connections between pultruded GFRP adherends, and (iv) the natural weathering of a pultruded GFRP structure after several years in service conditions.

Overall, the objectives defined for this investigation were accomplished and allowed characterising the influence of different external factors on the durability of GFRP profiles, providing also long-term estimates and correlations regarding the long-term behaviour of

different material properties. In addition, the long-term behaviour of two different structural adhesives and of single lap bonded joints between them and GFRP adherends was also successfully addressed and characterised, resulting in a vast set of experimental data (complemented with numerical results) that can be used as reference for design and for further investigations. Finally, the *SATU Oeiras* case study allowed quantifying changes experienced by pultruded GFRP beams in real service conditions at both structural and material levels.

The following subsections provide more specific conclusions and contributions for each of the aforementioned topics.

13.1.1 Durability of pultruded GFRP profiles

The research about the durability of pultruded GFRP profiles (Part II of this thesis) included a vast experimental programme that comprised physical, mechanical, chemical, and aesthetical characterisation tests on two different types of commercial pultruded GFRP profiles made of unsaturated polyester (UP) and vinylester (VE) resins (both unaged and aged), with identical fibre architecture.

The experimental investigations included three main types of ageing environments, which consisted of: (i) hygrothermal ageing, that comprised immersion in demineralised and salt water at 20 °C, 40 °C, and 60 °C, and continuous condensation at 40 °C, followed by a drying (desorption) period, (ii) outdoor (natural) and QUV (artificial accelerated) ageing, and (iii) thermal cycling ageing. In addition, the synergistic effects of different exposures (outdoor ageing, saturated environment, and indoor controlled environment) under sustained loads (10% and 20% of the failure load) were also addressed.

Concerning **hygrothermal ageing**, both GFRP pultruded profiles presented approximately Fickian behaviour regarding absorption in water and salt water immersion environments. In most of the immersions, small deviations were found with relation to a Fickian response and the sorption behaviour was better simulated considering a dual Fickian response. For both UP and VE profiles, temperature dependence was identified, with higher diffusivity values for higher temperatures. The presence of salt in the aqueous solution seemed to hinder water uptake to some extent; in addition, the continuous condensation environment reached saturation levels at an earlier time when compared to immersions at the same temperature. As expected, the VE profiles exhibited lower overall diffusivity and saturation levels when compared to the UP profiles for the same environment at the same temperature.

The thermo-mechanical response was consistent with the occurrence of plasticization effects, although the extent of this phenomenon was small. Post-curing phenomena were evident in the UP profile, and its glass transition temperature (T_g) consistently increased up to 12 months, being also temperature dependent (maximum increases of 27% at the higher temperatures). The T_g of the VE profile was not significantly affected through the ageing process with maximum variations of 4%, regardless of the immersion temperature.

Hygrothermal ageing negatively affected the mechanical properties of both profiles, with degradation being temperature dependent and affecting mostly strength related properties. Some property recovery during the ageing process also occurred, which was associated with the aforementioned post-curing effects, which had an offsetting effect with the degradation mechanisms. The drying period also contributed to attenuate the degradation, since it allowed reversing the physical degradation effects to some extent; this is suggested by higher overall degradation presented by the same material when this desorption period did not occur [13.2]. This "positive" influence of desorption was more noticeable in stiffness related properties. Overall, the highest changes in mechanical performance occurred at the highest immersion temperatures with reductions after 2 years of immersion being as high as 45-48% and 23-37% for the UP and VE profiles, respectively; again, this evidenced the higher resistance to degradation of the VE profile when compared to the UP profile. Salt water had similar, but slightly lower detrimental effects on the mechanical properties, which was also consistent with the diffusion behaviour of both profiles. Moreover, continuous condensation produced comparable results with immersion at the same temperature.

Arrhenius models were successfully applied to predict the long-term material properties of both profiles. The higher activation energy and the lower water incorporation calculated for the VE profile were in agreement with its overall better durability performance. The predicted mechanical properties for the UP profile after 100 years of water immersion at 23 °C were 50-60% of the initial values, while for the VE profile these figures ranged between 60-75%. In general, salt water immersions involved higher retention values compared to water immersion. For both types of immersion, predictions agreed well with the main trends highlighted by the experimental results. For immersion at a temperature of 23 °C (a quite aggressive exposure for FRP composites), none of the estimated properties fell below 50% after 100 years, which, considering the usually conservative Arrhenius approach, are a good indication of the high durability performance of these materials.

Regarding the effects of **outdoor ageing** up to 8.5 years and QUV artificial accelerated ageing, UV exposure caused significant photo-chemical degradation of the resin matrix due to this type

of exposure, which resulted in fibre blooming, yellowness, darkening and gloss reduction. When exposed to such environments, appropriate protections, such as UV stabilizers, surface veils, protective paintings or gel coats should be considered. FTIR analysis confirmed the occurrence of chemical changes, indicating also that the main effects of UV exposure are concentrated in the outer layers directly exposed to the radiation (few microns at the surface of the specimens). This resulted in much smaller changes in material properties when compared to hygrothermal degradation. The viscoelastic behaviour through DMA analysis showed only slight variations, and at some point it indicated post-curing effects, which should be prolific in the warmer outdoor seasons, with higher average temperatures.

Concerning mechanical characterisation, the failure modes in all types of characterisation tests were not changed. The most affected properties were flexural strength in the VE profile (22% maximum reduction) and tensile and flexural modulus in the UP profile (33% and 37% maximum reductions, respectively). Between 42 and 102 months of natural ageing, no significant differences were found. In general, the VE profile presented higher mechanical properties and stability to degradation compared with the UP profile, which was consistent with hygrothermal ageing. To a certain extent, the results obtained allowed correlating the effects of outdoor (natural) and QUV (artificial accelerated) ageing, especially in what concerns gloss and colour changes. In this regard, 2000 to 3000 hours of QUV exposure caused similar aesthetic degradation to 30 to 40 months of natural ageing in Lisbon city centre.

Concerning the effects of **thermal cycles** likely to be experienced by pultruded GFRP profiles in Mediterranean mild climates, the main results indicated low to moderate degradation of both UP and VE properties due to thermal cycles, particularly when compared to the hygrothermal degradation experienced by those same materials.

Both types of matrix and fibre-matrix interfaces presented no evident structural changes and the glass transition temperature of both profiles exhibited only slight variations. DMA results also suggested the existence of post-curing phenomena (as noted in the other types of ageing) between 200 and 600 thermal cycles. Overall, the VE profile presented better mechanical performance when compared to the UP profile. Regarding tensile and interlaminar shear strength, only slight variations occurred for both profiles: after 600 thermal cycles, the values were similar w.r.t the unaged values. Only the tensile modulus of the VE profile exhibited 12% changes at this period. In-plane shear strength and modulus suffered changes of 7% and 12% for the UP profile, whereas for the VE profile, the variations were ever lower due to its higher stability. For both profiles, a higher degradation was noted in the flexural properties, with the modulus and strength decreasing as much as 25% and 13%, respectively. The increased degradation of

the flexural properties when compared to the other mechanical properties is deemed to have been caused by the stronger dependency of the former on the resin matrix and the fibre-matrix interphase.

SEM observations allowed observing fibre debonding (adhesive rupture) and also cracking in the resin matrix (cohesive rupture); however, the latter was scarcely present in the VE profile and adhesive rupture was also present to a lesser extent, which confirmed the better resistance to thermal cycling of the VE profile (already suggested by mechanical characterisation).

Regarding the synergistic effects of sustained loading and different ageing environments, the experimental results obtained indicate that in general the loading conditions used do not influence to a high extent the level of degradation caused by the different environments: natural weathering, continuous condensation, and laboratory-controlled ageing. However, the effects of the different loading conditions were still visible. Loading the specimens in bending to 20% of their capacity caused higher degradation levels when compared to specimens loaded to 10% of their capacity - consistently lower flexural strength values were found when higher stress levels were applied during ageing. The specimens of both UP and VE profiles subjected to natural weathering also evidenced increases in flexural strength, which were attributed to post-curing effects. For the continuous condensation environment, considerably higher levels of degradation were observed at later stages of exposure, comparable with the results of immersion in demineralised water at 20 °C experienced during hygrothermal ageing.

Table 13.1 presents a summary of the main results obtained within this topic, which are useful for design purposes.

Table 13.1. Summary of results obtained for pultruded GFRP profiles, applicable for design purposes.

	Property retention (service life) for:									
	UP GFRP profile					**VE GFRP profile**				
	2 years	**50 years (predicted)**	**2 years**	**600 cycles**	**8.5 years**	**2 years**	**50 years (predicted)**	**2 years**	**600 cycles**	**8.5 years**
Exposure type	**Immersion [20 °C]**	**Immersion [23 °C]**	**Humid [40 °C]**	**Thermal cycles**	**Natural weathering**	**Immersion [20 °C]**	**Immersion [23 °C]**	**Humid [40 °C]**	**Thermal cycles**	**Natural weathering**
$T_{g\ tan\ \delta}$	105%[(a)]	-	115%	101%	101%	101%	-	104.6	103%	101%
Tensile strength	84%	66%	70%		85%	111%	-	105%	99%	100%
Flexural strength	88%	55%	69%	90%	92%	90%	64%	85%	100%	85%
Shear strength	87%	64%	85%	108%	-	87%	77%	84%	99%	-
Interlaminar shear strength	91%	75%	78%	89%	88%	93%	-	90%	91%	93%
Tensile Modulus	90%	65%	85%	98%	82%	99%	-	87%	88%	94%
Flexural Modulus	106%	-	114%	99%	105%	106%	-	114%	104%	86%
Shear Modulus	110%	-	98%	88%	-	104%	-	96%	106%	-

(a) this value refers to 12 months of immersion.

13.1.2 Durability of structural adhesives

Two different structural adhesives usually recommended for bonding operations involving GFRP components for civil engineering applications - epoxy and polyurethane - were experimentally studied regarding their durability (Part III of this thesis). In particular, the effects of hygrothermal ageing (immersions in salt and demineralised water at 20 °C and 40 °C, and also continuous condensation at 40 °C) and exposure to outdoor environment on the physical and mechanical properties of those adhesives was addressed.

The **sorption behaviour** during hygrothermal ageing did not follow a Fickian behaviour. In fact, after 2 years of immersion, water molecules were still being incorporated, in most cases causing significant mass gains, due to relaxation effects of the polymeric structure. For both adhesives, and both immersion media (water and salt water), as expected the higher temperature increased the diffusivity coefficients. Regarding the modelling of the sorption behaviours, the (non-Fickian) analytical models used provided an overall good fitting to the test data. In general, the polyurethane exhibited higher diffusivity when compared to epoxy at higher temperature, while at lower temperature comparable mass gains were measured. In addition, the water uptake in the salt immersions was lower, which was reflected in the lower diffusion coefficients obtained.

Regarding the **viscoelastic behaviour** of the epoxy adhesive, generalised reductions in the glassy plateau of the storage modulus curves were visible, due to water plasticization effects. In addition, the original peak of the tan δ curve experienced a split due to prolonged immersion times, which occurred with the widening of the curve. These changes were reflected in a detrimental effect on the T_g values, regardless of the exposure temperature (20% and 10% decreases in water and salt water, respectively, while in continuous condensation the reductions were smaller); insignificant changes were noticeable in outdoor ageing. On the contrary, the polyurethane adhesive presented only slight changes in the E' and tan δ curves up to one year of ageing; post-curing phenomena were noticed in all ageing environments. However, both adhesives presented fluctuations in the tan δ peak curve at about 100 °C, suggesting that the desorption period was not enough to fully remove the water content from the adhesive. Even considering the detrimental effects in the T_g of epoxy adhesive compared to the generalised increase in the polyurethane adhesive, the epoxy still presented higher T_g values after two years of immersion ($T_{g,\ tan\delta}$ never reduced below 62° C, while the highest value for polyurethane was 57° C). These differences were even higher in the $T_{g,E'onset}$ values.

In terms of **flexural properties**, both adhesives presented overall degradation trends during hygrothermal ageing, more noticeable with higher temperatures and longer exposure periods. Reductions as high as 24-30% and 30-36% in flexural strength and modulus were observed; the stress-strain behaviour of both adhesives also presented signs of water induced plasticization effects, in line with the DMA results, with increasing values of strain at failure (or maximum strain in case of the polyurethane). Some post-curing phenomena related effects were also identified at some periods, when the flexural properties presented increasing values. When compared to demineralised water, the salt water immersion had insignificant effects in the epoxy adhesive and caused slightly lower degradation effects in the polyurethane; continuous condensation showed similar results when compared to demineralised water at the same temperature. Comparing both adhesives, epoxy presented higher resistance to hygrothermal ageing when compared to polyurethane, and superior flexural performance (about 2.2 higher strength, and 2.8 higher moduli).

Similar plasticization effects were also observed in the **shear properties** of both adhesives, which affected the usual brittle failure of epoxy, changing it to a more progressive and less sudden failure, especially at higher temperatures and longer periods of exposure. In terms of in-plane shear strength and stiffness, the epoxy adhesive presented opposite trends - generalised increase in strength, as much as 28%, and decrease in modulus, as much as 43%. Outdoor ageing produced similar changes, but with lower magnitudes. Under hygrothermal ageing, the polyurethane adhesive presented reductions of both shear strength and modulus (26% and 44% maximum decreases, respectively). For outdoor ageing, the shear strength of polyurethane exhibited a slightly increasing trend, and practically no changes in modulus, which were attributed to post-curing effects during the warmer seasons; in addition, several specimens presented lower deformation capacity and collapsed prematurely. Comparing the shear performance of both adhesives, epoxy presented similar reductions in shear modulus, and better resistance to hygrothermal ageing in terms of shear strength. In addition, this adhesive presented an overall superior performance in terms of shear properties, especially in what concerns stiffness (around 2 times higher).

Globally, hygrothermal ageing negatively affected both the epoxy and the polyurethane adhesives, which suffered from irreversible degradation mechanisms, even in the presence of competing post-curing phenomena; the effects of natural weathering in both adhesives were less harmful.

Owing to its overall superior mechanical performance and its better resistance to both outdoor and hygrothermal ageing, in general, the epoxy adhesive was found to be more suitable to civil engineering structural applications, especially when considering exposure to relatively harsh

environments. However, the polyurethane adhesive can still be useful in applications with specific requirements, namely where high deformation capacity is needed or to increase the ductility of GFRP structures [13.3].

Similarly to the GFRP profiles, Table 13.2 summarizes the main results obtained within this topic, which are useful for design purposes.

Table 13.2. Summary of results obtained for epoxy and polyurethane adhesives, applicable for design purposes.

Property retention (service life) for:						
	Epoxy adhesive			**Polyurethane adhesive**		
	2 years	**1 year**		**2 years**	**1 year**	
	Immersion [20 °C]	**Humid [40 °C]**	**Natural weathering**	**Immersion [20 °C]**	**Humid [40 °C]**	**Natural weathering**
$T_{g\ tan\ \delta}$	81%	96%	98%	110%[(a)]	113%	108%
Flexural strength	92%	94%	-	80%	78%	-
Shear strength	119%	-	107%	74%	-	112%
Flexural Modulus	84%	88%	-	88%	89%	-
Shear Modulus	94%	-	87%	68%	-	103%

(a) this value refers to 12 months of immersion.

13.1.3 Durability of adhesively bonded connections between pultruded GFRP adherends

The research about the durability of adhesively bonded connections between pultruded GFRP adherends was the focus of part IV of the thesis document. The effects of hygrothermal (immersions in salt and demineralised water at 20 °C and 40 °C, and also continuous condensation at 40 °C), natural weathering and thermal cycles on single lap joints made of pultruded unsaturated polyester-GFRP laminates bonded with either epoxy (EP-GFRP) or polyurethane (PUR-GFRP) structural adhesives were addressed.

Despite the intrinsic differences between both adhesives, the mechanical performance of both EP-GFRP and PUR-GFRP unaged single lap joints was similar in terms of overall joint stiffness; the ultimate load was 12% higher for the polyurethane joints.

Hygrothermal ageing caused detrimental effects on the mechanical response of both EP-GFRP and PUR-GFRP bonded joints, especially at the higher immersion temperature. For the lower immersion temperature, overall, some increasing trends were noted in both failure load and local

stiffness at some point, which should be related with the occurrence of post-curing effects; after two years of immersion, the initial ultimate load was re-attained or even slightly exceeded. The maximum reductions that occurred were higher in the EP-GFRP joints in comparison to the PUR-GFRP joints (27% *vs.* 20%), while the opposite was noticed regarding the stiffness values (16% *vs.* 20%). The immersions at 40°C presented higher degradation in the initial periods and progressed towards a plateau. The maximum reductions of ultimate load were 35% and 30% for EP-GFRP and PUR-GFRP joints, respectively, while for the overall stiffness those figures were 40% and 22%. The presence of salt in the exposure medium did not seem to influence the overall joint degradation. Both salt fog spray and continuous condensation produced similar effects, which were comparable with immersion at the same temperature (40 °C).

Regarding **outdoor ageing**, small differences were found in the mechanical performance of bonded joints with both types of adhesives. Changes in stiffness never exceeded 5% in EP-GFRP joints and 14% in PUR-GFRP joints; in terms of ultimate load, changes were moderate, matching the seasonal cycles, comprising an alternate but overall increasing trend for both adhesives. After 2 years, the ultimate load increased 25% in EP-GFRP joints and 10% in PUR-GFRP joints.

In both types of single lap joint specimens, failure always initiated in one of the GFRP adherends, next to the extremity of the overlap. In the EP-GFRP specimens, only light-fibre tear and fibre tear failure was observed in the unaged specimens, which reflected the quality of the adhesion. However, in PUR-GFRP specimens, adhesive failure also occurred frequently. Hygrothermal and outdoor ageing produced changes in the percentage of the different failure modes that could be correlated with the changes in the mechanical performance of the bonded joints.

The numerical investigations allowed assessing the evolution of the internal stresses along the single lap joints, aiming to obtain a better understanding of the evolution of the load-transfer mechanisms in such joints. The results confirmed that the moduli degradation (considering a linear elastic analysis - *i.e.* valid for lower levels of loading) leads to a smoother stress distribution at the extremities of the overlaps and to a consequent reduction of the stress peaks. This effect should delay failure initiation, partly counterbalancing the potential strength degradation experienced by the constituents, which is in agreement with the experimental results. This smoothing effect was particularly noted in the peeling stresses.

Regarding the effects of **thermal cycles** on similar single lap bonded joints, detrimental effects were also found, and their magnitude was smaller compared to hygrothermal ageing. The maximum performance reduction occurred after 150 cycles for the EP-GFRP joints and after 250 cycles for the PUR-GFRP joints. Subsequently, little further changes occurred, which were partly attributed to the occurrence of post-curing phenomena in the adhesives during exposure to the higher temperatures of the cycling profile. The maximum reductions of ultimate load were 18% and 19%, for EP-GFRP and PUR-GFRP joints, respectively; the figures for overall stiffness were 22% and 11%.

In terms of failure modes, adhesive failure became more frequent in EP-GFRP joints, progressing (in terms of surface area) from 0% (unaged specimens) to 24% (350 cycles), which evidenced the detrimental effects that occurred between the epoxy and the GFRP adherends. In opposition, adhesive failure became less frequent in PUR-GFRP joints, decreasing from 40% (unaged specimens) to 8% (350 cycles). The higher degree of post-curing experienced by the polyurethane adhesive together with its lower shear modulus and T_g (allowing for more polymer chain mobility at the lower temperature cycles) may have contributed to improve the adhesion performance of PUR-GFRP joints.

Despite the aforementioned differences between both adhesives, the effects of thermal cycles were fairly similar at the bonded joint level, with experimental results being of the same order of magnitude. However, the specimens bonded with polyurethane adhesive seemed to be less susceptible to this type of ageing.

Numerical simulations provided further insights about the stresses developed during thermal cycling, namely due to mismatch between the coefficients of thermal expansion (CTE) of the adherends and the adhesive. Results indicated that internal stresses were found to be of relatively low magnitude, and suggested that the performance of the single lap joints should be mainly influenced by the effects of the thermal cycles on the properties of the constituent materials, and not to the severity of thermal stresses resulting from the thermal variations. Note that in the present study thermal amplitudes experienced in mild climates were considered, and that higher thermal variations may induce higher internal thermal stresses.

Table 13.3 presents a summary of the results obtained for the effects of ageing on the bond performance of adhesively GFRP bonded joints with epoxy and polyurethane adhesives, which may be helpful for design purposes.

Table 13.3. Summary of results obtained for EP-GFRP and PUR-GFRP bonded joints, applicable for design purposes.

	Property retention (service life) for:							
	EP-GFRP				**PUR-GFRP**			
	2 years	**1 year**	**2 years**	**350 cycles**	**2 years**	**1 year**	**2 years**	**350 cycles**
	Immersion [20 °C]	**Humid [40 °C]**	**Natural weathering**	**Thermal cycles**	**Immersion [20 °C]**	**Humid [40 °C]**	**Natural weathering**	**Thermal cycles**
Failure load	111%	79%	125%	86%	100%	77%	110%	83%
Local Stiffness	98%	-	106%	81%[(a)]	105%	-	105%	93%[(a)]

(a) this value refers to global stiffness.

13.1.4 Natural weathering of a GFRP structure: SATU Oeiras

Part V of the current work aimed to increase the knowledge of the durability of pultruded GFRP profiles under real service conditions. The case study of *SATU Oeiras* allowed assessing the performance of a GFRP structure under exposure to a mild Mediterranean climate and influenced by saline environment (close to the Atlantic Ocean). After 11 years of service, a detailed inspection was performed and complemented by full-scale and material level testing.

Overall, the GFRP components presented very low to moderate degradation of their mechanical properties and structural performance. The most frequent anomalies in the pultruded GFRP structure comprised the existence of surface marks (quite frequent), the local existence of biological colonisation and the corrosion of metallic elements. Only minor maintenance operations should be required in the near future.

In terms of structural characterisation, the flexural and shear stiffness of GFRP beams taken from the structure, as well as their ultimate load, showed an increasing trend over time. This fact should be associated with post-curing phenomena of the polymer matrix, well known in such materials. In fact, these phenomena were also observed in other parts of the present thesis.

At the material level, the mechanical properties of GFRP profiles exhibited a low level of degradation (8-10%) in terms of strength. Material stiffness seemed to remain unaffected after 11 years of use.

Moderate variation of colour was also identified, which, in the future, may justify the maintenance of the profiles. However, since the profiles in this specific structure were covered from direct exposure to UV (solar) radiation, fibre blooming did not occur.

Considering the results obtained, it is reasonable to assume that the structural safety of the GFRP profiles used in *SATU Oeiras* infrastructure is presently largely fulfilled, especially

considering the conservative values of safety factors included in design manuals. Accounting for the very low degradation trends highlighted by the experiments, safety related issues should not occur or become critical in the near future.

13.2. Future developments

The experimental, analytical and numerical studies presented in this thesis provided a better understanding of the durability and degradation mechanisms that affect pultruded GFRP components and their adhesively bonded connections when they are subjected to different types of environmental agents. However, some aspects of the investigation need to be complemented and/or deepened, requiring further research efforts. Those aspects are highlighted in the following paragraphs.

Concerning the ageing of pultruded components, it is well known that material properties can change considerably among different manufacturers. Thus, it would be useful to investigate profiles produced by different manufacturers and compare the results with those presented in this thesis. This would allow extending the current knowledge to a more extensive and generalised database on the long-term effects on these materials. Extending those similar studies to alternative combinations of fibre architectures, different polymeric resins for the matrix component (*e.g.* phenolic or epoxy matrices) or different reinforcing fibres (*e.g.* basalt or natural fibres, *e.g.* flax[17]) would also contribute to this goal. The consideration of compressive properties (not addressed here) in such durability studies should also be accounted for.

In addition, aiming to increase the renewable content while decreasing the relatively high embodied energy of GFRP resources, further efforts in the replacement of the polymeric resin matrices based on non-renewable resources can be made; alternative, less energy intensive materials produced from biological renewable resources such as bio-resins should be studied as possible replacements for bio-GFRPs. The study of their incorporation in the production of pultruded GFRP component, and their durability properties should be addressed.

A relevant issue about natural weathering consisted of the premature occurrence of fibre blooming. In fact, in current pultruded GFRP applications, such as hand-rails or gratings, fibre blooming may be quite harmful, since fibres can be in direct contact with users. This issue

[17] Note that flax fibres are less relevant for structural applications.

needs to be fully addressed, in order to model the phenomenon and to study cost-efficient ways of preventing it, such as the use of surface veils, UV stabilizers or protective coatings.

Furthermore, the study about the effects of natural weathering was limited to mild Mediterranean climates. Different outdoor ageing conditions (*e.g.* Alpine or desert climates) should be addressed, as they can have higher thermal variations, freeze-thaw cycles, snow and other characteristics that should produce different effects on the performance of GFRP structures.

Another issue concerning the natural weathering of (pultruded) GFRP structures is the inexistence of specific management systems available for these elements, despite the lesser maintenance operations that should be required. As such, developing inspection, diagnosis and rehabilitation systems for GFRP constructions is of paramount importance.

Also, the information about the effects of natural weathering on existent GFRP structures is still very limited. More case studies, such as that described in Chapter 12, are needed to fully understand the environmental degradation of GFRP structures, comprising different periods of exposure and different environments.

Other degradation factors that were not investigated in the current thesis should also be further studied, such as freeze-thaw cycles or the exposure to alkaline and acid environments. The latter type of exposure is quite relevant in different locations of waste water treatment plants. Here, it would also be useful to compare the performance of different resin systems.

Moreover, further developments on the synergistic combinations between different degradation factors are critical to increase the knowledge on how these components deteriorate, since civil engineering applications often experience a handful combination of different exposures.

Despite their inherent limitations, Arrhenius approaches are still widely used to predict and extrapolate the long-term behaviour of pultruded GFRP components [13.4, 13.5]. Despite the inherent difficulties, such as the uncertainty about environmental agents, the development of new degradation models that aim to predict more accurately the long-term behaviour of pultruded GFRP structures is also fundamental to increase their acceptability.

Regarding the different types of possible adherends and adhesively bonded connections, other adhesives and GFRP combinations (*e.g.* the use of vinylester resin in the pultruded GFRP component) are also recommended for further study. In addition, the effects of different types of ageing environments on other types of bonded connections, such as butt or tie joints, and

more complex forms, such as beam-to-column connections, should also be investigated. In addition, the durability of other substrate combinations should also be addressed, such as GFRP-to-metal or GFRP-to-concrete, since they are relevant for different types of hybrid structures.

The numerical investigations could also be extended to account for the influence of the cumulative effects of thermal cycles. The models may also be enhanced by considering cohesive elements to model the joint interfaces and material non-linear behaviour (particularly relevant for softer adhesives, such as polyurethanes). This would aim at predicting the degradation of joint strength.

Since civil engineering structures have relatively long service life periods, future studies should include longer periods of immersion and exposure to natural weathering. This applies to both pultruded GFRP elements and their adhesively bonded connections. Furthermore, parallel studies regarding the durability of bolted connections between pultruded GFRP profiles should be addressed. In addition, the effects of building details related to drilling, such as sealing operations, and how they can affect the durability of the bolted connections should also be included. Information on these subjects is presently very scarce and needs further attention.

The results presented in this thesis and in similar investigations are also expected to contribute to the future development of design codes for the design of pultruded GFRP structures, namely to the definition of reduction factors for different types of environmental exposure. Such guidance is of paramount importance to widespread the use of GFRP civil engineering structures.

Related to durability are also the topics of sustainability and life cycle assessment. Investigations about these subjects are also scarce and very much needed to increase the competitiveness of GFRP solutions compared to traditional structural applications. Some preliminary research available (such as [13.6]) already point out ecological advantages of composite bridges. Further research about the above-mentioned topics is needed and should include life cycle analysis (LCA) from cradle to cradle for several GFRP construction applications and service life periods, comparing them with conventional solutions.

13.3. References

[13.1] Witten E. The European GRP-market 2017. In: Witten E, Sauer M, editors. Compos. Mark. Rep. 2017, AVK - German professional association for fibre composite plastics/composites; 2017, p. 4–23.

[13.2] Cabral-Fonseca S, Correia JR, Rodrigues MP, Branco FA. Artificial accelerated ageing of GFRP pultruded profiles made of polyester and vinylester resins: Characterisation of physical-chemical and mechanical damage. Strain 2012;48:162–73.

[13.3] Castro J de, Keller T. Design of robust and ductile FRP structures incorporating ductile adhesive joints. Compos Part B Eng 2010;41:148–56.

[13.4] Keller T, Theodorou NA, Vassilopoulos AP, Castro J De. Effect of natural weathering on durability of pultruded glass fiber–reinforced bridge and building structures. J Compos Constr 2015;20:1–9.

[13.5] Sousa JM, Correia JR, Cabral-Fonseca S. Durability of glass fibre reinforced polymer pultruded profiles: Comparison between QUV accelerated exposure and natural weathering in a Mediterranean climate. Exp Tech 2016;40:207–19.

[13.6] Daniel RA. A composite bridge is favoured by quantifying ecological impact. Struct Eng Int 2010;20:385–91.

Appendix

This section presents, in a continuous manner, tables with the most relevant experimental data for each chapter.

A. Hygrothermal ageing of pultruded GFRP profiles experimental results

A.1 Sorption experimental results

Table A.1. UP water sorption experimental results.

T [days]	W20 [%]	std.dev [%]	S20 [%]	std.dev [%]	W40 [%]	std.dev [%]	S40 [%]	std.dev [%]
0.000	0.000	0.000	0.000	0.000	0.000	0.000	0.000	0.000
0.979	0.037	0.007	0.047	0.010	0.067	0.020	0.077	0.034
2.938	0.050	0.004	0.050	0.007	0.130	0.023	0.103	0.009
8.167	0.092	0.001	0.086	0.003	0.217	0.022	0.174	0.008
9.208	0.111	0.004	0.097	0.005	0.225	0.016	0.183	0.004
11.208	0.126	0.009	0.110	0.011	0.245	0.023	0.194	0.006
14.208	0.150	0.019	0.117	0.003	0.276	0.023	0.213	0.010
15.938	0.153	0.010	0.125	0.001	0.290	0.023	0.254	0.036
23.125	0.168	0.005	0.150	0.002	0.344	0.034	0.276	0.045
29.000	0.192	0.016	0.164	0.011	0.385	0.024	0.290	0.026
34.917	0.199	0.010	0.165	0.003	0.409	0.045	0.307	0.030
42.125	0.217	0.008	0.184	0.002	0.438	0.032	0.325	0.016
57.125	0.259	0.023	0.212	0.001	0.497	0.034	0.360	0.010
63.917	0.268	0.016	0.222	0.001	0.523	0.043	0.373	0.018
76.917	0.283	0.008	0.233	0.007	0.551	0.021	0.394	0.018
85.208	0.299	0.013	0.240	0.001	0.573	0.014	0.403	0.017
92.250	0.310	0.013	0.241	0.009	0.599	0.015	0.413	0.022
107.250	0.337	0.025	0.251	0.004	0.620	0.007	0.421	0.014
119.542	0.359	0.026	0.268	0.011	0.643	0.001	0.431	0.010
147.021	0.401	0.033	0.289	0.004	0.677	0.002	0.443	0.015
161.021	0.420	0.010	0.301	0.019	0.689	0.006	0.468	0.019
176.125	0.441	0.012	0.308	0.018	0.709	0.004	0.478	0.008
192.188	0.438	0.026	0.309	0.014	0.729	0.007	0.492	0.000
204.208	0.448	0.025	0.305	0.006	0.743	0.003	0.487	0.010
217.250	0.462	0.031	0.322	0.008	0.750	0.006	0.497	0.009
231.188	0.464	0.033	0.321	0.012	0.755	0.003	0.504	0.010
246.208	0.487	0.034	0.331	0.015	0.783	0.014	0.511	0.010
266.250	0.488	0.032	0.331	0.012	0.805	0.010	0.524	0.011
279.542	0.497	0.031	0.335	0.010	0.815	0.001	0.526	0.009
293.542	0.505	0.027	0.339	0.011	0.827	0.006	0.531	0.002
307.542	0.517	0.028	0.343	0.011	0.841	0.009	0.535	0.007
321.542	0.516	0.028	0.342	0.015	0.854	0.000	0.549	0.014
332.542	0.526	0.029	0.347	0.012	0.871	0.003	0.561	0.012
359.542	0.531	0.029	0.352	0.012	0.903	0.002	0.560	0.018
387.250	0.531	0.032	0.357	0.016	0.949	0.005	0.563	0.015
402.167	0.534	0.027	0.361	0.016			0.569	0.019
420.167	0.534	0.032	0.368	0.018			0.574	0.018
449.167	0.543	0.026	0.376	0.018			0.588	0.014
478.979	0.548	0.018	0.414	0.010			0.571	0.020
510.979	0.558	0.001	0.419	0.008			0.601	0.014
532.208	0.570	0.007	0.425	0.007			0.635	0.018
540.167	0.558	0.007	0.409	0.007			0.626	0.023

547.125	0.558	0.006	0.403	0.009			0.627	0.007
562.208	0.556	0.009	0.409	0.016			0.634	0.020
568.125	0.551	0.007	0.406	0.009			0.632	0.020
575.000	0.560	0.010	0.409	0.010			0.634	0.023
583.125	0.552	0.013	0.412	0.011			0.649	0.028
595.125	0.555	0.012	0.409	0.010			0.649	0.016
606.125	0.552	0.006	0.416	0.012			0.645	0.020
620.000	0.536	0.012	0.420	0.011			0.658	0.015
644.042	0.553	0.009	0.425	0.021			0.660	0.025
658.125	0.549	0.005	0.424	0.013			0.666	0.018
673.146	0.555	0.006	0.424	0.014			0.669	0.020
694.542	0.564	0.002	0.427	0.010			0.681	0.011
707.542	0.537	0.003	0.413	0.012			0.675	0.019
742.542	0.558	0.001	0.440	0.016			0.708	0.019

Table A.2. UP water sorption experimental results (cont.).

T [days]	W60 [%]	std.dev [%]	S60 [%]	std.dev [%]	C40 [%]	std.dev [%]
0.000	0.000	0.000	0.000	0.000	0.000	0.000
0.979	0.098	0.005	0.086	0.009	0.000	0.000
2.938	0.196	0.009	0.180	0.008	0.080	0.001
8.167	0.249	0.007	0.212	0.015	0.170	0.006
9.208	0.246	0.007	0.198	0.008	0.173	0.000
11.208	0.294	0.010	0.229	0.008	0.191	0.001
14.208	0.346	0.014	0.270	0.008	0.219	0.003
15.938	0.373	0.017	0.283	0.004	0.231	0.000
23.125	0.455	0.007	0.377	0.016	0.270	0.005
29.000	0.496	0.003	0.387	0.003	0.300	0.006
34.917	0.533	0.003	0.394	0.014	0.303	0.043
42.125	0.577	0.005	0.419	0.004	0.351	0.001
57.125	0.643	0.014	0.443	0.009	0.404	0.005
63.917	0.664	0.010	0.456	0.004	0.432	0.000
76.917	0.689	0.001	0.470	0.005	0.459	0.009
85.208	0.687	0.002	0.462	0.003	0.477	0.009
92.250	0.707	0.007	0.486	0.011	0.490	0.004
107.250	0.701	0.034	0.531	0.050	0.518	0.013
119.542	0.723	0.032	0.526	0.033	0.552	0.017
147.021	0.781	0.026	0.527	0.019	0.585	0.015
161.021	0.797	0.030	0.530	0.005	0.606	0.018
176.125	0.816	0.016	0.522	0.004	0.624	0.019
192.188	0.826	0.026	0.510	0.006	0.649	0.009
204.208	0.839	0.025	0.518	0.009	0.663	0.010
217.250	0.861	0.025	0.531	0.020	0.677	0.008
231.188	0.875	0.018	0.504	0.026	0.689	0.005
246.208	0.894	0.036	0.505	0.026	0.713	0.015
266.250	0.917	0.019	0.540	0.019	0.741	0.012
279.542	0.931	0.016	0.538	0.021	0.733	0.017
293.542	0.945	0.012	0.536	0.022	0.740	0.026
307.542	0.954	0.004	0.533	0.022	0.759	0.008
321.542	0.974	0.035	0.532	0.027	0.777	0.005
332.542	0.978	0.016	0.498	0.023	0.795	0.008
359.542	1.000	0.013	0.517	0.035	0.828	0.005
387.250	1.008	0.013	0.524	0.029	0.847	0.006

402.167			0.512	0.009		
420.167			0.564	0.011		
449.167			0.495	0.033		
478.979			0.526	0.034		
510.979			0.546	0.050		
532.208			0.561	0.057		
540.167			0.553	0.060		
547.125			0.571	0.038		
562.208			0.569	0.033		
568.125			0.553	0.040		
575.000			0.551	0.043		
583.125			0.587	0.034		
595.125			0.564	0.026		
606.125				0.057		
620.000				0.067		
644.042				0.063		
658.125				0.039		
673.146				0.039		
694.542				0.061		
707.542				0.052		
742.542				0.058		

Table A.3. VE water sorption experimental results.

T [days]	W20 [%]	std.dev [%]	S20 [%]	std.dev [%]	W40 [%]	std.dev [%]	S40 [%]	std.dev [%]
0.00	0.000	0.000	0.000	0.000	0.000	0.000	0.000	0.000
0.98	0.077	0.001	0.039	0.006	0.100	0.005	0.043	0.022
2.94	0.117	0.001	0.063	0.020	0.220	0.002	0.072	0.015
8.17	0.192	0.005	0.096	0.016	0.268	0.010	0.124	0.009
9.21	0.201	0.004	0.113	0.023	0.277	0.001	0.140	0.012
11.21	0.219	0.008	0.119	0.021	0.300	0.001	0.154	0.015
14.21	0.246	0.013	0.141	0.021	0.334	0.001	0.175	0.018
15.94	0.248	0.005	0.144	0.024	0.343	0.004	0.185	0.008
23.13	0.278	0.007	0.189	0.022	0.395	0.003	0.239	0.011
29.00	0.308	0.003	0.192	0.033	0.413	0.001	0.243	0.015
34.92	0.320	0.010	0.210	0.030	0.442	0.001	0.260	0.011
42.13	0.351	0.016	0.243	0.055	0.458	0.004	0.283	0.002
57.13	0.361	0.019	0.263	0.043	0.494	0.000	0.323	0.015
63.92	0.367	0.024	0.276	0.044	0.517	0.002	0.346	0.028
76.92	0.388	0.024	0.291	0.050	0.542	0.007	0.374	0.032
85.21	0.394	0.023	0.302	0.052	0.550	0.002	0.392	0.038
92.25	0.392	0.019	0.313	0.045	0.553	0.005	0.393	0.036
107.25	0.423	0.003	0.320	0.051	0.579	0.006	0.398	0.041
119.54	0.431	0.016	0.333	0.054	0.590	0.007	0.400	0.037
147.02	0.467	0.010	0.358	0.056	0.629	0.028	0.407	0.036
160.54	0.474	0.014	0.371	0.052	0.618	0.003	0.408	0.036
176.13	0.492	0.014	0.370	0.065	0.630	0.006	0.403	0.047
192.19	0.492	0.017	0.379	0.058	0.644	0.004	0.406	0.041
204.21	0.512	0.016	0.386	0.058	0.654	0.003	0.409	0.036
217.25	0.518	0.009	0.391	0.052	0.659	0.005	0.407	0.042
231.19	0.527	0.010	0.395	0.061	0.664	0.004	0.405	0.042
246.21	0.535	0.013	0.399	0.059	0.675	0.011	0.406	0.041

266.25	0.548	0.021	0.404	0.061	0.686	0.005	0.418	0.039
279.54	0.551	0.019	0.408	0.063	0.695	0.006	0.419	0.041
293.54	0.558	0.011	0.412	0.064	0.701	0.005	0.421	0.042
307.54	0.564	0.004	0.415	0.065	0.708	0.007	0.422	0.043
321.54	0.557	0.008	0.408	0.064	0.706	0.008	0.420	0.048
332.54	0.568	0.009	0.413	0.065	0.716	0.006	0.427	0.033
359.54	0.574	0.013	0.417	0.065	0.728	0.001	0.421	0.037
387.25	0.582	0.006	0.417	0.063	0.738	0.002	0.423	0.039
402.17	0.589	0.004	0.411	0.067	0.745	0.006	0.423	0.043
420.17	0.596	0.004	0.418	0.062	0.747	0.005	0.428	0.047
449.17	0.584	0.040	0.429	0.070	0.747	0.004	0.438	0.039
478.98	0.588	0.047	0.443	0.065			0.456	0.049
510.98	0.595	0.045	0.449	0.069			0.457	0.042
532.21	0.607	0.050	0.456	0.073			0.469	0.036
540.17	0.607	0.046	0.453	0.068			0.460	0.043
547.13	0.615	0.039	0.454	0.069			0.456	0.045
562.21	0.616	0.045	0.458	0.068			0.461	0.042
568.13	0.623	0.063	0.457	0.068			0.465	0.043
575.00	0.612	0.048	0.456	0.062			0.471	0.049
583.13	0.627	0.045	0.464	0.065			0.476	0.060
595.13	0.625	0.050	0.462	0.067			0.472	0.043
606.13	0.627	0.047	0.464	0.070			0.479	0.048
620.00	0.631	0.047	0.475	0.074			0.480	0.042
644.04	0.637	0.047	0.471	0.073			0.481	0.049
658.13	0.634	0.047	0.470	0.073			0.485	0.041
673.15	0.639	0.044	0.478	0.070			0.487	0.052
694.54	0.645	0.050	0.480	0.079			0.483	0.041
707.54	0.638	0.051	0.475	0.073			0.485	0.047
742.54	0.666	0.054	0.480	0.076			0.488	0.054

Table 4. A.4. water sorption experimental results (cont.).

T [days]	W60 [%]	std.dev [%]	S60 [%]	std.dev [%]	C40 [%]	std.dev [%]
0.00	0.000	0.000	0.000	0.000	0.000	0.000
0.98	0.102	0.001	0.106	0.004	0.082	0.000
2.94	0.201	0.002	0.184	0.007	0.176	0.002
8.17	0.260	0.008	0.241	0.014	0.188	0.012
9.21	0.250	0.004	0.225	0.009	0.219	0.016
11.21	0.321	0.042	0.263	0.002	0.242	0.016
14.21	0.334	0.004	0.292	0.001	0.253	0.024
15.94	0.351	0.000	0.310	0.011	0.315	0.018
23.13	0.406	0.002	0.353	0.021	0.332	0.026
29.00	0.418	0.003	0.366	0.021	0.345	0.032
34.92	0.419	0.005	0.374	0.040	0.363	0.015
42.13	0.429	0.011	0.371	0.041	0.400	0.028
57.13	0.438	0.006	0.374	0.042	0.414	0.028
63.92	0.447	0.010	0.367	0.047	0.433	0.034
76.92	0.460	0.007	0.362	0.049	0.449	0.037
85.21	0.460	0.007	0.360	0.068	0.462	0.033
92.25	0.483	0.004	0.365	0.056	0.466	0.039
107.25	0.498	0.010	0.351	0.050	0.475	0.039
119.54	0.511	0.008	0.352	0.057	0.490	0.041
147.02	0.548	0.024	0.332	0.045	0.504	0.051

160.54	0.552	0.018	0.355	0.045	0.507	0.055
176.13	0.566	0.001	0.355	0.049	0.515	0.056
192.19	0.575	0.012	0.356	0.056	0.521	0.062
204.21	0.597	0.016	0.352	0.053	0.523	0.060
217.25	0.595	0.026	0.355	0.058	0.534	0.060
231.19	0.608	0.019	0.360	0.042	0.529	0.054
246.21	0.616	0.019	0.355	0.045	0.548	0.062
266.25	0.633	0.019	0.345	0.041	0.549	0.065
279.54	0.643	0.010	0.346	0.035	0.550	0.064
293.54	0.652	0.005	0.347	0.030	0.551	0.063
307.54	0.658	0.000	0.347	0.027	0.557	0.062
321.54	0.683	0.011	0.331	0.043	0.567	0.062
332.54	0.685	0.014	0.332	0.041	0.579	0.060
359.54	0.692	0.018	0.332	0.039	0.582	0.062
387.25	0.702	0.008	0.356	0.035	0.590	0.057
402.17	0.709	0.017	0.340	0.030	0.592	0.061
420.17	0.710		0.339	0.035	0.600	0.057
449.17	0.710		0.322	0.027	0.615	0.055
478.98			0.334	0.033	0.615	0.043
510.98			0.349	0.019	0.613	0.045
532.21			0.353	0.025	0.614	0.051
540.17			0.354		0.624	0.057
547.13			0.360		0.624	0.052
562.21			0.355		0.625	0.052
568.13			0.351		0.630	0.060
575.00			0.349		0.641	0.057
583.13			0.354		0.632	0.032
595.13			0.353		0.632	0.050
606.13					0.643	0.045
620.00					0.638	0.041
644.04					0.648	0.040
658.13					0.655	0.039
673.15					0.666	0.037
694.54					0.653	0.028
707.54					0.654	0.027
742.54						0.024

A.2 Thermo-mechanical experimental results

Table A.5. UP profile glass transition temperature experimental results.

W20				
t [months]	T_g tan δ [°C]	std.dev [°C]	T_g E' [°C]	std.dev [°C]
0	136.6	0.4	112.3	3.6
3	137.2	1.7	109.8	3.6
6	139.7	1.0	111.1	5.3
9	141.7	0.8	109.2	1.1
12	143.2	0.8	118.0	9.1
18	123.4	0.4	108.6	3.0
24	124.0	0.8	106.8	1.8

S20				
t [months]	T_g tan δ [°C]	std.dev [°C]	T_g E' [°C]	std.dev [°C]
0	136.6	0.4	112.3	3.6
3	137.1	0.9	105.7	4.4
6	139.2	0.9	104.6	15.1
9	139.9	1.2	95.3	8.2
12	142.3	2.8	106.2	10.9
18	124.6	0.2	111.3	3.8
24	123.9	0.4	105.3	1.6
W40				
t [months]	T_g tan δ [°C]	std.dev [°C]	T_g E' [°C]	std.dev [°C]
0	136.6	0.4	112.3	3.6
3	144.7	2.3	113.9	9.5
6	149.9	1.2	121.5	3.5
9	157.0	5.8	111.9	8.2
12	159.9	0.9	122.5	3.1
18	123.8	0.5	105.5	1.7
24	123.9	0.4	108.2	4.6
S40				
t [months]	T_g tan δ [°C]	std.dev [°C]	T_g E' [°C]	std.dev [°C]
0	136.6	0.4	112.3	3.6
3	149.5	4.7	99.7	7.8
6	144.6	1.3	116.0	13.5
9	158.5	3.5	110.9	10.8
12	169.0	2.0	125.1	12.9
18	124.3	0.4	109.5	3.2
24	124.9	0.1	113.9	0.9
W60				
t [months]	T_g tan δ [°C]	std.dev [°C]	T_g E' [°C]	std.dev [°C]
0	136.6	0.4	112.3	3.6
3	169.6	3.9	106.1	15.7
6	175.8	2.9	126.4	11.0
9	175.8	2.4	118.8	9.7
12	173.8	1.3	129.5	13.4
18	125.6	0.2	105.7	4.0
24	125.5	0.6	109.7	2.2
S60				
t [months]	T_g tan δ [°C]	std.dev [°C]	T_g E' [°C]	std.dev [°C]
0	136.6	0.4	112.3	3.6
3	162.5	6.6	102.9	2.4
6	171.4	2.0	121.2	0.0
9	177.0	6.1	115.0	6.7
12	182.6	1.4	130.8	1.1
18	126.2	1.3	107.4	3.1
24	126.0	0.1	108.0	0.6
C40				
t [months]	T_g tan δ [°C]	std.dev [°C]	T_g E' [°C]	std.dev [°C]
0	136.6	0.4	112.3	3.6
3	141.2	1.6	107.0	10.1
6	145.9	2.2	111.8	6.2
9	151.6	0.4	104.7	7.3
12	156.9	1.8	121.9	8.7
18	124.0	0.8	105.4	1.6
24	124.4	0.4	111.0	5.5

Table A.6. VE profile glass transition temperature experimental results.

W20				
t [months]	T_g tan d [°C]	std.dev [°C]	T_g E' [°C]	std.dev [°C]
0	124.1	0.3	106.6	1.3
3	126.4	1.1	108.3	2.6
6	127.3	0.1	109.7	5.2
9	125.9	0.6	109.3	1.8
12	126.3	0.5	111.3	5.8
18	124.6	0.1	110.8	4.3
24	125.8	0.5	106.3	2.0
S20				
t [months]	T_g tan d [°C]	std.dev [°C]	T_g E' [°C]	std.dev [°C]
0	124.1	0.3	106.6	1.3
3	124.8	0.5	106.7	4.4
6	125.9	0.4	104.0	3.5
9	124.3	0.3	109.4	4.5
12	127.5	0.4	108.2	0.5
18	125.7	0.3	109.3	4.4
24	126.2	0.9	110.2	3.7
W40				
t [months]	T_g tan d [°C]	std.dev [°C]	T_g E' [°C]	std.dev [°C]
0	124.1	0.3	106.6	1.3
3	124.0	0.4	113.1	0.9
6	123.6	1.2	109.1	1.5
9	125.4	0.1	112.1	4.1
12	126.8	0.2	112.9	3.4
18	125.4	0.3	110.2	2.6
24	126.4	0.1	108.7	6.5
S40				
t [months]	T_g tan d [°C]	std.dev [°C]	T_g E' [°C]	std.dev [°C]
0	124.1	0.3	106.6	1.3
3	125.9	0.5	110.1	2.2
6	124.0	0.4	112.8	1.2
9	124.6	0.8	108.8	3.6
12	128.7	0.4	107.9	1.7
18	125.1	0.2	108.3	3.0
24	127.6	0.9	109.6	4.0
W60				
t [months]	T_g tan d [°C]	std.dev [°C]	T_g E' [°C]	std.dev [°C]
0	124.1	0.3	106.6	1.3
3	127.4	0.2	106.4	4.7
6	128.0	1.7	110.3	4.8
9	127.3	0.8	106.9	2.5
12	131.6	1.3	111.0	5.6
18	126.4	0.5	108.6	1.8
24	126.2	1.9	105.9	2.6
S60				
t [months]	T_g tan d [°C]	std.dev [°C]	T_g E' [°C]	std.dev [°C]
0	124.1	0.3	106.6	1.3
3	124.2	0.3	109.2	4.0
6	125.4	0.4	107.7	3.4
9	127.7	0.3	108.0	5.5
12	128.2	0.6	108.1	3.4
18	128.1	0.7	111.8	2.7

24	130.2	0.5	112.7	5.0
C40				
t [months]	T_g tan d [°C]	std.dev [°C]	T_g E' [°C]	std.dev [°C]
0	124.1	0.3	106.6	1.3
3	125.4	0.8	105.4	2.8
6	123.0	0.7	105.8	2.6
9	128.4	0.3	108.2	2.2
12	128.1	0.8	107.6	6.9
18	124.9	0.4	108.5	4.2
24	129.9	4.6	115.3	4.1

A.3 Tensile experimental results

Table A.7. UP profile tensile tests experimental results.

W20						
t [months]	σ_{tu} [MPa]	std.dev [MPa]	var.coef [%]	E_t [GPa]	std.dev [GPa]	var.coef [%]
0	479.4	28.9	6.0	37.4	2.3	6.1
3	442.7	40.3	9.1	38.6	1.6	4.1
6	441.6	42.3	9.6	36.5	2.5	7.0
9	427.9	40.8	9.5	34.2	2.4	7.0
12	435.9	40.7	9.3	33.9	2.7	8.1
18	409.1	37.5	9.2	33.3	0.8	2.3
24	405.3	12.4	3.1	33.6	0.9	2.6
S20						
t [months]	σ_{tu} [MPa]	std.dev [MPa]	var.coef [%]	E_t [GPa]	std.dev [GPa]	var.coef [%]
0	479.45	28.86	6.02	37.36	2.29	6.13
3	422.01	28.50	6.75	39.44	1.32	3.34
6	406.07	51.26	12.62	37.33	1.19	3.19
9	424.59	31.21	7.35	36.40	1.93	5.31
12	432.04	29.56	6.84	35.69	1.96	5.49
18	412.23	13.84	3.36	33.45	1.20	3.57
24	401.04	18.35	4.58	34.26	0.97	2.84
W40						
t [months]	σ_{tu} [MPa]	std.dev [MPa]	var.coef [%]	E_t [GPa]	std.dev [GPa]	var.coef [%]
0	479.45	28.86	6.02	37.36	2.29	6.13
3	381.21	30.89	8.10	36.86	2.23	6.04
6	368.15	38.13	10.36	35.25	1.43	4.07
9	346.09	27.50	7.95	33.71	1.43	4.23
12	346.47	27.29	7.88	33.15	1.30	3.92
18	336.14	20.11	5.98	31.85	1.06	3.34
24	301.06	19.24	6.39	31.15	0.32	1.03
S40						
t [months]	σ_{tu} [MPa]	std.dev [MPa]	var.coef [%]	E_t [GPa]	std.dev [GPa]	var.coef [%]
0	479.45	28.86	6.02	37.36	2.29	6.13
3	394.44	49.62	12.58	37.02	2.09	5.65
6	402.95	16.20	4.02	35.63	2.22	6.24
9	384.31	37.35	9.72	35.88	2.48	6.92
12	356.70	21.62	6.06	33.06	1.74	5.25
18	376.14	19.96	5.31	32.52	1.45	4.45
24	342.00	27.77	8.12	31.00	0.86	2.77
W60						
t [months]	σ_{tu} [MPa]	std.dev [MPa]	var.coef [%]	E_t [GPa]	std.dev [GPa]	var.coef [%]
0	479.45	28.86	6.02	37.36	2.29	6.13

3	355.45	8.91	2.51	35.45	1.12	3.17
6	313.95	14.15	4.51	34.56	0.78	2.24
9	282.92	24.71	8.74	33.80	1.69	4.99
12	271.33	23.73	8.75	31.02	1.97	6.36
18	267.11	39.50	14.79	31.12	1.72	5.53
24	262.02	6.52	2.49	30.50	1.94	6.36
S60						
t [months]	σ_{tu} [MPa]	std.dev [MPa]	var.coef [%]	E_t [GPa]	std.dev [GPa]	var.coef [%]
0	479.45	28.86	6.02	37.36	2.29	6.13
3	379.85	12.15	3.20	35.98	1.07	2.97
6	320.07	25.50	7.97	34.71	1.30	3.73
9	306.13	23.48	7.67	33.89	1.52	4.49
12	322.46	18.86	5.85	33.56	1.66	4.94
18	291.39	20.30	6.97	31.56	0.33	1.06
24	306.46	16.64	5.43	30.20	1.30	4.29
C40						
t [months]	σ_{tu} [MPa]	std.dev [MPa]	var.coef [%]	E_t [GPa]	std.dev [GPa]	var.coef [%]
0	479.45	28.86	6.02	37.36	2.29	6.13
3	402.69	26.33	6.54	38.97	1.61	4.12
6	352.29	18.20	5.17	35.79	2.51	7.02
9	400.98	27.12	6.76	34.84	1.52	4.37
12	380.66	17.94	4.71	35.02	1.09	3.12
18	347.47	23.31	6.71	35.04	2.18	6.22
24	335.80	23.39	6.97	31.55	1.47	4.67

Table A.8. VE profile tensile tests experimental results.

W20						
t [months]	σ_{tu} [MPa]	std.dev [MPa]	var.coef [%]	E_t [GPa]	std.dev [GPa]	var.coef [%]
0.0	430.0	33.8	7.9	39.2	0.5	1.2
3.0	389.9	24.2	6.2	35.3	1.1	3.1
6.0	385.3	26.5	6.9	35.1	0.8	2.4
9.0	399.0	16.5	4.1	34.3	1.1	3.2
12.0	411.7	19.7	4.8	33.0	1.1	3.3
18.0	493.2	26.1	5.3	34.9	2.1	5.9
24.0	477.5	21.7	4.5	38.7	0.9	2.3
S20						
t [months]	σ_{tu} [MPa]	std.dev [MPa]	var.coef [%]	E_t [GPa]	std.dev [GPa]	var.coef [%]
0	430.05	33.81	7.86	39.22	0.47	1.20
3	380.74	9.42	2.47	34.74	1.27	3.66
6	365.18	28.40	7.78	34.43	1.55	4.52
9	411.88	21.82	5.30	33.14	0.84	2.52
12	426.66	26.13	6.12	32.45	0.95	2.92
18	500.81	16.54	3.30	35.40	1.87	5.27
24	492.74	35.72	7.25	38.17	1.43	3.75
W40						
t [months]	σ_{tu} [MPa]	std.dev [MPa]	var.coef [%]	E_t [GPa]	std.dev [GPa]	var.coef [%]
0	430.05	33.81	7.86	39.22	0.47	1.20
3	362.32	23.94	6.61	35.52	0.83	2.35
6	369.60	25.06	6.78	34.24	1.51	4.40
9	412.61	11.17	2.71	33.32	1.18	3.53
12	403.08	17.79	4.41	32.14	1.10	3.44
18	435.28	34.94	8.03	36.40	2.37	6.50
24	386.74	31.46	8.13	34.59	0.85	2.46
S40						

t [months]	σ_{tu} [MPa]	std.dev [MPa]	var.coef [%]	E_t [GPa]	std.dev [GPa]	var.coef [%]
0	430.05	33.81	7.86	39.22	0.47	1.20
3	395.31	19.44	4.92	35.08	1.90	5.41
6	383.16	14.26	3.72	33.09	1.16	3.50
9	418.25	22.48	5.37	33.63	0.85	2.54
12	424.56	13.95	3.29	33.02	0.62	1.88
18	472.00	5.94	1.26	33.05	1.30	3.92
24	438.20	25.95	5.92	32.53	0.72	2.21
W60						
t [months]	σ_{tu} [MPa]	std.dev [MPa]	var.coef [%]	E_t [GPa]	std.dev [GPa]	var.coef [%]
0	430.05	33.81	7.86	39.22	0.47	1.20
3	381.66	16.86	4.42	35.47	1.28	3.61
6	377.15	22.23	5.89	33.77	1.37	4.05
9	366.22	16.37	4.47	32.62	0.70	2.14
12	350.62	15.87	4.53	33.45	1.05	3.13
18	371.32	32.38	8.72	36.53	1.58	4.32
24	296.23	26.22	8.85	33.64	1.05	3.11
S60						
t [months]	σ_{tu} [MPa]	std.dev [MPa]	var.coef [%]	E_t [GPa]	std.dev [GPa]	var.coef [%]
0	430.05	33.81	7.86	39.22	0.47	1.20
3	383.79	20.86	5.44	36.47	1.71	4.69
6	375.66	15.79	4.20	33.11	1.66	5.02
9	409.49	16.81	4.10	32.68	0.90	2.75
12	403.99	20.85	5.16	32.10	1.56	4.85
18	425.12	16.40	3.86	32.64	1.21	3.69
24	337.11	12.18	3.61	33.37	0.23	0.70
C40						
t [months]	σ_{tu} [MPa]	std.dev [MPa]	var.coef [%]	E_t [GPa]	std.dev [GPa]	var.coef [%]
0	430.05	33.81	7.86	39.22	0.47	1.20
3	382.65	19.18	5.01	34.27	1.12	3.28
6	369.91	22.24	6.01	34.39	1.06	3.07
9	372.56	23.62	6.34	33.20	1.12	3.37
12	417.22	14.57	3.49	32.85	0.96	2.93
18	424.76	14.26	3.36	31.44	1.44	4.57
24	450.99	27.09	6.01	34.00	2.47	7.27

A.4 Flexural experimental results

Table A.9. UP profile flexural tests experimental results.

W20						
t [months]	σ_{fu} [MPa]	std.dev [MPa]	var.coef [%]	E_f [GPa]	std.dev [GPa]	var.coef [%]
0	552.6	40.2	7.3	21.4	2.3	10.7
3	554.1	28.1	5.1	23.1	1.7	7.6
6	541.3	35.0	6.5	22.8	0.7	3.0
9	521.8	19.0	3.6	22.7	0.5	2.3
12	521.2	36.7	7.0	23.3	0.1	0.5
18	496.1	31.4	6.3	22.8	0.6	2.6
24	467.7	19.7	4.2	22.7	1.0	4.6
S20						
t [months]	σ_{fu} [MPa]	std.dev [MPa]	var.coef [%]	E_f [GPa]	std.dev [GPa]	var.coef [%]
0	552.62	40.16	7.27	21.38	2.28	10.67
3	573.58	50.65	8.83	22.96	0.53	2.33
6	524.43	15.97	3.04	22.90	1.25	5.47

9	510.36	54.37	10.65	21.96	2.34	10.68
12	525.46	15.38	2.93	22.93	1.48	6.44
18	500.36	22.76	4.55	24.37	1.04	4.27
24	501.45	21.60	4.31	23.66	1.13	4.78
W40						
t [months]	σ_{fu} [MPa]	std.dev [MPa]	var.coef [%]	E_f [GPa]	std.dev [GPa]	var.coef [%]
0	552.62	40.16	7.27	21.38	2.28	10.67
3	475.90	24.99	5.25	20.80	1.41	6.76
6	426.19	18.71	4.39	21.43	2.06	9.60
9	383.98	15.12	3.94	21.50	1.31	6.10
12	376.38	26.26	6.98	21.81	0.97	4.44
18	351.98	8.38	2.38	22.93	0.87	3.80
24	338.46	25.72	7.60	23.90	0.86	3.58
S40						
t [months]	σ_{fu} [MPa]	std.dev [MPa]	var.coef [%]	E_f [GPa]	std.dev [GPa]	var.coef [%]
0	552.62	40.16	7.27	21.38	2.28	10.67
3	500.24	17.80	3.56	22.16	1.40	6.31
6	445.05	19.39	4.36	21.91	1.64	7.50
9	406.15	34.47	8.49	20.86	0.61	2.92
12	414.47	21.88	5.28	20.96	1.08	5.14
18	383.36	24.08	6.28	22.95	1.11	4.85
24	378.54	26.51	7.00	23.32	1.22	5.21
W60						
t [months]	σ_{fu} [MPa]	std.dev [MPa]	var.coef [%]	E_f [GPa]	std.dev [GPa]	var.coef [%]
0	552.62	40.16	7.27	21.38	2.28	10.67
3	409.31	31.15	7.61	22.16	0.56	2.51
6	365.30	15.82	4.33	20.52	1.29	6.26
9	292.86	13.93	4.76	19.18	2.31	12.07
12	313.58	38.86	12.39	18.73	1.74	9.27
18	308.84	20.30	6.57	22.01	0.75	3.43
24	289.27	13.37	4.62	24.32	0.68	2.81
S60						
t [months]	σ_{fu} [MPa]	std.dev [MPa]	var.coef [%]	E_f [GPa]	std.dev [GPa]	var.coef [%]
0	552.62	40.16	7.27	21.38	2.28	10.67
3	426.39	21.61	5.07	21.28	0.80	3.77
6	358.47	8.07	2.25	21.40	1.41	6.59
9	348.70	39.66	11.37	22.66	2.84	12.54
12	335.61	13.81	4.11	21.27	0.63	2.98
18	321.80	31.64	9.83	22.09	0.24	1.10
24	337.51	29.88	8.85	22.72	1.12	4.92
C40						
t [months]	σ_{fu} [MPa]	std.dev [MPa]	var.coef [%]	E_f [GPa]	std.dev [GPa]	var.coef [%]
0	552.62	40.16	7.27	21.38	2.28	10.67
3	501.85	20.84	4.15	23.52	1.79	7.61
6	485.57	47.92	9.87	22.18	1.67	7.52
9	445.66	43.89	9.85	21.52	2.71	12.61
12	413.70	16.31	3.94	21.54	1.34	6.20
18	388.42	12.49	3.22	21.36	1.78	8.33
24	380.50	15.69	4.12	24.51	0.97	3.96

Table A.10. VE profile flexural tests experimental results.

W20						
t [months]	σ_{fu} [MPa]	std.dev [MPa]	var.coef [%]	E_f [GPa]	std.dev [GPa]	var.coef [%]
0.0	561.1	16.8	3.0	23.0	0.8	3.4
3.0	578.3	36.3	6.3	22.9	1.1	4.7
6.0	550.3	15.6	2.8	23.0	0.6	2.8
9.0	535.4	25.6	4.8	25.3	0.5	1.8
12.0	509.2	29.3	5.7	22.6	1.4	6.1
18.0	505.1	60.1	11.9	23.9	2.9	12.1
24.0	502.9	31.2	6.2	24.5	1.2	5.1
S20						
t [months]	σ_{fu} [MPa]	std.dev [MPa]	var.coef [%]	E_f [GPa]	std.dev [GPa]	var.coef [%]
0	561.11	16.84	3.00	23.02	0.77	3.37
3	534.00	38.64	7.24	23.24	1.41	6.05
6	522.25	38.56	7.38	22.84	1.73	7.57
9	509.19	34.67	6.81	24.38	0.41	1.70
12	519.80	37.78	7.27	23.18	0.69	3.00
18	528.46	17.84	3.38	25.24	3.03	12.02
24	506.80	29.60	5.84	25.86	0.69	2.66
W40						
t [months]	σ_{fu} [MPa]	std.dev [MPa]	var.coef [%]	E_f [GPa]	std.dev [GPa]	var.coef [%]
0	561.11	16.84	3.00	23.02	0.77	3.37
3	555.18	28.18	5.08	23.40	1.26	5.40
6	499.01	16.15	3.24	24.24	0.54	2.23
9	474.28	39.53	8.34	22.36	1.37	6.13
12	444.06	26.83	6.04	21.97	0.84	3.81
18	461.39	14.21	3.08	22.74	2.10	9.25
24	447.51	39.40	8.80	24.31	1.53	6.30
S40						
t [months]	σ_{fu} [MPa]	std.dev [MPa]	var.coef [%]	E_f [GPa]	std.dev [GPa]	var.coef [%]
0	561.11	16.84	3.00	23.02	0.77	3.37
3	500.79	24.30	4.85	21.23	0.40	1.88
6	486.00	26.37	5.43	21.75	0.27	1.26
9	439.08	13.73	3.13	22.57	1.00	4.43
12	475.10	31.63	6.66	22.16	0.82	3.70
18	434.69	27.11	6.24	21.89	2.75	12.57
24	463.08	18.83	4.07	23.86	1.14	4.77
W60						
t [months]	σ_{fu} [MPa]	std.dev [MPa]	var.coef [%]	E_f [GPa]	std.dev [GPa]	var.coef [%]
0	561.11	16.84	3.00	23.02	0.77	3.37
3	483.63	38.98	8.06	23.00	1.75	7.62
6	456.70	12.70	2.78	20.96	0.41	1.97
9	395.08	24.30	6.15	21.63	1.18	5.46
12	344.06	20.68	6.01	22.15	1.43	6.44
18	390.66	16.21	4.15	23.39	2.72	11.61
24	354.06	25.81	7.29	24.64	2.45	9.95
S60						
t [months]	σ_{fu} [MPa]	std.dev [MPa]	var.coef [%]	E_f [GPa]	std.dev [GPa]	var.coef [%]
0	561.11	16.84	3.00	23.02	0.77	3.37
3	424.96	37.98	8.94	21.68	0.99	4.57
6	465.41	31.29	6.72	22.49	1.28	5.69
9	457.44	26.53	5.80	21.25	1.45	6.81
12	383.80	32.88	8.57	21.18	0.99	4.66
18	408.01	26.33	6.45	22.01	1.55	7.03

24	433.29	11.99	2.77	24.62	1.28	5.19
C40						
t [months]	σ_{fu} [MPa]	std.dev [MPa]	var.coef [%]	E_f [GPa]	std.dev [GPa]	var.coef [%]
0	561.11	16.84	3.00	23.02	0.77	3.37
3	502.44	44.17	8.79	21.68	1.00	4.60
6	521.85	24.51	4.70	22.43	0.71	3.19
9	513.64	22.49	4.38	24.89	0.81	3.23
12	473.38	28.93	6.11	22.36	1.53	6.84
18	453.91	33.75	7.44	22.03	2.04	9.26
24	474.12	24.35	5.13	26.34	0.92	3.49

A.5 In-plane shear experimental results

Table A.11. UP profile in-plane shear tests experimental results.

W20						
t [months]	t_u [MPa]	std.dev [MPa]	var.coef [%]	G [GPa]	std.dev [GPa]	var.coef [%]
0	53.7	1.9	3.5	3.0	0.5	15.7
3	53.7	3.0	5.6	2.6	0.4	13.9
6	51.3	6.5	12.6	3.3	0.1	3.4
9	49.8	1.3	2.7	2.5	0.1	4.5
12	47.6	2.5	5.3	3.1	0.3	9.8
18	47.9	1.6	3.4	3.1	0.4	11.7
24	46.7	2.1	4.5	3.3	0.4	11.5
S20						
t [months]	t_u [MPa]	std.dev [MPa]	var.coef [%]	G [GPa]	std.dev [GPa]	var.coef [%]
0	53.72	1.88	3.51	3.04	0.48	15.68
3	54.79	2.62	4.79	2.89	0.24	8.40
6	52.89	1.82	3.44	2.70	0.16	6.09
9	52.46	3.97	7.57	2.87	0.18	6.32
12	52.56	2.06	3.91	2.94	0.02	0.72
18	50.56	1.84	3.63	2.88	0.29	10.11
24	51.60	0.57	1.10	3.17	0.14	4.49
W40						
t [months]	t_u [MPa]	std.dev [MPa]	var.coef [%]	G [GPa]	std.dev [GPa]	var.coef [%]
0	53.72	1.88	3.51	3.04	0.48	15.68
3	49.87	1.62	3.25	2.87	0.40	13.97
6	48.24	2.20	4.56	2.76	0.29	10.56
9	42.30	1.07	2.53	2.34	0.33	13.97
12	40.53	1.40	3.45	2.62	0.42	16.13
18	41.30	2.25	5.46	3.38	0.35	10.48
24	40.40	2.63	6.51	3.30	0.31	9.27
S40						
t [months]	t_u [MPa]	std.dev [MPa]	var.coef [%]	G [GPa]	std.dev [GPa]	var.coef [%]
0	53.72	1.88	3.51	3.04	0.48	15.68
3	54.38	2.70	4.97	3.10	0.25	8.18
6	48.89	5.52	11.30	2.69	0.37	13.89
9	45.16	3.72	8.23	2.32	0.34	14.58
12	42.43	3.26	7.68	2.35	0.05	2.14
18	38.79	1.62	4.17	2.68	0.06	2.16
24	39.40	2.34	5.93	2.98	0.18	6.15
W60						
t [months]	t_u [MPa]	std.dev [MPa]	var.coef [%]	G [GPa]	std.dev [GPa]	var.coef [%]
0	53.72	1.88	3.51	3.04	0.48	15.68

3	45.46	2.06	4.52	2.77	0.24	8.54
6	41.43	2.99	7.22	2.67	0.33	12.18
9	35.91	3.05	8.49	2.17	0.17	7.76
12	37.53	3.31	8.83	2.41	0.16	6.64
18	32.56	3.38	10.37	2.77	0.48	17.32
24	29.56	3.12	10.55	2.74	0.09	3.13
S60						
t [months]	t_u [MPa]	std.dev [MPa]	var.coef [%]	G [GPa]	std.dev [GPa]	var.coef [%]
0	53.72	1.88	3.51	3.04	0.48	15.68
3	46.41	4.12	8.88	2.36	0.26	10.90
6	45.71	5.11	11.17	2.96	0.50	17.00
9	39.79	2.02	5.08	2.45	0.25	10.38
12	40.30	1.06	2.63	2.57	0.10	3.74
18	38.56	1.38	3.57	2.75	0.28	10.30
24	34.22	0.80	2.35	2.92	0.25	8.42
C40						
t [months]	t_u [MPa]	std.dev [MPa]	var.coef [%]	G [GPa]	std.dev [GPa]	var.coef [%]
0	53.72	1.88	3.51	3.04	0.48	15.68
3	53.04	0.85	1.60	2.77	0.23	8.25
6	51.06	1.60	3.12	2.65	0.19	7.17
9	48.63	1.89	3.89	2.54	0.15	5.91
12	46.97	1.43	3.04	2.47	0.39	15.78
18	44.87	4.04	9.01	2.77	0.11	3.86
24	45.81	2.11	4.61	2.97	0.13	4.40

Table A.12. VE profile in-plane shear tests experimental results.

W20						
t [months]	t_u [MPa]	std.dev [MPa]	var.coef [%]	G [GPa]	std.dev [GPa]	var.coef [%]
0	67.6	2.1	3.1	3.8	0.6	14.6
3	63.4	3.8	6.0	3.5	0.3	7.6
6	61.5	1.6	2.6	3.1	0.3	9.9
9	61.6	2.8	4.6	3.2	0.1	3.8
12	61.0	1.1	1.8	3.6	0.2	5.1
18	61.3	2.0	3.3	3.7	0.2	6.3
24	59.0	1.7	2.8	3.9	0.2	6.3
S20						
t [months]	t_u [MPa]	std.dev [MPa]	var.coef [%]	G [GPa]	std.dev [GPa]	var.coef [%]
0	67.59	2.10	3.10	3.77	0.55	14.62
3	68.03	1.57	2.30	3.84	0.52	13.63
6	63.86	1.62	2.53	3.54	0.15	4.22
9	62.59	1.19	1.90	3.49	0.26	7.52
12	61.23	3.53	5.76	3.70	0.50	13.48
18	62.15	2.70	4.35	3.77	0.32	8.43
24	59.68	2.62	4.39	3.84	0.23	6.05
W40						
t [months]	t_u [MPa]	std.dev [MPa]	var.coef [%]	G [GPa]	std.dev [GPa]	var.coef [%]
0	67.59	2.10	3.10	3.77	0.55	14.62
3	62.46	2.03	3.25	3.65	0.25	6.85
6	60.88	3.05	5.02	3.28	0.27	8.10
9	60.42	1.89	3.14	3.37	0.26	7.73
12	60.34	3.92	6.49	3.65	0.14	3.71
18	56.30	1.43	2.54	2.79	0.31	11.27
24	53.30	2.14	4.01	3.70	0.29	7.88

S40						
t [months]	t_u [MPa]	std.dev [MPa]	var.coef [%]	G [GPa]	std.dev [GPa]	var.coef [%]
0	67.59	2.10	3.10	3.77	0.55	14.62
3	68.19	1.74	2.55	3.68	0.57	15.46
6	61.19	1.35	2.20	3.16	0.25	7.89
9	61.53	3.16	5.14	3.30	0.44	13.25
12	61.19	2.08	3.40	3.65	0.56	15.37
18	61.28	1.27	2.07	3.88	0.18	4.60
24	56.46	1.82	3.23	3.48	0.19	5.32
W60						
t [months]	t_u [MPa]	std.dev [MPa]	var.coef [%]	G [GPa]	std.dev [GPa]	var.coef [%]
0	67.59	2.10	3.10	3.77	0.55	14.62
3	62.65	2.52	4.01	3.61	0.36	9.94
6	60.41	2.76	4.57	3.29	0.39	11.85
9	59.17	1.75	2.95	3.09	0.26	8.43
12	58.24	2.62	4.50	3.50	0.24	6.87
18	54.96	0.89	1.61	3.23	0.27	8.30
24	52.53	1.99	3.79	3.21	0.33	10.42
S60						
t [months]	t_u [MPa]	std.dev [MPa]	var.coef [%]	G [GPa]	std.dev [GPa]	var.coef [%]
0	67.59	2.10	3.10	3.77	0.55	14.62
3	63.18	2.66	4.21	3.49	0.30	8.62
6	60.97	1.79	2.94	3.24	0.26	8.12
9	59.49	4.11	6.90	3.32	0.26	7.97
12	58.06	0.62	1.06	3.28	0.15	4.58
18	54.79	4.14	7.55	3.37	0.73	21.64
24	51.79	0.85	1.64	3.06	0.15	5.07
C40						
t [months]	t_u [MPa]	std.dev [MPa]	var.coef [%]	G [GPa]	std.dev [GPa]	var.coef [%]
0	67.59	2.10	3.10	3.77	0.55	14.62
3	63.64	4.35	6.84	3.76	0.31	8.16
6	62.15	1.35	2.17	3.65	0.20	5.48
9	60.56	1.90	3.14	3.62	0.14	3.87
12	58.80	1.33	2.26	3.57	0.06	1.79
18	57.92	1.05	1.81	3.41	0.10	2.89
24	57.12	0.44	0.78	3.61	0.47	12.89

A.6 Interlaminar shear experimental results

Table A.13. UP profile interlaminar shear tests experimental results.

W20						
t [months]	τ_u [MPa]	std.dev [MPa]	var.coef [%]	s_u [mm]	std.dev [GPa]	var.coef [%]
0	34.72	4.54	13.08	0.55	0.09	17.06
3	35.21	3.66	10.41	0.81	0.17	21.06
6	32.92	5.27	16.02	0.56	0.10	17.05
9	31.80	5.48	17.22	0.43	0.08	18.64
12	32.55	4.13	12.69	0.60	0.09	14.31
18	31.86	1.51	4.74	0.59	0.06	10.62
24	31.53	2.22	7.03	0.56	0.09	16.77
S20						
t [months]	τ_u [MPa]	std.dev [MPa]	var.coef [%]	s_u [mm]	std.dev [GPa]	var.coef [%]
0	34.72	4.54	13.08	0.55	0.09	17.06
3	34.75	2.25	6.49	0.85	0.14	17.01

6	33.44	5.91	17.68	0.62	0.15	23.46
9	32.82	2.14	6.53	0.51	0.08	16.22
12	33.08	4.06	12.28	0.60	0.09	15.63
18	32.56	2.66	8.16	0.60	0.09	14.37
24	32.05	1.32	4.11	0.70	0.12	17.74
W40						
t [months]	τ_u [MPa]	std.dev [MPa]	var.coef [%]	s_u [mm]	std.dev [GPa]	var.coef [%]
0	34.72	4.54	13.08	0.55	0.09	17.06
3	31.80	4.23	13.32	0.89	0.10	11.10
6	32.31	6.75	20.89	0.54	0.10	19.00
9	30.37	1.38	4.53	0.54	0.07	12.17
12	29.59	3.63	12.26	0.51	0.07	13.36
18	29.50	0.96	3.24	0.51	0.06	12.61
24	27.54	2.04	7.40	0.58	0.18	31.61
S40						
t [months]	τ_u [MPa]	std.dev [MPa]	var.coef [%]	s_u [mm]	std.dev [GPa]	var.coef [%]
0	34.72	4.54	13.08	0.55	0.09	17.06
3	32.92	4.01	12.19	0.75	0.09	11.63
6	31.83	5.74	18.04	0.54	0.13	24.13
9	32.03	4.32	13.49	0.59	0.10	16.22
12	29.35	4.06	13.84	0.52	0.06	11.17
18	28.84	1.47	5.11	0.52	0.11	22.01
24	30.03	1.05	3.48	0.49	0.07	15.09
W60						
t [months]	τ_u [MPa]	std.dev [MPa]	var.coef [%]	s_u [mm]	std.dev [GPa]	var.coef [%]
0	34.72	4.54	13.08	0.55	0.09	17.06
3	31.19	4.41	14.14	0.71	0.05	7.52
6	27.10	4.13	15.23	0.51	0.05	9.28
9	27.01	2.81	10.39	0.56	0.06	10.35
12	25.35	4.13	16.31	0.58	0.08	13.33
18	24.34	0.61	2.50	0.44	0.04	8.73
24	22.62	1.01	4.47	0.38	0.08	19.98
S60						
t [months]	τ_u [MPa]	std.dev [MPa]	var.coef [%]	s_u [mm]	std.dev [GPa]	var.coef [%]
0	34.72	4.54	13.08	0.55	0.09	17.06
3	29.50	2.71	9.19	0.74	0.12	15.96
6	28.11	3.18	11.30	0.49	0.07	13.65
9	29.24	6.33	21.65	0.47	0.10	22.25
12	24.40	3.85	15.76	0.50	0.06	12.00
18	22.90	2.94	12.82	0.48	0.02	5.10
24	22.62	2.3	10.17	0.49	0.05	10.20
C40						
t [months]	τ_u [MPa]	std.dev [MPa]	var.coef [%]	s_u [mm]	std.dev [GPa]	var.coef [%]
0	34.72	4.54	13.08	0.55	0.09	17.06
3	32.46	3.36	10.34	0.73	0.11	14.67
6	33.31	2.32	6.96	0.56	0.08	14.01
9	36.16	5.31	14.68	0.57	0.06	11.30
12	31.55	4.34	13.77	0.52	0.13	25.46
18	27.59	3.54	12.82	0.50	0.03	5.44
24	25.65	2.4	9.36	0.47	0.05	10.64

Table A.14. VE profile interlaminar shear tests experimental results.

W20						
t [months]	τ_u [MPa]	std.dev [MPa]	var.coef [%]	s_u [mm]	std.dev [GPa]	var.coef [%]
0	37.81	1.73	4.57	0.5356	0.040	7.52
3	34.21	2.30	6.73	0.72	0.09	12.67
6	34.48	0.86	2.50	0.53	0.08	14.27
9	35.05	1.57	4.48	0.52	0.04	7.38
12	34.20	1.61	4.69	0.57	0.07	12.41
18	37.64	2.86	7.59	0.51	0.02	4.43
24	35.17	0.63	1.79	0.53	0.04	7.55
S20						
t [months]	τ_u [MPa]	std.dev [MPa]	var.coef [%]	s_u [mm]	std.dev [GPa]	var.coef [%]
0	37.81	1.73	4.57	0.5356	0.040	7.52
3	34.72	3.21	9.24	0.75	0.05	7.16
6	32.75	1.25	3.81	0.58	0.07	12.09
9	34.86	1.11	3.19	0.50	0.02	3.09
12	32.94	1.34	4.06	0.51	0.03	5.71
18	37.27	2.88	7.74	0.61	0.06	10.00
24	36.44	2.77	7.60	0.57	0.09	16.10
W40						
t [months]	τ_u [MPa]	std.dev [MPa]	var.coef [%]	s_u [mm]	std.dev [GPa]	var.coef [%]
0	37.81	1.73	4.57	0.5356	0.040	7.52
3	33.86	1.50	4.44	0.73	0.04	6.00
6	33.27	1.36	4.09	0.53	0.04	7.86
9	35.14	1.08	3.09	0.53	0.03	6.45
12	33.68	1.46	4.34	0.53	0.03	6.14
18	37.70	0.93	2.45	0.47	0.04	8.25
24	32.81	1.55	4.73	0.56	0.06	10.24
S40						
t [months]	τ_u [MPa]	std.dev [MPa]	var.coef [%]	s_u [mm]	std.dev [GPa]	var.coef [%]
0	37.81	1.73	4.57	0.5356	0.040	7.52
3	33.86	1.83	5.39	0.73	0.07	8.92
6	34.74	2.12	6.10	0.54	0.05	9.71
9	31.77	0.95	2.99	0.46	0.04	9.54
12	33.64	1.43	4.25	0.56	0.04	7.14
18	36.40	0.98	2.69	0.52	0.06	12.22
24	32.72	1.77	5.42	0.52	0.09	16.58
W60						
t [months]	τ_u [MPa]	std.dev [MPa]	var.coef [%]	s_u [mm]	std.dev [GPa]	var.coef [%]
0	37.81	1.73	4.57	0.5356	0.040	7.52
3	33.42	1.98	5.91	0.68	0.04	5.14
6	31.57	1.19	3.77	0.52	0.03	5.06
9	31.03	2.31	7.45	0.52	0.05	9.26
12	31.66	2.10	6.63	0.49	0.03	6.24
18	34.58	0.77	2.23	0.52	0.03	6.31
24	29.38	0.86	2.93	0.44	0.04	9.71
S60						
t [months]	τ_u [MPa]	std.dev [MPa]	var.coef [%]	s_u [mm]	std.dev [GPa]	var.coef [%]
0	37.81	1.73	4.57	0.5356	0.040	7.52
3	34.40	0.85	2.47	0.79	0.11	14.02
6	33.44	2.40	7.17	0.57	0.04	7.57
9	31.18	2.87	9.22	0.53	0.04	7.99
12	32.05	1.17	3.66	0.54	0.09	16.09
18	35.05	0.88	2.50	0.57	0.05	7.92

24	29.38	0.80	2.73	0.48	0.17	35.48
C40						
t [months]	τ_u [MPa]	std.dev [MPa]	var.coef [%]	s_u [mm]	std.dev [GPa]	var.coef [%]
0	37.81	1.73	4.57	0.5356	0.040	7.52
3	36.09	2.03	5.61	0.79	0.10	12.75
6	34.18	0.92	2.69	0.56	0.05	8.82
9	34.21	2.85	8.33	0.48	0.02	4.21
12	31.66	4.01	12.68	0.56	0.04	7.05
18	35.24	0.74	2.09	0.50	0.02	3.01
24	34.13	3.22	9.42	0.55	0.07	13.44

B. Natural ageing of pultruded GFRP profiles experimental results

B.1 Temperature monitoring experimental results

Table B.1. Monthly variation of the air temperature between 2005 and 2017 in Lisbon.

Month	T_{min} [°C]	std.dev [°C]	T_{med} [°C]	std.dev [°C]	T_{max} [°C]	std.dev [°C]
Jan.	8.30	1.82	11.70	1.06	16.21	1.33
Fev.	8.44	1.67	11.76	1.14	16.26	1.42
Mar.	9.97	1.08	13.78	1.06	19.08	1.97
Apr.	12.02	0.84	15.98	0.88	21.70	1.69
May.	14.09	1.12	18.26	1.52	24.38	2.30
Jun.	16.96	1.19	21.38	1.61	27.48	2.51
Jul.	18.23	1.13	22.87	1.33	29.60	1.67
Aug.	18.56	1.17	23.25	1.43	30.20	2.05
Sep.	17.82	0.97	22.00	1.35	28.37	2.23
Oct.	15.93	1.09	19.13	1.18	23.96	2.04
Nov.	11.72	1.89	15.16	1.31	19.87	1.48
Dec.	9.07	1.54	12.24	1.13	16.56	1.26

B.2 Humidity monitoring experimental results

Table B.2. Monthly variation of the relative humidity between 2005 and 2017 in Lisbon.

Month	H_{min} [%]	std.dev [%]	H_{med} [%]	std.dev [%]	H_{max} [%]	std.dev [%]]
Jan.	59.00	10.44	80.44	6.89	93.33	4.56
Fev.	56.00	9.14	76.71	7.95	91.46	6.81
Mar.	49.17	7.63	71.92	6.41	89.63	5.74
Apr.	46.18	6.65	70.06	6.20	88.66	4.20
May.	39.58	9.73	63.80	5.51	83.31	5.87
Jun.	42.30	6.51	64.35	5.72	83.66	4.44
Jul.	39.32	6.18	63.13	5.32	82.34	5.21
Aug.	37.37	7.00	61.94	6.52	82.97	5.12
Sep.	42.37	7.97	65.53	8.05	84.82	6.35
Oct.	53.88	7.95	75.63	6.33	91.15	4.79
Nov.	57.39	8.86	77.54	8.18	91.58	6.76
Dec.	61.58	6.79	80.93	5.95	92.59	4.63

B.3 Radiation monitoring experimental results

Table B.3. Radiation values between 2005 and 2017 in Lisbon.

Solar radiation [kJ/m^2]						
Month	Global value			UV component [300-400 nm]		
	Total	Minimum	Maximum	Total	Minimum	Maximum
Jan.	366461	577.5	23865	10475	61.0	580.0
Fev.	355263	2001.0	24644	11916	151.5	697.5
Mar.	558947	2798.0	27103	19882	189.0	905.5
Apr.	604013	8099.5	26529	23434	385.5	973.0
May.	612812	6317.0	25612	25807	344.5	1024.5
Jun.	581996	6243.3	23922	25384	320.3	1027.3
Jul.	688161	11931.0	24452	29048	564.3	1018.3

Aug.	710821	8754.0	25677	27275	405.3	1000.3
Sep.	642735	7821.7	26020	22813	349.7	936.0
Oct.	562879	4000.3	25601	18203	238.0	814.3
Nov.	432776	1570.3	23355	12609	121.7	636.7
Dec.	332178	894.0	21333	9454	92.7	481.3

B.4 Tensile experimental results

Table B.4. UP profile tensile tests experimental results.

NE [months]	σ_{tu} [MPa]	std.dev [MPa]	var.coef [%]	QUV [hours]	σ_{tu} [MPa]	std.dev [MPa]	var.coef [%]
0	406.0	31.1	7.7	0	406.0	31.1	7.7
12	364.0	39.3	10.8	1000	413.6	15.8	3.8
24	348.0	25.3	7.3	2000	386.0	39.5	10.2
42	455.5	40.3	8.8	3000	322.0	89.8	27.9
102	344.5	18.5	5.4				

Table B.5. UP profile tensile tests experimental results (cont.).

NE [months]	E_t [GPa]	std.dev [MPa]	var.coef [%]	QUV [hours]	E_t [GPa]	std.dev [MPa]	var.coef [%]
0	37.6	2.6	6.9	0	37.6	2.6	6.9
12	25.2	2.6	10.3	1000	33.31	9.23	27.7
24	31.0	3.0	9.7	2000	39.96	5.7	14.3
42	31.4	7.0	22.3	3000	28.45	6.01	21.1
102	30.9	3.1	10.1				

Table B.6. VE profile tensile tests experimental results.

NE [months]	σ_{tu} [MPa]	std.dev [MPa]	var.coef [%]	QUV [hours]	σ_{tu} [MPa]	std.dev [MPa]	var.coef [%]
0	394.0	52.0	13.2	0	394.0	52.0	13.2
12	381.0	42.0	11.0	1000	389.6	50.4	12.9
42	455.0	87.0	19.1	2000	380.4	55.9	14.7
102	395.6	17.1	4.3	3000	392.8	21.2	5.4

Table B.7. VE profile tensile tests experimental results (cont.).

NE [months]	E_t [GPa]	std.dev [MPa]	var.coef [%]	QUV [hours]	E_t [GPa]	std.dev [MPa]	var.coef [%]
0	38.9	4.0	10.3	0	38.9	4.0	10.3
12	34.9	4.8	13.8	1000	39.3	5.0	12.7
42	39.8	3.6	9.0	2000	41.2	8.3	20.1
102	36.5	2.5	6.8	3000	33.8	4.1	12.1

B.5 Flexural experimental results

Table B.8. UP profile flexural tests experimental results.

NE [months]	σ_{fu} [MPa]	std.dev [MPa]	var.coef [%]	QUV [hours]	σ_{fu} [MPa]	std.dev [MPa]	var.coef [%]
0	472.2	76.4	16.2	0	472.2	76.4	16.2
12	475.9	42.1	8.8	1000	425.9	67.5	15.8
24	464.6	43.3	9.3	2000	443.1	58.2	13.1
42	414.1	65.8	15.9	3000	491.8	19.7	4.0
102	437.0	55.4	12.7				

Table B.9. UP profile flexural tests experimental results (cont.).

NE [months]	E_f [GPa]	std.dev [MPa]	var.coef [%]	QUV [hours]	E_f [GPa]	std.dev [MPa]	var.coef [%]
0	19.3	2.3	11.9	0	19.3	2.3	11.9
12	16.5	2.6	15.8	1000	17.3	1.7	9.8
24	17.1	1.1	6.4	2000	15.3	2	13.1
42	19.1	3.4	17.6	3000	20	2.8	14.0
102	20.3	2.8					

Table B.10. VE profile flexural tests experimental results.

NE [months]	σ_{fu} [MPa]	std.dev [MPa]	var.coef [%]	QUV [hours]	σ_{fu} [MPa]	std.dev [MPa]	var.coef [%]
0	537.0	73.0	13.6	0	537.0	73.0	13.6
12	496.1	13.5	2.7	1000	490.7	27.6	5.6
24	527.8	42.9	8.1	2000	488.5	34.7	7.1
42	418.8	86.4	20.6	3000	467.0	80.5	17.2
102	456.1	30.7	6.7				

Table B.11. VE profile flexural tests experimental results (cont.).

NE [months]	E_f [GPa]	std.dev [MPa]	var.coef [%]	QUV [hours]	E_f [GPa]	std.dev [MPa]	var.coef [%]
0	28.4	3.4	12.0	0	28.4	3.4	12.0
12	18.0	2.4	13.3	1000	24.8	2.8	11.3
24	22.0	2.7	12.3	2000	23.4	2.4	10.3
42	20.3	3.9	19.4	3000	25.6	2.8	10.9
102	24.5	1.5	6.0				

B.6 Interlaminar shear experimental results

Table B.12. UP profile interlaminar shear tests experimental results.

NE [months]	σ_{sbs} [MPa]	std.dev [MPa]	var.coef [%]	QUV [hours]	σ_{sbs} [MPa]	std.dev [MPa]	var.coef [%]
0	38.5	2.7	7.0	0	38.5	2.7	7.0
12	36.2	2.6	7.2	1000	37.6	1.7	4.5
24	33.4	8.0	24.0	2000	35.3	1.0	2.8
42	36.6	3.5	9.7	3000	35.3	3.7	10.5
102	34.1	1.9	5.6				

Table B.13. VE profile interlaminar shear tests experimental results.

NE [months]	s_{sbs} [MPa]	std.dev [MPa]	var.coef [%]	QUV [hours]	s_{sbs} [MPa]	std.dev [MPa]	var.coef [%]
0	39.2	4.2	10.6	0	39.2	4.2	10.6
12	40.5	2.7	6.7	1000	40.8	1.3	3.2
24	31.5	3.4	10.7	2000	38.2	2.2	5.8
42	41.0	0.8	2.0	3000	36.6	2.1	5.7
102	36.5	1.5					

C. Effects of thermal cycles on pultruded GFRP profiles experimental results

C.1 Thermo-mechanical experimental retention results

Table C.1. UP profile glass transition temperature experimental retention results.

TC [cycles]	T_g tan δ [%]	std.dev [%]	var.coef [%]	T_g E' [%]	std.dev [%]	var.coef [%]
0	100.0	0.8	0.8	100.0	1.5	1.5
70	101.5	0.9	0.9	96.3	5.0	5.2
120	100.8	0.7	0.7	92.6	3.0	3.2
190	100.7	0.5	0.5	99.4	5.0	5.0
200	105.9	0.4	0.4	104.3	2.0	1.9
400	107.0	0.4	0.4	108.0	4.0	3.7
600	100.6	1.1	1.1	102.1	4.0	3.9

Table C.2. VE profile glass transition temperature experimental retention results.

TC [cycles]	T_g tan δ [%]	std.dev [%]	var.coef [%]	T_g [%]	std.dev [%]	var.coef [%]
0	100.0	1.5	1.5	100.0	1.3	1.3
70	96.3	5.0	5.2	99.2	4.0	4.0
120	92.6	3.0	3.2	97.0	3.0	3.1
190	99.4	5.0	5.0	98.0	4.5	4.5
200	104.3	2.0	1.9	102.1	2.7	2.6
400	105.8	0.2	0.2	113.6	1.6	1.4
600	103.3	0.6	0.6	100.5	2.5	2.4

C.2 Tensile experimental retention results

Table C.3. UP profile tensile tests experimental retention results.

TC [cycles]	σ_{tu} [%]	std.dev [%]	var.coef [%]	E_t [%]	std.dev [%]	var.coef [%]
0	100.0	7.6	7.6	100.0	6.9	6.9
70	91.6	11.2	12.2	88.3	7.5	8.5
120	94.0	13.8	14.7	97.9	13.6	13.9
190	86.9	14.2	16.3	85.1	12.2	14.3
200	84.7	8.0	9.5	97.3	6.0	6.2
400	102.1	6.4	6.3	87.8	4.0	4.6
600	98.6	7.6	7.7	98.1	8.6	8.8

Table C.4. VE profile tensile tests experimental retention results.

TC [cycles]	σ_{tu} [%]	std.dev [%]	var.coef [%]	E_t [%]	std.dev [%]	var.coef [%]
0	100.0	13.2	13.2	100.0	7.0	7.0
70	102.7	6.9	6.7	95.1	8.1	8.5
120	103.6	5.0	4.8	100.3	9.2	9.2
190	107.8	3.7	3.4	92.5	8.1	8.7
200	108.2	4.3	4.0	91.0	4.5	4.9
400	103.0	3.4	3.3	79.9	4.8	6.0
600	99.3	3.1	3.1	88.5	2.8	3.2

C.3 Flexural experimental retention results

Table C.5. UP profile flexural tests experimental retention results.

TC [cycles]	σ_{fu} [%]	std.dev [%]	var.coef [%]	E_f [%]	std.dev [%]	var.coef [%]
0	100.0	16.2	16.2	100.0	19.5	19.5
70	87.3	16.3	18.6	85.4	17.6	20.6
120	90.3	19.9	22.0	81.0	10.4	12.8
190	89.8	17.8	19.8	76.5	20.2	26.4
200	88.4	1.7	1.9	80.7	6.7	8.3
400	85.4	4.5	5.3	78.3	14.7	18.8
600	88.5	9.8	11.1	81.2	6.8	8.4

Table C.6. VE profile flexural tests experimental retention results.

TC [cycles]	σ_{fu} [%]	std.dev [%]	var.coef [%]	E_f [%]	std.dev [%]	var.coef [%]
0	100.0	13.6	13.6	100.0	12.0	12.0
70	88.5	17.5	19.8	77.5	17.7	22.9
120	84.2	12.4	14.7	73.6	12.9	17.6
190	87.0	13.7	15.8	75.4	16.8	22.3
200	89.7	10.3	11.5	82.1	3.7	4.5
400	90.2	2.8	3.1	79.4	4.8	6.1
600	88.1	5.9	6.7	83.1	5.8	7.0

C.4 In-plane shear experimental retention results

Table C.7. UP profile in-plane shear tests experimental retention results.

TC [cycles]	t_u [%]	std.dev [%]	var.coef [%]	G [%]	std.dev [%]	var.coef [%]
0	100.0	3.5	3.5	100.0	15.7	15.7
200	94.5	8.6	9.1	93.9	8.4	9.0
400	92.8	9.4	10.1	90.1	10.3	11.5
600	93.2	6.6	7.0	87.7	12.3	14.0

Table C.8. VE profile in-plane shear tests experimental retention results.

TC [cycles]	t_u [%]	std.dev [%]	var.coef [%]	G [%]	std.dev [%]	var.coef [%]
0	100.0	3.1	3.1	100.0	14.6	14.6
200	96.8	2.9	3.0	96.9	12.6	13.0
400	97.6	2.7	2.8	93.9	10.4	11.0
600	99.4	1.5	1.5	95.3	13.1	13.7

C.5 Interlaminar shear experimental retention results

Table C.9. UP and VE profiles interlaminar shear tests experimental retention results.

TC [cycles]	STR [Mpa]	std.dev [°C]	var.coef [%]	STR [Mpa]	std.dev [°C]	var.coef [%]
0	100.0	7.0	7.0	100.0	10.7	10.7
70	91.4	15.6	17.1	94.9	12.1	12.7
120	93.5	5.8	6.2	91.8	6.7	7.3
190	88.6	11.4	12.9	97.7	6.0	6.1
200	87.2	9.5	10.9	94.6	5.2	5.5
400	92.3	4.3	4.6	93.4	4.1	4.4
600	88.6	11.8	13.3	91.0	7.3	8.0

D. Synergistic effects of different ageing environments and sustained loading on pultruded GFRP profiles experimental results

D.1 Natural weathering and flexural loading experimental results

Table D.1. UP profile flexure tests experimental results under 10% of the UFS load.

t [months]	σ_{fu} [MPa]	std.dev [MPa]	var.coef [%]	Ef [GPa]	std.dev [GPa]	var.coef [%]
0	552.62	40.16	7.27	21.38	2.28	10.67
3	604.10	24.57	4.07	23.93	0.43	1.81
6	581.14	12.86	2.21	22.78	0.60	2.65
12	595.56	26.50	4.45	23.27	0.90	3.88
18	601.43	53.96	8.97	23.75	0.15	0.63
24	580.97	48.56	8.36	23.12	0.53	2.29

Table D.2. VE profile flexure tests experimental results under 10% of the UFS load.

t [months]	σ_{fu} [MPa]	std.dev [MPa]	var.coef [%]	Ef [GPa]	std.dev [GPa]	var.coef [%]
0	561.11	16.84	3.00	23.02	0.77	3.37
3	567.21	9.80	1.73	25.27	0.26	1.01
6	536.29	10.96	2.04	25.21	3.81	15.11
12	524.00	43.49	8.30	23.40	2.19	9.35
18	561.66	30.33	5.40	24.97	2.87	11.50
24	585.50	10.75	1.84	24.34	2.84	11.68

Table D.3. UP profile flexure tests experimental results under 20% of the UFS load.

t [months]	σ_{fu} [MPa]	std.dev [MPa]	var.coef [%]	Ef [GPa]	std.dev [GPa]	var.coef [%]
0	552.62	40.16	7.27	21.38	2.28	10.67
3	583.46	32.19	5.52	23.44	0.71	3.01
6	558.73	17.20	3.08	21.60	0.80	3.70
12	579.50	22.44	3.87	22.89	0.56	2.45
18	560.40	48.50	8.65	23.01	1.35	5.87
24	575.15	34.67	6.03	22.26	0.09	0.42

Table D.4. VE profile flexure tests experimental results under 20% of the UFS load.

t [months]	σ_{fu} [MPa]	std.dev [MPa]	var.coef [%]	Ef [GPa]	std.dev [GPa]	var.coef [%]
0	561.11	16.84	3.00	23.02	0.77	3.37
3	517.43	40.71	7.87	22.77	2.52	11.05
6	488.24	8.13	1.67	22.50	0.80	3.57
12	519.19	26.55	5.11	23.22	2.09	9.00
18	558.75	28.75	5.15	24.95	1.95	7.82
24	560.43	32.59	5.81	23.78	3.21	13.51

D.2 Continuous condensation and flexural loading experimental results

Table D.5. UP profile flexure tests experimental results under 10% of the UFS load.

t [months]	σ_{fu} [MPa]	std.dev [MPa]	var.coef [%]	Ef [GPa]	std.dev [GPa]	var.coef [%]
0	552.62	40.16	7.27	21.38	2.28	10.67
3	575.39	15.82	2.75	23.81	0.99	4.16
6	555.95	32.38	5.82	22.37	1.25	5.59
12	535.18	27.67	5.17	22.36	0.30	1.33
18	520.35	24.91	4.79	23.75	0.28	1.17
24	515.69	11.60	2.25	23.78	0.28	1.17

Table D.6. VE profile flexure tests experimental results under 10% of the UFS load.

t [months]	σ_{fu} [MPa]	std.dev [MPa]	var.coef [%]	Ef [GPa]	std.dev [GPa]	var.coef [%]
0	561.11	16.84	3.00	23.02	0.77	3.37
3	512.15	16.78	3.28	23.96	2.95	12.31
6	548.33	4.47	0.81	24.28	1.93	7.94
12	524.27	50.60	9.65	22.40	3.39	15.12
18	519.41	20.83	4.01	23.88	2.30	9.63
24	525.63	32.31	6.15	22.46	2.73	12.17

Table D.7.UP profile flexure tests experimental results under 20% of the UFS load.

t [months]	σ_{fu} [MPa]	std.dev [MPa]	var.coef [%]	Ef [GPa]	std.dev [GPa]	var.coef [%]
0	552.62	40.16	7.27	21.38	2.28	10.67
3	568.36	34.25	6.03	23.63	1.18	5.01
6	542.01	30.40	5.61	21.33	0.41	1.92
12	530.03	20.23	3.82	22.16	1.98	8.93
18	486.50	45.60	9.37	21.49	1.14	5.33
24	480.54	52.79	10.99	22.89	1.00	4.36

Table D.8. VE profile flexure tests experimental results under 20% of the UFS load.

t [months]	σ_{fu} [MPa]	std.dev [MPa]	var.coef [%]	Ef [GPa]	std.dev [GPa]	var.coef [%]
0	561.11	16.84	3.00	23.02	0.77	3.37
3	553.26	38.65	6.99	23.47	2.28	9.70
6	533.77	29.75	5.57	23.92	2.58	10.78
12	499.91	13.08	2.62	22.23	2.87	12.90
18	541.74	30.66	5.66	23.32	1.75	7.50
24	521.32	21.05	4.04	22.14	3.13	14.16

D.3 Controlled environment and flexural loading experimental results

Table D.9. UP profile flexure tests experimental results under 10% of the UFS load.

t [months]	σ_{fu} [MPa]	std.dev [MPa]	var.coef [%]	Ef [GPa]	std.dev [GPa]	var.coef [%]
0	552.62	40.16	7.27	21.38	2.28	10.67
3	576.20	36.71	6.37	23.92	0.46	1.91
6	560.41	50.82	9.07	25.99	0.63	2.41
12	543.90	10.19	1.87	24.79	1.25	5.03
18	604.87	32.32	5.34	24.35	0.82	3.38
24	622.51	27.82	4.47	23.63	0.68	2.87

Table D.10. VE profile flexure tests experimental results under 10% of the UFS load.

t [months]	σ_{fu} [MPa]	std.dev [MPa]	var.coef [%]	Ef [GPa]	std.dev [GPa]	var.coef [%]
0	561.11	16.84	3.00	23.02	0.77	3.37
3	540.95	39.89	7.37	21.87	1.69	7.71
6	550.22	34.98	6.36	22.40	1.13	5.04
12	547.03	48.80	8.92	22.57	1.84	8.16
18	526.41	33.55	6.37	22.90	1.49	6.50
24	530.62	25.76	4.86	22.76	1.50	6.60

Table D.11. UP profile flexure tests experimental results under 20% of the UFS load.

t [months]	σ_{fu} [MPa]	std.dev [MPa]	var.coef [%]	Ef [GPa]	std.dev [GPa]	var.coef [%]
0	552.62	40.16	7.27	21.38	2.28	10.67
3	570.30	24.84	4.36	23.27	2.64	11.36
6	555.34	4.55	0.82	21.34	2.12	9.95
12	535.78	33.90	6.33	21.14	1.00	4.73
18	557.63	24.05	4.31	22.15	0.70	3.18
24	601.31	38.60	6.42	22.00	1.00	4.55

Table D.12. VE profile flexure tests experimental results under 20% of the UFS load.

t [months]	σ_{fu} [MPa]	std.dev [MPa]	var.coef [%]	Ef [GPa]	std.dev [GPa]	var.coef [%]
0	561.11	16.84	3.00	23.02	0.77	3.37
3	513.19	8.18	1.59	22.84	0.79	3.45
6	515.84	29.43	5.70	21.60	3.11	14.41
12	506.58	28.78	5.68	21.92	2.95	13.46
18	515.36	32.58	6.32	22.45	3.47	15.48
24	520.15	18.52	3.56	22.88	2.21	9.67

E. Hygrothermal ageing and natural weathering of a cold curing epoxy adhesive experimental results

E.1 Sorption experimental results

Table E.1. EP water sorption experimental results.

T [days]	W20 [%]	W40 [%]	S20 [%]	S40 [%]	C40 [%]
0	0	0	0	0	0
0.124704167	0.070065	0.45632	0.043246	0.289315	0.12365
0.250104167	0.073216	0.536548	0.053419	0.389786	0.15632
0.498816667	0.083645	0.623215	0.07562	0.432564	0.256843
1.020834378	0.10264	0.691454	0.091563	0.478923	0.31256
3.124997086	0.121253	0.836635	0.13574	0.576166	0.411134
4.083329261	0.138565	0.863702	0.075411	0.666116	0.538815
5.06249647	0.153151	0.944905	0.125685	0.641805	0.643514
7.541662129	0.170167	1.077782	0.168418	0.802256	0.827375
9.541671773	0.245527	1.154064	0.138253	0.841153	0.947395
12.16667024	0.301439	1.269716	0.228747	0.994311	1.075077
16.20832853	0.269837	1.429661	0.339349	1.042933	1.332993
17.54165892	0.291715	1.491178	0.336836	1.115865	1.363636
18.5416612	0.243096	1.518246	0.354432	1.147469	1.391726
22.16667591	0.296577	1.60437	0.276507	1.215539	1.501532
23.54166934	0.364644	1.663427	0.334322	1.315214	1.544944
25.54167326	0.410832	1.71018	0.389623	1.405164	1.603677
29.54165799	0.413263	1.81845	0.512795	1.458647	1.695608
32.54167313	0.447297	1.897192	0.417274	1.512131	1.74668
43.54166734	0.590723	2.079283	0.560555	1.631254	2.012257
46.20832886	0.55669	2.064519	0.578151	1.563184	1.963739
51.16666393	0.692824	2.158026	0.630939	1.570477	2.048008
57.54167177	0.653928	2.283521	0.63848	1.631254	2.1476
60.12500055	0.726857	2.167868	0.761651	1.740653	2.15526
73.24999795	0.763322	2.359802	0.749082	1.507269	2.277835
88.16666667	0.880008	2.536972	0.955206	1.675013	2.402962
103.1666616	1.127966	2.655085	1.020562	1.534011	2.586823
135.1666502	1.208187	2.832255	1.186466	1.606943	2.734934
164.9791771	1.407526	2.972514	1.206576	1.638547	2.959653
196.979179	1.456145	3.075863	1.297069	1.643409	2.967314
218.2083357	1.516919	3.225965	1.395103	1.653134	3.003064
226.1666555	1.584986	3.184133	1.457946	1.772257	3.069459
233.1249837	1.592279	3.233347	1.462973	1.709048	3.089888
248.2083074	1.597141	3.238269	1.558494	1.77955	3.347804
254.1249697	1.643329	3.331775	1.659042	1.730928	3.163943
261.000028	1.638468	3.31455	1.55598	1.947294	3.110317

269.1249729	1.626313	3.312089	1.626364	1.723635	3.16905
281.1249714	1.687087	3.336696	1.679151	1.726066	3.28907
292.1249691	1.757585	3.356382	1.666583	1.767394	3.217569
305.5416839	1.730844	3.408056	1.674124	1.774688	3.375894
330.1250353	1.747861	3.45727	1.824946	1.796567	3.355465
344.1249963	1.828082	3.474495	1.734453	1.796567	3.381001
359.1458149	1.913166	3.572923	1.804836	1.789274	3.406537
380.5416618	1.769739	3.715643	1.701775	1.871931	3.388662
393.5416679	1.798911	3.580305	1.686692	1.687169	3.470378
428.5416749	1.944769	3.659047	1.89533	1.852482	3.600613
442.5417013	1.825651	3.617215	1.704288	1.665289	3.403984
450.541702	1.842668	3.63444	1.779699	1.648272	
462.5416385	1.849961	3.609833	1.757076	1.740653	
476.5416619	1.874271	3.683654	1.767131	1.62153	
504.541653	1.893718	3.769778	1.777186	1.743084	
514.5416245	2.003112	3.77716	1.852597	1.721204	
521.5416727	1.888856	3.782081	1.789754	1.701755	
533.5416674	1.966647	3.816531	1.862651	1.728497	
554.5416734	2.066317	3.853441	1.920467	1.738221	
571.541696	2.107643	3.868205	2.041124	1.747946	
596.5416977	2.122229	3.959251	2.081343	1.876793	
606.5416339	2.131953	3.966633	2.086371	1.687169	
616.5416661	2.161124	3.983858	2.161782	1.745515	
647.5416958	2.183003	3.988779	2.196974	1.740653	
667.5416775	2.212174	3.993701	2.212056	1.728497	
694.5416503	2.241346	4.033072	2.19446	1.568046	
730.5417209	2.241346	4.033072	2.19446	1.568046	

E.2 Thermo-mechanical experimental results

Table E.2. EP adhesive glass transition temperature experimental results.

W20						
t [months]	T_g tan δ [°C]	std.dev [°C]	var.coef [%]	T_g E'$_{onset}$ [°C]	std.dev [°C]	var.coef [%]
0	78.1	0.2	0.2	59.4	0.2	0.3
2	72.2	1.0	1.4	56.3	0.6	1.0
4	69.8	0.6	0.9	54.4	0.6	1.1
6	67.8	1.4	2.0	51.8	0.9	1.8
9	70.9	0.8	1.1	54.9	0.6	1.1
12	72.1	0.7	0.9	56.2	1.0	1.8
18	63.5	1.0	1.5	51.7	0.5	1.0
24	63.2	0.1	0.1	50.5	0.0	0.0
S20						
t [months]	T_g tan δ [°C]	std.dev [°C]	var.coef [%]	T_g E'$_{onset}$ [°C]	std.dev [°C]	var.coef [%]
0	78.1	0.2	0.2	59.4	0.2	0.3
2	70.5	0.1	0.1	55.2	0.5	0.9
4	71.2	1.1	1.6	55.7	0.4	0.7
6	69.2	0.7	1.0	53.3	0.6	1.0
9	71.1	0.4	0.6	55.1	1.1	2.0
12	72.8	1.1	1.5	55.4	2.2	4.0
18	67.7	3.2	4.7	53.3	2.2	4.1
24	70.3	1.4	1.9	54.9	1.0	1.9
W40						
t [months]	T_g tan δ [°C]	std.dev [°C]	var.coef [%]	T_g E'$_{onset}$ [°C]	std.dev [°C]	var.coef [%]
0	78.1	0.2	0.2	59.4	0.2	0.3
2	75.0	0.1	0.1	58.1	1.9	3.3
4	74.3	1.3	1.7	58.2	2.8	4.8
6	73.1	0.6	0.8	55.2	5.5	9.9
9	72.7	0.9	1.2	56.6	0.5	0.9
12	77.0	2.0	2.5	59.6	0.3	0.6
18	69.6	4.3	6.2	53.1	7.7	14.5
24	62.2	2.6	4.1	47.8	1.4	2.9
S40						
t [months]	T_g tan δ [°C]	std.dev [°C]	var.coef [%]	T_g E'$_{onset}$ [°C]	std.dev [°C]	var.coef [%]
0	78.1	0.2	0.2	59.4	0.2	0.3
2	76.5	1.5	1.9	61.3	1.4	2.2
4	76.6	0.6	0.8	60.8	1.6	2.6
6	73.1	1.6	2.1	56.6	2.0	3.5
9	74.7	0.6	0.8	57.8	0.6	1.0
12	77.6	0.9	1.2	62.6	2.2	3.5
18	68.7	3.2	4.7	53.7	2.0	3.7
24	71.0	2.8	4.0	55.5	3.4	6.2
C40						
t [months]	T_g tan δ [°C]	std.dev [°C]	var.coef [%]	T_g E'$_{onset}$ [°C]	std.dev [°C]	var.coef [%]
0	78.1	0.2	0.2	59.4	0.2	0.3
2	74.6	0.8	1.0	58.8	1.5	2.6
4	75.6	0.4	0.6	61.2	0.6	0.9
6	73.8	1.1	1.4	56.9	3.1	5.5
9	73.9	2.1	2.9	55.1	6.6	11.9
12	75.1	0.5	0.7	60.3	2.1	3.4

NE						
t [months]	T_g tan δ [°C]	std.dev [°C]	var.coef [%]	T_g E'$_{onset}$ [°C]	std.dev [°C]	var.coef [%]
0	78.1	0.2	0.2	59.4	0.2	0.3
12	76.6	0.3	0.4	60.3	0.8	1.3

E.3 Flexural experimental results

Table E.3. EP adhesive flexural experimental results.

W20						
t [months]	σ_{fu} [MPa]	std.dev [MPa]	var.coef [%]	E_f [GPa]	std.dev [GPa]	var.coef [%]
0	71.7	7.9	11.1	3.9	0.2	5.6
2	63.7	3.1	4.9	3.5	0.4	10.7
4	70.4	3.3	4.7	3.5	0.1	3.2
6	63.9	8.1	12.7	3.2	0.2	7.0
9	62.0	4.6	7.4	3.1	0.2	5.4
12	63.6	5.7	9.0	3.3	0.3	8.8
18	65.2	5.9	9.1	3.1	0.5	16.1
24	65.8	5.6	8.6	3.3	0.3	9.4
S20						
t [months]	σ_{fu} [MPa]	std.dev [MPa]	var.coef [%]	E_f [GPa]	std.dev [GPa]	var.coef [%]
0	71.7	7.9	11.1	3.9	0.2	5.6
2	70.7	4.9	7.0	3.7	0.3	7.2
4	70.4	3.3	4.7	3.5	0.1	3.2
6	63.8	4.5	7.1	3.3	0.3	9.1
9	62.8	2.5	4.0	3.2	0.3	10.7
12	60.7	3.9	6.4	3.3	0.2	5.0
18	67.2	5.1	7.6	3.2	0.5	14.1
24	64.7	5.0	7.8	3.2	0.3	10.2
W40						
t [months]	σ_{fu} [MPa]	std.dev [MPa]	var.coef [%]	E_f [GPa]	std.dev [GPa]	var.coef [%]
0	71.7	7.9	11.1	3.9	0.2	5.6
2	62.1	2.6	4.3	3.4	0.2	5.2
4	65.9	2.1	3.2	3.5	0.2	4.6
6	63.9	3.9	6.1	3.5	0.4	12.5
9	58.8	7.4	12.5	3.2	0.3	9.9
12	65.5	3.5	5.4	3.5	0.2	5.6
18	63.1	4.8	7.5	3.3	0.5	15.3
24	54.4	3.1	5.8	2.7	0.3	9.4
S40						
t [months]	σ_{fu} [MPa]	std.dev [MPa]	var.coef [%]	E_f [GPa]	std.dev [GPa]	var.coef [%]
0	71.7	7.9	11.1	3.9	0.2	5.6
2	68.1	9.7	14.2	3.5	0.3	9.0
4	68.5	2.6	3.9	3.1	0.2	7.6
6	70.4	4.7	6.7	3.2	0.2	5.5
9	69.0	3.0	4.3	3.1	0.2	5.4
12	59.0	5.4	9.2	3.2	0.3	10.0
18	70.2	8.1	11.5	3.2	0.3	9.6
24	66.5	5.1	7.7	3.1	0.1	4.1
C40						
t [months]	σ_{fu} [MPa]	std.dev [MPa]	var.coef [%]	E_f [GPa]	std.dev [GPa]	var.coef [%]
0	71.7	7.9	11.1	3.9	0.2	5.6
2	68.2	7.5	11.0	3.7	0.5	12.8
4	68.1	5.1	7.6	3.3	0.2	7.6

6	64.4	7.0	10.8	3.2	0.1	2.9
9	64.4	5.6	8.7	3.0	0.3	10.8
12	67.5	6.9	10.3	3.5	0.4	12.2

E.4 In-plane shear experimental results

Table E.4. EP adhesive in-plane shear experimental results.

W20						
t [months]	τ_u [MPa]	std.dev [MPa]	var.coef [%]	G [GPa]	std.dev [GPa]	var.coef [%]
0	28.26	4.01	14.21	1.79	0.37	20.74
3	30.55	3.10	10.16	1.73	0.33	19.30
6	33.70	1.76	5.21	1.46	0.17	11.37
9	32.03	3.34	10.43	1.17	0.09	7.29
12	33.76	1.26	3.74	1.68	0.12	7.10
S20						
t [months]	τ_u [MPa]	std.dev [MPa]	var.coef [%]	G [GPa]	std.dev [GPa]	var.coef [%]
0	28.26	4.01	14.21	1.79	0.37	20.74
3	32.23	3.09	9.60	1.49	0.26	17.33
6	33.10	2.41	7.29	1.52	0.21	13.65
9	30.74	5.28	17.19	1.70	0.29	17.33
12	30.34	5.23	17.24	1.37	0.25	18.15
W40						
t [months]	τ_u [MPa]	std.dev [MPa]	var.coef [%]	G [GPa]	std.dev [GPa]	var.coef [%]
0	28.26	4.01	14.21	1.79	0.37	20.74
3	28.84	6.54	22.69	1.51	0.21	13.94
6	33.02	1.89	5.73	1.45	0.35	23.97
9	33.25	2.95	8.89	1.30	0.28	21.81
12	28.75	3.34	11.61	1.01	0.27	26.78
S40						
t [months]	τ_u [MPa]	std.dev [MPa]	var.coef [%]	G [GPa]	std.dev [GPa]	var.coef [%]
0	28.26	4.01	14.21	1.79	0.37	20.74
3	33.57	1.58	4.70	1.18	0.18	14.91
6	36.17	0.96	2.65	1.42	0.20	13.92
9	34.25	2.07	6.04	1.20	0.27	22.71
12	33.64	3.05	9.05	1.23	0.15	11.84
NE						
t [months]	τ_u [MPa]	std.dev [MPa]	var.coef [%]	G [GPa]	std.dev [GPa]	var.coef [%]
0	28.26	4.01	14.21	1.79	0.37	20.74
3	30.87	3.62	11.71	1.65	0.20	11.89
6	31.75	2.12	6.67	1.49	0.23	15.54
9	33.30	2.70	8.10	1.61	0.25	15.69
12	30.35	5.72	18.84	1.55	0.32	20.48

F. Effects of hygrothermal ageing and natural weathering on structural polyurethane adhesive experimental results

F.1 Sorption experimental results

Table F.1. PU water sorption experimental results.

T [days]	W20 [%]	W40 [%]	S20 [%]	S40 [%]	C40 [%]
0	0	0	0	0	0
0.124704167	0.2334	0.57789	0.12564	0.46597	0.23654
0.250104167	0.3678	0.9864	0.23548	0.69872	0.31424
0.498816667	0.4631	1.18659	0.32165	0.83659	0.40366
1.020834378	0.45586	1.44733	0.52078	0.97726	0.47892
3.124997086	0.55872	1.66503	0.6887	1.10155	0.9384
4.083329261	0.58444	1.76312	0.64733	1.10886	1.14018
5.06249647	0.62652	1.83967	0.65463	1.10155	1.24471
7.541662129	0.75276	2.0789	0.83471	1.17223	1.51699
9.541671773	0.7738	2.15784	0.78361	1.16248	1.61424
12.16667024	0.85094	2.33009	0.83228	1.18198	1.79171
16.20832853	1.01926	2.55736	0.99289	1.26971	2.12963
17.54165892	1.00991	2.7296	0.96126	1.20878	2.13449
18.5416612	0.99121	2.74156	1.01723	1.26727	2.11018
22.16667591	1.05433	2.89228	0.99776	1.30627	2.27063
23.54166934	1.0894	2.99993	1.06833	1.31845	2.3387
25.54167326	1.12212	3.11237	1.14621	1.33307	2.48213
29.54165799	1.18992	3.3181	1.22652	1.35744	2.64501
32.54167313	1.27408	3.43772	1.24355	1.35257	2.77143
43.54166734	1.4237	3.83962	1.25815	1.35257	3.16526
46.20832886	1.42136	3.87551	1.24355	1.38181	3.16283
51.16666393	1.50552	4.05014	1.35063	1.41837	3.33544
57.54167177	1.56162	4.20325	1.32629	1.43543	3.47644
60.12500055	1.61072	4.25827	1.48691	1.41106	3.36948
73.24999795	1.64578	4.60276	1.34333	1.23072	3.78519
88.16666667	1.84215	4.9951	1.50394	1.39887	4.15714
103.1666616	2.00814	5.32045	1.56235	1.32576	4.54126
135.1666502	2.15074	5.72953	1.52584	1.3087	5.12715
164.9791771	2.00112	6.22473	1.60859	1.30139	5.33865
196.979179	2.07827	6.42329	1.7108	1.35501	5.538
218.2083357	2.36581	6.65056	1.68889	1.42568	5.70574
226.1666555	2.3588	6.7606	1.7181	1.40375	5.78354
233.1249837	2.36815	6.84673	1.68403	1.394	5.81514
248.2083074	2.52946	6.87783	1.70836	1.40862	5.93913
254.1249697	2.50842	6.93285	1.71566	1.4135	5.85647
261.000028	2.49673	7.06442	1.70349	1.43299	5.9999
269.1249729	2.5692	7.04529	1.73026	1.39156	6.12875
281.1249714	2.58322	7.16251	1.69376	1.33064	6.14091
292.1249691	2.65569	7.13619	1.7619	1.32089	6.24058

305.5416839	2.65803	7.27495	1.72783	1.38669	6.3597
330.1250353	2.75856	7.44719	1.78137	1.39644	6.55176
344.1249963	2.78661	7.40891	1.75217	1.44518	6.4691
359.1458149	2.95025	7.80364	1.7619	1.44762	6.4302
380.5416618	2.9222	8.11225	1.69133	1.48417	6.76326
393.5416679	2.84272	7.90172	1.61102	1.39887	6.55419
428.5416749	3.01571	8.01655	1.73756	1.45736	6.77785
442.5417013	2.90584	7.89694	1.59398	1.31845	6.5396
450.541702	2.95259	7.99502	1.61102	1.31845	
462.5416385	2.93623	7.91847	1.58425	1.15029	
476.5416619	2.98999	8.08832	1.60128	1.26971	
504.541653	3.05545	8.73903	1.58425	1.23315	
514.5416245	3.07883	8.6242	1.63779	1.35013	
521.5416727	3.07649	8.57396	1.56478	1.39887	
533.5416674	3.14896	8.64573	1.62562	1.3745	
554.5416734	3.22611	8.81558	1.70349	1.40375	
571.541696	3.29858	8.85386	1.78867	1.36476	
596.5416977	3.38508	8.97586	1.87384	1.46224	
606.5416339	3.37105	9.12418	1.84221	1.20878	
616.5416661	3.43417	9.1505	1.84221	1.42812	
647.5416958	3.42248	9.16724	1.8057	1.3477	
667.5416775	3.41079	9.16964	1.75217	1.22828	
694.5416503	3.56508	9.19117	1.8057	0.90659	
730.5417209	3.56508	9.19117	1.8057	0.90659	

F.2 Thermo-mechanical experimental results

Table F.2. PU adhesive glass transition temperature experimental results.

W20		
t [months]	T_g tan δ [°C]	T_g E'_{onset} [°C]
0	49.8	9.2
2	51.9	12.6
4	50.0	14.5
6	51.0	13.2
9	57.0	14.5
12	54.5	16.1
S20		
t [months]	T_g tan δ [°C]	T_g E'_{onset} [°C]
0	49.8	9.2
2	56.5	18.2
4	51.0	17.5
6	52.5	17.9
9	53.7	18.1
12	55.4	18.5
W40		
t [months]	T_g tan δ [°C]	T_g E'_{onset} [°C]
0	49.8	9.2
2	49.8	8.3
4	52.0	14.4
6	49.9	15.1
9	56.8	16.9
12	56.9	20.0

S40		
t [months]	T_g tan δ [°C]	T_g E'$_{onset}$ [°C]
0	49.8	9.2
2	53.6	16.0
4	53.8	18.6
6	52.5	15.8
9	56.9	17.9
12	53.7	13.2
C40		
t [months]	T_g tan δ [°C]	T_g E'$_{onset}$ [°C]
0	49.8	9.2
2	52.9	12.8
4	51.9	15.7
6	49.0	14.2
9	55.3	17.4
12	56.1	19.6
NE		
t [months]	T_g tan δ [°C]	T_g E'$_{onset}$ [°C]
0	49.8	9.2
12	53.7	16.1

F.3 Flexural experimental results

Table F.3. PU adhesive flexural experimental results.

W20					
t [months]	σ_{fmax} [MPa]	std.dev [MPa]	var.coef [%]	E_f [GPa]	std.dev [GPa]
0	30.6	2.1	6.9	1.3	0.2
2	22.7	5.8	25.4	1.0	0.3
4	26.8	1.3	4.8	1.2	0.1
6	24.6	0.7	2.7	1.1	0.0
9	15.3	2.0	13.2	0.6	0.1
12	31.7	2.7	8.5	1.1	0.2
18	25.4	4.7	18.6	1.2	0.2
24	24.6	2.9	11.7	1.1	0.3
S20					
t [months]	σ_{fmax} [MPa]	std.dev [MPa]	var.coef [%]	E_f [GPa]	std.dev [GPa]
0	30.6	2.1	6.9	1.3	0.2
2	25.0	2.6	10.6	1.1	0.2
4	26.6	0.7	2.6	1.2	0.1
6	26.4	1.6	6.2	1.2	0.1
9	21.1	3.5	16.6	0.8	0.2
12	23.2	6.0	25.8	1.2	0.3
18	27.8	5.0	18.0	1.3	0.3
24	25.7	2.5	9.6	1.2	0.3
W40					
t [months]	σ_{fmax} [MPa]	std.dev [MPa]	var.coef [%]	E_f [GPa]	std.dev [GPa]
0	30.6	2.1	6.9	1.3	0.2
2	32.2	1.1	3.4	1.5	0.1
4	26.6	0.7	2.6	1.2	0.1
6	24.0	0.7	2.8	1.1	0.1
9	23.2	0.5	2.2	1.0	0.2
12	23.5	3.4	14.4	0.8	0.3
18	25.7	6.3	24.5	0.9	0.3

24	21.4	1.6	7.3	0.8	0.1
S40					
t [months]	σ_{fmax} [MPa]	std.dev [MPa]	var.coef [%]	E_f [GPa]	std.dev [GPa]
0	30.6	2.1	6.9	1.3	0.2
2	26.0	1.6	6.3	1.0	0.1
4	30.3	1.2	4.0	1.3	0.1
6	27.5	2.8	10.1	1.2	0.1
9	13.7	2.0	14.3	0.5	0.1
12	27.2	5.7	21.0	1.0	0.3
18	28.2	4.7	16.7	1.1	0.3
24	26.3	7.1	26.9	0.9	0.2
C40					
t [months]	σ_{fmax} [MPa]	std.dev [MPa]	var.coef [%]	E_f [GPa]	std.dev [GPa]
0	30.6	2.1	6.9	1.3	0.2
2	30.1	1.7	5.8	1.4	0.1
4	26.3	1.1	4.2	1.1	0.1
6	24.9	0.7	3.0	1.2	0.1
9	14.2	3.6	25.3	0.5	0.1
12	23.8	3.8	16.0	1.1	0.3

F.4 In-plane shear experimental results

Table F.4. PU adhesive in-plane shear experimental results.

W20						
t [months]	τ_{max} [MPa]	std.dev [MPa]	var.coef [%]	G [GPa]	std.dev [GPa]	var.coef [%]
0	24.71	1.42	5.76	0.84	0.14	17.17
3	21.21	0.82	3.85	0.73	0.05	6.67
6	19.79	0.64	3.23	0.64	0.07	10.65
9	22.02	0.74	3.37	0.79	0.13	16.70
12	18.34	1.19	6.51	0.57	0.08	13.71
S20						
t [months]	τ_{max} [MPa]	std.dev [MPa]	var.coef [%]	G [GPa]	std.dev [GPa]	var.coef [%]
0	24.71	1.42	5.76	0.84	0.14	17.17
3	23.77	0.74	3.11	0.79	0.19	24.07
6	19.69	0.36	1.82	0.75	0.10	13.60
9	21.91	1.35	6.16	0.63	0.18	28.32
12	19.44	1.40	7.19	0.61	0.13	22.13
W40						
t [months]	τ_{max} [MPa]	std.dev [MPa]	var.coef [%]	G [GPa]	std.dev [GPa]	var.coef [%]
0	24.71	1.42	5.76	0.84	0.14	17.17
3	26.15	0.91	3.49	0.89	0.11	12.13
6	21.22	2.26	10.63	0.73	0.11	15.07
9	24.67	1.26	5.10	0.73	0.12	15.91
12	19.70	1.13	5.72	0.49	0.07	14.19
S40						
t [months]	τ_{max} [MPa]	std.dev [MPa]	var.coef [%]	G [GPa]	std.dev [GPa]	var.coef [%]
0	24.71	1.42	5.76	0.84	0.14	17.17
3	27.10	0.88	3.24	1.04	0.11	10.55
6	22.80	1.38	6.05	0.74	0.09	11.88
9	21.21	3.66	17.26	0.61	0.09	14.66
12	21.15	1.26	5.97	0.47	0.03	5.88

NE						
t [months]	τ_{max} [MPa]	std.dev [MPa]	var.coef [%]	G [GPa]	std.dev [GPa]	var.coef [%]
0	24.71	1.42	5.76	0.84	0.14	17.17
3	24.05	1.32	5.50	0.91	0.14	15.21
6	25.19	1.09	4.33	0.84	0.21	24.60
9	26.25	1.05	4.01	0.77	0.12	15.63
12	27.82	0.35	1.25	0.86	0.19	22.43

G. Effects of hygrothermal ageing and natural weathering on structural polyurethane adhesive experimental results

G.1 Failure load experimental results

Table G.1. EP-GFRP bonded joint failure load experimental results.

Failure load [kN]								
Time [months]	W20 [MPa]	std.dev [MPa]	S20 [MPa]	std.dev [MPa]	W40 [MPa]	std.dev [MPa]	S40 [MPa]	std.dev [MPa]
0	10.7	1.4	10.7	1.3	10.7	1.3	10.	1.3
2	9.2	0.6	8.6	0.6	9.0	1.3	8.4	0.3
4	8.9	1.4	8.8	0.6	8.8	0.6	7.9	0.9
6	7.8	1.0	8.5	0.9	7.5	0.3	7.6	0.8
9	9.1	0.3	9.3	0.6	7.7	0.6	7.7	0.7
12	9.9	0.6	9.2	1.0	8.3	0.3	8.2	0.7
18	11.8	1.7	12.5	1.6	8.6	1.6	8.2	1.3
24	11.9	1.1	11.3	1.5	6.9	0.4	8.6	1.9
Failure load [kN]								
Time [months]	C40 [MPa]	std.dev [MPa]	NE [MPa]	std.dev [MPa]	t [hours]	SF35 [MPa]	std.dev [MPa]	
0	10.7	1.3	10.7	1.3	0	10.7	1.3	
2	8.8	0.9	8.6	0.7	500	9.7	0.5	
4	8.4	0.7	8.4	0.9	1000	8.0	0.8	
6	7.7	0.6	9.1	1.1	2000	7.2	1.0	
9	8.5	0.6	10.2	0.1				
12	8.4	0.7	9.9	0.4				
18			11.8	2.1				
24			13.4	1.8				

Table G.2. PU-GFRP bonded joint failure load experimental results.

Failure load [kN]								
Time [months]	W20 [MPa]	std.dev [MPa]	S20 [MPa]	std.dev [MPa]	W40 [MPa]	std.dev [MPa]	S40 [MPa]	std.dev [MPa]
0	0	12.0	2.3	12.0	2.3	12.0	2.3	12.0
2	2	13.7	1.5	14.0	1.8	11.4	1.2	11.1
4	4	11.7	1.3	10.6	1.1	10.6	1.1	8.8
6	6	9.6	1.2	10.3	0.8	8.4	0.4	8.5
9	9	9.8	1.3	11.0	2.0	9.4	1.0	9.2
12	12	10.2	0.8	11.8	2.0	9.2	0.6	8.9
18	18	12.1	1.4	13.1	1.4	9.7	2.1	9.1
24	24	12.1	1.6	12.1	1.9	8.7	2.7	8.8

Failure load [kN]								
Time [months]	C40 [MPa]	std.dev [MPa]	NE [MPa]	std.dev [MPa]	t [hours]	SF35 [MPa]	std.dev [MPa]	
0	12.0	2.3	12.0	2.3	0	12.0	2.3	
2	12.9	0.8	10.2	2.1	500	14.1	1.5	
4	9.1	0.4	8.1	1.5	1000	9.6	1.4	
6	8.4	0.4	9.7	0.6	2000	10.0	0.5	
9	9.1	1.9	9.7	2.0				
12	9.2	0.8	12.1	2.1				
18			13.9	1.3				
24			13.2	2.1				